INFORMATION TO USERS

This reproduction was made from a copy of a document sent to us for microfilming. While the most advanced technology has been used to photograph and reproduce this document, the quality of the reproduction is heavily dependent upon the quality of the material submitted.

The following explanation of techniques is provided to help clarify markings or notations which may appear on this reproduction.

1. The sign or "target" for pages apparently lacking from the document photographed is "Missing Page(s)". If it was possible to obtain the missing page(s) or section, they are spliced into the film along with adjacent pages. This may have necessitated cutting through an image and duplicating adjacent pages to assure complete continuity.

2. When an image on the film is obliterated with a round black mark, it is an indication of either blurred copy because of movement during exposure, duplicate copy, or copyrighted materials that should not have been filmed. For blurred pages, a good image of the page can be found in the adjacent frame. If copyrighted materials were deleted, a target note will appear listing the pages in the adjacent frame.

3. When a map, drawing or chart, etc., is part of the material being photographed, a definite method of "sectioning" the material has been followed. It is customary to begin filming at the upper left hand corner of a large sheet and to continue from left to right in equal sections with small overlaps. If necessary, sectioning is continued again—beginning below the first row and continuing on until complete.

4. For illustrations that cannot be satisfactorily reproduced by xerographic means, photographic prints can be purchased at additional cost and inserted into your xerographic copy. These prints are available upon request from the Dissertations Customer Services Department.

5. Some pages in any document may have indistinct print. In all cases the best available copy has been filmed.

University Microfilms International
300 N. Zeeb Road
Ann Arbor, MI 48106

8401337

Sager, William Warren

SEAMOUNT PALEOMAGNETISM AND PACIFIC PLATE TECTONICS

University of Hawaii PH.D. 1983

University
Microfilms
International 300 N. Zeeb Road, Ann Arbor, MI 48106

Copyright 1983

by

Sager, William Warren

All Rights Reserved

SEAMOUNT PALEOMAGNETISM

AND

PACIFIC PLATE TECTONICS

A DISSERTATION SUBMITTED TO THE GRADUATE DIVISION OF THE
UNIVERSITY OF HAWAII IN PARTIAL FULFILLMENT
OF THE REQUIREMENTS FOR THE DEGREE OF

DOCTOR OF PHILOSOPHY

IN GEOLOGY AND GEOPHYSICS

AUGUST 1983

By

William W. Sager

Dissertation Committee:

Barbara H. Keating, chair
David Epp
Frederick K. Duennebier
Murli H. Manghnani
Keith E. Chave

ACKNOWLEDGEMENTS

I am particularly indebted to Dr. Barbara Keating, my dissertation advisor, for constant support, encouragement, and sound advice. On the wall of her office Barbara has hung a sign that reads, "Heresy Thought Here". This is a spirit I find admirable and I hope it has shown in this work. David Epp, as well as serving as one of my committee members, has been a valuable source of insight and this manuscript has benefitted greatly from his thoughtful review. Richard Blakely and Don Plouff, of the USGS, were very kind to supply me with their computer program for modeling seamounts. My thanks also go to Richard Gordon, whose work parallels my own, for providing the computer program to calculate paleomagnetic poles and keeping me abreast of his latest ideas on Pacific tectonics. This study would have been impossible without the assistance of the captains, chief scientists, crew members, and scientific staff of the R/V Kana Keoki, with whom I have spent many a birthday at sea. A special thanks goes to Allen Clarke, my great uncle, who has stimulated by curiosity ever since childhood and has always been a source of encouragement in the quest for my doctorate. Dick Hey also deserves a mention here as it was a paper I did for his class in plate tectonics, as a first year graduate student, that first aroused my interest in seamount paleomagnetism. Last, but certainly not least, I am grateful to the scientists at the Office of Naval research, who have funded this project since its inception.

ABSTRACT

Thirty-four new seamount paleomagnetic models are presented in this study, doubling the amount of reliable seamount paleomagnetic data available from the Pacific, making it possible to re-interpret the apparent polar wander path (APWP) of the Pacific and to examine the temporal distribution of volcanism in the Line Islands and Musicians Seamounts. Paleomagnetic results from twenty-six dated seamounts were combined with Pacific paleomagnetic data from other sources to calculate seven mean paleomagnetic poles representing the Eocene, Maastrichtian, Campanian, Santonian, Turonian, Albian, and Barremian. The agreement of the seamount VGPs with the other paleomagnetic data is generally quite good, indicating that the seamount results are relatively free of any bias that might result from demagnetization or secondary magnetization components. The APWP begins near Greenland along the Late Jurassic DSDP Site 307 polar circle and moves more than 20^{o} southward to the Barremian and Albian poles. Between the Albian and the Campanian it turns to the north and then to the east to form a mid-Cretaceous loop before trending northward to the geographic pole in the Late Cretaceous and Tertiary. The rate of APW along the segments that form this loop are very high, and in one spurt from about 91 to 81 Ma. the paleopole appears to move over 22^{o} in only 10 Ma. Within the resolution of the data, the timing of the fast APW appears to be coincident with the Cretaceous Quiet Time.

The north Pacific paleomagnetic poles are compared to the positions predicted for them by a Pacific plate/hotspot motion model and a large discrepancy during the Early and Late Cretaceous is noted. These

differences could be caused by true polar wander, varying long term non-dipole geomagnetic field components, or by an inadequate model of plate/hotspot motion. The implications of the paleomagnetic data for each of phenomena is discussed and it is concluded that although true polar wander and non-dipole components probably have some effect on the APWP, most of the rapid APW is due to plate motion.

It is noted that a number of equatorial DSDP sediment paleocolatitudes record paleomagnetic poles significantly closer to the geographic pole than do the rest of the paleomagnetic data. These discrepant data show excellent agreement with the few south Pacific paleomagnetic data available, and it is suggested that the discrepancy may have a tectonic cause.

Seamount paleomagnetism gives some interesting insights into the processes of volcanism in the Line Islands and the Musicians Seamounts. The VGPs of Line Islands seamounts indicate that there was volcanic activity in the chain during both the Late Cretaceous and the Eocene. Few reliable ages are available for Musicians Seamounts, but the VGPs from these edifices are very consistent and so a magnetic age has been assigned to each volcano by the position of its VGP along the APWP. The paleomagnetic data indicates that volcanism occurred in the Musicians from the Santonian-Turonian to the Maastrichtian. The magnetic ages are inconsistent with all proposed models for the formation of the Musicians, but show a general younging trend from west to east.

TABLE OF CONTENTS

LIST OF TABLES

LIST OF FIGURES

CHAPTER 1: INTRODUCTION

1.1 THE PROBLEMATIC PACIFIC

More than fifteen years have passed since Morgan (1968) demonstrated that the earth's surface is made up of a network of crustal blocks, called "plates", that are constantly in motion and interacting with one another. The past motions of most of these plates are relatively well known. Perhaps the most notable exception is the Pacific plate. Despite being over 13,000 km. across at its widest, its evolution and past movements remain enigmatic. Not only is this lack of knowledge detrimental to the understanding of Pacific tectonics, but like a piece missing from a jigsaw puzzle, it detracts from the whole picture of plate tectonics. The tectonic evolution of plates and their margins is very important because of its social and economic ramifications, yet the margins of the plates around the Pacific will not be fully understood until the past motions of the Pacific are better known.

Several tools are available to the geoscientist who wishes to fit a plate into the tectonic framework of those surrounding it. Perhaps the most widely used of these are paleomagnetism and the correlation of magnetic lineations. The paleomagnetist seeks to locate the plate with respect to the spin axis using the geomagnetic field as an absolute

frame of reference. This is accomplished by measuring the direction of the geomagnetic field "frozen" in rocks at the time of their formation. It is assumed that the shape of the geomagnetic field that magnetized the rocks is the same as a dipole at the center of the Earth and aligned along the spin axis. Thus, from the inclination and declination of the preserved paleomagnetic field, the distance and direction of the geographic pole from the sampling site at a time in the past can be determined.

If the plate is left in its present-day position on the globe and the positions of the pole measured at different geologic periods are also plotted, one usually finds that the ancient poles are displaced from the geographic pole. The locus of positions of these poles in the past is called an apparent polar wander path (APWP). Figure 1.1 shows APWPs for Europe and North America from a classic text on paleomagnetism (McElhinny, 1973). Both paths have similar shapes, but are separated. This separation is evidence of the relative motion between the two plates caused by the opening of the Atlantic Ocean. In Figure 1.1 it can also be seen that both continents were once closer to the equator because the paleomagnetic poles of the APWPs are on the opposite side of the spin axis from the continents themselves. Thus both relative (plate versus plate) and absolute (plate versus spin axis) motions can be derived from a paleomagnetic APWP. Unfortunately, both relative and absolute past motions of the Pacific are uncertain because its APWP is poorly known (Jarrard and Sasajima, 1980). The primary reason for this problem is the fact that so little of the

Pacific plate is accessible to easy sampling. Most of it lies beneath several kilometers of ocean and cannot be sampled by traditional land paleomagnetic techniques.

The correlation of marine magnetic lineations also gives relative plate motions. If two plates separated by a spreading center are rotated towards one another by the same angle about their pole of relative motion, then magnetic lineations of the same age on each plate will line up with each other atop the location of the spreading ridge. In such fashion an extensional ocean (the Atlantic, for example) can be "closed" to represent previous configurations from its past. This technique does not work for most of the Pacific, however, as it is almost completely surrounded by subduction zones. As a consequence, tectonophysicists who would predict relative motions among Pacific basin plates must circumvent the Pacific by laborious "plate circuits" which tend to compound the errors inherent in the measurement of magnetic lineations and the calculation of rotation poles.

Magnetic lineations are also important as time markers. They represent the position of the edge of the plate that abuts a spreading ridge at the time of a magnetic field polarity change. Therefore, one need only measure these lineations with a magnetometer and identify them with a geomagnetic reversal time scale to determine the age of the underlying seafloor and the limits of the plate at that time in its past. In an area with plentiful linear anomalies, tectonic histories are usually easy to construct because fracture zones, ridges, and ridge jumps are well delineated. Because of the many high amplitude

lineations found there, the evolution of the Pacific plate east of Hawaii was fairly well deciphered (Atwater, 1970; Atwater and Menard, 1970; Herron, 1972; Handschumacher, 1976; Weissel et al., 1977) within a few years after geophysicists accepted the unifying theory of plate tectonics. In contrast, the evolution of the central and western Pacific remains an enigma because much of the seafloor in that area was formed during the Cretaceous Long Normal Period or contains poorly mapped, low amplitude magnetic lineations (Figure 1.2). Where magnetic lineations do exist in the western Pacific, they can often be confusing or misleading. For instance, neither of the spreading rates inferred from the Mesozoic and Cenozoic lineation sequences can be extrapolated through the seafloor formed during the Cretaceous Long Normal Period. The quiet zone is too wide. This fact has lead some authors to postulate that extremely fast spreading or large ridge jumps occurred during this time interval (Larson and Chase, 1972; Winterer, 1976). Recent studies, however, suggest that more complex tectonic events may have occurred in the quiet zone (Tamaki et al., 1979; Orwig and Kroenke, 1980; Farrar and Dixon, 1981).

Two other methods can be used to derive the past motion of the Pacific. These are the study of hotspot-derived volcanic chains and the study of the stratigraphy and distribution of equatorial sediments. Hotspot island and seamount chains are formed as the plate drifts over a magma source in the mantle. Volcanoes are built over the magma source and eventually carried away by the plate's motion. By studying the chronology of volcanism along the chain, the rate of movement of

the plate over the mantle can be determined. If several such chains are examined, then a pole of rotation of the plate with respect to the hotspots and mantle can be calculated. Evidence exists which suggests that most of the earth's hotspots are spatially fixed with respect to one another (Crough and Jurdy, 1980; Duncan, 1981; Morgan, 1981) and thus constitute a reference frame which may be used to compare plate motions. In the case of the Pacific, there are two problems with this method. Studies of worldwide plate motions in the hotspot reference frame suggest that either the Pacific hotspots are moving relative to the rest or that the plate reconstructions used to link the Pacific with its neighbors are incorrect (Duncan, 1981). The former is a possiblility, but the latter is less surprising considering that most of the Pacific's spreading margin abuts the Antarctic and Nazca plates whose motions are not well understood. The second problem is the scarcity of well-studied, hotspot-created seamount chains, particularly for the Cretaceous and Jurassic. The Hawaiian-Emperor chain is probably the best studied hotspot chain on Earth, but its oldest volcano, Meiji Guyot, is only about 70 Ma of age (Worsley, 1973). Other Pacific volcanic chains which appear to have been formed by hotspot-like volcanism are the Marquesas, Society, Caroline, Guadaloupe (Jarrard and Clague, 1977), and Pratt-Welker (Turner et al., 1980) chains. These seamount chains are generally young and not nearly as well constrained by data as the Hawaiian-Emperor chain. For the Cretaceous and Jurassic there is practically no constraint of the Pacific's motion from hotspots. Though some authors have attempted to

explain several Cretaceous Pacific seamount chains by hotspot volcanism (Henderson and Gordon, 1981; Epp, 1982), their interpretations are equivocal.

The Pacific plate's motion can also be measured from observations of the northward drift with time of equatorial sediments. A zone of intense organic sedimentation exists along the equator from approximately 5^{o} N to 5^{o} S because of the proliferation of aquatic micro-organisms in nutrient rich water brought up from the depths by the divergence of equatorial currents (Arrhenius, 1963). As the plate passes across the equator it acquires a thick accumulation of sediments as a result of the rain of organic detritus from these highly productive waters. This equatorial sedimentary sequence is a characteristic "fingerprint" that can be identified in Deep Sea Drilling Project (DSDP) cores (Heezen et al., 1973; van Andel et al., 1975). The age ot the equatorial deposits gives the time at which the DSDP site crossed the equator. If it is assumed that the biologic high productivity zone has remained about 90^{o} from the spin axis in the past, then this information is analogous to paleomagnetic data and can be treated similarly. This technique is limited by several factors. The geographic range of suitable sites to drill such a stratigraphic sequence is small. It is not certain how close to the equator the high-sedimentation belt has remained in the past. Also, the identification of the characteristic sediment sequence in the DSDP core may be difficult because of spotty coring, turbidites, and hiatuses.

Paleomagnetism is the primary tool used in this study to refine current thinking on the tectonics of the Pacific plate. Most of the emphasis is placed on paleomagnetic data derived from the inversion of seamount magnetic anomalies (called "seamount paleomagnetism" here); however, this data is combined with paleomagnetic data and equator transits from the literature. Seamount paleomagnetism is a method of estimating the overall magnetization vector of the lavas comprising a seamount using only a bathymetric and magnetic survey of the edifice (see Chapter 2). It has been used sparingly by geoscientists in the past; but, it is particularly useful for studying the Pacific for several reasons. All that is needed to measure the magnetization vector of a seamount is a survey at the sea surface. No oriented samples need be recovered from great depths of water. Any bathymetric chart of the Pacific shows that there is no scarcity of seamounts to be studied. Also, as many Pacific seamounts are found in linear chains, seamount paleomagnetic data not only gives information about the overall motion of the plate, but it also gives clues to the spatial and temporal distribution of volcanism in these seaount chains. Additionally, the seamount paleomagnetic technique is well suited for studying the quiet zone areas of the seafloor because the method works best on seamounts magnetized during a single geomagnetic polarity interval.

1.2 THE IMPORTANCE OF SEAMOUNT PALEOMAGNETISM

Seamount paleomagnetism has undeservedly been the neglected stepchild ot paleomagnetic research. It holds great potential for the understanding of oceanic plates such as the Pacific. The problem with oceanic plates, of course, is the difficulty of obtaining oriented paleomagnetic samples from the ocean depths. Only a tiny percentage of the Pacific's vast expanse is land area and almost all of this land is in the form of young islands. Thus it is not practical to use traditional land paleomagnetic techniques to obtain samples more than about 10-15 Ma. of age.

The paleomagnetist has at his disposal four primary methods of obtaining deep sea paleomagnetic samples: oriented piston cores, DSDP rotary drill cores, estimates of the skewness of seafloor magnetic lineations, and seamount surveys. Oriented piston cores give the most precise paleomagnetic data; however, they are severely limited in the range ot ages they can sample. Older sediments tend to be indurated and buried deep within the sediment column except in areas of chance erosional exposure. Thus it is rare that sediments older than a few tens of millions of years are recovered by this method. Oriented piston core paleomagnetism has brought to light some interesting insights in Pacific plate tectonics for the late Tertiary (Hammond et al., 1979, Hammond, 1980; Epp et al., 1982), but it has left untouched earlier periods which are most interesting segments of the Pacific's history.

The DSDP rotary drill cores cover a much wider range of ages than oriented piston cores; however, they too have several limitations. First, rotary cores are not azimuthally oriented--only paleolatitudes and polarity can be determined from them--and there is at least a 5^{o} uncertainty in their vertical orientation (Peirce, 1976). Second, the coring process sometimes jumbles and disturbs the samples it recovers (Peirce, 1976). Third, DSDP coring of basalts rarely recovers enough independent samples to average out secular variation (Kono, 1980). Rotary drill cores are also by far the most expensive method of paleomagnetic sampling.

Inclinations of the paleomagnetic field can be determined from the shape (called "skewness") of the magnetic anomalies caused by the crustal blocks of alternating polarity formed at a spreading ridge. This method is similar to the seamount paleomagnetic method, except that the magnetic source bodies are within the crust and the paleomagnetic data derived is azimuthally unoriented because the shape of the anomaly is only sensitive to the projection of the remanent magnetization perpendicular to the strike of the magnetic lineation. This sort of data has not been particularly helpful in delineating the motion of the Pacific mainly because only a few magnetic lineation groups have been studied. In addition anomaly skewness studies suffer from relatively large errors in the determination of the paleoinclination and there is often a systematic error, called "anomalous skewness", that must be determined in an ad hoc manner.

Seamount paleomagnetism is important because it has no theoretical age limitation and seamounts are scattered all over the Pacific. It also has its own limitations (see Chapter 2), but these problems have been over estimated in the past. The work presented here shows that the greatest limitation of the seamount paleomagnetic technique at present is the scarcity of such data. In this dissertation the number of seamount paleomagnetic poles from the Pacific is more than doubled and the result is very enlightening for Pacific tectonics.

1.3 THE EVOLUTION OF THE PACIFIC PLATE

As the main purpose of this dissertation is to clarify and extend our knowledge of Pacific plate tectonics, a brief summary of the history of the Pacific is in order. The following synopsis borrows heavily from Hilde et al. (1977), which is itself a summary of the evolution of the western Pacific. The reader wishing more detailed analyses is referred to the following sources: north Pacific, Hilde et al. (1976); northeast Pacific, Pittman and Hayes (1968), Atwater (1970), Atwater and Menard (1970), Woods and Davis (1982); east Pacific, Herron (1972), Handschumacher (1976); south Pacific, Winterer et al. (1974), Molnar et al. (1975), Weissel et al., (1977); central Pacific, Larson and Chase (1972), Larson (1976).

The Pacific began as a small plate which formed at a triple junction in the Late Jurassic. The infant Pacific was surrounded by ridges on all sides, except perhaps the west, and thus its area grew by accretion (Figure 1.3). It was flanked on the north by the Kula and Farallon plates and to the south by the Phoenix and Indian-Australian plates. The growth of the Pacific continued through the Cretaceous and approximately 100 Ma. its northwest corner began to subduct beneath Asia. About the same time the Tethys ridge, south of the Asian continent, was subducted causing spreading to begin further south, rifting India from Gondwanaland and bisecting the Indian-Australian plate by the Ninetyeast ridge transform. At the end of the Cretaceous all of the Pacific-Kula ridge west of the Emperor Trough had been subducted beneath Asia and the Aleutian Trench. Along the Pacific-Australian ridge massive volcanism formed the Ontong Java Plateau. At approximately 53 Ma., the Pacific-Australian ridge began to subduct beneath Asia and the spreading center jumped southward to rift Australia from Antarctica. At about 45 Ma. the last bit of Kula plate was subducted in the Aleutian Trench. Coincidentally, the motion of the Pacific plate switched from north northwest to west northwest, a change recorded by the bend in the Hawaiian-Emperor chain. In the late Tertiary, the Pacific-Farallon ridge evolved into the present East Pacific Rise and subduction of the Pacific plate began on its southwest margin.

The history summarized above is characterized by almost constant growth of the Pacific plate. This history provides a reasonable

framework for the Pacific's evolution; however, in many ways this story leaves much to be desired. Many of the most interesting features of the western Pacific are either not explained or are attributed to unusual circumstances. The Hess Rise, Shatsky Rise, and Emperor Trough are supposed to have formed by rapidly changing unstable configurations of the Pacific-Kula-Farallon triple junction (Larson and Chase, 1972; Hilde et al., 1976). The Manihiki Plateau, Magellan Plateau, and Ontong Java Plateau are attributed to unusual volumes of volcanism in the wake of the Pacific-Phoenix ridge and the Pacific-Phoenix-Farallon triple junction (Kroenke, 1974; Winterer et al., 1974; Winterer, 1976). Most of the seamounts and seamount chains are not included in this version of the Pacific's history, although, some authors would have many of them formed during a voluminious pulse of Late Cretaceous volcanism (Schlanger et al., 1981) the like of which has not been seen since. Even some of the Mesozoic lineations do not fit into this story. An example is the fan shaped anomaly sequence near the Magellan Rise (Tamaki et al., 1979).

Obviously, the formation of the Pacific was much more complicated than previously supposed. It is quite possible that the Pacific has not even been a single plate throughout its history. Much new work and data is needed to understand the processes and events which shaped the Pacific. Hopefully, the paleomagnetic results presented here represent a step in the this direction.

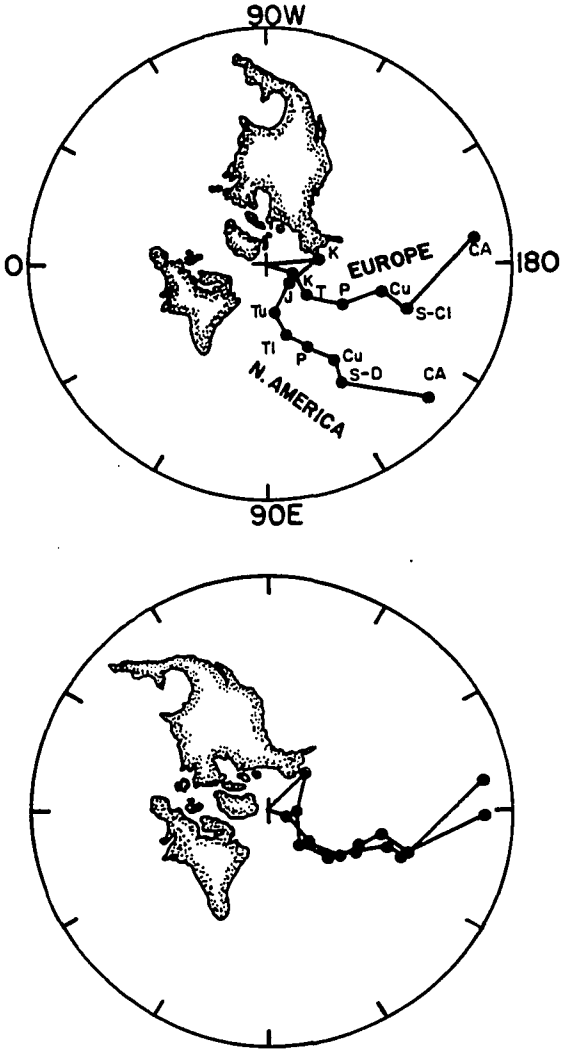

FIGURE 1.1 Apparent polar wander paths for Europe and North America. Top: The APWP are shown with present continental positions. Bottom: The APWP, shown with the continents backtracked to close the Atlantic Ocean, display an agreement demonstrating that the two continents were one during much of the Mesozoic and Paleozoic. Age Code: K, Cretaceous; J, Jurassic; T, Triassic; P, Permian; C, Carboniferous; S, Silurian; D, Devonian; CA, Cambrian; u, upper; l; lower. (redrawn from McElhinny, 1973)

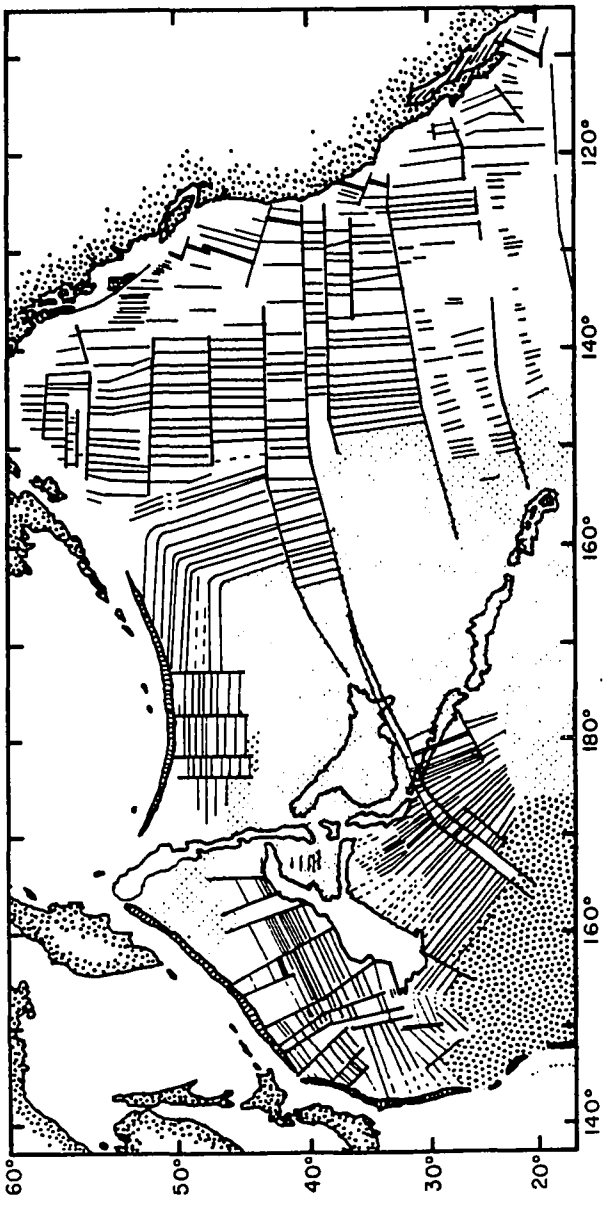

FIGURE 1.2 Pacific Quiet Zone seafloor. Map shows magnetic lineations indentified on the northern Pacific plate (Cenozoic lineations are to the east, Mosozoic, to the west) as well as Cretaceous Quiet Zone seafloor (cross hatched area). Also shown is area of seafloor probably formed during the Late Jurassic (stippled) on which magnetic lineations have not yet been identified. (redrawn from Hilde et al., 1976)

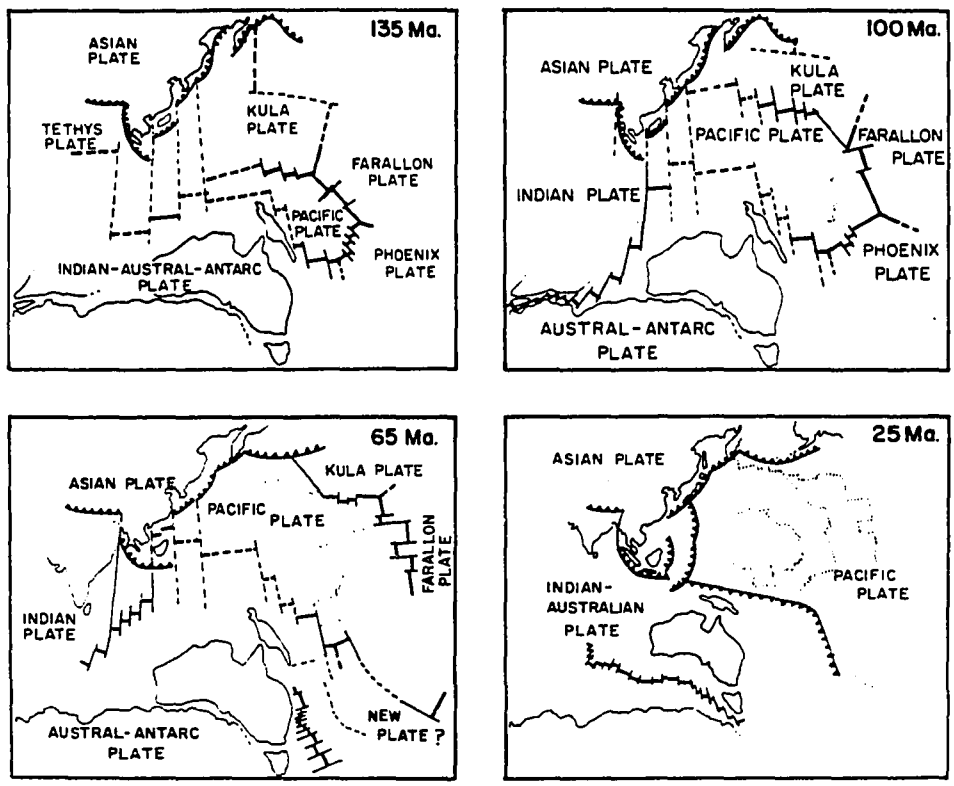

FIGURE 1.3 Evolution of the Pacific plate from 135 Ma. to 25 Ma. Heavy lines are spreading ridges, lighter lines are transforms. Dashed lines represent uncertain boundaries. Saw-tooth lines indicate subduction zones with the teeth pointing in the direction of underthrusting. Light dotted lines represent relict boundaries. (redrawn from Hilde et al., 1977)

CHAPTER 2: SEAMOUNT PALEOMAGNETISM: THE METHOD

2.1 A BRIEF HISTORY OF SEAMOUNT PALEOMAGNETISM

In 1962 Victor Vacquier devised a method for determining the average magnetization direction of a mountain using only a magnetic survey and the mountain's shape (Vacquier, 1962). It was first applied to seamounts by Van Voorhis and Walczak (1963). Variations of this method have been reported by Talwani (1965), Grossling (1970), Parker (1972), and Plouff (1976). Only the Vacquier, Talwani, and Plouff methods have been widely applied to seamount data.

Uyeda and Richards (1966) and Vacquier and Uyeda (1967) first applied the seamount paleomagnetic method to Pacific seamounts. They found a significant amount of apparent polar wander and hypothesized that the Pacific had undergone a large amount of northward displacement since the Cretaceous. Richards et al. (1967) analyzed Cretaceous seamounts from the area around Hawaii and found that these seamounts gave a different average pole than the seamounts south of Japan reported by Vacquier and Uyeda. Francheteau et al. (1970) added new seamount poles of Tertiary as well as Cretaceous age. They suggested that the difference between the poles of the seamounts near Hawaii and those south of Japan is due to an intervening plate boundary. Also, they were the first to estimate an APWP for the Pacific plate.

Harrison et al. (1975) raised the number of reliable Cretaceous seamount paleopoles from the Pacific to 30. They, too, noted a difference between the paleopoles of most Cretaceous seamounts and those south of Japan; however, they hypothesized that the separation is caused by a difference in seamount ages. Additionally, they calculated a Cretaceous paleomagnetic pole at 58.3° N, 350.3° E from 26 of the 30 seamounts. This pole has been widely used by geoscientists to measure the Pacific plate's motion since the Cretaceous. As few of these seamounts are reliably dated, this usage is probably unwise. All together the seamounts likely span a range of ages in the neighborhood of 60-90 m.y. and thus this pole does not accurately represent the Pacific plate's motion.

Few additions to the Pacific paleomagnetic data have been made since 1975. Most are by the author and coworkers (Keating and Sager, 1980; Sager et al., 1982; Sager, 1983a,b) who have published poles from seamounts in the Line Islands and Hawaiian chain.

A paper by Blakely and Christiansen (1978) is cited by many critics of the seamount paleomagnetic method as proof of the technique's inaccuracy. They determined a paleopole (44° N, 328° E) for Holocene-age Mt. Shasta volcano that is significantly removed from either the geomagnetic or geographic pole. Other authors have also attempted to analyze the magnetic anomalies of andesitic strato-volcanoes with varying degrees of success (Vaquier and Uyeda, 1967; Richards et al., 1967; Kodama and Uyeda, 1979). Since basaltic seamounts usually seem to give paleopoles with less scatter than

island-arc type volcanoes, the Blakely and Christiansen report should be regarded as further evidence that some andesitic volcanoes may violate one or more of the basic assumptions of the seamount paleomagnetic method. Considering the explosive nature and high ash content of the eruptions that build these volcanoes, the assumption that the entire edifice is homogeneously magnetized (discussed in Section 2.6) is probably the violated one. This study also demonstrates the weakness of using a single seamount paleopole as a basis for tectonic implications.

Seamounts have been analyzed paleomagnetically from only a few locations other than the Pacific. Vacquier and Uyeda (1967) studied several seamounts from the Shikoku Basin; Harrison (1970) and Miles and Roberts (1981), several from the Atlantic; and McNutt and Batiza (1981), several from the Cocos plate. The amount of seamount paleomagnetic data from plates other than the Pacific is so small that it is difficult to use these data for more than a cursory tectonic interpretation.

2.2 CALCULATION OF MAGNETIZATION PARAMETERS

Magnetic measurements at sea are usually made with a proton precession magnetometer that measures the magnitude of the earth's

magnetic field strength. Also called the magnetic flux density, the field strength is a vector quantity denoted by $\bar{B}$. It is measured in units of Webers./m.^{2}, known as Teslas (T.) in the SI system of units. In the c.g.s. system, $\bar{B}$ is measured in Gauss (G) and 1 G equals 10^{-4}T. For geophysical purposes a sub-unit called the gamma (γ), which equals 10^{-5}G., is more conveniently used. It follows that 1 γ equals 10^{-9}T., a unit called a nanoTesla and abbreviated nT. As SI units are simpler and more rational than other physical units, particularly in the field of electromagnetism, they are used here.

The B-field of the earth ranges from about 30,000 nT. at the equator to about 60,000 nT. at the poles. It consists of three basic constituents: the internal or core-produced field, the external field whose sources are in the upper atmosphere or space, and the field produced by crustal rocks. For geotectonic study, the latter is of primary interest. However, the other two are important because they must be removed from the observed field to obtain the part caused by the crust.

The core field is approximately 90% of the total field. Its changes usually take place on a time scale of years and are called secular variations. Both the core field and its variation can be calculated at most spots on the earth with fair accuracy by a spherical harmonic model. The coefficients for this model are recalculated at five year intervals and published by the International Association on Geomagnetism and Aeronomy. The theoretical field calculated from this model is referred to as the International Geomagnetic Reference Field

(IGRF). The most recent is IGRF 1980 (Fabiano et al., 1982). Once the IGRF is subtracted from the observed total field values (the remainder is called the total field anomaly), the task of removing variations caused by external sources remains. There are many such variations, some of which are nearly the same amplitude as the desired crustal anomalies and are thus difficult to completely remove. The special techniques for the exorcism of these unwanted variations are discussed in Chapter 3.

Our interest is specifically focused on the magnetic anomaly created by a seamount. Seamounts are composed mostly of basalts that often carry a relatively strong natural remanent magnetization (NRM). The magnetization, denoted $\bar{J}$, is also a vector quantity. It is expressed in SI units as amperes/meter (A./m.). Often magnetization appears in c.g.s. units (e.m.u./cc.) and 1 A./m. equals 10^{-3} e.m.u./cc. The seamount has its own magnetic anomaly by virtue of the contrast between its magnetic rocks and the non-magnetic water surrounding it. As shown in Figure 2.1, the shape of the magnetic anomaly depends on the direction of the magnetization "frozen" into the seamount's basalts.

The magnetization vector recorded by the seamount is the raw data for tectonic study. If averaged over a sufficiently long period of time (about 10^4 years), the earth's magnetic field is approximately that of an axial geocentric dipole (Figure 2.2) and the inclination and declination of the magnetization vector of the seamount give the distance and azimuth to the geographic pole at the time of its

formation. For an axial geocentric dipole field, inclination is simply related to latitude, tan(Inc)=2 tan(Lat). By simple formulas, the location of the paleopole recorded by the seamount, called a virtual geomagnetic pole (VGP), can be found from the direction of the seamount's magnetization (McElhinny, 1973, p. 25). The seamount VGP is used in the calculation of paleomagnetic poles for various periods and to infer plate motion (Figure 2.3).

Usually in simple physical problems one has a body with a known shape and magnetization direction. The magnetization is integrated over the volume of the body to obtain the magnetic field at a point in space. The problem addressed here is the inverse. The shape of the body and the magnetic field are known, but the magnetization direction is not. However, the observed magnetic field values can be mathematically expressed as a linear combination of the unknown magnetization components and volume integrals of the body. Thus simple linear least-squares inversion techniques can be applied to determine the magnetization components.

Suppose there is a body Q with a magnetization $\bar{J}$. This body will have a magnetic field filling the space around it as shown in Figure 2.1. Using the right-handed coordinate system shown in Figure 2.4, the magnetic potential W at the origin created by a small volume element (dx dy dz) of Q is written

$$W = \frac{\bar{m} * \bar{R}}{R^3}$$

where $\bar{m}$ is the magnetic moment of the volume element and $\bar{R}$ is the distance vector. If the magnetization of Q is assumed to be homogeneous, $\bar{m} = \bar{J}\ dx\ dy\ dz$ and the potential is

$$W = \frac{J_x x + J_y y + J_z z}{R^3}\ dx\ dy\ dz \qquad (1)$$

in which J_x, J_y, J_z are the components of vector $\bar{J}$.

Equation (1) is an expression for the potential, but the desired quantity is the magnetic field strength, so the gradient of the potential is taken, giving

$$X = -\iiint \frac{\delta W}{\delta x}\ dx\ dy\ dz$$

$$Y = -\iiint \frac{\delta W}{\delta y}\ dx\ dy\ dz \qquad (2)$$

$$Z = -\iiint \frac{\delta W}{\delta z}\ dx\ dy\ dz$$

In equation (2) X, Y, Z are the three components of the magnetic field created by Q (i.e. the magnetic anomaly). Although this derivation has followed Talwani (1965), similar formulas can be found in most any textbook on electromagnetism. Talwani reduces equations (2) to the following form:

$$X = J_x V_1 + J_y V_2 + J_z V_3$$

$$Y = J_x V_2 + J_y V_4 + J_z V_5 \qquad (3)$$

$$Z = J_x V_3 + J_y V_5 + J_z V_6.$$

The $V_1 \ldots V_6$ in (3) are volume integrals involving only the dimensions of the body Q and its distance from the point of observation:

$$V_1 = \iiint \frac{3x^2 - R^2}{R^5} \, dx \, dy \, dz$$

$$V_2 = \iiint \frac{3xy}{R^5} \, dx \, dy \, dz$$

$$V_3 = \iiint \frac{3xz}{R^5} \, dx \, dy \, dz \qquad (4)$$

$$V_4 = \iiint \frac{3y^2 - R^2}{R^5} \, dx \, dy \, dz$$

$$V_5 = \iiint \frac{3yz}{R^5} \, dx \, dy \, dz$$

$$V_6 = \iiint \frac{3z^2 - R^2}{R^5} \, dx \, dy \, dz \, .$$

Given the dimensions of Q, these volume integrals can be evaluated. Their value is constant for any given observation point. Thus in (3) X, Y, Z are measured and $V_1 \ldots V_6$ are calculated leaving the magnetization components J_x, J_y, J_z as the unknowns to be calculated. As stated previously, this problem readily lends itself to an over-determined linear least-squares regression.

The various routines used to solve (3) diverge in their evaluation of the volume integrals (4). Vacquier (1962) converted (4) to surface integrals using Green's theorem. The body, Q, was approximated by vertical, rectangular prisms with sides parallel to the x and y axes. By assuming the magnetization of each prism to be homogeneous, the magnetic effect of each prism face could be reduced to that of a single "free pole." The magnetic anomaly was the result of the sum of all the

free poles. Talwani (1965) approximated Q by horizontal polygonal laminas which followed the contours of the body. The approximation of the body could be improved by specifying more sides to each lamina and by increasing the number of laminas. The integration of (4) was carried out analytically for the horizontal dimensions and a numerical approximation was used for the vertical direction. Plouff (1976) extended Talwani's method by assuming that the polygonal laminas were the tops of vertical prisms (Figure 2.5) and performing an analytical integration of (4) in the z direction. This algorithm has the advantage of being computationally faster than Talwani's and it does not suffer from any error due to the numerical integration (Plouff, 1975).

The Vacquier method was used in seamount studies for several years until Talwani's routine superceded it. Today, the Talwani method is still widely used; however, the Plouff method has gained much popularity. The Plouff algorithm has been used for the studies of the seamounts whose models are presented in Chapter 4. These results should be no different than if they had been calculated by the other equivalent methods.

Equations (3-4) must be put into a form more convenient to the least squares process. The text now follows Plouff (1975). In general, the magnetization has two primary components, one remanent and one induced (actually there may be more, as discussed in Section 2.7). Thus the magnetization vector is written

$$J_x = kH_l + J_rL$$

$$J_y = kH_m + J_rM \qquad (5)$$

$$J_z = kH_n + J_rN$$

where k is the volume susceptibility, H is the magnetic field strength of the earth's main field (i.e. kH is the intensity of the induced magnetization, J_i), and J_r is the intensity of the remanent magnetization. L, M, N and l, m, n are the direction cosines of the remanent magnetization and the earth's field, respectively,

$$L = \cos(I_r)\cos(D_r) \qquad l = \cos(I_e)\cos(D_e)$$

$$M = \cos(I_r)\sin(D_r) \qquad m = \cos(I_e)\sin(D_e) \qquad (6)$$

$$N = \sin(I_r) \qquad n = \sin(I_e)$$

with the subscript r referring to the remanent magnetization and e referring to the main field. In (6) I is the inclination (positive downward) and D is the declination (positive clockwise from north).

The magnitude of the magnetic anomaly, T, is evaluated as

$$T = ((lH + X)^2 + (mH + Y)^2 + (nH + Z)^2)^{1/2} - H \qquad (7)$$

where H is the magnitude of the main field and X, Y, Z are the components of the magnetic field of the body Q. Magnetic anomalies measured at sea rarely exceed 5% of the magnitude of the main field, so it is sufficient (and mathematically much simpler) to approximate the magnetic anomaly by its projection along the direction of the Earth's field vector, so (7) becomes

$$T \doteq lX + mY + nZ = T'. \qquad (8)$$

Substituting the expressions for X, Y, Z from (3) into (8),

$$T' = J_x(lV_1 + mV_2 + nV_3) + J_y(lV_2 + mV_4 + nV_5) + J_z(lV_3 + mV_5 + nV_6). \qquad (9)$$

Letting $B_1 = (lV_1 + mV_2 + nV_3)$, $B_2 = (lV_2 + mV_4 + nV_5)$, $B_3 = (lV_3 + mV_5 + nV_6)$, and $B_4 = (lB_1 + mB_2 + nB_3)$, and substituting the values of J_x, J_y, J_z from (5), (9) becomes

$$T' = J_r(LB_1 + MB_2 + NB_3) + J_iB_4. \qquad (10)$$

Because it is necessary to allow for an offset between the observed and calculated anomalies, a constant term is added to (10),

$$T' = J_r(LB_1 + MB_2 + NB_3) + J_iB_4 + C_0. \qquad (11)$$

Plouff (1975) divides his algorithm into two separate parts, one for calculating the susceptibility and one for calculating the remanent magnetization. For the former, $J_r = 0$, and (11) is

$$T' = J_iB + C_0 .$$

This equation is solved (Appendix A) in a manner equivalent to a regression for a least-squares line with J_i as the slope and C_0 as the intercept. For calculating the remanent mangetization, k = 0 and (11) is reduced to

$$T' = J_1B_1 + J_mB_2 + J_nB_3 + C_0 . \qquad (12)$$

In this case, there are four unknowns, but this is easily solved using multivariate least-squares regression (Appendix A). Once (12) has been solved for the components of the remanent magnetization (J_l, J_m, J_n), the inclination, declination, and intensity of the magnetization vector can be calculated using simple trigonometry,

$$J_h = (J_l^2 + J_m^2)^{1/2}$$

$$J_r = (J_h^2 + J_n^2)^{1/2}$$

$$D_r = \tan^{-1}(J_m/J_l)$$

$$I_r = \tan^{-1}(J_n/J_h) \ .$$

Many of the authors of seamount paleomagnetic studies have calculated a planar regional field, of the form $Z = Ax + By + C$, in the least-squares inversion rather than just the constant offset used in (12). For a planar regional, (12) becomes

$$T' = J_l B_l + J_m B_2 + J_n B_3 + C_1 x + C_2 y + C_0 \qquad (13)$$

where x, y are distances in the direction of geographic north and east. The validity of using (12) versus (13) is discussed in Section 2.9.

It is also possible to calculate the magnetization parameters of more than one body simultaneously. Each additional body adds three more magnetization parameters to the number of unknowns. Equation (12) is then expressed

$$T' = J_{11}B_{11} + J_{m1}B_{21} + J_{n1}B_{13} + J_{12}B_{12} + J_{m2}B_{22} + J_{n2}B_{32} +$$

$$\ldots + J_{1j}B_{1j} + J_{mj}B_{2j} + J_{nj}B_{3j} + C_0$$

with j the number of magnetic bodies and 3j + 1 parameters to be determined. This variant of the inversion technique has been used successfully to determine the magnetizations of two or three seamounts in close proximity (Richards et al., 1967; Francheteau et al., 1970), but it has not been used to determine different magnetizations for various parts of the same seamount. There is no theoretical reason why this approach cannot be used for such a problem; however, if the seamount has a complicated magnetization this method may not be practical as the inherent non-uniqueness of the potental field will cause the solution to be ill-constrained.

2.3 THE MORPHOLOGY OF SEAMOUNT MAGNETIC ANOMALIES

In Figure 2.1 it can be seen that the shape of a seamount's magnetic anomaly depends not only on the shape of the seamount, but on the angle between its magnetization vector and the direction of the geomagnetic field vector as well. It is instuctive to examine the changes in the shape and morphology of the magnetic anomaly of a

homogeneous seamount with a simple shape as its magnetization direction and latitude are varied. For this demonstration the bathymetry of a nearly conical seamount (Tchaikovsky Seamount, Section 4.5.15) was approximated by stacking 10 polygonal prisms as shown in Figure 2.5. In Figure 2.6 the upper face of each prism used in the model is shown. The top is at 2125 m. and the bottom, at 5750 m. (for example, the 2125 m.-2375 m. prism follows the 2250 m. contour). The uppermost prisms are at 250 m. intervals (2250 m.-3500 m.), whereas the lower prisms are spaced at 500 m. intervals (3500 m.-5500 m.) because deeper changes in the seamount's shape have less effect on the magnetic anomaly measured at the sea surface (see Section 2.8). Each layer is assumed to have a homogeneous magnetization and a declination of zero, except in two cases as noted below. Anomalies were calculated assuming the seamount formed at 40° S, 20° S, 0°, and 20° N and was surveyed at 40° S, 20° S, 0°, 20° N, and 40° N. All but one of the examples are normally polarized.

Many of these anomalies should be similar to those measured over seamounts in the Pacific. For example a seamount formed at the equator during the Cretaceous might be surveyed at 20° - 40° N. On the other hand, it would be startling to find a Pacific seamount with a net southward displacement, say formed at 20° N and surveyed at 20° S, but the anomalies from these seamounts are interesting and are included with the others for comparison.

As seen in Figure 2.6, the anomalies commonly have one positive and one negative center. The relative amplitudes of the maximum and

minimum depend on the latitude of formation and observation. Some anomalies have only a minimum (e.g., formed at 40° S and observed at 40° N) whereas others have a minimum and two maxima (e.g., formed at 0° and observed at 0°). The reader can see how the anomaly arises by looking back to Figure 2.1. The seamount's magnetization produces a roughly dipolar field around the seamount and thus the direction of the seamount field varies with the position of the observer in relation to the volcano. Taking the $0^{\circ}/0^{\circ}$ anomaly as an example, one can imagine the magnetization vector in Figure 2.1 oriented horizontally, parallel to the main field vector. Thus the point at which the seamount field will be antiparallel to the main field vector will be directly over the top of the seamount and so the maximum negative of the anomaly will occur there. To the south and north the seamount field vector will make an increasingly large angle with the main field vector, eventually passing through 90° and thus augumenting the main field to cause a positive anomaly. As the distance from the seamount increases, the strength of its field, and hence the resultant anomaly, decreases. Because or this decrease, coupled with the fact that the seamount field vector is never exactly parallel with the main field vector at the sea surface, the positive parts of the anomaly are smaller in amplitude that the negative part. Thus the $0^{\circ}/0^{\circ}$ anomaly consists of a large negative over the seamount's summit and two positive centers, one to the north and one to the south. Because the magnetization's

declination is zero, the positive anomaly centers are roughly due north and south of the summit.

As the seamount formed at the equator moves north, the maxima and minimum move north of their positions in the equatorial anomaly. The amplitude of the southern maximum is greatly increased whereas the northern maximum is diminished. At 40^{o} N the minimum is only slightly more intense than the maximum and the summit is found in between the two features. If the same seamount is observed instead at more southerly latitudes, exactly the opposite effects are seen. The maxima and minimum move south of their equatorial positions and the northern maximum becomes dominant. Similar behavior of the maxima and minima the other anomalies in Figure 2.6 is observed.

Several subtle effects seen in Figure 2.6 deserve comment. None of the anomalies is symmetric about a north-south line across the summit. This symmetry would be observed if the seamount were a perfect cone and the magnetization and main field declinations were zero. Because the seamount is slightly elongated northwest-southeast, the anomalies are composed of maxima and minima with a similar bias. Another effect of the seamount's asymmetric shape is that the peak (marked by the cross in Figure 2.6) is never in the exact center of the anomaly. Two examples are given of seamounts whose magnetizations have non-zero declinations. The seamount formed and observed at the equator is given $\pm 30^{o}$ of declination. When the declination is positive, the minimum is elongated northwest-southeast rather than east-west as in the zero declination example. Also, a line running from the center of

the southern maximum to the center of the northern maximum has a decidedly eastward tilt. If the seamount had a symmetric shape, the negative declination anomaly would be a mirror image of the positive declination example. However, the northwest-southeast elongation of the seamount causes the northern maximum to vanish in the negative declination case; although, a line from the center of the southern maximum to the seamount summit has a westward tilt as expected.

One example of an anomaly produced by a reversely polarized seamount is given. By comparison with the normally polarized examples it is seen that the positive contours become negative and the negative contours become positive, but the shape of the anomaly remains the same.

An interesting ambiguity occurs in the example anomalies. The morphology of the anomaly formed by a seamount with a magnetization vector making a certain angle with the main field vector is exactly the same as a seamount whose magnetization vector and main field vector are separated by a negative angle of the same value. For example, the anomaly of the seamount formed at the equator and observed at 20^{o} N is the same as that of the seamount formed at 20^{o} N and observed at the equator. The angle between the magnetization and main field vectors for the former is 36.1^{o}, whereas the angle for the latter is -36.1^{o}. Thus one cannot tell at what latitude a seamount was formed knowing neither the magnetization direction nor magnetic field direction; however, the specification of either eliminates the ambiguity.

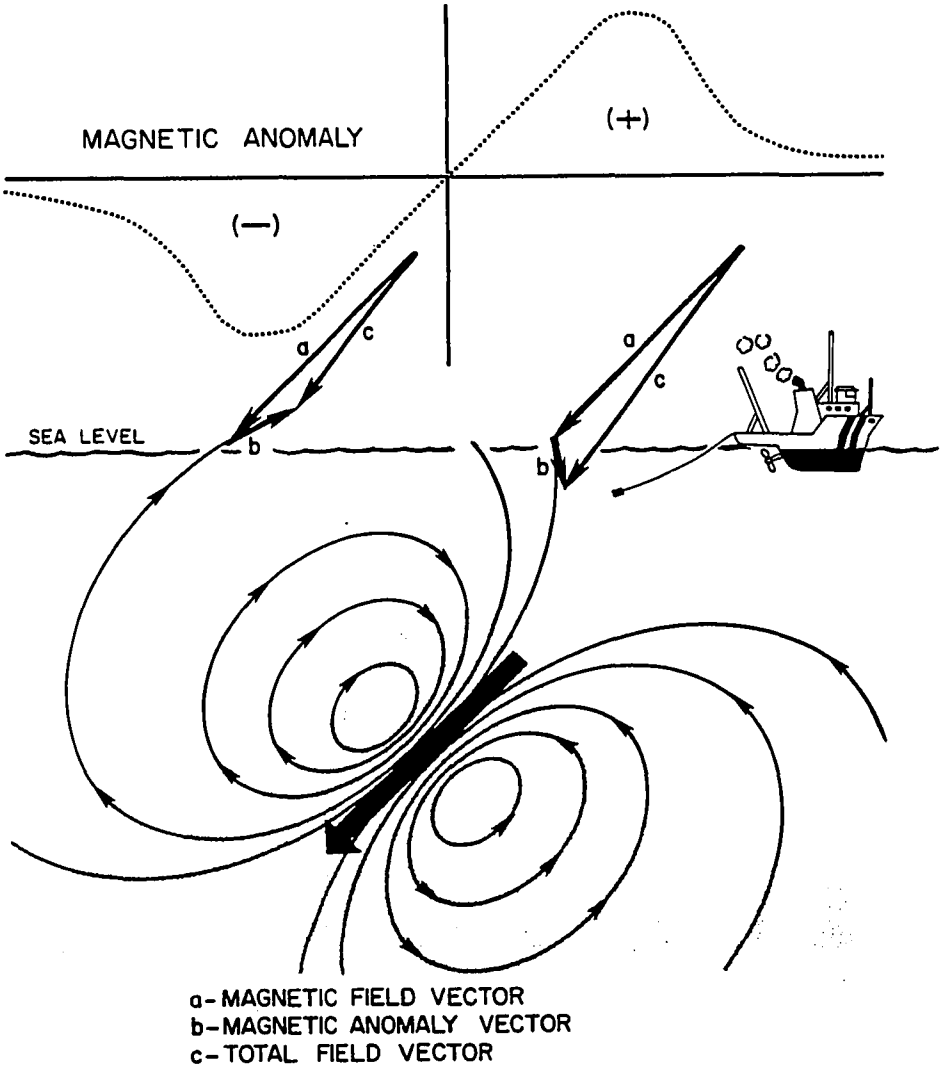

Figure 2.1 Explanation of the magnetic anomaly created by a seamount. The stippled area is a cross section of a seamount and the heavy arrow represents its average magnetization vector. The curved lines with arrow heads are a schematic representation of the magnetic field lines of the seamount. The magnetic field vectors of the seamount and the geomagnetic field add at the sea surface to make the total field vector. If the total field vector is shorter than the theoretical geomagnetic field, the magnetic anomaly is negative (left); if it is longer, the anomaly is positive (right). (redrawn from Uyeda, 1978)

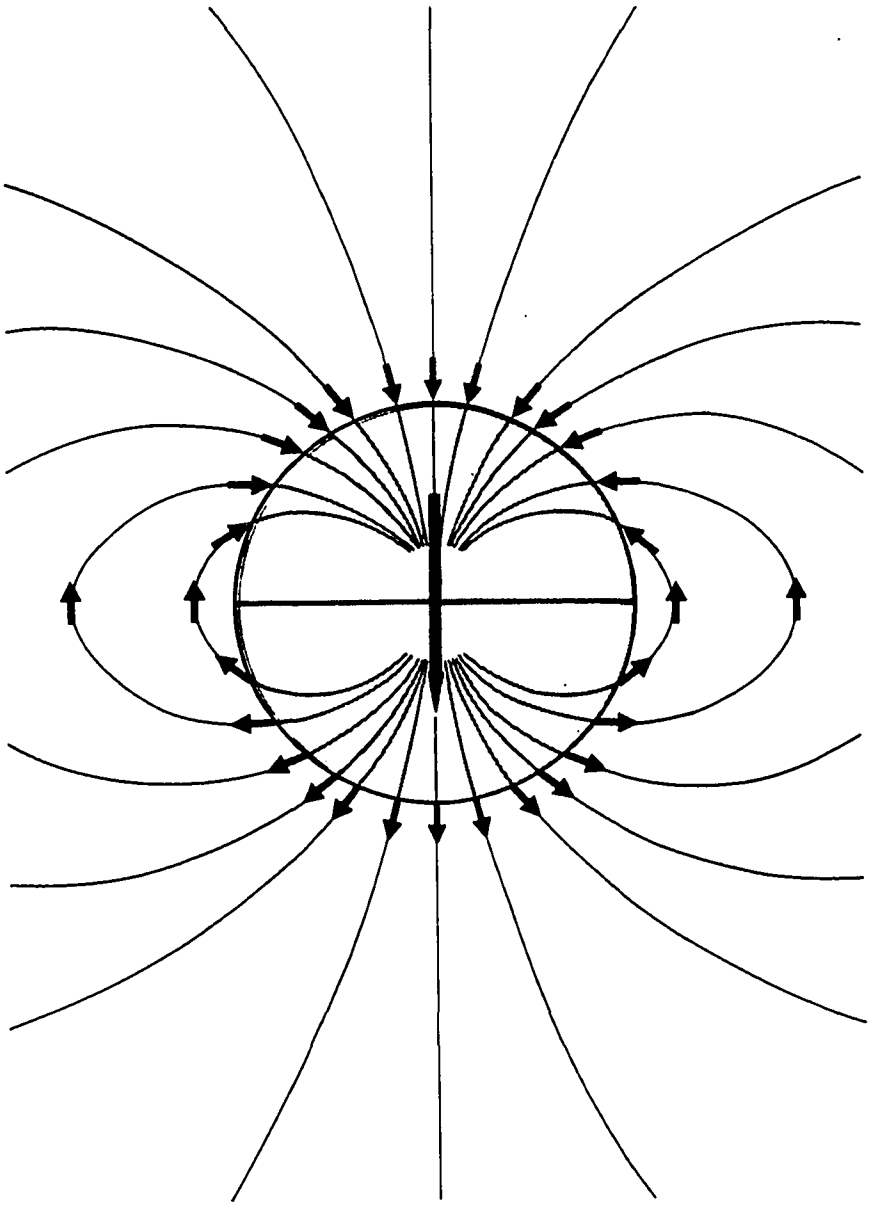

Figure 2.2 Schematic representation of a geocentric axial dipole magnetic field. The Earth's dipole moment points southward, so the field lines point upward in the southern hemisphere and downward in the northern hemisphere. During times of reversed field polarity, the converse is true. Note that the inclination of the magnetic field vector varies in a regular manner with latitude, being horizontal at the equator and vertical at the poles.

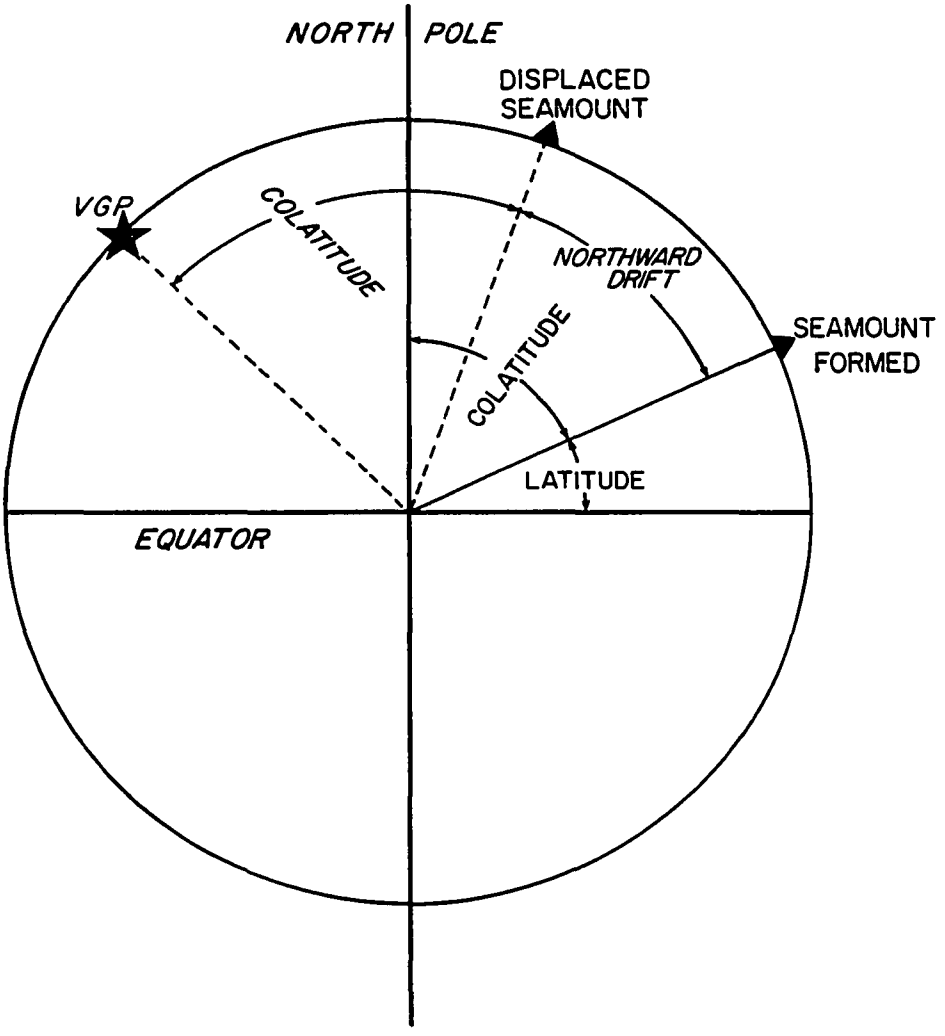

Figure 2.3 Explanation of the virtual geomagnetic pole (VGP). The seamount is formed at some latitude and its distance from the geographic pole is given by the colatitude. If the long term average of the geomagnetic field is that of a geocentric axial dipole field, then the seamount's VGP will be located at the geographic pole at the time of its formation. Some time later, the seamount will have been carried from the place of its origin by plate motion. In the Pacific the seamount will have moved northward by some amount. The distance from the seamount to its VGP remains constant, but since the volcano has moved northward towards the geographic pole, its VGP will be displaced a proportionate amount to the opposite side.

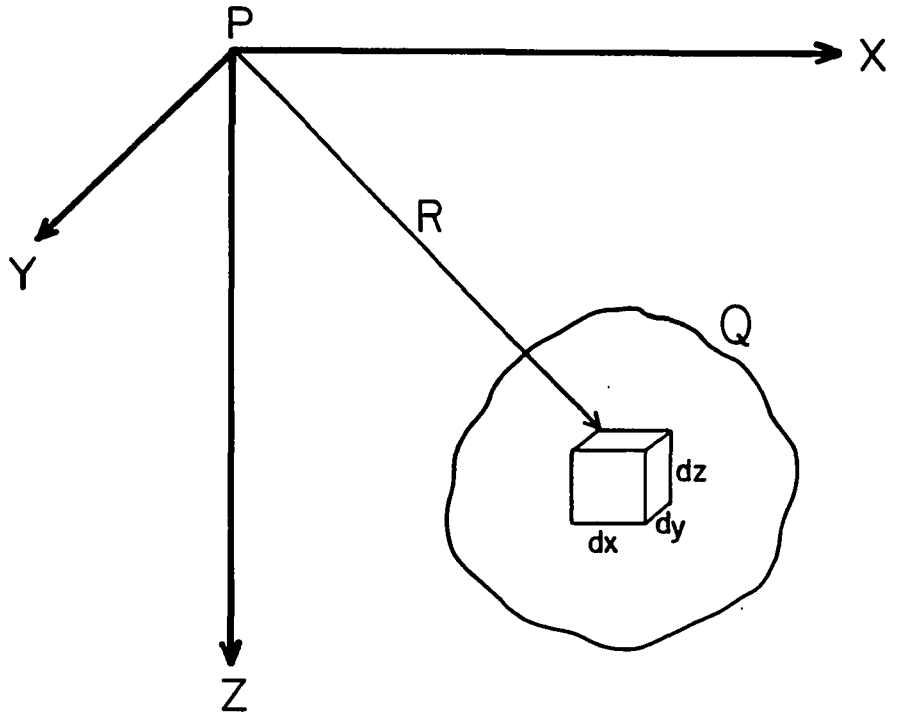

Figure 2.4 Coordinate system for the derivation of the magnetic field of a seamount. A right handed coordinate system with the vertical direction positive downward is used. An element dx dy dz of the volume of magnetized body Q is located at a distance R from the observation point P.

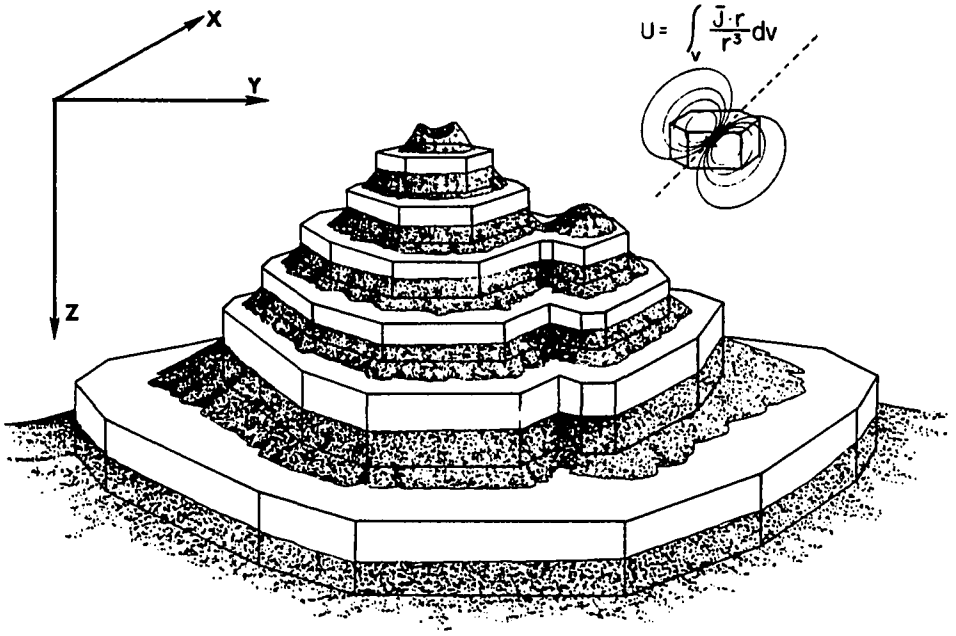

Figure 2.5 Approximation of a seamount by stacked prisms. The Plouff (1976) magnetic modeling method calculates the magnetic field of polygonal prisms with vertical sides. The shape of each prism in the x y plane is usually constructed to follow a contour of the seamount. The vertical dimensions of each prism are such that a stack of prisms is made that approximate the volume and shape of the volcano. The number of prisms and prism vertices may be increased to make the approximation more accurate; however, lower prisms are usually made taller and with less corners than upper level prisms because small variations in the shape of the body at depth do not greatly affect the magnetic anomaly measured at the sea surface.

Figure 2.6 (part 1) Examples of seamount magnetic anomaly morphology. A seamount with a relatively simple shape (Tchaikovsky Seamount) was used to calculate theoretical magnetic anomalies for the edifice given a magnetization inclination and a survey latitude. The anomalies in each row are all surveyed at the same latitude whereas those in the each column are formed at the same latitude. All seamounts are normally magnetized. Negative anomaly contours are dashed. The cross marks the position of the seamount summit (see part 2).

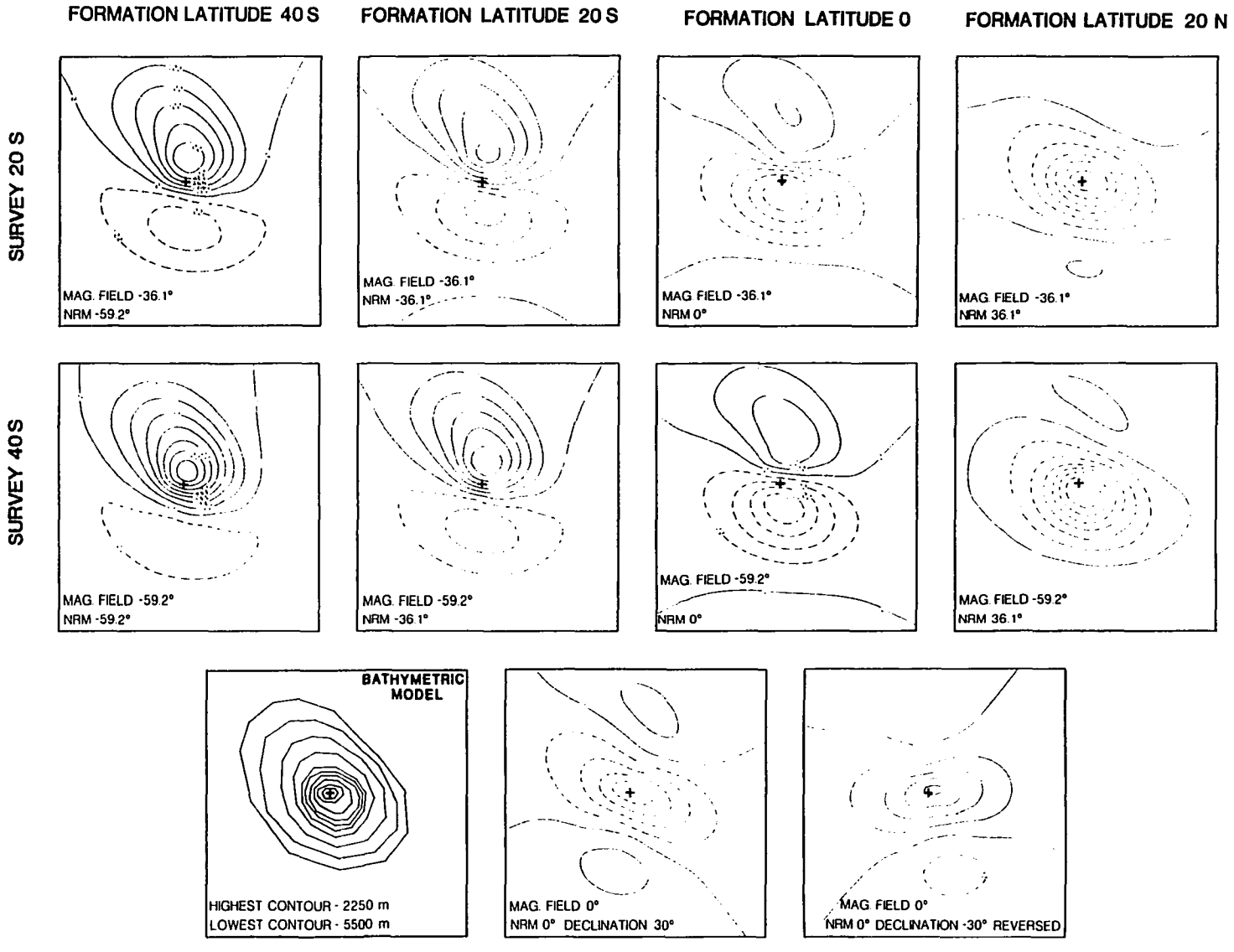
FORMATION LATITUDE 40 S
FORMATION LATITUDE 20 S
FORMATION LATITUDE 0
FORMATION LATITUDE 20 N
SURVEY 20 S
SURVEY 40 S
MAG. FIELD -36.1°
NRM -59.2°
MAG. FIELD -36.1°
NRM -36.1°
MAG. FIELD -36.1°
NRM 0°
MAG. FIELD -36.1°
NRM 36.1°
MAG. FIELD -59.2°
NRM -59.2°
MAG. FIELD -59.2°
NRM -36.1°
MAG. FIELD -59.2°
NRM 0°
MAG. FIELD -59.2°
NRM 36.1°
BATHYMETRIC MODEL
HIGHEST CONTOUR - 2250 m
LOWEST CONTOUR - 5500 m
MAG. FIELD 0°
NRM 0° DECLINATION 30°
MAG. FIELD 0°
NRM 0° DECLINATION -30° REVERSED

Figure 2.6 (part 2) Examples of seamount magnetic anomaly morphology. The examples in this figure complement the examples in part 1. All conventions are the same. A plan view of the prisms used to approximate the seamount's shape is shown in the lower left. Two examples of seamount anomalies with non-zero declinations are given at the bottom. The bottom right anomaly is reversely polarized.

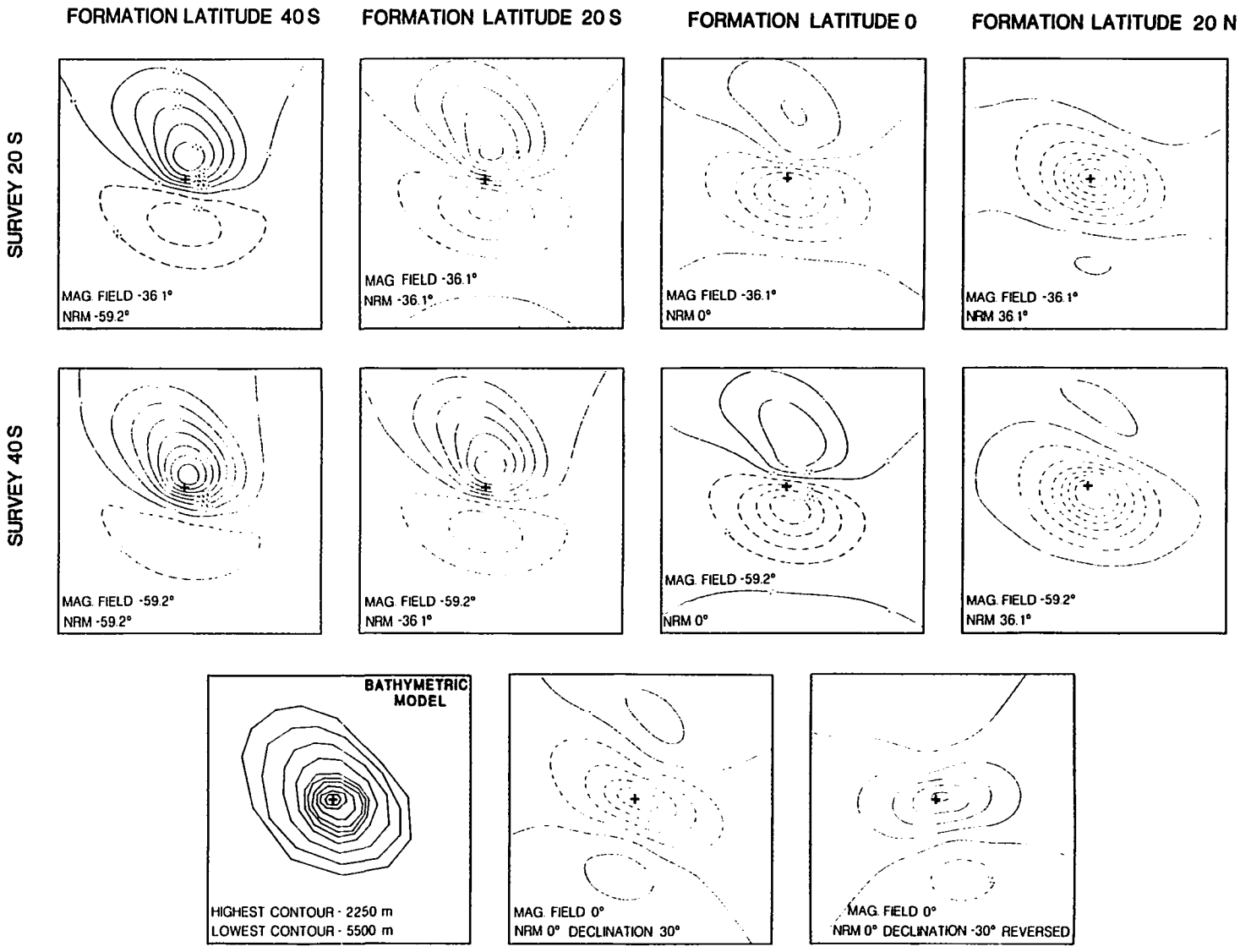
FORMATION LATITUDE 40 S
FORMATION LATITUDE 20 S
FORMATION LATITUDE 0
FORMATION LATITUDE 20 N
SURVEY 20 S
SURVEY 40 S
MAG. FIELD -36.1°
NRM -59.2°
MAG. FIELD -36.1°
NRM -36.1°
MAG. FIELD -36.1°
NRM 0°
MAG. FIELD -36.1°
NRM 36.1°
MAG. FIELD -59.2°
NRM -59.2°
MAG. FIELD -59.2°
NRM -36.1°
MAG. FIELD -59.2°
NRM 0°
MAG. FIELD -59.2°
NRM 36.1°
BATHYMETRIC MODEL
HIGHEST CONTOUR - 2250 m
LOWEST CONTOUR - 5500 m
MAG. FIELD 0°
NRM 0° DECLINATION 30°
MAG. FIELD 0°
NRM 0° DECLINATION -30° REVERSED

2.4 SEAMOUNT PALEOMAGNETIC ASSUMPTIONS

Several suppositions are made in the formulation of the seamount paleomagnetic method. The accuracy of the technique naturally depends on the validity of these assumptions, so a discussion of each is in order. The assumptions are the following:

(1) the magnetization is homogeneous,

(2) the magnetic anomaly is caused solely by the thermoremanent magnetization (TRM),

(3) the bottom of the seamount is flat,

(4) the seamount formed over a sufficiently long interval of time to average out secular variation.

The first three hypotheses are necessary to make the modeling of the seamount tractable. Without assumption (1) mathematical solutions of the equations in Section 2.2 become ill-defined because of the non-uniqueness of potential fields. An infinite number of solutions to the inversion are possible with no constraint on the direction or intensity of the magnetization. This assumption is examined in Section 2.6. Assumption (2), discussed in Section 2.7, solves a similar problem. The magnetic anomaly may be partially caused by induced or viscous magnetization components in addition to the thermoremanent magnetization . Practically, these additional components are difficult to separate from the TRM component without an extensive set of rock samples from the volcanic pile. The third assumption is a result of the shape of the geometric bodies used to approximate the volume of the seamount. Usually a flat bottom is used for no better reason than the

actual shape of the seamount's base is almost never known (see Section 2.8). Assumption (4) is shared with other forms of paleomagnetism. Since our interest is the tectonic motion of the Pacific plate, it is hoped that the rocks of each seamount record the geomagnetic field over a period of time long enough (usually 10^4 - 10^5 yr.) that the average field will be that of an axial geocentric dipole (Nagata and Uyeda, 1967).

2.5 SEAMOUNT FORMATION AND MORPHOLOGY

In order to examine the seamount as a recorder of the geomagnetic field it is necessary to have a clear picture of the process of seamount formation. This section summarizes current thought in this field. Because seamounts are generally inaccessible, the processes of submarine volcanism are not well known. Many hypotheses about seamount formation and structure are based upon studies of subaerial volcanoes or seamounts now found on land. Whether or not the inferences made from these studies truely apply to deep water volcanism is debatable.

According to Menard (1964, p. 55), "a seamount may be defined as a more or less isolated elevation of the sea floor with a circular or elliptical plan, at least 1 km. of relief, comparatively steep slopes, and a relatively small summit area." Batiza (1982) estimates that the Pacific may contain as many as 5.5×10^4 seamounts.

Submarine volcanoes may be divided into five primary types by their size and morphology: abyssal hills and knolls, seamounts, guyots, islands and atolls, and submarine ridges and plateaus. Abyssal hills and knolls are features, probably small shield volcanoes, less than 1 km. in height (Menard, 1964). Islands and atolls are seamounts that have reached sea level and either have not been eroded away or have coral caps that have remained at sea level. Abyssal hills and knolls are rarely suitable for seamount paleomagnetism because they are difficult to survey because of their small size and it is questionable whether or not they formed over a long enough period of time to average out secular variation. Islands and atolls, on the other hand, are usually too big to be useful for seamount paleomagnetic research. They are usually formed over a period of time long enough to include magnetic reversals and frequently are the products of volcanism from several coalesced edifices, thus producing a complicated magnetic signature. Likewise, submarine ridges and plateaus, massive outpourings of lava from multiple centers, are usually too big and too complex to be useful for seamount paleomagnetism. The edifices most amenable to seamount paleomagnetism are guyots and seamounts. Guyots are distinguished from seamounts by their flat tops, however, for most of the research in this volume they can be treated the same.

Seamounts may also be classified by their genetic type. As such they fall into three categories: convergent plate boundary volcanoes, melting anomaly (called "hotspot" here) volcanoes, and extensional or strike-slip plate boundary volcanoes. The first type are usually andesitic strato-volcanoes associated with island arcs. Although the

anomalies of some have been analyzed for paleomagnetic data, the results have not always been good. Probably, the drawback is their style of eruption which mixes lava flows with explosive ash deposits. This sort of eruptive pattern must lead to an internal magnetic fabric that is grossly inhomogeneous. As there are no confirmed convergent boundary volcanoes on the Pacific plate, they fall outside the scope of this report.

Melting anomaly volcanoes typically form long, linear chains or ridges. Often these volcanoes are rather large and initially form islands or atolls. The mechanism that gives rise to these edifices is not certain; they are possibly caused by mantle plumes, propagating fractures, or thermal feedback (Morgan, 1972; Shaw and Jackson, 1973; Jackson and Wright, 1970). Whatever the mechanism, the volcanoes seem to form at a spot that is fixed with respect to the mantle (Morgan, 1981), and seamount chains which are formed by melting anomalies are parallel to circles of latitude about the plate versus mantle rotation pole (Jarrard and Clague, 1973). The best studied example of a chain of hotspot volcanoes is the Hawaiian-Emperor chain (Jackson et al., 1980).

The third type of seamount is formed in the vicinity of a spreading ridge away from any hotspots. These volcanoes are often relatively small, only a few kilometers in height at most, and rarely reach sea level. Probably they are formed from melt from the magma chamber beneath the spreading ridge or a pocket of magma detached from this source (Batiza, 1977). However, it has been noted that their numbers seem to increase on older crust and many are found near

fracture zones (Batiza, 1982), so other magma sources may be responsible for some of them. These seamounts rarely form chains, except perhaps at spreading ridges abandoned by a ridge jump.

The relative numbers of these two types of volcanoes in the Pacific are unclear. Batiza (1982) states that the non-hotspot volcanoes are dominant in the north Pacific; although, the seamounts studied by Watts et al. (1980) fall equally into the two categories. In the eastern Pacific, the number of non-hotspot volcanoes is almost certainly vastly greater than hotspot volcanoes. In the western Pacific, the uncertainty in the origin of most seamounts and the deep sediment cover which may hide smaller edifices make it difficult to determine which type is predominant. For the purposes of seamount paleomagnetic work it probably makes little difference whether a seamount was formed by hotspot or spreading ridge volcanism as the two types of volcanoes probably have similar eruptive processes.

The shape and internal structure of a seamount will be important factors determining its magnetic recording properties. Extrusive and intrusive basalts generally acquire a large, stable magnetization when cooled in the magnetic field near the earth's surface, but breccias, sediments, and biologic deposits do not. Figure 2.7 is a schematic diagram representing many of the features that might be found inside a seamount. Any given seamount probably does not contain all the structural elements depicted in the figure; however, they are incorporated into a single edifice for discussion's sake.

A seamount is born when magma pushes its way through the crust to the ocean floor, rising through the lithosphere and crust by bouyant

force. The exact mechanism by which it transits the lithosphere and crust is unknown. It may melt its way through, open cracks, or move through the country rock by stoping. As it reaches the brittle part of the crust its upward pressure probably produces a series of en echelon fractures that become feeder dikes for the eruption of the lavas that will form the seamount (Bhattacharji, 1979). If the basaltic basement is covered by sediments the magma probably intrudes them as sills owing to the greater density of the basalt (McBirney, 1963). Eventually the sediments are incorporated into the sill complex or pushed aside and the lava breaks out onto the ocean bottom (Menard, 1964). In Figure 2.7 this sill complex is shown directly beneath the basaltic core of the seamount. It extends vertically from basaltic basement up to the approximate level of the seafloor at the time the seamount began to form. Actually, the dimensions of the sill complex are not known. Its lateral extent may be much larger or smaller than shown and its vertical boundary is probably transitional into the submarine basalt flows ot the seamount and not abrupt as shown. Additionally, the sills may extend downward into a dike and sill complex in the upper part of layer 2 caused by the fracturing of the crust by the rising magma.

In the deep ocean the volumetric expansion of the gases in erupting basalt lava is small. Thus explosive volcanism should be limited to depths less than about 500 m.-1000 m. (McBirney, 1963; G. P. L. Walker. personal communication, 1982), although vesiculation probably occurs to much greater depths. Lavas erupting at greater depths will be more fluid than otherwise because of the gases trapped in them by the pressure of the surrounding water (McBirney, 1971).

Consequently, the seamount builds initially by the succession of pahoehoe and pillow flows. Because of the greater thermal conductivity and heat capacity of sea water versus air, the lava flows are chilled more rapidly and form steeper slopes than their subaerial counterparts. Growing submarine shields generally maintain slopes in the neighborhood of 10°-15°, however, they may vary from as little as 5° or less to 25° or more (Menard, 1964; Jones, 1966; McBirney, 1971). The steepness of the slope depends on several factors: the rate of magma discharge during eruptions, the volume of lava extruded per eruption, the proportion of flows emanating from the summit versus the flanks, and the explosivity of the eruptions (Basaltic Volcanism Study Project, 1981). Steeper slopes are formed by eruptions with low discharge rates, low volume, and a high percentage of explosive activity. Volcanoes that erupt more from the summit tend to steepen upwards, whereas those with a high percentage of flank eruptions have the inverted-bowl shape characteristic of shield volcanoes.

In Figure 2.7 the pile of pillow and pahoehoe flows makes up the core of the seamount. In many cases, particularly small and medium size volcanoes, this pile probably represents the majority of the volume of the edifice. For seamounts which grow into shallow water, however, hyaloclastite breccias are important constituents of the volcano. Many authors agree that eruptions in shallow water can produce large volumes of pyroclastic material because of their explosive nature (McBirney, 1963; Jones, 1966; McBirney, 1971; Nordlie, 1973). The increased percentage of pyroclastic material tends to make

the upper portions of a seamount steeper than its lower flanks built primarily of basalt (Jones, 1966). The steepness is probably a result of the relatively large angle of repose of pyroclastic debris in water (Nordlie, 1973). Slopes as high as 40° are not uncommon on the upper flanks of Pacific guyots (Menard, 1964). Additionally, magnetic studies of seamounts often give results suggesting that the upper few hundred meters or more of most submarine volcanoes are made up of non-magnetic material that is often hypothesized to be hyaloclastite (Harrison, 1971; Harrison et al., 1975; Keating and Sager, 1980; McNutt and Batiza, 1981). The ubiquity of hyaloclastite breccias in dredge hauls from Pacific seamounts (Bonatti, 1967; Heezen et al., 1973; Barr, 1974; Natland, 1976b), including those which show no evidence of ever having reached sea level, supports this hypothesis.

Hyaloclastite material may be important in the construction of the lower layers of a seamount as well because explosive eruptions might not be necessary for the formation of hyaloclastite. Instead, this material may be derived from the granulation and fragmentation of basalt extruded in sea water caused by thermal shock (McBirney, 1963; Lonsdale and Batiza, 1980). It may form a veneer of varying extent on normal oceanic slopes (Lonsdale and Batiza, 1980) or it may slump or flow as a density current to the base of a seamount forming a thick apron with characteristic slopes of only a few degrees (McBirney, 1963; Jones, 1966; Sager et al., 1982).

In Figure 2.7, the seamount is pictured as a guyot. Although many large Pacific seamounts are guyots, most seamounts are not. The

majority of seamounts probably never grow past the submarine shield stage. These volcanoes usually have relatively sharply peaked summits, sometimes with several summit cones or a crater (Menard, 1964). Guyots, on the other hand, are characterized by their flat or slightly rounded tops. Most hypotheses of guyot formation require the proximity of sea level, however, some do not. The fact that most guyots are large seamounts seems to favor the former type of origin. Guyots formed in deep water may be the result of the filling of a summit crater or caldera by lava or hyaloclastite (Natland, 1976b), the filling of a summit depression surrounded by eruptive ring dikes (Simkin, 1972), or the growth of a flat top by a primary constructional process similar to the growth of a volcanic dome (Nayudu, 1962).

Shallow water guyots may form in several ways. The hyaloclastites making up the emergent volcano are capped by subaerial lava flows as the edifice builds past sea level and the phreatic eruptions characteristic of shallow water eruptions cease (Jones, 1966; McBirney, 1971). These flows have the characteristic low angle slopes of subaerial shields. The island may subside without substantial modification to form a guyot with a slightly rounded or terraced top, or more likely, it will be truncated by wave action to form a flat-topped guyot (Jones, 1966). If fringing reefs grow on the seamount during its shallow water or subaerial stage, the flat top may be caused by the growth of a ring of reefs on the subsiding volcano that is subsequently filled by lagoonal sediments. This process seems to form many atolls (Darwin, 1842), but it is not clear why some reef-covered seamounts are atolls and others are guyots. However, many Pacific

guyots appear to have carbonate caps (Hamilton, 1956; Heezen et al., 1973).

As shown in Figure 2.7, most guyots aquire a thin cap of pelagic sediments as a result of their long stint below sea level. It is interesting to note that the material directly below the pelagic caps may be basalt, hyaloclastite, or limestone, depending on which of the aforementioned mechanisms is responsible for the guyot's flat top.

Figure 2.7 shows several internal features which may be present inside seamounts. A magma chamber/conduit complex is shown rising from the underlying crust, through the volcano, up to the subaerially deposited lava flows. Many volcanologists seem to divide volcanoes into those that have magma chambers and those that do not. Magma chambers have been detected or inferred to be beneath many large oceanic volcanoes. Examples are Kilauea (Koyanagi et al., 1976), Krafla (Basaltic Volcanism Study Project, 1981), the Azores (Machado, 1970), and the Galapagos (Nordlie, 1973). Additionally, a magma chamber has been hypothesized beneath at least one seamount in the Atlantic (LePichon and Talwani, 1964). Etna, a convergent boundary volcano, is an example of a volcano considered to have no magma chamber. Instead, its magma reservoir appears to be a more or less cylindrical conduit (Basaltic Volcanism Study Project, 1981).

An extremely detailed study of earthquakes below the summit of Kilauea volcano (Ryan et al., 1981) incicates that such a dichotomy may be inappropriate. Their study shows that there is no single large magma chamber beneath Kilauea. Instead, it appears that there is a primary conduit rising from the mantle to the base of the volcano where

it bifurcates into two major feeder-conduit systems which rise to within 2 km. of the surface. The term "conduit" evokes images of hollow cylindrical pipes; however, the conduit system beneath Kilauea is not cylindrical and probably not hollow either. Ryan et al. show that the conduit is elliptical in cross section and that it appears to vary from 1-3 km. in width in the section within Kilauea. Most likely it is a series of interconnected dikes and sills with an occasional larger contiguous magma pocket separated from one another by hot, viscous rock. The magma chambers, mentioned by other authors, appear to be widenings of the conduit that behave somewhat elastically when infused with pressurized magma from below. Consequently, there may be no real difference between volcanoes with magma chambers and those without. Instead, small volcanoes are likely to have smaller, less complicated conduit systems than larger volcanoes. The plumbing of a volcano may evolve and change with time, growing with the volcano, or perhaps changing its course and abandoning some parts of the conduit system. Pockets of magma might be left behind to erupt as differentiated late-stage volcanics or possibly to remain in place and cool as stocks and bosses such as those mapped in the highly dissected west Maui volcano (Stearns and Macdonald, 1942; Diller, 1982).

Dikes are not limited to the area in and around the conduit system. They are probably the primary mechanism for feeding magma from the conduit to the surface. Flank eruptions occur on a volcano when the pressure from the magma in the reservoir exceeds the sum of the tensile strength of the volcanic pile and the tectonic forces acting on the volcano (Nakamura, 1977). The rock cracks and a dike is formed.

If the dike reaches the surface, an eruption occurs. Dikes are usually oriented more or less radially around the center of a volcano; however, in some instances they are oriented into dike swarms around zones of weakness called rift zones. Radial dikes seem to form most often in isolated volcanoes whereas rift zones appear to develop in volcanoes forming alongside existing edifices (Fiske and Jackson, 1972; Nakamura, 1977). Even in volcanoes with well developed rift zones, a portion of the dikes in the edifice away from the rift zones are found to be oriented obliquely (often perpendicular) to the rifts (Wentworth and Jones, 1940). The orientation of a volcano's dikes seems to have an effect on its shape. Radial dike volcanoes are often circular in plan view, but volcanoes with well-developed rift zones are usually elongated along those zones.

In rift zone areas of the dissected Hawaiian volcanoes, dike density is often very high. Macdonald (1972) estimates that the number of dikes per kilometer across the rift can reach 160-320. If the most common dike thickness on Oahu, 0.6 m. (Wentworth and Jones, 1940), is a good representation of an average width, then the volume of dike material in the rift zones is at least 23%. Diller (1982) indicates that dike density falls off rapidly in the few kilometers either side of a rift zone, but this observation is only valid near the surface, and the dike density at depth could be much greater. If Furumoto's (1978) geophysical interpretations are correct, the dike complex beneath Kilauea's east rift may represent much of the volume of the rift zone, implying that a large amount of the total volume of a volcano may be made up of dike material.

No caldera is shown in Figure 2.7 because the configuration of the seamount is such that most of the top has been planed off by erosion. However, caldera formation appears to be common among large basaltic volcanoes. For many years it was believed that these features were rare on deep sea volcanoes (Menard, 1964) and that they form only in the late stages of a volcano's growth (Macdonald, 1972). It appears that neither of these suppositions is true as calderas have been found on a number of seamounts (Hollister et al., 1978) and also on Loihi Seamount, which is generally considered to be the progenitor of the next Hawaiian Island (Malahoff et al., 1982). In basaltic volcanoes, calderas appear to be formed by the collapse of part of the edifice (usually, but not always, near the summit) caused by the withdrawal of magma from a near-surface reservoir. Their sizes are variable, but Hawaiian calderas, for example, have a range of diameters from 3.5-17.6 km. and are typically a few tens to a few hundreds of meters deep (Macdonald, 1972).

In Figure 2.7 a "magnetic root" is indicated in the upper part of layer 2 beneath the seamount. This is possibly an area of remagnetized crust or intrusions that may be important to seamount magnetic modeling. Many seamount models fit the observed anomaly better if the edifice is extended below the seafloor (Harrison, 1971). Although this depth extension may be partly a portion of the seamount buried in sediments, depth extensions of a kilometer or more are not uncommon and might be a result of crustal remagnetization. Seamount models are not very sensitive to changes in the shape of the bottom of the seamount

(see Section 2.8) and so the extent and shape of the root in Figure 2.7 is highly speculative.

2.6 HOMOGENEOUS MAGNETIZATION IN SEAMOUNT PALEOMAGNETIC MODELING

As mentioned in Sections 2.2 and 2.4, it is assumed that the magnetization vector of a seamount is constant in direction and intensity throughout the edifice. Although it is possible to solve equation (12) in Section 2.2 for as many different magnetization components as is desired, practically the problem is ill-defined if the number of components is too large. The reason is that it is practically impossible to determine a unique magnetization vector for a body whose dimensions are unknown or whose magnetic field cannot be separated from those of surrounding bodies. Consequently, the body being modeled is usually assumed to be homogeneously magnetized in order to render the problem solvable. Unfortunately, of all of the assumptions made in the method of seamount paleomagnetism, this one is perhaps one of the most important and hardest to justify.

Lack of knowledge of the length of time it takes to form a seamount is undoubtedly the greatest uncertainty in determining a seamount's homogeneity of magnetization. If the geomagnetic field reverses its polarity one or more times while a seamount is being formed, the edifice will obviously be far from homogeneously magnetized. Modeling by Lumb et al. (1974) which assumed a known but

grossly inhomogeneous magnetization for several seamounts, showed that such a magnetic structure will result in poor estimates of the true magnetization to be obtained if homogeneity is assumed.

Menard (1969) estimated that Pacific seamounts may take as long as 10 m.y. to form. On the other hand, extrusion rates estimated from the present-day Hawaiian Islands vary from about 0.01-0.11 $km.^3/yr.$ (Swanson, 1971; Macdonald and Abbott, 1972; Jackson, 1976; Dzurisin et al., 1980) suggesting that even large seamounts may be formed in the space of about 10^5-10^6 yr. Similarly, Duncan and McDougall (1975) report that the bulk of the Society Islands volcanoes were each typically formed in about 0.5 m.y. If a seamount formed during the mid-Cretaceous, the length of time it took to form may not be critical because the geomagnetic field was normally polarized during much of that time. In fact, the magnetic anomalies of many Cretaceous seamounts give good results when analyzed paleomagnetically. Tertiary seamounts, however, are often of mixed polarity because of the relatively rapid rate of field reversals during the period. The fact that many Tertiary seamounts give apparently reliable paleomagnetic information (Francheteau et al., 1970; Sager, 1983a) implies that some of these seamounts must have formed relatively rapidly.

Not all seamounts having lavas of mixed polarities are useless for paleomagnetic analysis. Good results are possible if the seamount is predominantly one polarity (Schimke and Bufe, 1968; Sager et al., 1982) or if the incoherent "noise" in the seamounts anomaly caused by inhomogeneities is not too great (Sager, 1983b, see also models in

Chapter 4). Various authors have used different methods to analyze inhomogeneous seamounts. Sager et al. (1982) assumed that the peak of a seamount was reversely polarized and the base was normal. The position of the polarity boundary was assumed horizontal, and the magnetization vectors of the top and bottom were taken to be opposite in direction and equal in magnitude. Schimke and Bufe (1968) attacked a similar problem by assuming the level of the polarity change and subtracting the field of the reversed base from the observed anomaly before inverting the remainder for the magnetization of the normal top. Emilia and Massey (1974) analyzed a seamount by assuming that it was made up of a number of horizontal layers with the same magnetization direction, but different intensities. They found this method to be unstable if too many independent layers were used. Kodama and Uyeda (1979) and Blakely and Christiansen (1978) used a similar method to analyze island arc-type volcanoes, except that in each of these two cases the model variation was assumed to be in two bodies of different magnetization intensity. Although the Kodama and Uyeda result was interpreted as reliable by the authors, the Blakely and Christiansen model of Mt. Shasta was patently in error as the volcano's paleopole was calculated to be 44^{o} away from the geographic pole even though the edifice is Holocene in age. This spurious result may arise from large inhomogeneities in the magnetization structure of the volcano due to the explosive nature of its volcanism. However, it serves as a useful reminder that paleomagnetic results derived from an inhomogeneously magnetized volcano may be in error if the inhomogeneities are large and

the modeling of the inhomogeneities is imperfect. Thus a single seamount paleopole is a weak basis for geologic interpretation.

Even if the length of time a given seamount is active is relatively short, there are several geological factors which may lead to inhomogeneity of magnetization. If a seamount has a large magma chamber or conduit, it may take quite some time after the cessation of volcanism for the body of magma to cool because of the low thermal conductivity typical of basalt. Using an equation designed to describe the cooling of a spherical body, Grossling (1970) estimated that a magma chamber with a radius of 1 km. should take a bit less than 1 m.y. to cool to 100° C. Such a body may cool partly in a polarity interval opposite to the rest of the seamount, or its long cooling time may lead to a phaneritic rock body with magnetic properties in contrast to the surrounding microcrystalline basalts. In either case the volume of inhomogeneous rock within the seamount will probably be small and the magnetic anomaly it creates will have a much shorter wavelength than the anomaly caused by the seamount as a whole. Thus its effect on the inversion of the entire seamount anomaly should be small.

Post-erosional volcanism has been documented on most of the Hawaiian Islands (Macdonald and Abbott, 1972). Typically these lavas erupt several million years after the cessation of the main shield building volcanism and are characterized by highly differentiated chemistries. On the islands of Rurutu and Aitutaki in the Austral-Cook chain, such volcanism appears to have occurred respectively 7-10 m.y. and 6 m.y. after the main shield building stage (Duncan and McDougall,

1976; Turner and Jarrard, 1982). In fact, there is evidence that some volcanoes may be active over many millions of years, as in the Canary islands (Abdel-Monem et al., 1971; 1972), or may be revived after a hiatus of many millions of years as in the Line Islands (Haggerty et al., 1982; Chapter 5) or Bermuda (Rice et al., 1980). In the case of post-erosional type volcanism, the lavas extruded or dikes intruded may very well have a polarity differing from the rest of the edifice, but in most cases the volume of such lavas are small (Macdonald and Abbott, 1972; Batiza, 1977) and hence they should not cause too much trouble for paleomagnetic analysis.

A seamount which has episodic volcanism or is reawakened after a long period of quiescence may have a much larger volume of the later material. Rice et al. (1980) report that at least 32% of the Bermuda edifice that they drilled was made of of mid-Tertiary sills intruded into the pre-existing Cretaceous edifice. In Chapter 5 it is shown that both Late Cretaceous and Eocene volcanism occurred in the Line Islands. Although it is not clear whether the Eocene edifices were wholly formed during the Eocene, evidence from the southern part of the chain (Haggerty et al., 1982) indicates that Eocene volcanism occurred on a Cretaceous seamount. Consequently, it may be possible that some seamounts contain rocks with the imprints of the geomagnetic field of different periods; although, Rice et al. (1980) suggest that hydrothermal remagnetization inside a seamount may be so efficient that only about 40% new intruded material is needed to effectively remagnetize the whole volcano.

Aside from the large scale inhomogeneities mentioned above, a seamount's lava flows and dikes, its basic recorders of the magnetic field, are undoubtedly inhomogeneous to some degree even when emplaced in a magnetic field of constant polarity. In part this is caused by the behavior of dikes and flows when they form and partly it is due to the behavior of the magnetic field. Most deep water lava flows consist of pillows, tubes, and sheets of massive basalt surrounded by a chilled glassy margin (Vuagnat, 1975). Hyaloclastite ash and sand as well as broken pillow rinds are often associated with underwater volcanism (McBirney, 1971; Lonsdale and Batiza, 1980) and are probably intercalated with the more solid basalt flows. Because the magnetic moments of the broken pillow rinds will be oriented more or less randomly, their magnetic fields should cancel. Hyaloclastite tuff may carry a stable magnetization, but it will be weak in magnitude (Harrison and Ball, 1975) and for the purposes of seamount paleomagnetism can be considered to be non-magnetic. As was previously mentioned, the occurrance of non-magnetic seamount tops is frequently attributed to the presence of hyaloclastite in the seamount (Harrison, 1971).

It is unclear how much of a seamount might be made up of ash, sand, and pillow fragments. Typical subaerial flows are mostly massive basalt with a minor amount of debris (Macdonald, 1972), but Lonsdale and Batiza (1980) suggest that the amounts of these materials on the flanks of a seamount, though variable from one edifice to another, may be great. Surely a large amount of these weakly magnetic materials would have a considerable effect on the overall magnetization of a

seamount. If the entire volume of a seamount is used to calculate the magnetization of a seamount, that value will be an average of the properties of all of the material in the volcano.

If the lava in a flow acquires its thermoremanent magnetization while the material is still in a fluid or plastic state, the overall magnetization will be weakened by a randomization of the orientations of individual small elements of the flow by any subsequent motion. However, this distortion is probably not a problem because most basaltic lavas are fluid at temperatures of 1000°-1100° C and solidify completely at temperatures below about 750° C (Macdonald, 1972) whereas typical basalts have Curie temperatures in the range of 100°-550° C. Thus basalt should be quite solid before its magnetization is locked in.

Dikes, if present in sufficient numbers, may also make a significant contribution to the magnetization of a seamount. Those exposed in most volcanoes are made up of massive cryptocrystalline basalt which should acquire a stable TRM and thus be an excellent recorder of the ambient magnetic field. However, unlike lava flows which are deposited serially one atop another, dikes break through older material. Thus a dike of one polarity may intrude lavas of the opposite polarity. Consequently, if the volume of dikes in a volcano is large, the modeling of a polarity reversal by a horizontal boundary in the seamount may not be entirely valid.

The direction of the magnetization vectors of individual lava flows in a seamount will not all have the same direction because of

secular variation. Normally, deflections of the magnetic field vector at the Earth's surface caused by secular variation are between 0^{o}-20^{o} but can be greater during periods of high non-dipole field activity (Cox, 1975). A common paleomagnetic assumption is that the magnetic field averages to be an axial, geocentric dipole over a period of about 10^{4}-10^{5} yr. (Nagata and Ozima, 1967). This period of time should be sufficiently short that the secular variation should be averaged out by a seamount's many lava flows. Similarly, archeomagnetic evidence (McElhinny, 1973) indicates that the Earth's dipole moment varies by at least 50% with a period of the order of 10^{4} yr., thus the intensity of magnetization of a seamount is an average of the various flow intensities.

2.7 EFFECTS OF INDUCED MAGNETIZATION AND OTHER NON-TRM COMPONENTS

Much of the oceanic rock suitable for paleomagnetic study is basalt or one of its close relatives. It is generally made up of plagioclase and pyroxenes with occasional olivine. As its texture is fine, individual minerals are only rarely seen with the naked eye. Usually basalt contains a few percent of titanomagnetite minerals in which its magnetic properties reside.

In the derivation of the seamount paleomagnetic method it was assumed that the seamount's magnetic field is produced by a

thermoremanent magnetization locked into its rocks parallel to the geomagnetic field at the time of its formation. However, several different magnetization components may combine to produce its magnetic field. In the laboratory various techniques can be employed to separate the desired magnetization from its spurious counterparts. In contrast, a magnetic survey of a seamount measures the sum of all of the different *in situ* magnetizations of its rocks and such discrimination is usually impossible. Thus it is important to assess the relative contributions of the various magnetization components to the overall magnetization calculated from survey data.

Thermoremanent magnetization (TRM) is the residual magnetization left in a rock at a temperature T after it has been cooled from a higher temperature T_o under the influence of an external magnetic field. In general the direction of the TRM is parallel to that of the applied field. Its intensity is proportional to the external field intensity provided the applied field intensity is not too great. Most of the TRM is acquired within about 100° C of the rock's Curie temperature. This temperature is the highest temperature to which a rock can be heated before it loses its TRM or conversely it is the temperature at which thermal agitation of the rock's constituent atoms decreases to the point that it begins to acquire TRM. Curie temperatures of titanomagnetites range from -150° C to 580° C, depending on the amount of titanium present (Nagata and Ozima, 1967), but most oceanic basalts have Curie points from about 150° to 450° C. For example, Steiner (1982) measured 49 basalt and diorite samples from

DSDP Leg 61 and found a range of Curie temperatures of 155° to 490° C, with an average of 280° C. A higher average, 320° C, was found for 62 basalt samples from seven DSDP drill cores by Marshall (1978). The Curie point of those samples varied from 125° to 430° C. Often the Curie temperature of fresh basalt is low, in the neighborhood of 100° to 200° C, but subsequent low temperature oxidation of the titanomagnetites substantially increase its value. This may be at least partially responsible for the high Curie temperatures of basalts from the Line Islands. Twenty-five samples from that seamount chain were found to have Curie temperatures ranging from 420° to 560° C, with an average of 495° C (Sager et al., 1982).

The stability of TRM depends (among other factors) on the size of the ferromagnetic grains in which it resides. It is "hardest" when the magnetic grains are small enough so that they contain only one magnetic domain. Larger grains tend to have many domains whose walls can be moved by thermal agitation and hence the magnetization in these grains is often unstable or "soft", changing or decaying with time (Nagata and Ozima, 1967). Because they are fine grained, basalts have generally stable magnetizations whereas coarser grained intrusive rocks often have unstable magnetizations.

Chemical remanent magnetization (CRM) occurs from the formation of magnetic minerals at temperatures below the Curie point in the presence of an external magnetic field. CRM may arise from the process of nucleation of hematite grains formed from solution (McElhinny, 1973).

A small hematite grain will be superparamagnetic and thus carry no remanence; however, at a critical size in its growth (called the blocking diameter) the magnetization will become fixed. This process is probably important for the formation of the magnetization of redbeds on land, but its importance for submarine basalts is unclear. Submarine oxidation of the titanomagnetite grains is probably the most important process producing a CRM in oceanic basalts and thus it may be an important factor for seamount paleomagnetism. Some authors maintain that the remanent magnetization observed in seafloor and seamount basalts may be entirely a CRM acquired because of rapid low temperature oxidation (Marshall and Cox, 1971; Hall, 1977). Even if the original TRM of a rock is supplanted by CRM, the desired geologic imformation is probably not destroyed. As long as the temperature at which the oxidation takes place is lower than the Curie point of the TRM, the new CRM will follow the direction of the TRM (Marshall and Cox, 1971). After the initial cooling of a seamount's lavas, such conditions should prevail unless volcanic activity is renewed within the edifice.

Isothermal remanent magnetization (IRM) is the residual magnetization left behind when the magnetic field is removed from a ferromagnetic substance without a change in temperature. IRM is usually confined to that remanence acquired by a rock at low temperature and in a short period of time. In an external field of low magnitude (such as the geomagnetic field), IRM is usually of negligible importance compared to other sources of rock magnetism (McElhinny, 1973).

However, if a rock remains in an external magnetic field for long periods of time, random thermal fluctuations in the ferromagnetic minerals will tend to realign the walls of magnetic domains to produce a greater magnetization in the direction of the applied field. A magnetization acquired in this manner is a type of IRM called viscous remanent magnetization (VRM). Magnetic viscosity is a property common to all forms of remanent magnetization. Given a magnetized collection of identical grains with a moment of magnitude M_o, the moment will spontaneously decay to zero in a field-free environment according to the relation

$$M = M_o \exp(-t/\mathcal{T}),$$

where t is the elapsed time and $\mathcal{T}$ is the relaxation time of the grains (McElhinny, 1973). For small applied fields the relaxation time can be expressed by the thermal activation equation,

$$\mathcal{T} = C \exp(\frac{v\ Hc\ Js}{2\ k\ T})$$

where Hc is the coercivity, v the grain volume (for sigle domain grains), Js the saturation magnetization, T the absolute temperature, k Boltzmann's constant, and C a quantity related to the atomic reorganization time, about 10^{-9} sec. (Dunlop and Hale, 1977). All other factors being equal, it is seen that magnetic grains have relaxation times that vary according to their volume and the temperature. Temperature is a very important quantity in determining the relaxation time of a magnetic grain. The equation above can be

used to relate the relaxation time τ_1 at temperature T_1 to the relaxation time τ_2 at temperature T_2 (McElhinny, 1973),

$$T_1 \ln(\tau_1/C) = T_2 \ln(\tau_2/C).$$

Thus a grain with a long relaxation time at a low temperature will have a much shorter relaxation time at higher temperatures. This factor must undoubtedly be important in those instances in which rocks are reheated or subjected to hydrothermal alteration. Similarly, grains with blocking temperatures on the order of 200° to 500° C will have very long relaxation times at seafloor temperatures. For example, the equation above shows that a grain with a relaxation time of 1000 sec. at 400° C will have a relaxation time of about 10^{12} yr. at 15° C.

Terrestrial igneous rocks contain magnetic minerals with a wide range of relaxation times. Many plutonic rocks have very unstable magnetizations as their magnetic properties reside in grains with short relaxation times. Basalts, on the other hand, usually contain titanomagnetites with long relaxation times and hence their magnetizations are usually stable. Even in basalts, however, there are often some magnetic grains whose magnetizations move viscously in geologically short periods. In some rare cases, the viscous part of the magnetization may be larger than the stable part (Lowrie, 1973), but in most basalts the viscous component is usually less than 5% - 10% of the stable fraction (Dunlop and Hale, 1977).

In the laboratory a rock sample can frequently be cleaned of its viscous magnetization by heating or by being tumbled in a strong

alternating magnetic field. When the magnetic field of a seamount is measured the average viscous properties of all of its rocks will be included. Grains with short relaxation times, say less than 1000 yr., will record the ambient magnetic field vector. Those with relaxation times between 10^3 yr. and 10^5 yr. will record a field vector somewhere between the ambient field direction and the dipole field direction for the site. Grains with relaxation times from about 10^5 yr. to 10^7 yr. should have directions that have been randomized to some extent by the frequent reversals characterizing the Tertiary geomagnetic polarity history. Those grains with longer relaxation times carry the geologic information that is sought in the modeling process.

When a ferromagnetic substance is placed in an external magnetic field it will acquire a magnetization made up of two parts. One part will be the remanent magnetization, J_r, discussed above. The other part, J_i, is that magnetization induced in a sample by the external magnetic field. It is usually proportional and parallel to the magnetizing field, $\bar{H}$,

$$\bar{J} = k \bar{H},$$

and disappears when the field is removed. The quantity k is called the magnetic susceptibility. It varies with the amount of magnetic material contained in a rock, but for oceanic basalts it typically ranges from 30-3600 x 10^{-5} SI (Sharma, 1978, p. 192).

Thus the magnetization of a rock is the vector sum of its induced and remanent components,

$$\bar{J}_t = \bar{J}_r + \bar{J}_i.$$

In the laboratory a sample can be measured in a field-free space, thereby eliminating the induced component. A seamount magnetic anomaly, however, is produced by the average total magnetization vector of its component rocks--including the induced magnetization. In the past, authors of seamount paleomagnetic studies have assumed that the induced magnetization is negligible compared to the remanent magnetization. One might well wonder just how valid this assumption actually is.

The relative strength of the induced and remanent components of rocks is usually quantified by the Koenigsberger ratio, Q_n, which is expressed as

$$Q_n = J_r/kH,$$

the ratio of the magnitudes of the remanent and induced magnetizations. Since Q_n depends on the magnetic field at the sampling site, the ratio is often expressed

$$Q_n' = J_r/k.$$

It has been known for many years that Q_n is usually high for most oceanic basalts. However, submarine alteration can greatly reduce its value in oceanic basalts (Marshall and Cox, 1972; Fox and Opdyke, 1973). Undoubtledly this process plays a part in the reduction of the magnetization intensity of seafloor anomalies as they age, but deep drilling of Suiko seamount suggests that deep sea oxidation and weathering may not be very important processes affecting the

magnetization of rocks inside seamounts (Kono, 1980a). Figure 2.8 shows a Q_n' histogram of 1124 samples of submarine basalt and related rocks older than 5 m.y. The selection is limited to older rocks because very young basalts have very high Koenigsberger ratios (Irving et al., 1970). It is seen that Q_n' values for oceanic basalts are generally high. The most common values of Q_n' are between 3.1 - 10.0. Even at the most northerly point in the Pacific (59° N, 145° W), where the geomagnetic field intensity is highest (55800 nT.), this range corresponds to Q_n values of 5.5 - 17.9. At the equator (0° N, 130° W) where the field strength is lower (32100 nT.) the Q_n values are even higher, 9.7 - 31.2. In Figure 2.8, 92.3% of samples have Q_n' values greater than 1.0. Additionally, few of the samples with low values of Q_n' are found alone. Usually they are associated with other rocks with higher Koenigsberger ratio values. Often the low Q_n' rocks are highly weathered pillow fragments or glassy samples that would naturally be expected to have small remanent magnetizations. Consequently, the assumption that most of a seamount's magnetic anomaly is produced by remanent magnetization is probably a good one in most cases.

However, this assumption has been made rather blindly in the past, so it would be interesting to examine the effect that induced magnetization will have on the paleomagnetic modeling of a seamount whose rocks have low Koenigsberger ratios. Figure 2.9 shows the effect

that the induced component will have on the overall magnetization direction for low values of Q_n. Pacific seamounts will have magnetization inclinations less than the current dipole field direction at their latitudes because of their northward drift. For normally magnetized seamounts (Figure 2.9 a,b), the induced component steepens the inclination of the magnetization giving the impression that the seamount formed further north than it actually did. The opposite is true for reversely polarized seamounts (Figure 2.9 c,d). The induced component makes it appear that the seamount formed further south than it actually did. Thus reversely magnetized seamounts will have greater northward drift values than normally magnetized seamounts of the same age if the induced component is an important part of their magnetization. Unfortunately, the number of reversely polarized seamounts that have been paleomagnetically analyzed is small and few seamounts of either polarity have reliable ages, thus it is impossible to perform this test convincingly with the data presently available.

Figure 2.10 shows the effect of the varying angle between the induced and remanent components of the magnetization. The deflection of the total magnetization vector is most when the remanent and induced components are perpendicular. In the Pacific, most seamounts have undergone 30° of northward motion or less (Harrison et al., 1975). Thus the angle between the two components is usually less than 60°. This factor tends to slightly lessen the effect of a low Q_n ratio on the direction of the total magnetization vector.

Figures 2.11 and 2.12 display the effects of varying Q_n ratios on ten seamount VGPs which are representative of most of those listed in Chapter 4. In Figure 2.11 it is assumed that the measured magnetization direction of each seamount is parallel to the remanent vector (i.e., $Q_n = \infty$). Decreasing the value of Q_n, the VGPs of normally magnetized seamounts tend to move toward the geomagnetic north pole. The one VGP of a reversely magnetized seamount (south pole shown) moves away from the geomagnetic north pole. As long as the overall Q_n of the seamount is greater than about 5, the movement of the VGP is only about 3 - 5° for the normally magnetized seamounts. However, if the Q_n is as low as 1, the VGP movement may be as much as 10 - 15°. In Figure 2.12 vector subtraction of the induced and remanent components has been performed (i.e., each point on the line corresponds to the true VGP of the seamount if the measured VGP is calculated from a magnetization vector with the given value of Q_n). In this case the normally magnetized seamount VGPs move away from the north geomagnetic pole with decreasing Q whereas the reversely magnetized seamount south pole moves toward the geomagnetic north pole. The VGPs are thus further north than they should be by about 5 - 8° in most cases if the Q_n is as low as 5. This behavior is what one might expect if the VGPs of the seamounts listed in Chapter 4 are calculated from an anomaly combining both induced and remanent magnetizations. Thus it is important to compare seamount paleomagnetic results to

paleomagnetic data measured from samples in the laboratory as a systematic difference of this sort would indicate that a significant induced component of magnetization is incorporated in the seamount results. In fact, as will be shown in Chapter 5, there is no apparent difference between Pacific seamount paleomagnetic data and other types of Pacific paleomagnetic data, and thus the assumption that the induced component of magnetization is small appears to be valid. However, the number of dated seamounts is small and the amount of reliable non-seamount paleomagnetic data from the Pacific is also small, so this finding is not conclusive and deserves a more rigorous test than is possible with the present data.

Is there any way to calculate the contribution of the induced component to the overall magnetization of a seamount? As explained in Appendix A, there is no theoretical barrier to calculating a value of the susceptibility in the inversion procedure. Practically, the remanent and induced vectors may be very difficult to separate. However, if the angle between the two component vectors is substantial, it may be possible to separate the two. One method is the aforementioned inversion procedure calculating a coefficient for the susceptibility as well as the usual three Cartesian components of the remanent magnetization. A better way might be to specify a value of the susceptibility, so that the inversion routine does not have to calculate it. One could either enter a value of the susceptibility determined from a dredge sample or try a series of test values to see which works the best. To the author's knowledge, no one has conducted such an investigation. In the modeling of several of the seamounts

described in Chapter 4 an induced anomaly was included to see if it improved the model's fit to the observed anomaly. In no case did this procedure improve a model, but the investigation was not extensive.

2.8 THE HORIZONTAL LAYER APPROXIMATION

In the Talwani (1965) and Plouff (1976) seamount modeling routines, the magnetic body is approximated by horizontal laminas or polygonal, plate-like prisms (see Figure 2.5). As a result, the bottom of the seamount is usually assumed to be horizontal as are any polarity transitions within the seamount. Truly horizontal layers within a volcano are probably rare, thus a discussion of this assumption is in order.

The assumption that a polarity transition within the layers of a seamount is horizontal is probably not very accurate. Even if the transition were instantaneous in time and the seamount's eruptions were distributed randomly on the upper surface of the seamount, the bottom of the lavas with the newer polarity should dip outward at the characteristic submarine lava slope of about 15^{o}. This angle implies that the transition should dip 270 m. vertically for every 1000 m. horizontally. Additionally, eruptions rarely occur completely at random on the surface of a volcano and the normal and reverse lavas may be separated by lavas of intermediate polarity. Also, the dikes which

fed the lavas of the later polarity will cool in the same field and have the same polarity, but will intrude the older lavas of opposite polarity to an unknown depth. Thus it is doubtful that the polarity transition within the seamount is truly horizontal.

Little is known about the configuration of the bottom of a seamount. If the first eruptions of a growing seamount were extruded on a flat, sediment-free ocean bottom, the horizontal bottom approximation might be valid for small volcanoes. Large volcanoes cause the underlying crust and lithosphere on which they lie to be warped downward. Geological and geophysical data are inconclusive as to the amount of the flexure, but it certainly depends on the mass of the volcano and the age of the underlying lithosphere (Suyenaga, 1979; Watts et al., 1980). Estimates of the amount of flexure under the island of Oahu range from 2 - 10 km. (Suyenaga, 1979), implying a maximum dip of about $4 - 5^{o}$. Edifices as large as Oahu commonly have complex magnetization distributions that make them unsuitable for magnetic anomaly studies. As the volcanoes amenable to such study are generally much smaller and much less massive, the flexure beneath them is probably much less.

Even if the flexure beneath a seamount is small, it is still uncertain whether the bottom is flat. Magma rising through the crust may remagnetize portions of layer 2 or intrude a series of dikes and sills into the crust forming a magnetic root. Such a root may explain some of the sub-sediment extensions which improve many magnetic models of seamounts. The shape of this root is uncertain and that shown in

Figure 2.7 is highly speculative. Additionally, if sediments cover the sea floor when a seamount begins to form, the magma should intrude the sediments as sills because it is more dense than the sediments. The areal extent of the sills formed in this manner is unknown and their configuration in Figure 2.7 is also speculative.

Given the lack of constraint on the true shape of the surfaces in question, the horizontal layer approximation is probably reasonable. In particular, the approximation of the seamount's bottom as a horizontal boundary probably has little effect on the magnetic model of a seamount because of the insensitivity of the modeling technique to changes in the shape of the deepest part of the edifice. The reason for this insensitivity can be seen by considering the vertical component of the magnetic field of a spherical body with a volume V observed at a distance R from the center of the sphere,

$$Z = \frac{2 J_z V}{R^3},$$

where J_z is the vertical component of the magnetization. Because the strength of the magnetic field falls off as the cube of the distance to the body, a large volume of material deep in the ocean is necessary to produce the same magnetic field as a smaller volume close to the sea surface. In fact, the magnitude of the anomaly produced by 1 km.^{3} of material at a depth of 1 km. is only just matched by a volume of 125 km.^{3} at a depth of 5 km.

2.9 REGIONAL FIELD REMOVAL

As explained in Section 2.2, equations (12) and (14), the magnetic anomaly T', for some point outside the magnetic body, can be expressed as

$$T' = J_1 B_1 + J_m B_2 + J_n B_3 + R,$$

where J_1, J_m, J_n are the Cartesian components of the magnetization, B_1, B_2, B_3 are volume integrals of the body, and R is a regional field. If one wishes to compare the calculated magnetic anomaly to the observed anomaly, the simplest R that can be used is a constant offset,

$$R = C_o.$$

In this case C_o is the value that, when added to the calculated anomaly brings the calculated and observed anomalies into best agreement in a least-squares sense. This offset is usually calculated in the inversion routine along with the magnetization components J_1, J_m, J_n. Instead, most authors use a planar regional field for R,

$$R = C_o + C_1 x + C_2 y,$$

where x and y are distances in the north and east directions. Harrison et al. (1975) claim that the addition of the plane in the inversion calculation rarely changes the magnetization direction significantly and that it helps to separate the field caused by the seamount from any spurious background field. This view is not unequivocally accepted and for reasons explained below magnetizations calculated with constant

offsets are preferred. Other authors have used more complicated regional fields, but these have ususally been removed from the observed data before insertion into the inversion routine and they have been used only in special circumstances when the data seemed to warrant such treatment.

To test the ability of the modeling technique to recover both the correct magnetization and planar regional, a model seamount was constructed with an assigned magnetization, its anomaly was calculated, and a planar regional was added. The computer program used for all of the paleomagnetic models described in Chapter 4, with a planar regional assumed in the inversion routine, displayed the ability to calculate both the magnetization and the planar regional to within about 2% or less. However, when used on real data, the planar regional seems to cause the magnetization directions to be more scattered than those calculated with the constant offset. Table 2.1 lists 38 seamounts with VGPs calculated using both kinds of regional field. The least difference between the two types of VGP is less than 1^{o}. On the other hand, 63% of the seamounts show more than 5^{o} of distance between the VGPs. The worst case is 32.9^{o}. Many of the seamounts which show large shifts have low GFR, small anomalies, or complex anomalies, but some of the large shifts occur for seamounts with well-defined, simple anomalies. Consequently, a large change in the magnetization direction of a seamount upon the addition of a planar regional field to the calculation cannot be blamed entirely on poor survey coverage, a complex anomaly, or a low GFR. In this study it has been found to be

practically impossible to predict a priori whether or not a seamount will show a large shift between the two VGPs.

Figure 2.13 shows the scatter of planar regional VGPs more graphically. Thirty-one of the seamounts from Table 2.1 were selected because their constant offset VGPs fall near calculated apparent polar wander paths for the Late Cretaceous - early Tertiary Pacific plate (see Chapter 5). The calculated apparent polar wander path of this age is a relatively smooth curve that probably cannot be distinguished from a great circle with the given seamount data. Such a distribution is well-suited for analysis with Bingham statistics. The best average position of these 31 seamount VGPs was calculated along with its 95% confidence ellipse using Bingham statistics for both the constant offset and planar regional cases. The average position, as seen in Figure 2.13, is nearly the same in each case (66.7° N, 1.2° E, constant offset; 66.0° N, 2.2° E, planar regional). However, the major and minor semi-axes of the 95% confidence ellipse are much smaller for the constant offset group (4.2°, 2.0°) than the planar regional group (5.2°, 3.5°). These numbers only serve to confirm what is readily visible in Figure 2.13--the planar regional VGPs are clearly more scattered.

The reader should be aware of a possible bias of the above test because of the somewhat circular logic used to produce it. The seamounts ananlyzed were picked because their constant offset VGPs fall close to a predicted APWP (i.e., becuase they did not show too much scatter). Some of these seamounts may be more appropriate for other

parts of the APWP, but because of scatter their VGPs fall in with the group used. A more valid test would be to use the same procedure with seamounts of the same age from an area of the Pacific that can be reasonably said to have no fossil plate boundaries that might have caused relative movement between the seamounts. Unfortunately, because the number of dated seamounts is small such a test remains inconclusive.

Because the seamounts whose magnetizations were calculated with planar regional fields seem to show more scatter than those calculated with a constant offset, the constant offset VGPs are used for the tectonic interpretations presented in Chapter 5. The other seamount VGPs have been used as published for consistancy's sake (and because constant offset VGPs are rarely published). Trying to justify using the planar regional in a case by case manner would only further confuse the issue. Both types of VGP have been included in Chapter 4 so that the reader may draw his own conclusions.

There might be occasions when the use of the planar regional is superior to the constant offset. If total magnetic field intensity values are used for the magnetization calculation rather than total field residual anomaly values, the planar regional may be helpful because the geomagnetic field sometimes has gradients amounting to a sizable percentage of the seamount anomaly over a distance appropriate to a seamount survey. In such a case, the gradient is usually smooth and nearly planar over a small area as it is caused by sources in the Earth's core. All of the magnetic interpretation done in this study made use of magnetic anomaly values, hence most of this type of

gradient should be removed. However, because spherical harmonic geomagnetic field models are not perfect, instances may occur in which there remains a significant gradient, even after the subtraction of the theoretical core field from the observed field. In such a case, the planar regional may be preferred over the constant offset; however, in all of the new seamount models presented in this study, none obviously fit this category.

Often seamounts occur close together and their anomalies impinge upon one another. If the interference is too great, the final paleomagnetic results must suffer. In many cases the seamounts' anomalies are separate enough so that a reasonable model can be made; however, for such a model a planar regional will not work well because the spurious anomaly is not planar. In fact, Table 2.1 indicates that the planar regional often causes a large shift of the VGP if the anomaly is complex. Likewise, the planar regional cannot be expected to cope with the non-seamount field if the edifice sits atop a large crustal anomaly. In such an instance it may be difficult to make a reasonable model at all. For example, Francheteau et al. (1970) obtained poor results modeling seamounts situated on high amplitude magnetic lineations in the eastern Pacific despite their best efforts to remove the unwanted magnetic field caused by the crustal anomalies.

2.10 THE DEMAGNETIZATION EFFECT

If a body whose length is much greater than its height is magnetized in a strong field, there will be a tendency for the induced magnetization vector to be more nearly horizontal than the magnetizing field vector (Grant and West, 1965, p. 318). This phenomenon is called the demagnetization effect and it was proposed by Vogt (1969) as an explanation for some or all of the paleomagnetic northward motion of Pacific seamounts. Although the effect strictly applies only to the induced magnetization of a body, Uyeda et al. (1963) demonstrated that if a rock has a marked defelection of its induced vector, there will be a similar effect on the TRM aquired by it. Vogt pointed out several factors which might lead to a significant demagnetization effect in seamounts. He reasoned that the magnetization of seamounts derived from magnetic models was an average of the magnetic properties of each edifice and that the actual magnetization of many individual flows might be much higher than the average. Additionally, he pointed out that lava flows are generally tablular in form and that seamounts themselves often have diameter to height ratios of 20 or more.

The demagnetization effect manifests itself as a fictional "equator fleeing force" because the deflection of the magnetization vector towards the horizontal makes seamounts formed north of the equator appear to have a greater amount of northward drift than they actually do whereas it makes seamounts formed south of the equator appear to have less northward drift. If the apparent motion of Pacific seamounts were due entirely to the demagnetization effect, then no

seamount could appear to cross the equator. In fact, 29 of the seamounts in Table 4.1 (Chapter 4) appear to have done so. This observation is not surprizing as there are many geophysical data of other types that also indicate a large amount of northward drift for the Pacific plate.

Could the demagnetization effect instead account for a small systematic bias of the seamount data? The magnitude of the magnetizations involved suggest that it should not. The largest seamount magnetization intensity from Table 4.1 is 15.6 A./m. This value suggests that the highest susceptibility should be in the neighborhood of 10% of that value. However, experimental results (Uyeda et al., 1963) indicate that the magnetic shape anisotropy of a rock would be negligible even if the susceptibility were of the same order of magnitude as the strongest remanent magnetization observed in seamounts.

Rather than leave this discussion completely in the academic realm, the data can be tested for the presence of the demagnetization effect. Uyeda et al. (1963) have shown that the inclination recorded in a rock can be related to the inclination of the magnetizing field,

$$\tan(I_{trm}) = f \tan(I_{ext}).$$

The factor f is inversely related to the bulk susceptibility and a shape factor. Its value is unity if the susceptibility is small or the body is equidimensional. Assuming that a number of seamounts of the same approximate age have all moved northward by the same amount (only an approximation at best because plate movement on a sphere is a

rotation), the expected inclination of a seamount, I, can be expressed in terms of the demagnetization factor, f, the seamount's present latitude, p, and its northward drift, d,

$$\tan(I_i) = 2\ f\ \tan(p_i - d),$$

where the values of f and d are assumed to be the same for all of the seamounts. Since I_i and p_i are known, the best values of f and d can be calculated by least-squares minimization of the function,

$$S = \sum_i (I_i - I_i')^2 ,$$

where I_i' is the model value of the inclination (Harrison et al., 1975). A proper test for the demagnetization effect would use only reliably dated seamounts, but as noted earlier, these are few in number. Sager (1983a) lists seven seamounts believed to be Late Eocene or Early Oligocene in age. For this group of seamounts, the RMS deviation, S, is minimized for d = 12° and f = 1.01 (Figure 2.14 a). This value of d agrees well with the amount of northward drift found by Sager and the f value is very close to unity. A similar test was performed on eight seamounts with radiometric ages between 72 - 83 m.y. In this case the preferred northward drift was 29° with an f of 0.79 (Figure 2.14 b). The variance of the data from the expected values with these values for f and d is 0.3250, whereas the variance for f = 1.0 is 0.2591. An F-test shows that the two variances are indistinguishable at the 95% confidence level implying that the 0.79 value for f is not significantly different than unity.

These two tests suffer from the small numbers of dated seamounts available. A further set of tests was performed on 20 seamounts whose VGPs fall close to the Maastrichtian paleomagnetic pole and 20 others whose VGPs fall close to the Campanian and Santonian poles (see Chapter 5). Although few of these seamounts are dated, one can assume that the position of a seamount's VGP along the Pacific APWP is related to its age. As some scatter is to be expected in the VGP positions, this inference is not always a good one. However, keeping in mind that not all of the VGPs in these two groups are necessarily the same age, each group can be examined for a systematic dispersion consistant with the demagnetization effect. The 20 seamounts of apparent Maastrichtian age gave $d = 21^{o}$, $f = 0.90$ and the Campanian - Santonian seamounts gave $d = 30^{o}$, $f = 0.96$. These results are shown graphically in Figure 2.14 c,d. The RMS deviation minima around the best f values are now a bit deeper, but there is still little difference in the variance of the data between, say, $f = 0.9$ and $f = 1.0$.

Using an F-test, it is possible to deduce a 95% confidence interval for f. The lower bound for the confidence interval is the lowest value of f that produces a variance indistinguishable at the 95% confidence level from the variance calculated with the best value of f. The upper bound of the confidence interval is determined in a similar fashion. For $N = 20$, the confidence interval for f is 0.68 - 1.28 for the Maastrichtian seamounts and 0.67 - 1.28 for the Campanian - Santonian seamounts. Note that the confidence region is asymmetric around the best value of f because the RMS minima in Figure 2.14 are

asymmetric. Although the 95% confidence intervals for f are fairly wide, the least squares solution for f has a propensity to fall close to unity in all of the data sets. This strongly suggests that the demagnetization effect is not large and that the data are not significantly biased by it.

2.11 GOODNESS OF FIT PARAMETERS

It is useful to have some measure of how well the calculated anomaly of a seamount matches the measured anomaly. An objective parameter measuring this "goodness of fit" would allow comparison among seamount paleomagnetic results and would give an indication of the reliability of the magnetization calculated for each seamount. The most widely used quality parameter is the "goodness of fit ratio" (GFR) (Richards et al., 1967), defined as

$$GFR = \sum_i |T_i| / \sum_i |E_i|.$$

The T_i are the observed anomaly values minus the regional field, the E_i are the residuals (observed minus calculated anomaly), and the sum is over the n observation points of the magnetic anomaly. The higher the value of the GFR, the better the match between the observed and calculated anomalies. A GFR of 2.0 implies that the residuals are about half the size of the observed anomaly, and 1.8 is usually

considered as the lower limit for a reliable paleomagnetic inversion of the anomaly (Harrison et al., 1975).

A similar quality parameter is the average residual (Francheteau et al., 1969),

$$R_{ave} = \sum_i |E_i| / n.$$

Low values of this parameter are to be desired. It has been used only rarely in the literature.

Harrison (1971) advocates the use of RMS residuals,

$$RMS = (\sum_i E_i^2/n)^{1/2},$$

or relative RMS residuals,

$$rms = (\sum_i E_i^2 / \sum_i T_i^2)^{1/2},$$

as quality parameters for seamount paleomagnetic analysis. Both indicate a better agreement of the observed and calculated anomalies by lower values. Acceptable values of the relative RMS residual are usually lower than about 0.4. These parameters have also been used sparingly in the literature.

Several quality parameters are derived from the standard deviations of components of the magnetization calculated by the inversion process. Francheteau et al. (1970) recommended SD_a and SD_m, the standard deviations of the direction and intensity of the components of the magnetization vector, as parameters to indicate its accuracy. These standard deviations are given by,

$$SD_a = S_a / M(n - 3m - k)^{1/2}$$

$$SD_m = S_a / (n - 3m - k)^{1/2}$$

where S_a^2 is the average variance of the three magnetization components, M is the magnitude of the magnetization, n, the number of observation points, m, the number of magnetic bodies, and k, the number of regional field constants. Acceptable values of SD_a are usually less than about 5^o, whereas SD_m has a wide range but should be below about 50 nT. to indicate reliability. Neither parameter is particularly good for comparing seamount anomaly inversions because the values calculated for both depend heavily on the number of observation points used.

Plouff (1976) suggests that the multiple correlation coefficient,

$$MCC = [(J_1 P_{41} + J_m P_{42} + J_n P_{43}) / P_{44}]^{1/2},$$

is a good indicator of the accuracy of a magnetic anomaly inversion. In this equation the P_{ii} are product moments used in the solution of the linear least-squares normal equations. The MCC ranges from 0 - 1 with a perfect match between the observed and calculated anomalies giving a value of unity. Most acceptable seamount inversions give MCCs greater than 0.9. This parameter is sometimes a useful complement to the GFR because its value depends more on the matching of the shapes of the observed and calculated anomalies than does the GFR.

No one of these quality prameters is clearly better than the rest for distinguishing reliable and unreliable results. The GFR carries

the weight of custom as it has been used in almost all seamount paleomagnetic studies. For this reason its use is continued in this study. Like any of these parameters, it must be used with its limitations in mind.

No theoretical basis exists for setting a lower limit on the GFR for a reliable seamount paleopole. The lower limit of 1.8 used by Harrison et al. (1975) was arbitrary. The limit could have been higher, but seamount paleopoles are few enough in number that it would be difficult to make tectonic interpretations if too much of the data is thrown out. Although no empirical or theoretical relation exists between the value of seamount GFRs and their VGP scatter, seamounts of about the same age having high GFR values generally have VGPs that group closer together than if they had lower GFR values. For example, most of the Musicians seamounts have high GFRs and their VGPs all fall fairly close to the Pacific APWP (Chapter 5). Conversely, the seamounts modeled from the Mid-Pacific Mountains all have low GFRs and their VGP scatter is high.

Below is a subjective classification of seamount paleopole reliability by GFR values based on the 36 seamount anomaly inversions described in Chapter 4. These classifications are not rigid and should be used only as guidelines.

GFR	RELIABILITY
< 2.0	Poor
2.0 - 2.5	Fair
2.5 - 3.5	Good

3.5 - 5.0	Very Good
> 5.0	Excellent

Two seamount VGPs with the same value of the GFR may not have the same degree of reliability. It has been shown that as the distance from a magnetic body increases, so does the GFR (Kodama and Uyeda, 1979). A similar effect has been noted for the relative RMS residual and the MCC (Blakely and Christiansen, 1978). Partly this effect is caused by the attenuation of short wavelength components of the magnetic anomaly, that might be present because of magnetization inhomogeneities, with distance from the magnetic body. Also it is a result of the fact that it becomes increasingly more difficult with increasing distance to distinguish the magnetic fields of two dipoles whose moments are not separated by a large angle.

Although the GFR (and any of the other quality parameters mentioned above) is usually a reliable indicator of the relative reliability of a seamount anomaly inversion, there are instances in which it can be misleading. Blakely and Christiansen (1978) reported a paleopole for Mt. Shasta volcano which lies at a significant distance from either the geographic or geomagnetic north poles even though the mountain is clearly of Holocene age and the goodness of fit parameters indicated a reliable inversion. Similarly, seamounts Line 3 and WP7 in Table 4.4 have high GFR (6.8 and 3.1), but their magnetization directions are considered unreliable because they do not agree with any other seamounts and they fit no reasonable model of Pacific plate motion.

With additional geologic information it is possible to pinpoint reasons why each of the models mentioned above did not work. The modeling of Mt. Shasta indicated that the volcano is grossly inhomogeneous in its magnetization. As mentioned in Section 2.6, it is often difficult to obtain reliable results from such seamounts and thus their magnetization directions should always be treated with a certain amount of skepticism. Seamount Line 3 had several troublesome features. It is a small ridge, standing barely 1 km. above the surrounding seafloor, and its position near Christmas Island and the Line Islands Ridge virtually guarantees that much of it is buried beneath a deep cover of sediments. Also, the magnetization of Line 3 is very inhomogeneous (the best model has nearly equal parts of normal and reversed polarity) and there is no constraint on the positions of the polarity boundaries. Additionally, the magnetic anomaly is very small (110 nT.) and shows no obvious relation to the position or shape of the source body.

The first sign of trouble in the modeling of Line 3 was an instability of the solution of the magnetic inversion. Small changes in the postion of polarity boundaries within the seamount model produced wild variations in the declination of the calculated magnetization declination. Seamount WP7 also has a very small anomaly (120 nT.), particularly considering the volcano is over 3 km. in height. Like Line 3, WP7 has an anomaly which does not appear as one might expect from a homogeneously magnetized seamount. These two observations suggest that the seamount may also be inhomogeneously magnetized to a great degree with lavas of opposing polarities nearly

cancelling each other and producing a low amplitude anomaly. The VGP of this seamount (1.4° N, 231.2° E) fits no known pattern of Pacific seamount VGPs and is thus suspect.

Occasionally a low value of the GFR occurs in a model that appears to be good. Chapman Seamount (L6 in Table 4.1) has an anomaly that is complicated by inhomogeneities of magnetization. In this case, however, the anomaly has a large amplitude and an overall form consitent with the shape of the seamount. A model assuming the edifice to be homogeneous had a low GFR of 2.6, but subsequent modeling of the volcano as an inhomogeneous body (see Section 4.5.7) produced a GFR of 4.3. The magnetization direction of the latter model differs very little from the former model and the VGP of Chapman seamount is in excellent agreement with the VGPs of other seamounts in the Line Islands.

These problems indicate that the only sure measure of the reliability of a seamount VGP is its consistency with other VGPs of the same age from volcanoes in the same tectonic province. They also demonstrate the problems inherent in trying to make tectonic interpretations of the VGPs of seamounts whose ages are unknown. Although most of the VGPs of seamounts with high GFRs are reliable, a few may not be, and hence interpretations based on undated seamounts must be carefully made.

Table 2.1: Angular Difference Between VGPs Calculated With A Constant Offset Or Planar Regional Field.

	Const. Off. VGP		Planar Reg. VGP			
Name	Lat(°N)	Long(°E)	Lat(°N)	Long(°E)	Del(°)	Comments
H5	68.0	10.0	67.8	5.7	1.6	
H6	65.5	16.6	65.6	14.6	0.8	
H10	68.0	8.9	68.6	356.7	4.5	CA
W7	58.6	342.3	58.5	344.8	1.3	
W10	71.0	281.3	58.4	282.8	12.6	PS,LAA
W11	57.0	4.8	56.4	4.0	0.7	
W12	71.7	246.5	67.8	248.0	3.9	
W13	55.0	312.9	52.3	301.3	7.4	CA, low GFR
W14	74.5	6.4	69.2	357.4	6.0	CA, low GFR
W15	55.8	296.6	61.1	293.0	5.6	
W16	57.4	340.3	59.3	350.5	5.7	CA
W17	63.2	2.2	57.0	43.8	21.2	CA
C1	61.0	31.2	56.3	40.6	6.8	CA
P1	50.9	277.9	39.6	273.3	11.8	CA, CI, low GFR
P2	68.1	21.9	64.7	354.3	11.5	CI, low GFR
P3	73.3	324.2	73.6	350.6	7.5	CI, low GFR
P4	69.2	328.6	61.3	333.8	8.2	CI
L1	68.3	38.7	65.7	37.2	2.7	
L2	65.6	6.1	61.6	4.0	4.1	
L4	75.6	356.5	54.3	312.3	27.1	IM, SA
L5	78.2	14.6	78.4	37.8	4.7	IM, SA
L6	75.7	37.8	78.9	32.3	3.4	IM, CA
L7	80.0	20.4	82.5	63.6	6.8	IM, SA, PS
L8	68.5	345.6	75.9	352.2	7.7	CA
J1	42.1	331.8	49.4	337.1	8.2	TFA, low GFR
J2	55.4	349.4	56.4	359.4	5.7	TFA, low GFR
HR1	75.5	4.6	73.9	334.2	8.1	
M1	59.4	358.8	56.6	339.5	10.6	
M2	56.0	342.6	61.0	5.6	12.9	
M5	67.2	26.9	66.3	15.2	4.7	CA
M7	65.7	355.3	56.4	331.3	14.7	CA
M9	67.3	3.1	67.8	30.5	10.4	CA
M10	62.4	356.6	42.6	41.9	32.9	
M11	59.2	333.8	57.0	330.9	2.8	CA
M12	69.3	10.2	69.5	28.9	6.6	
M13	70.1	0.0	65.3	327.0	13.2	
M14	67.7	1.8	67.9	4.0	0.9	
M15	64.9	9.5	63.6	358.6	4.9	

Comment Code:
SA = small anomaly
PS = poor survey
CA = complex anomaly
IM = inhomogeneous magnetization
TFA = total field anomaly
LAA = low amplitude anomaly
CI = crustal anomaly interference

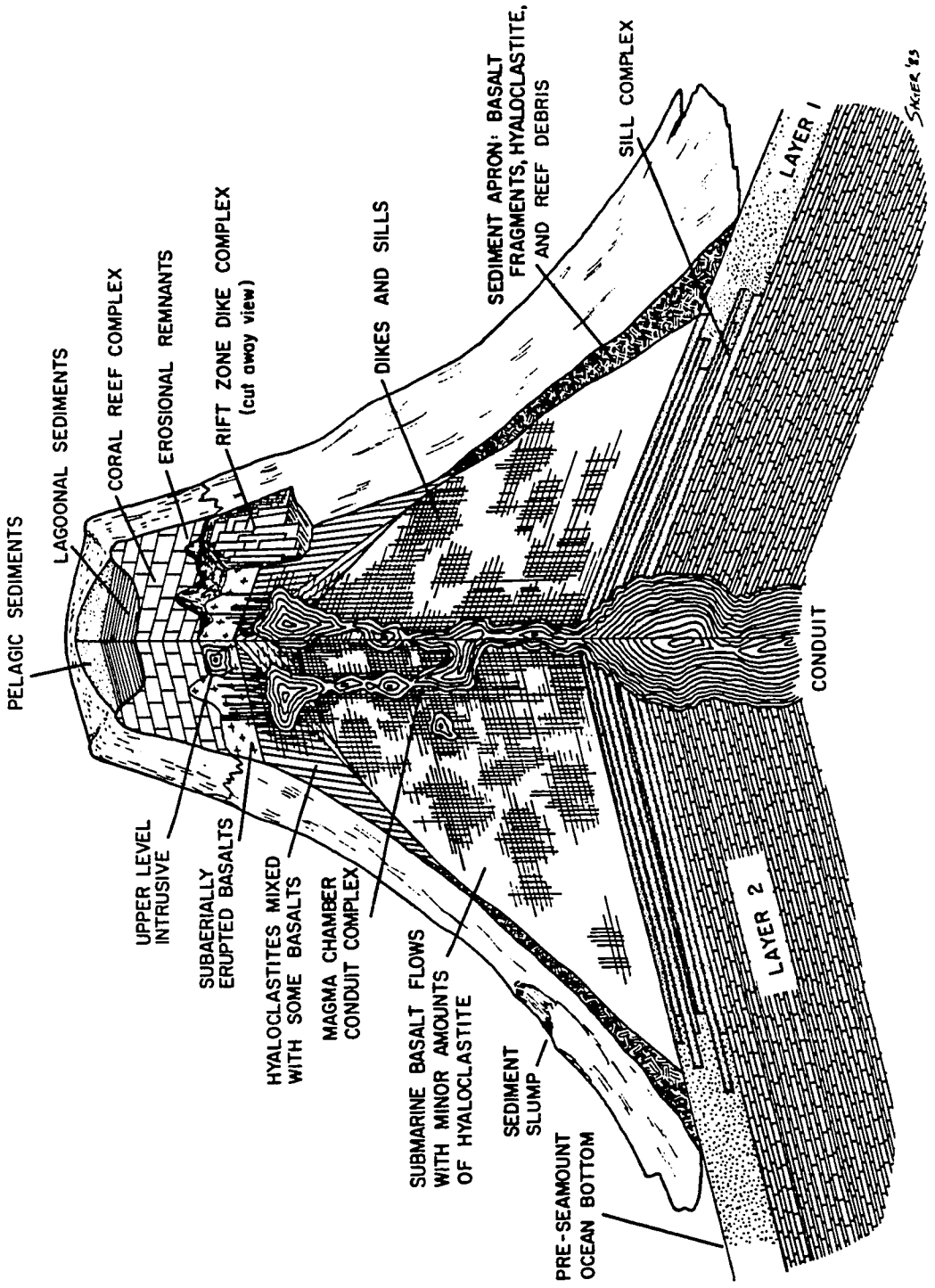

Figure 2.7 Schematic diagram of features that might be encountered on the inside and outside of a guyot. The features shown are not necessarily to scale and the drawing includes a large amount of vertical exaggeration. The information from which this seamount was envisioned was drawn from many sources mentioned in Section 2.5.

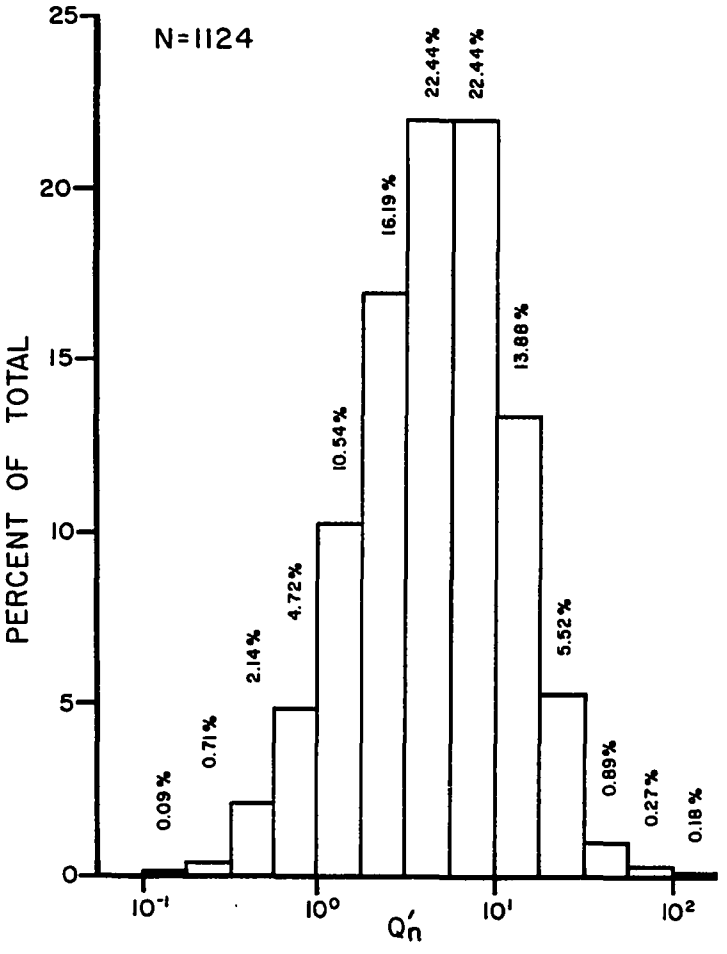

Figure 2.8 Histogram of Q'_n values of oceanic basalts and diorites greater than 5 m.y. of age. The total population consists of 1124 samples taken from the following sources: Cox and Doell (1962) [26/1], Ozima et al. (1968) [6/6], Vacquier (1972) [5/1], Fox and Opdyke (1973) [52/15], Lowrie et al. (1973) [27/4], Lowrie and Hayes (1975) [32/4], Cockerham and Hall (1976) [20/2], Ade-Hall et al. (1976) [36/3], Marshall (1978) [111/7], Petersen (1978) [48/1], Petersen et al. (1978) [22/1], Petersen et al. (1979) [22/3], Kono (1980b) [444/3], Steiner (1981) [271/2], Sager et al. (1982) [2/1]. The numbers in brackets refer to the number of samples and the number of sites from which the Q values were taken. About two thirds of the samples come from DSDP Leg 55 and DSDP Leg 61.

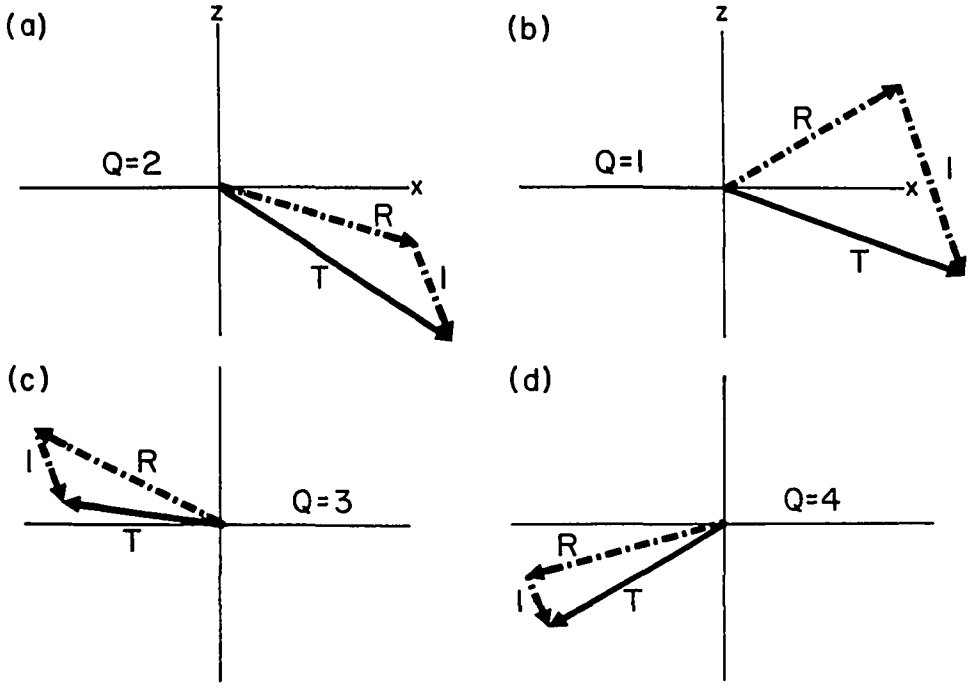

Figure 2.9 The effect of induced magnetization on the direction of the total magnetization vector. Induced (I), remanent (R), and total (T) magnetization vectors are shown for four cases: (a) a normally magnetized seamount formed north of the equator, (b) a normally magnetized seamount formed south of the equator, (c) a reversely magnetized seamount formed north of the equator, and (d) a reversely magnetized seamount formed south of the equator. In each case it is assumed that the seamount has undergone northward displacement since the remanent vector was aquired. A different Koenigsberger ratio (Q) is assumed for each case.

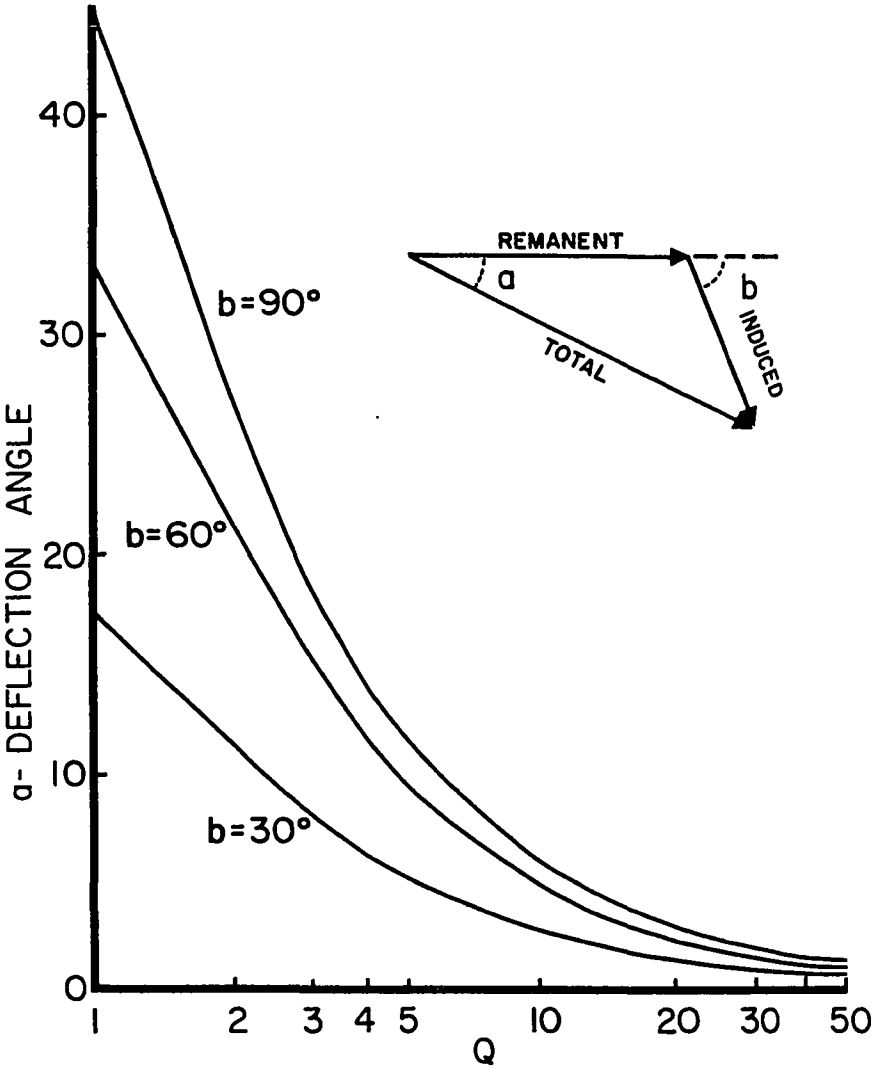

Figure 2.10 The deflection of the total magnetization vector by an induced vector making various angles with the remanent vector. The deflection of the total magnetization vector from the remanent vector depends on the angle between the remanent and induced vectors and the Koenigsberger ratio, Q. Deflection curves are shown for angles of 90°, 60°, and 30° between the remanent and induced magnetization vectors.

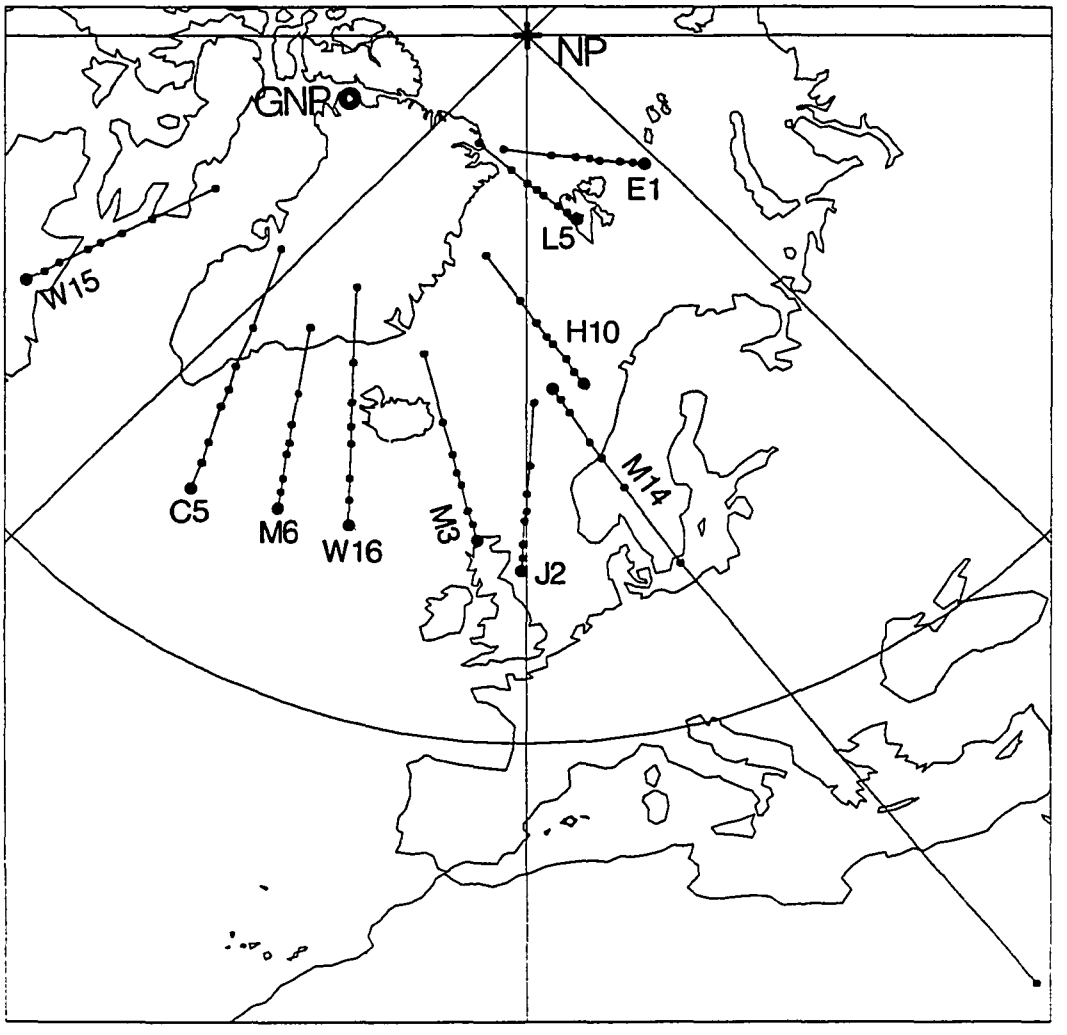

Figure 2.11 Movement of seamount VGPs with increasing Koenigsberger (Q) values. The large dots are the VGPs of ten seamounts from Chapter 4. In each case this VGP is assumed to be the result of magnetization that is entirely remanent. The smaller dots connected by a line to each VGP are the positions of the VGP if Q values of 20, 10, 5, 4, 3, 2, and 1 are assumed. Q decreases moving along the line away from the large dot. GNP is the geomagnetic north pole. All of the seamounts, except for M14, are normally magnetized.

Figure 2.12 Movement of VGPs with increasing Koenigsberger ratio (Q) values. As in Figure 2.11, the large dot is the VGP of each of ten seamounts from Chapter 4. In this figure each of those VGPs is assumed to be affected by a certain amount of induced magnetization; and, the small dots are the position of the remanent VGP assuming that the orignal VGP has the given Q value. Once again the small dots represent Q values of 20, 10, 5, 4, 3, 2, and 1. The displacement of the two VGPs increases with decreasing Q. For example, if the true Q value of the magnetization which produced the VGP shown by each large dot is 1, then the remanent magnetization VGP will be the most distant dot on the line connected to the large dot. All of the seamounts are normally magnetized except for M14.

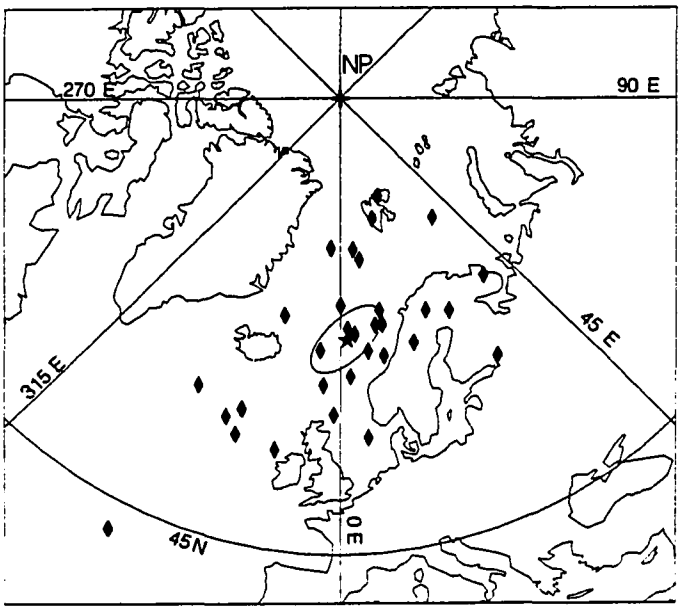

a

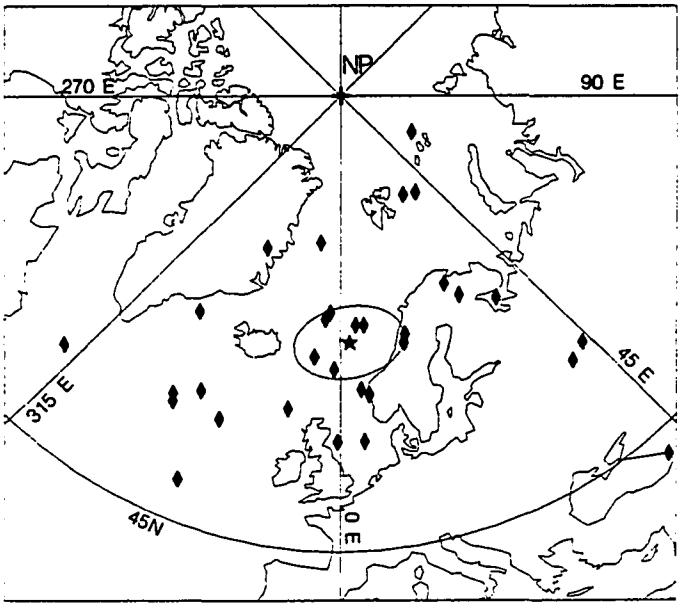

b

Figure 2.13 Pacific seamount VGPs calculated with constant offset and planar regionals. The diamonds in (a) show VGPs calculated with a constant offset regional and in (b) show the planar regional VGPs. The star in each case is the average position and the ellipse is the 95% confidence region, both calculated by Bingham statistics.

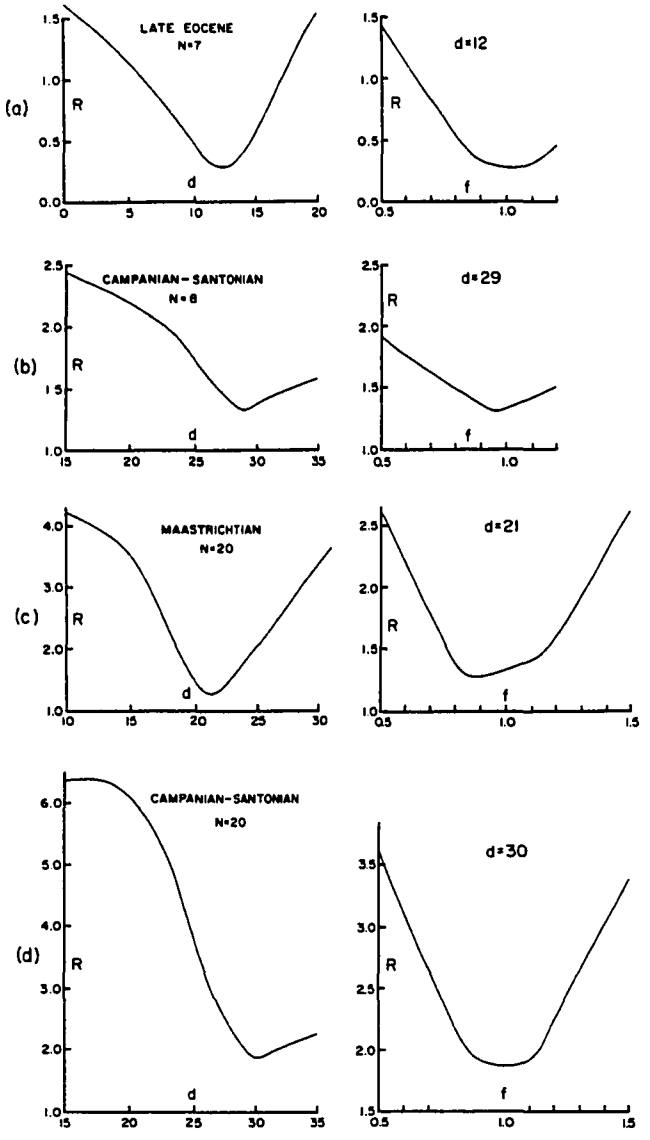

Figure 2.14 RMS residuals for the test of the demagnetization effect. The graphs in the left column show the variation of the RMS residual of the inclination data with different amounts of northward drift, d, whereas the graphs in the right column show the variation of the RMS residual at the best value of d for various values of f, the demagnetization factor. Row (a) is the results of seven seamounts of Late Eocene age, (b), the results of eight seamounts ranging from Campanian to Santonian age, (c), the results of the test using 20 seamounts of approximately Maastrichtian age, and (d), the results of 20 seamounts of approximately Campanian to Santonian age.

CHAPTER 3: MAGNETIC FIELD VARIATIONS AND CORRECTIONS

In Chapter 2 the procedure by which a paleomagnetic pole can be calculated from the shape and magnetic anomaly of a seamount was described. It was assumed that good contour maps of the seamount's bathymetry and magnetic anomaly are available, but no mention was made of the procedure of producing such maps. Before paleomagnetic modeling of a seamount can begin, three tasks must be performed: the seamount must be surveyed and its bathymetry and magnetic anomaly contoured. Space limitations do not allow this study to delve too deeply into the details of obtaining geophysical data at sea and the contouring of bathymetry, although seamount surveying is briefly discussed in Appendix B. However, because of the broad spectrum of fluctuations that occur in the geomagnetic field, marine magnetic survey data is often difficult to contour. Thus it is appropriate to discuss these variations and the steps that can be taken to remove them from the survey data.

Magnetic field measurements at sea are usually made with a proton precession magnetometer towed a few hundred meters behind the ship to escape the magnetic field of the vessel. Generally, such magnetometers have a sensitivity of about one nanoTesla (Telford et al., 1976), but because of the difficulties of precise navigation in the open ocean and the imperfect removal of geomagnetic field variations from the data, the mean magnetic track-crossing error of most seamount surveys is much

larger. Fortunately, the paleomagnetic analysis of seamounts is not particularly demanding of the magnetic data and a mean crossing error on the order of 25 nT. is acceptable; although, one would naturally desire to reduce this error as much as possible.

3.1 THE GEOMAGNETIC FIELD AND ITS VARIATIONS

The geomagnetic field is a dynamic entity that is constantly changing due to myriad sources within the Earth and in space. It can be divided into three basic parts: the primary (core generated) field, the field caused by crustal anomalies, and the field arising from ionospheric and magnetospheric currents. The crustal source field is the quantity of paleomagnetic interest. Although it remains relatively constant, it must be separated from the core field and the external field which are constantly in a state of flux. Figure 3.1 shows the broad spectrum of variations that perturb the geomagnetic field. Many of these variations have effects that must be removed from marine magnetic data in order to allow contouring and interpretation. A brief discussion of these variations and their effects on magnetic survey data is given in the following two sections.

3.1.1 THE PRIMARY FIELD AND SECULAR VARIATION

Most of the geomagnetic field is generated by a dynamo-like mechanism in the Earth's core. It is called the primary or main field and is described mathematically by a spherical harmonic model called the International Geomagnetic Reference Field. The IGRF is convenient because it allows the main field to be subtracted out of magnetic measurements leaving only the anomalies due to crustal sources and external sources. About 90% of the geomagnetic field at the Earth's surface closely resembles a terrestrially centered dipole tilted 11.5^{o} away from the rotation axis (Vestine, 1967). Much of the rest of the field is in the form of non-dipole fields that also have their origin in the core. These non-dipole fields are usually seen as broad centers, thousands of kilometers across, that either augument or detract from the dipole field. Neither the dipole nor non-dipole fields are constant; rather, they undergo slow changes called secular variation. The causes of secular variation remain the source of much speculation, but conceptually the variation can be envisioned in three parts: changes in the strength of the central dipole, changes in the orientation of the dipole axis, and changes in the strength and direction of the non-dipole field (McElhinny, 1973). Because the characteristic periods of these variations are on the order of hundreds to thousands of years, their effect on a seamount survey done over a period of days will be negligible. However, if one wishes to combine magnetic data collected at different times, secular variation must be

taken into account. The yearly change in geomagnetic field intensity can be as high as 120 nT. in some locales. In the Pacific, the change is not nearly so large, amounting to about 20 to 40 nT./yr. (Chapman and Bartels, 1940). Nonetheless, these changes can be troublesome when combining data obtained over several years' time.

The IGRF includes secular change coefficients so that data taken in different years may be compared (Vestine, 1967). However, in practice most magnetic track crossings taken on different cruises show errors as a result of several problems. First, the IGRF is only a mathematical model, constructed of a limited number of coefficients calculated from incomplete data, and thus its representation of the secular change is imperfect. Consequently, two coincident magnetic tracks measured a few years apart and reduced to the same IGRF may not have identical values. Second, each time the IGRF is recalculated (usually once per decade), its coeffiecients are changed by the utilization of new and different data. As a result, matching magnetic tracks reduced to two different IGRFs may not be identical. A partial solution to this problem is a new, long-term IGRF derived from Magsat and magnetic obervatory data by Peddie and Fabiano (1982). Third, some of the track crossing error comes from magnetic field changes caused by external sources (discussed in Section 3.1.2).

Both of the errors caused by IGRF imperfections usually manifest themselves as a more or less constant offset in a small survey area. The first type of error is usually relatively small, but the difference in a magnetic measurement resulting from the use of two different IGRFs can amount to several hundred nanoTeslas. However, because of the

third of these problems, one cannot simply go back to the original total field data and reduce it to the same IGRF. Instead, the most practical solution to these problems, at least for a small survey area, is the following. The data must first be corrected for short period variations caused by external field sources as explained in Section 3.2. One track or a group of tracks is selected as a datum and a constant value is added to or subtracted from each of the rest of the tracks to make it agree with the datum tracks. In most cases, one has a seamount survey similar to those pictured in Figure B.1 (Appendix B) combined with several previous tracks across the seamount. It is usually a simple matter to determine the offset between the newer and older data. However, sometimes if the navigation of an older track is poor, it may be difficult to merge it with the newer data. In some instances, one may have several tracks that cross a seamount, but do not intersect. Unless there is a cross-track that intersects most of the tracks, one should be wary of using the data to calculate a magnetization direction for the seamount. The reason for this caution is the fact that differences in the base level of each track, as a result of IGRF errors or magnetic field variations, will cause distortion of the shape of the highs and lows of the magnetic anomaly resulting in the calculation of an erroneous magnetization direction.

3.1.2 THE EXTERNAL MAGNETIC FIELD AND ITS VARIATIONS

Only about 1% of the geomagnetic field is attributable to sources outside the Earth, but that 1% is very important because its rapid fluctuations are a nuisiance for magnetic surveys. In order to properly contour marine magnetic data, most of these fluctuations should be removed from the observed field values. For this purpose it is necessary to know the characteristic periods and amplitudes, at the Earth's surface, of the different types of variations.

The primary sources of the external magnetic field are electric currents in the ionosphere and magnetosphere. These currents are constantly varying because of stimuli provided by solar radiation, the solar wind, the interplanetary magnetic field, and their complex interactions. The following discussion deals primarily with those variations that might appear on marine magnetic data obtained at mid and low latitudes. Other variations, seen only in the magnetically active polar and auroral zones, are not mentioned.

Looking at Figure 3.1, the shortest period fluctuations are atmospherics and pulsations. Atmospherics arise principally from lightning strokes in the lower atmosphere (Campbell, 1967). Because of their short periods and low amplitudes, they are not generally measurable with proton precession magnetometers; although, they are a contributor to the background noise seen on magnetograms. Pulsations are typically small fluctuations of several nanoTeslas amplitude and several seconds to several minutes duration (Chapman and Bartels, 1940). Campbell (1967) gives a good review of their characteristics

and causes. Pulsations can appear to be very coherent oscillations or impulsive fluctuations with no apparent periodicity. Their occurance is often correlated with high solar activity and they may occur singly or in groups. The origin of many pulsations appears to be trapped, resonating hydromagnetic waves in the magnetosphere. Except for the largest pulsations, that may be seen on magnetic records at widely separated stations, the station-to-station correlation of most pulsations is poor over distances more than about 1000 km. Pulsations are generally divided by their periods into five categories, PC1 through PC5. PC1, PC2, and PC3 pulsations have short periods (0.2 to 45 sec.) and amplitudes generally less than 1 nT. PC4 pulsations have periods between 45 to 150 sec. and amplitudes averaging less than 10 nT. The PC5 are large pulsations with periods up to 600 sec. and amplitudes that can be as great as 60 to 70 nT.

Four different fluctuations of importance have durations in the neighborhood of one to several hours. They are DP1 and DP2 disturbances, solar flare effects, and slow oscillations. DP1 and DP2 are disturbances of the polar ionosphere whose magnetic field effects often reach to low and middle latitudes. The DP1 phenomena originates in the auroral zone as a result of plasma movement into the polar regions brought about by magnetospheric instabilities that are often triggered by sudden changes in the interplanetary magnetic field (Mayaud, 1978). DP1 events, also called "bays" or substorms, usually last from one to several hours and show up on magnetic records as a positive or negative departure from normal undisturbed field values followed by a subsequent recovery (Chapman and Bartels, 1940). They

attain their maximum intensities (200 to 300 nT.) in the auroral zone at midnight; but, their effects, though widespread, fall off rapidly with decreasing latitude (Mayaud, 1978). At mid to low latitudes the magnetic excursion associated with substorms is usually only about 15 to 25 nT. (Mayaud, 1978).

DP2 variations are caused by ionospheric currents across the polar region. Their periods typically range from minutes to hours. The amplitudes of these variations are small at most latitudes, usually amounting to less than 10 nT.; however, in the auroral zone and at the dip equator their effects can be much larger, 50 nT. or more, because of enhancement by the electrojet currents (Mayaud, 1978).

Solar flare effects, called sfe or "crochets", typically appear in a magnetic record as a sudden departure (usually an increase) from normal undisturbed field values followed by a gradual return to normal over a half to several hours (Chapman and Bartels, 1940). The phenomenon is caused by a sudden increase in the conductivity of the ionosphere due to increased ionization by solar flare X-rays. For many years they were believed to be the result of an enhancement of the Sq diurnal variation currents (discussed below), but are now thought to arise from a separate current system in the lower ionosphere (Matsushita, 1967b). Like the Sq daily variation, the sfe has its maximum intensity near the geomagnetic equator (Mayaud, 1978) where it typically has amplitudes of tens of nanoTeslas (Matsushita, 1967b). Sfe are usually correlatable from one station to another over the entire daylight hemisphere (Mayaud, 1978).

Slow oscillations are smooth rises and dips of the base level of a magnetogram over the period of several hours. Unless magnetograms from several locations are compared, their effects are usually so gradual as to escape notice. These variations are seen worldwide and commonly have amplitudes of 10 to 20 nT. Their source appears to be fluctuations in the equatorial ring current (Mayaud, 1978).

Figure 3.2 shows magnetic field values for 29 days in August and September 1979 at Christmas Island in the Pacific Ocean. The most noticeable feature of the magnetic values are their large, regular daily variation. Diurnal variations such as these are very troublesome for magnetic surveys because they generally have large amplitudes as well as wavelengths that are very similar to those of crustal anomalies measured by a towed magnetometer at common ship speeds. There are three basic components of the low to mid latitude daily variations: solar quiet day variations (Sq), lunar semi-diurnal variations (L), and equatorial electrojet variations.

The Sq and L variations arise from current dynamos in the ionosphere (Matsushita, 1967a). Solar X-rays cause ionization of the atmosphere in the region of 90 to 130 km. and solar heating of the same region causes thermal convection. The convection and solar tidal movements within the ionosphere in the presence of the geomagnetic field induce two giant current vortices, one either side of the equator (Matsushita, 1967a). The position of these vortices remains approximately beneath the sun, about 30^{o} from the equator on the average, and their intensities are relatively constant (Mayaud, 1978).

On a magnetically quiet day, the Sq field causes the magnetic field to rise smoothly from night values beginning about sunrise (about 0600 local solar time [LST]) to a maximum between 1000 and 1400 LST (usually at local noon) and then decay back to night values at sunset (about 1800 LST)(Rastogi and Iyer, 1976). Figure 3.3 shows average Sq variations for several Pacific island magnetic stations. The daily range of Sq varies with latitude as shown in Figure 3.4. The northward component of the Sq reaches maximum at the mean equator (halfway between the geographic and geomagnetic equators). To the north and south the range of the northward component decreases until it changes sign at about 30° to 35° from the equator, approximately beneath the Sq current vortices (Onwumechilli, 1967). The vertical component of the Sq has a smaller maximum range. It is zero at the equator and reaches a maximum of about 20 nT. at 10° from the equator (Onwumechilli, 1967). The eastward component of the Sq diurnal variation is negligible.

As seen in Figure 3.2, the daily range of Sq can vary greatly from day to day. This variation is complex and has many causes. Some of these are day-to-day fluctuations in the ionospheric dynamo electric fields (Schlapp, 1973), lunar semi-diurnal variation effects (Osbourne, 1966), equatorial electrojet and counter-electrojet effects (Mayaud, 1977), and solar activity perturbations (Matsushita, 1967a). Solar activity also has an effect on the long term amplitude of the Sq daily range. It increases linearly with sunspot number (Matsushita, 1967a; Rastogi and Iyer, 1976) and can amount to approximately 10 to 40 nT. difference over the course of a solar cycle (Bhargava and Yacob, 1969).

The Sq variation also changes with the seasons. Its maximum daily range occurs during the equinoctial months (March, April, September, October) whereas the average variation is somewhat lower during the solstitial months (May to August, November to February)(Matsushita, 1967a).

As seen in Figure 3.4, there is a sharp intensification of the northward component of the Sq variation at the dip equator. This intensification is caused by the equatorial electrojet. The electrojet is an intense ionospheric current about 600 km. in width (Yacob, 1966) that is usually located at or very near the dip equator (Onwumechilli, 1967). Figure 3.5 shows the latitude of the electrojet at various longitudes around the globe. The electrojet is generated by a Hall current polarization of the ionosphere caused by the crossed electric and magnetic fields in the upper atmosphere. At most latitudes the Hall polarization can leak away along the geomagnetic field lines, but at the dip equator the polarization is trapped because the magnetic field lines are horizontal (Onwumechilli, 1967). The electrojet current is at the same altitude as the Sq currents and is considered as an intensification of them rather than a separate current system (Hutton, 1967).

The electrojet variation can be troublesome for magnetic surveys near the dip equator. It is very similar to the normal Sq diurnal variation except that its effects are localized to the region surrounding the dip equator. Because of its influence, the amount of diurnal variation near the dip equator can be doubled (Onwumechilli, 1967). Not only does the electrojet greatly increase the normal quiet

day variation, but it also amplifies the lunar semi-diurnal variation (Mayaud, 1977), geomagnetic storms, bays, and solar flare effects (Rastogi et al., 1966; Mayaud, 1978). Consequently, wild variations of the geomagnetic field are not uncommon near the dip equator, and the marine scientist who wishes to conduct a magnetic survey in this region must take particular care to record and remove these variations.

The lunar semi-diurnal variation, L, arises in a manner similar to the Sq variation. High and low pressure systems in the upper atmosphere are created by the Moon's tidal forces and their resultant air motions give rise to electric currents that produce a perturbational magnetic field (Matsushita, 1967a). The L current system is similar to the Sq system except that it usually consists of two to eight vortices (Chapman and Bartels, 1940). The L variation has a period of 12.5 hours (Arora and Sastri, 1977), with an amplitude that is usually much smaller than the Sq variation, rarely amounting to more than a few nanoTeslas (Matsushita, 1967a). However, as mentioned above, the L variation is sometimes greatly amplified in the region of the dip equator owing to the high ionospheric conductivity found there (Onwumechilli, 1967). At such times the L variation can rival the amplitude of the Sq variation (Chapman and Raja Rao, 1965; Onwumechilli, 1967).

Magnetic storms typically affect the geomagnetic field for a period of several days. These events are global in nature and affect magnetic recordings the world over. Although magnetic storms are variable in duration, amplitude, and form, they generally follow a characteristic morphology that was delineated by Chapman and Bartels

(1940). The storm usually (but not always) begins with a sudden enhancement of the magnetic field over the period of several minutes. The sharp increase is called a sudden storm commencement or ssc. It is often followed by a period of one to several hours during which the field remains elevated many tens of nanoTeslas above its pre-storm level. This period during which the field is enhanced is called the initial phase. It is followed by a drastic decrease of the field below its pre-storm level that lasts for several hours to a day or more, and is called the main phase. For small storms, the decrease may be less than 100 nT., but great storms may lower the magnetic field by more than 1000 nT. The main phase is followed by a recovery phase during which the magnetic field slowly regains its pre-storm level over one or more days' time. The magnetic storm is a time of profound disruption of the normal ionospheric current systems that results in large, irregular, unpredictable variations. The equatorial magnetic field is particularly susceptible to wild storm variations because of the enhanced conductivity in the dip equatorial inonsphere (Rastogi et al., 1966).

A small storm is seen in the magnetic values of August 29 - 30, 1979 at Christmas Island (Figure 3.2). No obvious ssc occurs, but the magnetic field decreases by about 100 nT. from 0000 to 1200 hours UT on the 29th. No Sq peak is seen on August 29 - 30. Instead, several large irregular fluctuations are recorded. The normal Sq variation returns after a lapse of a little more than a day, on August 30 - 31.

Magnetic storms are caused by the interaction of the magnetosphere and solar plasma ejected from intense solar flares. The initial phase

begins as a plasma shock wave, produced in the solar wind by the flare, strikes the magnetosphere. The ssc and initial phase arise mainly from compression of the magnetospheric cavity by the shock wave (Akasofu and Chapman, 1967), whereas the main phase is caused principally by an enhancement of the equatorial ring current by the injection of solar plasma from the magnetotail (Akasofu and Chapman, 1967; Piddington, 1967).

Because they are intimately related to solar activity, magnetic storms are most common in high sunspot number years (Chapman and Bartels, 1940). Not only are storms more common in these years, but they also tend to be larger and longer (Matsushita, 1967b). Additionally, there appears to be a tendency for storm effects to recur at 27 day intervals (Chapman and Bartels, 1940). The recurrence is probably caused by the rotation of the sun returning an active, plasma emitting region to the Earth-facing side of the sun.

Several long period variations of the magnetic field have been found. Such variations bring about base level differences in magnetic survey data obtained at different times. A semi-annual variation, probably caused by the ring current, imparts a modulation of usually less than 10 nT. to the magnetic field (Currie, 1966). An annual variation, caused by seasonal changes in the Sq base level, accounts for a somewhat smaller modulation (Currie, 1976). The solar cycle also gives rise to a variation of the Sq base level. This 11 year variation can have an amplitude on the order of 60 - 70 nT. in the equatorial zone and is sympathetic with sunspot number (Rastogi and Iyer, 1976).

Additionally, another solar cycle effect is a 5.5 year harmonic which may cause a variation of about 10 to 15 nT. (Currie, 1966).

3.2 CORRECTIONS FOR GEOMAGNETIC VARIATIONS

Considering all of the possible magnetic field variations reviewed in the preceeding section, their range of amplitudes, and their unpredictability, the correction of magnetic survey data must seem an impossible task. It is not. In mid and low latitudes only two of these variations are of primary importance: diurnal variations and magnetic storms. The former is somewhat predictable and relatively easily measured, so its removal from raw magnetic data is not too difficult. The latter is unpredictable and often characterized by wild geomagnetic fluctuations. It presents problems best solved by refraining from making magnetic surveys during magnetic storms.

Although it is not always possible to avoid magnetic storms, several measures can be taken to detect their presence. Aboard ship the magnetometer output can be monitored for symptoms of the beginning of a storm. As mentioned in the previous section, storms usually begin with an ssc, a sharp rise of many tens of nanoTeslas in a few minutes, followed after several hours by a precipitous drop in the intensity of the magnetic field. Even though it is not always possible to distinguish these features from the variations caused by crustal magnetization, their characteristic signature is usually distinctive. Another method of avoiding magnetic storms is to have storm warnings

radioed to the ship. The Hawaii Institute of Geophysics communications center routinely receives daily radio propagation and geomagnetic activity reports from the Space Environmental Services Center at Boulder, Colorado. Additionally, information about the current state of the magnetic field can be had from the Honolulu Magnetic Observatory at Ewa Beach, Hawaii.

There are a number of ways to remove field fluctuations from marine magnetic data. Basically they differ by the manner that the variations are determined. Once the fluctuations are measured, they can be subtracted from the observed total magnetic field values. The following discussion briefly reviews some of these methods, found to be most useful for seamount surveys, in decreasing order of efficiency and reliability.

Perhaps the best method of correcting magnetic surveys is to have one or more nearby base station magnetometers constantly recording the magnetic field during the time of the survey operations. Roden and Mason (1964) show that a good estimate of the magnetic variation at a survey site can be made by using the weighted average of two base station magnetometers in the vicinity. Similarly, a single base station may be used for the same purpose if its diurnal range is scaled to the latitude of the survey site, its time is shifted to correspond to local solar time at the survey site, and it is not too distant from the survey site.

As a very accurate recording of the geomagnetic field behavior can be made at a base station, in principle practically all of the fluctuations could be removed from survey data. However, the use of

base stations for correcting marine survey data has several drawbacks. Islands suitable for a base station are not always close to the area of the survey and establishing base stations on remote islands can be prohibitively expensive. Also, the accuracy of the corrections determined from the base station data suffers with increasing distance from the survey site. Although Riddihough (1971) found excellent station-to-station correlation (0.91 for freqencies greater than 10 min.) over a range of about 200 km., Mason (1963) found that the correlation over larger distances could be much lower. Mason's study only examined periods limited to 3 to 60 min. from several island stations in the Pacific and hence its comparison to Riddihough's study of a broader spectrum of magnetic fluctuations in Ireland may be a bit tenuous. However, Osbourne (1966) and Schlapp (1968) both addressed the station-to-station correlation of Sq and obtained results similar to those of Mason. Schlapp found that the correlation coefficient of Sq fell to 0.5 in about 1500 km. latitudinally and 2000 km. longitudinally and Osbourne discovered the correlation to be poor if a station was under one of the Sq current foci (usually in the neighborhood of 21^{o} to 33^{o} from the equator).

A particularly troublesome problem with island and coastal base stations is a perturbation called the "island effect". It is caused by the deflection of electric currents, induced in the ocean by magnetic field variations, around non-conducting structures such as islands (Roden, 1964; Lines and Jones, 1973). This effect can cause a change in the amplitude, phase, and shape of the measured fluctuations (Lines

and Jones, 1973; Jones, 1974) and can be detected several hundred kilometers inland from the ocean (Bennett and Lilly, 1973). Because the island effect primarily affects the vertical component of magnetic field variations (Price, 1967; Hobbs and Dawes, 1979), its perturbation of the Sq variation will be least near the equator. Hence, the best island base station would be located at a low latitude (to minimize the island effect), but at some distance from the dip equator to steer clear of the electrojet enhancement of magnetic field disturbances.

Often one does not have base station data to use in making magnetic survey corrections. Several courses of action are open in such instances. If the survey data is plentiful, night time values may be compared with daytime values. Figure 3.3 shows that magnetic measurements made at night do not vary much on the average. Consequently, the night values can be used as a sort of base level. The difference in the magnetic field measured at track crossings where day values (0600 - 1800 LST) cross night values (1800 - 0600 LST) can be assumed to be the result of diurnal variation providing that the survey navigation is good. If these differences are plotted on a graph against the day times corresponding to the track crossings, a curve showing the daily variation can be drawn. For surveys in which only a few such crossings are available, the crossing error can be used along with an average daily range curve, such as those in Figure 3.3, to make an estimate of the diurnal variation. The average curve is simply scaled so that it best matches the plotted crossing differences. This idealized version of the diurnal variation may then be used to correct magnetic survey measurements.

Occasionally no track crossing differences will be suitable to help constrain the scaling of the ideal daily range curve. In such an instance one might be tempted not to make any corrections at all. However, if the expected diurnal range is fairly large, then it may have a rather deletereous effect on the paleomagnetic information derived from that survey. Even if a seamount's magnetic anomaly is relatively large, diurnal corrections are still desirable. In Figure 2.6 it is seen that even seamount anomalies with deep minima often have flanking maxima of much lower amplitude. These lower amplitude anomaly features will be distorted by the diurnal variation and perhaps bias the magnetization calculation. If no track crossing information can be used to establish a daily variation curve, then one of the average diurnal variation curves can be scaled to the proper amplitude using the daily range versus latitude curves in Figure 3.4 and centered with its maximum at local noon. At best this method provides only an educated guess of the true diurnal variation, but even so it should still remove a sizeable percentage of the variation.

These methods of estimating a diurnal variation curve should be used with care. During periods of geomagnetic quiet, they may work well enough. However, if the geomagnetic field is disturbed there may be many fluctuations that cannot be predicted by such procedures. This will be particularly true near the dip equator and auroral zones where large, unpredictable variations are most common. It is always a good idea to obtain the magnetic records of one of closest of the world-wide network of magnetic observatories for the days during which the

surveying was done and check for magnetic storms or other large perturbations.

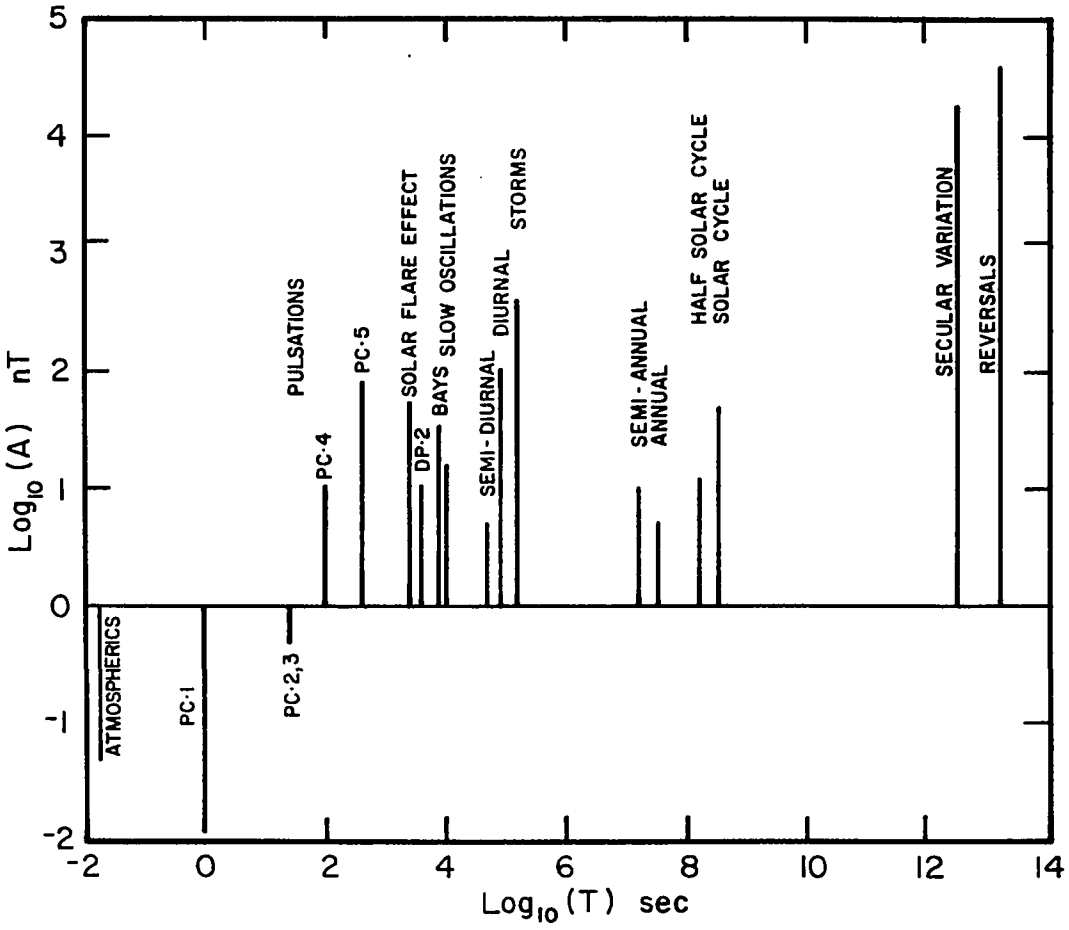

Figure 3.1 Typical periods and amplitudes of geomagnetic variations. Along the ordinate are plotted the logarithms of the variation amplitudes and along the abcissa are plotted the logarithms of the variation periods. Data compiled from various sources.

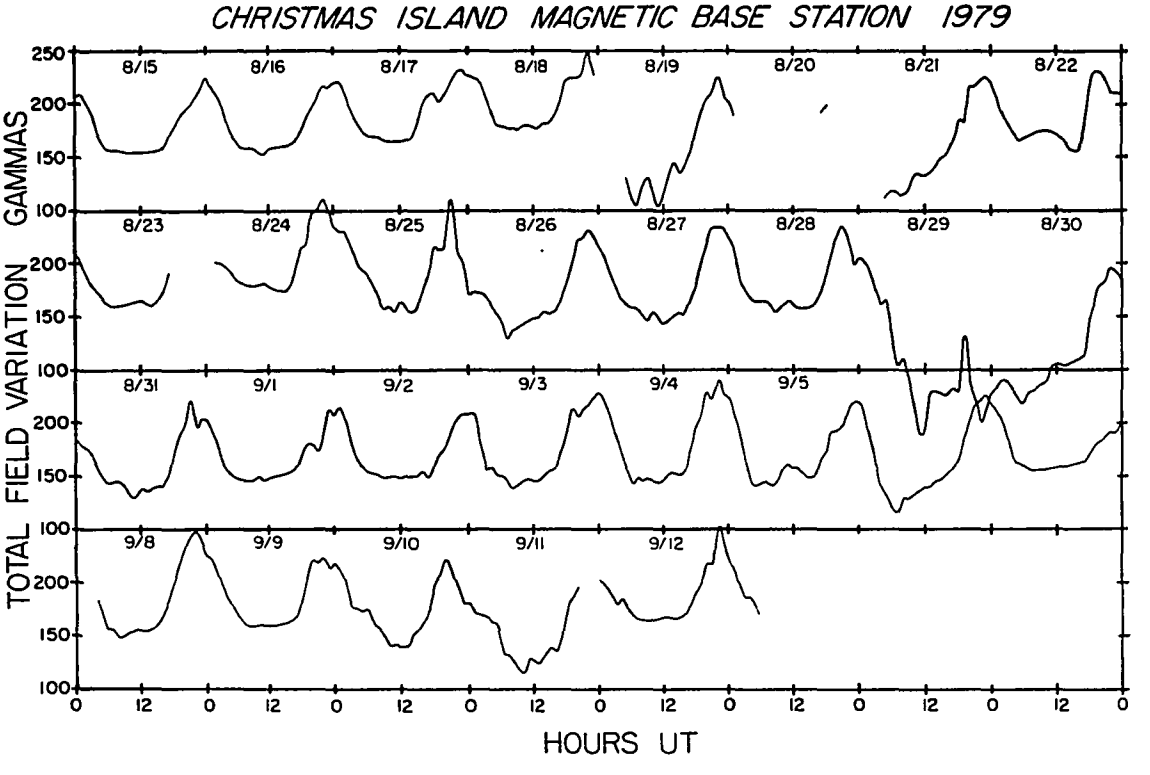

Figure 3.2 Magnetic base station records from Christmas Island in the Pacific Ocean (1° 59.2′ N, 157° 28.8′ W) obtained from August 15 to September 12, 1979. Total magnetic field measurements were made using a proton precession magnetometer to allow corrections to be made to magnetic survey data collected in the Line Islands. Gaps in the recording are due to power outages. The variations shown are from a base level of 33,500 nT.

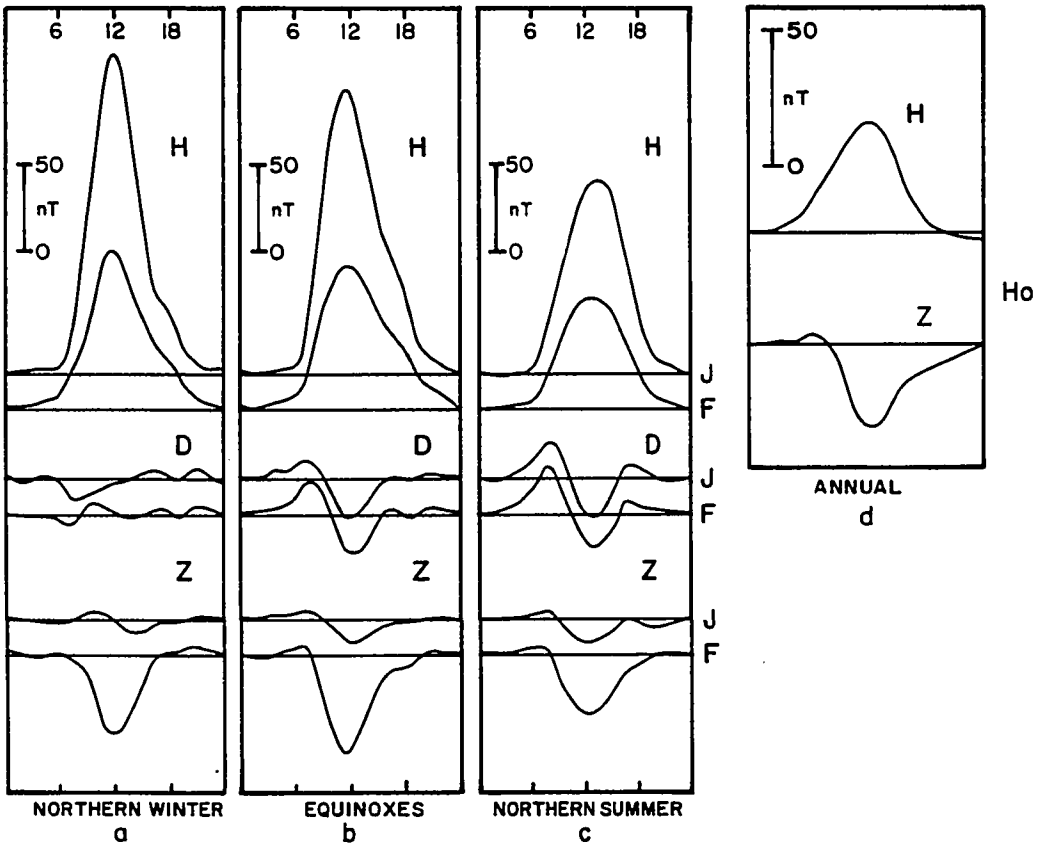

Figure 3.3 Average diurnal variation curves for three Pacific islands. Parts (a), (b), (c) show variations in the H, D, and Z components at Jarvis (J) and Fanning (F) islands for northern winter, equinoxes, and northern summer quiet days during the IGY (from Mason, 1963). Part (d) shows the annual average variation of H and Z at Honolulu for quiet days during the IGY (from Chapman and Raja Rao, 1965).

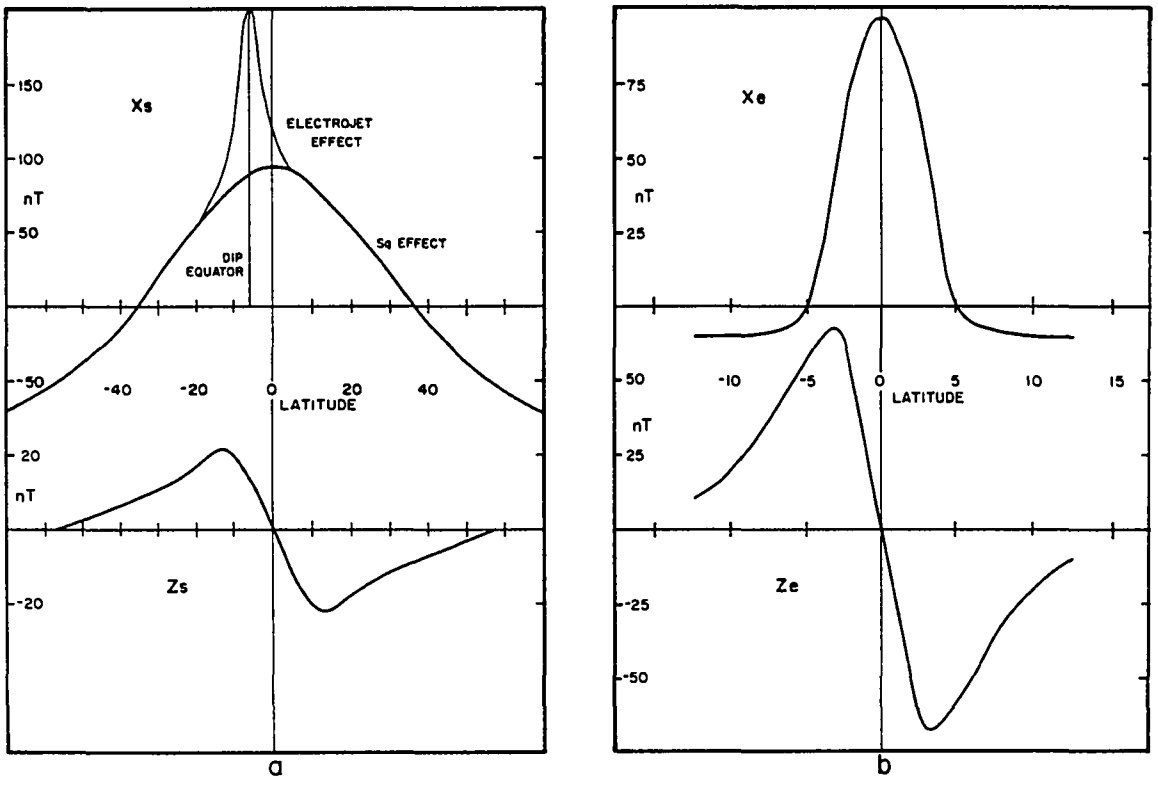

Figure 3.4 Sq and equatorial electrojet variation amplitude changes with latitude. Part (a) is the average quiet day Sq variation to be expected in the H (top) and Z (bottom) components at different latitudes. The electrojet H variation is shown superimposed on the Sq variation. It is centered on the dip equator, shown here for 76° W. Part (b) is the average quiet day electrojet variation to be expected in the H (top) and Z (bottom) components. In part (a) the abcissa is mean latitude (halfway between geographic and geomagnetic) whereas the abcissa in part (b) is geomagnetic latitude. (after Onwumechilli, 1967).

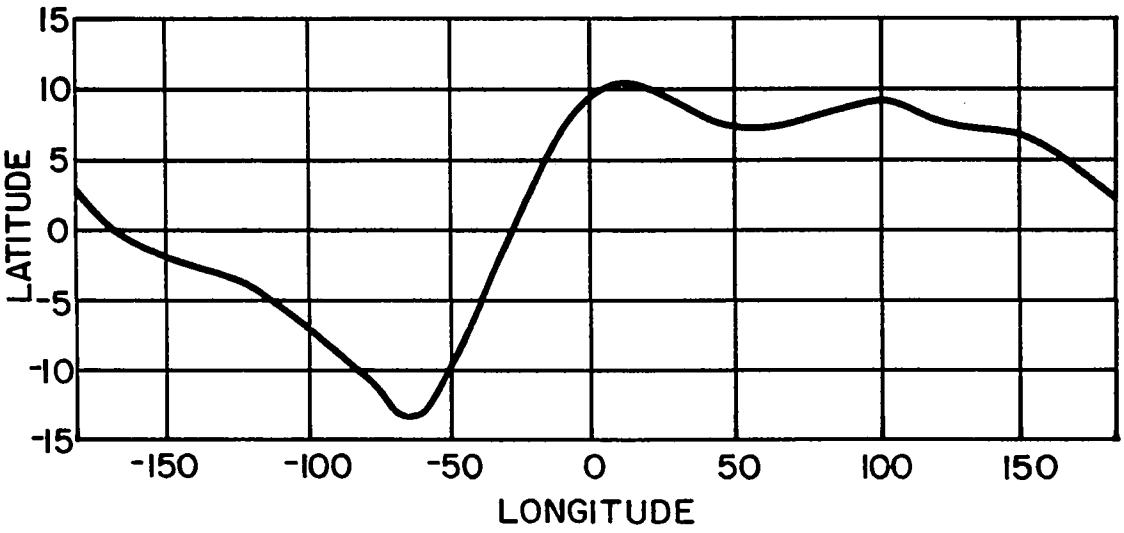

Figure 3.5 Equatorial electrojet positions. The average latitude of the center of the electrojet current is shown as observed by the POGO satellite. (after Cain and Sweeney, 1973).

CHAPTER 4: DATA

It would be inappropriate to examine the tectonic implications of the seamount paleomagnetic data for the Pacific without also considering other available types of paleomagnetic data: DSDP paleocolatitudes, paleoinclinations from magnetic lineation skewness, and DSDP equator transits. Consequently, a systematic search was conducted to find reliable paleomagnetic data to complement the results from the seamounts modeled paleomagnetically in this study. All of these types of data are used here for two primary purposes, to determine the APWP of the Pacific plate and to explain the origins of seamounts and seamount chains. All four types of data can be used to determine the historical motion of the Pacific by plotting its APWP. This polar curve can be used to find the past latitudes and orientations of the plate as well as looking for relative tectonic motions between various provinces of the Pacific. Moreover, the seamount paleomagnetic data is particularly well suited for investigating the sequence of volcanism in a seamount chain or province and giving an insight to the source mechanism of the volcanism.

Of the four types of data presented here, the most abundant are the seamount paleopoles that are the primary interest of this study. They are the only fully oriented paleomagnetic data, constraining both the latitude and longitude of the paleomagnetic pole, available

for the Cretaceous and early Tertiary. The other data types only constrain the distance to the paleomagnetic pole. DSDP paleolatitudes and paleoinclinations from lineation skewness are two different methods of measuring the magnetization of the seafloor. In contrast, DSDP equatorial transits have nothing to do with paleomagnetism. Instead, they are sedimentological determinations of the time that a DSDP site crossed the equator. Given certain assumptions. they can be treated the same as paleomagnetic paleocolatitudes.

The range of time that is of primary interest in this study is from the Early Cretaceous through the Eocene. Although the Pacific contains seafloor of Jurassic age (Hilde et al., 1977), Pacific paleomagnetic data of that age is practically non-existant. On the other end of this range, a detailed APWP is being delineated by several workers using orented piston core paleomagnetic data (F. Theyer and D. Wilson, personal communiction. 1982). They have much data in the interval from the Oligocene to the present, a time for which reliable seamount paleomagnetic data is sparse. Most of the seamount paleopoles appear to be Cretaceous or early Tertiary in age and thus this study focuses primarily the the paleomagnetic data of that age.

In the sections that follow, each of these data types will be discussed briefly. Following these discussions are tables containing the seamount and other paleomagnetic data that is used to make tectonic interpretations in Chapter 5. The last part of this chapter contains brief descriptions of each of the newly analyzed seamounts and their models, providing future workers in this field both a guide

to seamount modeling techniques and a record of the steps taken to obtain the new seamount paleopoles.

4.1 SEAMOUNT PALEOPOLES

The seamounts which have given reliable paleopoles are listed in Table 4.1 with their positions. magnetization parameters. VGPs. and quality parameters. Seventy-six seamount are listed in Table 4.1; 34 of these have models presented here for the first time and three others were modeled in the course of this study but were published previously. For consistency, the VGPs and magnetization parameters of these seamounts have been taken as published. Table 4.2 lists bathymetric modifications and other salient features of the seamount models and Table 4.3 contains the measured and inferred ages available for the seamounts in Table 4.1. In Figure 4.1 the locations of the seamounts in Table 4.1 are shown and in Figure 4.2 their VGPs are plotted. The seamounts and their models that have not been previously published are discussed in Section 4.5.

The bathymetry of each seamount modeled in this study was contoured at 250 m. intervals using ocean bottom depths measured with a 3.5 kHz. or 12.0 kHz. echo-sounder and corrected for the variation of acoustic velocity in sea water using Matthews' (1939) tables. Navigational points on most shiptracks were determined using Doppler

satellite positioning and dead reckoning between fixes. A small amount of data navigated by other means was used in a few surveys.

Magnetic anomalies were generally calculated by subtracting the 1975 IGRF (Barraclough and Fabiano, 1977) from the observed total field values (in one or two surveys the 1965 IGRF was used as the reference field if the principal survey data was collected before 1975). The resulting total field residual anomaly was corrected for diurnal variations as described in Chapter 3 and contoured at 50 nT. or 100 nT. intervals.

The seamount modeling process is described in detail in Appendix C, but a brief recapitulation is as follows. The bathymetric contours of the seamount are approximated by polygons that represent the sides of stacked prisms (Figure 2.5). Most of the seamount models use 250 m. prisms for the upper 1.5 to 2.0 km. of the volcano, and 500 m. prisms below. The magnetic anomaly values to be used in constraining the magnetization are digitized on a grid over the seamount. For most of the seamounts a one nautical mile grid spacing was sufficient to completely describe the magnetic anomaly. The area of the gridded anomaly is made as large as possible, without including areas of the anomaly disturbed by adjacent magnetic bodies, in order to give the best possible constraint to the magnetization parameters. If the magnetic survey data is very sparse, it is digitized only along the shiptracks, instead of in a grid, to minimize any bias that might be caused by contouring.

The seamount model is often modified by removing layers from the top and adding layers to the bottom as discussed in Chapter 2. This

is the most common bathymetric modification of seamount paleomagnetic models. Such modification is usually needed because many seamounts have magnetic anomalies whose wavelength is longer than can be reproduced using the volume of the seamount seen above the ocean bottom. The longer wavelength anomaly can only be the result of a deeper magnetic body, so the seamount is "lowered" by removing some of the top and adding to the bottom (Harrison, 1971; Harrison et al., 1975). Usually the non-magnetic top is attributed to a large percentage of hyaloclastite material within the upper layers of the seamount, whereas the bottom extension may be a part of the seamount hidden by sediments or a magnetic root resulting from intrusions or remagnetization of the crust beneath the seamount (Harrison, 1971). In the course of the modeling of a seamount, the top and bottom layers are adjusted to give the GFR a maximum value and the best model is usually taken to be the one with the highest GFR. This sort of bathymetric modification rarely changes the calculated magnetization significantly; however, it often greatly improves the match between the observed and calculated magnetic anomalies.

The seamounts modeled in this study have had their magnetizations calculated with both a constant-offset regional and a planar regional. As discussed in Chapter 2, the former is preferable, but the latter has been extensively used for published models. In Table 4.1, the seamounts whose magnetizations were calculated with a planar regional are flagged by an asterisk. The listed magnetization parameters for each of these seamounts correspond to the planar regional model,

whereas the magnetization parameters of the unflagged seamounts correspond to a constant-offset regional model.

In order to assist other scientists in future seamount studies, a comprehensive listing of seamounts that have been surveyed or modeled but gave unreliable results is provided in Table 4.4.

4.2 DSDP PALEOCOLATITUDES

Aside from seamount paleopoles, the largest amount of Pacific paleomagnetic data comes from DSDP rotary drill cores. Unlike the seamount paleomagnetic results, such cores are not oriented in azimuth, so only the paleoinclination and polarity of the sample material can be determined. Consequently, only the paleocolatitude of the DSDP site (i.e., its distance from the paleomagnetic pole) can be calculated. The declination of the palemagnetic pole is unknown and thus it must lie on a circle, centered at the drill site, with a radius equal to the paleocolatitude. Twenty-one Cretaceous paleocolatitudes from DSDP drill cores are listed in Table 4.5 and shown in Figure 4.3 (the twenty-second paleocolatitude, GPC3, comes from a piston core). Because this data is to be combined with the seamount paleomagnetic data to constrain the APWP of the Pacific, a discussion of its limitations and the process by which the most reliable data was chosen is in order.

Peirce (1976) discussed several limitations that make it difficult to attain the same accuracy with DSDP paleomagnetic data as might be expected from a land-based study. He cites: (1) errors in the assumption that the drill core is vertical, (2) the disturbance of some of the cored material by the rotary coring process, (3) the sometimes limited amount of material available at any given stratigraphic level in the core, (4) the statistical problems caused by the lack of azimuthal orientation, and (5) the statistical problems caused by an incomplete knowledge of the secular variation recorded by the samples.

Only rarely is the deviation of the drill core from the vertical recorded, but it is usually less than about 5^{o} (Wolejszo et al., 1974). Material disturbed by the coring process can usually be avoided, however, it is not always possible to detect. In fact, it has been suggested that some of the core material that gives a large scatter of inclinations, despite being otherwise magnetically stable, may be the result of such disturbances (Peirce, 1976). The limited amount of core material available within a given stratigraphic section may make it impossible to determine reliable paleolatitudes for some sequences. Thus scientists interpreting paleolatitude data from DSDP material must be wary of relying too heavily on a small amount of data.

Normally, a DSDP paleolatitude is calculated from the mean inclination of the sample magnetizations using the dipole formula, $\tan(Inc) = 2 \tan(Lat)$. However, because there is no constraint on the paleodeclination of the magnetization vector, the average

inclination consistently underestimates the true inclination. The bias stems from the fact that the arithmetic mean is only an approximation of the true inclination of the average magnetization vector (Briden and Ward, 1966; Kono, 1980b; Cox and Gordon, 1983). Cox and Gordon (1983) have derived a correction factor, dependent on latitude, that may be used to obtain a better estimate of the true paleoinclination. All of the paleocolatitudes listed in Table 4.5 have been corrected for this bias; although, in most cases the correction was small because of the low paleolatitudes of the sites.

Kono (1980b) determined that about 30 basalt flows had to be sampled on Suiko Guyot in order to statistically average out secular variation. Only rarely are so many flow units cored in a single DSDP hole. For this reason many paleomagnetic studies of DSDP basalt samples may not be well suited for tectonic study. In Table 4.6, almost all of the rejected DSDP paleoinclination data were basalt studies with too few independent samples. Of the five paleocolatitudes in Table 4.5 calculated from basalts, only the Site 433C (Suiko) study has sampled more than 30 flows. The other four basalt paleocolatitudes were retained because they have more independent samples than most and because they sample the paleomagnetic field of periods in which the available data is scarce.

The secular variation problem is not as severe for most sediment cores and so most of the paleocolatitude data in Table 4.5 is of this type. Because abyssal sedimentation rates are generally low, usually on the order of 2 to 34 mm./10^4 yr. (Prince et al., 1980), sediment samples commonly record the magnetic field for a period of 10^4 yr. or

more, except in areas of very high sedimentation rates. As the longest known periods of secular variation are of the order of 10^4 yr. (Cox, 1975), each sample may itself nearly average out secular variation. Even so, one should be wary of paleocolatitudes calculated from a small number of sediment samples as measurement errors must be averaged out as well. For this study, only paleocolatitudes calculated from 9 or more samples were considered usable. This limit is an attempt to strike a balance between the need for Pacific paleomagnetic data to be interpreted and the risk of including poor data in the interpretations. Future workers may wish to raise this limit as more reliable data becomes available. The paleocolatitudes were not judged solely on the number of samples used to calculate them. The dispersion of each data set was also examined. Occasionally, a paleocolatitude derived from more than the required number of samples was rejected because its individual inclinations were highly scattered.

The paleocolatitudes and error bounds in Table 4.5 are not always the values published by the original authors. As mentioned previously, all of the paleoinclinations were corrected for bias inherent to azimuthally unoriented data. In several instances, the original data was subdivided into smaller time intervals more suitable for the tectonic interpretations in Chapter 5. Also, each paleocolatitude was recalculated as the average of the paleocolatitudes of the individual samples rather than from the average of the sample paleoinclinations. Cox and Gordon (1983) suggest that the former method is preferable as a result of the

symmetry of secular variations; although, the difference between the paleocolatitudes calculated by either method is usually much smaller than the standard deviation of the data.

Data errors have been calculated following Cox and Gordon (1983). The error listed for each paleocolatitude in Table 4.5 is the standard error of the mean. It is approximately half of the half width of the 95% confidence range. The variance of each paleocolatitude is made up of three parts: S^2_{bf} the between flow variance, S^2_{if} the intra-flow variance, and S^2_s the variance caused by systematic errors. In a study of basalt flows, S^2_{if} is calculated as the mean of the individual flows, whereas S^2_{bf} is calculated as the variance of the average inclination of all of the flows. If the magnetization direction of each flow is accurately represented by its mean, then S^2_{bf} is mainly caused by secular variation. In fact, Cox and Gordon (1983) recommend replacing S^2_{bf} by the variance expected at the site latitude from their global model of secular variation in order to prevent underestimating the variance as a result of the limited number of samples.

If the number of independent flows sampled is N,

$$S^2_r = (S^2_{bf} + S^2_{if})/N$$

(Cox and Gordon, 1983). As systematic errors are not decreased by

increasing the number of samples, the total variance is the sum of the variances caused by the data dispersion and the systematic errors:

$$S^2_t = S^2_r + S^2_s$$

(Cox and Gordon, 1983).

For sediment samples it is not as easy to separate the errors caused by secular variation from the experimental errors. One could assume that each sediment sample perfectly averages out secular variation so that $S^2_{bf} = 0$. On the other hand, one could assume that no secular variation averaging occurs within each sample and use the values of S^2_{bf} given by the secular variation model of Cox and Gordon (1983). The true situation is somewhere between the two extremes. In Table 4.5 the standard errors for the sediment samples were calculated from the above equations in the following manner. S^2_{bf} values were taken directly from the model values tablulated by Cox and Gordon (1983). Although this tacitly assumes no secular variation averaging by the sediment samples, it seems the most conservative approach to take as it tends to slightly overestimate the data errors. S^2_{if}, on the other hand, is taken as the variance of the measured magnetization directions. Peirce (1976) instead used a fixed value of 10^o for S_{if}, but this assumption means that S^2_r would be the same for all DSDP sediment paleocolatitudes calculated from the same number of samples. This assumption ignores the fact that the dispersion of some DSDP paleomagnetic studies is greater than others. Using the measured

variance for S^2_{if} has the advantage of giving smaller error bounds to those samples with lesser scatter.

The largest source of systematic error is probably the off-vertical tilt of the drill pipe. As the tilt is rarely measured, the value for S^2_s must be assumed. The errors tablulated in Table 4.5 were calculated using $S_s = 2.0^o$, as suggested by Cox and Gordon (1983).

As discussed in Chapter 2, secondary magnetization caused by VRM can be a significant part of the NRM measured from sea floor samples. Many paleomagnetic studies of DSDP cores have shown that the NRM is often an unreliable indicator of the paleoinclination (Lowrie, 1974; Peirce et al., 1974; Lowrie and Hayes, 1975). Changes in the measured inclination of 20^o upon performing magnetic cleaning are common for DSDP samples, and occasionally much larger changes occur (Peirce, 1976). Consequently, only paleocolatitudes calculated from samples that have undergone demagnetization cleaning were considered acceptable for inclusion in Table 4.5 to be used for tectonic interpretation.

4.3 PALEOINCLINATIONS FROM MAGNETIC LINEATION SKEWNESS

In a manner analogous to the calculation of a seamount's magnetization direction, the paleoinclination of the seafloor can be estimated from the shape of the magnetic anomalies caused by crustal blocks of alternating polarity formed at a spreading ridge. The shape of a seafloor lineation anomaly depends upon the paleolatitude and orientation of the magnetic source body at the time it was formed as well as the present direction of the Earth's magnetic field in relation to the body (Schouten and Cande, 1976). By varying the paleolatitude of the source body, the shape asymmetry or skewness of the anomaly is changed. Thus it is possible to determine the latitude at which a magnetic lineation formed by examining the anomaly's shape. Because the shape of the anomaly depends on the projection of the magnetization and geomagnetic field vectors perpendicular to the strike of the source body, the paleodeclination is indeterminate. Thus only the distance to the paleopole is determined and the locus of the pole is a half great circle on the Earth's surface (Schouten and Cande, 1976).

The effective inclination (the projection perpendicular to the lineation strike) of the Earth's field vector, I', and the effective inclination of the remanent vector, I_r', are expressed as

$$\tan I' = \tan I/\sin(A-D)$$

$$\tan I_r' = \tan I_r/\sin(A-D_r)$$

where A is the azimuth of the lineations, I. D are the inclination and declination of the geomagnetic field. and I_r, D_r are the inclination and declination of the remanent vector (Schouten and Cande, 1976). The values for A, I, and D are known and I′ is calculated. After reducing the magnetic lineation to the pole, the phase shift, θ, that gives the anomaly its most symmetrical shape, is determined. I_r' is found from

$$I_r' = \theta - I' + 180^\circ$$

(Schouten and Cande, 1976). Thus only I_r and D_r are left as unknowns and the paleopole is somewhere along the locus of poles corresponding to the various possible values of these two parameters.

Although anomaly skewness has been used widely to infer the general motion of several lithospheric plates. only recently has skewness analysis been used in a quantitative manner and so there are only a few usable examples of this data. Table 4.7 contains paleoinclinations from two studies of Pacific lineations. The loci of possible pole positions for these skewness measurements are shown in Figure 4.4. Cande (1976) determined effective inclinations for Cenozoic anomalies 27 through 32 in five areas of the Pacific. Larson and Chase (1972) determined the skewness of three sets of Mesozoic anomalies M1 through M10. Larson and Chase did not report the position, azimuth, or present day geomagnetic field parameters that were used, however. these were reconstructed from the figures in their report.

Cande (1976) claimed that the effective remanent inclinations derived from his data are biased by "anomalous skewness" because the loci of paleomagnetic poles for his northern Pacific anomalies did not match those of his southern Pacific anomalies. The argument he used to determine the amount of anomalous skewness made the ad hoc assumption that the paleopole loci of these widely separated sets of anomalies should intersect. The amount of anomalous skewness was that needed to bring the polar loci into agreement. Such an argument, of course, ignores the possibility of relative motion between the locations of the lineations used, and thus these paleomagnetic data should be treated with caution.

The error bounds listed in Table 4.7 are basically those quoted by the authors. These errors are generally larger than the errors associated with most seamount paleopoles or DSDP paleocolatitudes. When there is anomalous skewness present, the errors should reflect both the contribution of the variance of the determination of the skewness parameter as well as the variance of the determination of the anomalous skewness (Gordon and Cox, 1980). However, Cande (1976) reports an error of only about $\pm 1^{o}$ in the determination of the anomalous skewness, and thus the error bounds are mainly the error in determining the skewness parameter.

A locus of paleomagnetic poles can also be found from the relative amplitudes of two sets of lineations assuming the average geomagnetic field to be dipolar. The anomaly amplitudes depend not only on the paleofield strength, but also on the spreading rate, thickness of the magnetic layer, and the depth of the sea floor

(Schouten, 1971; Blakely and Cox, 1972). Consequently, the resolution of the relative amplitudes is far less than the resolution of the skewness (Schouten and Cande, 1976). In view of the inaccuracies involved and the fact that there is only one relative amplitude datum from the Pacific (Schouten and Cande, 1976) this datum is not used in the tectonic interpretations of this study.

4.4 DSDP EQUATORIAL TRANSITS

Another form of azimuthally unoriented data comes from studies of the sediment facies found in DSDP drill cores. As the Pacific plate crosses the equator where the productivity of biologic material in the ocean increases sharply, a distinctive pile of organic sediments is deposited on the sea floor (van Andel et al., 1975). Several authors have used the occurrance of thse deposits in DSDP cores to infer the northward motion of the Pacific (Winterer, 1973; van Andel, 1974; Lancelot and Larson, 1975; Suarez and Molnar, 1980; Gordon and Cape, 1981). If the zone of high biologic productivity has remained close to the equator in the past, then the identification of an equatorial transit in sediments of a given age are roughly equivalent to a paleomagnetic paleocolatitude of 90° for that time.

The equator crossing is usually identified by the occurrance of one or more of three possible changes in the sediment column: (1) a sharp increase in the bulk sedimentation rate, (2) a change in the

lithology of the sediments to predominantly calcareous. and (3) the appearance of rare calcareous tests in an otherwise siliceous section (Suarez and Molnar, 1980). This method makes several important assumptions. It relies on the past latitudinal stablility of the currents that control the high productivity zone. It assumes that the sedimentation has been pelagic in nature and undisturbed by turbidites or hiatuses. Also, it assumes that the DSDP coring has recovered most of the stratigraphic section in question. Space limitations do not permit an in depth discussion here of the determination of paleoequators; however, the reader is referred to van Andel et al. (1975) and Suarez and Molnar (1980) for further information.

Only four equatorial transits of Cretaceous age appear in the literature. These are given in Table 4.8 and their predicted polar loci are shown in Figure 4.4. All of these transits suffer from spotty coring or the occurance of hiatuses in the section containing the equatorial sediments. Thus these paleoequator determinations could be somewhat in error. Additionally, it has not been determined whether or not the biologic high productivity zone was located precisely at the equator during the Cretaceous. The circulation of Cretaceous ocean currents may have been significantly different than today.

No systematic study of equatorial transits has been made to determine the magnitude of the errors to be expected in such a determination. As the high productivity zone appears to extend from about 5° N to 5° S (Arrhenius. 1963). a standard error of 2.5° is used in the tectonic interpretation of these data.

TABLE 4.1 SEAMOUNT PALEOPOLES AND MAGNETIZATION PARAMETERS

NAME	ID	POSITION LAT(N)	POSITION LON(E)	INC (+Down)	DEC (+East)	INT (A./m.)	VGP-A LAT(N)	VGP-A LON(E)	VGP-B LAT(N)	VGP-B LON(E)	GFR	MCC	SDa	SDm	PLANAR REGIONAL C0	PLANAR REGIONAL C1	PLANAR REGIONAL C3	REF
CENTRAL PACIFIC SEAMOUNTS																		
Magnet	C1	12.3	173.2	-20.9	342.3	9.5	61.0	31.2	56.3	40.6	3.9	0.97	0.9	15.1	200	-1.43	-4.38	1
Dixon	C2 *	12.6	180.9	-18.9	0.0	6.7			68.0	1.0	5.6		2.8	33.0				2
L1	C3 *	6.2	186.0	-24.3	352.5	7.1			69.7	27.5	2.8		2.6	32.0				3
L2	C4 *	2.7	186.0	37.3	180.2	7.5			66.5	5.5	3.8		2.4	31.0				3
L3	C5 *	1.0	180.5	-45.1	22.4	10.5			54.9	324.1	4.3		1.9	35.0				3
EAST PACIFIC SEAMOUNTS																		
Moonless	E1 *	31.9	218.2	38.0	359.4	10.2			79.4	41.3	4.2		1.5	27.0				4
39131	E2 *	39.0	229.0	47.1	5.9	1.3			78.0	23.0	2.0				-114	2.89	1.45	5
Tripod E7	E3 *	21.3	247.5	30.9	350.0	7.3			79.5	133.0	3.0		2.4	31.0				4
Tripod E8	E4 *	21.3	247.5	36.2	32.9	3.3			59.3	333.7	3.0		5.0	29.0				4
Tripod E9	E5 *	21.3	247.5	21.2	11.6	4.2			74.8	18.6	3.0		6.4	47.0				4
Tripod A1	E6 *	20.7	247.3	33.0	331.2	6.9			62.7	156.5	2.0		6.7	81.0				4
Tripod A2	E7 *	20.7	247.3	45.0	1.1	4.4			84.1	256.6	2.0		7.9	61.0				4
Tripod A3	E8 *	20.7	247.3	26.3	354.5	7.0			81.4	105.8	2.0		3.6	44.0				4
Tripod A4	E9 *	20.7	247.3	29.5	351.5	8.2			80.6	127.0	2.0		5.0	71.0				4
HAWAIIAN AREA SEAMOUNTS																		
Kaulunkalana	H1	23.3	201.6	40.8	5.2	2.0	85.2	289.9			5.7	0.96	3.1	10.5				1
Chatauqua	H2	22.2	197.4	12.7	189.3	4.8	60.0	358.7			(good)							6
HD1	H3 *	18.3	198.2	-24.2	21.8	1.9			52.0	342.0	4.7				35031	6.62	0.43	5
HD4	H4 *	20.0	201.8	-6.7	350.7	4.3			66.0	40.0	3.4				35946	1.95	-2.38	5
Finch	H5	17.7	203.3	-7.7	4.6	8.3	68.0	10.0	67.8	5.7	4.4	0.98	0.8	11.3	-69	0.83	2.19	1
Unnamed	H6	17.4	202.1	-13.8	2.3	4.1	65.5	16.6	65.6	14.6	3.0	0.89	2.9	20.4	-47	0.23	0.28	1
Kona 4N	H7 *	17.3	205.8	-8.4	13.5	5.8			64.6	352.8	2.9							4
Kona 5S	H8 *	17.1	205.8	35.3	196.4	0.9			49.8	1.5	2.9							4
Show	H9 *	17.9	207.3	18.0	199.8	3.8			56.5	350.1	3.2		2.6	16.0				4
Bushnell 1S	H10*	19.0	206.2	0.2	2.9	3.9			70.9	17.1	2.3							4
Unnamed	H11	26.5	182.2	9.2	357.5	4.7	68.0	8.9	68.6	356.7	3.6	0.94	1.7	14.4	-76	0.16	2.67	1
Paumakua	H12	24.9	202.9	-7.8	187.0	4.0	67.7	1.8	67.9	4.0	4.9	0.96	1.3	9.4	-50	-0.67	-0.85	1
HAWAIIAN RIDGE SEAMOUNTS																		
Abbott	HR1	31.8	174.3	-32.2	177.3	3.1	75.5	4.6	73.9	334.2	6.6	0.99	0.5	3.0	61	0.13	-1.26	7
JAPANESE SEAMOUNTS																		
A	J1 *	41.3	146.0	2.4	352.8	15.6	42.1	331.8	49.4	337.1	1.8							8
Sisoev	J2 *	40.9	144.9	22.2	341.3	10.4	55.4	349.4	56.4	359.4	2.0							8
Ryotu	J3 *	38.0	146.0	2.2	343.2	9.4			53.0	352.7	3.4							8
D	J4 *	36.0	143.5	7.0	320.0	8.3			40.9	21.6	2.7		2.1	31.0				3
Maiko	J5 *	34.0	145.9	-10.9	359.3	12.2			50.5	327.1	4.7		1.1	23.0				3
LINE ISLANDS SEAMOUNTS																		
Watkins	L1	17.5	190.8	-3.9	350.0	5.8	68.3	38.7	65.7	37.2	5.2	0.93	1.2	11.9	-14	-3.31	-0.35	9
Nagata	L2 *	12.5	193.0	-29.0	4.4	3.8	65.6	6.1	61.6	4.0	3.7	0.96	0.8	5.3	11	-2.05	0.36	10
Kapsitotwa	L3 *	12.0	194.2	-36.6	28.0	5.1			47.5	333.5	3.7		3.1	28.0				3
Stanley	L4	8.2	198.1	-10.5	5.3	3.2	75.6	356.5	54.3	312.3	4.7	0.96	2.4	16.0	157	-1.77	1.35	1
Willoughby	L5	7.9	198.1	-7.8	0.7	3.5	78.2	14.6	78.4	37.8	4.4	0.96	1.0	5.7	113	0.45	-1.92	1
Chapman	L6	3.4	199.9	-19.7	355.6	4.7/8.0	75.7	37.8	78.9	32.3	4.3	0.95	1.6	19.2	31	3.50	0.88	1
Clarke	L7	-3.3	206.0	-25.3	1.0	3.3	80.0	20.4	82.5	63.6	4.0	0.94	2.1	11.8	-45	1.25	1.78	1
Uyeda	L8	-7.5	208.5	40.1	195.7	6.9	68.5	345.6	75.9	352.2	3.1	0.94	1.6	19.1	383	-5.12	0.06	1

TABLE 4.1 (Continued) SEAMOUNT PALEOPOLES AND MAGNETIZATION PARAMETERS

NAME	ID	POSITION LAT(N)	POSITION LON(E)	INC (+Down)	DEC (+East)	INT (A./m.)	VGP-A LAT(N)	VGP-A LON(E)	VGP-B LAT(N)	VGP-B LON(E)	GFR	MCC	SDa	SDm	PLANAR REGIONAL C0	PLANAR REGIONAL C1	PLANAR REGIONAL C2	REF
MUSICIANS SEAMOUNTS																		
Berlin	M1	32.9	194.0	5.1	7.1	12.1	59.4	358.8	56.6	339.5	3.9	0.96	1.4	28.4	-106	-5.71	6.56	1
Mahler	M2	31.8	195.0	4.1	17.5	6.0	56.0	342.6	61.0	5.6	6.7	0.97	1.0	10.8	-11	3.83	-5.89	1
Mussorgski	M3 *	30.4	196.1	0.9	11.2	5.6			58.2	354.5	3.3		2.3	22.0				3
Rachmaninov	M4 *	29.6	196.7	11.9	26.6	9.3			55.6	324.6	2.5		2.7	43.0				3
Paganini	M5	28.7	197.4	12.2	356.3	8.3	67.2	26.9	66.3	15.2	3.2	0.95	2.4	34.1	-53	1.66	1.33	1
Khatchaturian	M6 *	28.1	197.7	5.9	23.0	12.8			56.5	332.5	5.3		3.4	75.0				3
Schubert	M7	31.9	197.9	17.9	9.2	6.4	65.7	355.3	56.4	331.3	4.3	0.95	1.9	20.1	111	-7.21	3.91	1
Brahms	M8 *	31.2	197.9	19.8	11.6	7.4			66.3	348.2	2.0		4.0	52.0				3
Debussy	M9	30.3	197.9	16.2	5.7	5.9	67.3	3.1	67.8	30.5	3.2	0.95	1.7	17.2	239	-6.56	-8.71	1
Tchaikovsky	M10	29.4	197.7	6.7	9.6	7.8	62.4	356.6	42.6	41.9	3.4	0.95	1.1	15.6	286	-3.30	-4.57	1
Liszt	M11	29.0	197.7	10.6	20.9	7.0	59.2	333.8	57.0	330.9	5.1	0.96	1.4	17.6	-186	0.94	2.19	1
Handel	M12	27.5	200.1	14.0	3.5	4.2	69.3	10.2	69.5	28.9	7.4	0.99	0.7	5.0	-44	0.55	-2.17	1
Rimsky-Korsakov	M13	25.3	200.2	12.8	6.8	2.9	70.1	0.0	65.3	327.0	9.3	0.98	2.8	14.5	-173	3.12	0.20	1
Gluck	M14	26.9	199.9	4.3	4.4	6.7	64.9	9.5	63.6	358.6	5.2	0.97	0.6	6.4	-179	0.17	1.85	1
MID-PACIFIC MOUNTAIN SEAMOUNTS																		
Woollard South	P1	18.0	171.2	7.7	37.2	3.6	50.9	277.9	39.6	273.3	2.0	0.86	1.5	9.1	-115	-1.19	2.76	1
Harvey	P2	17.8	172.7	-3.0	349.5	4.3	68.1	21.9	64.7	354.3	2.7	0.91	2.1	15.7	51	-3.37	1.86	1
Thomas	P3	17.3	173.9	5.3	8.2	3.5	73.3	324.2	73.6	350.6	2.5	0.87	2.8	16.7	92	-0.44	-1.97	1
Allen	P4	18.3	174.1	-1.2	8.8	4.1	69.2	328.6	61.3	333.8	3.6	0.92	1.5	10.6	285	-4.01	-0.71	1
Darwin	P5 *	22.1	171.6	36.2	207.8	1.9			39.9	316.8	2.4		4.5	15.0				3
WESTERN PACIFIC SEAMOUNTS																		
Z-4-1	W1 *	28.8	148.4	9.0	334.0	1.8			55.0	19.0	2.3							11
Z-4-2	W2 *	28.4	148.2	5.0	28.0	4.2			53.0	278.0	2.6							11
Z-4-3	W3 *	27.1	148.7	-13.0	16.0	6.4			53.0	302.0	4.1							11
Z-4-4	W4 *	27.8	146.7	-1.0	11.0	3.0			60.0	306.0	1.8							11
Makarov	W5 *	29.5	153.5	6.4	1.0	8.4			63.7	331.3	3.4		2.1	31.8				3
Miami	W6 *	21.7	161.9	-30.8	0.3	7.5			51.7	341.5	2.6		3.0	39.0				3
Birdseye	W7	20.9	165.7	-20.4	1.8	13.0	58.6	342.3	58.5	344.8	8.1	0.99	0.5	11.9	42	-0.19	-1.11	1
Aries 4	W8 *	21.2	166.5	-25.7	358.2	11.2			55.2	349.5	3.2		2.2	44.0				3
K	W9 *	19.4	165.9	-20.3	349.5	6.2			58.4	5.9	2.2		3.0	32.0				3
Unnamed	W10	16.7	162.4	13.7	16.7	1.6	71.0	281.3	58.4	282.8	5.5	0.94	3.1	8.3	65	-2.33	-0.05	1
Seascan	W11	15.1	159.3	-27.9	346.0	8.9	57.0	4.8	56.4	4.0	4.2	0.97	0.8	12.1	-12	-1.14	0.17	1
Unnamed	W12	15.5	153.3	26.0	18.8	1.8	71.7	246.5	67.8	248.0	9.5	0.98	0.9	3.0	-97	-0.55	0.39	1
Campbell	W13	16.5	149.0	31.8	189.6	4.8	55.0	312.9	52.3	301.3	2.4	0.92	1.6	13.6	60	-0.29	-2.32	1
Unnamed	W14	11.2	146.8	-1.7	350.2	7.5	74.5	6.4	69.2	357.4	2.7	0.91	1.4	17.8	265	-5.98	-0.88	1
Winchester	W15	10.3	156.7	-29.8	22.1	2.8	55.8	296.6	61.1	293.0	4.1	0.92	2.6	12.4	-155	1.69	1.01	1
Heezen	W16	8.8	163.2	-41.3	1.7	5.4	57.4	340.3	59.3	350.5	3.4	0.92	1.5	14.5	70	1.70	-3.67	1
Von Valtier	W17	7.3	172.3	-34.7	355.3	7.4	63.2	2.2	57.0	43.8	4.4	0.92	2.2	27.8	-172	17.22	-7.10	1

ABBREVIATIONS: INC, inclination, positive downward; DEC, declination, positive eastward; INT, intensity; VGP-A, paleopole calculated with constant offset regional; VGP-B, paleopole calculated with planar regional; GFR, goodness-of-fit ratio; MCC, multiple correlation coefficient; SDa, SDm, standard deviation of magnetization angle and intensity

* Note: Asterisk by seamount ID indicates that the magnetization parameters listed are those calculated with a planar regional.

REFERENCES: (1) This volume, (2) Francheteau et al. (1969), (3) Harrison et al. (1975), (4) Francheteau et al. (1970), (5) Richards et al. (1967), (6) Schimke and Bufe (1968), (7) Sager (1983b), (8) Uyeda and Richards (1966), (9) Keating and Sager (1980), (10) Sager et al. (1982), (11) Vacquier and Uyeda (1967)

TABLE 4.2 SEAMOUNT MODEL NOTES

ID	COMMENTS	REF
C1	Top removed (872 m.), bottom extended (500 m.)	1
C2	Bottom extended (100 m.)	2
C3	Top removed	3
C4	Reversed polarity, top removed	3
C5	Top removed	3
E1	Model could be improved by removing top. extending bottom	4
E2	Marginal reliability (GFR = 2.0)	4
E6	Marginal reliability (GFR = 2.0)	4
E7	Marginal reliability (GFR = 2.0)	4
E8	Marginal reliability (GFR = 2.0)	4
E9	Marginal reliability (GFR = 2.0)	4
H1	Magnetization may be largely induced	1
H2	Reversed polarity, inhomogeneous magnetization	5
H3	Bottom extended	6
H5	Top removed (750 m.)	1
H6	Top removed (500 m.)	1
H8	Reversed polarity	4
H9	Reversed polarity	4
H11	Top removed (1750 m.), bottom extended (500 m.)	1
H12	Top removed (500 m.)	1
HR1	Reversed polarity, top removed (400 m.), bottom extended (1000 m.)	7
J1	Marginal reliability (GFR = 1.8). model could be improved by removing some of top and extending bottom	8
J2	Marginal reliability (GFR = 2.0), model could be improved by removing some of top and extending bottom	8
J3	Top removed	8
J5	Top removed	3
L1	Top removed (750 m.), bottom extended (1300 m.)	9
L2	Bottom extended (1100 m.), inhomogeneous magnetization	10
L4	Bottom extended (1750 m.). inhomogeneous magnetization	1
L5	Bottom extended (1750 m.), inhomogeneous magnetization	1
L6	Top removed (550 m.), bottom extended (1750 m.), magnetization of upper half of seamount lower than bottom half	1
L7	Bottom extended (750 m.), inhomogeneous magnetization	1
L8	Top removed (750 m.), bottom extended (1375 m.)	1
M1	Top removed (475 m.)	1
M2	Top removed (700 m.), bottom extended (950 m.)	1
M3	Top removed	3
M5	Top removed (250 m.)	1
M6	Top removed	3
M7	Top removed (500 m.)	1
M9	Top removed (750 m.), bottom extended (250 m.)	1
M10	Top removed (600 m.)	1
M11	Top removed (825 m.), bottom extended (500 m.)	1
M12	Bottom extended (500 m.)	1

TABLE 4.2 (Continued) SEAMOUNT MODEL NOTES

ID	COMMENTS	REF
M13	Magnetization declination may be unstable	1
M14	Top removed (425 m.), bottom extended (250 m.)	1
P1	Top removed (500 m.), marginal reliability (GFR = 2.0), anomaly very complex and may be affected by deeper body	1
P2	Top removed (450 m.), anomaly may be affected by deeper body	1
P3	Top removed (350 m.), anomaly may be affected by deeper body	1
P4	Top removed (750 m.), anomaly may be affected by deeper body	1
P5	Reversed polarity, top removed, bottom extended	3
W1	Large regional removed from observed field values prior to inversion	11
W4	Marginal reliability (GFR =1.8), model might be improved by removing some of top and extending bottom	11
W7	Top removed (500 m.)	1
W8	Top removed	3
W10	Top removed (1125 m.), bottom extended (700 m.), survey data sparse, anomaly small	1
W11	Top removed (500 m.)	1
W12	Top removed (250 m.), magnetization may be induced	1
W13	Top removed (265 m.), bottom extended (250 m.)	1
W14	Top removed (1000 m.), bottom extended (1000 m.)	1
W15	Top removed (250 m.), bottom extended (500 m.)	1
W16	Top removed (750 m.)	1
W17	Top removed (626 m.), bottom extended (250 m.), only south 2/3 of anomaly used for inversion due to complications in north part	1

References: (1) This study; (2) Francheteau et al. (1969); (3) Harrison et al. (1975); (4) Francheteau et al. (1970); (5) Schimke and Bufe (1968); (6) Richards et al. (1967); (7) Sager (1983b); (8) Uyeda and Richards (1966); (9) Keating and Sager (1980); (10) Sager et al. (1982); (11) Vacquier and Uyeda (1967).

TABLE 4.3 SEAMOUNT AGES

ID	AGE(Ma.)	TYPE	COMMENTS
C3	130	SFL	Maximum age. Near lineation M14
C4	120	SFL	Maximum age. Near lineation M4 and M5
C5	120	SFL	Maximum age. Near lineation M4 and M5
E1	45	SFL	Maximum age. Near lineation 20 and 21
E2	37	SFL	Maximum age. Near lineation 13
E3	19	SFL	Maximum age. Near lineation 6
E4	19	SFL	Maximum age. Near lineation 6
E5	19	SFL	Maximum age. Near lineation 6
E6	3	K/Ar	Minimum age. (Ozima et al., 1968)
E7	19	SFL	Maximum age. Near lineation 6
E8	19	SFL	Maximum age. Near lineation 6
E9	19	SFL	Maximum age. Near lineation 6
H1	80	K/Ar	Minimum age. (M. Pringle, pers. comm., 1982)
H2	82	INF	Seamount reversed polarity, probably formed during Gubbio A- interval.
H3	88-91	K/Ar	Minimum age. (Dymond and Windom, 1968)
H8	82	INF	Seamount reversed polarity, assigned to Gubbio A- interval.
H9	82	INF	Seamount reversed polarity, assigned to Gubbio A- interval.
H11	74±4.3	K/Ar	Minimum age. (M. O. Garcia and J. Naughton, pers. comm., 1981)
H12	65	K/Ar	Minimum age. (M. Pringle, pers. comm., 1982)
HR1	41.5-42.5	INF	Age inferred from reversed polarity and position in Hawaiian chain. (Sager, 1983b)
J1	122	SFL	Maximum age. Near lineation M8.
J2	80.7-82.1	K/Ar	Minimum age. (Ozima et al., 1970)
	70-90	F	Minimum age. Gastropod fossils. (Harrison et al., 1975)
J3	72.9-73.9	K/Ar	Minimum age. (Ozima et al., 1970)
J4	131	SFL	Maximum age. Near lineation M14.
J5	5-22	F	Minimum age. Planktonic foraminifera (Matthews et al., 1974)
	135	SFL	Maximum age. Near lineation M17.
L2	81-89	K/Ar	Minimum age. (Sager et al., 1982)
	85	Ar/Ar	(Schlanger et al., 1982)
	83	INF	Probable reversal in seamount may record beginning of Gubbio A- interval.
L3	84.4±0.9	Ar/Ar	(Saito and Ozima, 1977)
	72-87	F	Planktonic foraminifera. (Saito and Ozima, 1976)
L4	41.9±1.1	Ar/Ar	(R. A. Duncan, pers. comm., 1982)
L5	42	INF	This seamount is adjacent to L4 and their VGPs are very close together. (Sager, 1983a)
L8	65-84	F	Minimum age. Pelecypod shell fragment indicates later part of Maastrichtian-Campanian interval. (J. A. Haggerty, pers. comm., 1982)
	68-72	INF	Seamount reversed polarity, probably Gubbio E- interval.

TABLE 4.3 (Continued) SEAMOUNT AGES

ID	AGE(Ma.)	TYPE	COMMENTS
M4	88.8±5.2	K/Ar	Minimum age. (Clague and Dalrymple, 1975)
M6	66.9±2.6	K/Ar	Minimum age. (Clague and Dalrymple, 1975)
P3	150	INF	Seamount age close to that of sea floor by gravity flexure study (A. B. Watts, pers. comm., 1981). Age of seafloor is uncertain, but lineation M29 is nearby.
P5	106-109	F	Minimum age. Coral fragments. (Harrison et al., 1975)
W2	65.1-81.2	K/Ar	Minimum age. (Ozima et al., 1970)
W3	89.5-97.9	K/Ar	Minimum age. (Ozima et al., 1970)
	120	INF	Maximum age determined from flexure study (Watts et. al., 1980)
W4	18.2	K/Ar	Minimum age. (Ozima et al., 1970)
W5	93.9±1.3	Ar/Ar	(Ozima et al., 1977)
	87-100	F	Minimum age. Planktonic foraminifera. (Heezen et al., 1973)
	120	INF	Maximum age determined from flexure study. (Watts et al., 1980)
W6	43-49	F	Minimum age. Planktonic foraminifera. (Heezen et al., 1973)
W15	89-92	F	Minimum age. Planktonic foraminifera of probable Turonian age dredged approximately 100 km. to the north on a ridge connected to seamount. (J. A. Haggerty, pers. comm., 1983)
W17	78-82	F	Minimum age. Planktonic foraminifera. (J. A. Haggerty, pers. comm., 1983)

AGE TYPE CODE: F, fossil age; INF. inferred age, SFL, sea floor lineation age; K/Ar, potassium-argon age; Ar/Ar, 40Argon-39Argon age.

NOTE: K-Ar ages have been corrected for new decay constants (Dalrymple, 1979).

TABLE 4.4 PACIFIC SEAMOUNTS GIVING UNRELIABLE PALEOMAGNETIC RESULTS

NAME	LAT(N)	LON(E)	REASON FOR REJECTION	REF
B	40.6	146.9	Low GFR (1.4). Model could be improved.	1
Z-3-1	37.1	163.8	Low GFR (1.1).	2
Z-3-2	36.6	163.9	Odd VGP (21.0, 91.0) depite GFR of 2.5.	2
HD3N	19.1	198.0	Low GFR (1.6), poor survey, small anomaly.	3
HD5E	19.3	197.5	Low GFR (1.4), poor survey.	3
HD5W	19.3	197.7	Low GFR (1.4). poor survey.	3
HD6	20.1	197.3	Low GFR (1.3). poor survey, small anomaly.	3
Unnamed W	36.8	234.4	Low GFR (1.8). large crustal anomaly interference.	3
Unnamed M	36.8	234.6	Same as Unnamed W	3
Unnamed E	36.8	234.8	Same as Unnamed W	3
Fieberling #2	32.3	232.8	Model looks good except high declination seems unneccessary. Reference 5 published significantly different pole for same data under name of Hoke Seamount.	3
Bushnell 2N	19.2	206.2	Poorly surveyed. small anomaly. GFR of 2.3 applies to three seamounts.	4
Bushnell 3E	19.0	206.4	Poorly surveyed. small anomaly. GFR of 2.3 applies to three seamounts.	4
Marie	30.7	217.3	Low GFR (1.1).	4
Maher	29.5	211.2	Poor goodness of fit.	5
Boutelle	39.0	228.9	Poor goodness of fit.	5
Hoke	32.3	232.8	Same as Fieberling #2.	5
Tripod A5	20.7	247.3	Low GFR (2.0) and high SDa, SDm.	4
Tripod A6	20.7	247.3	Low GFR (2.0) and high SDa, SDm.	4
Tripod F10	20.2	243.6	Low GFR (1.2).	4
Tripod G11	20.5	243.3	Low GFR (1.2).	4
Tripod H12	21.0	240.6	Low GFR (1.4).	4
Pioneer 3	45.8	231.2	Low GFR (1.1).	4
Pioneer 4	47.3	229.3	Low GFR (1.0).	4
Pioneer 5	47.9	204.7	Low GFR (1.1).	4
Pioneer 6	49.6	227.7	Low GFR (1.0).	4
Pioneer 7	49.6	227.3	Low GFR (1.1).	4
Pioneer 8	48.7	228.2	Low GFR (1.0).	4
Pioneer 9a	48.5	230.5	Low GFR (1.2).	4
Pioneer 9b	48.5	230.5	Low GFR (1.2).	4
Pioneer 9c	48.5	230.5	Low GFR (1.2).	4
Pioneer 10	49.8	226.5	Low GFR (1.3).	4
Pioneer 11	48.9	227.8	Low GFR (1.2).	4
Pioneer 12	50.6	228.9	Low GFR (1.0).	4
Pion. 13a	49.8	228.1	Low GFR (1.2).	4
Pion. 13b	49.8	228.1	Low GFR (1.2).	4
Pion. 13c	49.8	228.1	Low GFR (1.2).	4

TABLE 4.4 (Continued) PACIFIC SEAMOUNTS GIVING UNRELIABLE PALEOMAGNETIC RESULTS

NAME	LAT(N)	LON(E)	REASON FOR REJECTION	REF
Pion. 14a	48.0	229.9	Low GFR (1.2).	4
Pion. 14b	48.0	229.9	Low GFR (1.2).	4
Pioneer 15	46.8	229.2	Low GFR (1.1).	4
Pioneer 16	46.7	228.7	Low GFR (1.0).	4
Pioneer 17	48.0	228.0	Low GFR (1.1).	4
Pioneer 18	46.4	229.0	Low GFR (1.2).	4
Pioneer 19	45.8	230.5	Low GFR (1.7).	4
Pioneer 20	46.5	227.8	Low GFR (1.0).	4
Pioneer 21	48.0	227.2	Low GFR (1.4).	4
Pioneer 22	48.4	230.0	Low GFR (1.0).	4
Pioneer 23	47.9	230.3	Low GFR (1.7).	4
Pion. 24a	47.6	228.4	Low GFR (1.1).	4
Pion. 24b	47.6	228.4	Low GFR (1.1).	4
Cobb	46.8	229.2	Complex anomaly. Survey magnetization differs greatly from hand samples.	6
Mauke	-20.2	202.7	Low GFR (1.1).	7
Mitiaro	-19.9	202.3	Low GFR (1.2).	7
Takutea & Atiu	-20.0	201.9	Low GFR (1.1).	7
Rarotonga	-19.8	201.7	Low GFR (1.8).	7
Manihiki	-10.4	199.0	Odd VGP despite GFR of 2.8.	7
Mangaia	-21.9	203.0	Low GFR (1.5).	8
Niihau	21.8	200.0	Renewed volcanism.	9
Eveline	10.3	192.1	Low GFR (1.9). anomaly affected by large nearby ridge.	9
Derickson	53.0	198.8	Low GFR (1.7).	9
Nova 1	-26.7	185.4	Low GFR (1.5).	9
Nova 2	-26.0	185.0	Low GFR (1.5).	9
Donna	-16.3	183.9	Low GFR (1.4).	9
Aries 1	19.2	180.2	Low GFR (1.4).	9
Aries 2	19.3	176.7	Low GFR (1.3).	9
Bonatti	-8.0	252.0	Low GFR (1.2).	9
7Tow 137	14.4	191.0	Low GFR (1.2).	9
Silas Bent	27.8	145.9	Low GFR (1.1).	9
Stu 1	9.3	201.5	Low GFR (1.1).	9
Stu 2	9.3	201.5	Low GFR (1.1).	9
DSD 66	2.7	195.0	Low GFR (1.1).	9
Dvorak	30.5	198.8	Low GFR (1.1).	9
Musician 1	32.0	197.5	Low GFR (1.1).	9
Musician 2	32.0	197.5	Low GFR (1.1).	9
Musician 3	32.0	197.5	Low GFR (1.1).	9
Suiko	44.5	170.5	Low GFR (1.7).	10

TABLE 4.4 (Continued) PACIFIC SEAMOUNTS GIVING UNRELIABLE PALEOMAGNETIC RESULTS

NAME	LAT(N)	LON(E)	REASON FOR REJECTION	REF
Line 3	-0.6	202.6	Despite high GFR (6.8). anomaly is very small, magnetization inversion unstable.	11
Line 6	9.6	196.0	Very complex anomaly.	11
Line 7	10.5	195.1	Very complex anomaly.	11
Line 10	2.1	195.6	Low GFR (0.5).	11
Ravel	27.2	198.4	Low GFR (1.6).	11
MP5	17.5	173.5	Odd VGP (30.0, 313.5) despite GFR of 3.6.	11
WP7	14.3	160.0	Odd VGP (1.4, 231.2) despite GFR of 3.1, poor survey.	11
Harrie	5.6	172.3	Low GFR (1.7).	11

REFERENCES: (1) Uyeda and Richards (1966), (2) Vacquier and Uyeda (1967), (3) Richards et al. (1967), (4) Francheteau et al. (1970), (5) Grossling (1970), (6) Merrill et al. (1972), (7) Woodward and Hochstein (1970), (8) Lumb et al. (1973), (9) Harrison et al. (1975), (10) Kodama et al. (1978), (11) This study.

TABLE 4.5 CRETACEOUS PACIFIC PALEOCOLATITUDE DATA

SITE NO.	POSITION LAT(N)	LON(E)	COLAT	STAND. ERROR	N	AGE (Ma.)	CORES NO.	TYPE	REF
L. PALEOCENE - MAASTRICHTIAN (60 - 74 Ma.)									
GPC-3	30.3	202.2	79.1	2.3	78?	65		S	1
165	8.2	195.1	99.6	3.2	60	65-73	18-22	S	2
199	13.5	156.2	99.5	4.1	9	60-73	9-11	S	2
288A	6.0	161.8	98.6	4.5	9	60-78	8-12	S	2
315A	4.2	201.5	98.9	2.4	60	65-73	15-21	S	3
433C	44.8	170.0	63.0	3.5	40	64.7±1.1		B	4
CAMPANIAN - TURONIAN (74 - 85 Ma.)									
167	7.1	183.2	102.8	3.2	40	73-89	57-59	S	5
170	11.8	177.6	106.2	3.9	25	72-80	6-8	S	5
171 *	19.1	190.5	97.8	3.5	12	84-88	22	S	5
315A	4.2	201.5	102.1	3.5	18	73-88	22-26	S	3
317A	-11.0	197.7	114.3	3.2	24	83-93	6-7	S	2,3
462, 462A	7.2	165.0	96.7	2.5	41	78-87	9-11,55-57	S	6
462, 462A	7.2	165.0	114.2	5.0	6?	73-84	14-32	B	7
CENOMANIAN - ALBIAN (92-110 Ma.)									
164	13.2	198.5	105.0	3.5	12	100-108		B	8
166	3.8	184.9	116.6	4.2	31	92-108	20-21	S	5
288A	6.0	161.8	119.9	3.0	44	88-108	15-28	S	2
317A	-11.0	197.7	118.4	3.2	27	92-108	8-10	S	2,3
463	21.4	174.7	107.4	2.7	32	102-112	55-64	S	9
OLDER THAN ALBIAN (> 110 Ma.)									
307 *	28.6	161.0	83.3	4.5	6	142	13	B	10
317A	-11.0	197.7	124.1	2.3	130	108-122	11-15	S	2,3
462	7.2	165.0	112.4	5.0	8?	115	41-71	B	7
463	21.4	174.7	101.9	2.6	42	108-122	65-78	S	9

NOTES: The asterisk shows sites whose polarity could be in error. N is an estimate of the number of independent samples. TYPE B refers to igneous samples; TYPE S to sediment samples. AGE is the approximate age span of the samples (usually biostratigraphic ages) in millions of years before present. CORES denotes the DSDP core numbers from each hole from which the samples were taken.

REFERENCES: (1) Prince et al. (1980); (2) Keating. personal communication, (1983); (3) Cockerham and Jarrard (1976); (4) Kono (1980b); (5) Jarrard (1973); (6) Steiner (1981a); (7) Steiner (1981b); (8) Marshall (1978); (9) Sayre (1981); (10) Larson and Lowrie (1975).

TABLE 4.6 REJECTED CRETACEOUS PACIFIC PALEOCOLATITUDE DATA

SITE NO.	POSITION LAT(N)	LON(E)	REASON FOR REJECTION	TYPE	REF
61	12.1	147.1	Too few samples. N<3.	B	1
63	0.8	147.9	Too few samples. N<2.	B	1
66	2.6	193.9	High scatter, poor age control.	S	2
163	11.2	209.7	Too few samples. N<6.	B	1
169	10.7	173.6	Too few samples. N=7.	S	3
192A	53.0	164.7	Too few samples. N<6.	B	1
289	-0.5	158.5	Too few samples. N<8 in all age ranges.	B,S	4
303A	40.8	154.5	Too few samples. N<3.	B	5
304	39.3	155.1	Too few samples. N=1.	B	5
313	20.2	189.0	Too few samples. N<2.	B	5
430A	38.0	170.6	Too few samples. N<5.	B	6
432A	41.3	170.6	Too few samples. N<3.	B	6
465A	33.8	178.9	Polarity of samples indeterminate.	B,S	7

REFERENCES: (1) Marshall (1978); (2) Sclater and Jarrard (1971); (3) Jarrard (1973); (4) Hammond et al. (1975); (5) Larson and Lowrie (1975); (6) Kono (1980b); (7) Sayre (1981).

TABLE 4.7 MAGNETIC LINEATION SKEWNESS DATA

SITE	POSITION LAT(N)	POSITION LON(E)	AGE (Ma.)	EFFECTIVE INCLINATION	CORRECTED EFF. INC.	ERROR	AZ.	REF
N1	47	187	62-71	26	40	5.1	88.0	1
N2	28	211	62-71	37	51	7.6	170.0	1
SW1	-51	192	62-71	-65	-79	4.2	215.0	1
SW2	-56	181	62-71	-68	-80	6.3	250.0	1
SW3	-58	187	62-71	-72	-79	5.2	250.0	1
PHO *	2	182	116-125	-51		10.0	258.0	2
JAP *	41	154	116-125	-98		15.0	72.0	2
HAW *	27	172	116-125	-18		10.0	143.0	2

* Positions of sites and lineation azimuths of these anomalies had to be estimated from figures in original reference.
References: (1) Cande (1976), (2) Larson and Chase (1972).

TABLE 4.8 CRETACEOUS EQUATORIAL TRANSIT DATA

DSDP SITE NO.	POSITION LAT(N)	LON(E)	AGE (m.y.)	CRITERIA	REF
171	19.1	190.5	67-76	1	1
199	13.5	156.2	56-76	2	2
313	20.2	189.0	69-76	1,3	3
463	21.4	174.7	68-72	1	4

EQUATOR TRANSIT IDENTIFICATION CRITERIA:
(1) Increase in bulk sedimentation rate.
(2) Change in lithology.
(3) Increase in $CaCO_3$ content of sediments.

REFERENCES: (1) Suarez and Molnar (1980); (2) Gordon and Cape (1981); (3) Lancelot and Larson (1975); (4) Thiede et al. (1981).
NOTE: All of these equatorial transits suffer from partial obscuration due to spotty coring and lacunas.

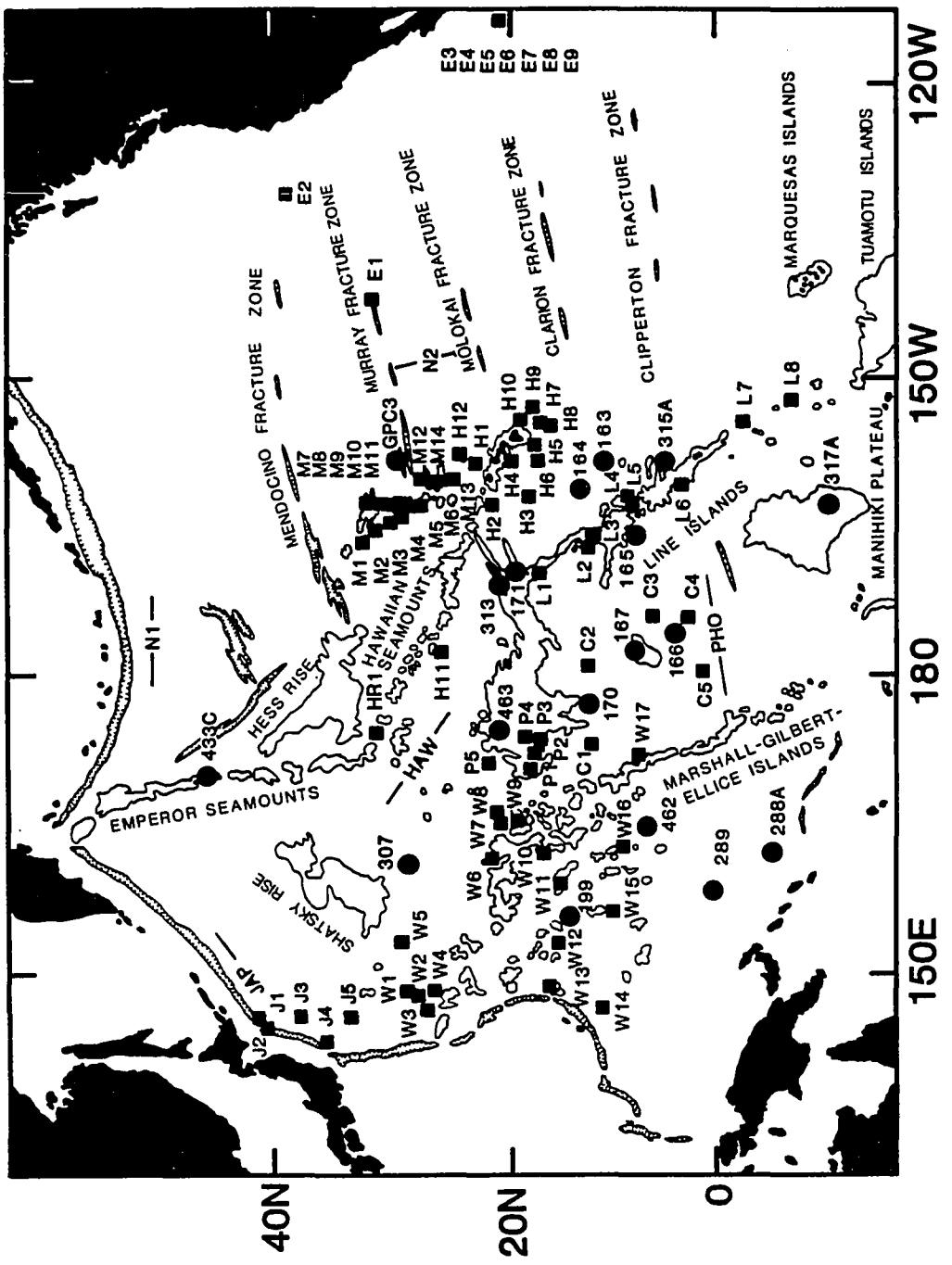

Figure 4.1 Sampling locations for data discussed in text. Solid squares are the seamounts studied paleomagnetically and the solid circles are DSDP sites (except for GPC3, a piston core paleocolatitude). Magnetic lineation groups analyzed for skewness are indicated by solid lines approximately parallel to the strike of the lineations.

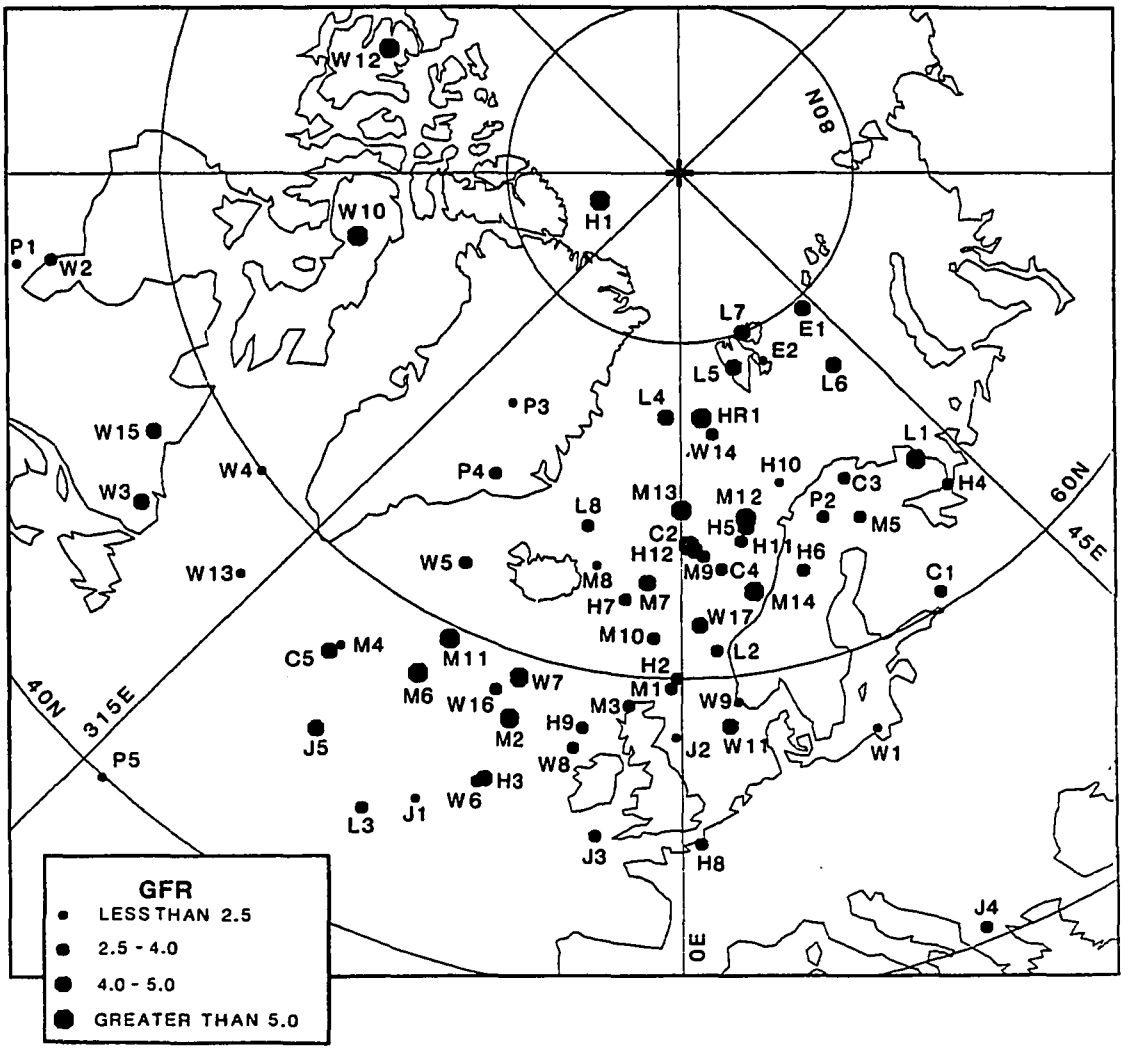

Figure 4.2 VGPs of Pacific seamounts. All of the VGPs from Table 4.1 are shown except for those from the Tripod Seamounts (see Chapter 5). The size of the symbol is proportional to the seamount's GFR, with the largest symbols indicating the highest GFRs. The high GFR paleopoles should be the most reliable.

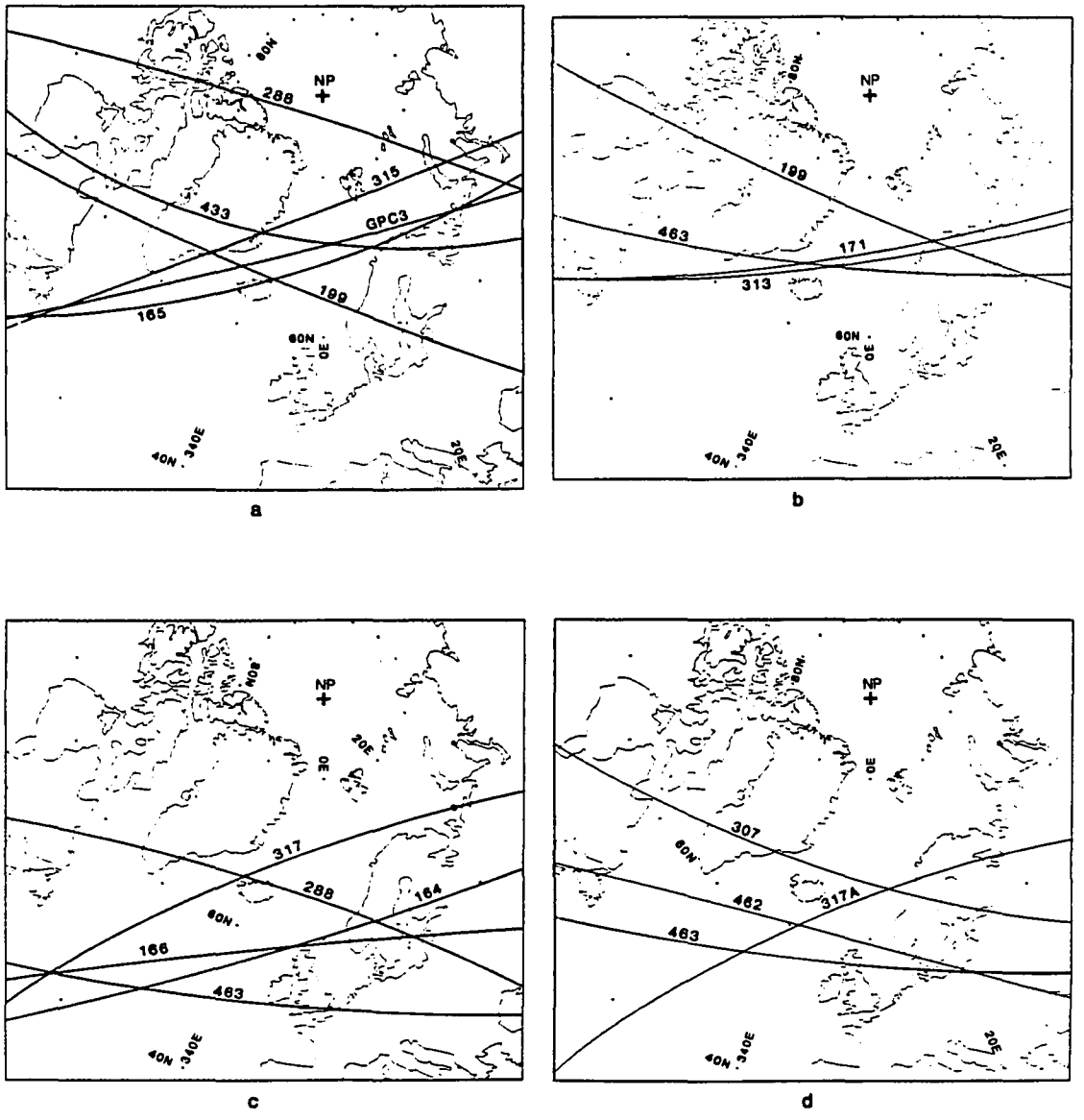

Figure 4.3 Paleocolatitude data. Polar circles of paleocolatitudes are shown as solid line arcs. Numbers identify DSDP sites (except for piston core GPC3). (a) Maastrichtian; (b) Campanian to Turonian (462B is from intrusives, 462S is from sediments); (c) Cenomanian to Albian; (d) older than Albian.

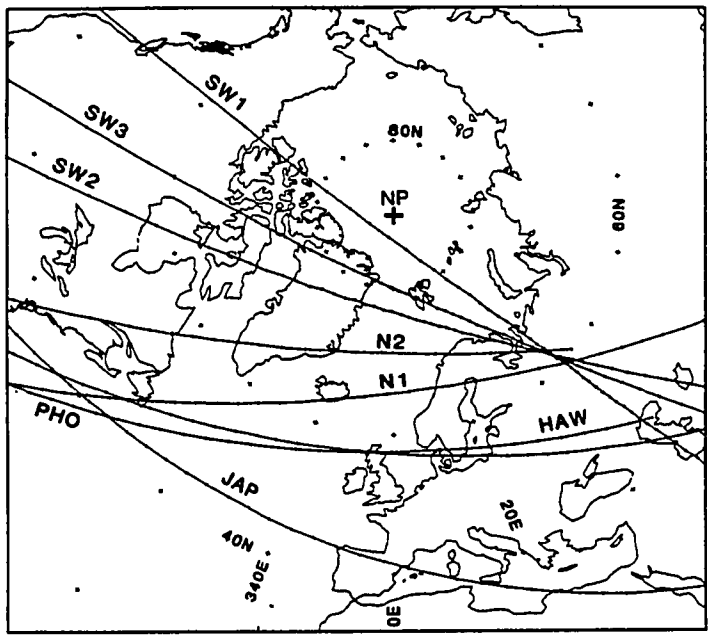

a

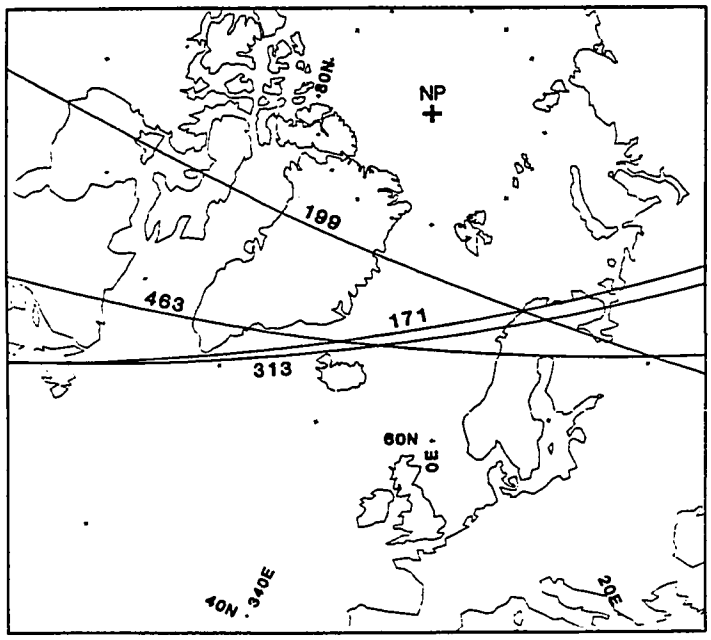

b

Figure 4.4 Lineation skewness and equator transit data. Polar circles of skewness paleoinclinations are shown by the arcs in (a). See Table 4.7 for ages. Polar circles from DSDP equator transits are shown in (b). Ages are given in Table 4.8. Numbers and letters identifying polar circles in (a) and (b) refer to the DSDP site numbers or anomaly groups listed in the tables.

4.5 SEAMOUNT MODELS

In this section each of the seamounts and paleomagnetic models analyzed in the course of this study are discussed in order to give the reader an insight to the methods and procedures used in calculating seamount magnetizations. The seamount paleopoles and models have been divided by geographic region for ease of reference. Seamounts in the central Pacific basin and eastern Pacific have been given identifiers beginning with C and E, respectively. The model for seamount C1 is given in Section 4.5.1. Those seamounts in the neighborhood of the Hawaiian Islands are prefixed by an H. They are discussed in Section 5.2.2 and the paleomagnetic models of H1, H5, H6, H11, and H12 are presented in sections 4.5.2 - 4.5.5. Seamounts from the Line Islands are designated by the letter L. Models for these seamounts (L4 - L8) are discussed in sections 4.5.6 - 4.5.9 and their tectonic implications are covered in Section 5.2.1. Ten Musicians seamounts (M1, M2, M5, M7, M9 - M14) have models in sections 4.5.10 - 4.5.19. Their inferences for the tectonics of the Musicians Seamounts are discussed in Section 5.2.2. The Mid-Pacific Mountains and western Pacific seamounts are indicated respectively by P and W. Models for P1 - P4 are given in sections 4.5.20 - 4.5.23 whereas those for W7 and W10 - W17 are covered in sections 4.5.24 - 4.5.32.

4.5.1 MAGNET SEAMOUNT (C1)

Magnet seamount was discovered by an aeromagnetic survey that noted its large magnetic anomaly at 12.3° N, 173.2° E. As the large anomaly was not associated with any charted bathymetric feature, it was surveyed during 1981 on Leg 5 of the Western Pacific Seamounts cruise by the R/V Kana Keoki. The bathymetry and magnetic anomaly are shown in Figure 4.5.

The seamount has two peaks, one to the south that has a minimum depth of 1378 m., and one to the north that is seen on only one ship track and has a minimum measured depth of 2750 m. The regional sea floor depth is in excess of 5600 m. The magnetic anomaly has a large minimum approximately over the south peak that reaches -1250 nT. To the north and south of this minimum are two maxima of +148 nT. and +144 nT. North of the northern maximum is a minimum of -314 nT. associated with the northern peak. The northern maximum is probably modified by the anomaly of the northern peak. The minimum values of the anomaly are not centered over the peak, but are located instead slightly to the west. As the minimum is crossed by several ship tracks this displacement appears to be a real feature and perhaps indicates inhomogeneity in the magnetization of the seamount's peak.

The best paleomagnetic model of C1 has an addition of 500 m. to the bottom of the seamount and a removes of 872 m. from the top. The fact that so much of the top is removed may reflect the fact that the minimum of the anomaly is not centered over the peak. Thus not all of the 872 m. removed from the top is necessarily non-magnetic. The

northern peak was included in the bathymetric model and assumed to have the same magnetization direction and intensity as the southern peak; however, the north peak and its anomaly are mostly outside the area of the anomaly used to constrain the magnetization of the south peak. The calculated magnetic anomaly and residuals are shown in Figure 4.6. The model's GFR of 3.9 indicates a good reproduction of the observed anomaly by the calculated anomaly. Magnet Seamount's VGP is at 61.0° N, 31.2° E. The seamount has not been dredged and its age is unknown.

4.5.2 KAULUAKALANA SEAMOUNT (H1)

This seamount is located approximately 240 km. north-northwest of Oahu at 23.3° N, 201.6° E. Most of the survey data for Kauluakalana was collected in 1980 by the R/V Kana Keoki on Leg 2 of the Musicians Seamounts cruise. As seen in Figure 4.7, the survey of this seamount contains more data than most. The regional sea floor depth is approximately 4600 m., however at least 800 m. of sediment can be seen just to the south on seismic reflection records. The minimum recorded depth is 1827 m. The seamount is approximately conical except for a long lobe extending to the west from its lower flanks.

The magnetic anomaly consists of a maximum of +61 nT. to the south of the peak and a -258 nT. minimum to the north. The best model has a GFR of 5.7 suggesting that the magnetic anomaly inversion has produced

excellent results. The calculated anomaly and residuals are shown in Figure 4.8. The inclination and declination of the magnetization vector are 40.8° and 5.2° whereas the geomagnetic field vector has an inclination of 41.0° and a declination of 11.4° in the area of the seamount. If the magnetic anomaly is caused by remanent magnetization, the seamount has had practically no northward drift, a situation that seems unlikely considering its 80 Ma. K/Ar age (M. Pringle, personal communication, 1982). Instead, the seamount's anomaly is more likely a result of induction caused by the geomagnetic field. Kauluakalana seamount appears to be one of those rare cases in which the remanent magnetization of a seamount is much smaller than its induced magnetization.

4.5.3 FINCH SEAMOUNT (H5) AND UNNAMED SEAMOUNT (H6)

Finch and the small unnamed seamount nearby are located at 17.7° N, 202.3° E and 17.4° N, 202.1° E, approximately 250 km. south-southwest of the island of Hawaii. They were surveyed in 1978 by the R/V Kana Keoki on cruise KK780807. The bathymetry and magnetic anomalies of these seamounts are shown in Figure 4.9. Finch is the larger of the two seamounts rising from a regional ocean floor depth of about 4800 m. to a minimum recorded depth of 1000 m. As no ship track appears to have actually crossed the summit, the minimum depth of the

seamount is probably somewhat less. Finch is approximately conical, but its smaller neighbor is elongated north to south. The unnamed seamount is much smaller than Finch and only rises to a depth of about 2727 m. As seen in Figure 4.9, there is another small seamount to the southeast of Finch. The data over this edifice was felt to be too sparse for a reliable inversion of its magnetic anomaly.

The magnetic anomaly over Finch is very large (1481 nT. peak to peak). A minimum of -1011 nT. is just to the north of the summit and a maximum of +470 nT. is to the south. The large magnetic anomaly appears to be caused by a large magnetization intensity (8.25 A./m.) of the seamount's basalts. The magnetic anomaly of the unnamed seamount resembles that of Finch except that it is much smaller. It has a maximum of +76 nT. to the south of the summit and a minimum of -244 nT. to the north.

The best depth to the bottom for the models of both seamounts was at 4750 m., approximately the level of the sea floor; however, the GFR was maximized by removing the upper 750 m. of Finch and the upper 500 m. of the unnamed seamount. The magnetization directions of the two seamounts are very similar. Finch gave an inclination and declination of -7.7° and 4.6°, whereas its companion gave -13.8° and 2.3°. The GFRs of 4.4 and 3.0, respectively for Finch and the unnamed seamount, suggest good results. The calculated and residual anomalies are shown in Figure 4.10 and 4.11.

4.5.4 UNNAMED SEAMOUNT (H11)

Located at 26.5° N, 182.2° E, approximately 220 km. south-southwest of Salmon Bank (Hawaiian chain), this seamount was surveyed in 1976 by the R/V Kana Keoki during cruise KK76080601. The survey data is a bit sparse, particularly in the southwest quadrant of the seamount; however, this problem did not unduly complicate the modeling of the volcano. The seamount is roughly conical and rises from the sea floor at about 5000 m. to a minimum depth of 801 m. as shown in Figure 4.12. The magnetic anomaly, however, is rather complicated. It has a large minimum of -658 nT. on the northern flank of the seamount and a maximum of +391 nT. on the south flank. In between these features, over the peak, is a zone of large amplitude, short wavelength anomalies. There are two relative minima, -530 nT. and -368 nT., and a relative maximum of +225 nT. These short wavelength anomalies are somewhat unusual and are perhaps related to highly magnetized intrusions high up in the volcanic edifice.

A large area of the magnetic anomaly was used in the inversion routine in order to ameliorate the detrimental effects of the short wavelength anomalies. The inversion was constrained mostly by the larger minimum and maximum to produce a magnetization vector that is believed to represent the bulk of the seamount. Figure 4.13 shows the calculated anomaly and residuals. Figure 4.14, a north-south magnetic transect over the seamount, graphically shows that the modeled anomaly follows the broad trend of the seamount anomaly while ignoring the short wavelength portion.

The best model had 1750 m. of the top removed and 500 m. added to the bottom. The large amount of top removed undoubtedly reflects the complicated magnetization of the upper layers of the seamount and the fact that this model made no attempt to duplicate the short wavelength anomaly features. The seamount's GFR, 3.6, is surprisingly high considering the confused portion of the anomaly. It suggests that the portion of the anomaly outside the complex region is closely matched by the calculated anomaly. H11 has been K/Ar dated at 74 $\pm$ 4 m.y. (M. Garcia and J. Naughton, personal communication, 1981).

4.5.5 PAUMAKUA SEAMOUNT (H12)

Located at 24.9° N, 202.9°E, Paumakua Seamount is 165 km. south of the eastern end of the Rameau Ridge in the Musicians Seamounts and 390 km. north of Oahu. It was surveyed by the R/V Kana Keoki on Leg 2 of the Musicians Seamounts cruise. Shiptracks from NOAA cruises CMAPPI1A and CMAPSU1A as well as Lamont-Doherty cruises C1220, C1303, and V2112 were also used to complete the survey.

Paumakua is slightly elongated in an east-west direction and has a eastward trending spur from its lower flanks as seen in Figure 4.15. At its shallowest, the seamount reaches 1880 m. and the deepest closed contour is 4500 m. The magnetic anomaly is relatively simple. It has a minimum, -414 nT., south of the peak and a maximum, +375 nT., north of the peak, indicating that the volcano is reversely polarized. The eastern end of the Rameau Ridge, slightly more than a degree of

latitude to the north, is also reversely polarized. It is the only clearly identifiable reversed edifice in the Musicians Seamounts.

Modeling of Paumakua seamount favored the bottom of the seamount at 4625 m., approximately the level of the ocean bottom, and the top of the seamount at 2375 m., a reduction of 500 m. The model's GFR, 4.9, indicates excellent results. The calculated and residual anomalies are displayed in Figure 4.16.

4.5.6 STANLEY (L4) AND WILLOUGHBY (L5) SEAMOUNTS

Stanley and Willoughby seamounts are located in the north central Line Islands at 8.2° N, 198.1° E and 7.9° N, 198.1° E. They were surveyed by the R/V Kana Keoki on cruise KK79080801. As seen in Figure 4.17, Stanley Seamount is elongated north-northwest to south-southeast whereas Willoughby Seamount consists of two cones. Stanley Seamount rises from 4500 m. to a minimum depth of 2970 m. The two peaks outlined by the 3000 m. contour along with the elongate shape of the seamount suggest that it may be the product of two coalesced volcanic cones. Willoughby Seamount consists of two edifices that are mostly separate, but join at a depth of about 4000 m. The northern peak is well surveyed and appears to be the larger of the two. It reaches a minimum depth slightly shallower than 2500 m. The southern cone is not well surveyed. Its minimum recorded depth is 3000 m., but a more complete survey of this cone would likely find a shallower summit.

Seismic reflection records penetrate at least 800 m. of sediment burying the flanks of both seamounts. In the area between the two seamounts, the penetration is not as great, suggesting that the edifices may be connected at their bases.

Both seamounts have relatively low amplitude magnetic anomalies. Small magnetic anomalies seem to be typical of many of the Line Islands seamounts surveyed for paleomagnetic study. The low amplitude anomalies might be a result of the petrologic character of the Line Islands basalts or an effect caused by the magnetic field at the time of the formation of these seamounts. Perhaps the magnetic field strength at the time of volcanism was low. Alternatively, it will be shown in Chapter 5 that some of the Line Islands seamounts appear to be Tertiary in age, so the magnetic field may have reversed frequently during the time that the lavas forming these seamounts were erupted, causing a partial cancellation of the magnetizations of opposing polarities.

The magnetic anomaly of Stanley Seamount is a broad low of about -75 nT. that is centered over the northern half of the seamount. Two relative maxima, just over +150 nT., are located to the northeast and southeast of the seamount. The magnetic anomaly of Willoughby Seamount is more complex. The northern peak has a small dipolar anomaly associated with it. A low of -178 nT. is to the north of the summit and a high of +24 nT. is to the south. The southwest cone of Willoughby Seamount has a large low associated with it that, unfortunately for modeling purposes, impinges upon the magnetic anomaly of the northern cone.

Both seamounts were first modeled as being homogeneous; however, the results were poor, even when the buried flanks were included. Preliminary modeling indicated that the magnetic field of Stanley Seamount observed at Willoughby seamount, and vice-versa, was small. Thus each seamount was modeled as if the other was not nearby. The model of Stanley Seamount gave an inclination of 13.5^{o} with a declination of 55.3^{o}, whereas the model of Willoughby Seamount gave 13.9^{o} and 11.0^{o}, respectively. Both had low GFRs of 2.2 and the calculated anomalies did not closely resemble the observed anomalies.

Some workers may have been satisfied with these results and quit at this point because the GFRs, although low, indicated marginally acceptable results. However, these seamounts are small and have broad. low amplitude magnetic anomalies that would tend to give artificially high GFR values even for poor models, as explained in Chapter 2. In this case the dissimilarity of the calculated and observed anomalies suggested that better results could be obtained.

The fact that the magnetic low associated with Stanley Seamount is centered over the northwestern part of the edifice suggests that the southeastern part has a lower magnetization. Several models were tried assuming varied amounts of the southeastern flank of the seamount to be non-magnetic. The best model was assumed to be the one that produced the highest GFR. As shown in Figure 4.18, this model assumes that most of the southeastern part of the seamount, down to 4125 m., is non-magnetic. The boundary between the two parts of the model is assumed to slope towards the non-magnetic section. This model gave better

results than a model with a vertical boundary between the two sections. It may indicate that the magnetic section was the original seamount and that the non-magnetic part was a later addition. The best model also has a sub-bottom extension of 1750 m. down to a depth of 6300 m. The accuracy of the determination of the bottom depth is low because of the limited areal coverage of the magnetic anomaly used for the inversion and the insensitivity of the modeling technique to changes in the magnetic body at large distances from the plane of observation.

The best model of Willoughby Seamount is similar to that of Stanley Seamount in that part of this seamount is also considered to be non-magnetic. For this seamount, approximately the southern third of the north peak down to a depth of 3400 m. was removed (Figure 4.18). The original magnetic model of the seamount, with the entire seamount present, produced a magnetic anomaly low centered over the peak of the seamount and a low GFR. The best model, lacking the aforementioned part of its south flank. produced an anomaly with a low to the north of the peak and a small high to the south of the peak closely resembling the observed anomaly (Figure 4.19). In all of the models of Willoughby seamount the southwest peak was included and assumed to have the same magnetization direction and intensity as the main peak. However, the area of the magnetic anomaly used for the inversion was kept small to minimize the effect of the poorly constrained southwest peak on the magnetization parameters calculated.

The non-homogeneous models of these two seamounts gave inclinations of -10.5° and -7.8° and declinations of 5.3 and 0.7.

respectively, for Stanley and Willoughby seamounts. Both seamount models have high GFRs. 4.7 and 4.4, and similar intensities, 3.2 A./m. and 3.5 A./m. Their VGPs fall close together well north of the VGPs of Cretaceous seamounts suggesting a younger age for the two volcanoes. Stanley seamount was dredged and a 41.9 $\pm$ 1.1 m.y. age was determined using Ar^{40}/Ar^{39} techniques (R. Duncan, personal communication, 1982) supporting the evidence of the VGPs. The VGPs from both of these seamounts were used in the calculation of a Late Eocene paleomagnetic pole for the Pacific (Sager, 1983a).

4.5.7 CHAPMAN SEAMOUNT (L6)

Chapman Seamount is a large volcano with two peaks located at 3.4° N, 199.9° E about 100 km. southwest of Fanning Island. Kana Keoki cruise KK79080801 crossed the summit and made an unsuccessful dredge attempt. In addition, nine other ship tracks cross the seamount from earlier Hawaii Institute of Geophysics and Scripps Institute of Oceanography cruises. This data was combined to form the basis for the bathymetric and magnetic contour maps in Figure 4.20.

The western peak is the larger of the two. The minimum depth recorded there is 1311 m., whereas the minimum depth of the eastern peak is somewhat deeper at 1608 m. The regional seafloor depth is greater than 4250 m. on the west side of the seamount, but it decreases

to the east because of the thick sediment apron draped on the nearby Line Islands ridge. Over 500 m. of sediments are clearly seen on airgun seismic reflection records around the seamount. These sediments are probably deeper as acoustic basement is often marked by an Eocene chert layer in this region (Orwig, 1981).

The magnetic anomaly produced by Chapman Seamount is rather complex. Associated with the western peak is a large amplitude minimum which reaches -560 nT. on the north side of the summit. To the north and south are maxima of +360 nT. and +315 nT. The minimum and two maxima make up the main anomaly. It is perturbed by two short wavelength features, both relative maxima that intrude the large minimum. One of these maxima nearly cuts the large minimum into two parts. Its maximum value is -155 nT. near 3.53° N, 199.85° E. The other maximum has a value of 109 nT. on the northwest flank of the seamount near 3.63° N, 199.73° E.

The best model of Chapman Seamount, assuming it to be homogeneously magnetized. gave an inclination of -20.2°, a declination of -1.4°, and a GFR of 2.6. This model included an extension of the bottom to 6000 m. and a removal of the top down to 1875 m. The eastern peak was included in the model and assumed to have the same magnetization direction and intensity as the western peak. The area of the observed magnetic anomaly used in the inversion was limited in its east-west extent so that the eastern peak would have little effect on the magnetization solution.

It seemed that an inhomogeneous model might increase the resemblance of the observed and calculated anomalies. With two small reversely magnetized areas accounting for the two short wavelength relative maxima and a small amount of the southeast flank assumed to be non-magnetic (Figure 4.18). the GFR improved to 3.3. The inclination changed only 0.9^{o} to -19.7^{o} and the declination changed 3.0^{o} to -4.4^{o}, so the magnetization direction was changed very little by the complications to the model.

The same model was divided into two parts, from the summit down to 2500 m. and from 2500 m. down to 6000 m. The magnetization vector of each part was assumed to have the same direction as before, but the intensity of the magnetization of each of the two parts was adjusted to obtain the best fit to the observed anomaly in a least-squares sense. The intensity of the top was found to be only about half that of the base, 4.7 A./m. versus 8.0 A./m. The calculated anomaly and residuals of this model are shown in Figure 4.21. These intensities are, of course, dependent on the assumed depth of the boundary between the two parts, which admittedly is arbitrary. However, the model demonstrates that the overall intensities of the seamount's base and summit are very different.

This model suggests that the magnetization of Chapman seamount may have formed in a complex manner. Apparently the seamount formed during two polarity epochs as evidenced by the reversed polarity sections in the normally magnetized bulk of the seamount. The difference in the magnetization intensity of the top and bottom may reflect an actual decrease of the intensity of the geomagnetic field at the time the

seamount formed, it might indicate that revesely polarized basalts have intruded the normally polarized top of the volcano, weakening its magnetization, or it may reflect a change in the petrology of the rocks that make up the summit (perhaps a greater abundance of non-magnetic hyaloclastite). The best model has a GFR of 4.3, indicating that the calculated anomaly is a good match to the observed anomaly. The seamount's VGP falls close to those of Stanley and Willoughby seamounts, also from the Line Islands. It was used in the calculation of the Late Eocene paleomagnetic pole for the Pacific (Sager, 1983a).

4.5.8 CLARKE SEAMOUNT (L7)

Located at 3.3° S, 206.0° E, Clarke Seamount was surveyed by cruises KK79080801 and KK79080802. The seamount appears to consist of two coalesced cones. The eastern peak is only crossed by one ship track and thus its bathymetry and magnetic anomaly is very poorly constrained (Figure 4.22). The western peak is crossed by three ship tracks and seems to be a simple cone elongated northwest to southeast. The minimum depth recorded over the western peak is 2990 m.; over the eastern peak it is 3317 m. The regional sea floor depth is about 5000 m. The depth of the sediments in this region is poorly known as the seismic reflection records in the area of the survey show poor penetration.

Like Stanley and Willoughby seamounts, this seamount has a very small magnitude anomaly. The magnetic anomaly consists of a simple minimum of about -165 nT. associated with the western peak. The eastern peak seems to have no discernible magnetic expression. Normally it would be difficult to obtain a good magnetic survey of a seamount with such a small anomaly so close to the magnetic equator (about 2^{o} to the north) because the diurnal variations at this geomagnetic latitude should be nearly as large as the anomaly. However, Clarke Seamount was surveyed at night when the diurnal variation is small, the magnetic field was quiet at the time of the survey, and a magnetic base station had been set up on Christmas Island (580 km. to the north) to aid in removing magnetic field variations. Consequently, the magnetic crossing errors for this survey were on the order of 2 nT.

The best magnetic model of Clarke Seamount assumed that the eastern peak is non-magnetic. The eastern flank of the western peak was drawn to keep the same shape and symmetry as the rest of the seamount (Figure 4.18). The bottom was extended 750 m. below the sea floor and none of the top was removed. An inclination and declination of -25.3^{o} and 1.0^{o} were calculated for the magnetization vector. The model's GFR is 4.0, indicating good results. The calculated anomaly and residuals are shown in Figure 4.23. The seamount's VGP falls near those of Stanley, Willoughby, and Chapman. It was used in the calculation of the Late Eocene paleomagnetic pole for the Pacific (Sager, 1983a).

4.5.9 UYEDA SEAMOUNT (L8)

Uyeda Seamount, located at 7.5° N, 208.5° E, is a large seamount, just over 4 km. in height, in the southern Line Islands near the Galapagos Fracture Zone. It was surveyed and dredged on cruises KK79080801 and KK79080802. The seamount appears as an isolated edifice on most bathymetric charts; however, it is actually part of a long aseismic ridge running from about 200 km. to the northwest of the seamount to the vicinity of Caroline Island, about 450 km. to the southeast (J. Mammerickx, map in preparation, 1982). As seen in Figure 4.24, the survey data shows that Uyeda Seamount is connected to the ridge on its southeast side at a depth of approximately 3500 m. Unfortunately, its connection to the ridge on its northwest side was not determined by the survey. The minimum depth of the seamount is 1177 m. on top of a small cone that sits atop the main edifice. The regional seafloor depth is approximately 5250 m.

Uyeda Seamount has a large magnetic anomaly, over 1100 nT. peak to peak. The anomaly is characterized by a large low, -549 nT., to the north of the seamount and a large high, +610 nT., to the south that indicate that the bulk of the seamount is reversely polarized. This high amplitude dipolar anomaly is perturbed by the anomaly associated with the ridge to the southeast and a short wavelength high of +220 nT. midway between the maximum and minimum. The short wavelength high is

centered very near the small cone on top of the main edifice. Although the cone itself is too small to be the likely source of this small anomaly without an unreasonably high magnetization intensity (at least several times the highest magnetization intensity listed in Table 4.1). both the cone and the small anomaly may be the result of a small magma chamber or intrusive body, now solidified. in the upper layers of the seamount. With no constraint on the position and shape of the source body for this small anomaly, it is difficult to extract any useful paleomagnetic information from it other than to suggest that the causative body might have been formed somewhat later than the bulk of the seamount because of its apparentl opposite polarity.

The best model of Uyeda Seamount extended the magnetic bottom 750 m., to a depth of 6000 m., and removed 1375 m. of the top. down to 2875 m. The 1375 m. of the summit that was removed may not necessarily be completely non-magnetic because the magnetic anomaly has two features that place conflicting constraints on the depth of the magnetic portions of the seamount. The wavelength of the anomaly is longer than can be produced by the seamount that appears above the ocean bottom. To reproduce the long wavelength, the bottom is extended and part of the top is removed. However, when the source body is lowered in this manner, the sharpness or "peakedness" of the high and low of the calculated anomaly are less than that of the observed anomaly. The model producing the highest GFR is the one that provides the best least-squares compromise.

An inhomogeneous model similar to that used for Chapman Seamount, with the top and bottom having different magnetization intensities. was

tried for Uyeda Seamount. It confirmed that the portion of the top that had been previously removed has a small magnetization, but it did not significantly improve the GFR. The best model has a GFR of 3.1 indicating an acceptable agreement of the calculated and observed magnetic anomalies. The calculated anomaly and residuals are shown in Figure 4.25.

Both fossils and basalts were dredged from Uyeda Seamount. The oldest fossils appear to be Maastrichtian or Campanian foraminifera and shell fragments (Haggerty et al., 1982; J. Haggerty, personal communication, 1982). A K/Ar age of 44.9 $\pm$ 4.5 m.y. was determined from the basalts (J. Naughton and M. Garcia, personal communication, 1981). This age is much younger than the fossil age and may result from the heavy submarine alteration of the basalt samples (M. Garcia, personal communication, 1981), or it might indicate that there was a pulse of volcanism on this seamount in the Eocene concurrent with such volcanism seen elsewhere in the Line Islands. The seamount's VGP agrees with a Late Cretaceous age, so if there was Eocene volcanism on the edifice, it must have been small in volume.

The reversed polarity of the seamount can be used to help establish its age. The reversed epochs occur that occur during the Campanian and Maastrichtian are those between anomalies 30 - 34 (Lowrie and Alvarez, 1981). The fossil evidence seems to favor the existence of shallow water fauna on the seamount during the Maastrichtian or late Campanian (J. Haggerty, personal communication, 1982), so the reversed intervals between anomalies 32 - 33, spanning 68-72 m.y., are the most likely intervals for the formation of the seamount.

4.5.10 BERLIN SEAMOUNT (M1)

Berlin Seamount is located at 32.9° N, 194.0° E in the northwest part of the Musicians Seamounts. It was surveyed by the R/V Kana Keoki during cruise KK800402, but was not dredged. The seamount is a simple cone with a small secondary cone attached to its northwest flank (Figure 4.26). As the secondary cone is only seen on one ship track. its shape is poorly constrained. The minimum depth of the main peak is 3392 m. and the regional sea floor depth is approximately 5800 m.

Berlin's magnetic anomaly is a simple dipole with a minimum of -498 nT. to the north of the summit and a maximum of +334 nT. to the south. The magnetic anomaly shows that the volcano is normally polarized and its simplicity suggests that the seamount's magnetization is homogeneous.

The best model assumes a homogeneous magnetization with no depth extension and a removal of 475 m. of the top. The GFR of 3.9 indicates a good match of the observed and calculated anomalies as shown in Figure 4.27. The calculated inclination of 5.1° suggests that the seamount formed close to the equator.

4.5.11 MAHLER SEAMOUNT (M2)

At 31.8° N, 195.0° E. 200 km. southeast of Berlin Seamount, lies Mahler Seamount. Mahler was also surveyed by the R/V Kana Keoki on cruise KK800402. As seen in Figure 4.28, Mahler consists of two seamounts connected at a depth of about 5000 m. The northeast peak has a minimum depth of 2427 m. and the southwest peak. 2710 m. The regional sea floor depth is approximately 5800 m. The survey data is rather sparse and the southwest peak is poorly surveyed as is the southeast flank of the northeast peak. Basalts were dredged from the southwest peak, but no age has been determined as yet.

Mahler's magnetic anomaly is relatively simple and smooth. A maximum of +186 nT. and a minimum of -653 nT. are associated with the northeast peak. Their positions indicate that the seamount is normally polarized. Because of the encroaching magnetic anomaly of the southwest peak, the area of the magnetic anomaly over the northeast peak used for the magnetization inversion was kept small. For this reason it was difficult to determine the best depth for the bottom of the model. The GFR was highest for a bottom depth of 7500 m., but this value seems much too deep. Since neither the GFR nor the magnetization direction changed significantly for bottoms in excess of 6750 m. depth, the model bottom was arbitrarily set at 6750 m. The GFR was sensitive, however. to the removal of portions of the summit. The best model had 700 m. of the top removed and a GFR of 6.7 indicating excellent agreement between the observed and calculated anomalies. The calculated anomaly and residuals are shown in Figure 4.29. The

inclination of the remanent magnetization vector, 4.1°, suggests that this seamount was also formed near the equator.

4.5.12 PAGANINI SEAMOUNT (M5)

Paganini Seamount is located at 28.7° N, 162.6° N near the Murray Fracture Zone. The seamount was not surveyed with the intent of applying the seamount paleomagnetic technique; however, a ship track from NOAA cruise CMAPPI1A crosses the seamount from north to south near the summit and two others cross the flanks. These tracks are crossed obliquely by a track from Lamont-Doherty cruise C1303 and Scripps cruise ARES07WT that passed near the summit (Figure 4.30). This data is rather sparse, but the seamount's magnetic anomaly is simple, so it suffices for a useable survey.

The seamount is elongated north to south. The main peak reaches a minimum recorded depth of 2862 m. The regional sea floor depth is approximately 5500 m. Paganini's magnetic anomaly has a maximum of +445 nT. to the south of the summit and a minimum of -340 nT. to the north. A large anomaly from a small seamount northwest of Paganini impinges upon the minimum to the north of Paganini's peak. Otherwise, Paganini's magnetic anomaly is simple and smooth.

Because the survey data is so sparse, the normal procedure of using gridded magnetic anomaly data to constrain the magnetization inversion was not used. The magnetic anomaly values were digitized

along the ship tracks at one nautical mile intervals. This procedure should minimize any bias that might result from contouring the sparse data. In all other aspects the modeling procedure was the same as that used for the seamounts discussed above. The best model had no sub-bottom extension and only 250 m. of the top was removed. The effect of the small peak to the north of Paganini appears to be small and the best model assumes that it is non-magnetic. The match of the calculated and observed anomalies along the north-south track over the summit is shown in Figure 4.31. The model's GFR, 3.2, indicates acceptable results.

The calculated magnetization is 12.2^{o}, indicating that the seamount formed at about 6^{o} north of the equator. Paganini's declination, at -3.7^{o}, is the most westerly of all of the Musicians Seamounts. As the magnetic field is better constrained north to south than east to west due to the orientation of the ship tracks, the declination is not as well constrained as the inclination and may be somewhat in error.

4.5.13 SCHUBERT SEAMOUNT (M7)

Schubert Seamount is a complex volcano located at 31.9^{o} N, 197.9^{o} E on the Musicians Horst. Scubert was not surveyed for paleomagnetic study; however, four north-south NOAA ship tracks from cruise CMAPPI2A

and one southwest-northwest track from Lamont-Doherty cruise C1303 are complemented by data from cruise KK800402 and constitute a useful magnetic survey. The seamount was dredged twice, but no age has yet been determined from the collected samples.

Elongated east to west, the main edifice of Schubert Seamount has four peaks on its summit (Figure 4.32). These reach mimimum depths of 2285 m., 2371 m., 2237 m., and 2367 m. The regional sea floor depth is difficult to determine because of the complex bottom topography in the area, but it appears to be about 5500 m. Schubert has a number of projections and spurs from its lower flanks. The most notable of these is south of the western part of the main edifice at a depth of about 3100 m.

The magnetic anomaly of the seamount is rather complex. A high of +190 nT. and a low of -660 nT. are associated with the main edifice. Their postions show that the seamount is normally polarized. The anomaly low trends to the east and connects to another low tht appears to be caused by the extension of Schubert to the east. The large southern spur of the seamount also has a relatively large anomaly associated with it.

Because the anomaly is so complex, the area of the anomaly used to constrain the magnetization inversion was limited to the vicinity of the main edifice. The bathymetric model included the main edifice and the extensions to the east and south. The best model has no extension of the bottom of the seamount below 5500 m.,but 500 m. was removed from the top. The model's GFR is 4.3, indicating very good results. The calculated anomaly and residuals are shown in Figure 4.33. As its

paleoinclination is 17.9°, Schubert Seamount appears to have formed about 9° north of the equator.

4.5.14 DEBUSSY SEAMOUNT (M9)

This seamount is located at 30.3° N, 197.9° E between the Musicians Horst and the Murray Fracture Zone. The survey data consists of several crossings made by the R/V Kana Keoki on cruise KK800402, two NOAA ship tracks from cruise CMAPPI2A. and a track from Scripps cruise GECS-BMV.

Debussy has two peaks, north and south, that reach depth of 2298 m. and 1766 m., respectively. Neither peak is well surveyed. although the southern one has the most data. In Figure 4.34, the two cones coalesce at a depth of 3500 m., but this is only an estimate from the sparse data. The regional sea floor depth is approximately 5700 m.

As might be expected from Debussy's complex bathymetry, the magnetic anomaly is also complicated. A maximum and minimum of +510 nT. and -628 nT. are associated with the south peak. A large minimum of -833 nT. is located just north of the northern peak and its corresponding maximum is low in intensity, +107 nT. This maximum is not on a line from the minumum through the summit as one would expect from a homogeneously magnetized seamount, but this skewness may be at least partially caused by the sparse survey data.

Because of the interference of the anomaly of the northern peak with that of the southern peak, the area of the anomaly used to constrain the magnetization inversion was kept small. Even so, the proximity of the northern peak is worrisome and the results of this inversion should be treated with some caution. The best model has a bottom 250 m. below the seafloor and 750 m. of the top removed. The GFR of the model is 3.2 indicating that the calculated anomaly (Figure 4.35) is a reasonable facsimile of the observed anomaly. Debussy's magnetization vector, with an inclination of 16.2° and a declination of 5.7°, agrees very well with those of nearby Schubert and Brahms seamounts, implying that the paleomagnetic results from this survey are reliable despite the aniticipated problems from the anomaly complexity.

4.5.15 TCHAIKOVSKY SEAMOUNT (M10)

Tchaikovsky Seamount is found approximately 100 km. south of Debussy Seamount and an equal distance north of the Murray Fracture Zone at 29.4° N, 197.7° E. Like several of the other Musicians Seamounts analyzed, this one was not surveyed specifically for paleomagnetic study. Cruise KK800402 crossed several of the pre-existing NOAA CMAPPI1A ship tracks over Tchaikovsky allowing the data to be contoured for paleomagnetic study.

Tchaikovsky is a simple conical volcano with a top at 2007 m. and a bottom at 5250 m. Its shape is not well constrained in the northwest and southeast quadrants, but the seamount is "boxed" by bathymetric data that suggests that a more complex shape is unlikely (Figure 4.36).

The magnetic anomaly of Tchaikovsky Seamount also appears to be very simple. The minimum, -845 nT., is located just to the north of the summit and is flanked by two highs. +400 nT. to the south and +84 nT. to the north. From the positions of the maxima and minimum, the seamount is seen to be normally polarized. No bottom extension was favored by the modeling process. although 600 m. of the top was removed. The GFR of the model is 3.4 and implies good results. The calculated anomaly and residuals are shown in Figure 4.37.

4.5.16 LISZT SEAMOUNT (M11)

Fifty kilometers to the south of Tchaikovsky seamount, at 29.0° N, 197.7° E, lies Liszt seamount. It was dredged by the R/V Kana Keoki on cruise KK800402. The underway geophysical data taken from that cruise was combined with NOAA cruise CMAPPI1A and Lamont-Doherty cruise C1303 for paleomagnetic study. Once again, the survey data is rather sparse. Liszt appears to have two peaks. the larger northern one reaches a shallowest recorded depth of 1556 m. whereas the smaller one only reaches 3119 m. The shape of the northern peak is fairly well constrained as two perpendicular tracks cross the summit (Figure 4.38).

The shape of the southern peak, however, is not well constrained. The regional ocean bottom depth is approximately 5500 m.

The magnetic anomaly shows contributions from both peaks. Associated with the northern one is a low of -780 nT. and a high of +365 nT. The southern peak has a low and a high of -360 nT. and +308 nT. Of these anomaly features, the minimum associated with the northern peak is the best constrained by the ship data. The maximum caused by the same peak is not as well constrained and the maximum and minimum of the southern peak are poorly mapped. Both peaks appear to be normally magnetized.

The magnetic model includes both peaks and uses only magnetic values digitized along the ship tracks for the magetization inversion. The best model has 825 m. removed from the top and 500 m. added to the bottom. The GFR, 5.1, indicates an excellent match between the observed and calculated anomalies. Figure 4.39 shows the agreement between the calculated and observed magnetic values along one of the north-south ship tracks.

Normally the high GFR would be taken as evidence that the magnetization parameters are of the highest quality. However, in this case, the declination should be accepted with some caution because the ship tracks are oriented north-south, and thus the inclination should be constrained better than the declination. The inclination, 10.6°, is very nearly the same as several of the seamounts analyzed in the vicinity. The declination, 20.9°, is about 10° higher than most seamounts in the Musicians and would be probably considered to be

erroneous were it not for two nearby seamounts. Khatchaturian (M6) and Rachmaninov (M4), that also have declinations greater than 20^{o}.

4.5.17 HANDEL SEAMOUNT (M12)

Handel Seamount is located in the eastern Musicians Seamounts province at 27.5^{o} N, 200.1^{o} E. just north of the area characterized by east-west trending ridges. It was surveyed and dredged by the R/V Kana Keoki on cruise KK800715. This data was combined with pre-existing NOAA CMAPPI1A and CMAPSU1A cruise tracks to make maps suitable for paleomagnetic analysis.

There is quite a bit of data in this survey, so the bathymetry and magnetic anomaly are well constrained (Figure 4.40). Handel is a simple conical feature, elongated slightly in a northeast direction. A 300 m. depression, that may be a caldera, is found at the summit. The shallowest recorded depth is 2525 m. and the regional seafloor is in the neighborhood of 5250 m. Scarlatti Seamount is close by Handel to the northwest and there is an unnamed cone to the northeast as well, but Handel is sufficiently isolated for easy modeling.

Handel's magnetic anomaly is very smooth, simple, and well sampled by the ship tracks. The minimum, north of the summit, reaches -486 nT. and the maximum, to the south, is +220 nT. Handel is normally polarized.

The best magnetic model of Handel has a very high GFR value of 7.4, undoubtedly a result of the simple shape of the anomaly and the good survey. No material was considered to be non-magnetic at the seamount's summit, but 500 m. of sub-bottom extension was needed. In this case the layers added to the bottom were strongly preferred by the modeling procedure as their inclusion increased the GFR by 14%. As seen in Figure 4.41, the calculated anomaly looks very similar to the observed anomaly and the residuals are very small considering the large amplitude of the seamount's anomaly.

4.5.18 RIMSKY-KORSAKOV RIDGE (M13)

Rimsky-Korsakov is a small ridge in the eastern Musicians Seamounts. It is found at 25.3° N, 200.2° E, about 60 km. south of Schumann Seamount and 390 km. north of Kauai. It was surveyed in detail during cruise KK800715 of the R/V Kana Keoki. Ship tracks from cruise KK800402, NOAA cruises CMAPPI1A and CMAPSU1A, and Lamont-Doherty cruise C1303 also cross the small ridge and were merged into the survey.

Rimsky-Korsakov is an east-west trending ridge (Figure 4.42) about 13 km. across north to south and about 70 km. in length. At its summit, roughly in the middle of the edifice, the shallowest recorded depth is 3267 m. On its eastern end, the ridge splits into two low

parallel ridges. The ocean bottom depth in the region is approximately 5000 m.

Like the ridge, its magnetic anomaly is also elongated east-west. The anomaly has a small amplitude (only 224 nT. peak to peak) that appears to be primarily a result of the ridge's small size and great depth. Rimsky-Korsakov is normally polarized with a -219 nT. anomaly minimum to the north of the ridge's summit and a 5 nT. maximum to the south. The magnetic survey data was somewhat difficult to contour properly as the ridge was surveyed from one end to the other. The eastern part of the ridge was measured at night whereas the western part was surveyed during the day, a situation that tended to maximize the amount of distortion of the small anomaly by diurnal variations. Because the daily range of the geomagnetic field variation near Rimsky-Korsakov should be close to the amount detected at Honolulu, about 45 nT. (see Figures 3.3 and 3.4), the maximum was shifted westward and the minimum was shifted eastward in the uncorrected data. This apparent shift caused a large, spurious declination to be calculated by the magnetization inversion routine. Corrections for the diurnal variation were made by determining the differences in the magnetic values at track crossings where day values were superimposed on night values and using these differences to constrain the scaling of the average diurnal variation curve for Honolulu.

Even with the diurnal corrections, the calculated declination seemed to be unstable. Depending on the amount of magnetic anomaly input into the inversion routine, the declination varied from about 6^{o} to 26^{o}. The reason for the occurance of the instability is that it

takes a large declination to significantly displace the magnetic contours from due east-west for an east-west trending ridge. Consequently, small errors in the determination of the positions of the east-west contours tend to cause large declination values to be calculated by the magnetization inversion. In the magnetic anomaly shown in Figure 4.42, the maximum and minimum values are lined up almost due north and south of one another, suggesting that the true declination is not large. The area of the magnetic anomaly used as input for the magnetization inversion was reduced until the declination settled into an apparently reasonable value. The small area of magnetic anomaly used for this calculation is partly responsible for the extremely high value of the GFR, 9.3. Throughout all of the model modifications the inclination varied little. The inclination and declination of the best model, with no top removed or bottom layers added, were 12.8° and 6.8°, comparing favorably with the magnetization parameters of nearby Handel Seamount. The calculated anomaly and residuals are shown in Figure 4.43.

4.5.19 GLUCK SEAMOUNT (M14)

Gluck Seamount is found in the eastern Musicians Seamounts at 26.9° N, 199.9° E, about 50 km. southwest of Handel Seamount. Data from cruise KK800715, NOAA cruise CMAPSU1A, and Lamont-Doherty cruise C1303 were combined to make the bathymetric and magnetic anomly maps

shown in Figure 4.44. Gluck was not intentionally surveyed for paleomagnetic analysis; however, three NOAA ship tracks cross the seamount in a north-south direction, one of them taking a jog over Gluck's northern flank, and the HIG track passes east-west over the summit. Fortunately, the shape of the seamount and its magnetic anomaly are simple, so this data suffices for a useful paleomagnetic survey. Gluck was succesfully dredged on cruise KK800715, but as yet it has not been dated.

The seamount appears to have a relatively simple conical shape. Its peak reaches to 1700 m. and the regional sea floor depth is about 5000 m. A smaller seamount, about 1.7 km. in height, is located to the northeast of Gluck. This smaller seamount is not surveyed well enough to be analyzed paleomagnetically.

Gluck is normally magnetized. Its magnetic anomaly is relatively smooth with a minimum of -650 nT. and a maximum of +505 nT. The small seamount to the northeast has a sizeable anomaly that impinges upon the northern part of the Gluck anomaly. In hopes of reducing the possible bias due to the interloper, the magnetic anomaly values used for the determination of Gluck's magnetization parameters were not taken from very far to the north of Gluck's summit. Both methods of inputting the observed anomaly values into the magnetization inversion, digitizing along the ship tracks and gridding the anomaly, were tried. The difference in the magnetization directions determined was insignificant (0.3^{o} in inclination and 1.9^{o} in declination). The best model has a bottom at 5250 m., an extension of about 250 m., and a top at 2125 m., a reduction of 425 m. By including the small seamount to the northeast

in the model and assuming its magnetization to have the same intensity and direction as that of Gluck, the GFR was improved substantially, but the inclination and declination of Gluck's magnetization was changed little. The GFR of this model is 5.2 indicating excellent results. The calculated anomaly and residuals are shown in Figure 4.45.

4.5.20 WOOLLARD GUYOT SOUTH PEAK (P1)

Situated at the western end of the Mid-Pacific Mountains province at 18.0° N, 171.2° E, Woollard Guyot was surveyed and dredged by HIG cruise KK81062605. It is a large feature that has several peaks which have likely evolved from several centers of volcanism. The data over most of the guyot is too sparse for paleomagnetic analysis; however, several ship tracks cross the southern peak. This feature is slightly elongated north-south and coalesces into the main part of the guyot at about 2250 m. depth (Figure 4.46). It has a flat top at a depth of about 1300 m. that is 17.5 km. across at its widest point. Approximately 0.5 sec. (two-way travel time) of carbonate and sediment material can be seen in seismic reflection records taken across the top (K. Nemoto, in preparation).

The data in this survey is rather sparse, particularly on the east flank of the peak; however, a bathymetric map of the feature having better control in that area (K. Nemoto, in preparation) was used to constrain the shape of the seamount where no other data was available.

The vertical dimensions of the peak are also ill-constrained because it is difficult to determine the whereabouts of the base of the south peak. Woollard Guyot, and other guyots in this area, appear to be built upon an older oceanic plateau (K. Nemoto, in preparation). This seamount is near the southern edge of this plateau and it is difficult to determine where the seamount ends and the plateau below it begins.

The magnetic anomaly of the south peak is complex. An east-west elongated minimum of -253 nT. is found over the south central part of the summit. Over the northern part of the peak are two more lows, of -221 nT. and -154 nT. Further to the north are several highs and lows caused by the main guyot. To the south of the peak is found a maximum of +198 nT. and another low of -207 nT. further to the south. The numerous highs and lows cannot be attributed to magnetic field variations as they are consistent from one track to another. They are undoubtedly caused by a complicated magnetization structure of the seamount. For the most part, the south peak appears to be normally magnetized.

For the purpose of magnetic modeling the area of the observed anomaly used for constraining the magnetization inversion was limited to the area over the south peak in hopes of minimizing the effect of the larger guyot body to the north and the edge of the plateau to the south. The south flank of the main guyot was included in the bathymetric model of the south peak and assumed to have the same magnetization intensity and direction; although, because it is well north of the magnetic anomaly analyzed its effect on the magnetic model of the south peak is small. The plateau underlying the seamount was

not modeled as its shape and magnetization direction are unknown. The best model has the northern half of the upper two layers (500 m.) non-magnetic. Its base is at 4250 m. The GFR of this model is only 2.0 and the calculated magnetic anomaly (Figure 4.47) is less complex than the observed anomaly. The low GFR value and the complexity of the seamount's magnetic anomaly indicate that caution is warranted in interpreting the magnetization direction calculated from this seamount.

4.5.21 HARVEY GUYOT (P2)

Harvey Guyot is located at 17.8° N, 172.7° E, about 100 km. to the east of Woollard Guyot in the western Mid-Pacific Mountains. It was surveyed and dredged on cruise KK81062605 of the R/V Kana Keoki. The guyot's top reaches a minimum depth of 1050 m. and has as much as 0.35 sec. (two-way travel time) of carbonate and pelagic material forming its cap (Kroenke, 1981). The top appears to be elongated northwest to southeast (Figure 4.48); although, only the northern half is surveyed well. Like Woollard Guyot, Harvey sits upon the south edge of the Mid-Pacific Mountains plateau. On its north side, the ocean bottom is only about 3200 m. deep whereas it is 5200 m. deep to the south. The shallowness of the ocean bottom to the north of Harvey Guyot is partially the result of a deep sediment pond found there (Kroenke, 1981).

Harvey Guyot's magnetic anomaly is as simple as any of those of the Mid-Pacific Mountains seamounts analyzed, but not nearly as simple as those of seamounts in other provinces (e.g., the Musicians Seamounts). The overall structure of the anomaly is a -504 nT. minimum flanked by maxima of +30 nT. and +326 nT., showing the guyot to be normally polarized. The minimum, however, is not symmetrically shaped. The lowest anomaly values occur over the northwest corner of the flat summit and a reentrant of higher values protrudes into the minimum from the east.

The best magnetic model has a top at 1500 m., a removal of 450 m., and a bottom of 4750 m. As the lowest closed contour around the seamount is at 3000 m., this sub-bottom extension requires some explanation. Two model layers were added below 3000 m., one having its top at 3500 m. (the bottom depth of the 3000 m. layer) and the other with its top at 4000 m. The 3500 m. contour is seen around much of the guyot and so the 3500 m. layer was assumed to keep the same slope on the north flank of the seamount as is observed on the south flank. As there is no 4000 m. contour around the seamount, the 4000 m. layer was constructed to maintain the same slope estalished by the two layers above it. The depth of the bottom of the model preferred by the modeling process is notable in the respect that it is significantly deeper than the apparent top of the underlying plateau at 3200 m. Although, the 4750 m. depth of the model seamount's bottom may not be accurate because of the uncertainties of the shape of the seamount at depth and the unknown magnetic effects of the underlying plateau, it indicates that the roots of the seamount are deep. The deep material

included in the model may not necessarily be part of the seamount itself; rather, it might be a magnetic root of remangetized material as disussed in Chapter 2. The best model's GFR of 2.7, while acceptable, is not particularly good. Figure 4.49 shows the calculated anomaly and residuals.

4.5.22 THOMAS GUYOT (P3)

At 17.3° N, 173.9° E, 330 km. southeast of Woollard Guyot and 150 km. southeast of Harvey Guyot, lies Thomas Guyot. Data from HIG cruise KK81062605, Scripps cruise IIOECGS, and DSDP Leg 62 were merged to make the bathymetric and magnetic maps shown in Figure 4.50. The seamount was dredged on cruise KK81062605.

Thomas Guyot is another of the medium size guyots of the western Mid-Pacific Mountains. Its flat top is about 22 km. in length, north-south, and 15 km. in width, east-west. It has a thick cap of carbonate and pelagic material, seen as 0.7 sec. (two-way travel time) of penetration on seismic reflection records (Kroenke, 1981). The minimum depth is 1287 m. near the center of the flat top. The slopes around the cap are relatively steep, but grade into shallower slopes further down the edifice. Like Harvey and Woollard guyots, Thomas is perched on the south side of the Mid-Pacific Mountains plateau and its southern flank blends into the scarps that constitute the southern edge of the plateau. The sea floor to the south of the plateau reaches a depth of

5000 m. To the north of the guyot, is a deep sediment filled trough with 0.9 - 1.2 sec. (two-way travel time) of sediment seen on seismic reflection records (Kroenke, 1981). The north flank of Thomas is buried in these sediments and the ocean bottom depth in that area is about 4000 m. A small subsidiary cone, reaching a depth of 2481 m., is found to the northwest of the main edifice of the guyot. It is isolated from the bulk of Thomas guyot to a depth of about 3750 m. Unfortunately, it is too sparsely surveyed for paleomagnetic study.

The magnetic anomaly over Thomas Guyot is rather complex. Six highs and lows can be seen in a single north-south line over the seamount. A deep minimum of -550 nT. is over the northern edge of the flat top. North of it is a high of +107 nT. and over the southern part of the flat top is another high of +82 nT. On the south flank of the guyot is a low of -151 nT. Further to the south are another low and a high that are poorly sampled. The first four features of the anomaly are probably a result of the guyot body, but the latter two may be caused by the edge of the underlying plateau to the south. The magnetic anomaly map in Figure 4.50 was difficult to contour because of its complexity, the sparseness of the survey data, and large track crossing errors. The latter problem probably results from navigational errors and the difficulty of making magnetic diurnal corrections with no base station and poorly navigated ship tracks. The seamount appears to be normally polarized.

The magnetic model has its base at 5250 m. and its top at 1625 m., a reduction of 338 m. The area of the magnetic anomaly used for the magnetization inversion was restricted to the part north of the -151

nT. low to lessen the bias caused by the anomaly of the edge of the underlying plateau. The slope of the northern flank of the model was constructed to maintain the same slope as the other sides of the model that follow the bathymetric contours. The small seamount to the northwest was included in the model with the same magnetization intensity and direction as the main edifice; however, it is well outside the area of the magnetic anomaly used for the inversion and thus has only a small effect on the model.

A homogeneously magnetized model had a marginally acceptable GFR of 2.1. Subsequent modeling reversed the polarity of the south half of the upper two layers in an effort to duplicate the +82 nT. high over the south section of the top. This feature improved the GFR to 2.5 without changing the magnetization direction significantly. This value of the GFR is still rather low and indicates that the magnetization derived from Thomas Guyot may not be very accurate. The calculated anomaly and residuals are shown in Figure 4.51.

Like the models of the other Mid-Pacific Mountains, this one has its bottom deeper than the apparent depth of the underlying plateau. The top of the model, however, is not like those of the other Mid-Pacific Mountains. Although 0.7 sec. (two-way travel time) of sediments are seen on reflection records taken across the summit of Thomas Guyot (Kroenke, 1981), the modeling process prefers magnetic material up to the flat top. Perhaps this discrepancy is not too surprizing considering the complexity of the anomaly, the sparseness of the data, and the low GFR.

4.5.23 ALLEN GUYOT (P4)

Allen Guyot is located at 18.3° N, 174.1° E, about 300 km. due east of Woollard Guyot in the western Mid-Pacific Mountains. It was surveyed and its pelagic cap was cored during cruise KK81062605. A single track from DSDP Leg 62 also crosses this seamount and was added to the survey data.

The guyot has a small flat top about 12 km. across at its widest. The minimum recorded depth is 1376 m. near the center, and a cap of 0.45 sec. (two-way travel time) depth is seen on seismic reflection records (Kroenke, 1981). The edifice is somewhat elongated east-west and appears to be on a small ridge that includes larger guyots to the east and west. The deepest closed contour is only 2750 m., but the sea floor drops off to 4000 m. to the north and south (Figure 4.52). As the survey data is sparse, Nemoto's bathymetric map (K. Nemoto, in preparation) was used to further constrain the shape of the seamount. To the south of the guyot is the same deep sediment basin mentioned in the discussion of Thomas Guyot.

The magnetic anomaly consists of a -350 nT. minimum over the top of the seamount, flanked by a +237 nT. maximum to the south and a +101 nT. maximum to the north, showing the seamount to be normally polarized. The area of the magnetic anomaly used to constrain the magnetization inversion was limited in the east-west direction because most of the magnetic information comes from two closely spaced north-south ship tracks over the seamount.

The best magnetic model has 750 m. of its top considered non-magnetic and its base extended to 6000 m. The bottom of this model is much deeper than any of the other Mid-Pacific mountains analyzed. This feature is caused by the long wavelength of the magnetic anomaly. Two different types of sub-bottom extensions were tried for this model. In both, layers deeper than the last closed contour down to 4000 m. were assumed to maintain the same slope on the east and west flanks as are seen on the north and south flanks (i.e., the contours were closed through the east west ridge). In one model the layers deeper than 4000 m. were assumed to have the same area as the 4000 m. layer (i.e., the extension had vertical sides). The other model assumed that the slope of the layers above 4000 m. was extended to the bottom of the model. The GFR of the second model was significantly better than that of the first (3.6 versus 3.0), but the magnetization parameters changed little. Thus the modeling procedure favors a deep sloping extension of the bottom of the seamount. The calculated anomaly and residuals are shown in Figure 4.53.

4.5.24 BIRDSEYE SEAMOUNT (W7)

Birdseye Seamount is located at 20.9° N, 165.7° E, about 300 km. north of Wake Island. It was discovered by D. Handschumacher who located its large magnetic anomaly during an aeromagnetic survey. Birdseye was surveyed and dredged by the R/V Kana Keoki on cruise KK81062602. As seen in Figure 4.54, the seamount is a simple conical feature rising from the sea floor at 5500 m. to its peak at 2382 m. The summit of the seamount is rough, displaying several hyperbolas on seismic reflection records, suggesting that little sediment is to be found there. Except for a portion of the southeast flank, most of the seamount is well covered by the survey.

The magnetic anomaly is very large (1422 nT. peak-to-peak), yet it is very smooth and simple. A deep minimum of -1153 nT. occurs over the peak and is flanked on the north and south by maxima of +210 nT. and +269 nT. The seamount is normally polarized.

Modeling Birdseye Seamount was very easy. The GFR peaked sharply for a top depth of 2875 m. (500 m. removed) and preferred a bottom depth of 5500m. (no extension). The GFR of 8.1 is very high, suggesting excellent results. Comparing the observed anomaly and the calculated anomaly (Figure 4.55) it is difficult to tell the two apart.

4.5.25 UNNAMED SEAMOUNT (W10)

Seamount W10 is found at 16.7° N, 162.4° E, approximately 500 km. southwest of Wake Island. It was surveyed by Kana Keoki cruise KK81062604. As seen in Figure 4.56, the survey of this seamount is very sparse, constraining neither the bathymetry nor magnetic anomaly well. Fortunately, the seamount appears to be a simple conical feature with a smooth magnetic anomaly. The seamount rises from the ocean bottom at 5500 m. to its summit at about 2247 m. It appears to be elongated in the east-west direction; although, data on the north and south are non-existant and the contouring may be misleading.

The magnetic anomaly is small, only about 225 nT. peak to peak, but once again there is no information about the anomaly to the north and south. It is interesting to compare this anomaly to that of Birdseye Seamount. Birdseye is a few meters shorter than W10, but its magnetic anomaly is larger by a factor of seven. W10 appears to be normally polarized with a minimum of -188 nT. over its summit and a maximum of more than +37 nT. to the south.

Because of the long wavelength magnetic anomaly, the magnetic source body for the model must be deep. The best model has a bottom extension of 750 m. and 1125 m. removed from the top. It is difficult to assess the effect of the sparseness of the data on these values. The GFR of the best model is 5.5, indicating an excellent match between the observed and calculated anomaly (Figure 4.57); however, this value is probably inflated by the apparent smoothness of the magnetic anomaly and its low amplitude.

The inclination, 13.7°, and declination, 16.7°, of the magnetization vector calculated from the W10 data are sufficiently close to the present day geomagnetic field values of 19.4° and 6.3° to make one suspect that most or all of W10's magnetic anomaly may be induced by the geomagnetic field rather caused by the seamount's remanent magnetization. The VGP for this seamount falls at 71.0° N, 281.3° E, near the north magnetic pole, but also not far from the scatter of VGPS of old western Pacific seamounts. Consequently, W10 might be an old seamount whose magnetization direction just happens to be close to the present field direction or it could be a very young seamount that has not been significantly displaced from the latitude of its origin. As there is no reason to expect volcanism of such a young age in this part of the Pacific, the latter hypothesis seems improbable. The low intensity of magnetization, 1.6 A./m. favors the induced magnetization hypothesis.

4.5.26 SEASCAN GUYOT (W11)

Seascan Guyot was also discovered by D. Handschumacher during an aeromagnetic survey. It is located at 15.1° N, 159.3° E, about 950 km. due north of Ponape Island. Seascan was surveyed and dredged during cruise KK81062602. As seen in Figure 4.58, this seamount is a small guyot with a simple conical shape. The flat top is elongated slightly northwest to southeast and is 11 km. across at its widest point. Very

little penetration of the top was seen on seismic reflection records. The minimum depth is 1157 m. and the ocean bottom depth is about 5500 m. Several subsidiary cones, no more than 500 m. in height, are scattered around the seamount's base.

The magnetic anomaly is extremely large, 1907 nT. peak to peak. It consists mostly of a large minimum that is nearly cut in two by a sharp maximum. The maximum reaches -520 nT. over the central portion of the top, whereas the minima, -1106 nT. and -1442 nT., are located over the northwest and southeast sections of the summit. To the north and south of the main low are maxima of +465 nT. and +175 nT. Seascan Guyot is normally polarized.

The best model of the guyot has a GFR of 4.2 indicating very good results. The GFR would undoubtedly be higher were there no short wavelength structure within the minimum. The cause of the relative maximum protruding into the minimum is probably a reversely magnetized body within the upper layers of the edifice. A model with a top at 1725 m. (550 m. removed) and a bottom at 5250 m. (250 m. above the sea floor) produces the highest GFR. The portion of the top removed may reflect a non-magnetic hyaloclastite or carbonate cap; however, it is not clear whether the base of the seamount is not very magnetic or the method is not accurate enough to determine the level of the bottom within 250 m. The calculated anomaly and residuals are shown in Figure 4.59.

4.5.27 UNNAMED SEAMOUNT (W12)

W12 is located 960 km. northeast of Guam at 15.5° N, 153.3° E. It was surveyed and dredged during Lamont-Doherty cruise V3401. An additional ship track from Scripps cruise CIRC02AR crosses the seamount and was added to the survey data.

Figure 4.60 shows that the seamount is a simple conical feature. Its base is at a depth of 5750 m. and its summit reaches 2135 m. Its magnetic anomaly is also simple, though low in amplitude (261 nT. peak to peak). The anomaly is characterized by an elongate east-west minimum of -250 nT. to the north of the seamount and a similar maximum of 11 nT. to the south of the seamount.

The very simple shape of the seamount and its magnetic anomaly help to make for a very high GFR of 9.5 for the best model. Comparing the calculated anomaly (Figure 4.61) with the observed anomaly (Figure 4.60), the two are seen to be virtually identical. This model has 250 m. removed from the summit and no sub-bottom extension. As shown in Figure 4.2, W12's VGP falls far from most of the other seamount VGPs, but not far from the north magnetic pole. The magnetization direction (26.0° inclination, 18.8° declination) is somewhat different than the present day field direction at the site of the seamount (15.8° inclination, 3.4° declination), so it is not clear whether the magnetization is induced or remanent or a combination of the two. A model was tried using the same data, assuming the magnetization to be

wholly induced, but its GFR was only 2.3. Perhaps a small amount of remanent magnetization is sufficient to make such a model seem untenable. The magnetization intensity is low, 1.8 A./m., as would be expected of a seamount whose magnetization is mostly induced.

4.5.28 CAMPBELL SEAMOUNT (W13)

Campbell Seamount is located at 16.5° N, 149.0° E, about 600 km. northeast of Guam. It was surveyed during Lamont-Doherty cruise V3401. Data from Lamont cruise C1107 and HIG cruises KK760102 and KK770303 were merged into the survey.

The seamount is roughly conical in shape with a small summit that attains a shallowest depth of 1609 m. The lowest closed contour around the seamount is 4750 m.; however, as seen in Figure 4.62, the sea floor slopes down to 5000 m. not far to the north and south. On the northeast flank of the seamount, 3000 m. and deeper, there is the suggestion of a spur or lobe. Around the seamount are several smaller edifices. One to the northeast reaches up to 3965 m., one to the east reaches 3167 m., and another on the west has a minimum depth of 4119 m. The cone to the east may be connected to Campbell near the sea floor, but this is impossible to ascertain with the present data coverage. Campbell and the seamounts on the east and west form a line of volcanoes. Whether or not this lineation is fortuitous is unclear.

Campbell's magnetic anomaly is not simple. It consists mainly of a maximum over the south flank of the peak. The maximum has two peaks itself, one of over +450 nT. and the other over +600 nT. Neither of these twin maxima are clearly related to the summit of the seamount. North of the bulk of the seamount is a broad minimum of less than -200 nT. This configuration of lows and highs indicates that the seamount is reversely polarized. Unfortunately, the minimum is not well surveyed, making the modeling of the seamount somewhat of a problem. To the east and west of the anomaly maxima are minima of -129 nT. and -100 nT. These minima are elongated east-west and might join were it not for the maximum caused by the body of Campbell Seamount. These two magnetic anomalies suggest that there might be some kind of buried magnetic body related to the line of seamounts.

Modeling of this seamount was difficult because of the complexity of the anomaly and the lack of data on the north flank of the seamount. The inclination calculated from the magnetization inversion is somewhat dependent on the magnetic gradient over the north flank, but because there is no north-south track over the summit, this gradient is not well known. Thus the final results will be dependent on the contouring of the magnetic anomaly in that region. Digitization of the anomaly along track lines was tried in an effort to reduce the bias caused by contouring; however, the calculated magnetization was found to be dependent on the extent of the tracks used in the northern part of the survey area. Consequently, the magnetization derived using the usual gridding procedure was considered better.

The best model has a top at 1875 m. (a reduction of 265 m.) and a bottom at 5250 m. (about 250 m. below the sea floor). The GFR of this model is very low, 2.2. The shape of the maximum of the anomaly is elongate to the northwest and not to the northeast as expected from the shape of the seamount. The northeast spur of the seamount was removed from the model improving the GFR to 2.4 with little change of the magnetization direction. The calculated anomaly and residuals are shown in Figure 4.63. Because of the low GFR of this model and the problems constraining the shape of the anomaly, the results from this seamount should be treated with caution.

4.5.29 UNNAMED SEAMOUNT (W14)

W14 is a medium size seamount located at 11.2° N, 146.8° E, 330 km. southeast of Guam. It was surveyed during Lamont-Doherty cruise V3611. As seen in Figure 4.64, the seamount has two peaks that coalesce into a single edifice. The base of the seamount is at about 5250 m. and the two peaks reach 2044 m. and 2095 m.

The magnetic anomaly has two highs and two lows. The minima coalesce into a broad low over the seamount and are flanked by maxima to the north and south. The minima descend to -689 nT. and -545 nT. The first is slightly northwest of the north peak, whereas the second is slightly south of the south peak. The maxima reach +206 nT. and

+270 nT. on the north and south flanks of the seamount. The seamount is normally polarized.

The best model has 1000 m. of the top removed and 1000 m. added to the base. It is doubtlful that so much of the summit is non-magnetic; however, the complex, twin-peaked minimum does not have a shape entirely consistent with homogeneous magnetization of the summit layers. The removal of the two bathymetric peaks from the top of the model helps the model to fit the anomaly better on the whole, even though the best model predicts only a single deep minimum (of -350 nT.) rather than two deep minima observed (Figure 4.65). The complex anomaly also keeps the GFR low, 2.7, indicating acceptable, but not good results. The magnetization vector gives a VGP at 74.5^{o} N, 6.4^{o} E, very near the Late Eocene paleomagnetic pole (Sager, 1983a). Eocene volcanism is unexpected in this part of the Pacific. As this seamount has not been dated it is unclear whether the seamount is actually Eocene in age or whether it is older but has a VGP that just happens to fall near the Eocene pole.

4.5.30 WINCHESTER GUYOT (W15)

This seamount is located at the end of a 300 km. long north-south line of seamounts about 420 km. north of Ponape Island. The survey, at 10.3° N, 156.7° E, was made during cruise KK81062602.

Winchester seamount is nearly conical and rises from the ocean bottom at 5250 m. to a minimum recorded depth of 1551 m. It is slightly elongated to the west as is shown in Figure 4.66. The summit has three peaks. One is a broad dome of pelagic sediments, reaching 1726 m., in the center of the summit. The other two are sharp pinnacles, reaching to 1551 m. and 1594 m., on the northwest and south edges of the summit. These pinnacles appear to be part of a rampart that surrounds more than half of the summit.

Although Winchester Seamount is fairly large, its magnetic anomaly is only 490 nT. peak to peak. It consists of a -364 nT. minimum over the south side of the summit and a +123 nT. maximum over the seamount's north flank. The anomaly configuration shows that it is normally magnetized.

The best model has 250 m. of the top removed and a bottom 500 m. below the ocean floor. Its GFR is 4.1 indicating a good match of the calculated anomaly (Figure 4.67) and the observed anomaly.

4.5.31 HEEZEN GUYOT (W16)

Heezen Guyot is a medium size guyot at 8.8° N, 163.2° E, on the edge of the Nauru Basin, approximately 380 km. due north of Kosrae Island. It was surveyed during Lamont-Doherty cruise V3401 as an alternate drilling site for DSDP Leg 61. The guyot was never drilled, however, the D/V Glomar Challenger did make a pass over it on that cruise.

The guyot has a relatively simple shape as seen in Figure 4.68. It is a truncated cone 80 km. across the base with a flat top 14.5 km. in diameter. The minimum recorded depth is 1091 m. and the lowest closed contour is 5000 m. On seismic reflection records taken by the Glomar Challenger (Schlanger and Larson, 1981, p. 798) the guyot is seen to be surrounded by at least 0.5 sec. (two-way travel time) of sediments; although, considering the results of the Leg 61 drilling that cored many sills, it is not clear whether the seismic profiles around the guyot actually record the acoustic basement. The same seismic records show that there is a carbonate/pelagic cap of at least 0.25 sec. (two-way travel time) depth.

Heezen Guyot's magnetic anomaly is very complex. Its overall appearance is that of a broad, complicated minimum over the summit of the edifice flanked by maxima on the north or south. This configuration indicates that the guyot is normally polarized. As seen in Figure 4.68, the anomaly low is actually made up of four relative minima. Three of them, lows of -884 nT., -823 nT., and -952 nT., are located over the northern part of the volcano's summit and the flank

just to the east. The fourth minimum is just over -1000 nT. and is found over the bathymetric spur protruding from the southwest side of the summit. Within the broad low are three relative maxima of -644 nT., -246 nT., and -304, nT. that are located over the central and southern part of the summit. To the north of the main low is a maximum of +417 nT. and to the south, is another relative maximum of -37 nT.

One might expect from the complexity of the anomaly that the seamount is not homogeneously magnetized. However,as seen from the calculated anomaly (Figure 4.69), even a homogeneous seamount of this shape produces a complex magnetic anomaly at this latitude. In the best model, none of the top was removed and the base was extended 750 m. below the sea floor. The GFR is 3.4 and indicates good results. The complexity of this seamount's magnetic anomaly tends to keep the GFR somewhat low because it is difficult to exactly match all of the highs and lows. Upward continuation of the seamount's anomaly would tend to smooth out these bumps and would improve the GFR of the model.

4.5.32 VAN VALTIER GUYOT (W17)

Von Valtier is a small guyot located at 7.3° N, 172.3° E, 120 km. east of Majuro Atoll in the Marshall Islands. It was surveyed and dredged by the R/V Kana Keoki during cruise KK81062602. Planktonic foraminifera of Campanian age were among the fossil material recovered from the guyot (J. Haggerty, personal communication, 1983).

The guyot has a small flat top about 8 km. across as shown in Figure 4.70. The minimum recorded depth of the summit is 1252 m. and about 0.25 sec. (two-way travel time) of penetration is seen on seismic reflection records across the summit. Although slightly elongate east-west, the guyot is roughly conical. It appears to be attached to a small seamount to the east that is poorly surveyed. The regional seafloor depth varies from about 4250 m. on the southwest side of the survey area to deeper than 4750 m. on the east side of the survey area. This bathymetric gradient may be caused by a sediment apron whose source is the Marshall Islands.

Von Valtier's magnetic anomaly is more complex than expected from a homogeneously magnetized edifice. There is a large low with two peaks of -173 nT. and -621 nT. over the top of the seamount. These are flanked by maxima of +335 nT. to the north and -16 nT. to the south.

The double peaked minimum poses a problem for paleomagnetic modeling. It appears that the northern of the two minima is anomalous and may result from some sort of magnetization inhomogeneity. Models in which most of the magnetic anomaly was used for the magnetization inversion tended to have large declinations on the order of 20°. In

these models the calculated anomaly tended to follow the northern maximum which is elongated northwest to southeast. However, such models predicted no northern minimum and a displayed a southern minimum that was also elongated northwest to southeast and not east-west as observed. Several models were tried with reversals near the summit in an attempt to account for the northern minimum, but these models were no improvement on the homogeneous models. Another model was tried in which only the southern two thirds of the anomaly were used to constrain the magnetization inversion. This was done in the belief that the northern minimum was modifying the shape of the northern maximum and causing a spuriously large declination to be calculated. In this model, the calculated anomaly followed the southern minimum (Figure 4.71) and the declination changed from 18.9^{o} to -4.7^{o}. The position and shape of the calculated anomaly for this model looks more like the observed anomaly and the GFR was improved from 2.9 to 4.4. The model's top is at 1875 m. (626 m. removed) and its bottom is at 5000 m.

Figure 4.5 Bathymetry and magnetic anomaly of Magnet Seamount (C1). (left) Bathymetric contours shown as solid lines; contour interval is 250 m. Dashed lines are ship tracks with magnetic and batymetric data; dotted lines (in following figures) are ship tracks with only bathymetric data. (right) Magnetic contours shown as solid lines; contour interval is 100 nT. Magnetic anomaly is total field residual anomaly (total field minus IGRF) corrected for diurnal variations. Dashed box is area of magnetic anomaly used to calculate magnetization parameters. This area corresponds to the area of the calculated anomaly and residuals in Figure 4.6.

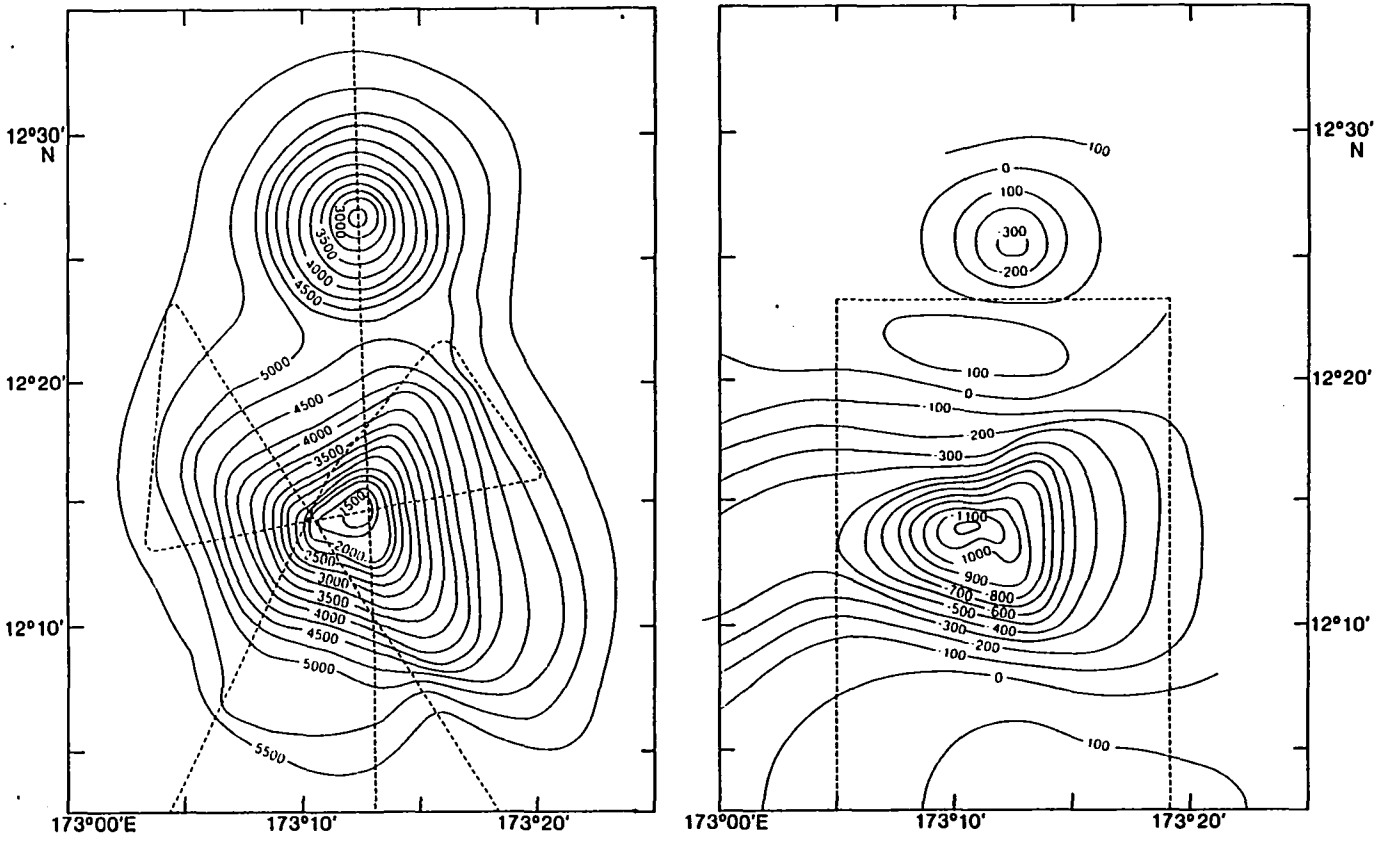
12°30' N
12°20'
12°10'
173°00'E
173°10'
173°20'
1000
3500
4000
4500
5000
4500
4000
3500
3000
2500
2000
1500
3000
3500
4000
4500
5000
5500
100
0
100
300
200
100
0
100
200
300
1100
1000
900
800
700
600
500
400
300
200
100
0
100
12°30' N
12°20'
12°10'
173°00'E
173°10'
173°20'

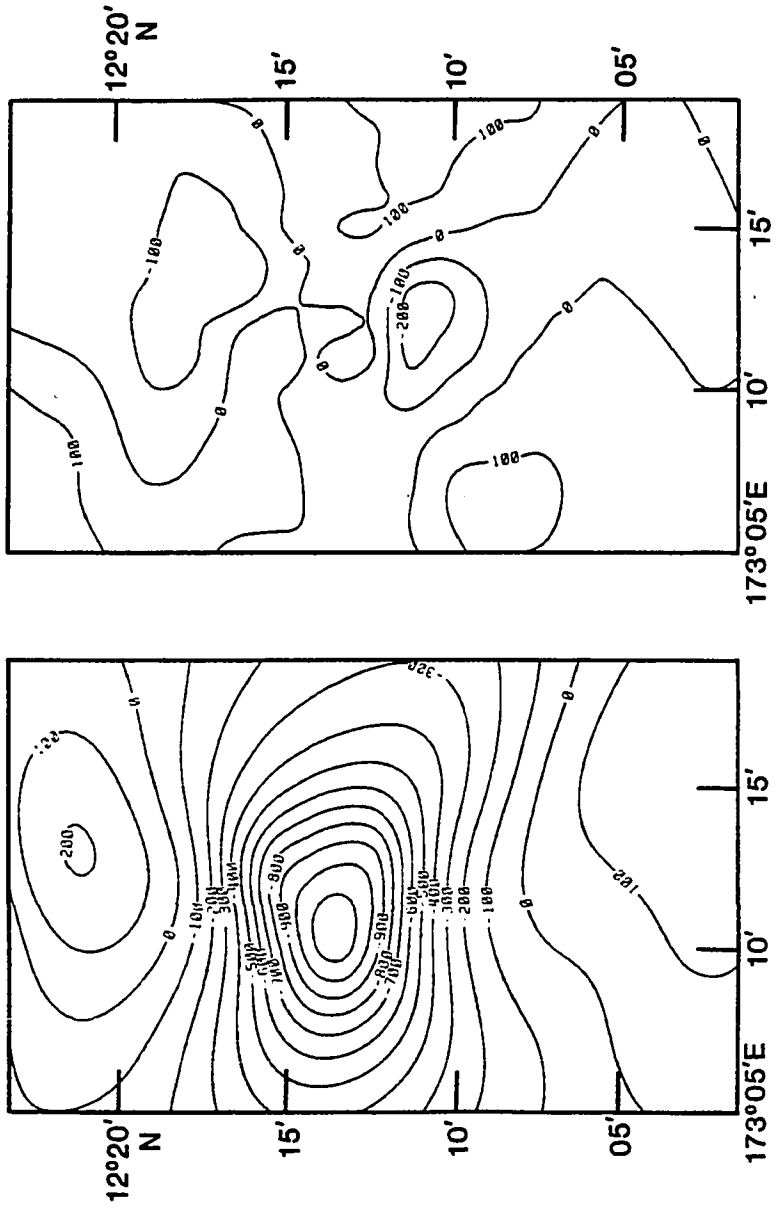

Figure 4.6 Calculated anomaly and residuals for Magnet Seamount (C1). (left) Magnetic anomaly calculated using the bathymetric model of Magnet Seamount with its magnetization parameters from Table 4.1. Contour interval is 100 nT. (right) Residuals (observed minus calculated anomaly) contoured at 100 nT. intervals.

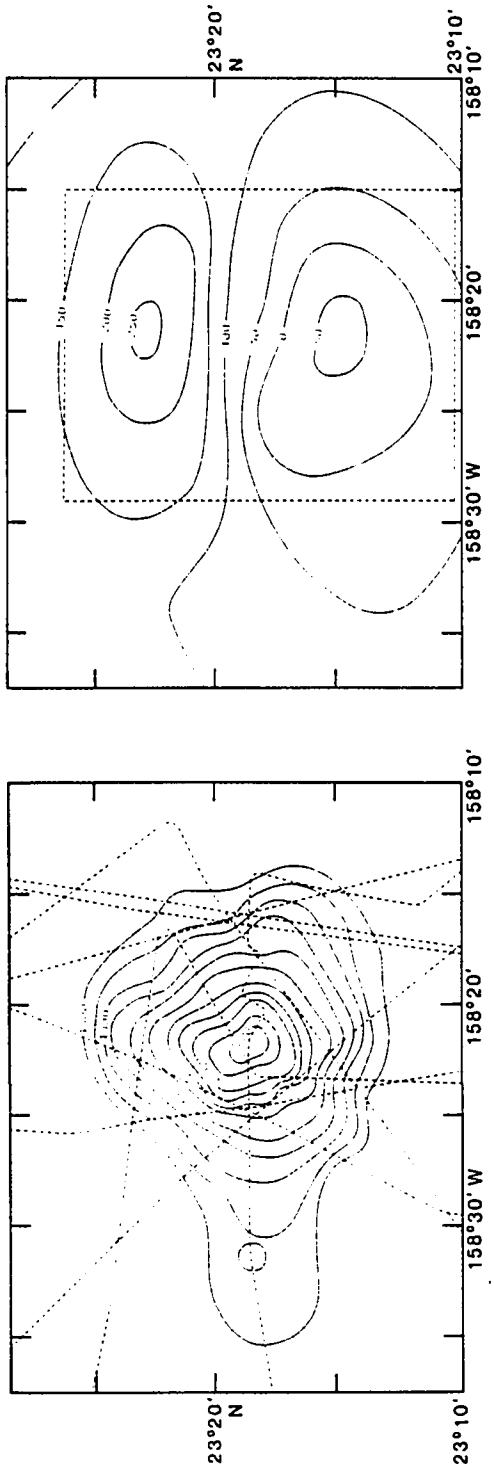

Figure 4.7 Bathymetry (left) and magnetic anomaly (right) of Kauluakalana Seamount (H1). See Figure 4.5 for explanation of charts. Magnetic contour interval is 50 nT.

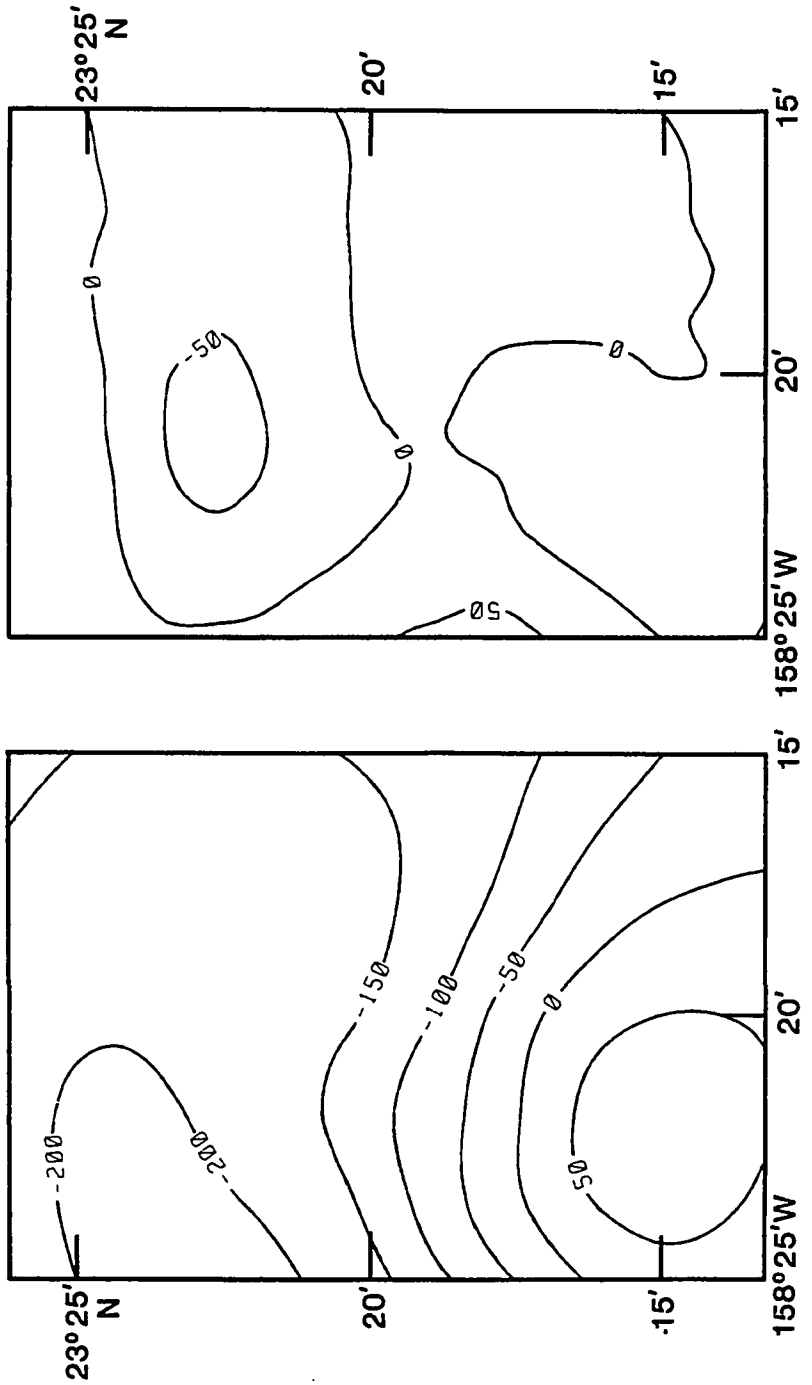

Figure 4.8 Calculated anomaly (left) and residuals (right) for Kauluakalana Seamount (H1). Contour interval is 50 nT.

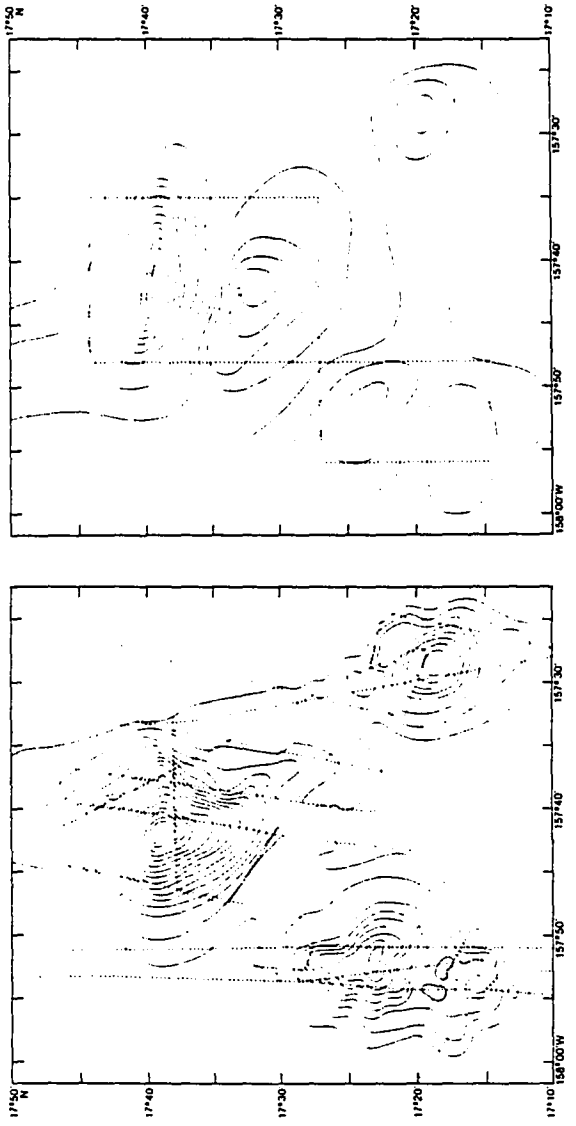

Figure 4.9 Bathymetry (left) and magnetic anomaly (right) of Finch (H5) and H6 seamounts. See Figure 4.5 for explanation of charts. Magnetic contour interval is 100 nT.

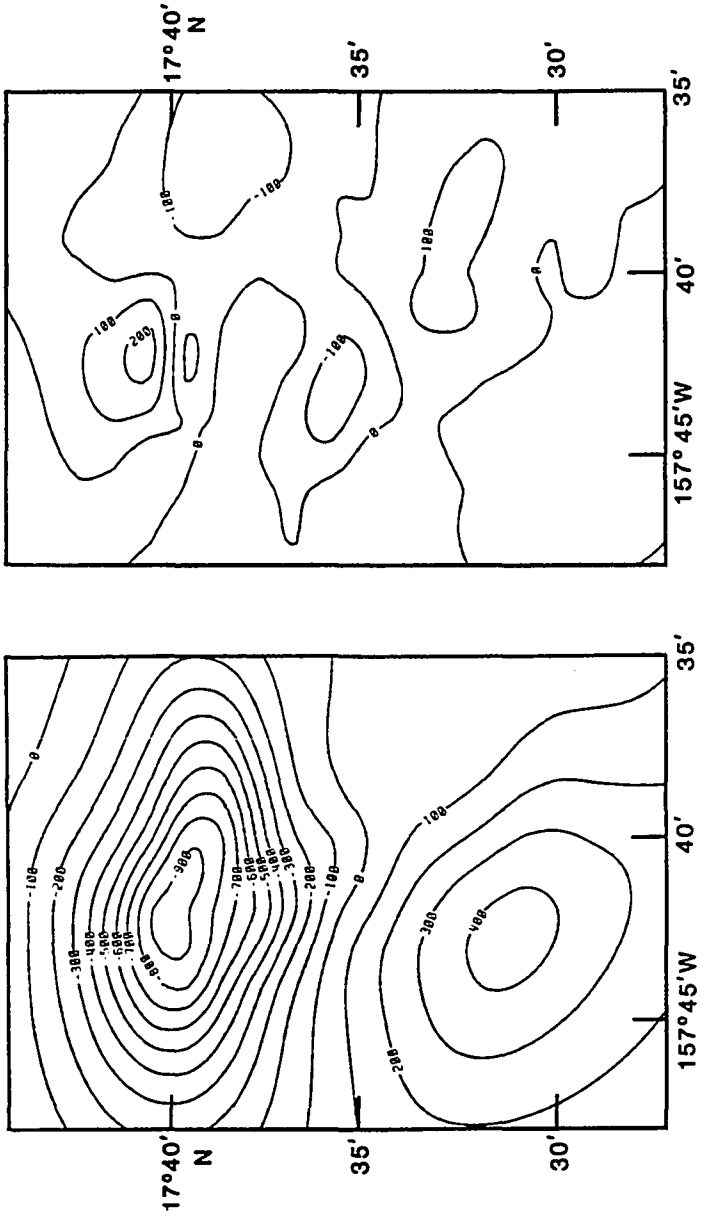

Figure 4.10 Calculated anomaly (left) and residuals (right) for Finch Seamount (H5). Contour interval is 100 nT.

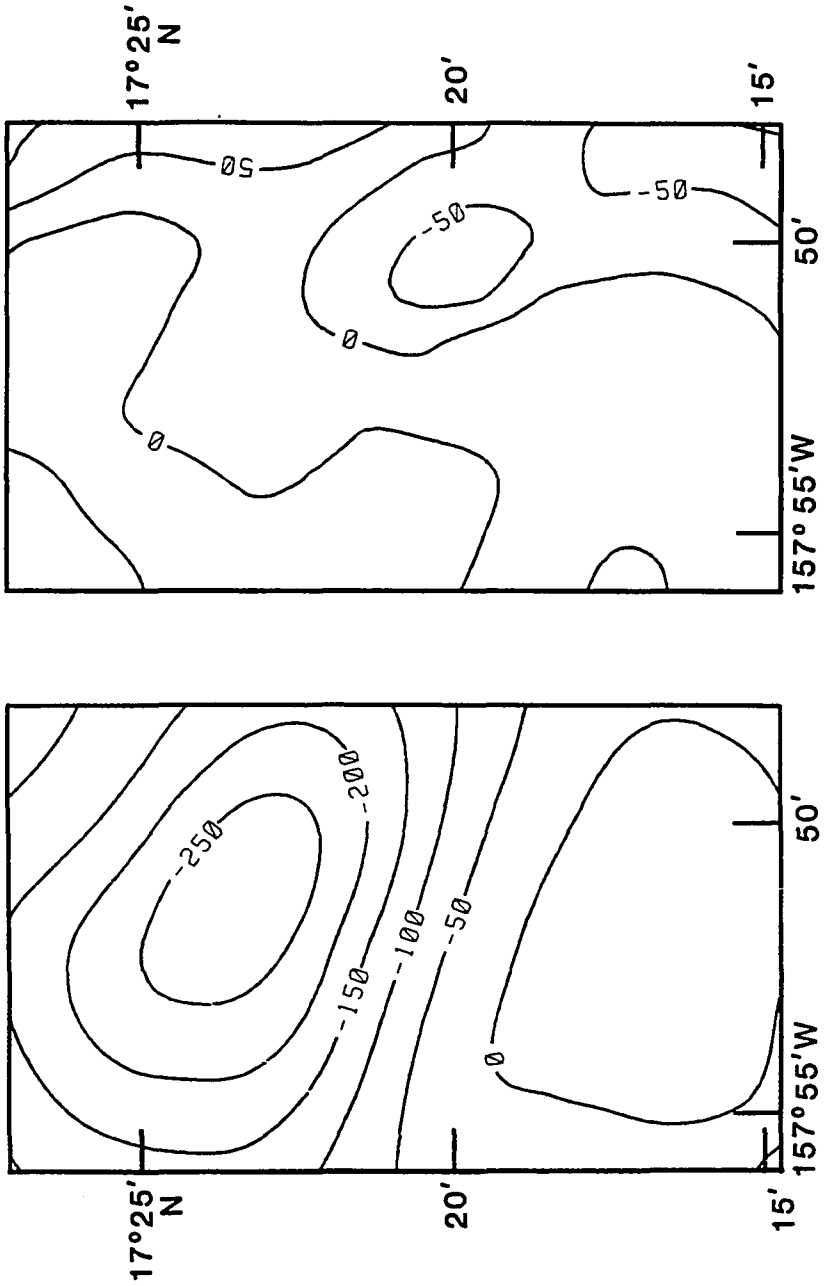

Figure 4.11 Calculated anomaly (left) and residuals (right) for seamount H6. Contour interval is 50 nT.

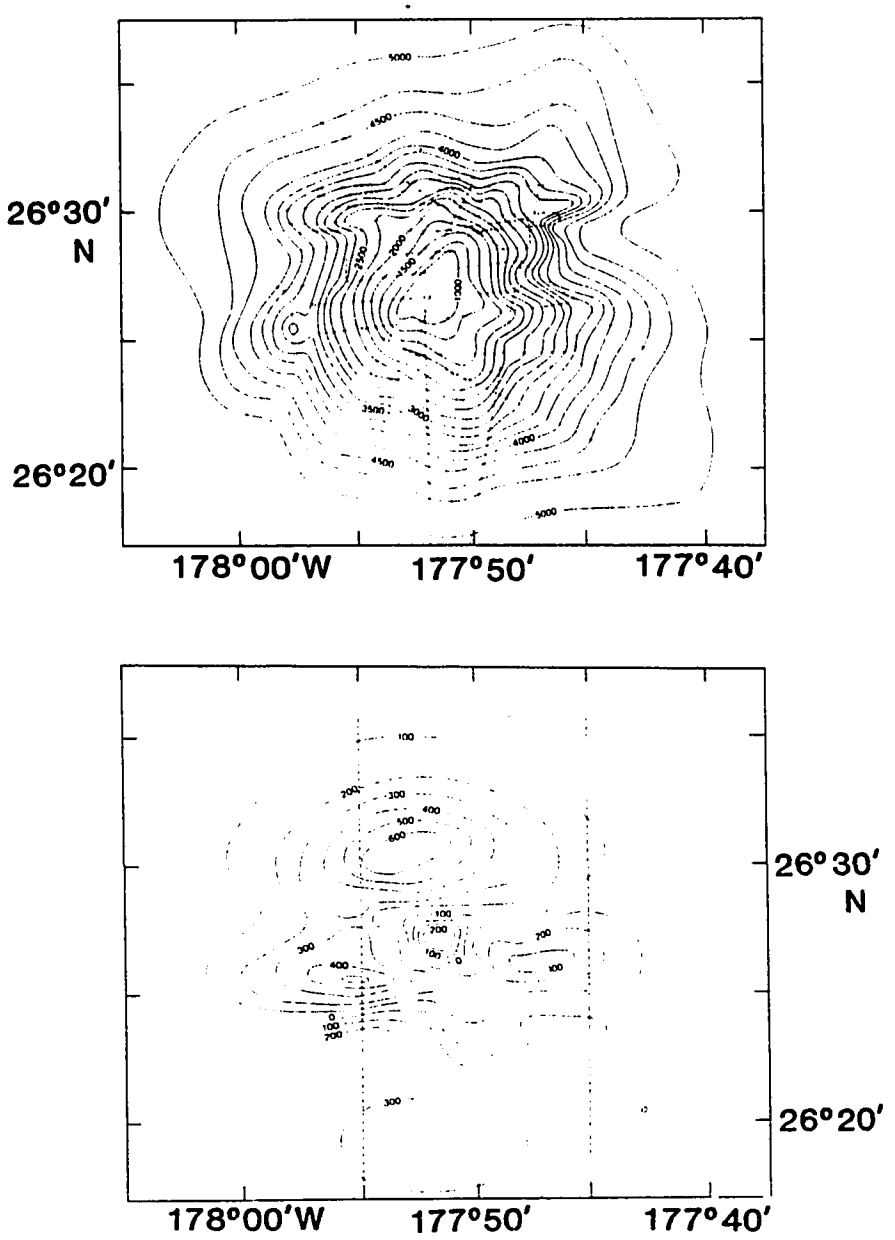

Figure 4.12 Bathymetry (top) and magnetic (bottoml anomaly of seamount H11. See Figure 4.5 for explanation of charts. Magnetic contour interval is 100 nT.

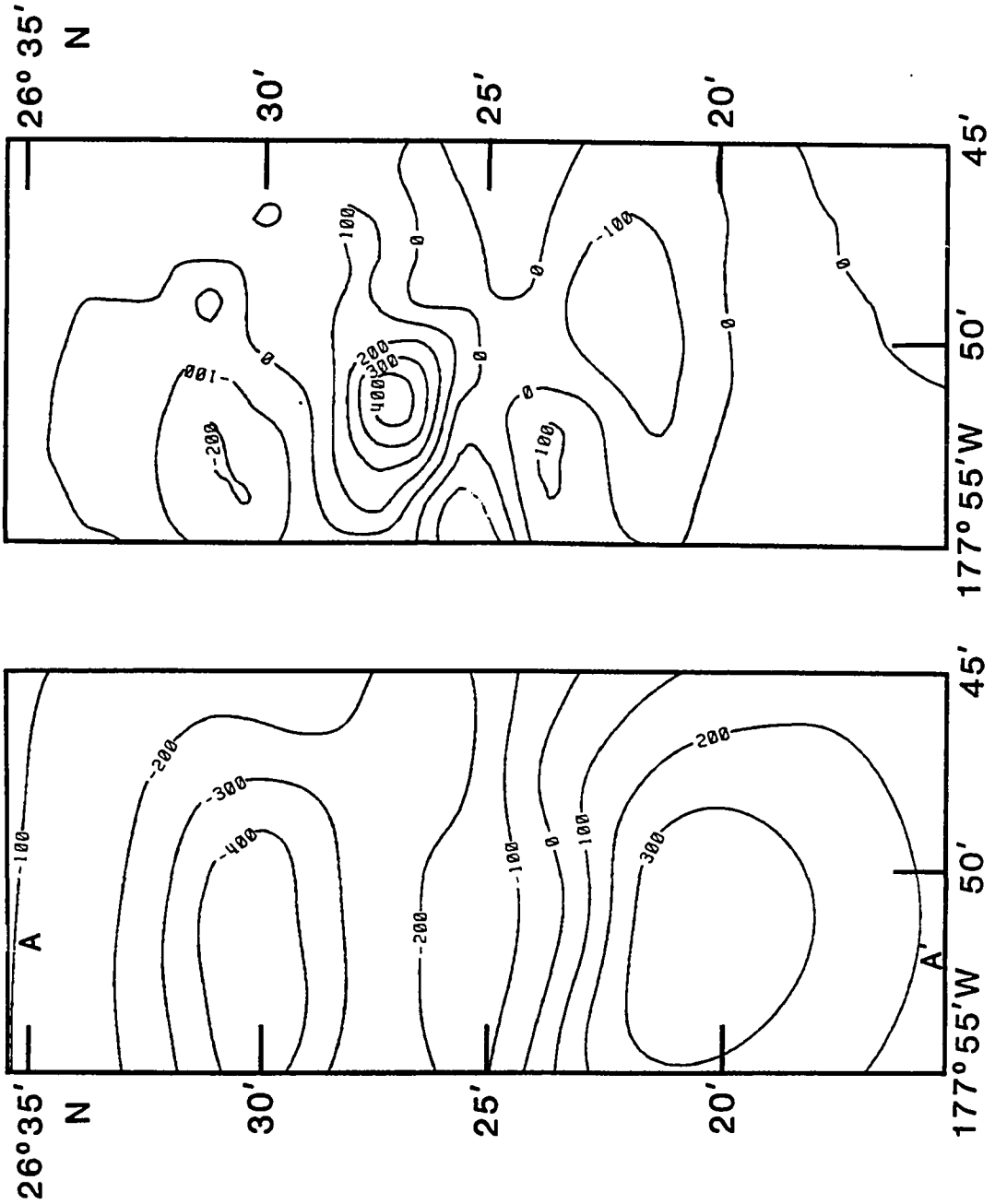

Figure 4.13 Calculated anomaly (left) and residuals (right) for seamount H11. Contour interval is 100 nT. Transect A - A' is shown in Figure 4.14.

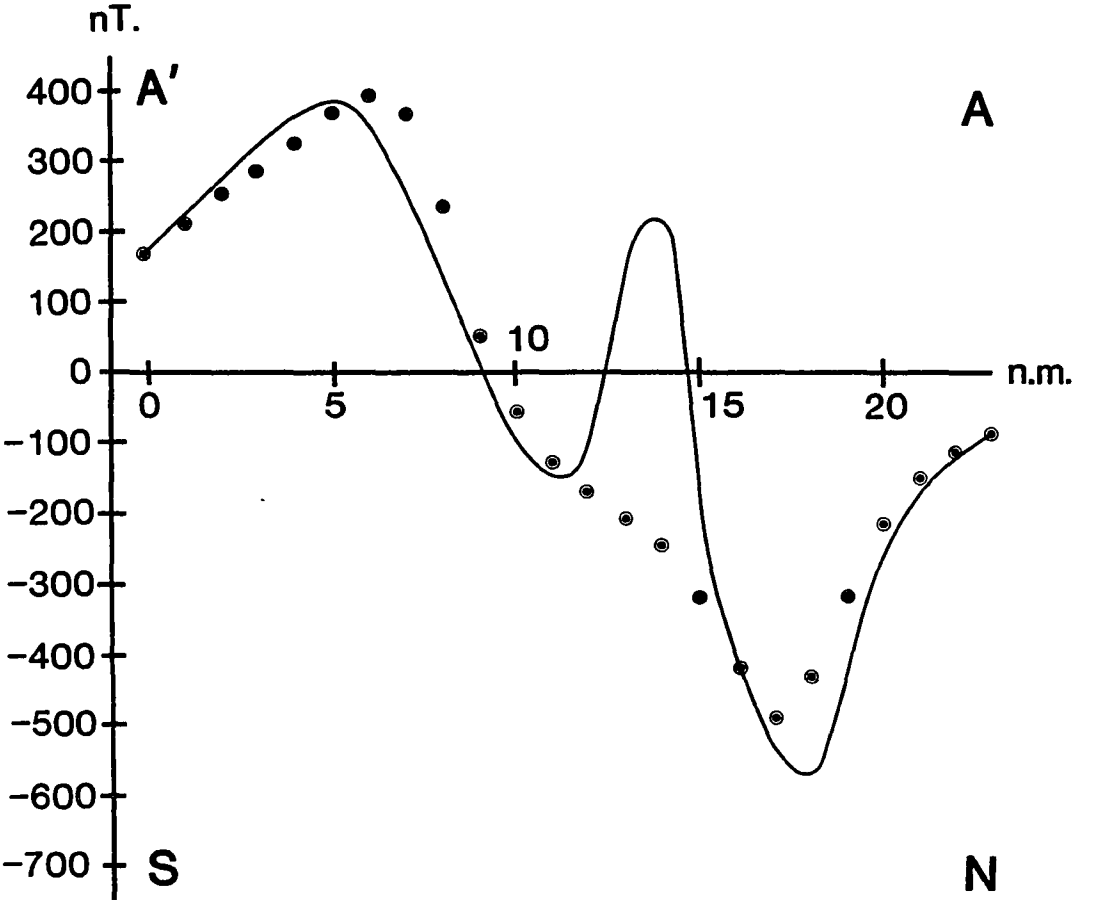

Figure 4.14 North-south transect over the magnetic anomaly of seamount H11 showing agreement of observed and calculated anomalies. The solid line is the observed anomaly and the dots are values of the calculated anomaly. The location of the transect is shown by A - A′ in Figure 4.12. Note that the calculated anomaly matches the long wavelength part of the anomaly, but ignores the short wavelength part. Abcissa labeled in nautical miles; ordinate, in nanoTeslas.

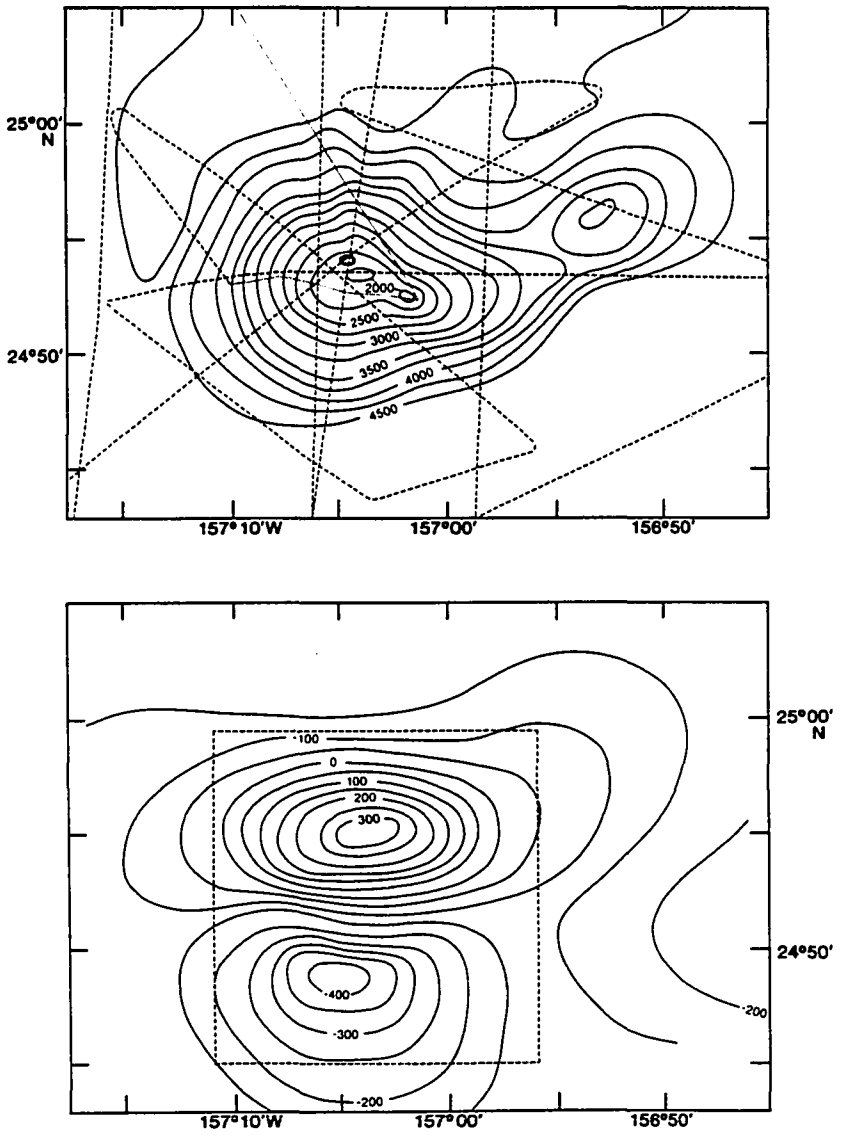

Figure 4.15 Bathymetry (top) and magnetic anomaly (bottom) of Paumakua Seamount (H12). See Figure 4.5 for explanation of charts. Magnetic contour interval is 50 nT.

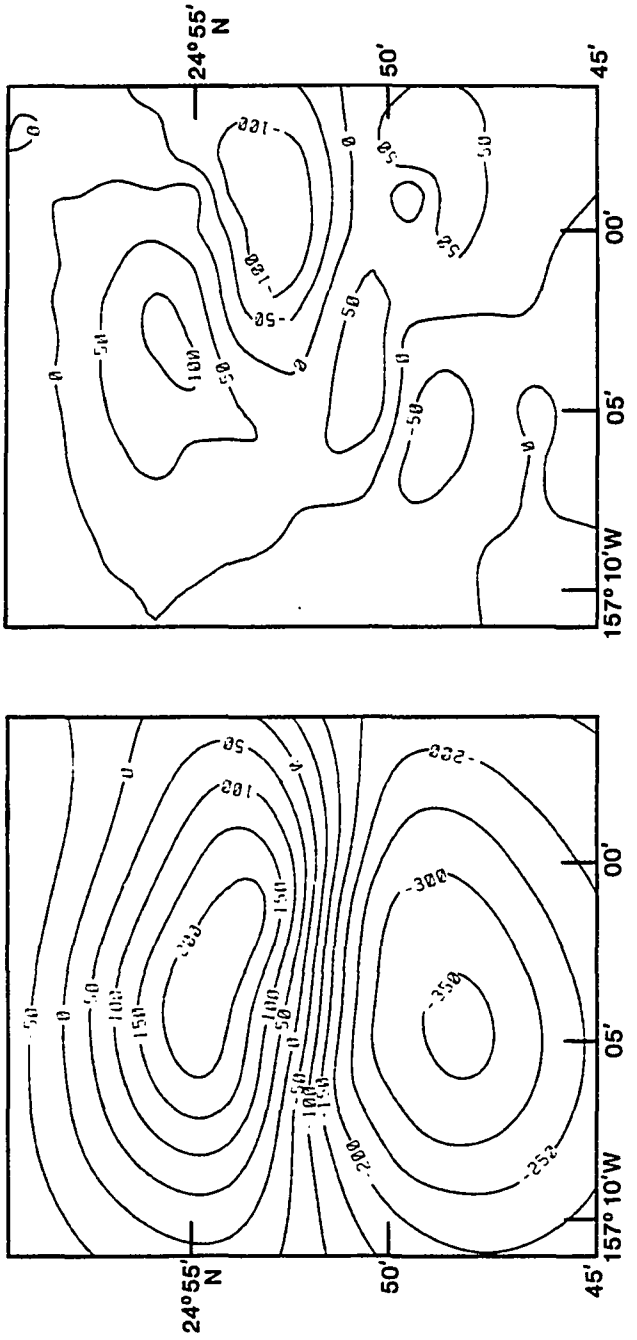

Figure 4.16 Calculated anomaly (left) and residuals (right) of Paumakua Seamount (H12). Contour interval is 50 nT.

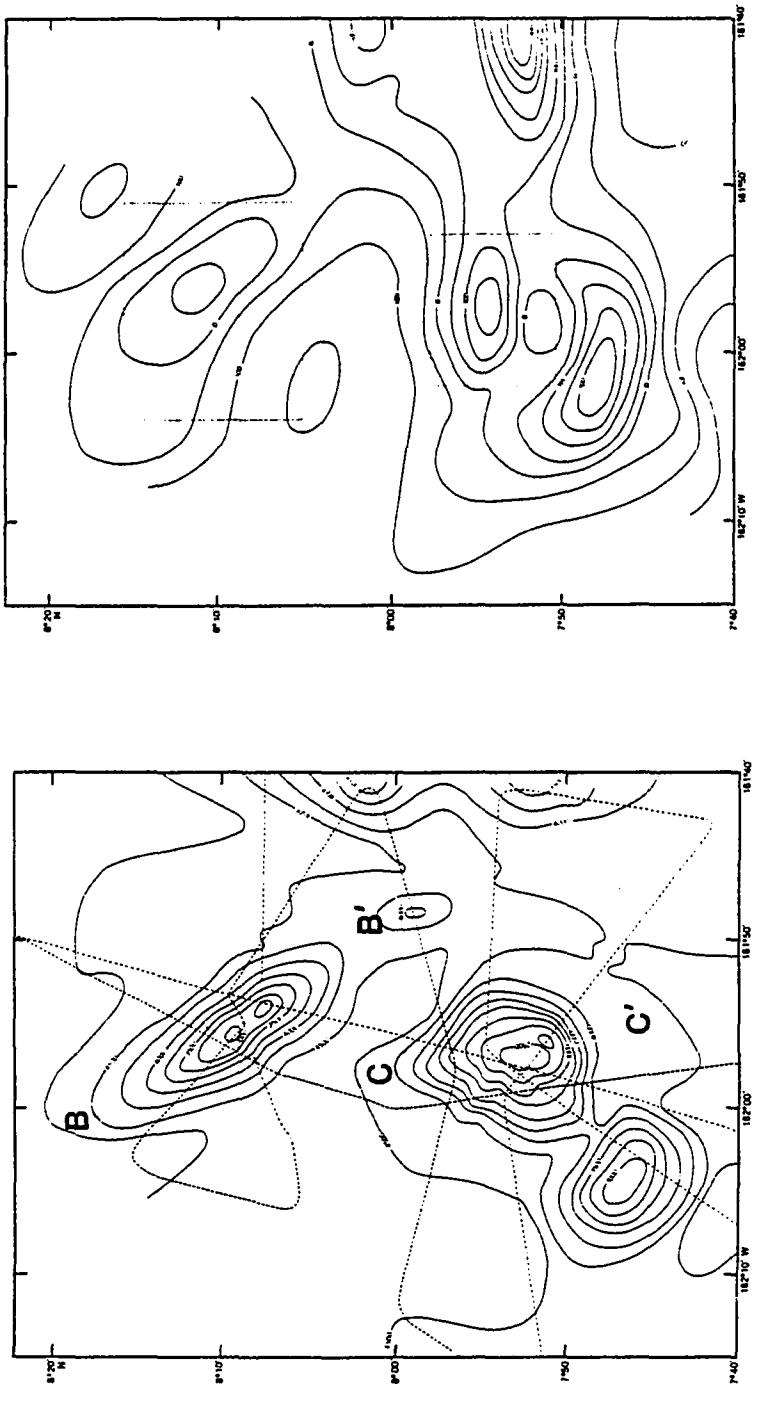

Figure 4.17 Bathymetry (left) and magnetic anomaly (right) of Stanley (L4) and Willoughby (L5) seamounts. Stanley Seamount is at top; Willoughby Seamount is at bottom. See Figure 4.5 for explanation of charts. Magnetic contour interval is 50 nT.

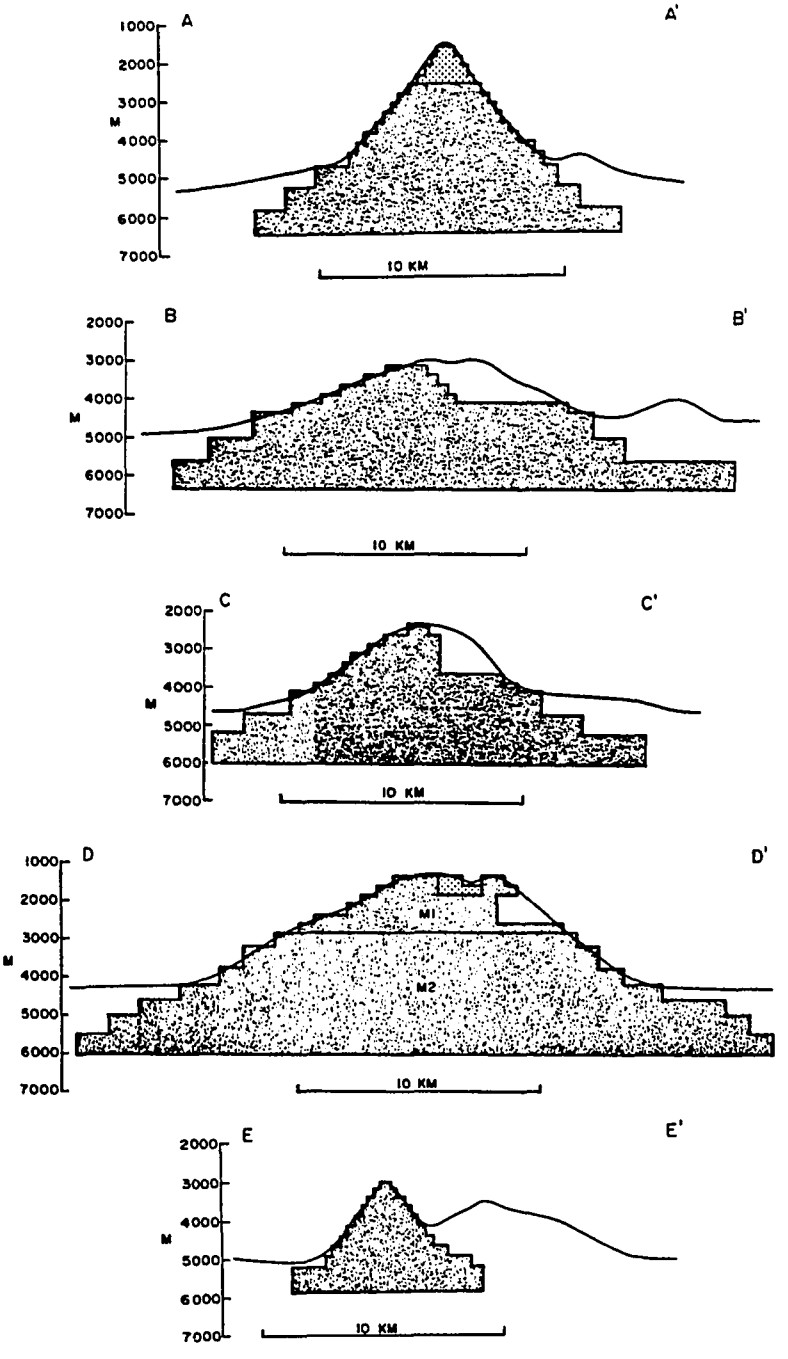

Figure 4.18 Inhomogeneous magnetization models of Line Islands seamounts. Solid line is the observed bathymetry and the blocks represent a cross-sectional view of the prisms used to approximate the bathymetry of the seamount. Vertical exaggeration 1.5:1. Stippled pattern indicates normal polarity; dotted pattern indicates reversed polarity; non-magnetic sections are clear. A - A′: Nagata Seamount (L2) from Sager et al. (1982); B - B′: Stanley Seamount (L4) (Figure 4.17); C - C′: Willoughby Seamount (L5) (Figure 4.17); D - D′ Chapman Seamount (L6) (Figure 4.20); E - E′ Clarke Seamount (L7) (Figure 4.22).

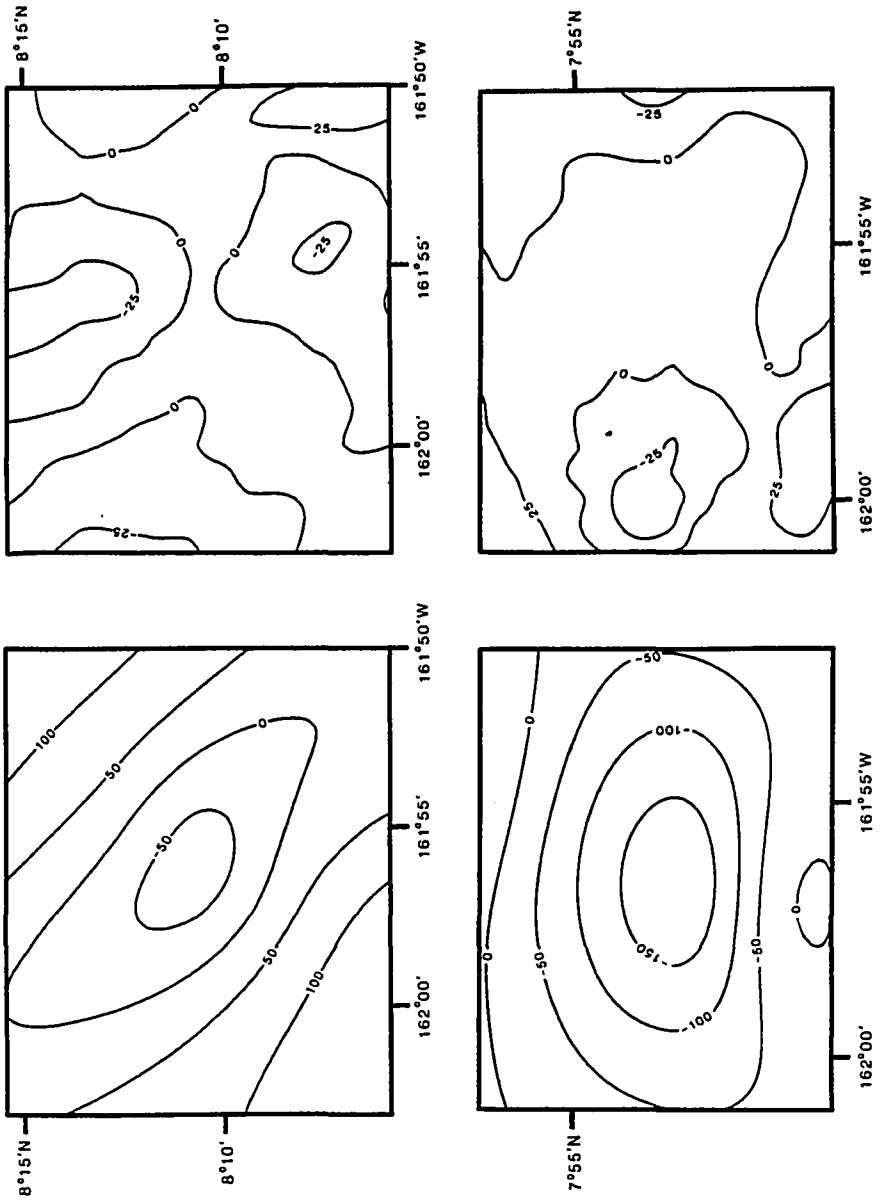

Figure 4.19 Calculated anomalies (left) and residuals (right) of Stanley (L4) and Willoughby (L5) seamounts. Upper pair are for Stanley Seamount; lower pair are for Willoughby Seamount. Contour interval is 50 nT.

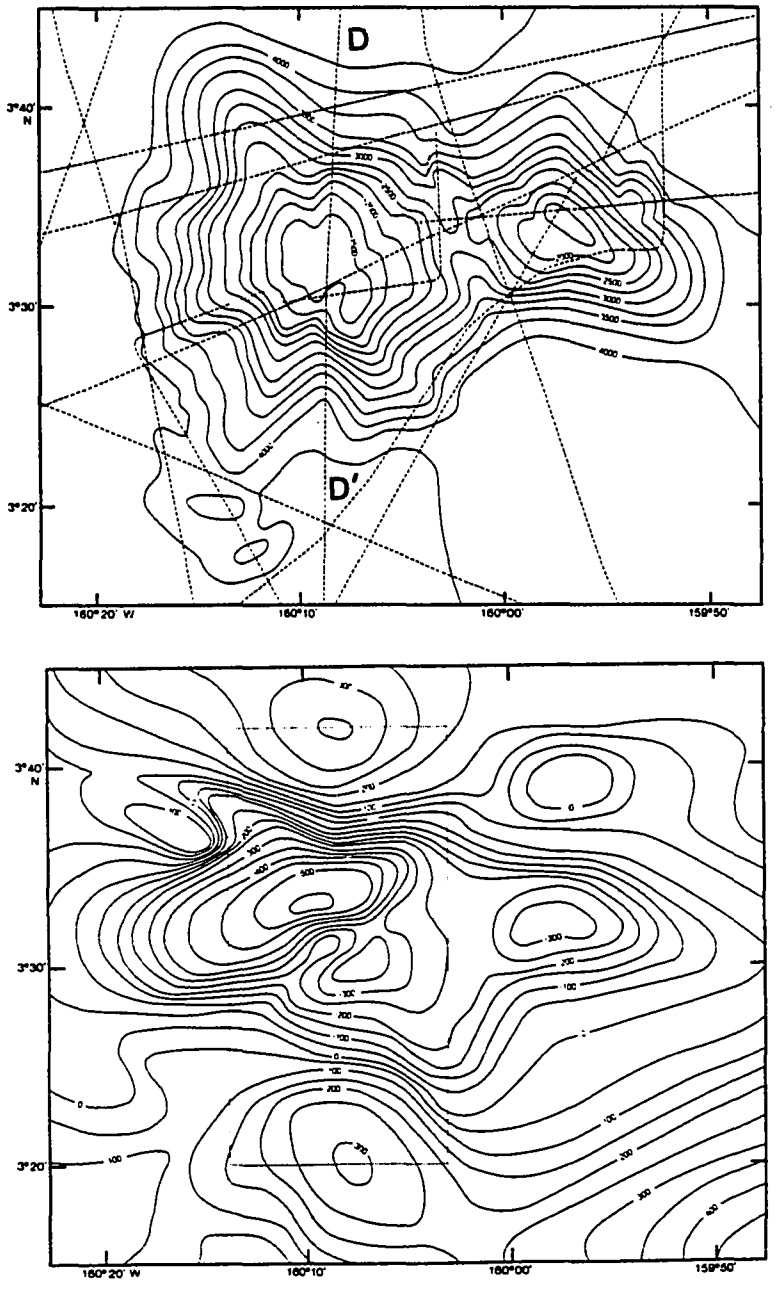

Figure 4.20 Bathymetry (top) and magnetic anomaly (bottom) for Chapman Seamount (L6). See Figure 4.5 for explantion of charts. Magnetic contour interval is 50 nT.

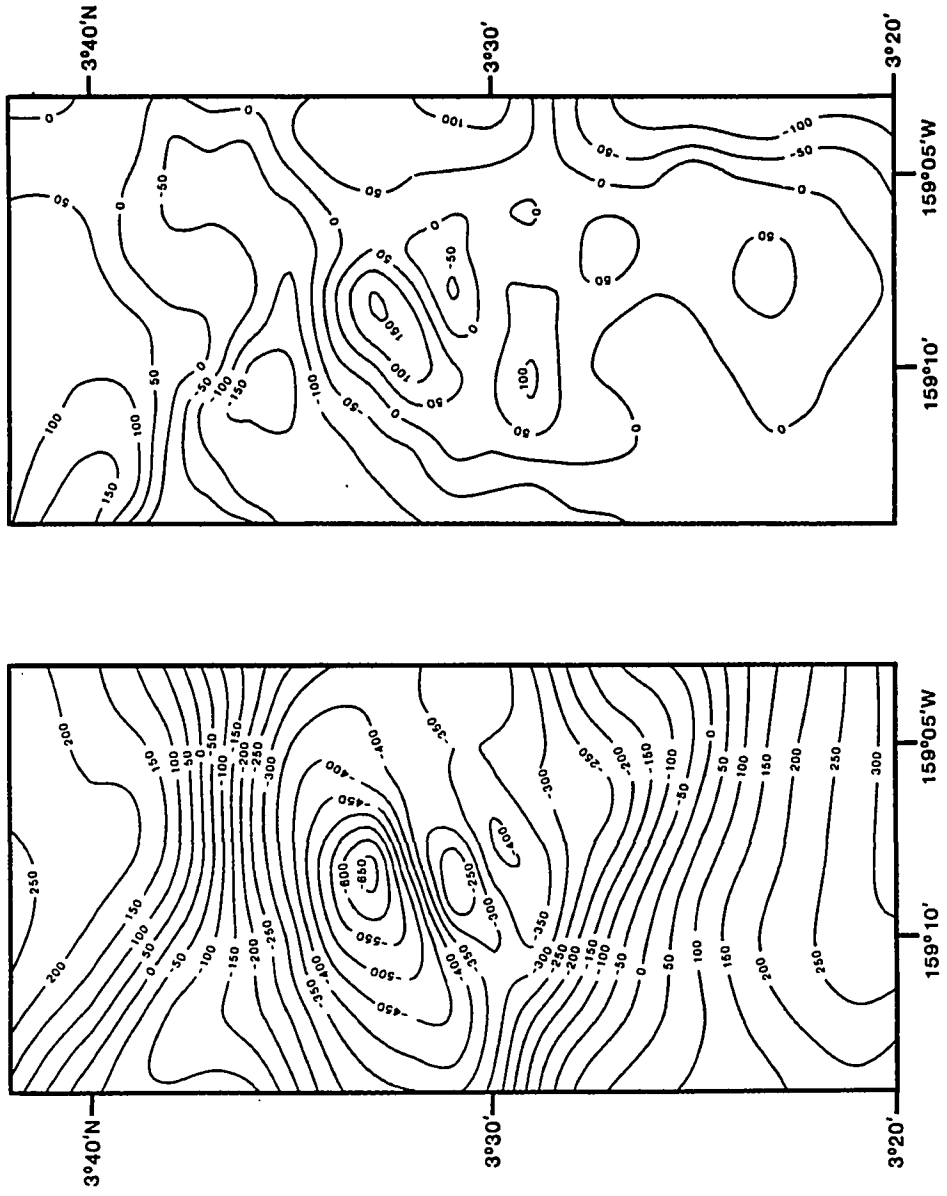

Figure 4.21 Calculated anomaly (left) and residuals (right) for Chapman Seamount (L6). Contour interval is 50 nT.

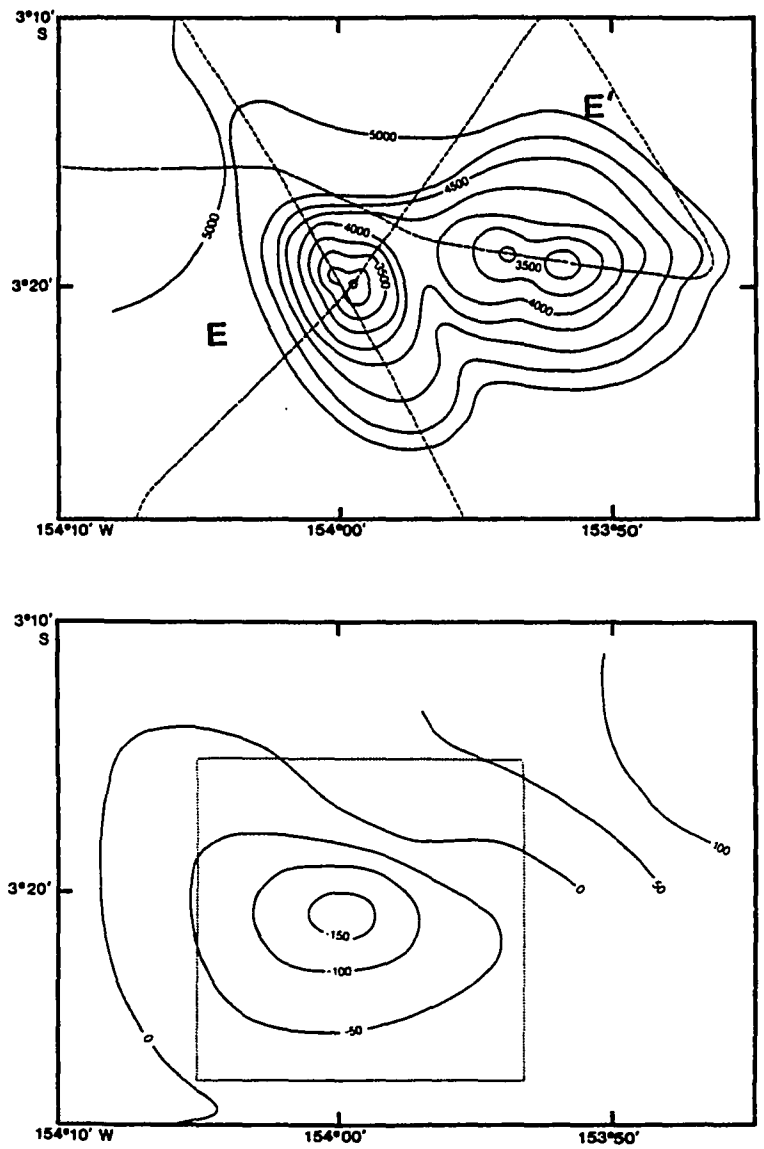

Figure 4.22 Bathymetry (top) and magnetic anomaly (bottom) for Clarke Seamount (L7). See Figure 4.5 for explanation of charts. Magnetic contour interval is 50 nT.

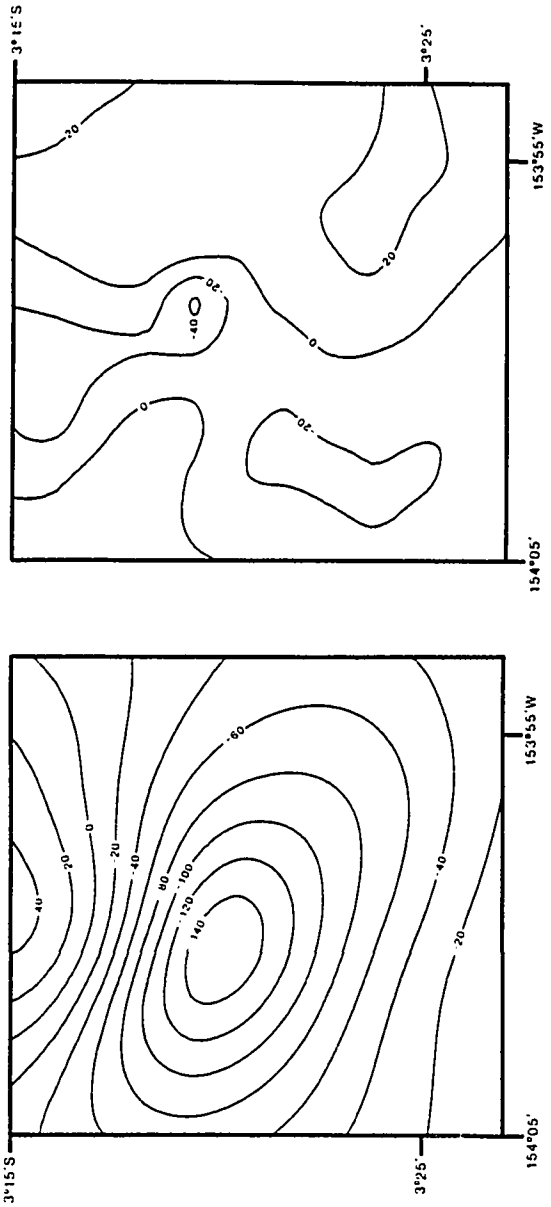

Figure 4.23 Calculated anomaly (left) and residuals (right) for Clarke Seamount (L7). Contour interval is 20 nT.

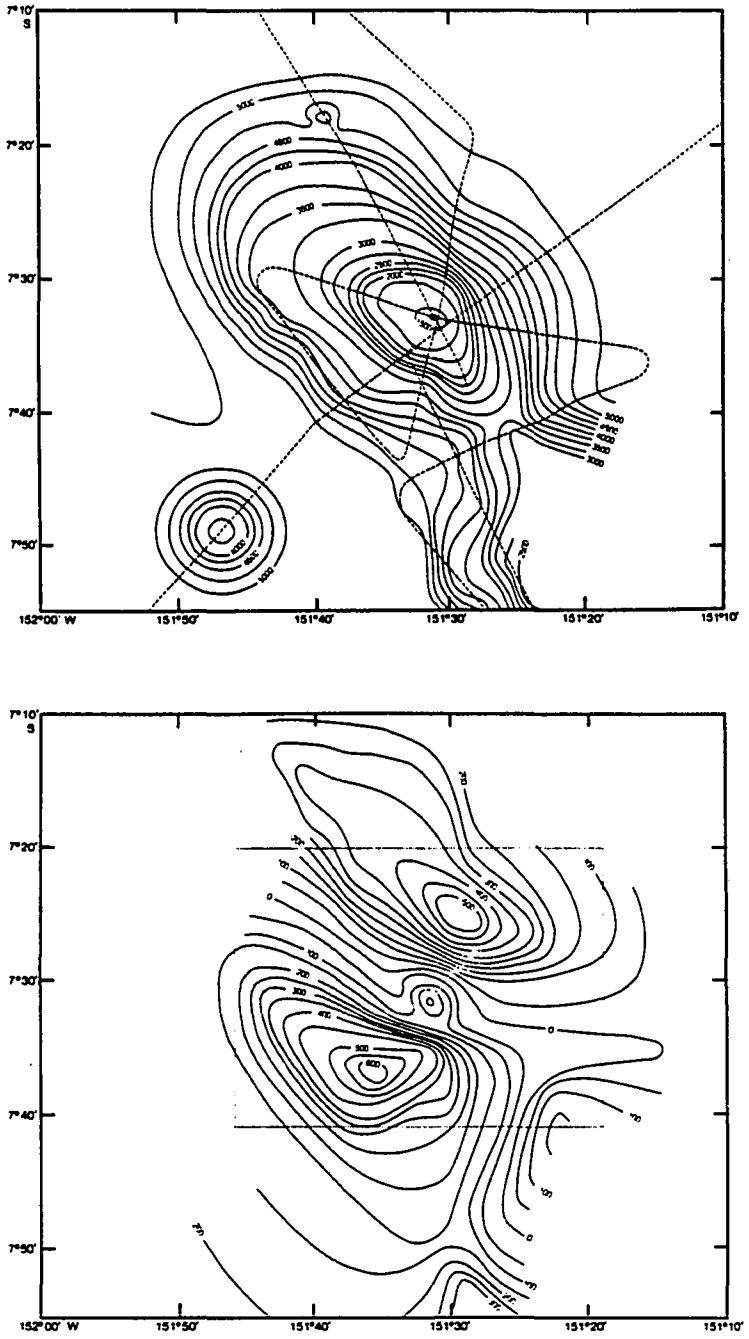

Figure 4.24 Bathymetry (top) and magnetic anomaly (bottom) for Uyeda Seamount (L8). See Figure 4.5 for explanation of charts. Magnetic contour interval is 50 nT.

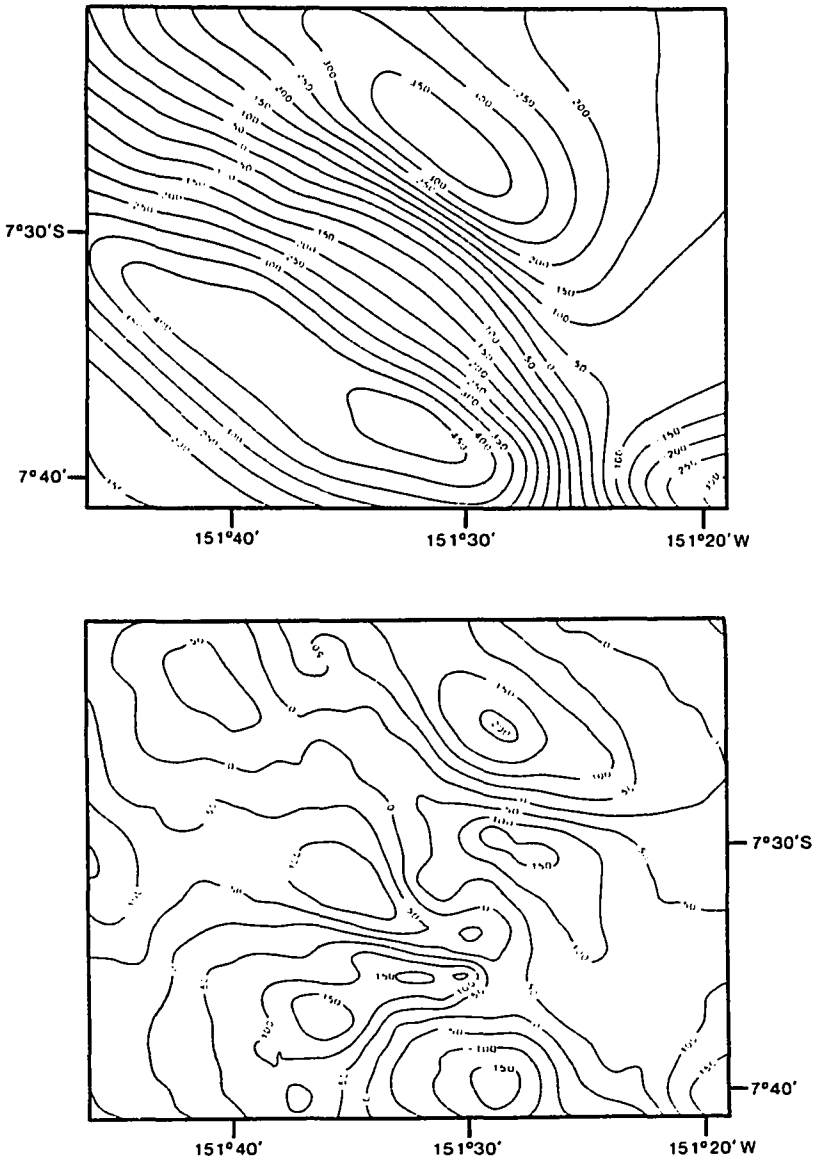

Figure 4.25 Calculated anomaly (top) and residuals (bottom) for Uyeda Seamount (L8). Contour interval is 50 nT.

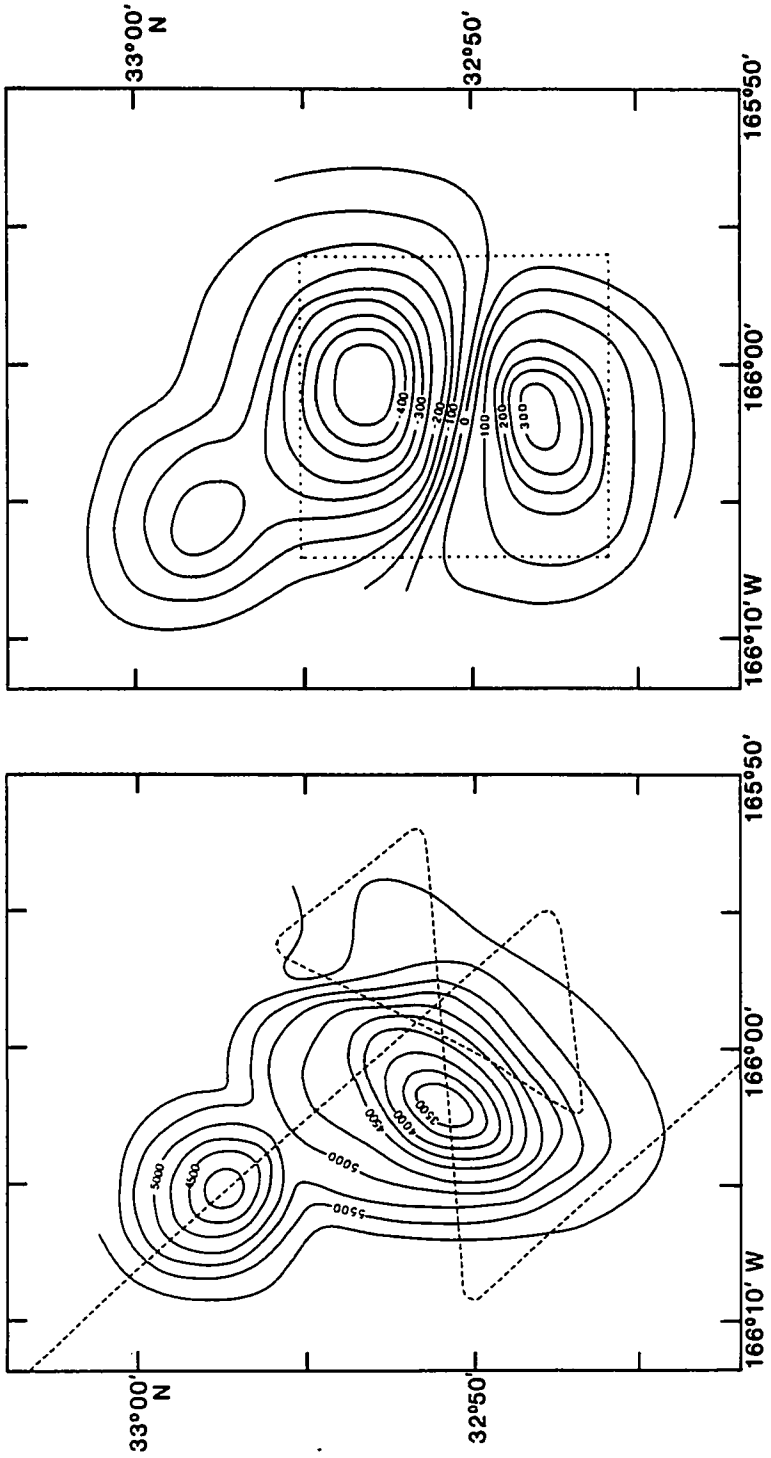

Figure 4.26 Bathymetry (left) and magnetic anomaly (right) of Berlin Seamount (M1). See Figure 4.5 for explanation of charts. Magnetic contour interval is 50 nT.

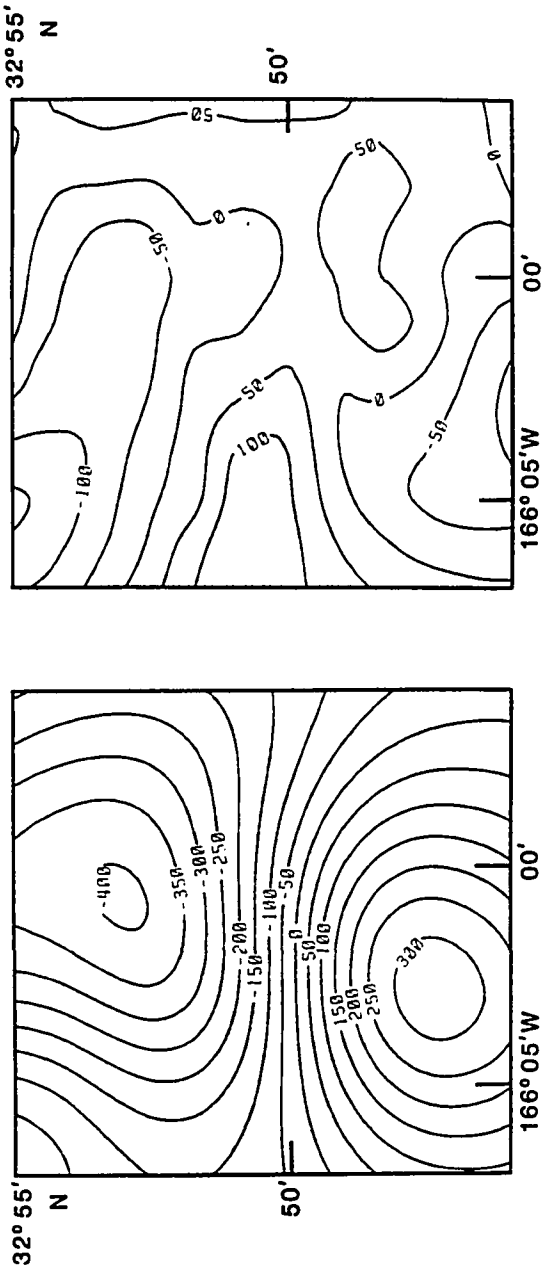

Figure 4.27 Calculated anomaly (left) and residuals (right) of Berlin Seamount (M1). Contour interval is 50 nT.

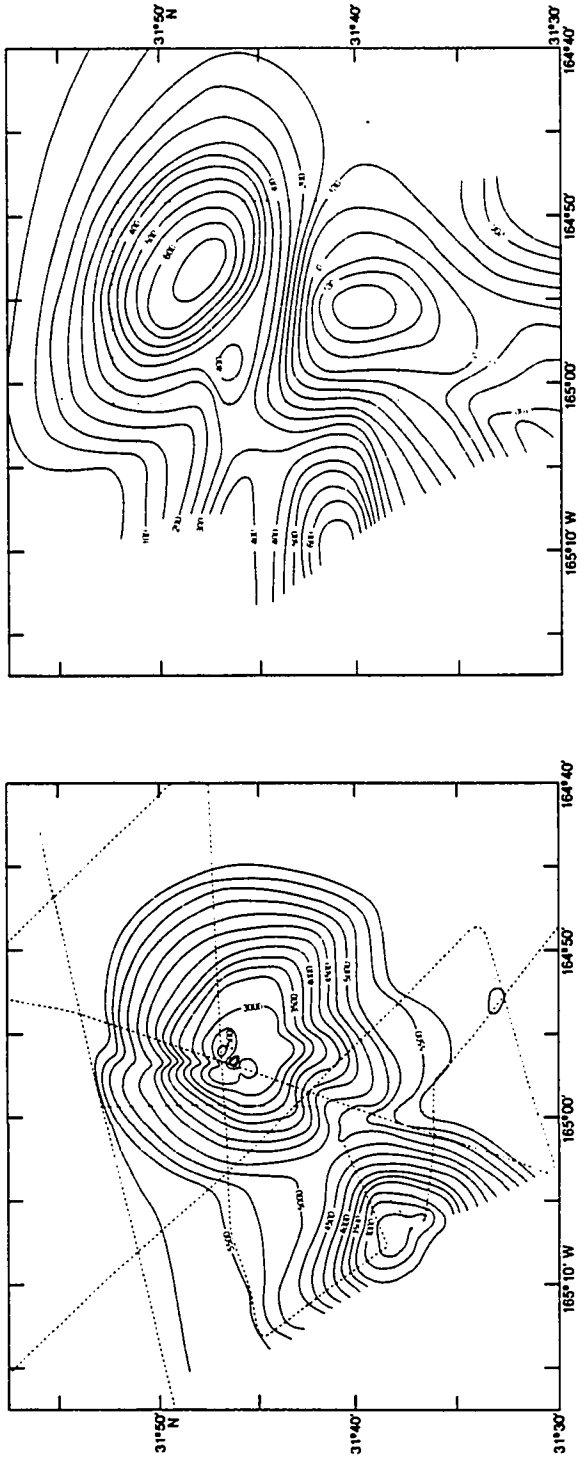

Figure 4.28 Bathymetry (left) and magnetic anomaly (right) of Mahler Seamount (M2). See Figure 4.5 for explanation of charts. Magnetic contour interval is 50 nT.

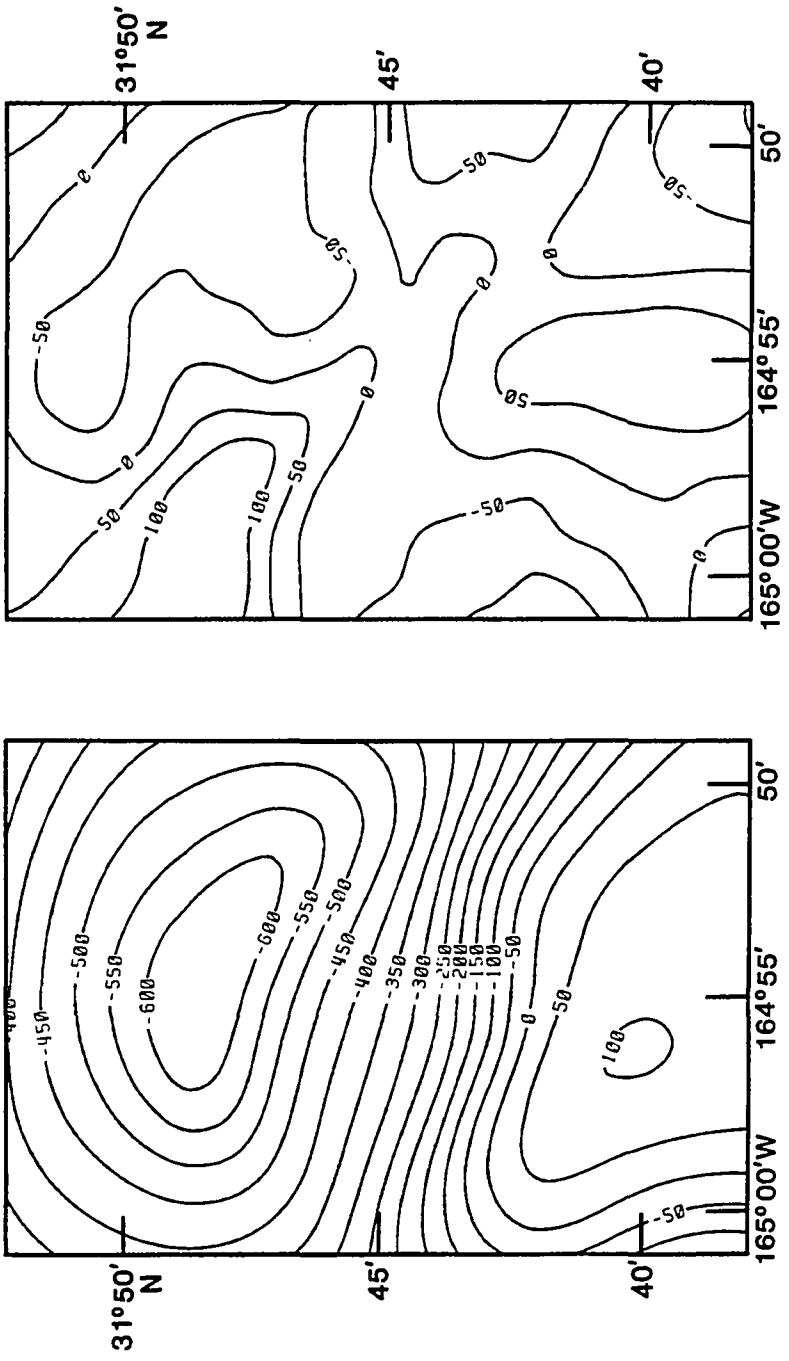

Figure 4.29 Calculated anomaly (left) and residuals (right) of Mahler Seamount (M2). Contour interval is 50 nT.

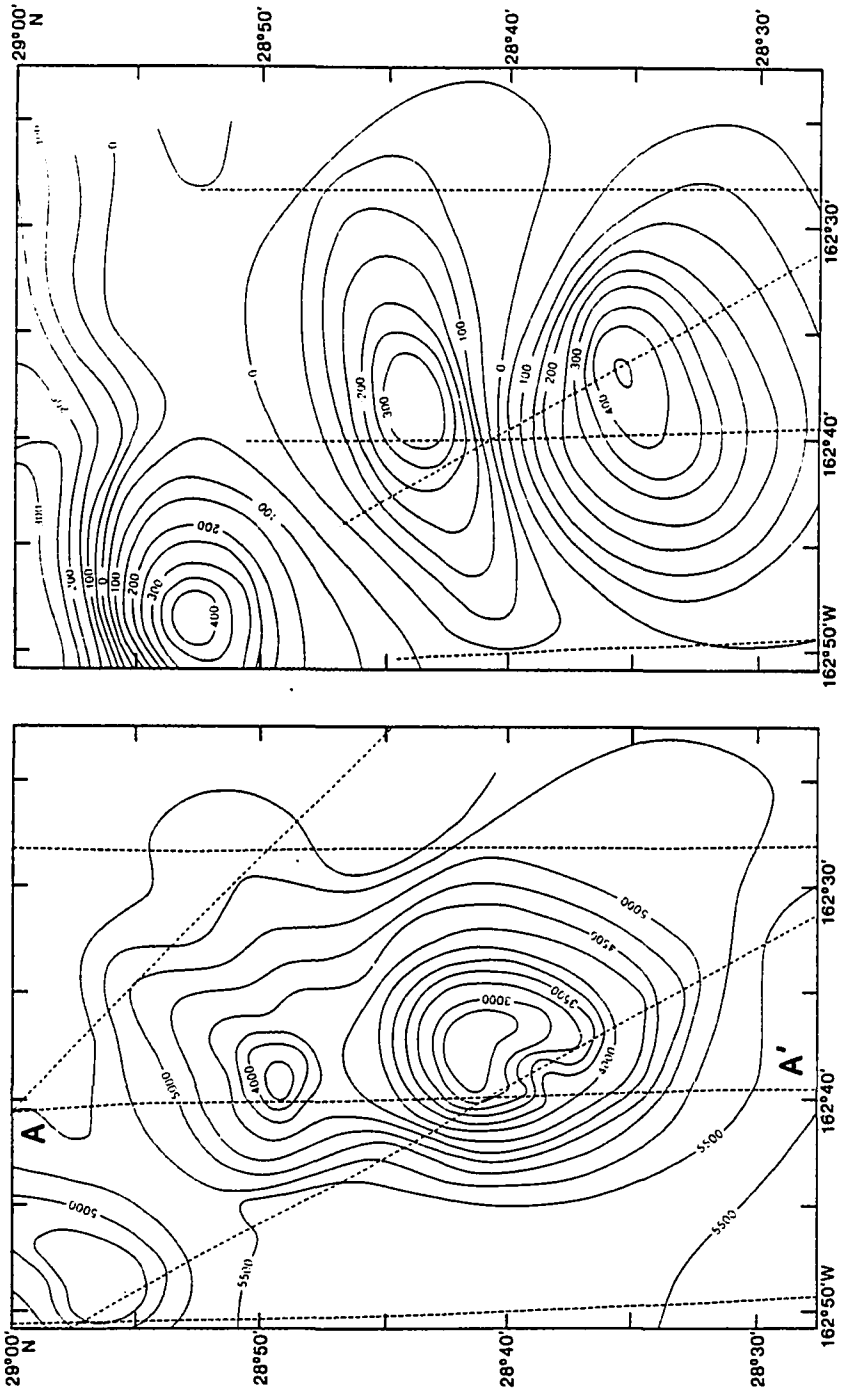

Figure 4.30 Bathymetry (left) and magnetic anomaly (right) of Paganini Seamount (M5). See Figure 4.5 for explanation of charts. Magnetic contour interval is 50 nT. Dashed lines in the magnetic anomaly chart are track lines along which the anomaly was digitized for constraining the magnetization inversion. Transect A - A' is shown in Figure 4.31.

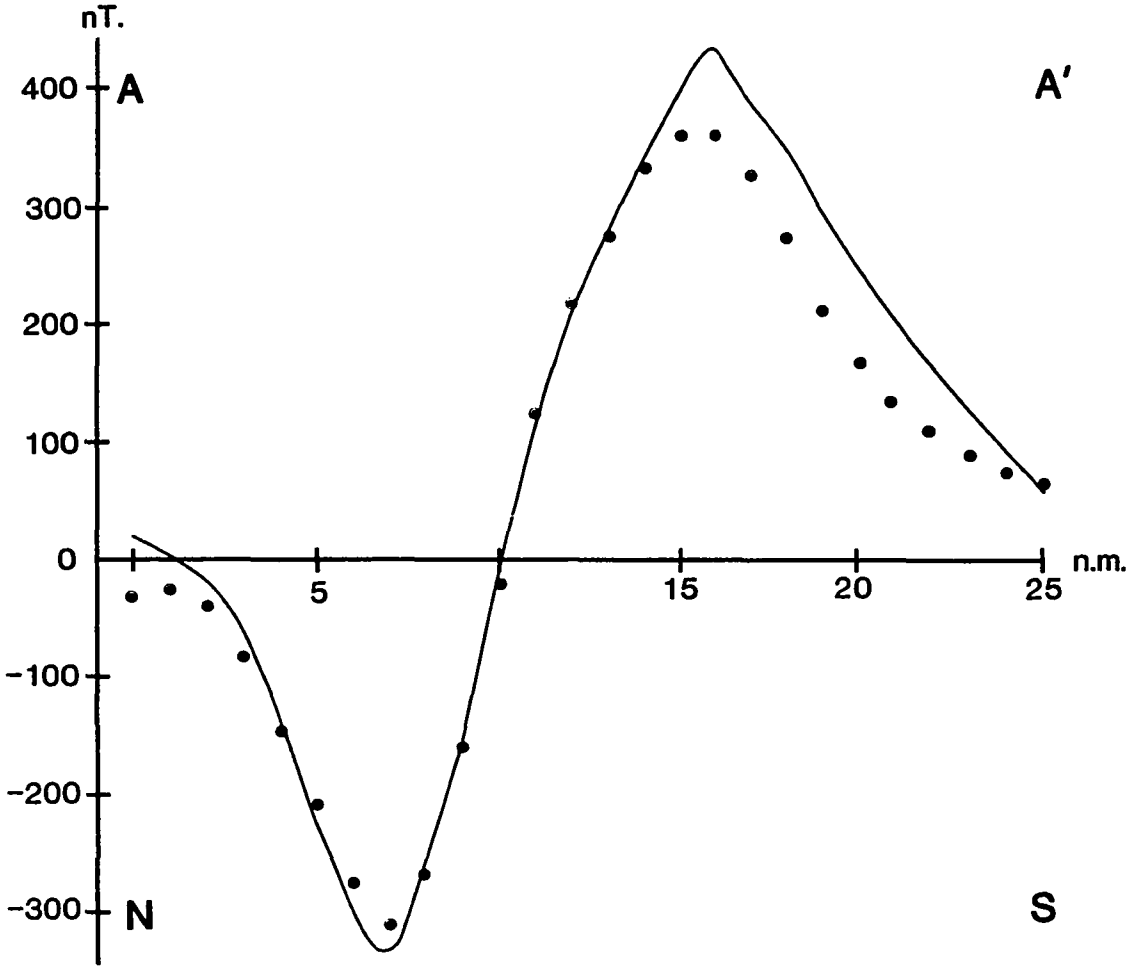

Figure 4.31 North-south transect across Paganini Seamount (M5) showing agreement of observed anomaly (solid line) and calculated anomaly values (dots). A - A' refers to transect line shown in Figure 4.30. Abcissa in labeled in nautical miles; ordinate, in nanoTeslas.

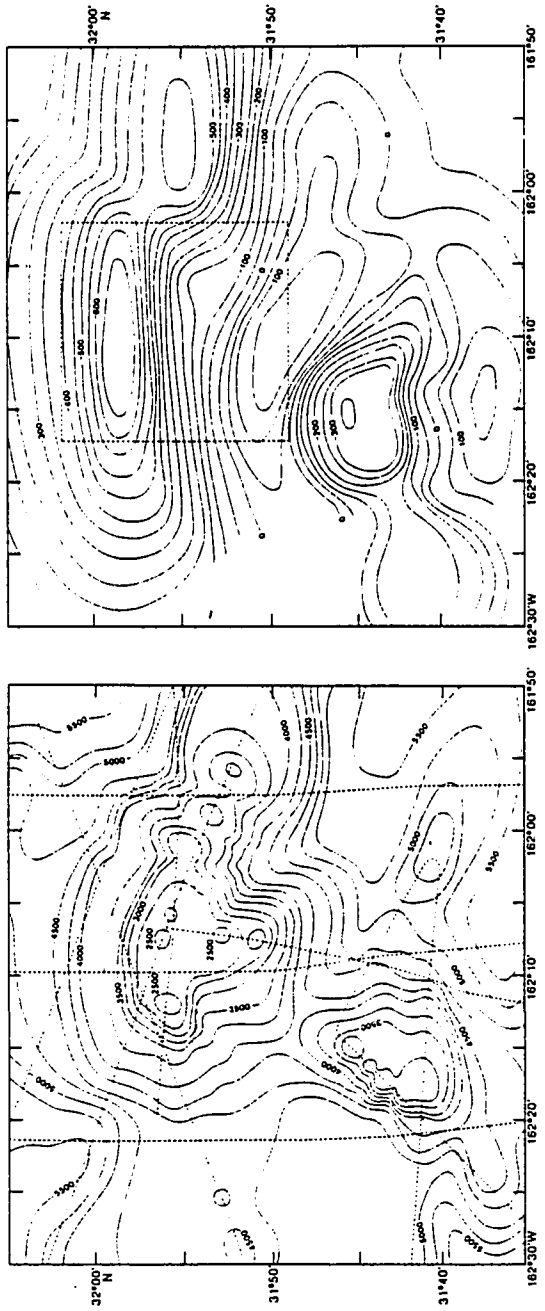

Figure 4.32 Bathymetry (left) and magnetic anomaly (right) of Schubert Seamount (M7). See Figure 4.5 for explanation of charts. Magnetic contour interval is 50 nT.

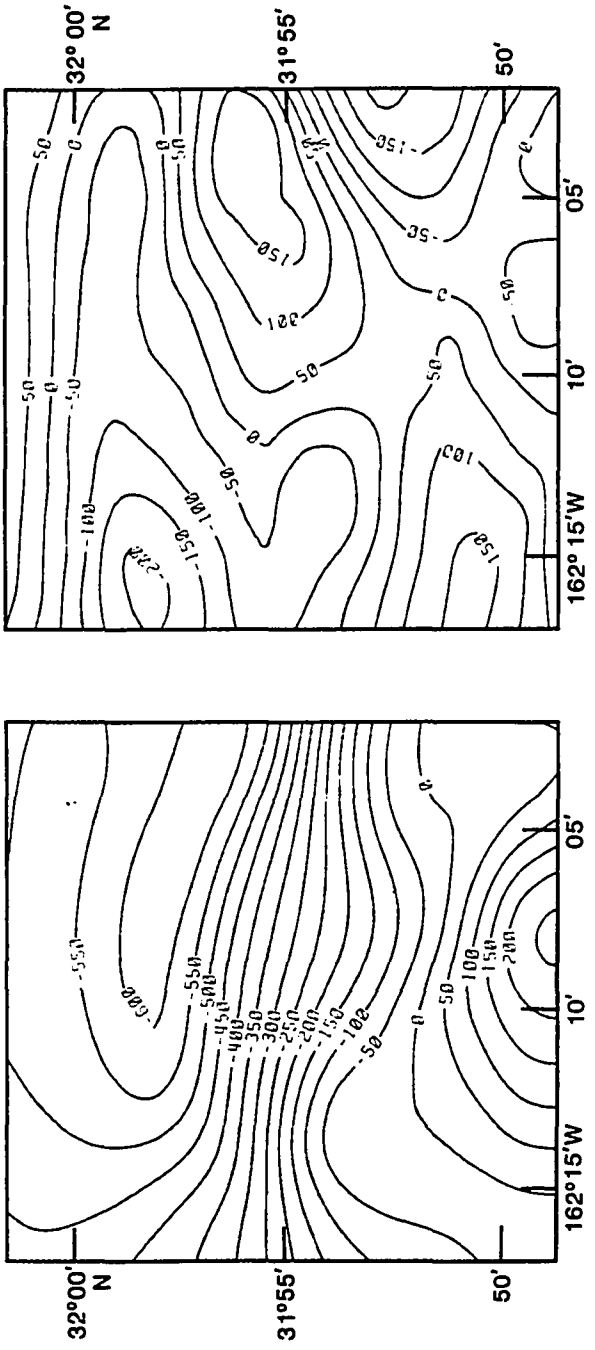

Figure 4.33 Calculated anomaly (left) and residuals (right) of Schubert Seamount (M7). Contour interval is 50 nT.

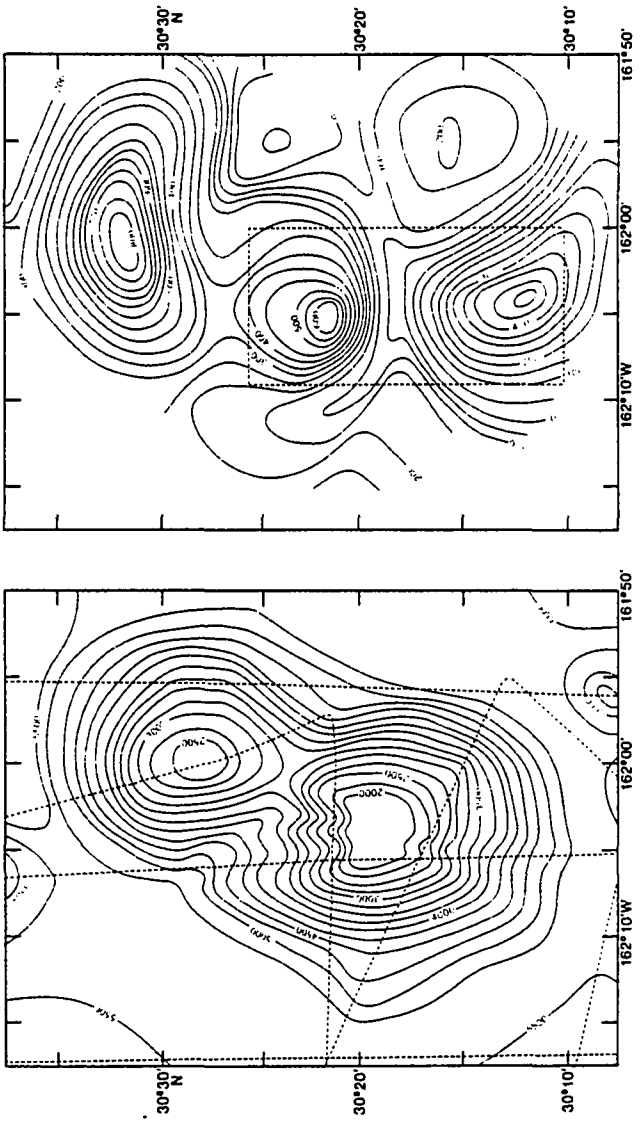

Figure 4.34 Bathymetry (left) and magnetic anomaly (right) of Debussy Seamount (M9). See Figure 4.5 for explanation of charts. Magnetic contour interval is 50 nT.

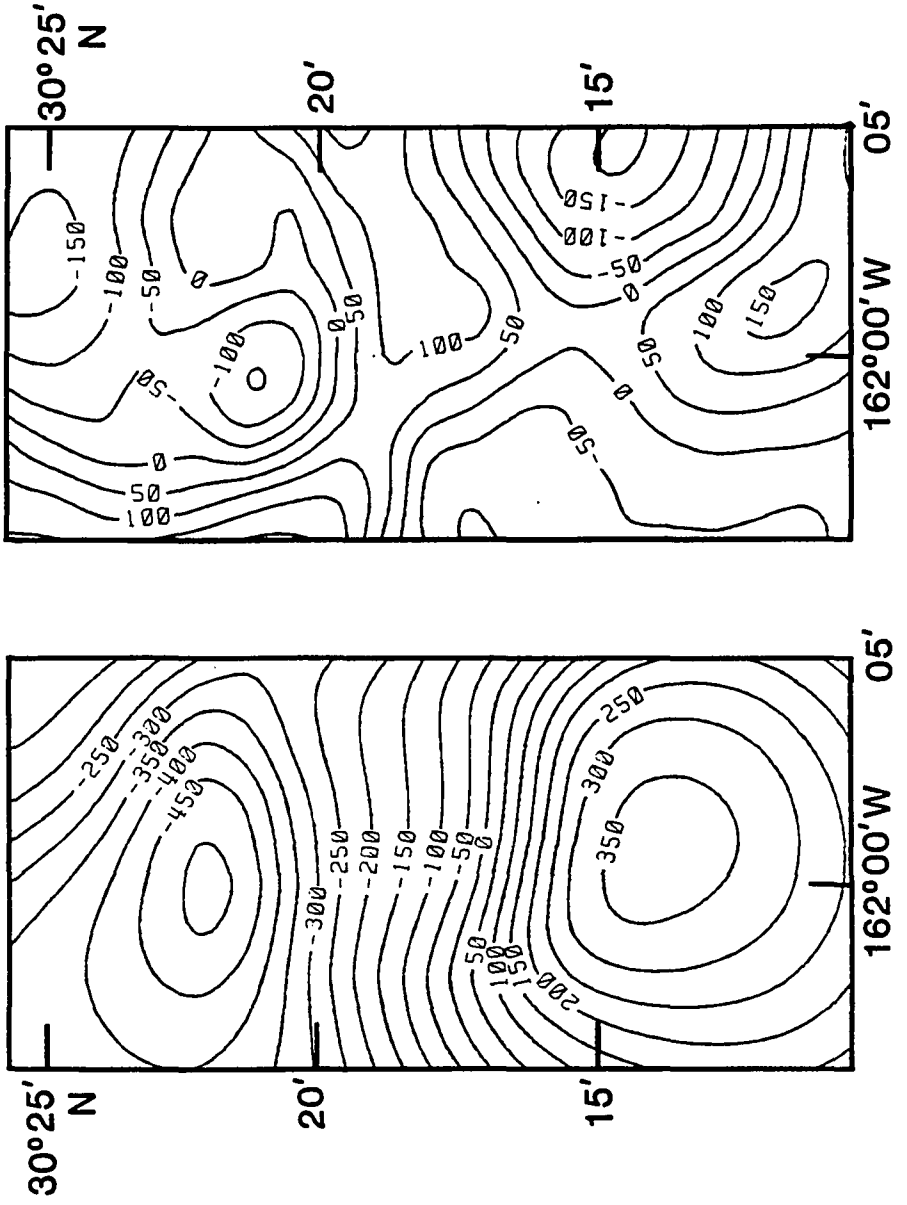

Figure 4.35 Calculated anomaly (left) and residuals (right) of Debussy Seamount (M9). Contour interval is 50 nT.

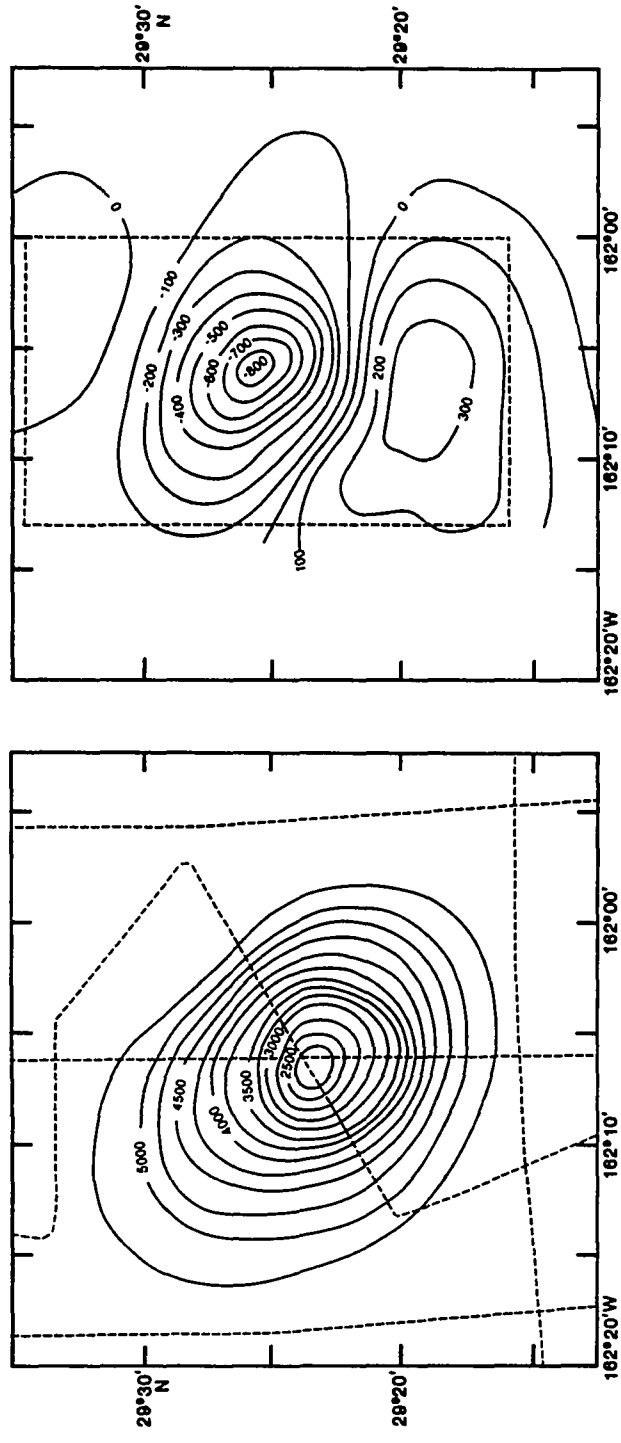

Figure 4.36 Bathymetry (left) and magnetic anomaly (right) of Tchaikovsky Seamount (M10). See Figure 4.5 for explanation of charts. Magnetic contour interval is 100 nT.

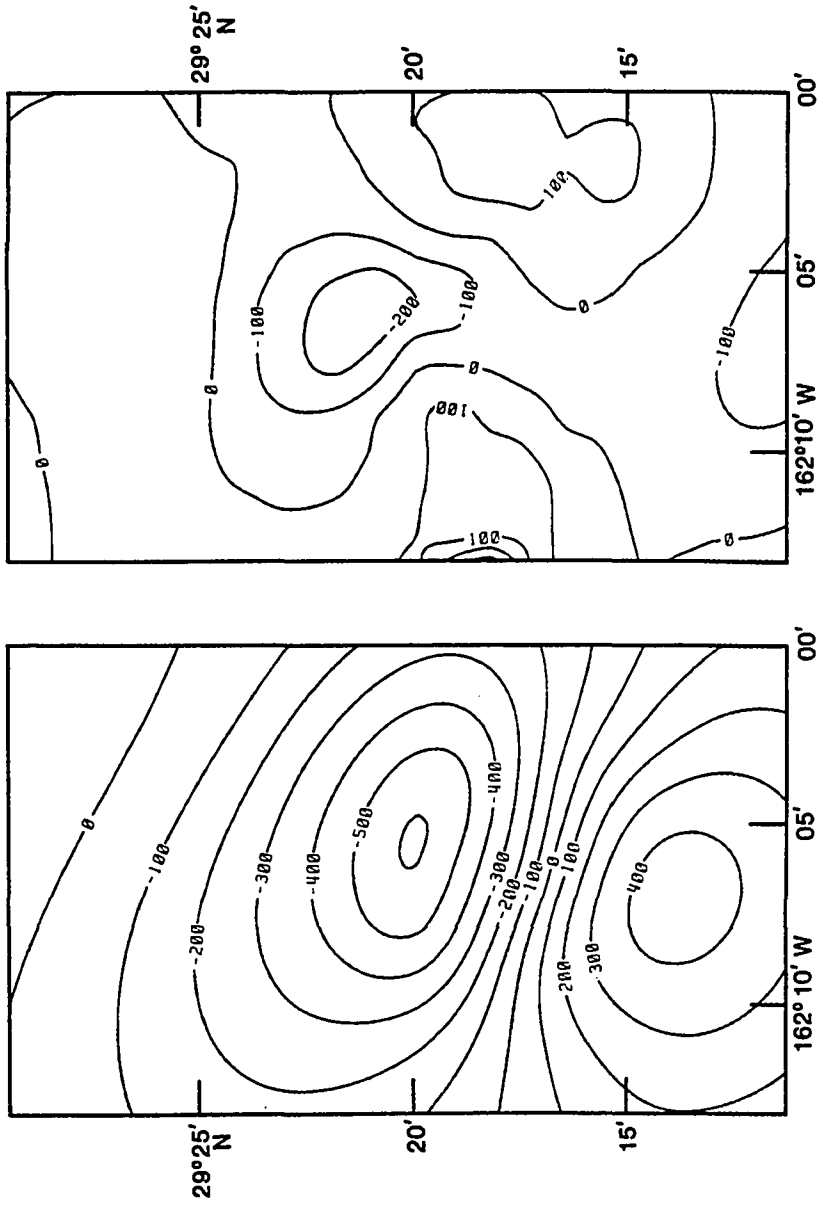

Figure 4.37 Calculated anomaly (left) and residuals (right) of Tchaikovsky Seamount (M10). Contour interval is 100 nT.

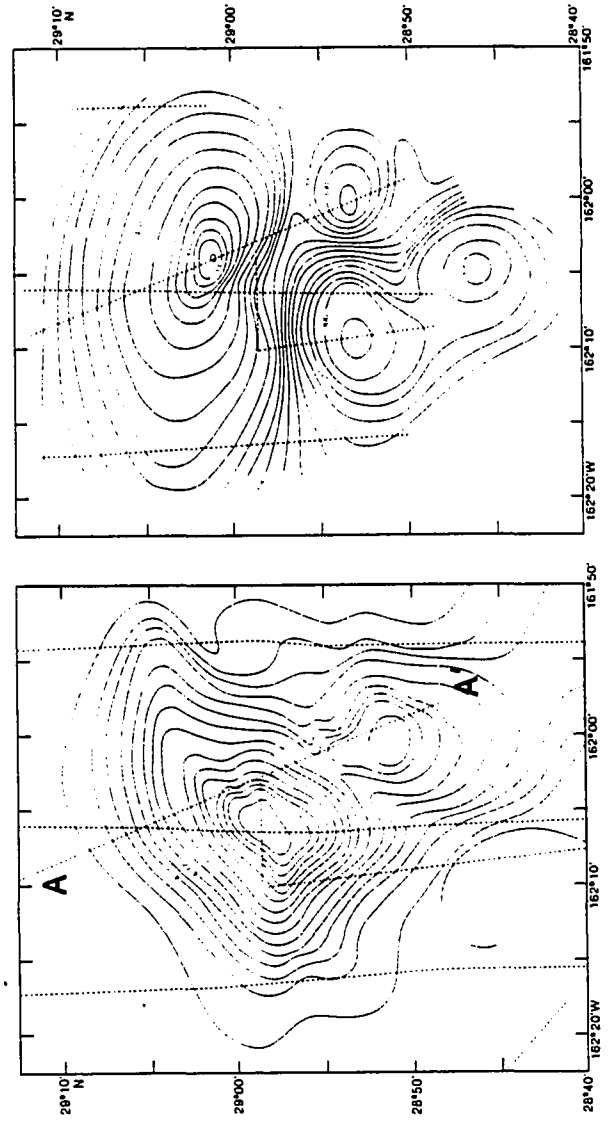

Figure 4.38 Bathymetry (left) and magnetic anomaly (right) of Liszt Seamount (M11). See Figure 4.5 for explanation of charts. Dashed lines in magnetic anomaly are track lines along which the anomaly was digitized for use in constraining the magnetization inversion. Transect A - A′ is shown in Figure 4.39.

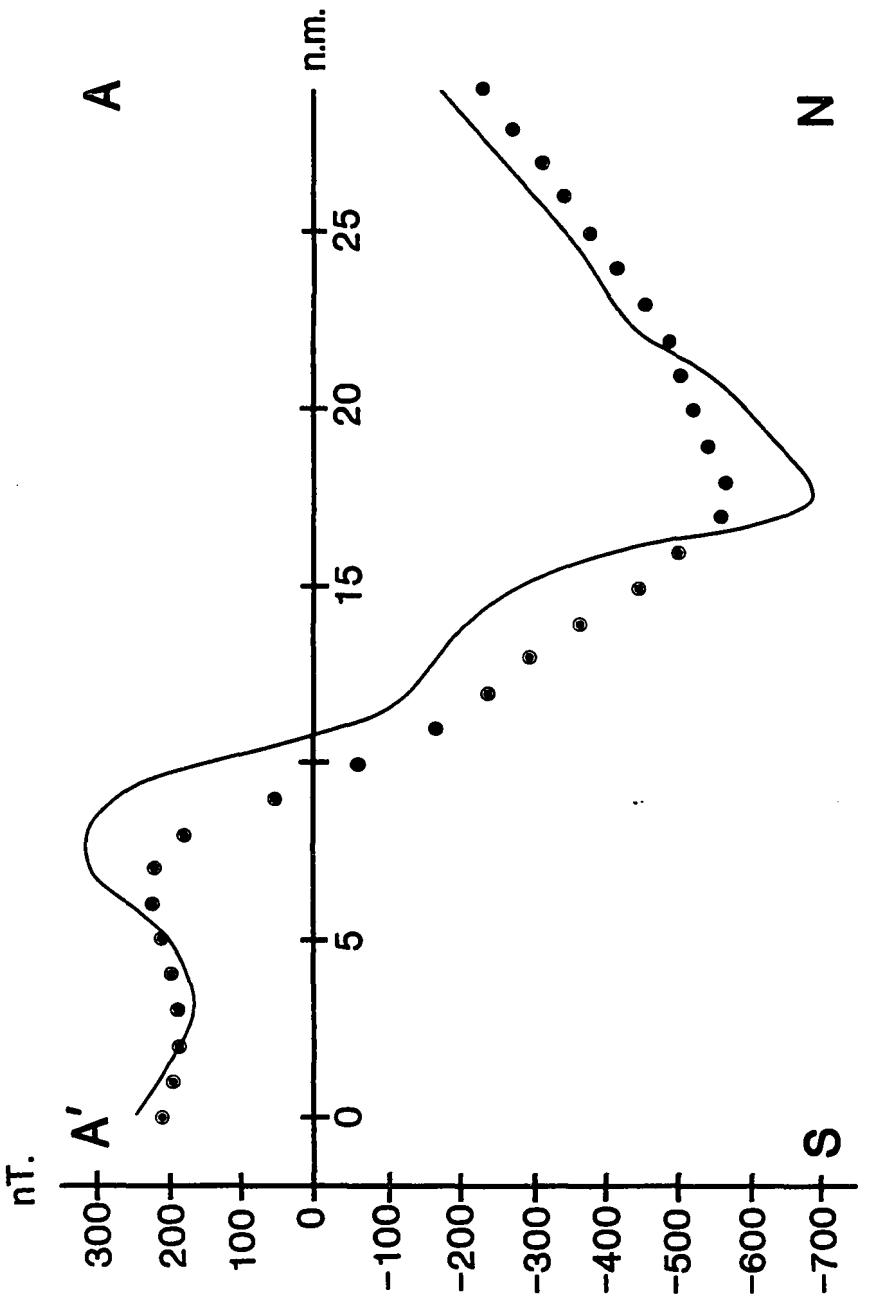

Figure 4.39 North-south transect across Liszt Seamount (M11) showing agreement between observed anomaly (solid line) and calculated anomaly (dots). Abcissa labeled in natutical miles; ordinate, in nanoTeslas.

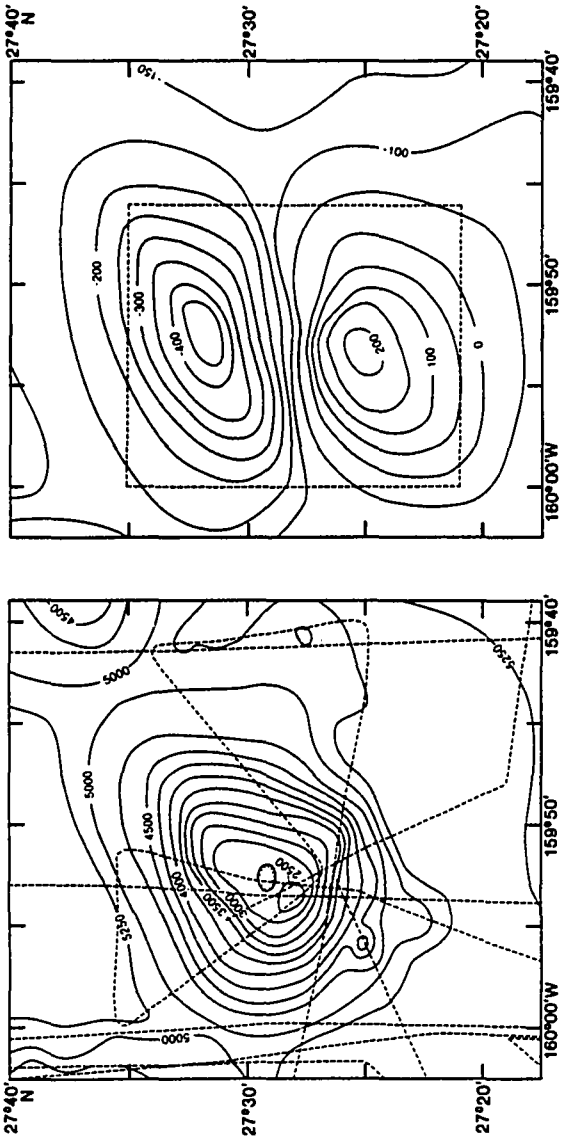

Figure 4.40 Bathymetry (left) and magnetic anomaly (right) of Handel Seamount (M12). See Figure 4.5 for explanation of charts. Magnetic contour interval is 50 nT.

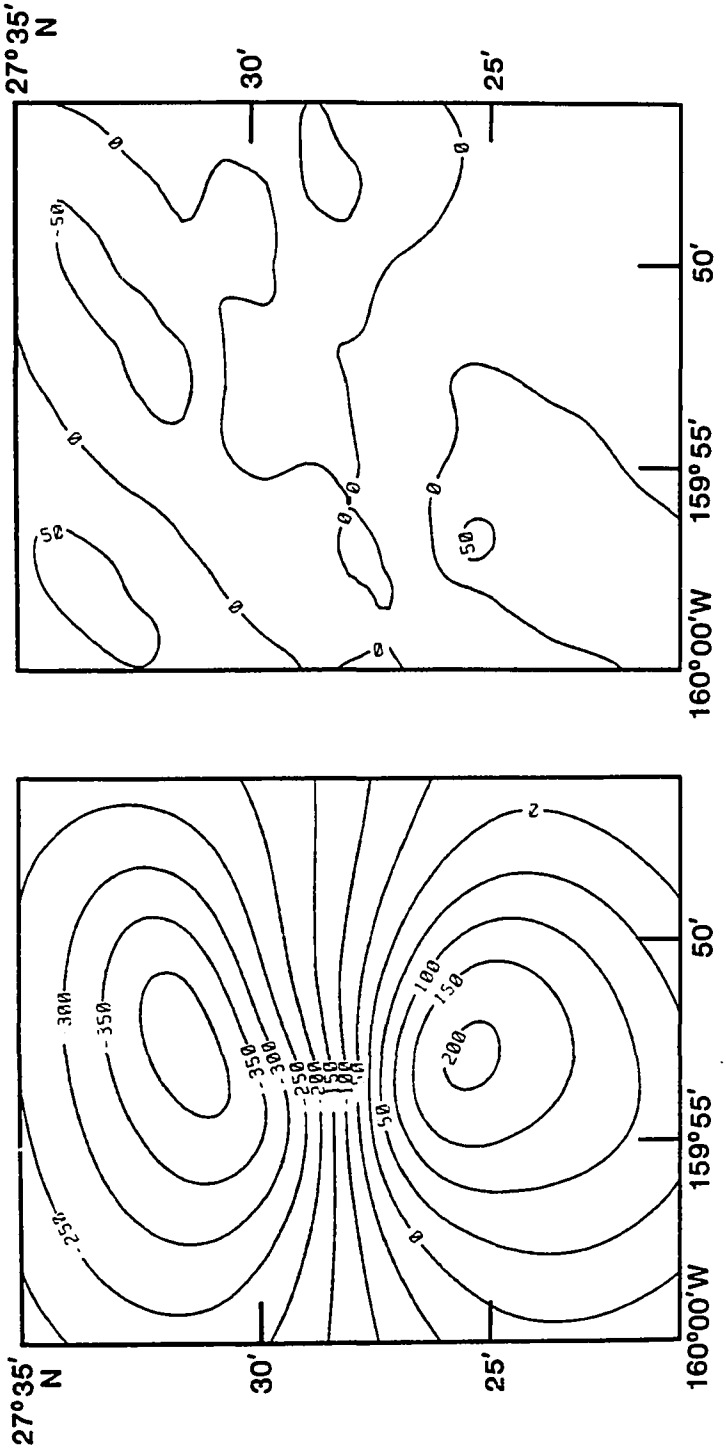

Figure 4.41 Calculated anomaly (left) and residuals (right) of Handel Seamount (M12). Contour interval 50 nT.

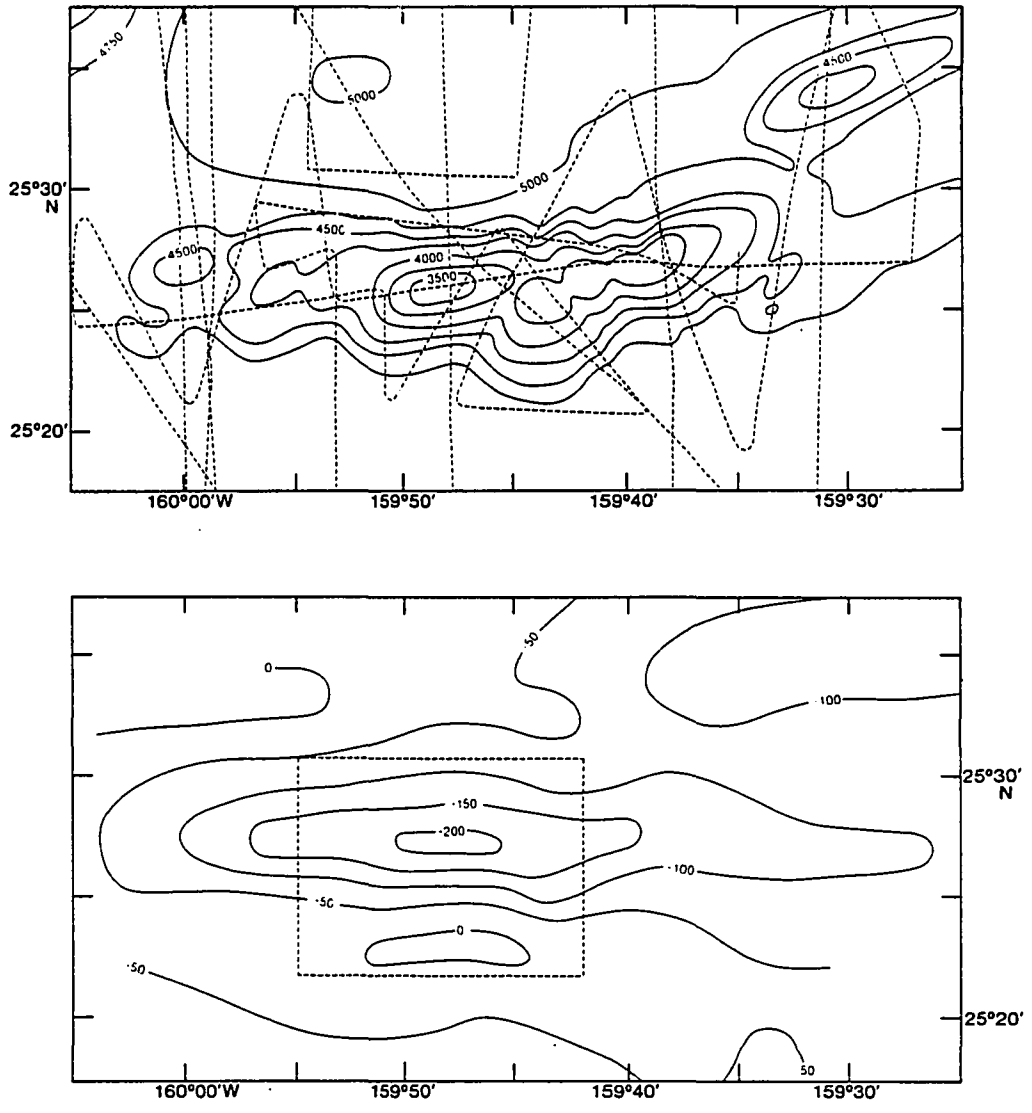

Figure 4.42 Bathymetry (top) and magnetic anomaly (bottom) of Rimsky-Korsakov Ridge (M13). See Figure 4.5 for explanation of charts. Magnetic contour interval is 50 nT.

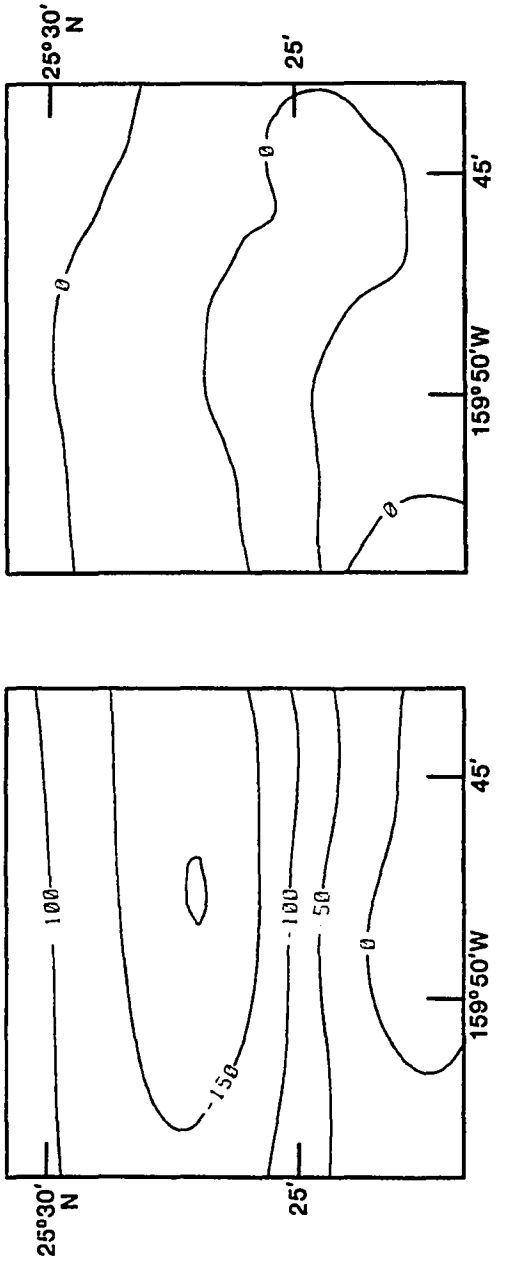

Figure 4.43 Calculated anomaly (left) and residuals (right) of Rimsky-Korsakov Ridge (M13). Contour interval is 50 nT.

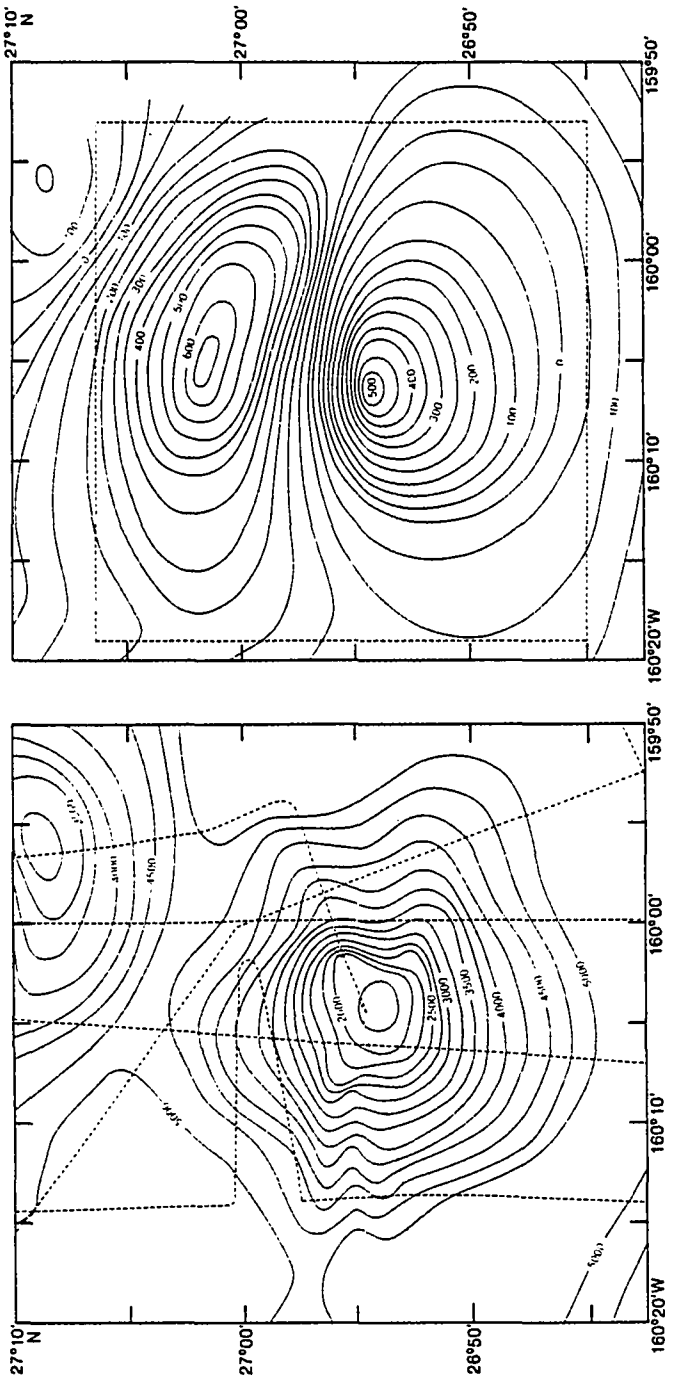

Figure 4.44 Bathymetry (left) and magnetic anomaly (right) of Gluck Seamount (M14). See Figure 4.5 for explanation of charts. Magnetic contour interval is 50 nT.

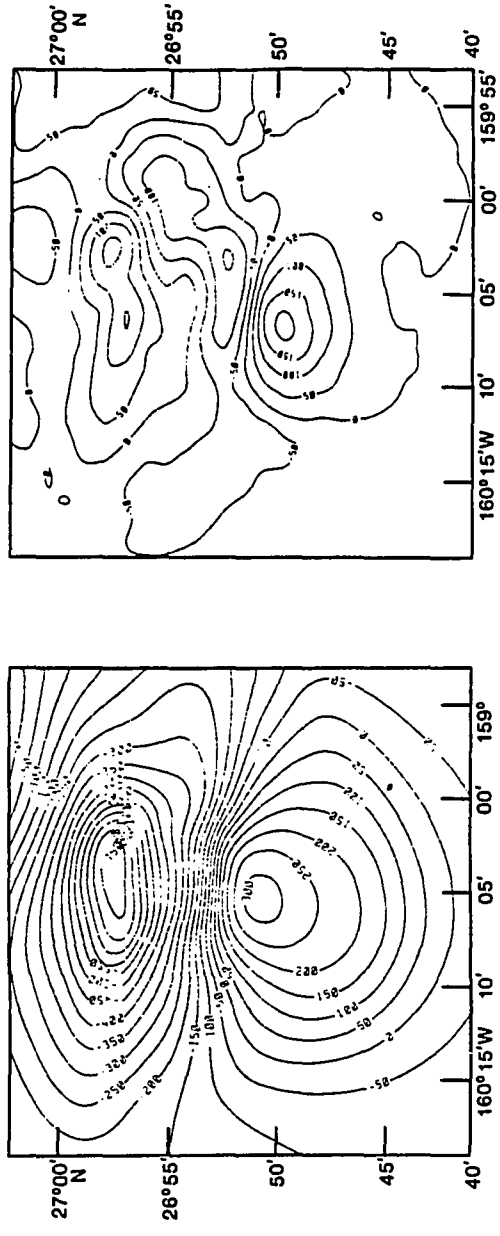

Figure 4.45 Calculated anomaly (left) and residuals (right) of Gluck Seamount (M14). Contour interval is 50 nT.

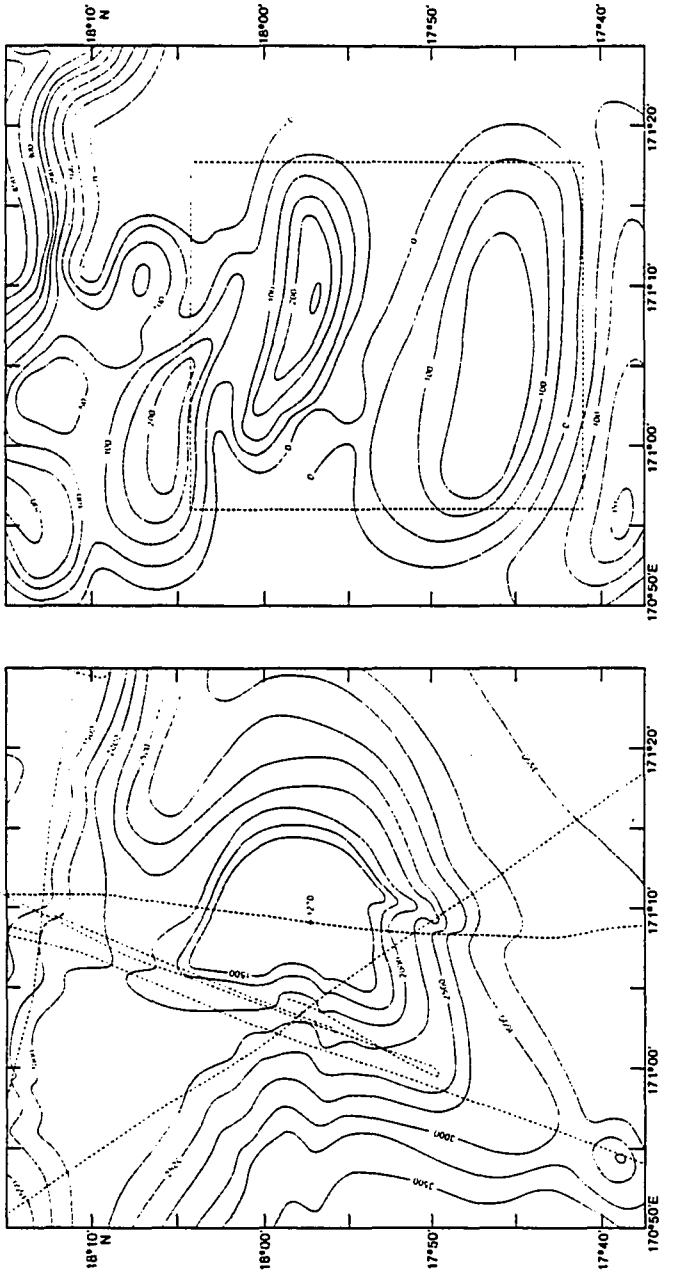

Figure 4.46 Bathymetry (left) and magnetic anomaly (right) of Woollard Guyot south peak (P1). See Figure 4.5 for explanation of charts. Magnetic contour interval is 50 nT.

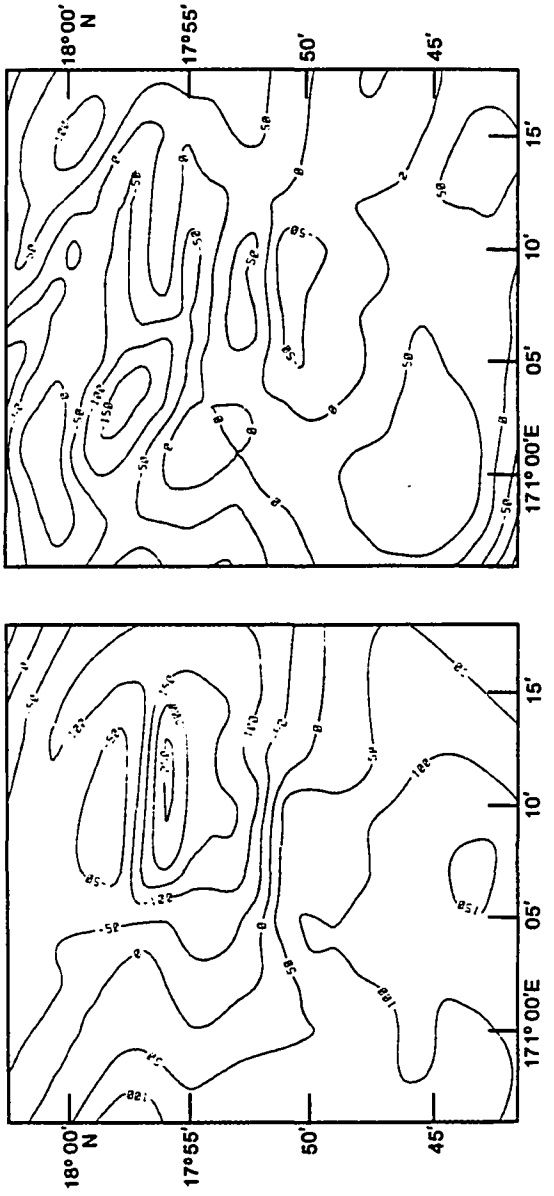

Figure 4.47 Calculated anomaly (left) and residuals (right) of Woollard Guyot wouth peak (P1). Contour interval is 50 nT.

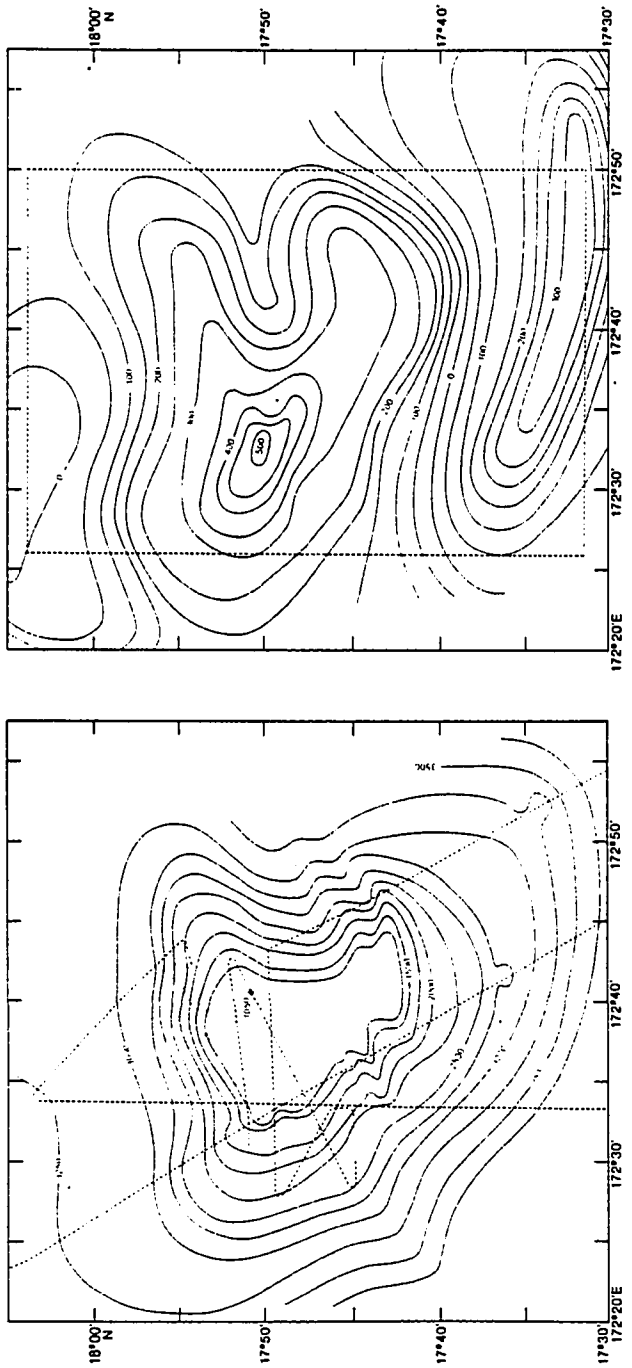

Figure 4.48 Bathymetry (left) and magnetic anomaly (right) of Harvey Guyot (P2). See Figure 4.5 for explanation of charts. Magnetic contour interval is 50 nT.

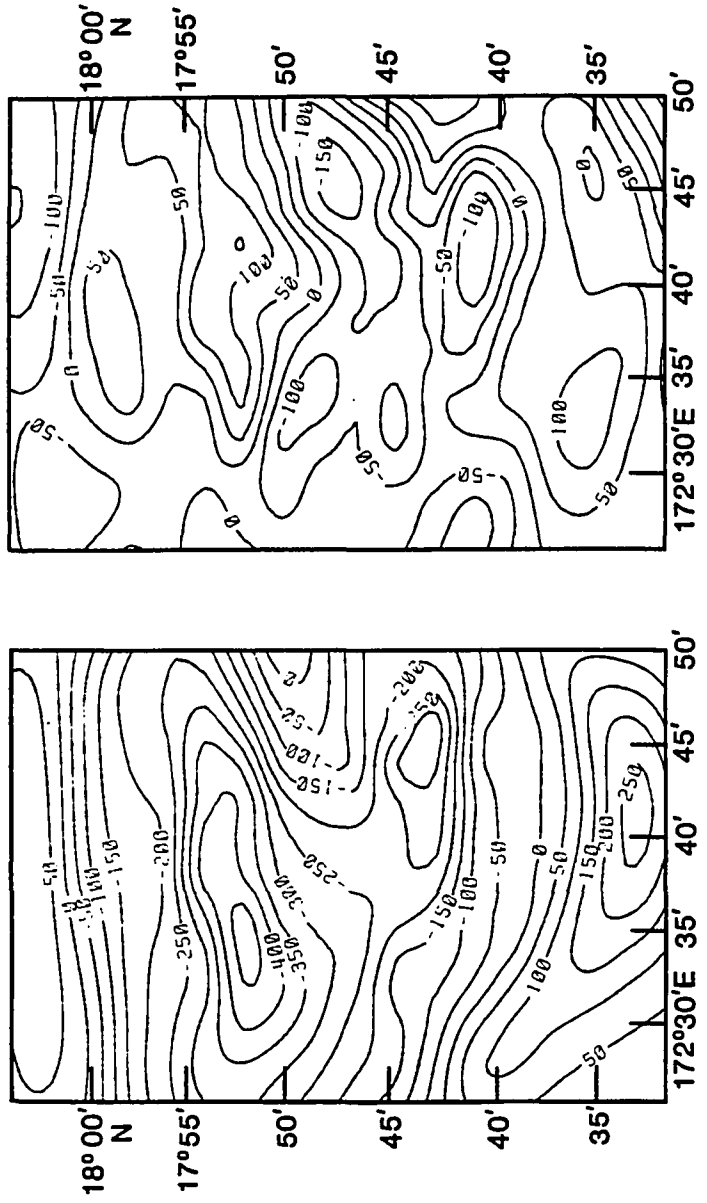

Figure 4.49 Calculated anomaly (left) and residuals (right) of Harvey Guyot (P2). Contour interval is 50 nT.

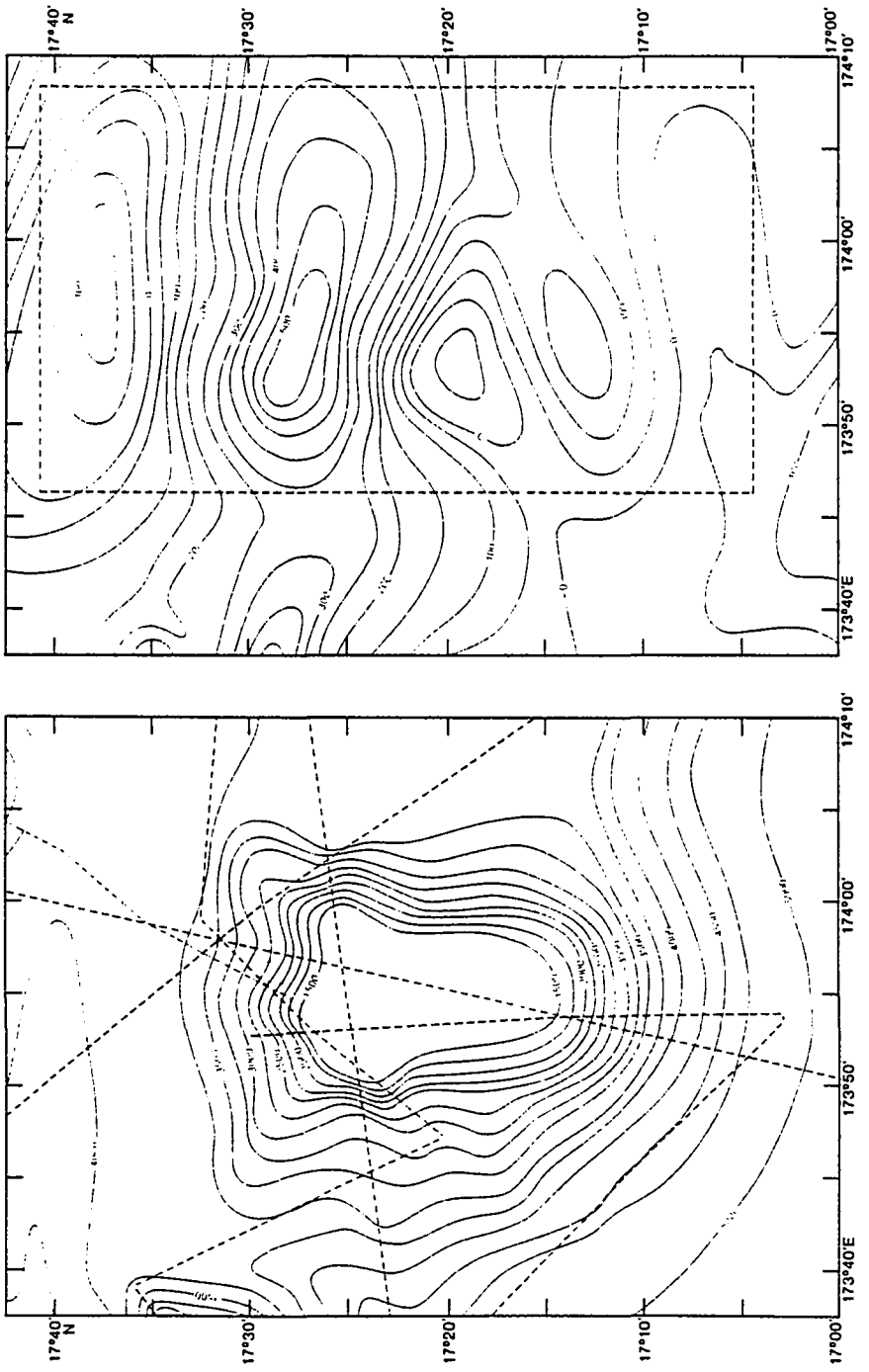

Figure 4.50 Bathymetry (left) and magnetic anomaly (right) of Thomas Guyot (P3). See Figure 4.5 for explanation of charts. Magnetic contour interval is 50 nT.

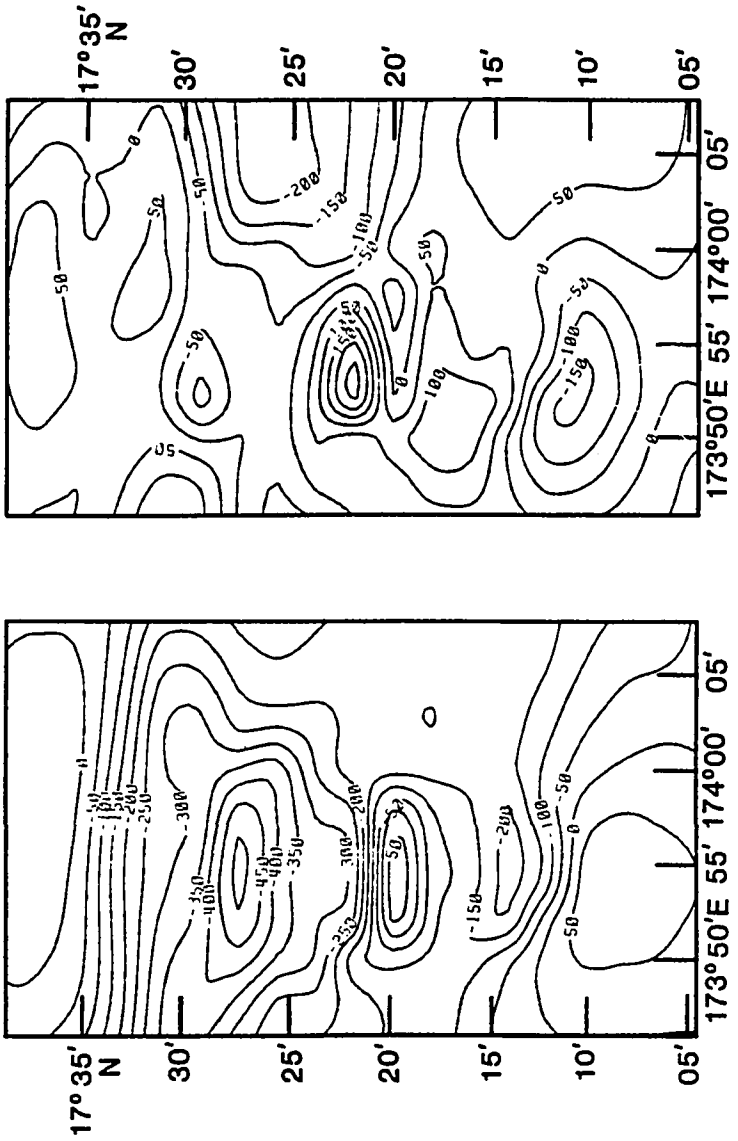

Figure 4.51 Calculated anomaly (left) and residuals (right) of Thomas Guyot (P3). Contour interval is 50 nT.

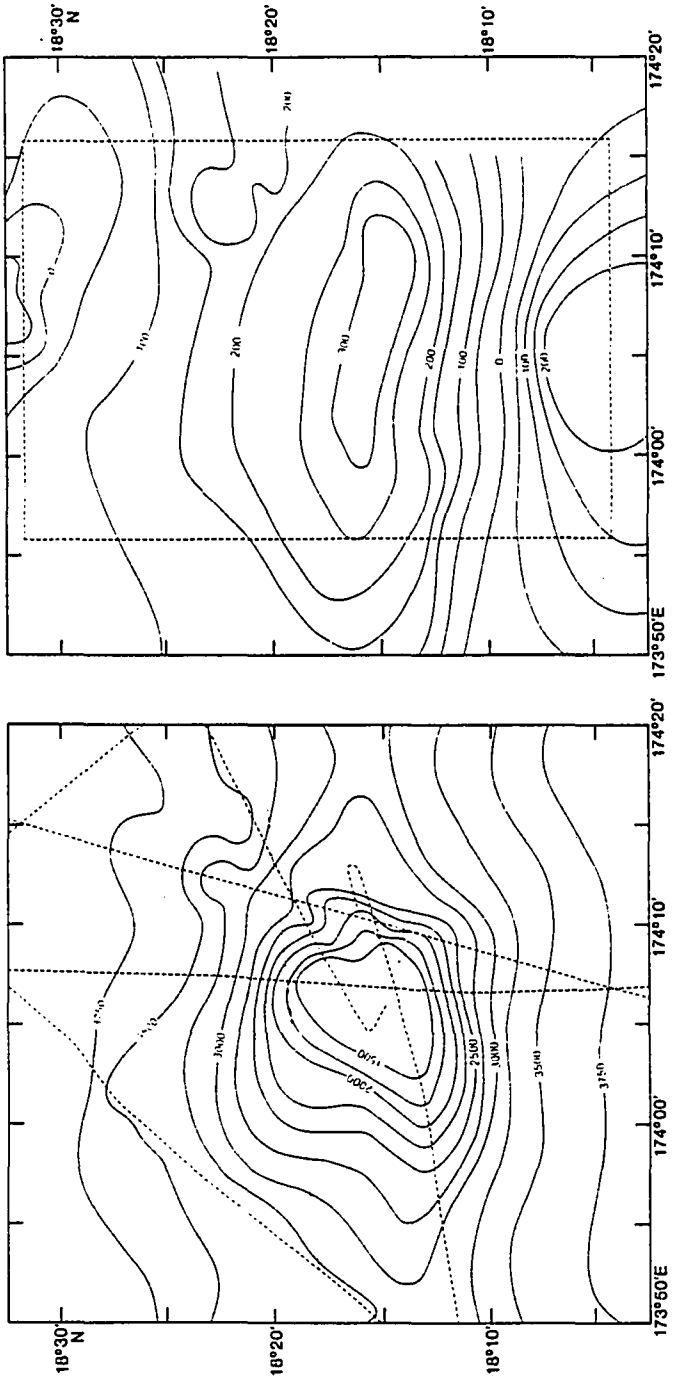

Figure 4.52 Bathymetry (left) and magnetic anomaly (right) of Allen Guyot (P4). See Figure 4.5 for explanation of charts. Magnetic contour interval is 50 nT.

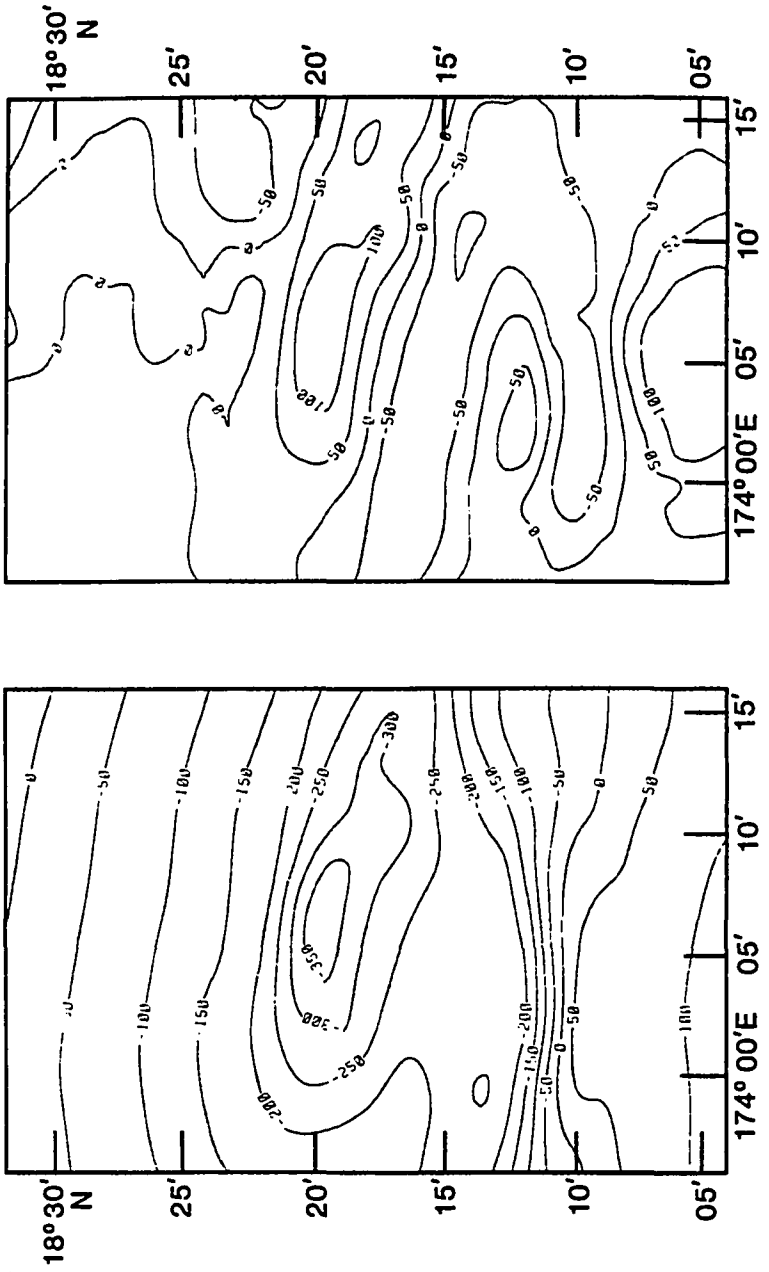

Figure 4.53 Calculated anomaly (left) and residuals (right) of Allen Guyot (P4). Contour interval is 50 nT.

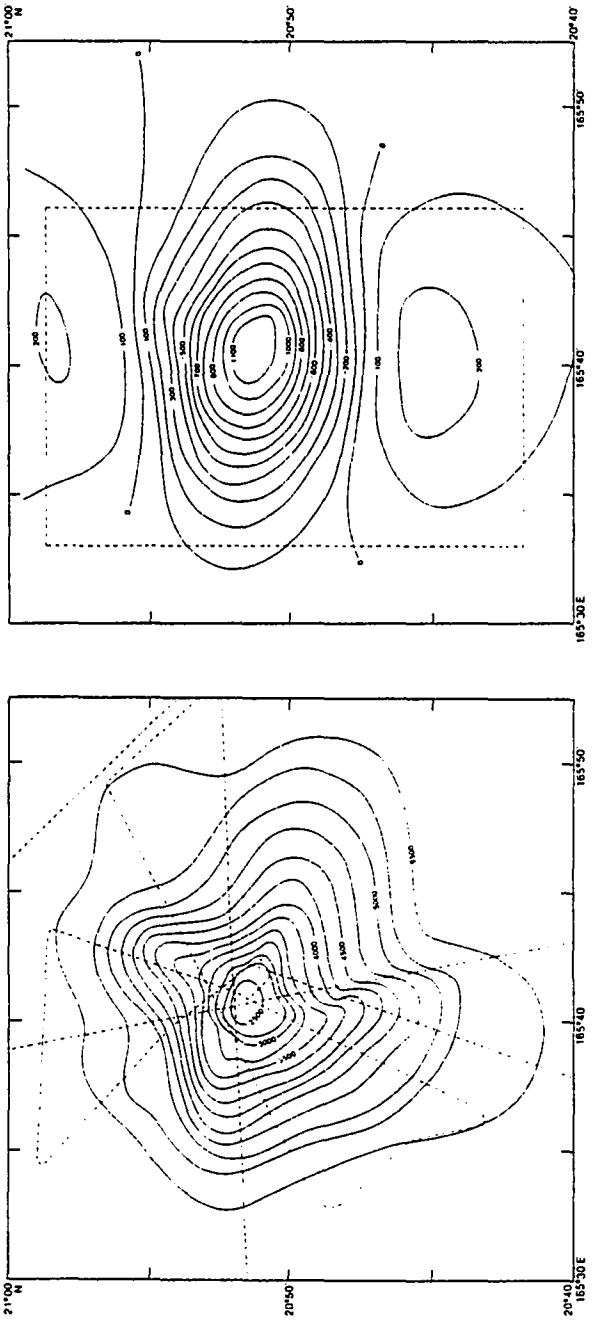

Figure 4.54 Bathymetry (left) and magnetic anomaly (right) of Birdseye Seamount (W7). See Figure 4.5 for explanation of charts. Magnetic contour interval is 100 nT.

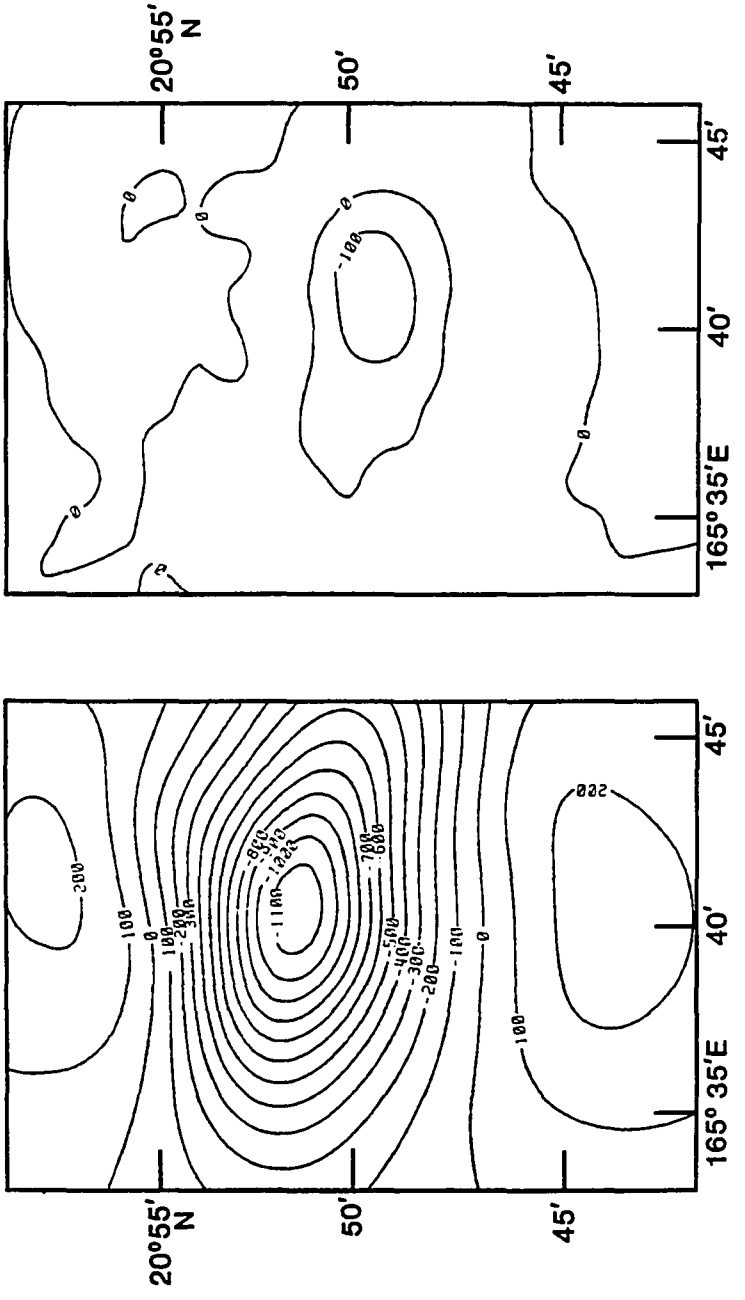

Figure 4.55 Calculated anomaly (left) and residuals (right) of Birdseye Seamount (W7). Contour interval is 100 nT.

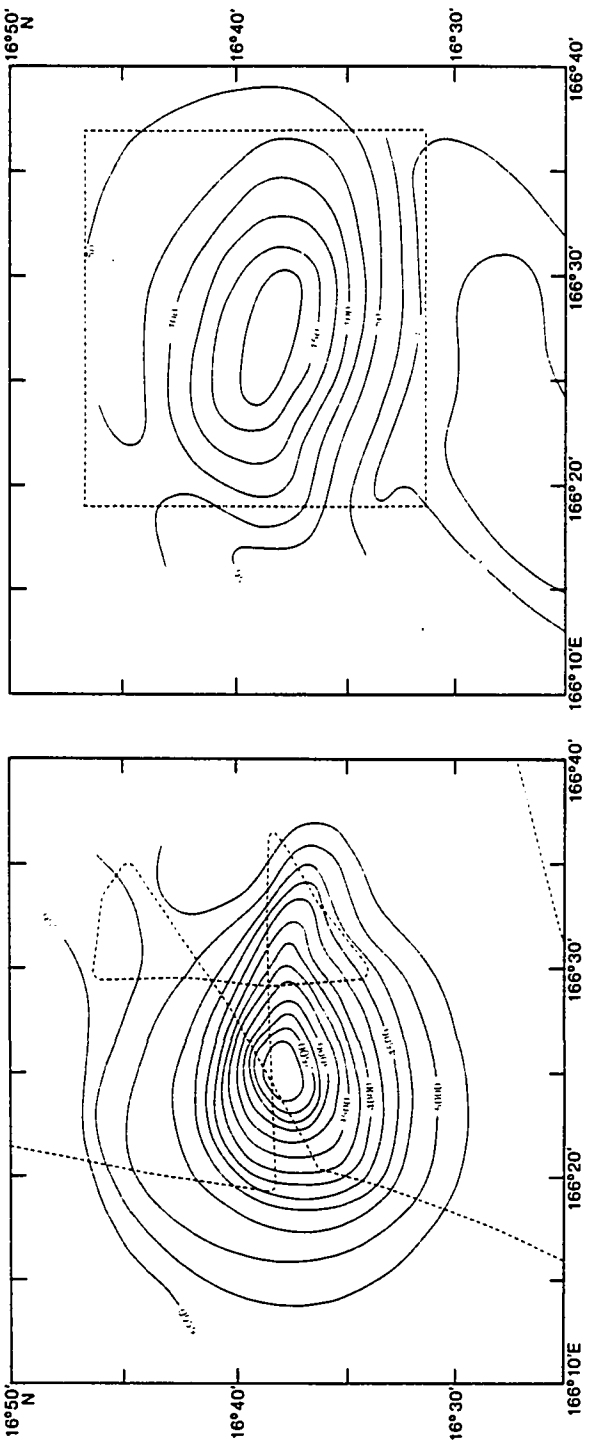

Figure 4.56 Bathymetry (left) and magnetic anomaly (right) of seamount W10. See Figure 4.5 for explanation of charts. Magnetic contour interval is 25 nT.

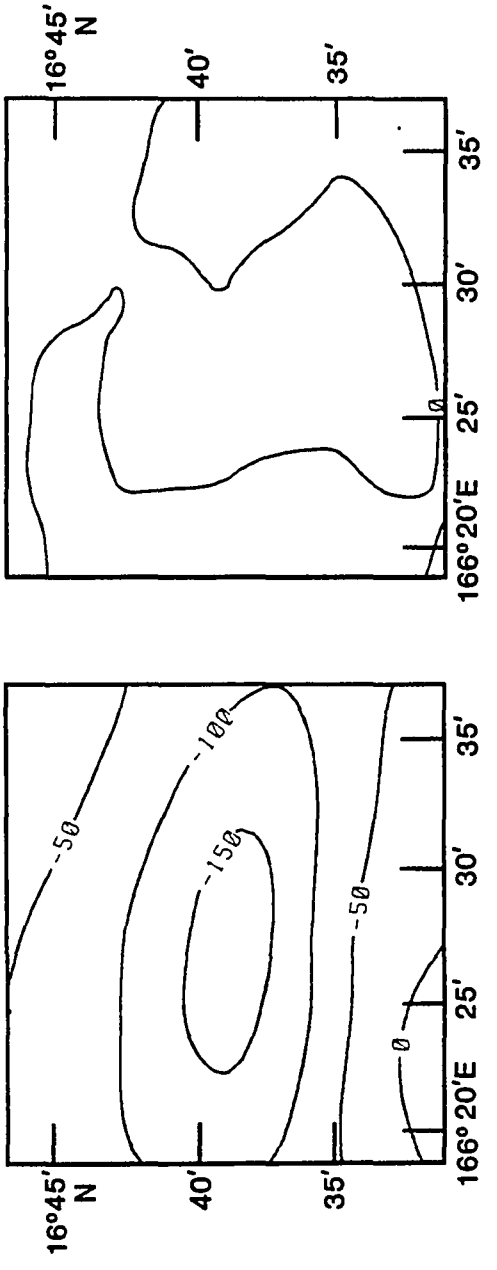

Figure 4.57 Calculated anomaly (left) and residuals of seamount W10. Contour interval 50 nT.

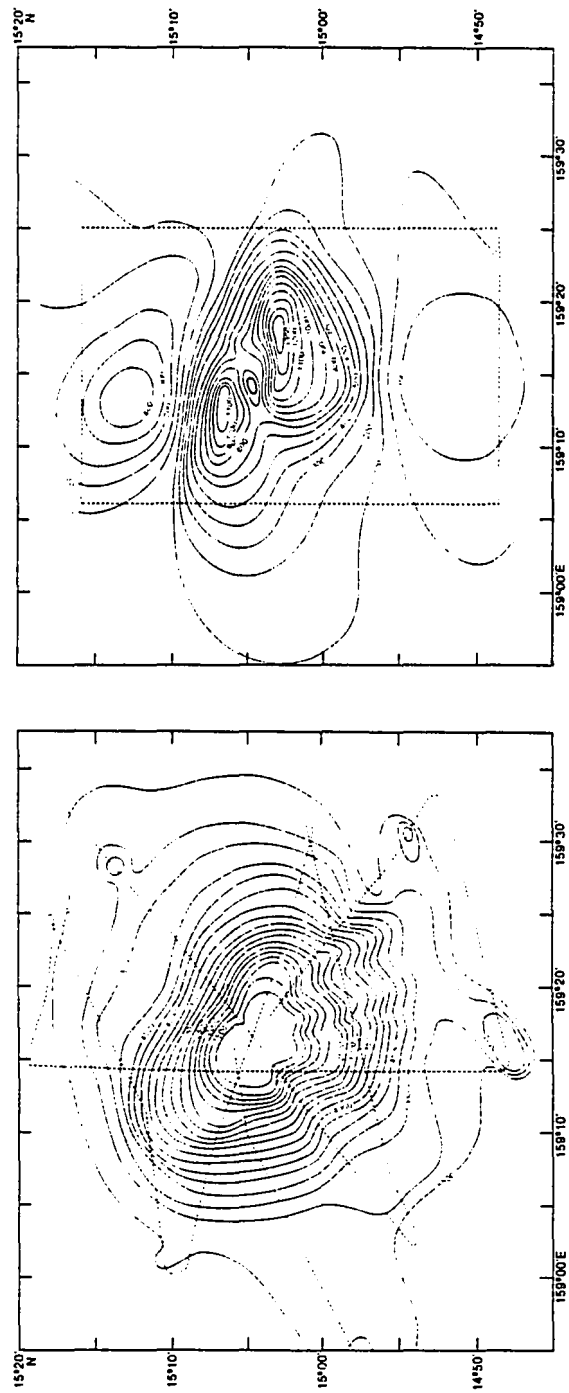

Figure 4.58 Bathymetry (left) and magnetic anomaly (right) of Seascan Guyot (W11). See Figure 4.5 for explanation of charts. Magnetic contour interval is 100 nT.

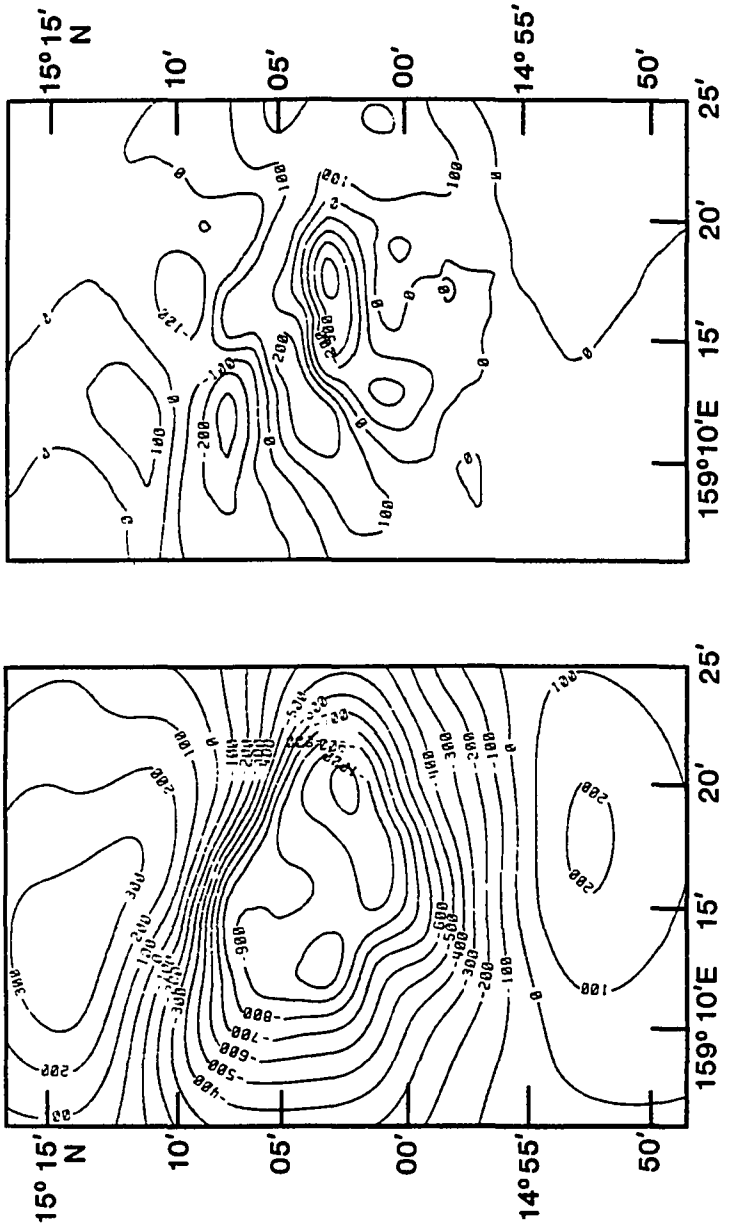

Figure 4.59 Calculated anomaly (left) and residuals (right) of Seascan Guyot (W11). Contour interval is 100 nT.

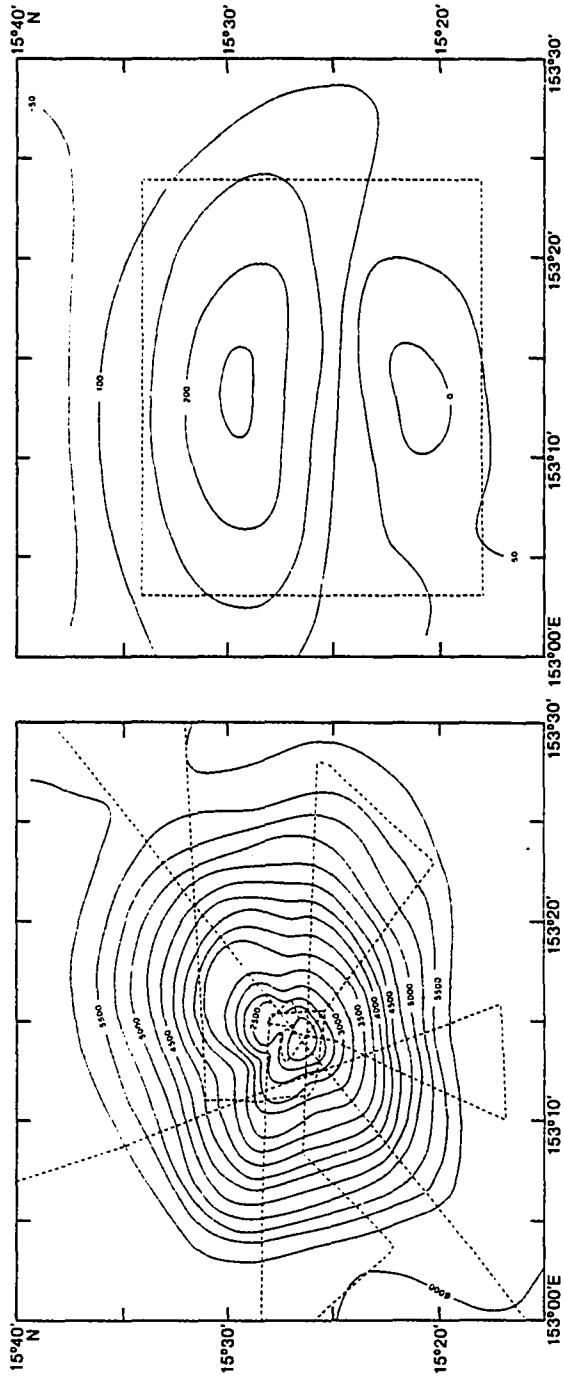

Figure 4.60 Bathymetry (left) and magnetic anomaly (right) of seamount W12. See Figure 4.5 for explanation of charts. Magnetic contour interval is 50 nT.

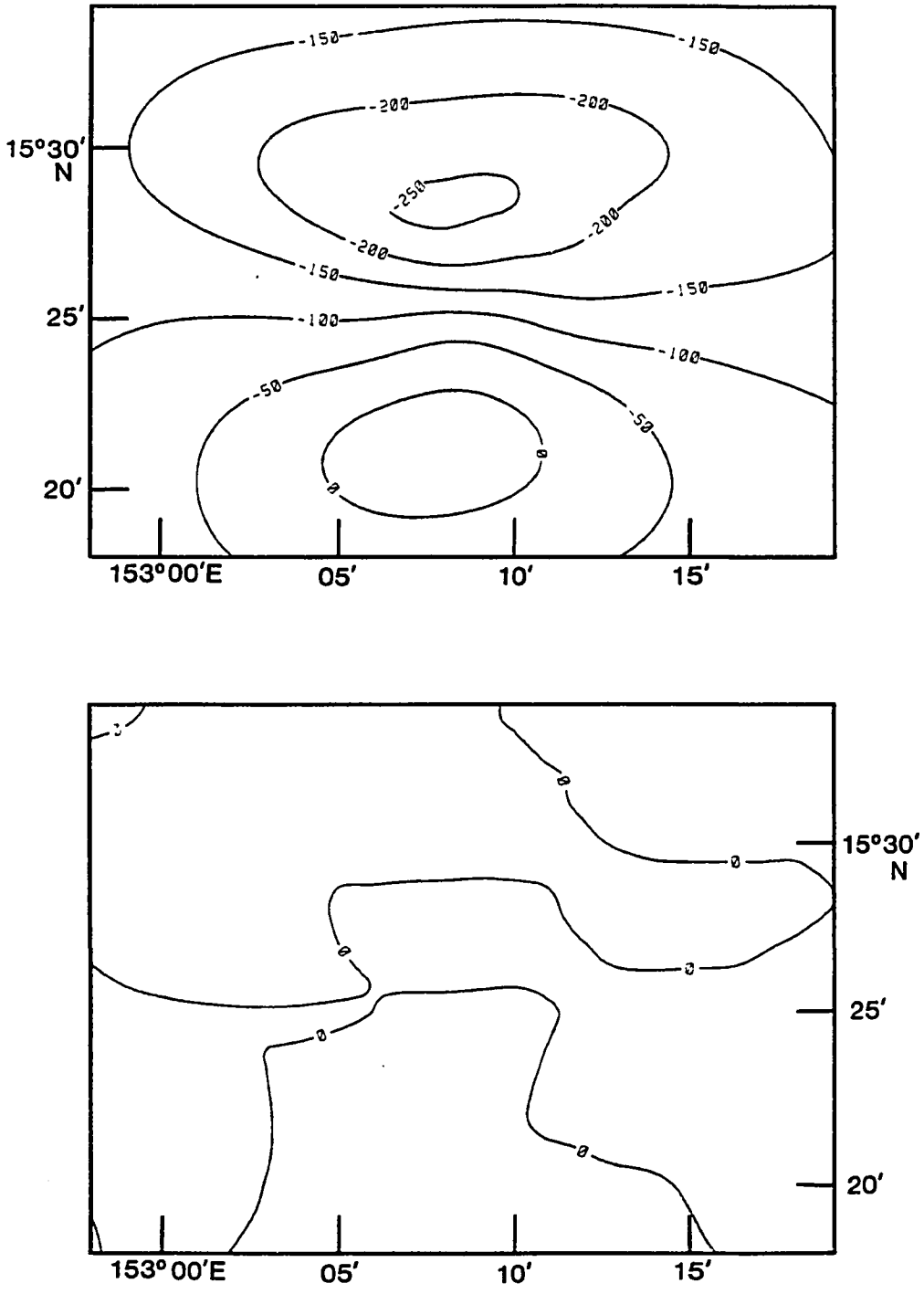

Figure 4.61 Calculated anomaly (top) and residuals (bottom) of seamount W12. Contour interval is 50 nT.

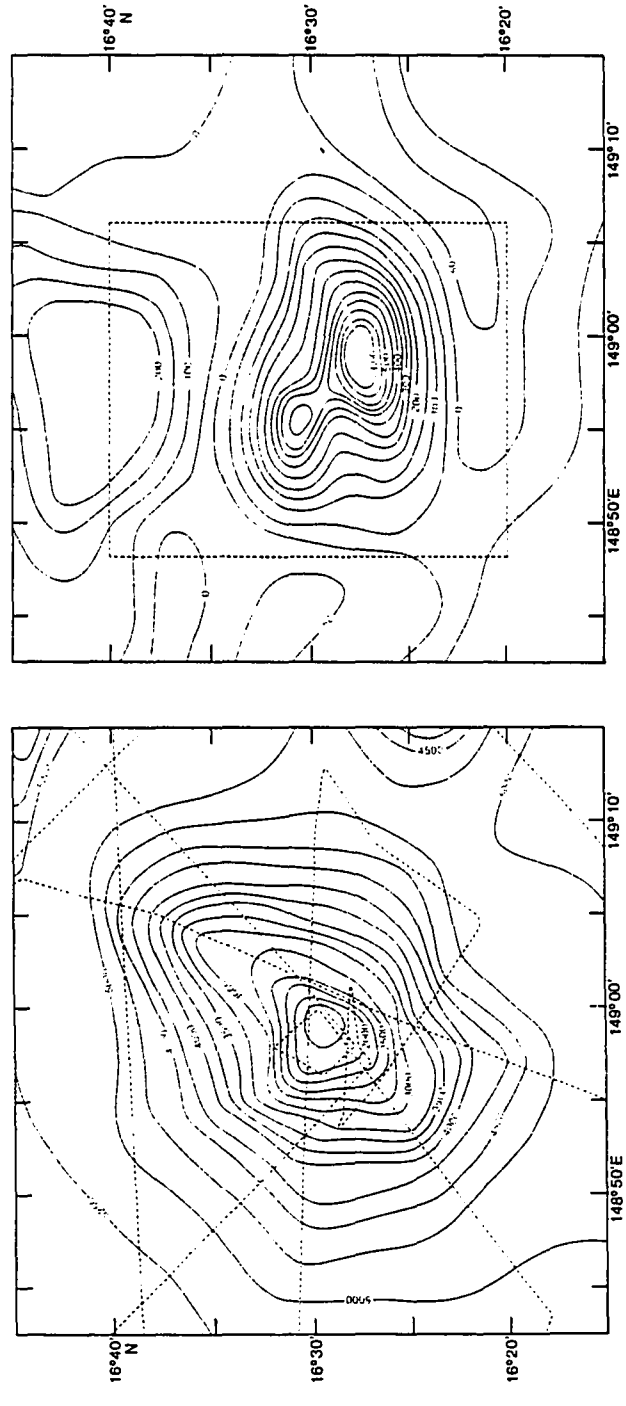

Figure 4.62 Bathymetry (left) and magnetic anomaly (right) of Campbell Seamount (W13). See Figure 4.5 for explanation of charts. Magnetic contour interval is 50 nT.

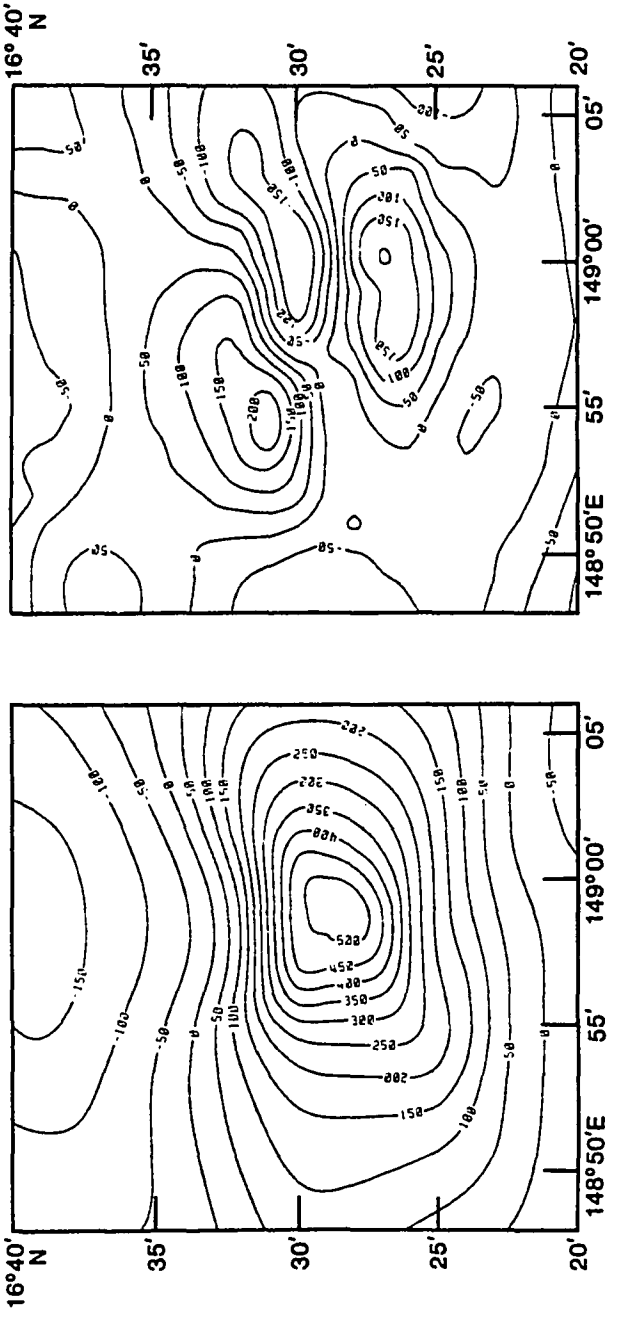

Figure 4.63 Calculated anomaly (left) and residuals (right) of Campbell Seamount (W13). Contour interval is 50 nT.

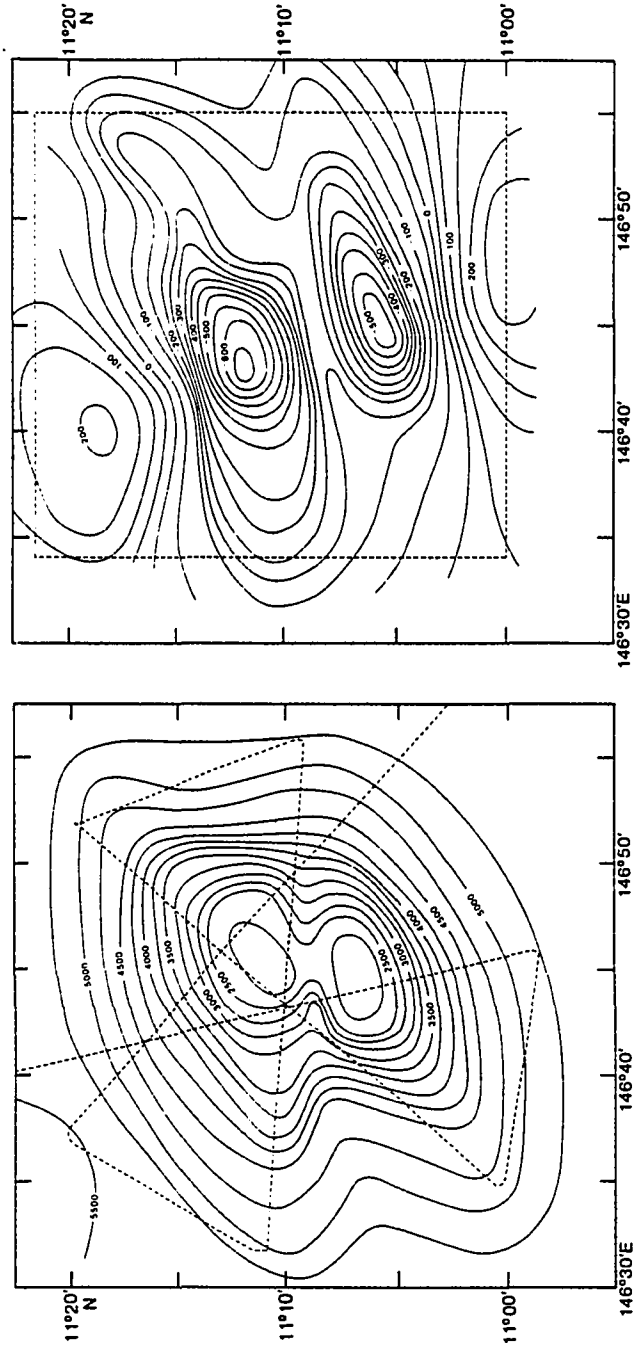

Figure 4.64 Bathymetry (left) and magnetic anomaly (right) of seamount W14. See Figure 4.5 for explanation of charts. Magnetic contour interval is 50 nT.

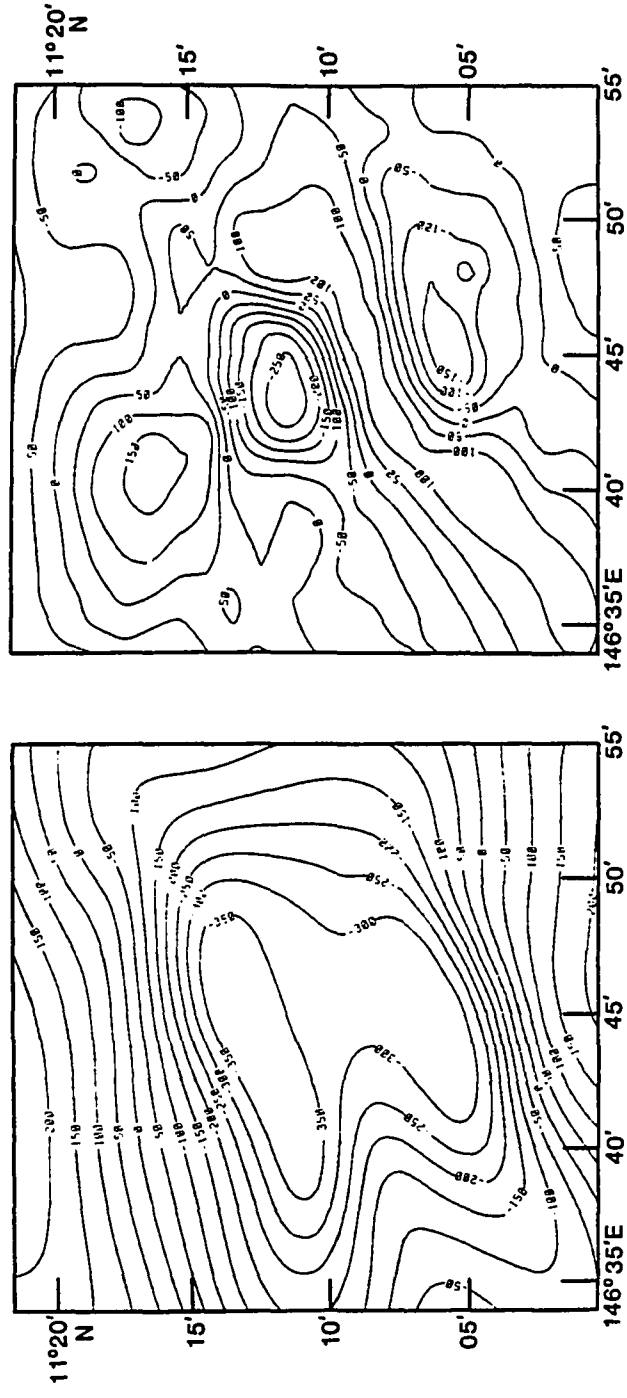

Figure 4.65 Calculated anomaly (left) and residuals (right) of seamount W14. Contour interval is 50 nT.

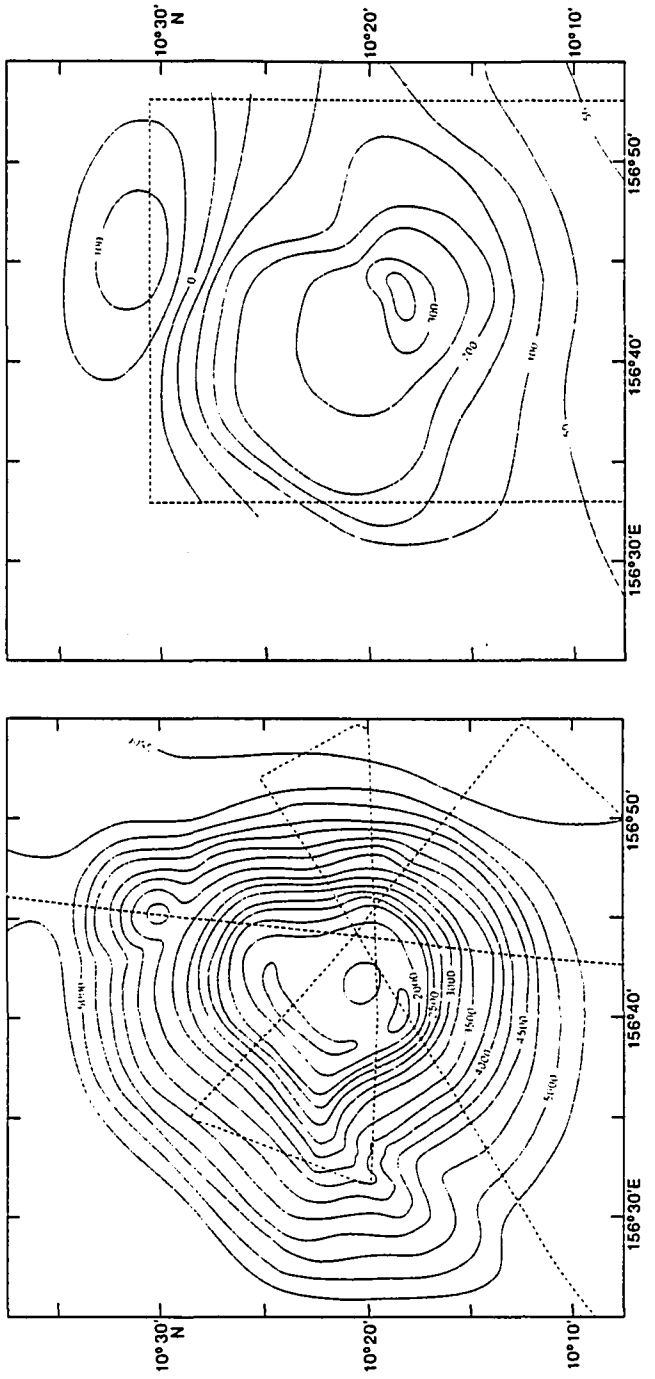

Figure 4.66 Bathymetry (left) and magnetic anomaly (right) of Winchester Guyot (W15). See Figure 4.5 for explanation of charts. Magnetic contour interval is 50 nT.

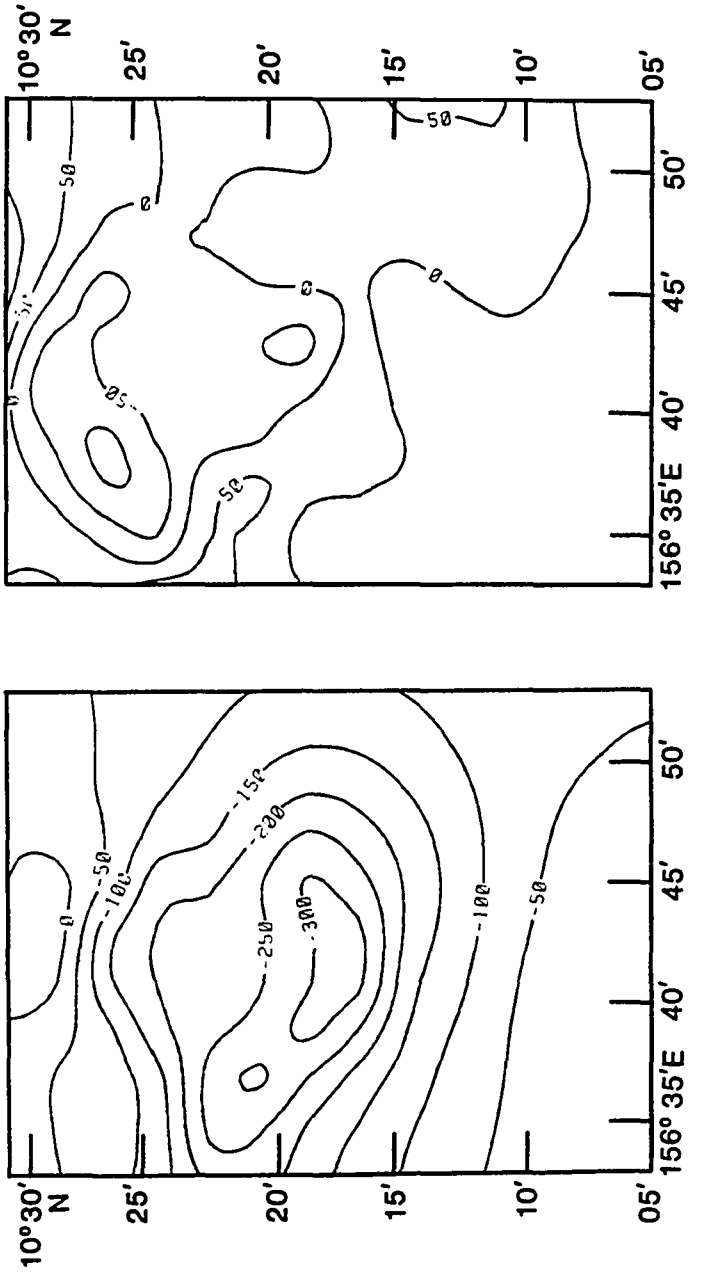

Figure 4.67 Calculated anomaly (left) and residuals (right) of Winchester Guyot (W15). Contour interval is 50 nT.

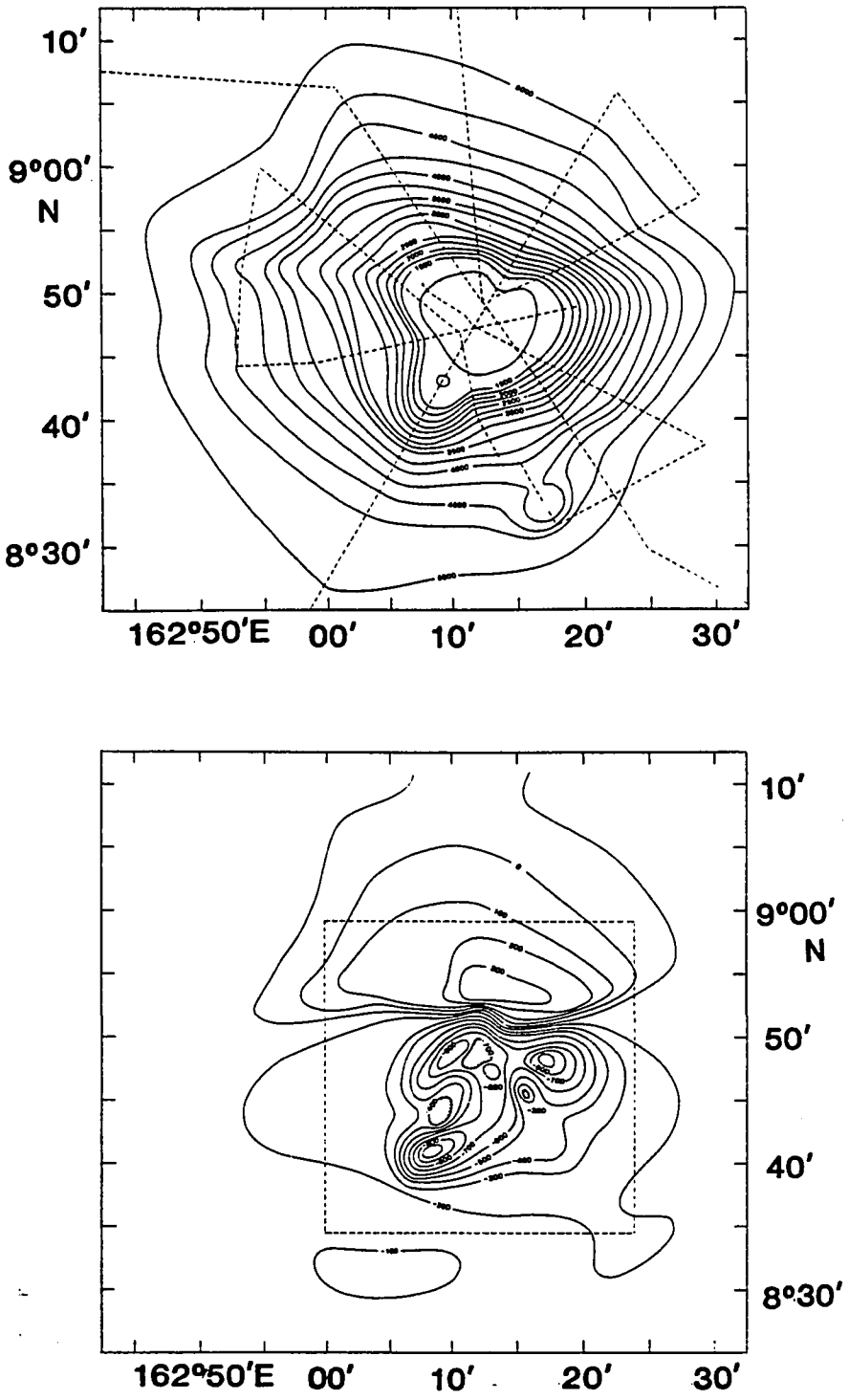

Figure 4.68 Bathymetry (top) and magnetic anomaly (bottom) of Heezen Guyot (W16). See Figure 4.5 for explanation of charts. Magnetic contour interval is 100 nT.

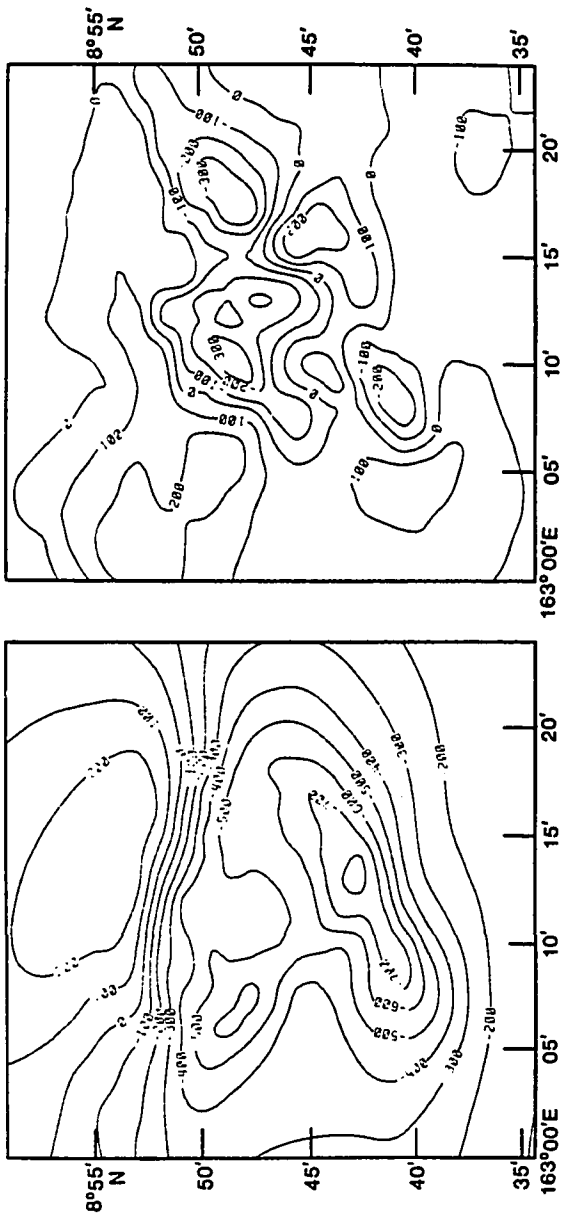

Figure 4.69 Calculated anomaly (left) and residuals (right) of Heezen Guyot (W16). Contour interval is 100 nT.

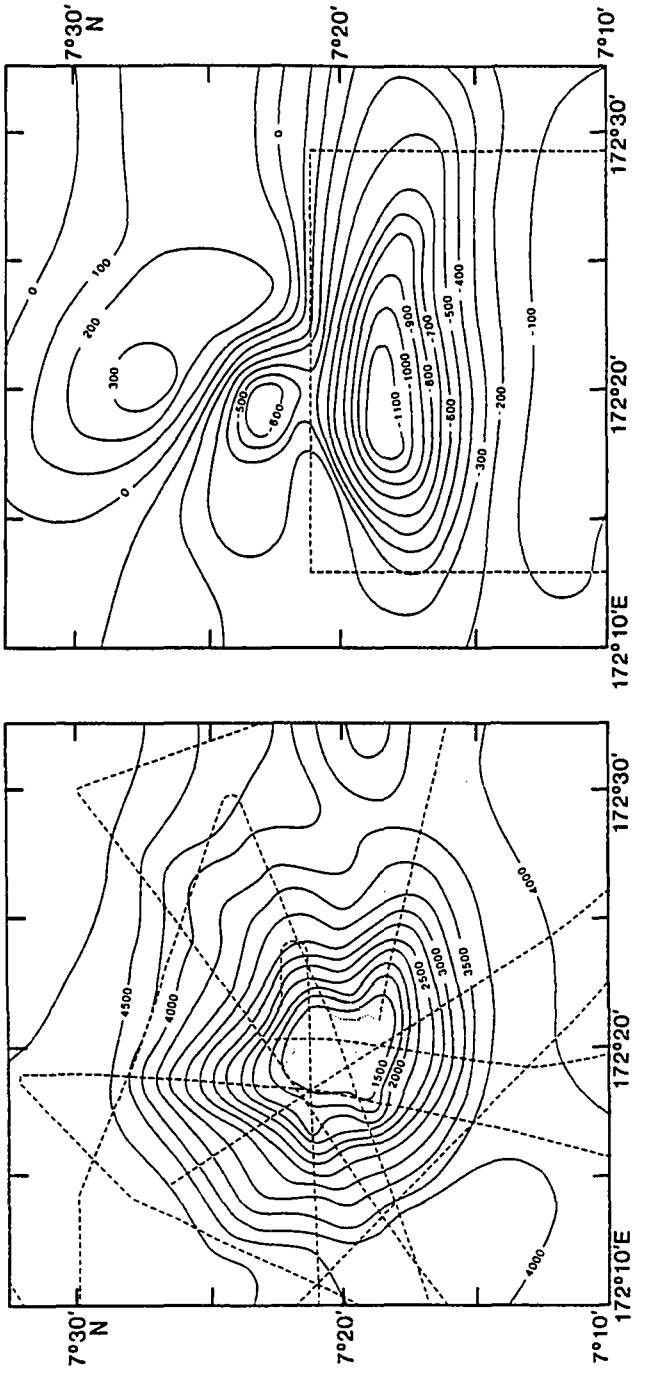

Figure 4.70 Bathymetry (left) and magnetic anomaly (right) of Von Valtier Guyot (W17). See Figure 4.5 for explanation of charts. Magnetic contour interval is 100 nT.

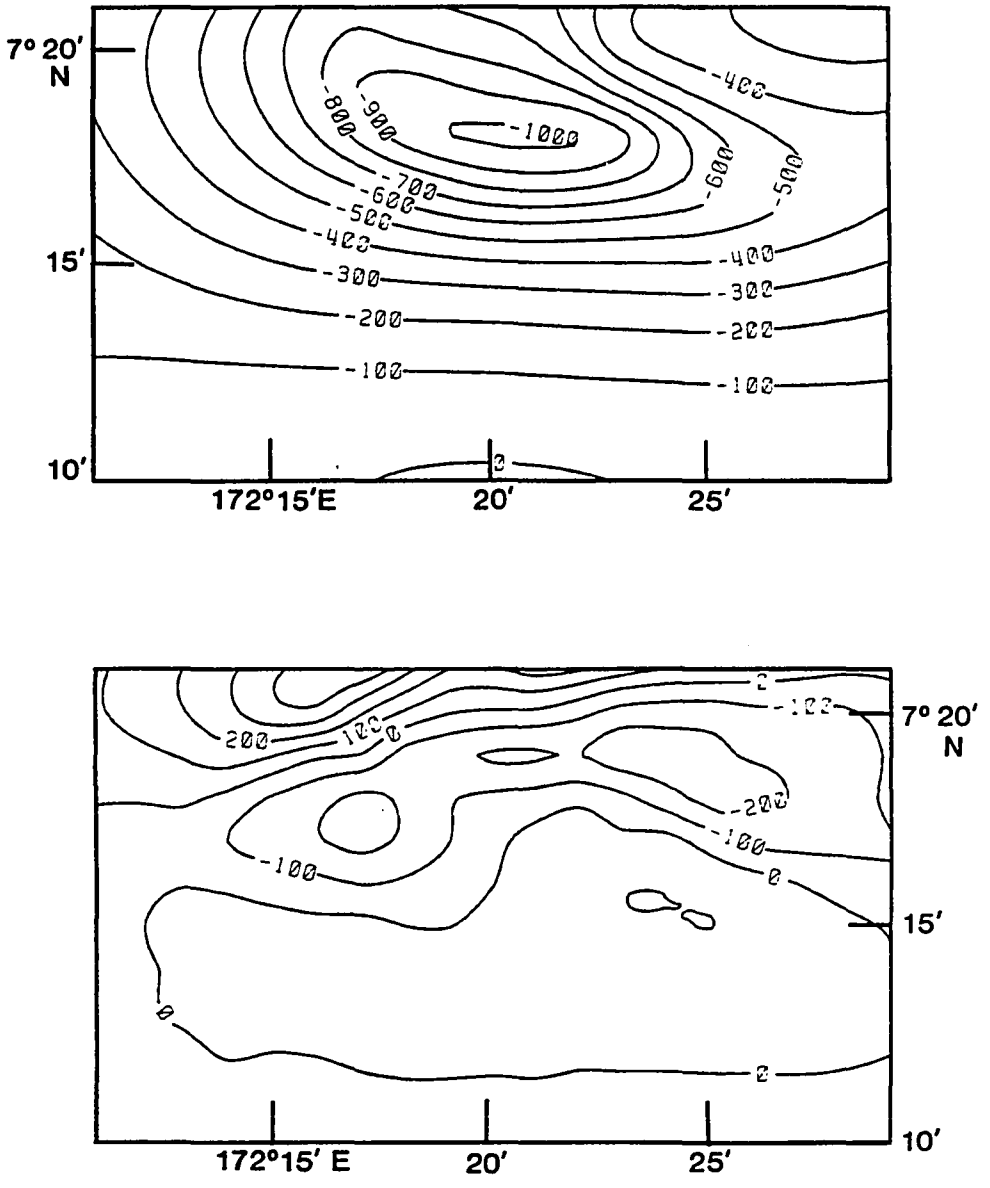

Figure 4.71 Calculated anomaly (top) and residuals (bottom) of Von Valtier Guyot (W17). Contour interval 100 nT.

CHAPTER 5: RESULTS AND INTERPRETATIONS

In this chapter the tectonic implications of the data listed in Chapter 4 are discussed. The syntheses that follow have two main thrusts: (1) to refine the APWP of the Pacific where it has already been outlined and to extend it as far back in time as possible, and (2) to use the seamount paleomagnetic data to place constraints on the tectonic evolution of individual seamount chains and groups.

5.1 AN APPARENT POLAR WANDER PATH FOR THE PACIFIC PLATE

The APWP of the Pacific plate has been a subject of much interest to geophysicists for nearly two decades, yet its details remain sketchy. The problem has been the scarcity of reliable paleomagnetic data from the Pacific resulting from the difficulty of obtaining oriented samples from the deep ocean. During the periods of interest to this study, the Cretaceous and early Tertiary, the paleomagnetic data consist primarily of seamount VGPs and DSDP paleocolatitudes along with a few DSDP equator transits and inclinations estimated from the skewness of magnetic lineations. Each of these types of data has limitations to its usefulness for determining the APWP. Few of the seamount VGPs have been useable as the vast majority are undated. DSDP paleocolatitudes, DSDP equator transits, and skewness inclinations are all azimuthally unoriented, so they place little constraint on the

longitude of the paleopole. Additionally, the DSDP paleocolatitudes sometimes contain systematic errors because of the manner of coring and the uncertainty of secular variation averaging in basalt cores (Peirce, 1976). Another problem has been the difficulty of comparing these varied data types and using them to calculate a paleomagnetic pole and its error bounds. However, this problem has recently been solved by Gordon and Cox (1980b) who developed a method for calculating an average paleomagnetic pole and its 95% confidence ellipse using both fully oriented and azimuthally unoriented data.

Unfortunately, the scarcity of data has forced many investigators to calculate Pacific paleopoles based on small amounts of data that is often of uncertain quality or widely dispersed in age. The result has been a scatter of paleopoles that does little more than allow the general trend of the APWP to be estimated. Figure 5.1 shows many of the Pacific paleopoles published in the literature. Some of these paleopoles have been calculated using a single data type. Some have utilized several different types. Some are based on only a few independent data whereas others have been calculated from many data. To give the reader a better insight to the reliability and scope of these paleomagnetic poles. they are discussed briefly below.

The pole labelled "27" and the curve labelled "22" are a virtual pole from two azimuthally oriented segments of the Midway Atoll drill core (Gromme and Vine, 1972) and a polar circle from a central Pacific basin piston core (Hammond et al., 1979). It is commonly assumed that the APWP continues from this point towards a Cretaceous pole; however, Sager (1983a) calculated an Eocene pole (labelled "41") from seven

seamount VGPS, a DSDP paleocolatitude, and an equatorial transit that suggest that mid-Tertiary paleopoles were stationary at about that latitude and longitude for nearly 25 Ma. This stationary behavior appears to have been the result of a "far-sided" bias of the Neogene data caused by persistent non-dipole geomagnetic field components (Sager, 1983a; Epp et al., 1983).

Cande (1976) determined a Paleocene-Maastrichtian pole (labelled "63-71") from the skewness of anomalies 27-31 in the north and south Pacific. This pole position depends on the assumption that the north and south Pacific lineation groups have skewness parameters affected by "anomalous skewness" and that the value of this bias is the amount needed to make the polar curves of the north and south Pacific anomalies intersect. A better estimation of the Maastrichtian pole (labelled "66") was made by Gordon (1982) from three paleocolatitudes, two equatorial transits, two skewness inclinations, and a magnetic lineation relative amplitude datum. Although the latitude of this pole is well constrained, its longitude relies heavily upon the single relative amplitude datum whose resolution is not considered to be very good by its originators (Schouten and Cande, 1976). Nonetheless, it will be shown in Section 5.1.3 that this pole is in excellent agreement with the Maastrichtian pole calculated in this study with much more data.

The pole labelled "70-110" is the average of 26 Cretaceous seamount VGPs calculated by Harrison et al. (1975). Despite the fact that this pole ignores Pacific plate motion during the Late Cretaceous, it has been widely used to estimate the Pacific plate's motion since

the Cretaceous. The poles labelled "81" and "90" were calculated by Gordon (1983) from eight seamount VGPs and 7 DSDP paleocolatitudes. Although the seamount VGPs seem sound, six of the seven paleocolatitudes are from basalt cores that have either too few samples to adequately average out secular variation or are of indeterminate polarity.

Two areas, labelled "LK" and "EK", were determined by Peirce (1976) as the probable locations of the Late and Early Cretaceous poleopole from DSDP paleocolatitudes. The Late Cretaceous pole was derived from six paleocolatitudes whereas the Early Cretaceous pole relies on only three such data. Two of the paleocolatitudes used to determine the former pole are from basalt cores that probably do not average out secular variation and the rest span a considerable range of ages in the Late Cretaceous. It will be shown in the analysis that follows that rapid apparent polar wander (APW) occurred during the Late Cretaceous and thus an average of paleomagnetic data representing a large range of ages can be misleading. Of the data used to calculate the Early Cretaceous pole, two of the three paleocolatitudes are from basalt cores sampling only a few eruptive units, thus precluding any averaging out of secular variation.

The "108-125" polar area is the intersection of three magnetic polar curves calculated from the skewness of Mesozoic anomalies M0-M10 (Larson and Chase, 1972). Considering the fact that the skewness for each of these lineations was determined by eye from data that was not reduced to the pole, this estimate of the paleomagnetic pole's location may not be reliable. The "133-143" polar area was also determined from

skewness (Jarrard and Sasajima, 1980), in this case from anomalies M15-M21. As no details of its calculation are given, its reliability is impossible to assess.

The pole labelled "120-150" is the Fisherian average of the VGPs of the four "South Japan" seamounts (W2-W5 in Table 4.1) from Harrison et al. (1975). Jarrard and Sasajima (1980) mistakenly assumed a Late Jurassic age for these seamounts claiming that Watts et al. (1980) had determined that they were formed soon after the sea floor upon which they rest. Instead, the Watts et al. (1980) lithospheric flexure study concluded that these seamounts formed well after the underlying lithosphere and are probably no more than 120 Ma. in age. In fact, two of these seamounts have radiometric ages of about 94 Ma.

Denoted by "K" in Figure 5.1 is a Cretaceous pole calculated from 16 paleocolatitudes ranging in age from 144 Ma. to 72 Ma. by Cox and Gordon (1983). They also divided these paleocolatitudes into two groups spanning smaller time intervals. 144-113 Ma. and 94-72 Ma., but the poles calculated from these two groups are not significantly different from the pole shown in Figure 5.1. All of the paleocolatitudes used by Cox and Gordon are from DSDP basalt cores. few of which have sampled enough independent flow units to average out secular variation properly. Given a large number of individual basalt paleocolatitudes within a small range of ages and covering a small area of a plate, Cox and Gordon's method should effectively average out secular variation. However, because of the large span of ages and wide geographical scatter of the paleocolatitudes used in the calcuation of this pole, it may also average out interesting tectonic motions.

The paleopoles shown in Figure 5.1 appear to be scattered and in some cases mutually inconsistent. No doubt this confused picture has deterred many investigators from speculating about the Pacific's APWP. for few have done so. One of the first attempts to define an APWP for the Pacific was made by Francheteau et al. (1970). This study was one of the first to note the large amount of northward motion of the Pacific since the Late Cretaceous. Their APWP was based on only two points, the virtual pole from the Midway Atoll core and an average pole for some seamounts around Hawaii, but the result was surprisingly very similar to APWPs calculated recently with much more data.

Using many of the paleopoles depicted in Figure 5.1, Jarrard and Sasajima (1980) noted that the northward drift of the Pacific did not begin until sometime in the Late Cretaceous. They reported that earlier paleopoles were no further south, but much further west, and explained the observation by suggesting that the Pacific underwent a large clockwise rotation during the Cretaceous. With his 66, 81, and 90 Ma. paleopoles, Gordon (1983) more firmly established the bend in the APWP suggested by Jarrard and Sasajima. Gordon rejected the rotation hypothesis in favor of a shift of the paleomagnetic dipole axis (i.e., true polar wander, see Section 5.1.9) to explain the bend in the APWP.

Cox and Gordon (1983) extended their APWP back into the Jurassic. They began their polar path in the vicinity of the eastern tip of Baffin Island along the polar circle of the Kimmeridgian age DSDP Site 307 paleocolatitude. The APWP moves southward through their Cretaceous pole (shown in Figure 5.1) and then eastward towards England at about

80 Ma. For younger ages it essentially follows Gordon's (1983) path. Cox and Gordon's (1983) polar curve is notable in that it incorporates a southward motion of the Pacific plate during the Early Cretaceous--a feature suggested previously by Larson and Lowrie (1975), Peirce (1976), and Sager and Keating (1982).

The seamount models presented in Chapter 4 double the number of available seamount paleopoles and thus the Pacific APWP is ripe for reinterpretation. Figure 5.2 shows the Pacific APWP delineated in this study. This APWP begins with the Site 307 paleocolatitude as did Cox and Gordon's polar wander curve. It moves southward to approximately 58°N, 339°E, at 119 Ma. and continues its southward motion, but with a westward component, to a pole at about 41°N, 318°E at 104 Ma. For the period 104-91 Ma. the APWP moves rapidly northward by 10° to 55°N, 316°E. It then begins an extremely rapid easterly shift with almost no latitudinal change. From 91 to 87 Ma. it shifts 15° to 54°N, 343°E and from 87 to 81 Ma. the movement is 10° to 60°N, 357°E for a total shift of 25° in about 10 Ma. This east-west segment crosses over the Early Cretaceous path creating an unprecedented mid-Cretaceous loop in the motion of Pacific the paleopole.

For the Late Cretaceous the APWP is very similar to Gordon's (1983) path. The paleopole moves rapidly northward to 70°N, 2°E at about 68 Ma. and 78°N, 21°E at 41 Ma. The paleopole remains in the vicinity of the Eocene pole until the Early Miocene (about 22 Ma.) at which time it begins a rapid shift towards the geographic pole.

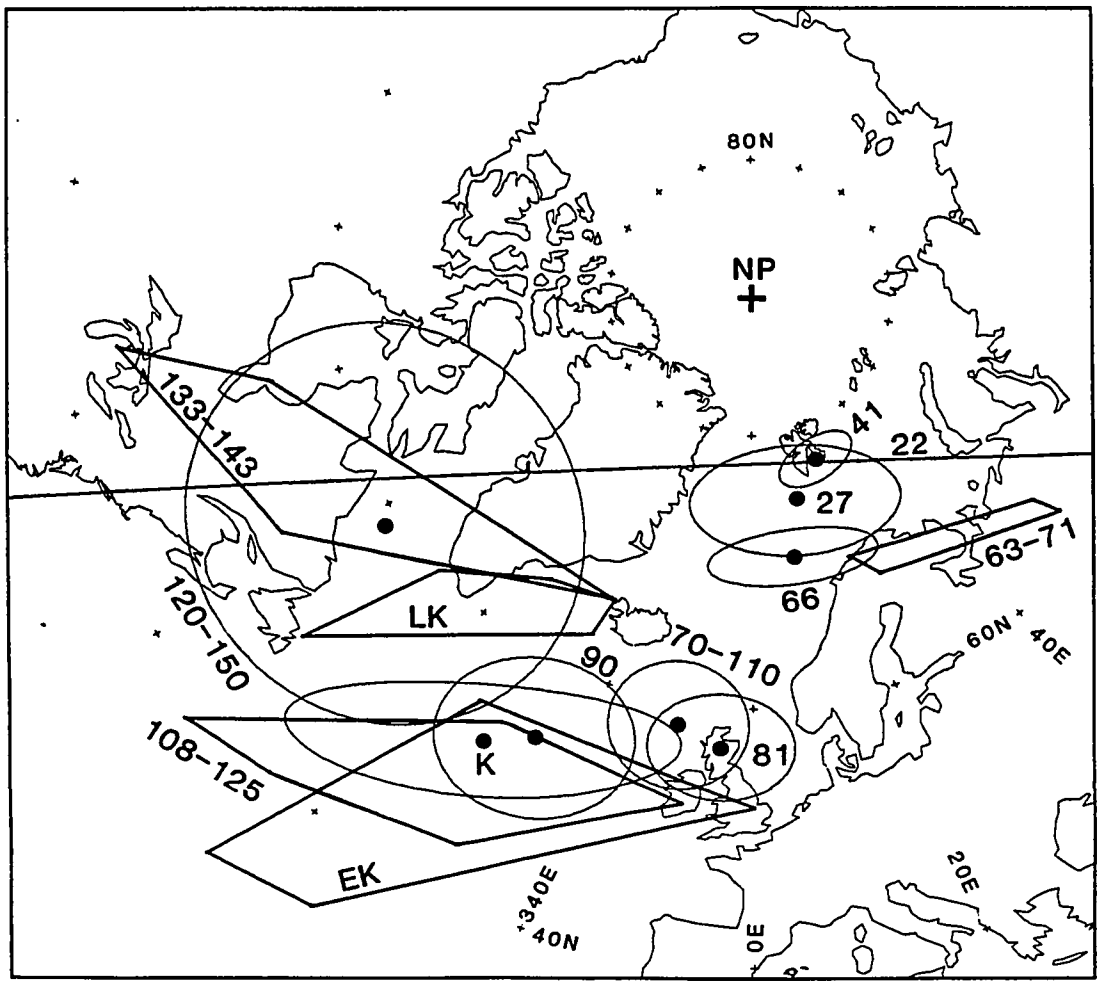

Figure 5.1 Published Pacific paleomagnetic poles. Dots indicate pole locations and surrounding ellipses are their 95% confidence regions. Polygons are polar areas and the line labeled 22 is a segment of a polar circle of a piston core. The numbers indicate the pole ages in Ma. K, EK, and LK label Cretaceous, Early Cretaceous, and Late Cretaceous poles. See text for discussion. Map projection is polar equal area.

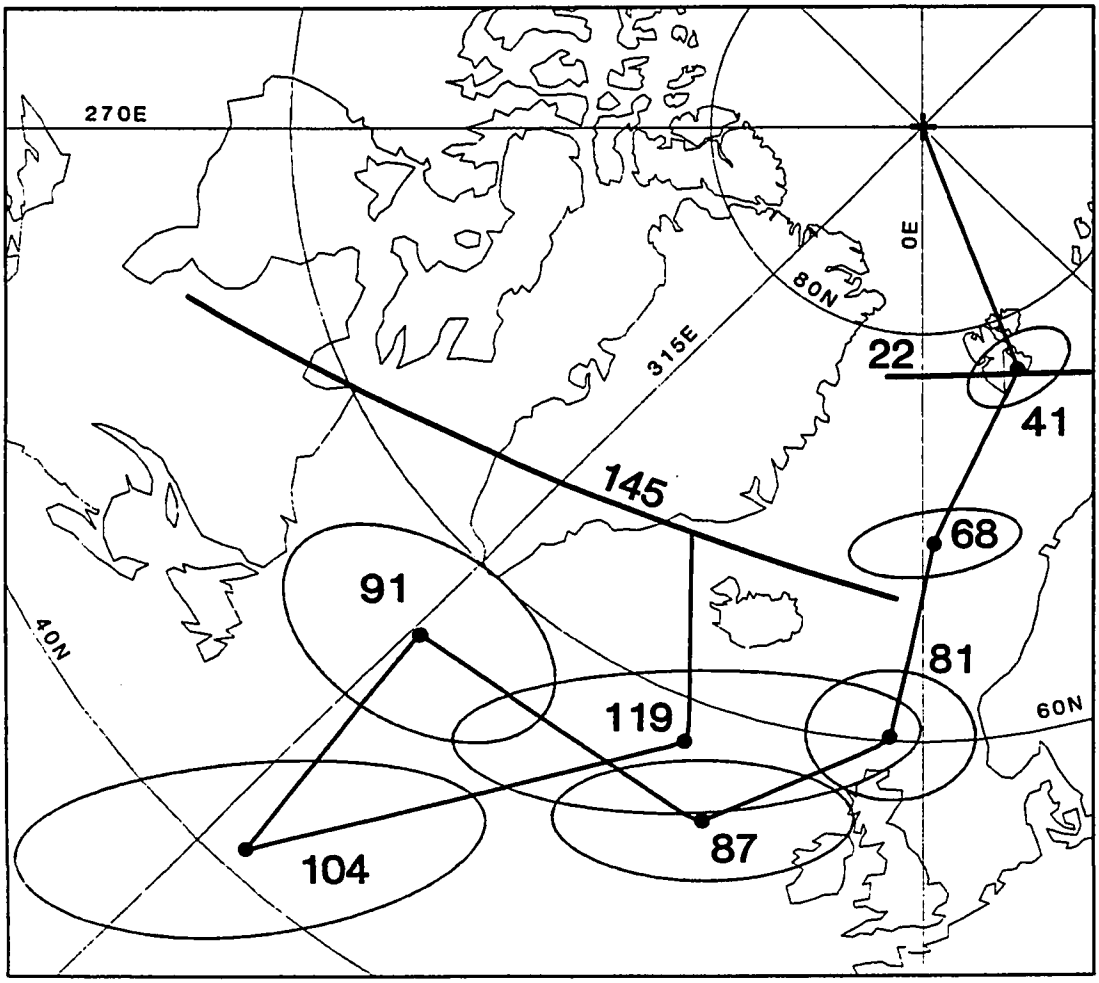

Figure 5.2 An apparent polar wander path (APWP) for the north Pacific. Dots represent the locations of the mean poles calculated in this study and the surrounding ellipses are their 95% confidence regions. The heavy lines labeled 145 and 22 are segments of polar circles from azimuthally unoriented cores. The numbers are ages in Ma. Straight line segments are shown connecting the poles to indicate the direction of APW which may be more complex than implied by these lines. Map projection is polar equal area.

5.1.1 THE CALCULATION OF AVERAGE PALEOMAGNETIC POLES

All of the average paleomagnetic poles presented in the following sections were calculated using the method of Gordon and Cox (1980b) and are listed in Table 5.1. This method makes it possible to combine the information afforded by both completely oriented and azimuthally unoriented paleomagnetic data as well as anomaly skewness inclinations, relative amplitudes, and paleoequator transits. The average pole is found by minimizing the distance between the average pole and the pole predicted by each datum in a maximum-likelihood, least-squares sense. The method has the desirable property of weighting each datum inversely to its error (i.e., the most accurate data places the most constraint on the average pole). It also allows the calculation of a 95% confidence ellipse around the average pole by the linear propagation of the individual datum errors.

In order to use the Gordon and Cox method, an error value must be assigned to each input datum to be used in the calculation of an average pole and its 95% confidence ellipse. The errors for the paleocolatitudes, equator transits, and skewness inclinations were explained in Chapter 4. No study, however, has adequately investigated the error to be expected in the position of each seamount VGP. To make a proper study of seamount paleopole errors, it is necessary to have a large number of seamounts of the same age and probably having similar GFR values. No such large group of well-dated seamount VGPs exists; consequently, the seamount VGP errors must be derived in one of two ways. Either the seamount VGPs of each age group can be used to

calculate a standard deviation to be used as the error for each VGP or, if too few seamounts belong to the group. an error may be assumed from other seamounts of similar age or geographic location.

Harrison et al. (1975) stated that seamount VGPs are not dispersed in Fisherian (Fisher, 1953) distributions (i.e., not in a circular distribution around the mean pole). Instead, they claimed that Cretaceous seamounts appeared to have about twice the scatter due to errors in the paleodeclination than in paleoinclination. However, much of the scatter they discussed can be attributed to tectonic motion. so their conclusion may not be valid. In the following sections it will be seen that the shape of the seamount VGP distribution of each age appears to be different. In some cases the scatter appears to be more or less Fisherian. but in others the distribution of VGPs seems decidedly elliptical. In most cases. however, the long axis of the VGP error ellipse is along the direction of polar wander, and thus tectonic motion may be at least partially responsible for the errors. The Tripod seamounts (Francheteau et al., 1970). because of their low mean GFR (2.4). provide an estimate of the maximum error to be expected from seamount VGPs with acceptable goodness-of-fit parameters. These seamounts have an A_{95} of 14.4^{o}. This value is rather large and most other groups of seamount VGPs tend to have 95% confidence limits less than half that value.

The most difficult task in the calculation of the paleomagnetic poles that define the APWP is dividing the data into age groups and deciding which data in any given group is reliable. Errors are to be expected in the determination of a paleomagnetic datum and its age.

Therefore, some age groups may contain data with misleading ages or paleopoles. This problem is particularly troublesome for the seaount data because the seamount VGP errors are so poorly known and because reliably dated seamounts are so scarce that one is forced to use many different methods for dating or inferring the ages of seamounts.

In order to separate out the misleading data it is necessary to examine the positions of the paleopoles recorded by the data of a given age group and look for mutual agreement. Usually most of the data will cluster, but sometimes there will be a few data that fall well outside the cluster. In some cases the difference may be the result of systematic errors in the age (e.g., K-Ar and fossil ages are minimum ages) or systematic errors in the measured paleomagnetic pole such as might be caused by relative tectonic displacements. In other cases the difference may result from large random errors in the determination of a paleomagnetic datum. Whatever the cause, it is desirable to eliminate the misleading data from the average pole calculation if it is located very far from the cluster of the majority of the data. If Pacific paleomagnetic data were more abundant, such discrepant data would not pose any great problem. However, as most of the mean paleomagnetic poles in this study have been calculated from a small amount of data, a few misleading data in any given age group could significantly bias the calculated postion of the mean pole.

Care must be excercised in the exclusion of discrepant data in order to prevent circular reasoning. Basically, one must examine a paleopole that shows a large difference from the average postion of the majority of the data of the same age group to see if the difference is

compatible with the error assigned to the datum. If this difference is greater than the 95% error bounds of the datum, then it is probably suspect. The pole calculation method makes it possible to put this test on a more rigorous footing. In the pole calculation, data "importance" values (Minster et al., 1974; Gordon and Cox, 1980b) can be calculated. The importance of a datum ranges from 0 to 1 with a value of unity implying that it completely constrains one degree of freedom of the mean pole position. If a paleopole lies well outside the scatter of most of the data of the same age and it also has a high importance value, its distance from the mean pole position that would be calculated without it is probably large compared with its error limits. Such a datum may bias the position of the mean pole if it is included in the calculation, so it is best excluded. In contrast, a datum that displays a large discrepancy with the rest of the data of the same age, but also has large error limits, will have a small importance value and will not significantly affect the mean pole position because its constraint of the pole in the Gordon and Cox method is inversely proportional to its assigned error.

Another test can be used to examine the mutual consistency of the data. According to Gordon and Cox (1980b), the data used to calculate a paleomagnetic pole, if free from systematic error, shoule be chi-square distributed. Their pole determiniation method also makes a provision to calculate a chi-square statistic for the input data. This parameter may be compared to standard tables of the 95% confidence limits of a chi-square variable for the appropriate number of degrees of freedom. If the chi-square statistic is too low, the data errors

are over-estimated; but, if it is too high, the indication is that the errors are underestimated (Gordon and Cox, 1980b). The latter problem may arise when data whose distance from the average pole is large compared to its assigned error are used in the pole calculation. The chi-square statistic may still be within its 95% confidence range even if some discrepant data is used. For such instances, Gordon and Cox (1980b) outline a procedure by which a datum's contribution to the chi-square statistic can be found and tested for consistency with the rest of the data being used for the calculation of the pole.

5.1.2 THE TERTIARY APPARENT POLAR WANDER PATH

Few data are available to be used for constraining the mid to late Tertiary APWP. The Tripod Seamounts (E3-E9) are located on sea floor of Miocene age. A K-Ar date from one of these seamounts (E6) is 3 Ma. (Ozima et al., 1968). Because these seamounts are located very close to one another, they are likely to be about the same age. The Tripod VGPs display a fairly large scatter around the geographic pole. The average position is 87^{o}N, 90^{o}E with an A_{95} of 14.4^{o} (Figure 5.3). In agreement with the apparent young age of these seamounts, this pole is not significantly different from the geographic pole and its large 95% confidence cone is probably a result of the low GFRs of the seamount models (Francheteau et al., 1970) and the location of these seamounts near high amplitude magnetic lineations.

Sager (1983a) calculated a Late Eocene paleomagnetic pole from seven seamounts (E1, E2, L4-L7), a paleocolatitude from DSDP Site 166, and an equatorial transit from DSDP Site 163. The average pole is at 77.5°N, 21.2°E and has a 95% confidence ellipse with a minor axis of 1.5° and a major axis of 2.9° trending 77.0° clockwise from north (Figure 5.4). It is assigned an age of 41+5 Ma.

Perhaps the most interesting aspect of the Tertiary APWP is the fact that the Oligocene age Midway Atoll drill core (Gromme and Vine, 1972) and seven Miocene central Pacific piston cores (Hammond et al., 1979) all predict the paleopole to have the same latitude as the Eocene pole (Sager, 1983a). It appears that this agreement is a coincidence caused by persistent non-dipole geomagnetic field components in the Early Miocene. Epp et al. (1983) made a detailed examination of high resolution piston core paleomagnetic data spanning the Oligocene to the present. Their data (Figure 5.5) showed a disagreement between the observed paleolatitudes and those predicted by Pacific plate/hotspot relative motion studies. A large difference of about 4° to 6° accumulated rapidly at about 24 Ma. The sense of the discrepancy is such that the paleoinclinations are too low and thus paleomagnetic poles from this data appear farther from the spin axis than they should. The rapid build-up of this bias suggests that it is not caused by true polar wander as the implied rate of plate/mantle or plate/spin axis motion is unreasonably high (Epp et al., 1983).

The geographical distribution of the data used to calculate this pole suggests that the northern part of the Pacific plate has remained

single rigid since the Eocene. The calculation of this pole is discussed at length by Sager (1983a).

5.1.3 THE MAASTRICHTIAN POLE (68 Ma.)

A considerable amount of data is available for estimating the Pacific's Maastrichtian pole (Figure 5.6). Six paleocolatitudes, four equator transits, five anomaly skewness inclinations, and five seamounts all have ages falling between 64 and 74 Ma. The paleocolatitudes are from GPC3 and DSDP Sites 165, 199, 288A, 315A, and 433C. The last of these was obtained from basalt samples from approximately 65 flow units (Kono, 1980b) whereas the others are from sediment samples. As shown in Figures 4.3a and 4.4b, the paleocolatitude and paleoequator data, with the exception of the Site 288A paleocolatitude, are in excellent agreement predicting a paleopole within a small region of the north Atlantic bounded by Greenland, Scandinavia, Spitzbergen, and Iceland. The Site 288A paleocolatitude predicts a paleopole significantly closer to the geographic pole than the rest of the data. In this way it is similar to paleomagnetic data of the same age from nearby DSDP sites 289 (Hammond et al., 1975) and 462 (Steiner, 1981a) as well as some other equatorial paleocolatitudes (discussed in Section 5.1.9).

Two of the five groups of magnetic lineations, N1 and N2 from the north Pacific, have semi-great circle pole loci that pass through the

same area of the north Atlantic favored by the other data. The other three anomaly groups, SW1, SW2, and SW3 are all located in the south Pacific. Like the Site 288A paleocolatitude, they record inclinations compatible with a pole closer to the geographic pole (Figure 4.4a).

Of the five seamounts with Maastrichtian ages, three (H11, H12, L8) have VGPs that fall near the center of the area where the polar curves of the other data intersect (Figure 5.6). The other two (J3, M6) have VGPs far to the south near the Campanian and Santonian poles. This difference (18^{o} and 19^{o}, respectively, from the mean Maastrichtian pole) is greater than would be expected from the normal scatter of reliable seamount VGPs. It is not uncommon for K-Ar ages of submarine basalts to be lower than the true age because of the loss of argon during submarine alteration (Ozima et al., 1977). Considering the large distance separating the VGPs of M6 and J3 from the area indicated as the probable location of the Maastrichtian pole by the other data, it seems likely that these two seamounts are probably somewhat older than their K-Ar ages imply and that they should therefore not be used in the calculation of the Maastrichtian pole.

The three remaining seamount VGPs all have nearly the same latitude, but vary in longitude by 24^{o}. The implication is that their longitudinal error greatly exceeds their latitudinal error. Although this reasoning may be correct, the three VGPs are too few to be used to derive a statistically meaningful error limits. Consequently, the standard deviation ellipse of each VGP was assumed to be the same as that calculated for the distribution of Eocene seamount VGPs (Sager,

1983a), an ellipse with a major semi-axis length of 5.0° striking 71° from north and having a minor semi-axis length of 2.9°. This error ellipse was calculated from the VGPs of seven seamounts of probable Eocene age. The distribution of these VGPs was assumed to be elliptical and the standard deviation ellipse was calculated by solving for the eigenvectors of the latitude-longitude covariance matrix of the VGP positions. The planar standard deviations thus derived were corrected so as to be applicable to a sphere by multiplying by $\sqrt{2}$ (Cox and Gordon, 1983).

Unfortunately, because the longitude of the average pole is not as well constrained by the azimutually unoriented data as the pole's latitude, the position and 95% confidence ellipse of the Maastrichtian pole are somewhat dependent on the errors assigned to the seamount VGPs. This occurs because, of all of the Maastrichtian data, the VGPs place the most constraint on the average pole longitude. For example, if the semi-axes of the standard deviation ellipse of each seamount are increased by 50% and rotated so that the major axis is nearly parallel to latitude lines, the average pole moves only about 0.2° north, but 4.0° of longitude to the west. The effect of the increase of the input errors on the 95% confidence ellipse is to increase the minor semi-axis length by 0.2° and the major semi-axis length by 1.6°.

The best Maastrichtian pole was calculated to be at 69.8°N, 1.6°E and have a 95% confidence ellipse with a minor semi-axis length of 1.6° and a major semi-axis length of 4.1° trending 83° clockwise from north.

This pole is situated only 2.8° away from Gordon's (1982) Maastrichtian pole. As shown in Figure 5.7. the error ellipses of these poles display a large amount of overlap, but the new Maastrichtian pole is to be preferred as it was calculated from twice the data used for Gordon's (1982) pole.

Besides seamount M6 and J3, four other data were left out of the calculation of the average pole. They are the southern Pacific skewness inclinations (SW1, SW2, SW3), the seamounts M6 and J3, and the poleocolatitude from Site 288A. The 288A paleocolatitude was rejected because its polar circle is much farther away from the average pole than its 95% confidence limits (about 9°) indicate it should be. The semi-great circle polar loci of the south Pacific skewness inclinations fall just to the north of the scatter of the other data. Although the error limits of the SW2 datum nearly intersect the Maastrichtian pole confidence ellipse, the SW1 and SW3 data are even further away. If all three skewness inclinations are used in the pole calculation. then the chi-square statistic describing the data distribution exceeds its 95% confidence region implying that these data may be incompatible with the rest using the given error limits. Additionally, there is the possibility that a plate boundary exists in the Pacific that may have caused relative motion between the north and south Pacific (Gordon and Cox, 1980a; Section 5.1.10). Discretion in the use of these three data appears to be called for and hence they were excluded from the pole calculation.

The pole listed in Table 5.1 for the Maastrichtian included four equatorial transits as mentioned above. Although these paleoequators

are not paleomagnetic data, their agreement with the paleomagnetic data is excellent. suggesting that the high biologic productivity zone in the Pacific was 90^{o} from the paleomagnetic dipole axis during the Maastrichtian. The inclusion of these paleoequators in the pole calculation does not bias the Maastrichtian pole significantly. If they are excluded. the Maastrichtian pole moves to 69.4^{o}N, 359.8^{o}E whereas the minor and major semi-axis of the confidence ellipse increase to 4.3^{o} and 1.8^{o} and the azimuth changes to 78^{o}.

The 68 ± 3 Ma. age of the Maastrichtian paleomagnetic pole is the mean of the ages of all of the data used in the pole calculation. The geomagnetic polarity time scale of Lowrie and Alvarez (1981) was used for correlating geomagnetic. radiometric and biostratigraphic ages for the Maastrichtian pole as well as all other poles up to 100 Ma. of age. The age of each paleocolatitude and paleoequator was assumed to be the middle of the age range spanned by its samples. The error in the age of the pole given in Table 5.1 is the mean of the estimated standard deviations of the ages of each datum. The standard deviation of each K-Ar date was taken as published or assumed to be 5% of the age. For the age of each paleocolatitude, the median age of is samples was used. Peirce (1976) claimed that biostratigraphic ages for the Late Cretaceous DSDP paleocolatitudes should be good to about 3 Ma., so this value was used as the error for each Maastrichtian paleocolatitude.

As seen in Figure 5.6 the mutual consistency of the data used to calculate the Maastrichtian pole is very good despite the fact that the data came from widely scattered locations in the north Pacific (Figure

5.8). There is no evidence in this data set for major relative tectonic movement among two or more sections of the north Pacific such as that suggested by Farrar and Dixon's (1981) hypothesis of 1400 Km of dextral shear along the Line Islands lineament during the early Tertiary. Rather, it appears that the north Pacific has remained a rigid plate since the Late Cretaceous.

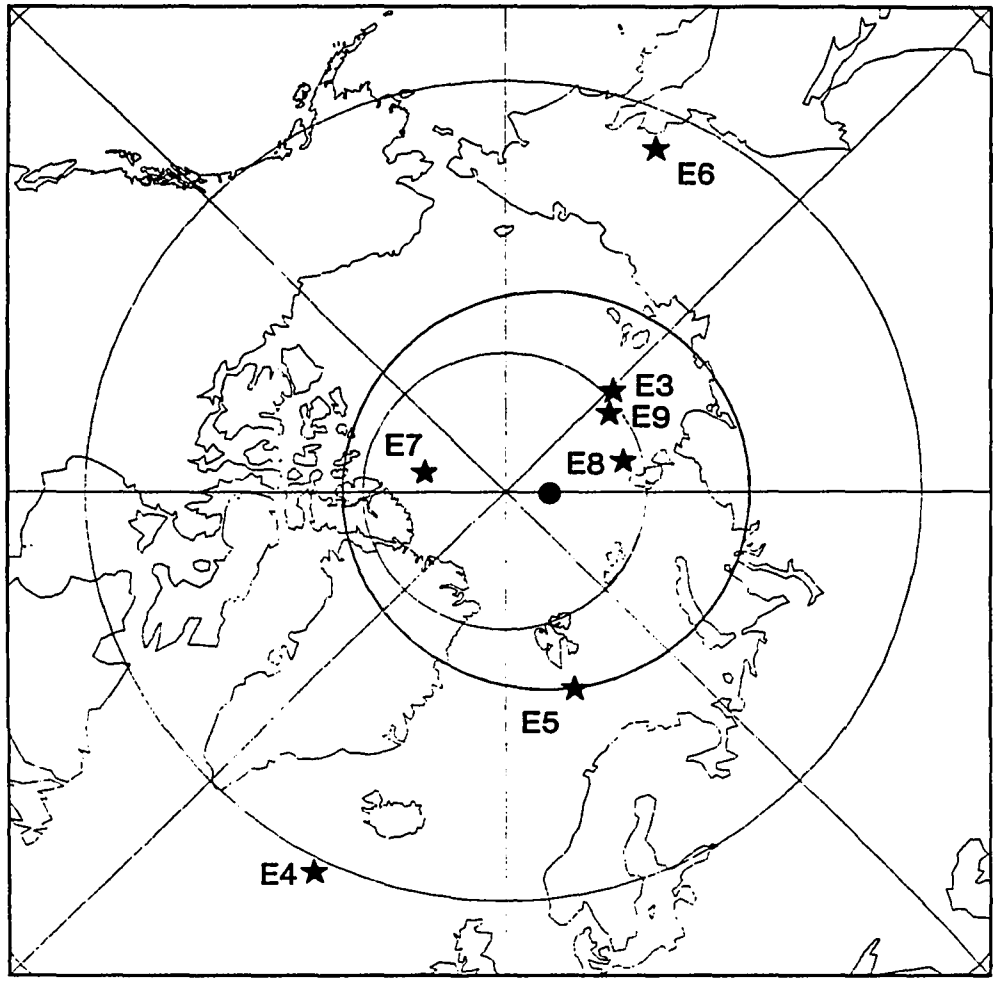

Figure 5.3 VGPs of Tripod Seamounts. VGP locations are shown by stars. The mean postion, calculated by Fisher statistics, is shown as a filled circle. The circle around the mean pole is its 95% confidence circle. Map projection is polar equal area. (after Francheteau et al., 1970).

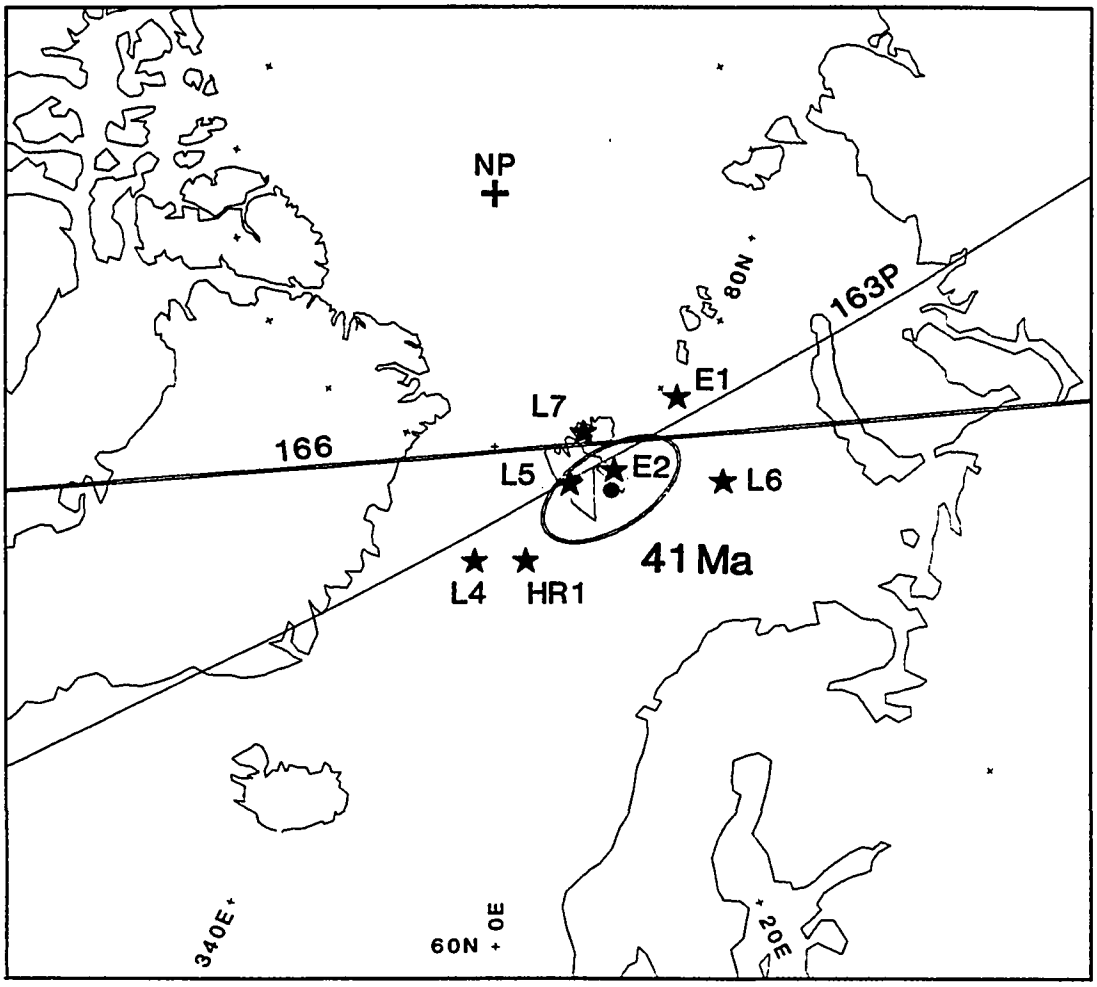

Figure 5.4 Eocene paleomagnetic pole. VGPs are shown as stars and labeled by their identifiers from Table 4.1. The thick line is a segment of the polar circle of a DSDP paleocolatitude and the thin line is the polar circle of a DSDP equator transit. The labels of these polar circles give the site number. The filled circle is the location of the mean pole and the ellipse is its 95% confidence region. Map projection is polar equal area. (after Sager. 1983a)

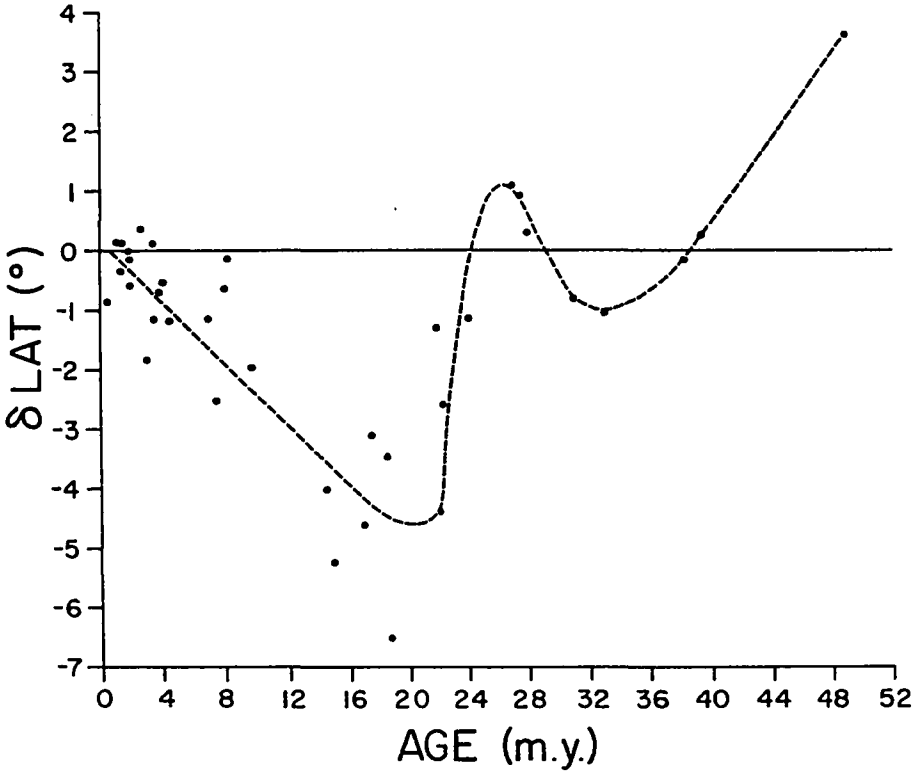

Figure 5.5 Late Tertiary "far-sided-effect". Observed paleolatitudes of central Pacific basin piston cores are plotted versus predicted latitudes from plate/hotspot motion. A large discrepancy occurs during the Early Miocene that has been attributed to persistent non-dipole geomagnetic field components. (from Epp et al., 1983)

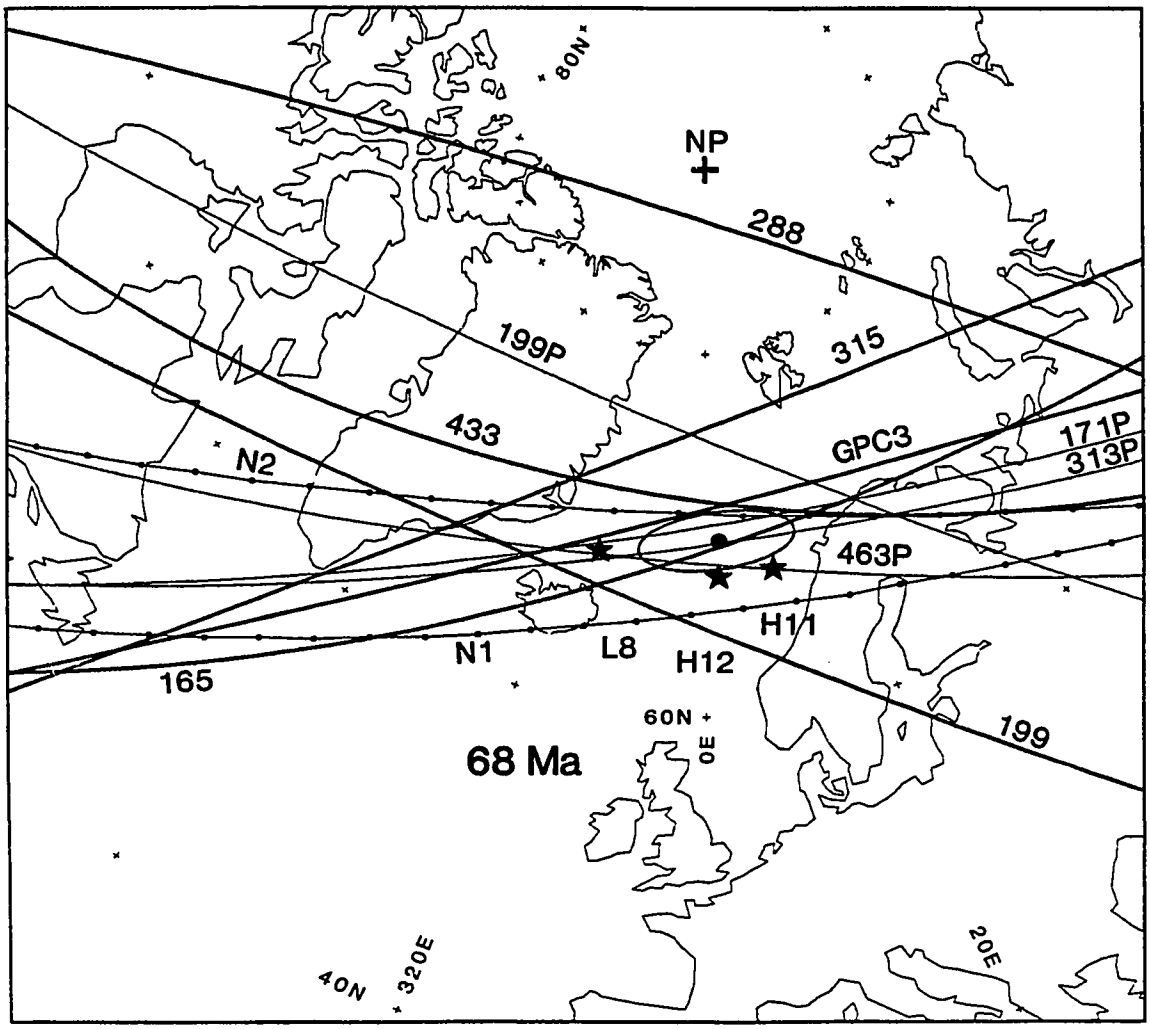

Figure 5.6 Maastrichtian paleomagnetic pole. Lines with dots represent semi-great circles of skewness inclinations. All other conventions as in Figure 5.4.

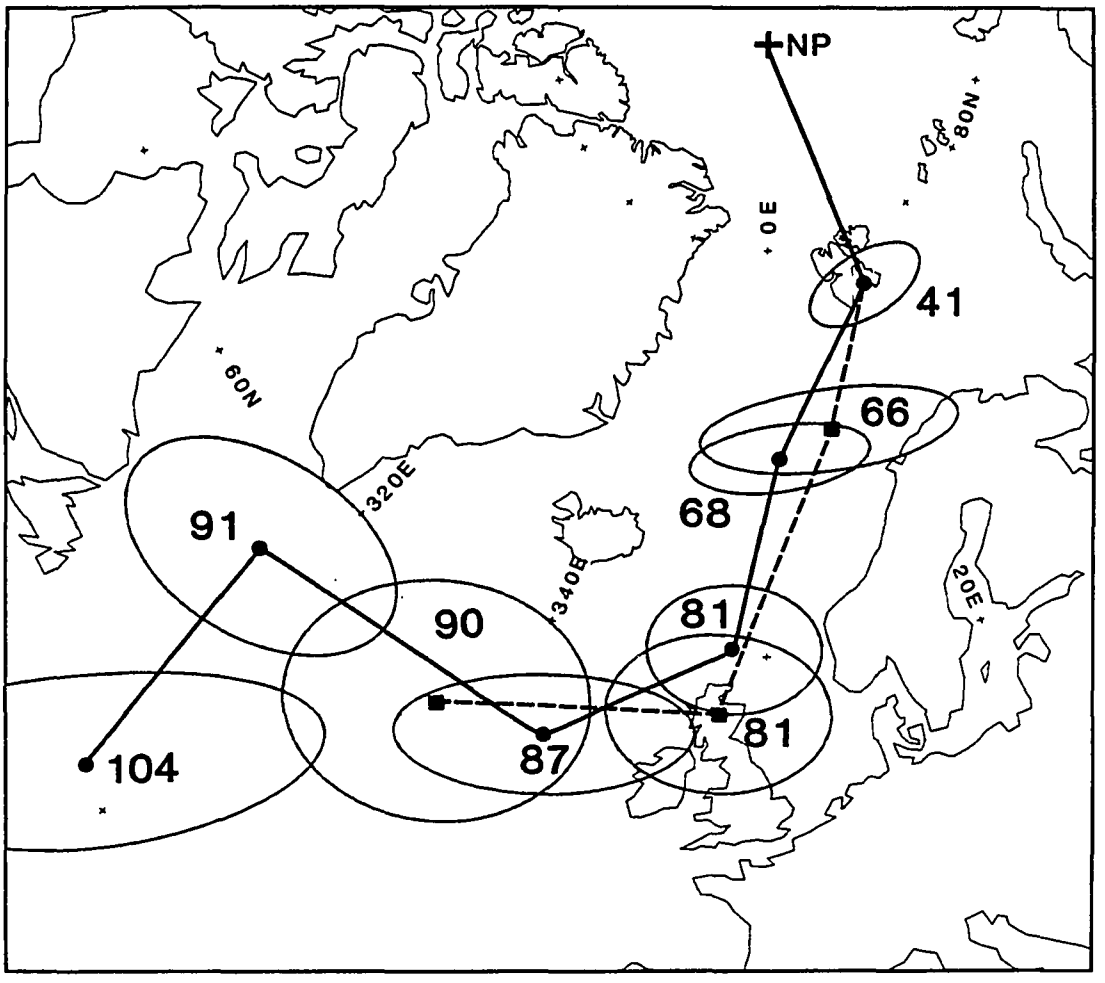

Figure 5.7 Comparison of north Pacific APWP with APWP calculated by Gordon (1983). Gordon's poles are shown by filled squares and connected by a dashed line. Conventions as in Figure 5.4.

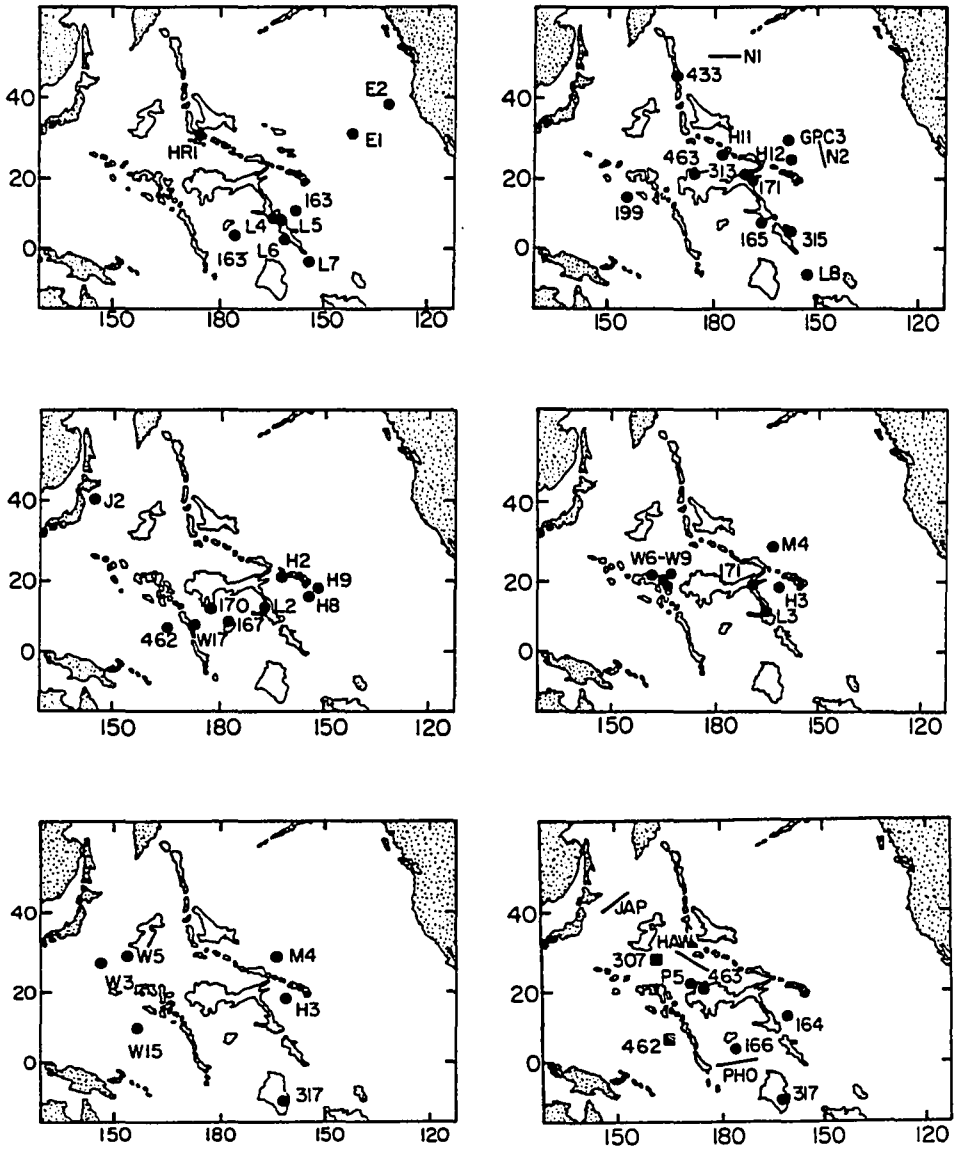

Figure 5.8 Sampling locations for data used in the paleomagnetic pole calculations. (upper left) Eocene; (upper right) Maastrichtian; (middle left) Campanian; (middle right) Santonian; (lower left) Turonian; (lower right) Albian and Barremian. Locations of seamounts and DSDP sites are shown by dots and magnetic lineation locations are shown by short line segments. In the Albian-Barremian plot the sites used for the Albian and/or Barremian poles are shown as dots; whereas the exclusively Barremian data are shown by squares.

5.1.4 THE CAMPANIAN POLE (81 Ma.)

As seen in Figure 5.2, the time from Turonian to Campanian is a time of rapid APW. Consequently, it is necessary to segregate the data into age groups spanning only a few million years. To do otherwise is to risk losing the details of this exceptional spurt of APW by averaging them out. Therefore, the paleomagnetic data of this age must be pushed to the limit of its resolution both in age and in paleopole postion and it is necessary to be cautious in selecting the data to be used in the calculation of the mean paleomagnetic poles.

Figure 4.3b shows that the paleocolatitude data of Campanian-Santonian age are not very consistent. The polar circles intersect in a large area of the north Atlantic between England and Spitzbergen, Greenland and Scanidinavia. In one instance, (Site 462) there is a difference of nearly 18^{o} between the paleocolatitude calculated from basalts and sediments of approximately the same age from the same DSDP hole.

Seventeen seamounts have, or can be inferred to have, ages in the Turonian-Campanian interval. One of these, W2, has a VGP 22^{o} to the west of the Turonian paleomagnetic pole despite its 73 Ma. K-Ar age (Ozima et al., 1970). This seamount may belong with the 91 Ma. Turonian pole, but its VGP is so far from any pole that both the seamount's age and paleomagnetic direction are suspect. The other 16 seamount VGPs are shown along with their ages in Figure 5.9. Seven of these seamounts are dated radiometrically. Of these, four have K-Ar

ages (W3,M4,H3,J2) and three have $^{40}Ar-^{39}Ar$ ages (L2,L3,W5). The K-Ar ages, are of course, minimum ages, but all of these give an age that is consistent with the seamounts' VGP locations and thus these ages are assumed to correctly represent the true age of the seamount. The 40Ar-39Ar age of 85 Ma. for L2 is believed to be slightly high because this seamount appears to have a reversely magnetized summit (Sager et al., 1982). If so, the seamount can be no older than the beginning of the reversal between anomalies 33 and 34. The beginning of this reversal is reported to be anywhere from 79 Ma. (Van Hinte, 1978) to 86 Ma. (Ness et al., 1980) depending on the geomagnetic reversal time scale being used. A median age of 83 Ma. is assumed here as the age for seamount L2.

This same reversal is also used to place an age on three other seamounts (H2,H8,H9). All of these seamounts are reversely polarized and found on Late Cretaceous crust near Hawaii. The most likely time for them to have formed is during the reversed interval between anomalies 33 and 34. They are unlikely to be older because the next older reversal (M0) occurred during the Albian and the sea floor upon which they sit, although of uncertain age, is probably not that old. A younger age is also unlikely because the next younger reversal is between anomalies 32 and 33 at 71 Ma. The VGPs of these three seamounts are relatively close together but average 15^{o} away from the Maastrichtian pole. Therefore, either a large systematic error in the determination of these VGPs or an extremely rapid shift of the Pacific paleopole from 71 to 68 Ma. would be necessary to justify a 71 Ma. age for these seamounts.

Four of the seamounts in Figure 5.9 are assigned an age of 86 Ma. by by assuming they have the same age as nearby edifices. Seamounts W6 through W9 are located within a 200 km. by 500 km. area near Wake Island. Two other seamounts in this area. Wilde Guyot and Lamont Guyot, have $^{40}Ar-^{39}Ar$ ages of 86.4±1.9 Ma. and 86.6±3.7 Ma. (Ozima et al., 1977). Although it is possible that the seamounts studied paleomagnetically could have been formed at a different time, they all seem to be part of a somewhat irregular chain of volcanoes and so this age assignment is at least a reasonable first approximation. The fact that the VGPs of these seamounts fall relatively close together and near those of more reliably dated seamounts of similar age adds credibility to this assumption.

Two of the seamounts in Figure 5.9 are dated by fossils. Planktonic foraminifera 78-82 Ma. of age were recovered from seamount W17 and probable Turonian age planktonic foraminifera were recovered from a seamount approximately 100 Km. north of seamount W15 (J. Haggerty, personal communication. 1983). The Turonian seamount is part of a north-south trending ridge, several hundred kilometers in length, of which W15 appears to be the southernmost edifice, so this age is assigned to W15. Strictly speaking. these fossil ages are minimum ages and sometimes fossil ages greatly underestimate the true age of a volcano, but in this case they appear to be reasonably accurate because the VGPs of these two seamount are in excellent agreement with the VGPs of seamounts of similar ages as shown in Figure 5.9. The VGP of W17 falls very near the VGPs of other seamounts whose ages are in the 80-83

Ma. range whereas the VGP of W15 falls near seamount poles about 94 Ma. old.

As seen in Figure 5.9, the consistency among seamount VGPs of the same age is generally very good. All but one of the VGPs from seamounts in the 80-83 Ma. age range are located just to the northwest of England. All but one of the seamount poles of edifices aged 84-89 Ma. are found just to the east of England. Likewise, all but one of the VGPs of seamounts 89-94 Ma. old are found near the south end of Greenland. This distribution of VGPs is evidence for a rapid eastward shift the Pacific paleopole during the Campanian to Turonian interval of the Cretaceous.

Six seamounts (H2,H8,H9,J2,L2,W17) and three paleocolatitudes (Sites 167,170,462[intrusives]) were used to calculate the Campanian paleomagnetic pole. The seamounts give a Fisher pole at 58.0°N, 359.3°E with an A_{95} of 4.5°. Because these seamount VGPs do not seem to have a decidedly elliptical distribution. Fisher statistics can be used to calculate their standard deviation for the pole calculation. The appropriate quantity to use is the ψ_{63} of the Fisher pole (McElhinny, 1973) which is 6.3° in this case. Including the DSDP paleocolatitudes, the Campanian pole was found to be at 60.3°N, 357.0°E. Its 95% error ellipse has a minor semi-axis length of 3.2° and a major semi-axis length of 3.9° with an azimuth of 89°. This pole and the data used to calculate it are shown in Figure 5.10. As seen in Figure 5.7. this pole and Gordon's (1983) Campanian pole have

overlapping 95% confidence ellipses; the two poles being separated by 3.3^{o}. Most of the difference between these poles is the result of the new data available for this study and the exclusion here of the VGP for L3 from the Campanian pole calculation. The new pole is to be preferred as it is calculated from more data and does not use the L3 VGP which appears to be more appropriate for the Santonian pole.

Two DSDP paleocolatitude determinations of Campanian age from Table 4.5 were left out of the pole calculation. Sediment samples from DSDP Sites 462 and 315A both imply much less northward motion than the rest of the data. In Figure 5.10 it is seen that the polar circles from these two poleocolatitudes are much nearer the geographic pole than the other Campanian data. In fact they intersect in the area of the Maastrichtian pole. The Site 167 paleocolatitude is also somewhat north of the rest of the data used to calculate the Campanian pole, although it is not so far removed as the paleocolatitudes of sites 315A and 462.

It would be tempting to attribute the discrepant data to poor age control, particularly in light of the rapid APW that occurred during this time. However, the ages of the paleocolatitudes from sites 462 and 315 appear to be well-constrained. Although the discrepancy of Sites 167 and 315 might be eliminated if their ages were assumed to be Turonian, the polar circle from DSDP Site 462 sediments never comes close to the poles of Campanian to Turonian age. A possible tectonic explanation for the discrepancy displayed by this data is discussed in Section 5.1.10.

To use the paleocolatitudes from Sites 462 and 315 sediments in the pole calculation biases the average pole 5° north of the position calcuated without these two data. Also, if the paleocolatitudes from Sites 315 and 462 are included in the Campanian pole calculation, the distribution of the data fails to be chi-squared at the 95% confidence level. In contrast, even if the Site 167 datum is included, the chi-squared statistic remains within its 95% confidence limits and the average pole position is not unduly biased from its position without the Site 167 datum. Consequently, the Site 315 and 462 paleocolatitudes were left out of the Campanian pole calculation whereas the Site 167 datum was retained.

The 81±3 Ma. age of the Campanian pole is somewhat dependent on the assumption that the reversely polarized seamounts formed at approximately 82 to 83 Ma. These seamounts comprise half the data in this group, so the average age of the group will be somewhere between the 79 Ma. average age of the rest of the data and the age assigned to the reversal between anomalies 33-34. Likewise the error limits of the average age will be affected by the assumed error for this reversal. In this study it was assigned a standard deviation of 3 Ma.

5.1.5 THE SANTONIAN POLE (87 Ma.)

For the calculation of the Santonian paleomagnetic pole seven seamount VGPs (H3,L3,M4,W6-W9) and the paleocolatitude from DSDP Site 171 were used (Figure 5.11). A Fisher pole for the VGPs of these seamounts is located at 54.7° N, 342.2° E and has an A_{95} of 6.2°. However, these VGPs do not appear to have a Fisherian distribution, instead they are more scattered in the direction of APW, almost due east-west. As a consequence, the latitude of the mean pole is probably better constrained by these VGPs than is its longitude.

The distribution of the VGPs was assumed to be elliptical and a standard deviation ellipse was calculated in the manner described in Section 5.1.3. The error ellipse for the seven VGPs has a minor semi-axis of 4.8° and a major semi-axis of 11.0°. The azimuth of the major semi-axis is 73° clockwise from north. This error ellipse was used for each seamount VGP in the the pole calculation.

The pole calculated from the seven VGPs and the paleocolatitude is located at 54.5°N, 342.6°E, 9.7° from the Campanian pole. Its 95% confidence ellipse has minor and major semi-axis lengths of 3.0° and 6.8°. The strike of the major axis is 71° clockwise from north (Figure 5.11). The 87±3 Ma. age of the pole is dependent on the 87±2.8 Ma. age assigned to seamounts W6-W9, although the average age of the other data is also 87 Ma.

5.1.6 THE TURONIAN POLE (91 Ma.)

Five seamounts (W3,W5,W15,H3,M4) and one paleocolatitude from DSDP Site 317A were used to calculate an average paleomagnetic pole representing the Turonian (Figure 5.11). Two of these seamounts, H3 and M4, were used in the calculation of the Santonian pole as well, but they have K-Ar ages (88.8 and 89.5 Ma., respectively) that are transitional between the Turonian and Santonian and their VGPs are also in the middle of the "smear" of VGPs between the two mean poles caused by the rapid APW that occurred during this interval of time. In the calculation of the Santonian pole, four seamounts had ages assigned from their proximity to dated edifices, so these two reliably dated seamounts provided a valuable constraint on the age and postion of that mean pole. Likewise, there are only a few seamounts with Turonian ages, so it was felt that these two seamounts would once again add a valuable constraint to the age and postion of this pole as well.

A Fisher pole for the five seamounts is located at 55.3°N, 319.0°E. It has a large A_{95}, 11.2°, because of the smearing of the VGPs along the APWP, so a standard deviation ellipse with a minor axis of 6.5° and a major axis of 15.2° and an azimuth of 93° was calculated for the VGP distribution of the seamounts as described in Section 5.1.3 and used as the error for each VGP in the pole calculation. Including the DSDP paleocolatitude from Site 317A, the Turonian pole was calculated to be at 55.4°N, 315.7°E, a distance of 15.4° away from the Santonian pole (Figure 5.11). Its 95% confidence ellipse has a major

semi-axis of 6.7° and a minor semi-axis of 4.5°. The major axis trends 76° clockwise from north. The average age for the data is 91+4 Ma.

Gordon's (1983) 90 Ma. pole at 54.0°N, 334.0°E falls midway between the Santonian and Turonian poles determined here (Figure 5.7). The difference between the 90 and 91 Ma. poles largely results from the use of slightly different data sets. Gordon did not have W15, and he used basalt paleocolatitudes from DSDP Sites 61, 315A, 462A, and 465A, rather than the sediment paleocolatitude from Site 317A used here. Of the paleocolatitudes used by Gordon, the Site 462 datum is the only one that might have enough eruptive units to average out secular variation, but the time distribution of its samples is uncertain. Also, the Site 465A samples were formed near enough to the equator to be of uncertain polarity.

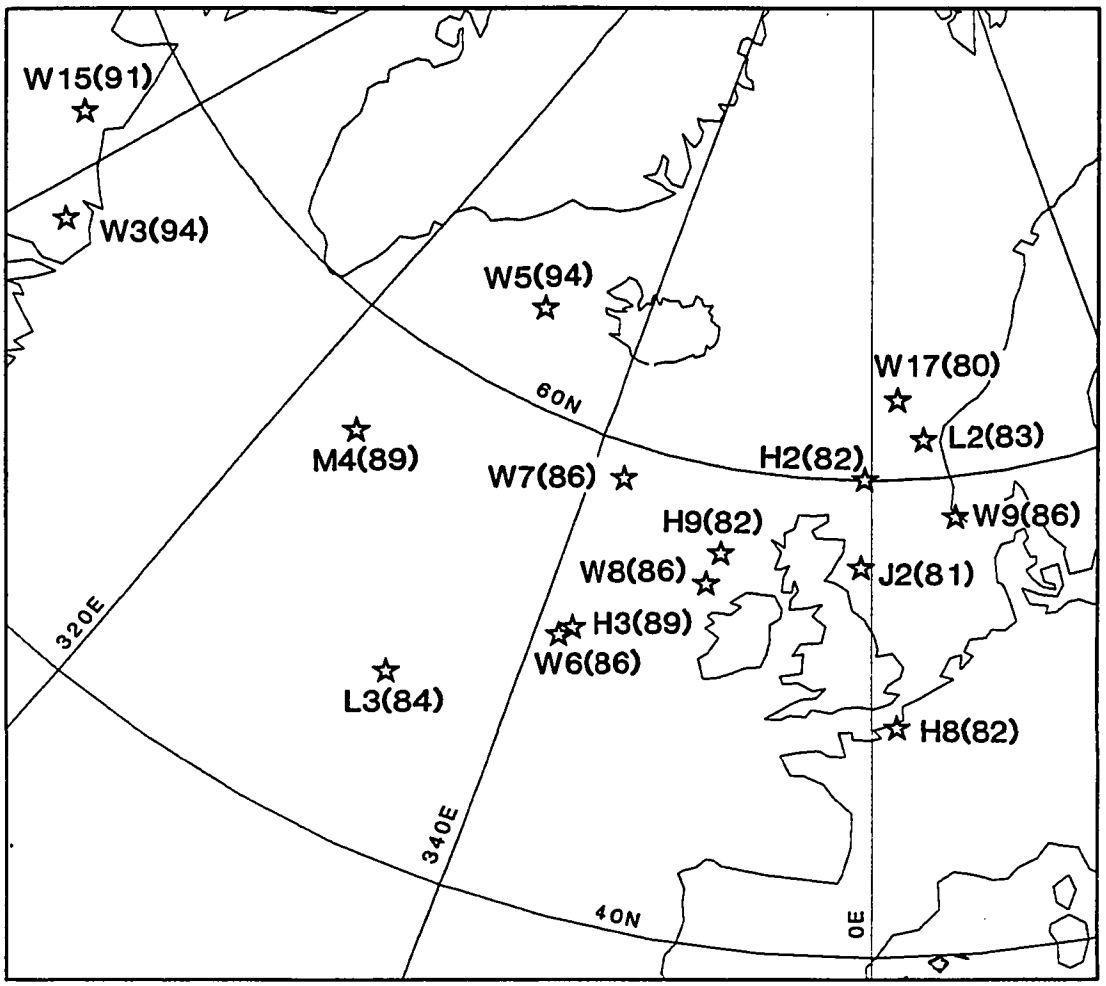

Figure 5.9 VGPs of seamounts with Campanian to Turonian ages. VGPs are shown by stars and labeled by the seamount identifiers from Table 4.1. Ages are given in parenthesis. Map projection is polar equal area.

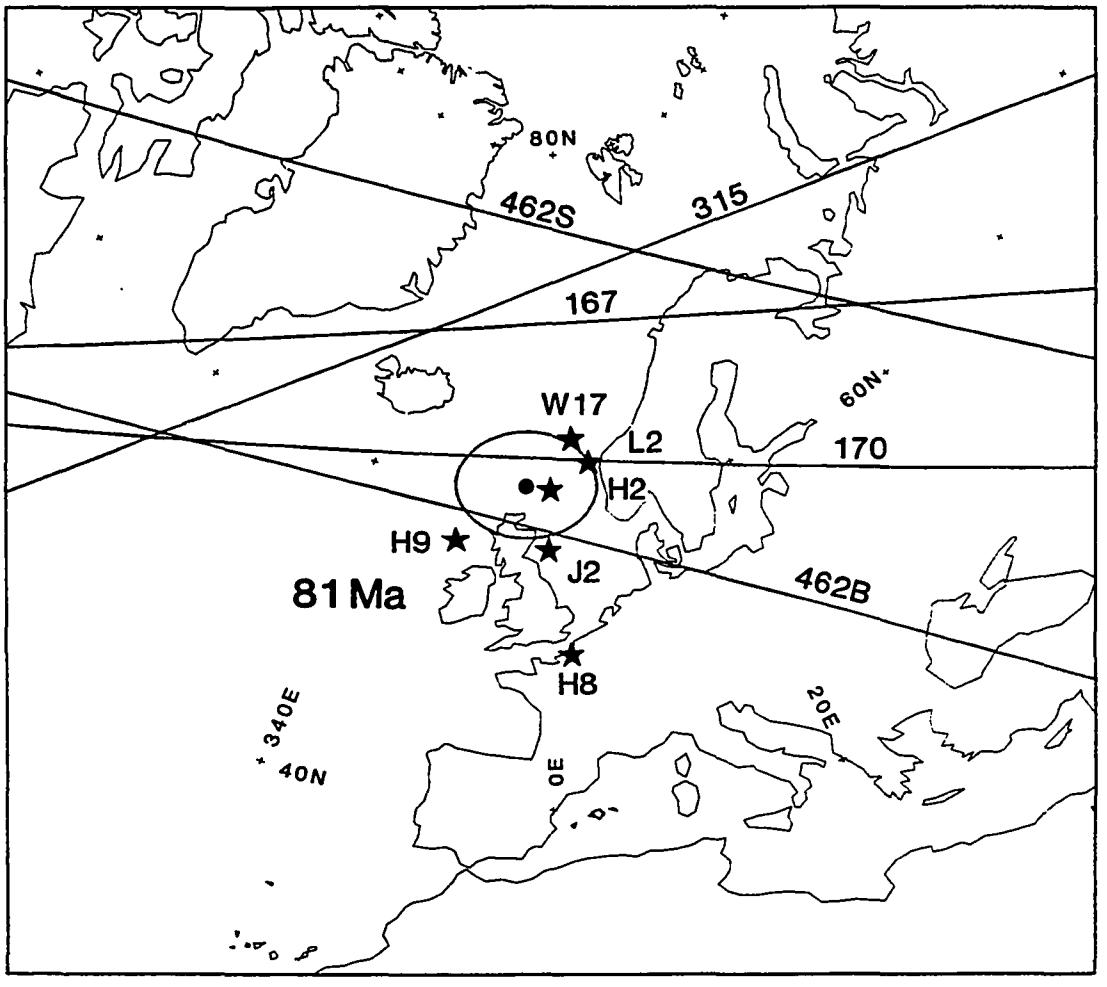

Figure 5.10 Campanian paleomagnetic pole. 462S refers to sediments cored at Site 462 whereas 462B refers to intrusives cored at the same site. Conventions as in Figure 5.4.

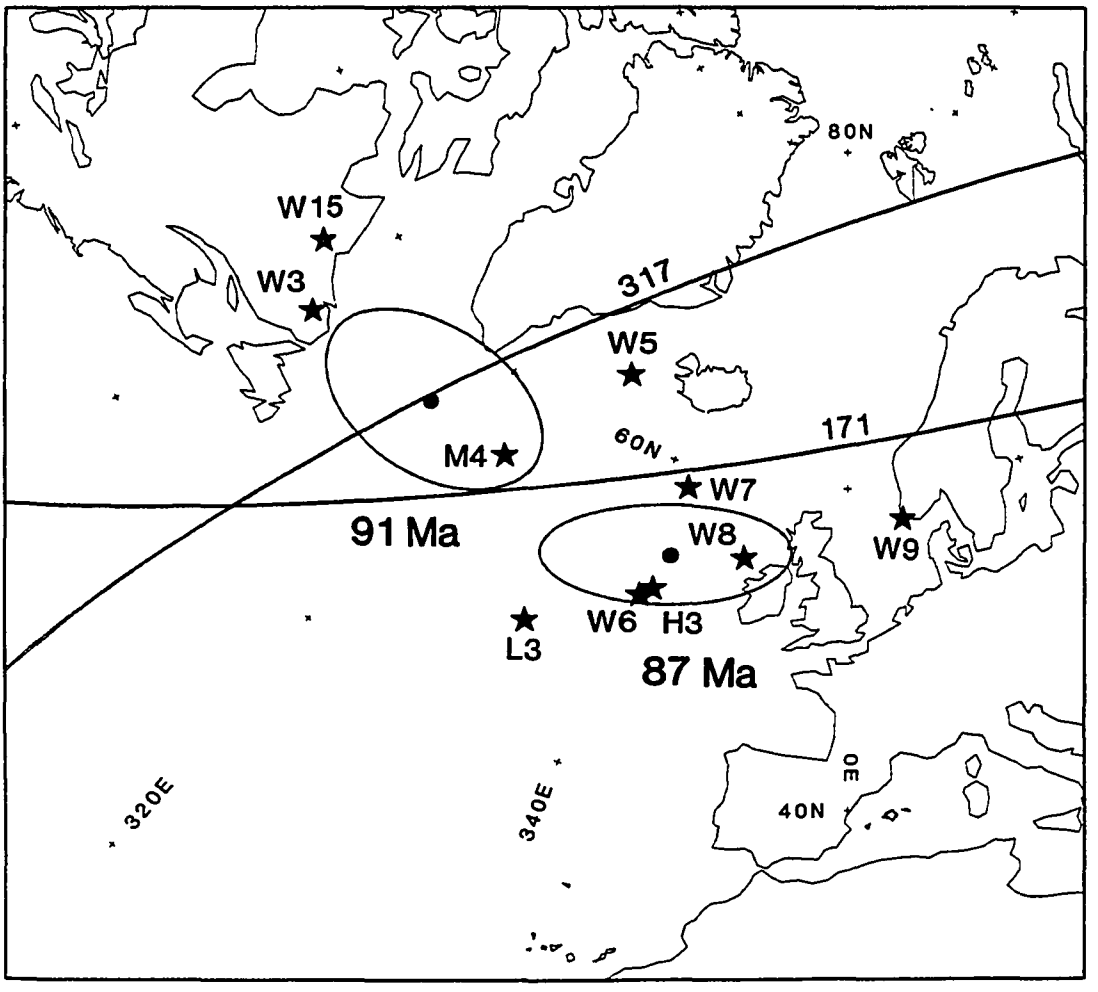

Figure 5.11 Santonian and Turonian paleomagnetic poles. Seamounts M4 and H3 were used in the calculation of both poles. The paleocolatitude from Site 171 was used for the Santonian pole; the Site 317 paleocolatitude, for the Turonian pole. Conventions as in Figure 5.4.

5.1.7 THE ALBIAN POLE (104 Ma.)

The Albian data consists mainly of four paleocolatitudes from DSDP sites 164, 166, 317A, and 463, ranging in age from about 98-107 Ma. These data show remarkably good agreement as the polar circles of all of the paleocolatitudes intersect in a relatively small area of the central north Atlantic (Figure 5.12). A paleocolatitude from Site 288A also has an Albian age, however, the locus of the paleomagnetic pole it records is significantly displaced from the other Albian data as was the case for the Maastrichtian data from this site. Only one seamount, Darwin Guyot (P5), has an Albian age. Its age, 106-109 Ma., was determined from coral fragments (Harrison et al., 1975), and although this age is only a minimum age, its VGP is consistent with the paleocolatitude data of the same age. The Albian pole is the farthest south and farthest west of all of the Pacific paleopoles. Likewise, the Darwin Guyot VGP is the farthest southwest of all of the seamount VGPs (Figure 4.2), and in fact is the only seamount VGP in the vicinity of the Albian pole. The probable cause of the lack of other seamount VGPs around the Darwin VGP is the fact that the paleopoles of seamounts only 10 Ma. older or younger should be located well to the north according to the APWP in Figure 5.2.

As there is only one seamount VGP of Albian age, the procedure used to estimate the VGP errors for the Campanian through Turonian poles could not be used. Instead the standard deviation of the Darwin VGP had to be estimated from undated seamount VGPs. A Fisher pole was calculated from the twelve seamount VGPs west of longitude 331^{o}E and

south of latitude 74°N (excluding W10 and W12). These VGPs appear to be scattered about the Turonian pole although most of their ages are uncertain. The A_{95} for these poles is 7.4° giving a ψ_{63} of 10.7° that was used for the standard deviation of the Darwin VGP in the pole calculation. Judging from the seamount VGP distributions examined previously, this error may be a bit large. However, because there is only one seamount VGP constraining the Albian pole, it is better to be conservative in assigning errors so that the end result is not unduly biased by the single seamount pole.

The Albian pole is located at 41.4°N, 317.5°E. Its 95% confidence ellipse has a major semi-axis of 11.3 aligned 35° clockwise from north and a minor semi-axis of 4.1°. This pole and the data used to calculate it are shown in Figure 5.12. As seen in Figure 5.2, the 95% confidence ellipse of the Albian pole does not intersect the confidence ellipse of either the Turonian pole or the Barremian pole. Thus, the Albian pole appears to be significantly different from these two poles.

The age of the Albian pole was calculated as the mean of the median ages of all of each paleocolatitude and the age of Darwin Guyot. All of these ages are biostratigraphic ages that can vary according to the time scale used. A variation of 4-6% in the published dates for the stage boundries of the middle and Early Cretaceous appears to be common (Van Hinte, 1978). Thus a 6% standard deviation was assumed for the age of each datum. The Early Cretaceous-Late Jurassic time scale of Van Hinte (1978) was used to assign absolute ages to the biostratigraphic ages of the data for this pole and the Barremian pole.

5.1.8 THE BARREMIAN POLE (119 Ma.)

Very few paleomagnetic data older than Albian are available from the Pacific plate. There are no dated seamounts of this age. Three DSDP sediment paleocolatitudes sample the Albian-Barremian geomagnetic field. These are from Sites 317A. 462, and 463. Another DSDP paleocolatitude from Site 307 probably sampled basalts from sea floor of Kimmeridgian age (approximately 145 Ma.). Larson and Chase (1972) calculated skewness parameters for the Japanese, Hawaiian, and Phoenix lineations from M0-M10 (approximately 120-126 Ma. using Van Hinte's (1978) time scale). Although they did not publish the effective inclinations for these lineations, they can be reconstructed with reasonable accuracy using their figures to determine the average locations and azimuths of the lineations and the 1965 IGRF to calculate the magnetic field directions at each site. The effective inclinations thus derived are listed in Table 4.7.

All of these data are shown in Figure 5.13. The polar circles from sites 462 and 463 agree well with the semi-great circles from the Hawaiian and Phoenix lineations. About 6^{o} to the north of these intersecting polar circles is the polar circle recorded by the Site 307 core. To the southwest lies the polar circle predicted by the Japanese lineations. Because five of these polar circles are nearly parallel, they constrain the longitude of the average pole very poorly. Most of the longitude constraint is provided by the Site 317A polar circle which crosses the others obliquely. Consequently, the longitude of the Barremian pole is highly dependent on the accuracy of the Site

317A paleocolatitude. On the other hand, the latitude of the average pole is much less affected by any one datum because of the relatively good latitudinal agreement of the data.

The Barremian pole is located at 57.9°N, 339.2°E. Its 95% confidence ellipse has a minor axis of 3.5° and a major axis of 10.8° striking 66° east of north. Because the Early Cretaceous data is so scarce, the calculation included the Site 307 paleocolatitude even though it appears to be about 20 Ma. older than the other data. As seen in Figure 5.2 there is quite a bit of overlap of the Barremian pole error ellipse over the error ellipses of the Campanian. Santonian, and Turonian paleomagnetic poles. Thus the APWP cannot be used to infer an unambiguous age for undated western Pacific seamounts whose VGPs lie in the vicinity of these four mean paleomagnetic poles as there may be a mixture of VGPs of very different ages.

The 119±12 Ma. age assigned to the Barremian pole is the mean of the data ages excluding Site 307. The standard deviation of this age is assumed to be 10% or 12 Ma. This value is greater than that used for the younger data because the uncertainty of the correlations between biostratigraphic, geomagnetic, and absolute abes increases from the Late Cretaceous to the Early Cretaceous (Van Hinte, 1978). Of course, the absolute age of this pole depends on the geomagnetic time scale used to give absolute ages to lineations M0-M10 and the biostratigraphic time scale used to give ages to the DSDP cores; Van Hinte's (1978) scale was used here.

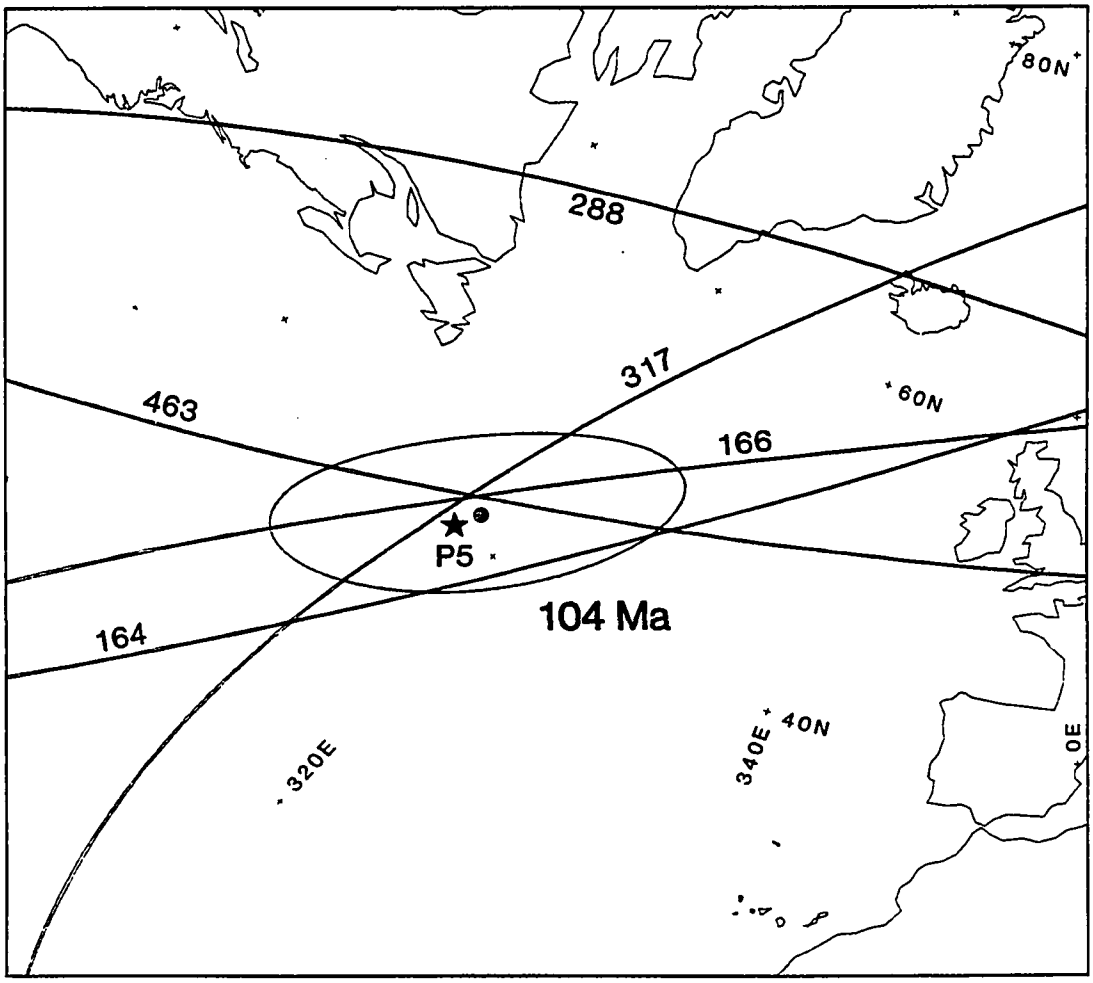

Figure 5.12 Albian paleomagnetic pole. Conventions as in Figure 5.4.

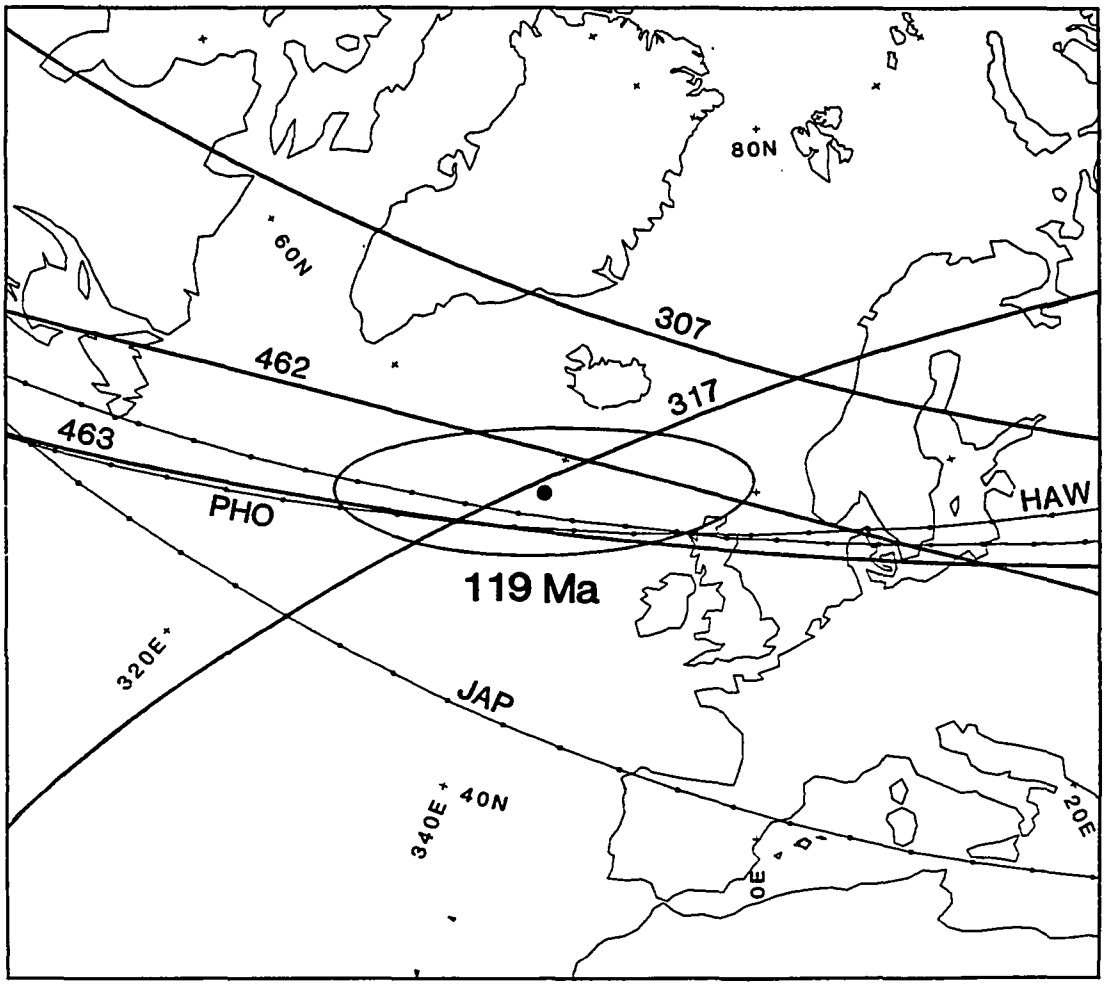

Figure 5.13 Barremian paleomagnetic pole. Conventions as in Figures 5.4 and 5.6.

5.1.9 IMPLICATIONS OF THE APPARENT POLAR WANDER PATH

The APWP shown in Figure 5.2 has many ramifications for the tectonic history of the Pacific plate. Perhaps the first question to be answered is "how reliable is the data?". All of the paleocolatitudes and seamount VGPs used in the calculation of the mean paleomagnetic poles have been screened for reliability to some degree. Paleocolatitudes with high scatter or too few samples to average out secular variation have not been used. Seamounts with GFR values less than 2.0 were not used for tectonic interpretation. Moreover, the GFR values of the dated seamounts used in the pole calculations are usually much higher; in fact, their mean value is 3.8. The reliability of the skewness inclinations and the paleoequators is hard to assess, but these data seem to show excellent agreement in most cases among themselves and with the other data types.

Despite the many possible sources of systematic error for seamount paleopoles discussed in Chapter 2, there is little evidence of any consistent bias of the seamount data used to calculate the poles in Table 5.1. In each case where both seamount poles and other data were combined, the seamount VGPs agreed with the other data within the expected error limits. Good examples of this agreement are the Eocene and Maastrichtian poles. In Figure 5.4 it is seen that the paleocolatitude and paleoequator polar curves pass through the distribution of seamount VGPs for the Eocene pole and in Figure 5.6 the seamount VGPs fall in the middle of the area of the intersection of the polar curves from skewness inclinations, paleocolatitudes, and

paleoequators used for the calculation of the Maastrichtian pole. Most of the discrepant data examined in the preceeding sections are paleocolatitudes from DSDP sites in a small area of the equatorial Pacific. Possible reasons for this discrepancy are be discussed in the following section.

The APWP in Figure 5.2 has some familiar features as well as some startling new ones. From 81 Ma. to present. it is mainly a refinement of paths found by previous investigations (Jarrard and Sasajima, 1980; Gordon, 1983). The paleopole moves away from the geographic pole with increasing age in a direction nearly diametrically opposite the geographic pole from the Pacific plate itself. A relatively continuous northward drift of the Pacific plate since the Campanian appears to adequately explain most of this part of the APWP. An exception is the apparent stationary behavior of the Pacific paleopole from the Eocene to Miocene pointed out earlier. The distances between the Campanian and Maastrichtian poles and the Maastrichtian and Eocene poles are $9.7^{\circ}\pm2.4^{\circ}$ and $9.4^{\circ}\pm2.1^{\circ}$ implying APW rates of $0.75^{\circ}\pm0.18$ $^{\circ}$/Ma. and $0.35^{\circ}\pm0.08$ $^{\circ}$/Ma. respectively. These rates are of the same order as those predicted by the plate/hotspot Euler poles listed in Table 5.2.

In the Late Jurassic and Early Cretaceous. the APWP shows a similar APW rate between the 145 Ma. polar curve and the 119 Ma. pole, except that in this case the pole decreases its distance from the geographic pole with increasing age, implying a southward drift of the Pacific plate. This southward motion of the Pacific plate is clearly shown for the Aptian by the inclinations of limestone samples from DSDP

Site 463 (Sayre, 1981, Figure 10) which steepen with decreasing age, indicating a southern hemisphere site drifting further south.

Between 81 and 119 Ma. a substantial increase in the rate of APW took place and three sharp bends in the path occurred. This period of time is only 26% of the total time span of the APWP. yet the fraction of the path between 81 and 119 Ma. is nearly as long as the combined remainder. The polar wander rates are 1.1 ± 0.4 °/Ma., 1.4 ± 0.7 °/Ma. and 1.6 ± 0.8 °/Ma. for the periods 91-104 Ma., 104-119 Ma., and 81-87 Ma. For the period of 87-91 Ma. the APW rate is even higher. 3.5 ± 1.5°/Ma.

The timing of this rapid phase of APW is very suggestive. Its beginning and end are very nearly conicident with the beginning and end of the Cretaceous Quiet Time. The first large change in the direction of the APWP and the rate of APW occurred at about Barremian to Albian time as evidenced by the 104 and 119 Ma. paleomagnetic poles. Because the data used to calculate the Barremian pole is sparse and the absolute age control is only fair, the beginning of the rapid APW and the change from a south trending to a north trending APWP is poorly resolved. However, within the estimated age errors of the paleomagnetic poles, the beginning of these changes are coincident with the beginning of the Cretaceous Quiet Time. The end of the Cretaceous Quiet Time appears to have occurred almost simultaneously with a large bend in the APWP at the 81 Ma. pole and a substantial reduction of the rate of APW. At this end of the Cretaceous Quiet Time the resolution of the paleomagnetic data is much better because the data is more abundant and the age control is better. In fact, the synchroneity of

the 81 Ma. pole and the reversal that ended the Cretaceous Quiet Time is well-established because this reversal was used to assign ages to four of the seamounts used in the calculation of this pole.

The Cretaceous Quiet Time is a notable period in the evolution of the Pacific plate for many other reasons. During this time the size of the Pacific increased substantially and the configuration of its borders underwent significant changes (Hilde et al., 1977)(see Figure 1.3). This period was also characterized by widespread volcanism in what is today the western Pacific and the rest of the world (Schlanger and Premoli-Silva, 1981; Schalanger et al., 1981; Haggerty et al., 1982) and high rates of spreading or large ridge jumps in the Pacific (Larson and Chase, 1972). These observations suggest that large changes in the core and mantle, as evidenced by the behavior of the geomagnetic field and the occurrence of volcanism, may also bring about substantial changes in plate motion as indicated by the APWP. Further evidence along this line comes from Cox (1975) who noted that the two largest changes in the frequency of geomagnetic field reversals during the last 100 Ma. occurred at the end of the Cretaceous Quiet Time and at about 45 Ma. The latter date is, of course, nearly coincident with the large change in the direction of the motion of the Pacific plate recorded by the Hawaiian-Emperor bend.

Several profound changes in the direction and rate of Pacific APW have been discussed. Before interpreting these findings further, it is appropriate to examine how well these changes are determined. The 95% confidence ellipses for the Early and mid-Cretaceous mean poles are relatively large because of the scarcity of Pacific paleomagnetic data

of that age, but for the younger poles the confidence ellipses are much smaller. In the estimation of the errors for the data used to calculate each one of these poles care was taken to make sure that the error assigned to each datum is conservative, so that if the errors is mistaken, it overestimates the actual error. For instance, in most cases a bivariate analysis was used to derive elliptical confidence limits for each seamount VGP. This method gives more reasonable estimates of the error than does Fisher statistics if the VGP distribution is non-circular and it also seems to give larger estimates of the error than Bingham statistics (Bingham, 1964). Likewise, in the calculation of the error of each DSDP paleocolatitude, an attempt was made to include the contributions of secular variation and off-vertical orientation to the error (see Section 4.2). As a result, the calculated 95% confidence ellipse for each mean paleomagnetic pole should also be, if mistaken, an over-estimate of the true error. Looking at Figure 5.2, there is very little overlap of the 95% confidence ellipses of the paleomagnetic poles except where the APWP doubles back on itself, so the poles appear to be significantly different. Also, even if each pole postion is allowed to be anywhere inside its 95% confidence ellipse, the overall trends dipicted by the APWP in Figure 5.2 are not greatly changed. Undoubtedly future studies with more and better data will refine and improve this APWP, but its overall shape appears to be relatively well-determined. It would be necessary to delete large portions of the data used to derive the APWP in order to bring about profound changes it its shape.

APWP have often been interpreted solely in terms of plate motion, but can all of the APW discussed above be attributed to the tectonic movement of the Pacific plate? The answer is not simple. APW may be caused by three phenomena: (1) plate motion, (2) variable long term non-dipole geomagnetic field components, and (3) true polar wander (TPW). In general it is difficult, if not impossible, to uniquely separate these phenomena using only the paleomagnetic data from a single plate. Studies of global paleomagnetic data sets (e.g., Coupland and Van der Voo, 1980; Morgan, 1981) appear to be the only way to do so. However, it is appropriate to examine here the Pacific's APW for the constraints it can place on these phenomena.

Although the causes of plate motion are not well understood, the two primary forces driving the plates seem to be the pull of subducting slabs (slab-pull) and the push exerted by spreading ridges (ridge-push)(Forsyth and Uyeda, 1975; Gordon et al., 1978). Plate motions are often measured, in an absolute sense, by paleomagnetism and the study of hotspot-generated seamount and island chains. The former defines the motion of the plate by using the geomagnetic field as a frame of reference. The basic assumption of paleomagnetism is that the geomagnetic field has the same form as that of an axial geocentric dipole when averaged over a few tens of thousands of years (McElhinny, 1973). Thus paleomagnetism gives the direction and distance of the paleomagnetic pole from a site on a plate and the paleomagnetic pole is usually assumed to be coincident with the spin axis. Studies of hotspot seamount chains can be used to delineate the motion of a plate with respect to the mantle. Morgan (1981) showed that hotspots tend to

remain fixed with respect to one another, so they can be used as a reference frame to which plate motion can be tied. If there were no TPW and no long term non-dipole magnetic field components affecting the paleomagnetic data, the motion of a plate in the paleomagnetic reference frame would be equivalent to that measured with respect to the hotspots. However, because of the existence of these phenomena, the two motions are generally not equivalent.

It has become apparent that the axial geocentric dipole hypothesis is invalid if examined closely. A long term average of the geomagnetic field at the Earth's sruface contains field components that cannot be explained by a single dipole centered within the earth (e.g., Wilson and McElhinny, 1974; Merrill and McElhinny, 1977; Coupland and Van der Voo, 1980), thus interpretations of paleomagnetic data made with the dipole assumption may give erroneous results. Moreover, these non-dipolar components appear to be persistant and time-varying (Coupland and Van der Voo, 1980) and hence a rapid change in the non-dipole field structure might be misconstrued as a tectonic event because of its effect on a plate's APWP.

True polar wander (TPW) has been defined in several ways in the literature. It has been hypothesized to be (1) relative motion between the spin axis and the entire lithosphere (Jurdy and Van der Voo, 1975), (2) relative motion between the spin axis and the hotspot-mantle reference frame (Gordon and Cape, 1981; Jurdy, 1981; Jurdy, 1983), and (3) relative motion between the geomagnetic axis and the spin axis (McElhinny, 1973). Most studies of (1) and (2) tacitly assume that (3) is negligible and use paleomagnetic data to define the position of the

spin axis. This assumption is probably correct because most hypotheses of the mechanisms by which the geomagnetic field is generated by the core dynamo imply some degree of long term symmetry of the field around the spin axis (e.g., Elsasser, 1955), so large amounts of (3) seem unlikely. Studies of global paleomagnetic data sets tend to find that (1) is insignificant (Jurdy and Van der Voo, 1975) whereas large amounts of (2) have accumulated since the Mesozoic (e.g., Morgan, 1981; Jurdy, 1981; Harrison and Lindh, 1982b). It is not clear why the amount of TPW referenced to the lithosphere should be less than that found with respect to the mantle. However, as most authors define TPW by (2), this usage will be followed in the discussion below in order that the results obtained here may be compared with previous studies.

TPW is most often measured by the mis-match between the positions of observed paleomagnetic poles and their positions predicted by plate/hotspot motion models. In Figure 5.14 the north Pacific paleomagnetic poles are compared with a predicted APWP calculated from the Pacific plate/hotspot rotation poles in Table 5.2. These rotation poles were derived in a detailed study of several Pacific hotspot seamount chains (Epp and Tuthill, in preparation) and are representative of most other Pacific plate/hotspot motion models. Consequently, the discussion that follows would not be significantly changed by a different choice of published rotation poles. As mentioned previously, the hotspot predicted APWP should agree with the observed APWP only if TPW and long term non-dipole magnetic field components have been negligible. Figure 5.14 shows that the observed and hotspot-predicted APWPs only agree in one place where the 95%

confidence ellipse of the 41 Ma. paleomagnetic pole just touches the predicted APWP at its 40 Ma. point. At every other point there is a substantial difference between the observed and predicted postions of the paleomagnetic poles. The 41, 68, and 81 Ma. poles follow the trend of the APWP, but the 22 Ma. polar circle and the 68 and 81 Ma. poles are located 5^{o} - 12^{o} away from their predicted postions. Prior to 81 Ma. even the trends are different as the predicted and observed APWP diverge with the predicted APWP continuing its north-south trend and the observed APWP bending to the west.

In two instances the Late Cretaceous - Tertiary paleopole data is abundant enough to allow the effects of TPW and non-dipole components to be distinguished. The discrepancy between the observed and hotspot-predicted paleolatitudes of late Tertiary age was attributed to time varying non-dipole magnetic field components (Epp et al., 1983) because central Pacific piston core paleomagnetic data with high resolution in both age and paleolatitude showed that the onset of the magnetic field bias was extremely rapid, accumulating 4^{o} - 6^{o} of offset between the two reference frames in little more than 1 Ma. (Figure 5.5). TPW was ruled out because it was felt that the rapid onset of the discrepancy between the two frames of reference implied an unbelievable acceleration of the mantle with respect to the core. For the 68 Ma. paleomagnetic data, non-dipole components were ruled out as the cause of the difference between the predicted and observed pole locations because the equator transit data (which is not affected by non-dipole magnetic field components) agrees with the paleomagnetic data (Figure 5.6). The paleomagnetic data appears to accurately record the postion

of the spin axis and thus the difference was attributed to TPW (Gordon and Cape, 1981).

Unfortunately, for times prior to 68 Ma. such distinctions are difficult to make at present, and one must keep in mind that the observed configuration of the APWP is the result of Pacific plate motion combined with both TPW and time-varying long term non-dipole geomagnetic field components. In fact it seems logical that TPW and changes in plate motion should occur simultaneously. Much of the driving force for plate motion is supplied by the pull of subducting slabs (Forsyth and Uyeda, 1975). Also, it appears that changes in subduction zones may trigger TPW as the spin axis attempts to track the prinicpal axis of inertia of the mantle mass anomaly caused by the subducting slabs and hotspots (Crough and Jurdy, 1980; Jurdy, 1983). Consequently, changes in plate motion may go hand-in-hand with TPW. Additionally, Coupland and Van der Voo (1980) have found that persistent time-varying non-dipole components are characteristic of much of the Cretaceous and all of the Tertiary. The implication is that paleomagnetic data of all ages is biased to some degree by these non-dipole components, and that this bias is constantly changing.

Figure 5.15 shows the north Pacific paleomagnetic poles backtracked using the plate/hotspot rotation poles in Table 5.2. A paleomagnetic pole whose observed postion agrees with its hotspot-predicted postion will be backtracked to the geographic pole. This procedure defines an APWP in the hotspot reference frame that is useful for examining the differences between the motions predicted by the plate/hotspot rotation poles and the paleomagnetic data. As seen in

Figure 5.15, only the Eocene pole is located near the geographic pole; all the others are 8^{o} - 27^{o} distant. The differences between the backtracked poles in similar diagrams have been attributed to TPW (Gordon, 1983), but because this data only comes from a single plate, non-dipole components, errors in the plate/hotspot motion model, and errors in the determination of the paleomagnetic poles also contribute to the discrepancies.

It seems unlikely that the observed large deviations of the paleomagnetic poles from the plate/hotpsot motion model can be attributed entirely to non-dipole field bias of the paleomagnetic data. Non-dipole errors of approximately 5^{o} have been documented in late Tertiary paleomagnetic data (Wilson and McElhinny, 1974; Epp et al., 1983), and there is little solid indication that they have been much higher since the Paleozoic (Irving, 1977; Coupland and Van der Voo, 1980). Additionally, Figure 5.15 shows that much of the mis-match occurs as a result of the rapid east-west phase of APW that occurred between 91-81 Ma. If attributed to non-dipole components, this shift would imply that the paleomagnetic data from the Pacific record a persistent declinational error in excess of 20^{o}. However, most studies of long term non-dipole field behavior agree that the dominant non-dipole components are zonal, affecting only the inclination and not the declination (Creer et al., 1973; Wilson and McElhinny, 1974). Furthermore, such a declinational error would imply, as noted by Gordon (1983), the implausible existence of a large persistent toroidial magnetic field at the Earth's surface.

Having dismissed non-dipole errors as the major source of the discrepancies between the observed and hotspot-predicted postions of the paleomagnetic poles, let us examine TPW as the cause of these differences. The agreement between the TPW implied by Figure 5.15 and that found in other studies of Pacific data of Late Cretaceous - Tertiary age is very good. The figure shows that the 68 Ma. pole is located about 12° away from the geographic pole towards the Pacific in accord with the findings of Gordon and Cape (1981), Jurdy (1981), and Gordon (1983). For earlier times, the agreement is not as good. Morgan (1981), for instance, did an analysis of a world-wide paleomagnetic data set, backtracking it in the hotspot reference frame in the same manner as the poles in Figure 5.15. His analysis showed that about 25° of TPW occurred between 120 and 45 Ma., but his results indicated that the rate and direction of the TPW during that interval changed little, unlike the rapid and erratic TPW implied by Figure 5.15. Also, the direction of the TPW in Morgan's study was somewhat different. His 45-120 Ma. paleopoles trend towards the northeast Atlantic with increasing age, whereas the paleopoles of the same age range in Figure 5.15 trend towards 270° E from 81-91 Ma., towards the Atlantic from 91-104 Ma., and then towards the Pacific from 104-119 Ma. Harrison and Lindh (1982b) also examined the offset between the paleomagnetic and hotspot reference frames using a global paleomagnetic data set. Although they did not define the direction of the TPW, their results indicate that approximately 20° of offset has occurred since 200 Ma. with only small variations occuring in the rate of the TPW. No

large, rapid shifts of the spin axis, such as those implied by the Pacific data in Figure 5.15, were found.

If TPW is the cause of the observed Pacific polar motion in the hotspot reference frame, then its effects should be visible in the paleomagnetic data of other plates, particularly considering the magnitude (in excess of 20°) and rates (more than 2°/Ma.) of the TPW epsiodes implied by Figure 5.15. Several of the better constrained continental APWP were examined for these effects. Although the poles of these APWP are often averaged over 20-40 Ma. to smooth out short term fluctuations in APW, the implied magnitude of the Pacific TPW suggests that its effects should nonetheless be visible to some extent despite such smoothing. The two APWP that are undoubtedly the richest in data are those of North America (Irving, 1977; Briden et al., 1981; Harrison and Lindh, 1982a) and Eurasia (Irving, 1977; Briden et al., 1981). Neither displays more than about 10° of APW during the interval of 60-120 Ma. and in both cases the direction of the APW is opposite to that implied by the 91-81 Ma. shift in the Pacific paleopoles (Figure 5.16). APWP from India, Australia, and Africa (Briden et al., 1981) were also examined with similar results. No consistent, rapid APW, that might correspond to the TPW implied by the Pacific data, is evident in any of these APWPs. Thus it appears that TPW is not a satifactory explanation for all of the observed differences between the Pacific paleomagnetic poles and their hotspot-predicted positions. Of course, TPW cannot be dismissed entirely. There are too many studies that have measured significant amounts of TPW to ignore it.

Consequently, the APWP should be the result of TPW (about 7^{o} - 10^{o} in the Late Cretaceous and another 7^{0} - 10^{o} in the Tertiary if the results of Morgan (1981) and Harrison and Lindh (1982b) are correct) combined with plate motion and the effects of long term non-dipole magnetic field components.

If TPW and non-dipole components are not the primary source of the discrepancies between the observed and hotspot-predicted paleopole postions, then these differences must arise either from the errors in the determination of the paleomagnetic poles or errors in the plate/hotspot motion model. The former source of error is probably not the cause either. As mentioned previously, care was taken in the estimation of the error limits of each of the individual paleomagnetic data that these limits are, if mistaken, overestimates of the true error. Consequently, the 95% confidence ellipses calculated for the paleomagnetic poles should also be conservative estimates of the errors. Figure 5.15 shows that these 95% confidence ellipses rarely intersect suggesting that these poles are significantly different. Additionally, even if the postions of the paleomagnetic poles are allowed to be located anywhere inside their 95% confidence ellipses, the APWP in the hotspot reference frame described here would not be changed significantly. Thus, although some of the discrepancies between the observed and hotspot-predicted pole postions indicated in Figure 5.15 may result from data errors, it appears that the possibility of significant errors in the plate/hotspot motion model must be entertained as well.

Let us briefly examine the Pacific plate/hotspot rotation poles in order to see where and why errors might occur. Much of our knowledge about the motion of the Pacific with respect to the mantle comes from the Hawaiian-Emperor chain. many of its edifices have been reliably dated (Dalrymple et al., 1980) and most are well-surveyed so that the trend of the chain is clear. The mid to late Tertiary motion of the Pacific is particularly well constrained because it can be determined from several other seamount chains as well as the Hawaiian chain (Turner et al., 1980). For the early Tertiary, the rotation pole is not quite as well constrained because its derivation relies heavily on the trend and ages of the Emperor Seamounts (Jarrard and Clague, 1977; Epp, 1978). However, the Late Cretaceous plate/hotspot rotation pole is undoubtedly the most poorly constrained because no Cretaceous seamount chains in the Pacific have been unequivocally demonstrated to have been formed by a hotspot. Because the Hawaiian-Emperor chain disappears into the Kamchatka Trench just to the northeast of Meiji Guyot, which has a fossil age of approximately 70 Ma. (Worsley, 1973), no earlier constraint of the plate/hotspot motion is available from it.

The Late Cretaceous plate/hotspot rotation pole in Table 5.2 was determined from the trends of several seamount chains of probably Cretaceous age: the Wentworth, North Gardner, north Emperor, Musicians, and Line Islands chains (Epp, 1978). All of these seamount chains are very nearly parallel to small circles (i.e., copolar) around the 36° N, 284° E rotation pole, so this pole probably represents a valid estimate of plate/hotspot motion for some time in the Cretaceous; however, its limits and rotation rate are poorly constrained because of

the scarcity of reliable age determinations of the edifices of these chains. Two of the seamount chains used to determine this rotation pole have no dated edifices at all (Wentworth, North Gardner); one has two dated edifices that place conflicting constraints on the age of the chain (Musicians) (Clague and Dalrymple, 1975); one is poorly dated and is so short that its azimuth is somewhat ambiguous (north Emperor); and one has radiometric dates, paleomagnetic poles, and other geologic information that indicate that its volcanic history has been complex (Line Islands, see Section 5.2.1). In addition, the 127 Ma. age of a volcano in the northern Line Islands, used to constrain the rate and beginning of the rotation around the Late Cretaceous pole, has recently been found to be too high by about 35 Ma. (D. Clague, personal communication, 1983).

Perhaps the most troublesome aspect of the Pacific plate/hotspot motion model is the fact that it cannot account for the large changes in the Cretaceous plate/spin axis motion observed in the north Pacific APWP (Figure 5.2). Usually models of Pacific plate/hotspot motion call for two major changes in the direction of the plate's motion. One of these occured at approximately 43 Ma. and corresponds to the Hawaiian-Emperor bend. The other is hypothesized to have occurred at about 67 Ma. and corresponds to the bend in the northern part of the Emperor chain. In Figure 5.14, the 43 Ma. change shows up in the trend of the hotspot-predicted APWP as a change from a southeasterly trend to a southwesterly trend. In contrast, the change from the Emperor rotation pole to the Late Cretaceous pole at 67 Ma. produces little change in the trend of the predicted APWP. However, according to the observed

APWP. there are three major changes in the plate/spin axis motin that are not satisfactorily explained by either TPW or non-dipole components and thus may be the result of changes in the motion of the Pacific plate with respect to the mantle. These changes occurred at approximately 104, 91, and 81 Ma. The first was a change from an apparent southward drift of the Pacific plate to a northward drift; the second indicates that the plate's motion switched from northward to westward; and the third returned the plate to a northward drift.

If these changes in the APW can be attributed to plate motion. in what ways must currently accepted plate/hotspot rotation models be modified to better account for the observed APW? First of all, it must be kept in mind that a plate's APW can only be used to indirectly infer plate/mantle motion because paleomagnetic data measures the relative motion of the plate with respect to the spin axis. not the mantle. As discussed previously, the agreement between APW and plate/mantle motion depends on the amount of TPW and non-dipole field affecting the paleomagnetic data. In general, neither TPW or the long term non-dipole structure of the magnetic field are known with sufficient accuracy during the Cretaceous to correct the paleomagnetic data for these effects. However, for the main period of interest, approximately 104-81 Ma., during which time the rate of APW was high and the APWP displays three major directional changes. TPW and non-dipole field bias may have fortuitously cancelled one another to some degree. Between 90 and 60 Ma. Morgan's analysis indicates that roughly 10^{o} of TPW occurred with the spin axis moving towards the Pacific. During the same

interval, evidence has been found for a large g_2^0 geomagnetic field component. If this finding is correct, Pacific paleomagnetic poles of this period should be biased 5^o - 12^o away from the Pacific. Additionally, evidence has been cited here that suggest that most of the Pacific's APW is a result of the motion of the plate and not time-varying non-dipole errors or TPW. Consequently, an examination of the Pacific APWP should provide some valuable clues to its past motions with respect to the hotspot reference frame.

Prior to approximately 104 Ma. the APWP indicates that the Pacific plate's motion was southward with respect to the spin axis and probably the mantle as well. Because no Early Cretaceous seamount chains have been positively identified, it is impossible to make any reasonable esimate of the location or rotation rate of the plate/hotspot Euler pole for this period. Between about 104-91 Ma. the plate/hotspot motion should probably impart a large component of northward drift to the plate. It is interesting to note that the 104 and 91 Ma. paleomagnetic poles very nearly lie on the same small circle of the 36^o N, 284^o E plate/hotspot rotation pole (Figure 5.17). This observation suggests that this pole is valid, but for a shorter period of time than given in Table 5.2. However, if this hypothesis is true, the rotation rate of this pole would have to be on the order of 2^o/Ma., about three times the rate given in Table 5.2. Also, it should be noted that both of these paleomagnetic poles have relatively large 95% confidence ellipses and thus their agreement with this pole of rotation may be fortuitous.

Th APW between 91 and 81 Ma. suggests a rapid east-west drift of the Pacific plate. A rotation pole to reproduce this phase of APW must be carefully chosen because of the high rate of APW involved. In Figure 5.18a it is seen that the 81, 87 and 91 Ma. paleomagnetic poles are nearly parallel to small circles of a pole at 69° N, 329° E. However. this rotation pole is so close to the paleomagnetic poles that it must rotate through an angle in excess of 90° in only 10 Ma. If the 91-81 Ma. shift of the paleomagnetic pole is attributed to plate motion, then such a rotation pole would imply absurdly high rates of plate/hotspot relative motion. Therefore. a rotation pole with these paleomagnetic poles near its equator would seem to be a better choice. Such a pole would not fit the trend of the paleomagnetic poles as well, but it would reduce the rotation rate to 22° in 10 Ma. However, as shown in Figure 5.18b, this pole must be located within the boundaries of the Pacific plate itself. The rotation of a large plate. such as the Late Cretaceous Pacific. around a pole within its boundaries appears to be unlikely because it is at odds with currently accepted ideas about plate driving forces. An improbable configuration of spreading ridges and trenches would be required to produce the ridge-push and slab-pull to drive the plate into a rapid rotation around an Euler pole within itself (Gordon, 1983). Thus the only reasonable position for the rotation pole, if it is to correspond to plate/hotspot motion. is between these two extremes, as shown in Figure 5.18c.

If the APW changes described here correspond to shifts in plate motion. then there should be hotspot-generated seamount chains in the

Pacific whose trends record these changes. Currently accepted plate/hotspot motion models recognize no such shifts prior to 67 Ma., but the APWP implies that a Cretaceous seamount chain formed by a hotspot should have a north-south trend for that part of it formed between 104-91 Ma. and just after 81 Ma. and an east-west trend for the segment formed between 91-81 Ma. The age of the bend in the northern Emperor chain (67 Ma.) is suspiciously close to the age of the 81 Ma. bend in the APWP. The two may actually record different changes in the Pacific plate's motion, but perhaps they are actually coincident. Because the age of Meiji Guyot (approximately 70 Ma.) is a minimum age, the currently accepted age of the north Emperor bend was derived by the extrapolation of the rate of the propagation of volcanism along the Hawaiian-Emperor chain. When plotted against the distance from Kilauea volcano (the approximate location of the Hawaiian hotspot), the ages of the Hawaiian-Emperor edifices fit remarkably well to a single line with a slope of 8.0 cm./yr. (Dalrymple, et al., 1980; Figure 7). This line implies an age of 67 Ma. for the north Emperor bend. However, this line is only a first approximation to the actual rate of volcanic propagation. There is no reason why the rate should have remained constant, as it appears to have done, for more than 70 Ma. Moreover, most of the ages of the Emperor Seamounts lie above this reference line, and if the line were allowed to bend at the Hawaiian-Emperor bend so that it more nearly follows the trend of the Emperor ages, the extrapolated age of the north Emperor bend would increase to about 78 Ma.--very close to the 81 Ma. age of the bend in the APWP.

This hypothesis has interesting implications for TPW. Much of the mis-match between the observed and hotspot-predicted postions of the 68 Ma. and 81 Ma. paleomagnetic poles is a result of the fast rate of rotation around the Emperor pole. However, if the age of the north Emperor bend is taken to be approximately 80 Ma., then the rate of rotation for the Emperor pole must be reduced by about 33%, to 0.5^{o}/Ma. An APWP is shown in Figure 5.17 using this rotation rate for the segment corresponding to the Emperor chain. The difference between the observed and hotspot-predicted postion of the 81 Ma. pole is reduced to within the error of the paleomagnetic pole; however, there is still a discrepancy of about 6^{o} between the observed an predicted postions of the 68 Ma. paleomagnetic pole. If these observations are correct, they imply that the spin axis may have moved away from its 81 Ma. position only to return to nearly the same spot at present.

If the proposed age of the north Emperor bend is correct, there may be other seamount chains in the Pacific that record the change in plate motion but have gone unidentified because previous workers have looked for a change from a trend corresponding to the Emperor pole to a trend corresponding to the 36^{o} N, 284^{o} E pole rather than the more nearly east-west trend indicated by the APWP. There are no obvious examples of another seamount chain that records this bend; but, this is not too surprising because such a chain would likely be located in the present day western Pacific, a region that appears to be the confluence of a number of seamount chains and groups of varied ages.

One possibility for such a seamount chain is the Marshall-Gilbert-Ellice (MGE) Islands. The easternmost edifices of the MGE group form a long, linear chain sub-parallel to small circles of the Emperor rotation pole. This fact has led some authors to speculate that it may have formed by a hotspot coevally with the Emperor chain (Morgan, 1972; Epp, 1978). At its northern end, near Wake Island, the MGE chain bends to the west northwest and continues as a diffuse chain of seamounts through Marcus Island to the Bonin Trench (Figure 5.19). The west northwest trending seamount chain is unnamed, however, it is referred to here as the Marcus-Wake (MW) chain as it contains these two islands.

Assuming that the MW chain was formed by a hotspot, a plate/hotspot rotation pole can be found whose small circles parallel the trend of the chain. Because the MW chain is so diffuse, alone its constraint on the position of this pole is poor. However, this pole should also account for the general trend of the APWP between 91-81 Ma., it should be far enough away from the paleomagnetic poles so that in accounting for the APW of 91-81 Ma. the rotation rate is not too high, and if the hypothesis that the north Emperor bend is coeval to the MGE-MW bend is correct, small circles of this pole should match the trend of the north Emperor chain.

A pole fitting these requirements is located at 65^{o} N, 190^{o} E. In Figure 5.19 it is seen that small circles of this pole do indeed agree well with the trend of the largest volcanoes in the MW chain. Also, Figure 5.20 shows that this pole also predicts the trends of the north Emperor chain and the 91-81 Ma. paleomagnetic poles reasonably well.

Neither the trend of the north Emperor chain nor that of the 91-81 Ma. paleomagnetic poles is exactly matched by the small circles of this pole; however, the fit is good considering that the north Emperor chain is short and poorly surveyed and the paleomagnetic poles are almost certainly affected to some extent by TPW and non-dipole field errors.

Only two seamounts in the MW chain have been reliably dated. These are Lamont and Wilde guyots. located a few hundred kilometers west of Wake Island (Figure 5.29). with $^{40}Ar-^{39}Ar$ ages of 86.6 and 86.4 Ma. (Ozima et al., 1977). Their ages agree remarkably well with the age of the chain implied by the proposed hotspot model. However, because these are the only reliably dated edifices in the MW chain, the paleomagnetic poles are the only source of constraint on the amount and rate of rotation around the 65° N, 190° E pole. The 81 and 91 Ma. paleomagnetic poles are separated by $22.1^{\circ}\pm5.3^{\circ}$ implying a rotation around the pole of $27.3^{\circ}\pm6.6^{\circ}$ and a rate of $2.7^{\circ}\pm0.7^{\circ}$ Ma. Likewise. if this estimate of the plate/hotspot pole and its rate of rotation are valid. the length of the MW chain should be approximately 2300 +600 km. in length, very close to the 2600 km. of MW chain visible between Wake Island and the trench. These estimates provide a means for future studies to test the validity of this hotspot hypothesis for the formation of the MW chain. If dated reliably, seamounts in the eastern part of the chain should have ages in the neighborhood of 81 Ma. and the ages of the seamounts should increase westward to about 91 Ma. at the trench.

It is interesting that two seamounts, W3 and W5, near the intersection of the MW chain and the trench have radiometric ages of 93.9 Ma. (^{40}Ar–^{39}Ar)(Ozima et al., 1977) and 93.7 Ma. (K-Ar)(Ozima et al., 1970). Although these seamount ages are very close to the values predicted for MW seamounts near the trench by the hospot model, neither of thse two seamounts appears to actually be a part of the chain (Figure 5.19), so it is unclear whether or not they are related to its formation.

There are several troublesome aspects of the hotspot model for the origin of the MGE-MW chain. The hotspot model is not universally accepted for the origin of the MGE chain. Only one seamount among the eastern MGE edifices has been dated (W17) and it has a fossil age of 80 Ma. (J. Haggerty, personal communication. 1983), much older than predicted by the hotspot model. Likewise, from volcanic sediments recovered at DSDP Site 462, Schlanger and Premoli-Silva (1981) infer that the Marshall Islands formed during the Late Cretaceous as a part of a widespread pulse of volcanism affecting most of the western Pacific. Also, the trend of the MGE chain is not exactly parallel to small circles of the Emperor rotation pole. Instead, it deviates by about 10° from the hotspot-predicted trend and some segments of the southern part of the chain are actually parallel to small circles of the 36° N, 284° E pole (Epp, 1978).

The discrepant ages in the MGE seamounts are not surprising because the volcanic history of the province is complex (Larson and Schlanger, 1981) and the incorporation of older edifices into younger

seamount groups should be common. The trend of the MGE chain is more difficult to explain. Its deviation from the Emperor pole trend was cited as evidence by Morgan (1972) that there may be small relative motions between hotspots; although, his more recent studies (Morgan, 1981) indicate that the amount of relative motion among hotspots is negligible. Epp (1978) examined the trend of the MGE chain and concluded that its deviation from the Emperor pole trend may be a result of the interaction of the hotspot volcanism with older structural trends.

Also troublesome are the facts that the MW chain is more diffuse than most hotspot chains. that nowhere is there an obvious example of a seamount chain parallel to small circles of the 36^{o} N, 284^{o} E pole (suggested here to apply to 104-91 Ma.) connected to a seamount chain parallel to small circles of the 65^{o} N, 190^{o} E pole, and that the proposed rates of rotation around these poles imply much faster plate/mantle velocities (approximately 23 cm./yr. for the MW chain) than have been measured for the Hawaiian-Emperor chain (8.0 cm./yr.). Unfortunately, if there existed a connection of the western end of the MW chain to any other chain, the evidence has been lost to subduction in the Bonin Trench. Perhaps the third of these problems is the cause of the first two. The high inferred velocity of the plate with respect to the mantle may tend to make a hotspot chain more diffuse than might be observed at slower rates of plate/mantle motion. Also, the high plate/mantle velocity combined with large changes in the direction of plate motion, may have been unfavorable circumstances for the recording of the bends in such chains. For example. bathymetry from the

Hawaiian-Emeperor bend indicates that the volume of volcanism was drastically reduced after the change in the direction of the plate at 43 Ma. for more than 1000 km. to the east along the Hawaiian chain (Bargar and Jackson, 1974). Perhaps a similar phenomenon may be resposible for the fact that most of the chains following the trend of the 36° N, 284° E pole small circles appear to terminate with no obvious connection to any other chain (e.g., North Gardner, Wentworth, Musicians, and perhaps the Line Islands chains).

Many observations have been made in this section concerning plate motion, TPW, and long term non-dipole geomagnetic field components. Because of the uncertainty in the amount of TPW and non-dipole error in the Jurassic. Cretaceous, and early Tertiary, these observations must be regarded as speculations at present. However, they should provide added impetus for future studies of hotspot seamount chains and global paleomagnetic data sets for these periods of time. Until better constrained plate/hotspot motion models are available for the Pacific. and more robust estimates of the past non-dipole structure of the geomagnetic field are derived. it will remain difficult to uniquely interpret the Pacific APWP (or any other APWP for that matter) in terms of the plate's motion.

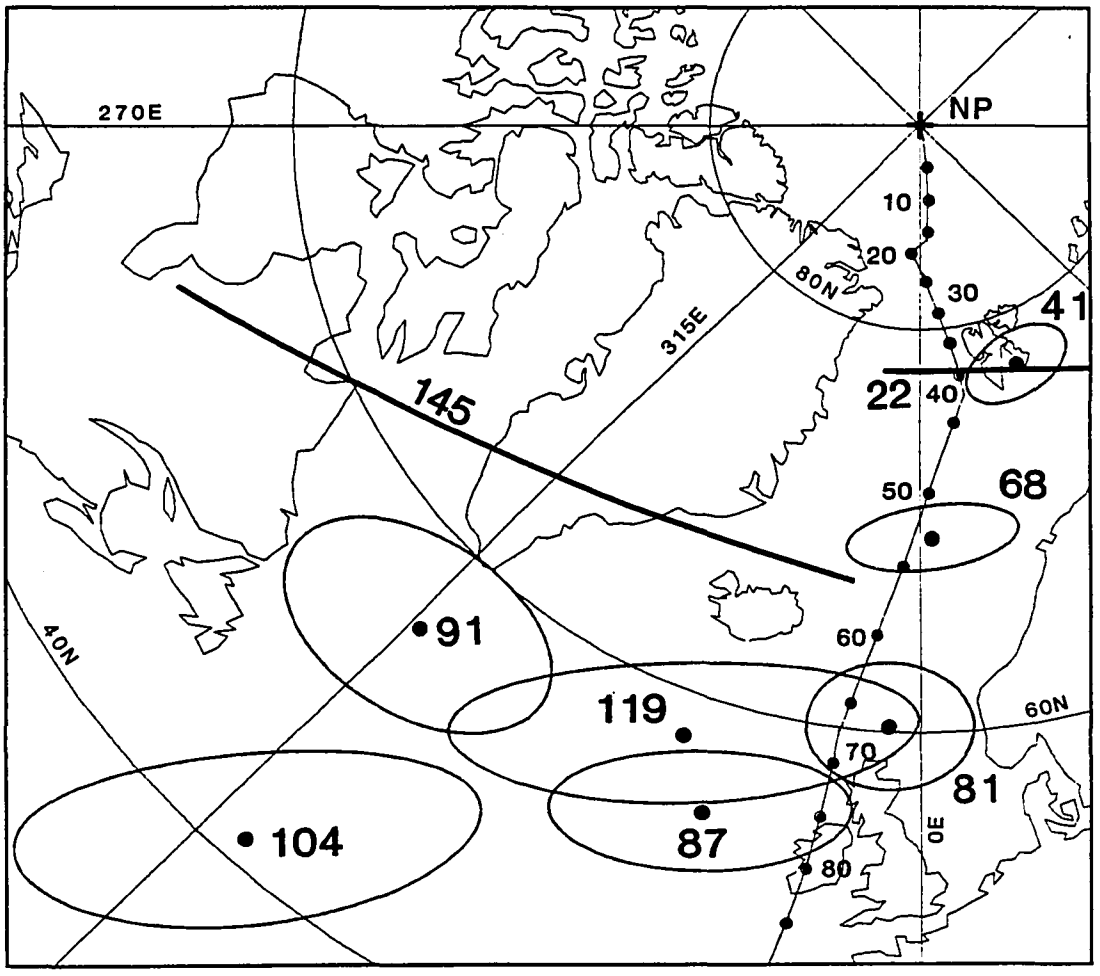

Figure 5.14 Comparison of observed APWP with one predicted by a Pacific plate/hotspot motion model (Table 5.2). The observed paleomagnetic poles are as in Figure 5.2. Dots connected by a line are the hotspot-predicted postions of the paleomagnetic poles and are labeled at 10 Ma. intervals.

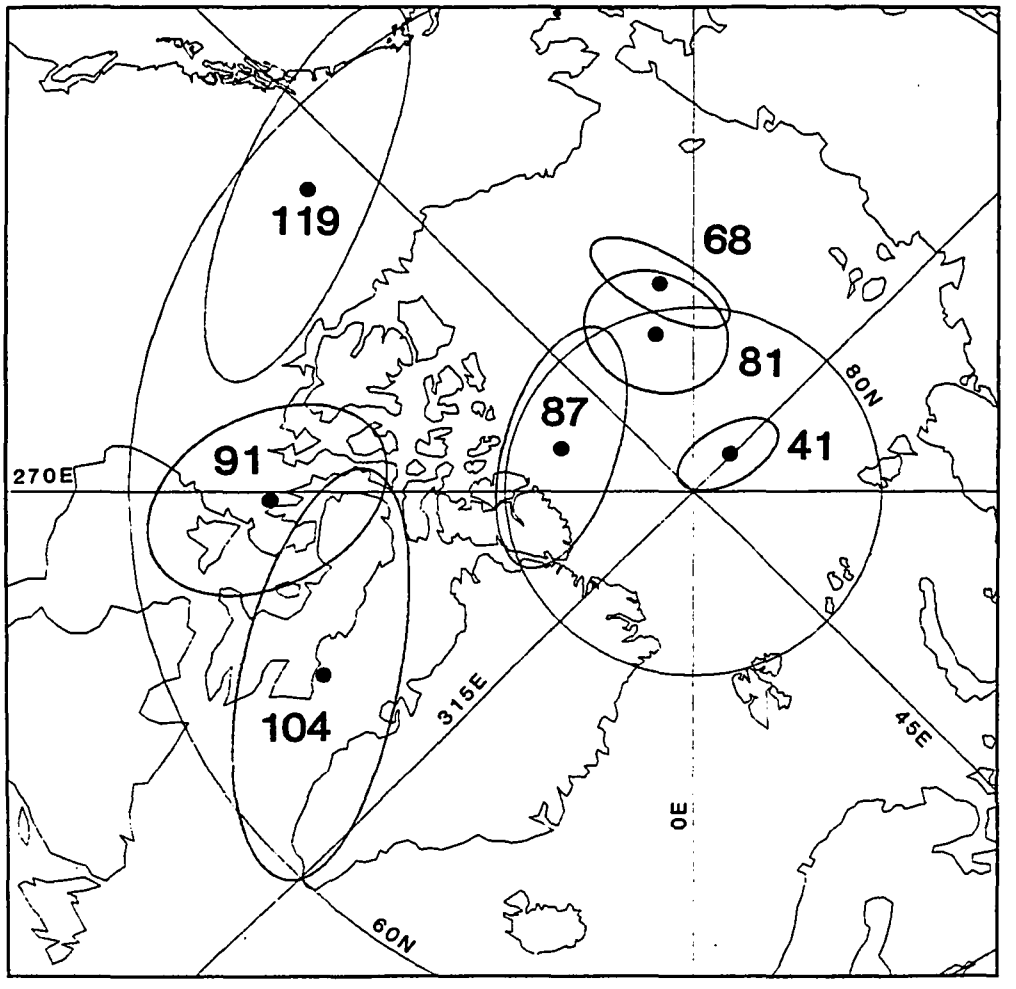

Figure 5.15 North Pacific APWP in the hotspot reference frame. The paleomagnetic poles from Figure 5.2 have been backtracked in the hotspot reference frame using the plate/hotspot rotation poles listed in Table 5.2. The displacement of a paleomagnetic pole from the geographic pole shows the amount and direction of mis-match between the observed and hotspot-predicted paleomagnetic pole postion. Map projection is polar equal area.

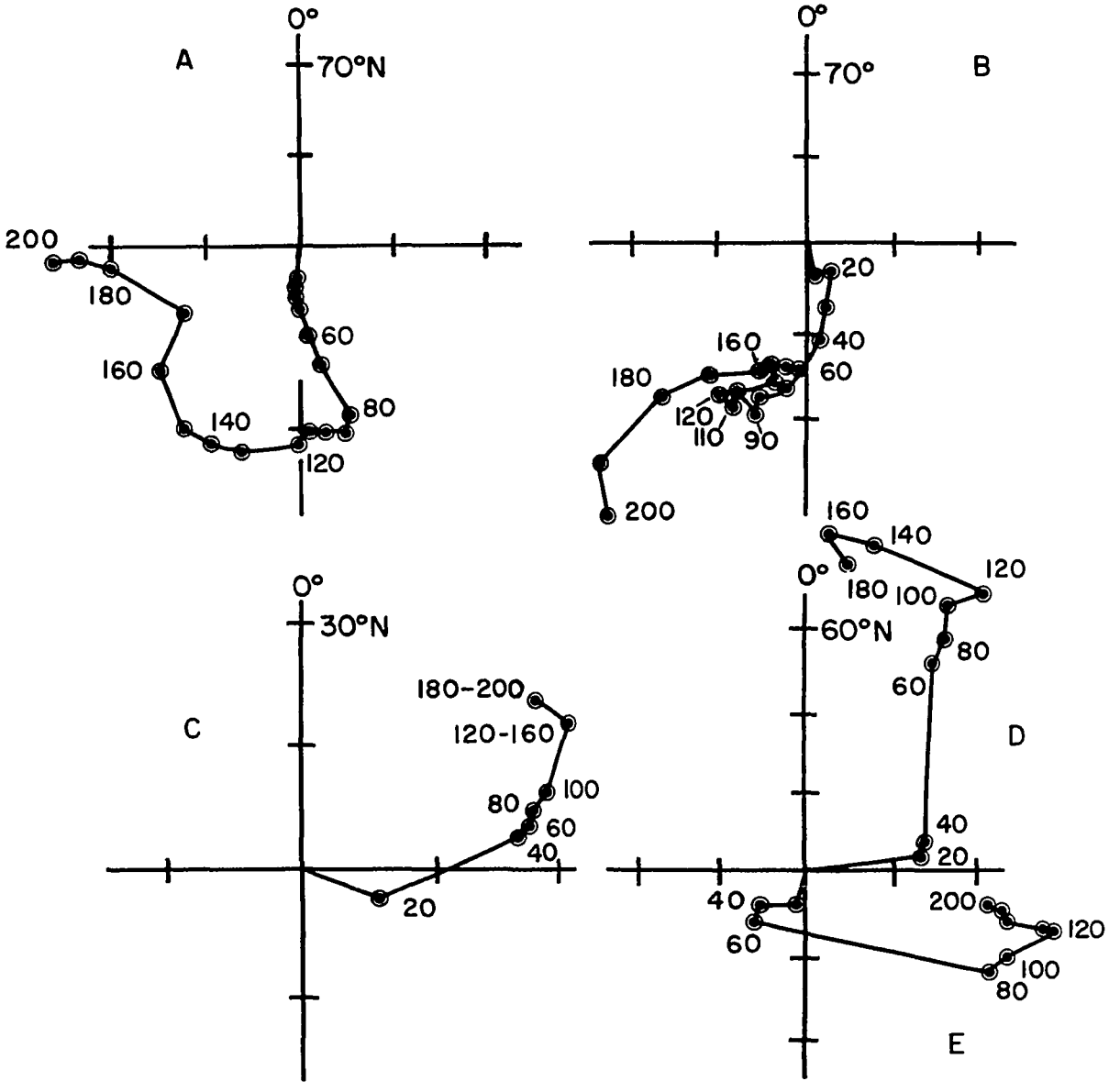

Figure 5.16 Continental APWPs. (a) North America (Harrison and Lindh, 1982a); (b) Eurasia (Irving, 1977); (c) India, (d) Australia, (e) Africa (Briden et al., 1981).

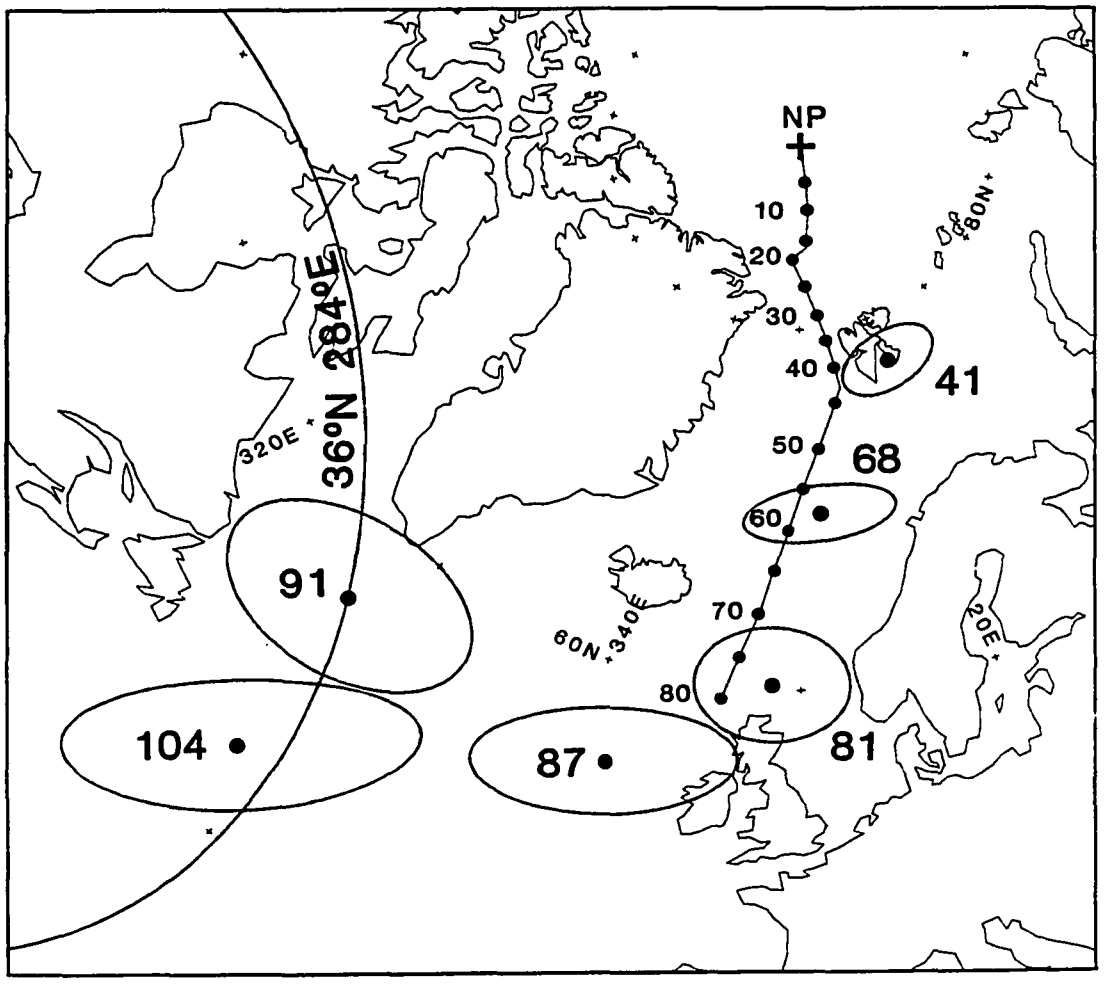

Figure 5.17 Comparison of paleomagnetic poles with small circle of 36° N, 284°E rotation pole and a predicted APWP with a reduced rate of rotation for the Emperor pole (15° N, 255°E). The 91 and 104 Ma. poles lie nearly on a small circle of the 36° N, 284° E pole. The hotspot-predicted APWP with the rotation rate of the Emperor pole reduced by 33% (to give the north Emperor bend an age of about 80 Ma.) displays better agreement with the 81 Ma. pole than before, but still disagrees with the 68 Ma. pole.

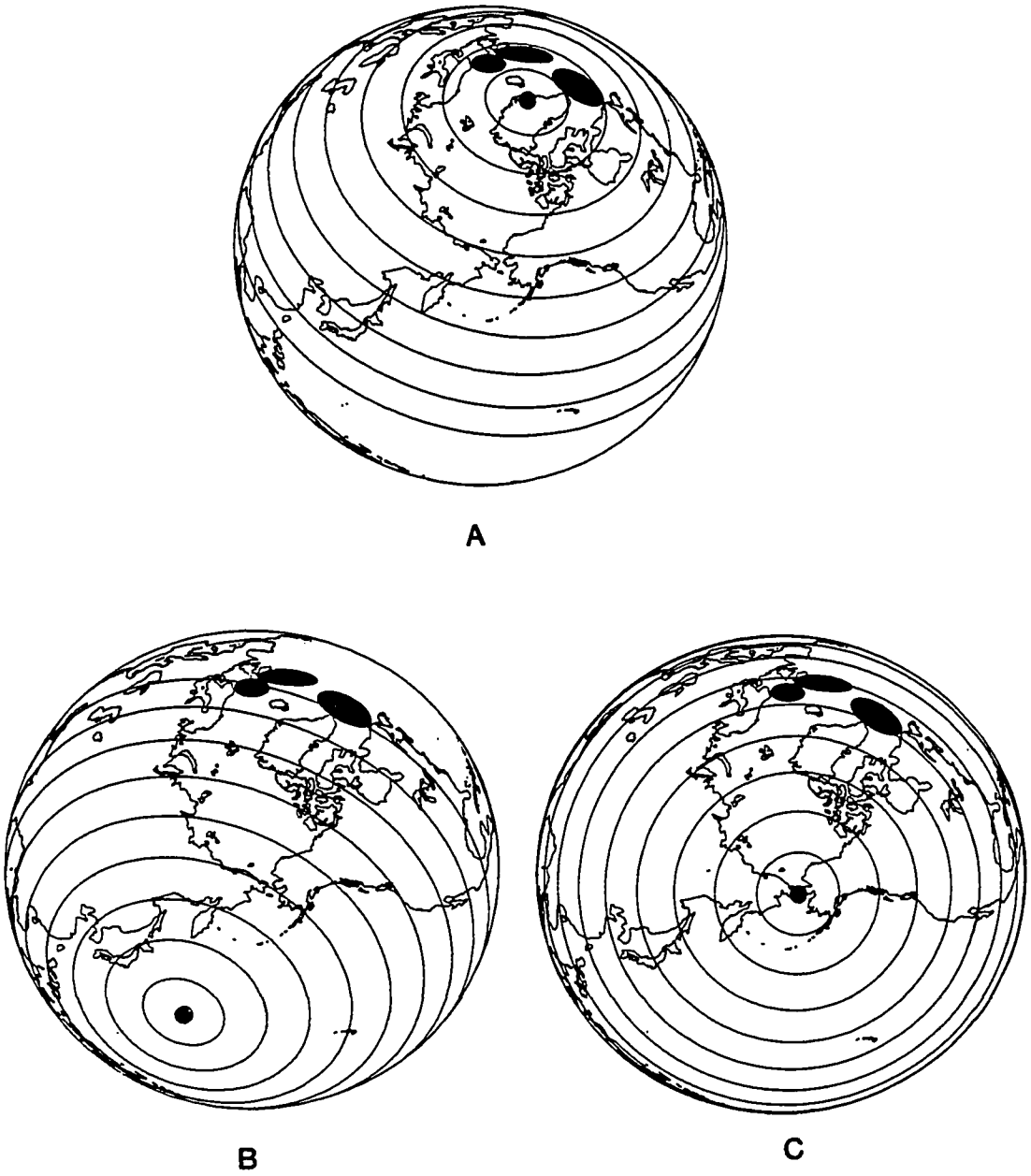

Figure 5.18 Examples of plate/spin axis rotation poles that could account for the rapid APW between 91-81 Ma. The ovals represent the 81, 87, and 91 Ma. paleomagnetic poles and the solid circle is the location of the pole. The small circles shown around each pole are at 10^{o} increments. (a) pole at 69^{o} N, 329^{o} E; (b) pole at 25^{o} N, 170^{o} E; (c) pole at 65^{o} N, 190^{o}E. The text explains possible implications of these poles for Pacific plate/mantle motion.

Figure 5.19 Possible hotspot trends for the Marshall-Gilbert-Ellice and Marcus-Wake seamount chains. Heavy solid lines are small circles of the Emperor plate/hotspot rotation pole and proposed plate/hotspot rotaion pole at 65° N, 190° E. It is postulated here that the Marcus-Wake seamount chain was formed by a hotspot between about 91 to 81 Ma. at which time the Pacific plate/hotspot motion was described by the 65° N, 190° E pole. Seamount ages from Ozima et al. (1977) are shown in parenthesis. Boxes show locations of seamounts that have given apparently reliable paleomagnetic results and are listed in Table 4.1. Filled circles show locations of DSDP sites mentioned in text.

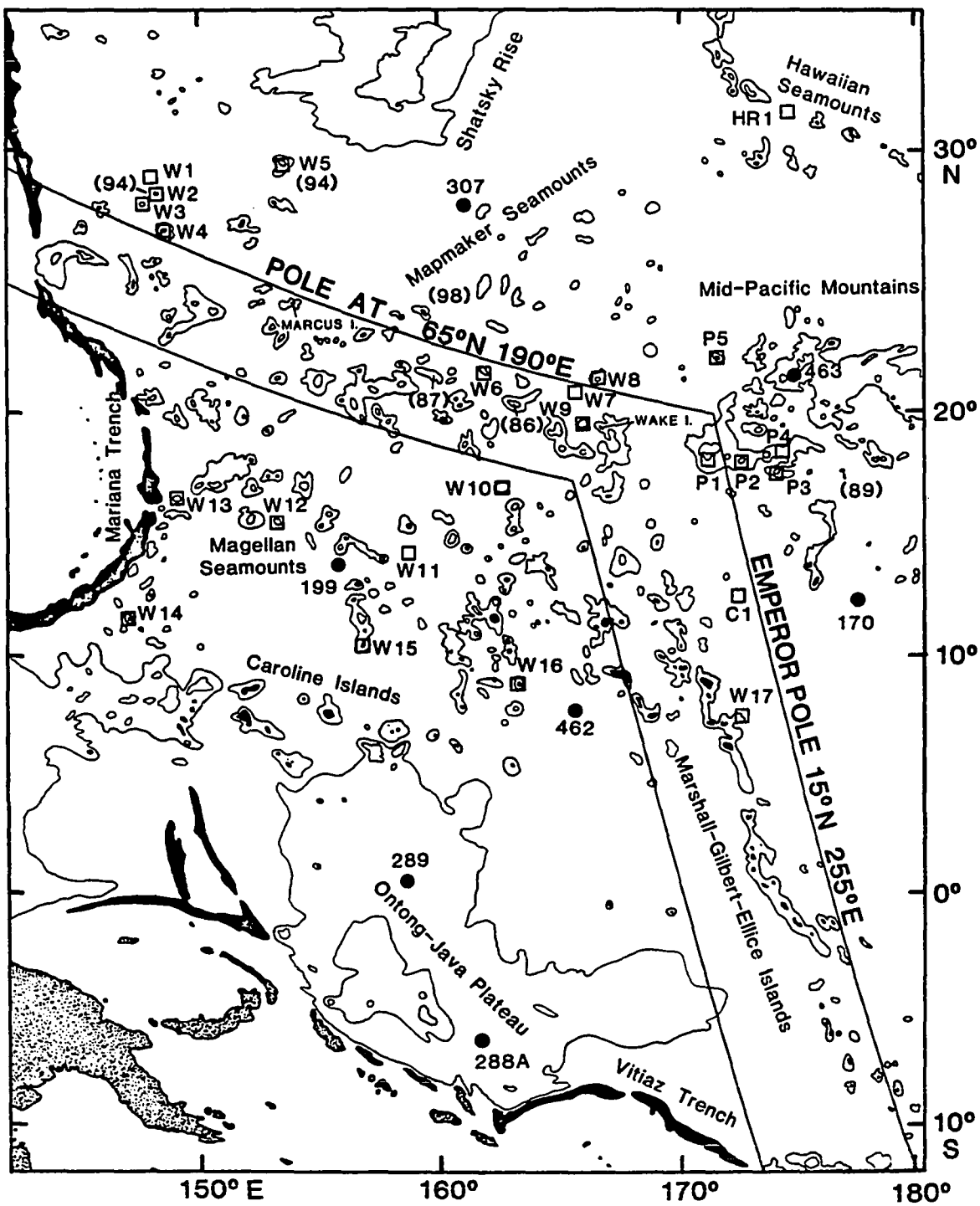
Shatsky Rise
Hawaiian Seamounts
HR1
30° N
W1
(94)
W2
W3
W4
W5
(94)
307
Mapmaker Seamounts
(98)
POLE AT 65°N 190°E
Mid-Pacific Mountains
MARCUS I.
P5
463
W8
W6
(87)
W9
W7
(86)
WAKE I.
20°
P4
P1
P2
P3
1
(89)
Mariana Trench
W13
W12
W10
Magellan Seamounts
199
W11
EMPEROR POLE 15°N 255°E
C1
170
W14
W15
W16
Caroline Islands
W17
462
Marshall-Gilbert-Ellice Islands
10° N
289
Ontong-Java Plateau
0°
288A
Vitiaz Trench
10° S
150° E
160°
170°
180°

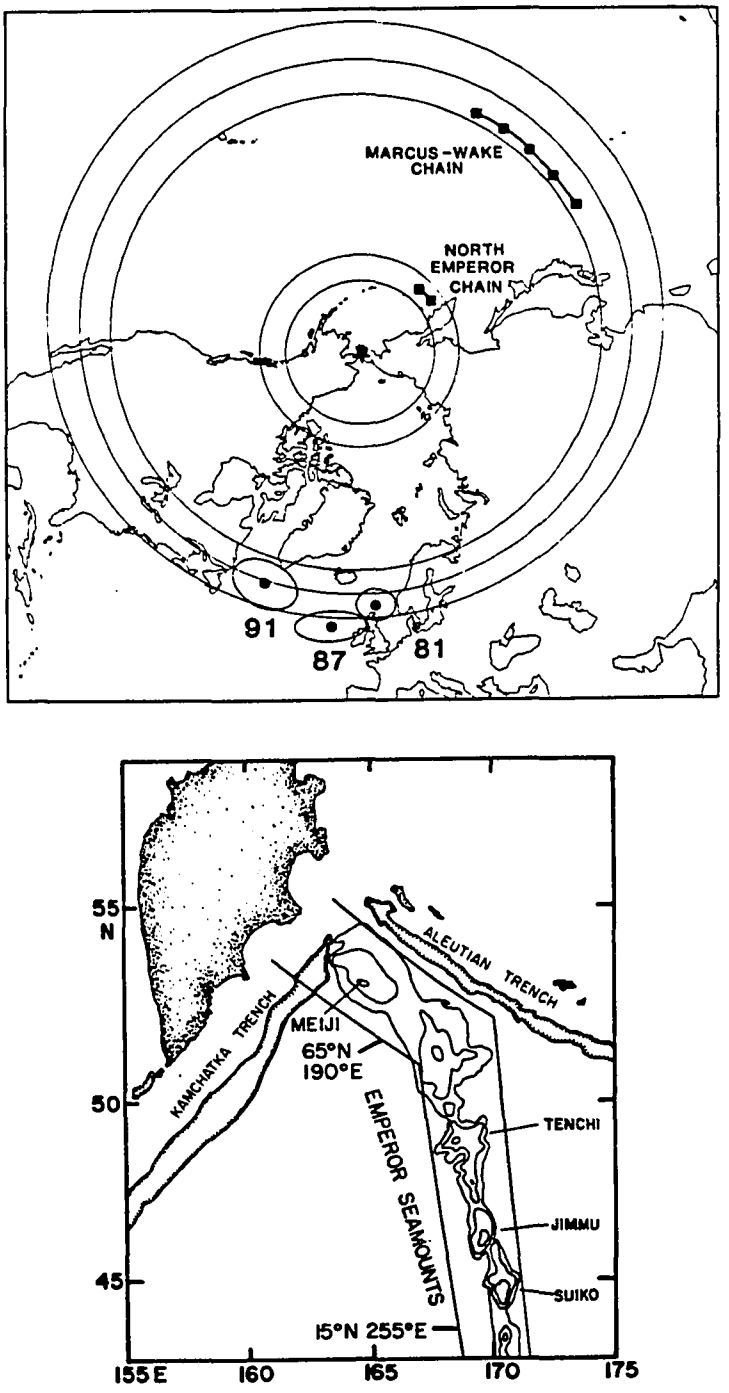

Figure 5.20 Fit of rotation pole at 65° N, 190° E to trends of Marcus-Wake seamount chain, north Emperor seamount chain, and paleomagnetic poles. (top) Small circles of rotation pole are seen to fit azimuths of both chains as well as the general trend of the 91-81 Ma. paleomagnetic poles. (bottom) The heavy solid lines are small circles of this pole showing their fit to the azimuth of the north Emperor chain.

5.1.10 A POSSIBLE APPARENT POLAR WANDER PATH FOR THE SOUTH PACIFIC

The preceeding analysis is based on the tacit assumption that the APWP in Figure 5.2 represents a single rigid Pacific plate. In other words, it was assumed that there has been no relative tectonic motion among the sampling sites of the data used to calculate each pole. Likewise, the differences between the average poles have not been attributed to relative motion between parts of the Pacific plate. The validity of these assumptions is naturally a question of great interest.

Looking at the distribution of the site locations for the Eocene and Maastrichtian poles (Figure 5.8). it can be seen that the data used for these poles come from widely scattered parts of the north Pacific. Thus, the rigid plate assumption for the north Pacific seems reasonable from the Maastrichtian to the present. The earlier poles were calculated from much less data. Most of this data comes from an area of the western Pacific north of the northern border of the Fiji Plateau and south of a line between Japan and Hawaii (Figure 5.8). The agreement of most of the data comprising the pre-Maastrichtian poles is very good. implying that the portion of the Pacific sampled has been a single rigid plate. However. as this conclusion is based on a limited area of sampling, it may not apply to the entire Pacific plate.

There has been a growing suspicion among many investigators that the Pacific may have been broken into two or more parts at some time in the past. Cox and Gordon (1980a) postulated a strike-slip motion between the north and south parts of the Pacific. They were uncertain

of the position of the boundary between the two sections. but hypothesized that it may have occurred along the Louisville Ridge or Eltanin Facture zone. Orwig and Kroenke (1980) postulated north-south spreading in the central Pacific basin during two episodes. one about about 110 Ma. and the other at 85 Ma. Their model called for northward displacement of the section of the Pacific north of the spreading center, southward displacement of the Pacific to the south of the spreading center, and strike-slip motion along the Line Islands to decouple this spreading from the eastern Pacific. Farrar and Dixon (1981) also hypothesized that the Line Islands mark a strike-slip boundary. However, their tectonic model indicated a Pacific plate divided into two parts. east and west, separated by a strike-slip boundary trending along the Emperor Trough and the Line Islands. They postulated that over 1700 Km of dextral shear occurred between these two parts of the Pacific between 70-40 Ma.

There is also evidence in the paleomagnetic data interpreted here for some sort of break between the north and south Pacific. Several times during the calculation of the paleomagnetic poles in Table 5.1 data were rejected because they did not agree with the majority of the data. In calculating the Eocene pole (Sager, 1983a). a paleocolatitude from 12 sediment samples cored at DSDP Site 289 was rejected because it predicted a paleopole much closer to the geographic pole than did the other data. The Site 288A paleocolatitude was omitted from the Maastrichtian data for the same reason in Section 5.1.3. A paleocolatitude derived from seven sediment samples of the same age from Site 289 shows the same bias; although, this paleocolatitude was

rejected from the useable data in Table 4.5 because the number of samples used to calculate it fell below the minimum felt necessary for reliability. The same tendency to record a paleopole nearer to the geographic pole than expected is displayed by Campanian age sediment paleocolatitudes from Sites 315A and 462 as well as Albian age sediment paleocolatitudes from Sites 288A and 289 (four samples). It should be noted, however, that the Site 462 sediment paleocolatitude is at odds with a paleocolatitude of approximately the same age calculated from intrusive bodies from the same site that was used in the calculation of the Campanian and Barremian poles. Some of these data must be in error. Since the basalt paleocolatitudes are calculated from an uncertain number of independent flows, they should be the more suspect.

Gordon (1983) suggests that DSDP sediment paleomagnetic results show this bias because of some systematic error. This explanation may be correct, but this systematic error only appears to occur in sediment cores from a small area of the equatorial Pacific and the paleocolatitudes derived from this data agree with other non-DSDP data from the south Pacific. The discussion that follows accepts these paleomagnetic measurements as such and attempts to explain the discrepant data in tectonic terms. If, in fact, the difference is the result of a systematic inclination error, these conclusions will be invalid. The problem will not be cleared up until more reliable paleomagnetic data is available from the south Pacific.

In Figure 5.21 the polar circles of the DSDP data mentioned above (288A, 289, 315A, 462[sediments]) are plotted along with semi-great circles from the south Pacific lineation groups SW1-SW3, the pole from

78 Ma. basalts from Chatham Island near New Zealand (Grindley et al., 1977) and a Fisher pole from seamounts M1-M3. The three seamounts, M1-M3, are in the northwest part of the southeast trending seamount chain found in the Musicians seamounts. Although none of these seamounts has been dated their VGPs fall very close to the Campanian pole; but, according to a tectonic model of the evolution of the Musicians seamounts (Moberly et al., 1983; see section 5.2.2), these seamounts should be at least 90-100 Ma. in age. Therefore, their VGPs would be expected to occur much further to the west near the Turonian or Albian poles.

The agreement of the data shown in Figure 5.21 is remarkably good. The 98 and 106 Ma. palecolatitudes from Sites 288A and 289 have polar circles that intersect the 95% confidence circle around the Fisher pole for seamounts M1-M3, hypothesized to be approximately the same age. Likewise, the 81 and 82 Ma. polar circles from sites 315 and 462 show good agreement with the 78 Ma. pole from Chatham Island. Further to the north, the Maastrichtian aged paleocolatitudes from Sites 288A and 289, as well as the skewness inclinations from lineation groups SW1-SW3 suggest a pole in the North Atlantic in the vicinity of Spitzbergen. In addition, the 39 Ma. paleocolatitude from Site 289 has a polar circle that crosses near the geographic pole, much further north than the north Pacific Eocene paleomagnetic pole. Thus the mechanism that caused this discrepancy appears to have been active at least as recently as 40 Ma.

Figure 5.21 shows a tentative APWP (called APWP2 here to distinguish it from APWP1 shown in Figure 5.2) for the sampling sites

in question. It is seen to be similar in shape to APWP1, except that it is shifted north, towards the geographic pole, very nearly along the trend of APWP1. However, the data constraining APWP2 is so sparse that no unique tectonic model can be derived to explain the shift of these poles. Because APWP2 is shifted nearly along APWP1, it appears that most of the tectonic motion has been along a strike-slip boundary between two parts of the Pacific. However, the paucity of south Pacific paleomagnetic data makes it difficult to estimate a relative rotation pole to shift APWP2 into coincidence with APWP1. For example, Gordon and Cox (1980a) showed that the area in which a relative rotation pole that would bring their 81 Ma. pole into coincidence with the Chatham Island pole is a large lune-shaped area covering most of North and South America.

One of the most attractive possibilities for the relative pole of rotation between these two APWPs is at 36°N, 284°E. This pole lies within the area of suitable poles defined by Cox and Gordon. As shown in Figure 5.21 a 13° rotation around this pole will shift most of the APWP1 poles, except for the 91 and 104 Ma. poles, into agreement with the APWP2 data. A similar 30° rotation around a pole at 59°N, 306°E will also accomplish the same thing and bring the 91 and 104 Ma. poles into better agreement. The 36°N, 284°E pole is particularly attractive because small circles about it are parallel to the Line Islands and many other Pacific bathymetric features (Epp, 1978). In fact, Farrar and Dixon (1981) hypothesized that relative motion between east and west Pacific plates occurred around virtually the same pole (36°N,

290°E) with 15.5° of rotation between 67 and 42 Ma. However, the details of their model do not precisely agree with the implications of Figures 5.21 and 5.8. The 39 Ma. paleocolatitude from DSDP Site 289 records a pole very close to the present geographic pole, showing that the relative motion was occurring later than the Eocene after their hypothesized relative motion ends. Also, their model had the plate west of the Line Islands moving north at a fast rate while the plate east of the Line Islands remained practically stationary during this time.

In Figure 5.22 it is evident that the distribution of the low northward drift data cannot be simply explained. Three sites west of the Marshall-Gilbert-Ellice chain (288A, 289, 462) show low northward drift as do those in the far south Pacific. Although the three seamounts (M1-M3) and DSDP Site 315A east of the Line Islands also have a low amount of northward drift, there are data from between these locations that appear to fit APWP1. However, the inclusion of Site 315A and seamounts M1-M3 in the APWP2 data set is problematic. Site 315A produced a Maastrichtian age paleocolatitude that displays less northward drift than most of the other data used to calculate the 68 Ma. pole, but it was not sufficiently displaced from the average pole position to be rejected from the pole calculation (Section 5.1.3). Also, the age assigned to the Musicians Seamounts M1-M3 may be incorrect and hence they may not actually disagree with the north Pacific paleomagnetic data.

In the central Pacific basin, between the Marshall-Gilbert-Ellice and Line Island chains, it is unclear which block the crust belongs to.

Sites 165, 166, 170, and 317A as well as seamount W17 and the Phoenix lineations agree with the northern Pacific data. However, the Site 167 paleocolatitude records a pole somewhat north of the other Campanian data (Figure 5.10) and the four undated seamounts (C1-C4) have VGPs near the Maastrichtian pole indicating that they are either very much younger than the underlying crust or they have not shared the total northward motion of the north Pacific data (Section 5.2.3).

A more detailed analysis with the sparse data in Figure 5.21 would do little good. More data is needed from the south Pacific and from the low northward drift areas shown in Figure 5.22. In this study it is only possible to point to the discrepancy between the north and south Pacific data and suggest that although Gordon (1982) apparently disproved Farrar and Dixon's (1981) hypothesis, it still has merits even though its details may be in error.

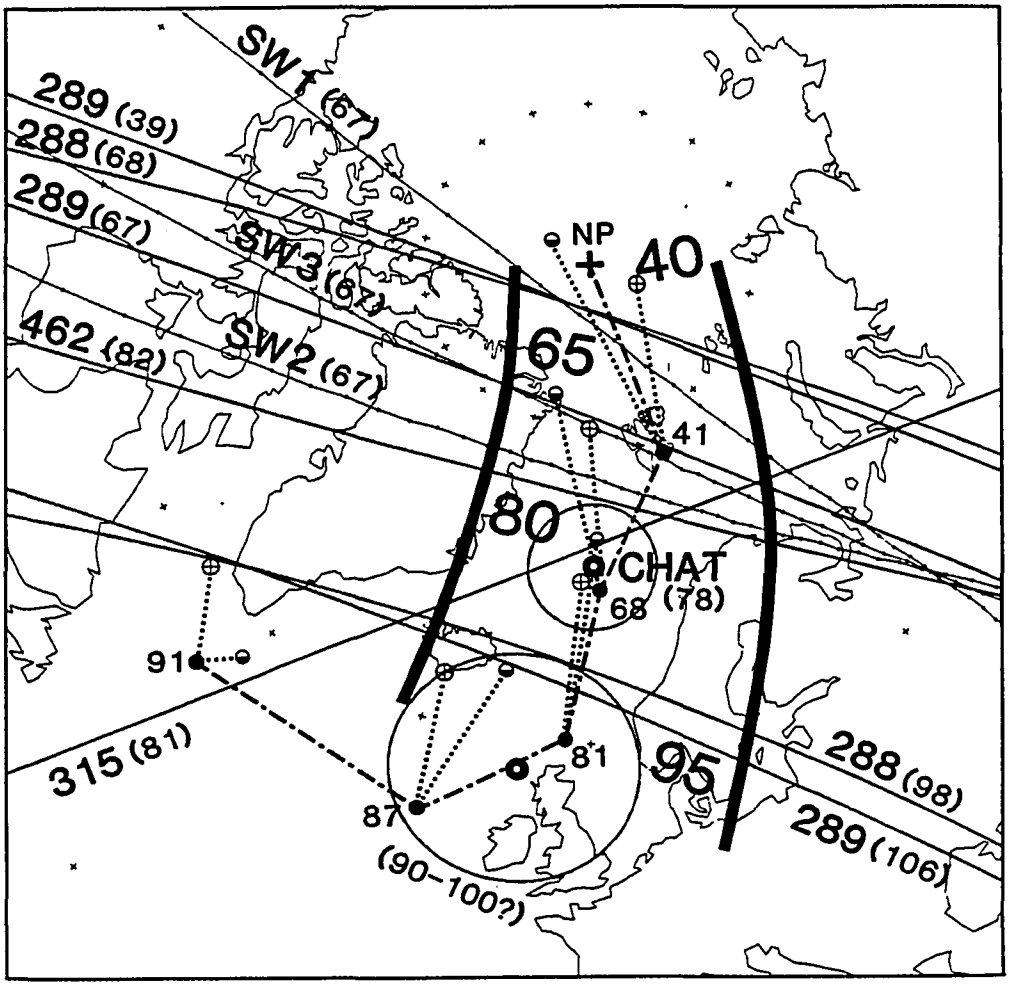

Figure 5.21 Possible APWP for south Pacific sites. North Pacific APWP shown by solid cricles connected by dash-dot line. Solid lines are polar circles from DSDP sites and lines with small dots are semi-great circles from skewness inclinations. Large circles are circles of 95% confidence of Chatham Island pole and Fisher pole of seamounts M1-M3. Data ages are given in parenthesis. Heavy lines indicate area of agreement of data and possible location of south Pacific APWP. Rotated postions of north Pacific paleomagnetic poles are shown. Circle with cross represents 13° of rotation around a pole at 36° N, 284° E; half filled circle represents 30° or rotation around a pole at 59° N, 306° E. Map projection is polar equal area.

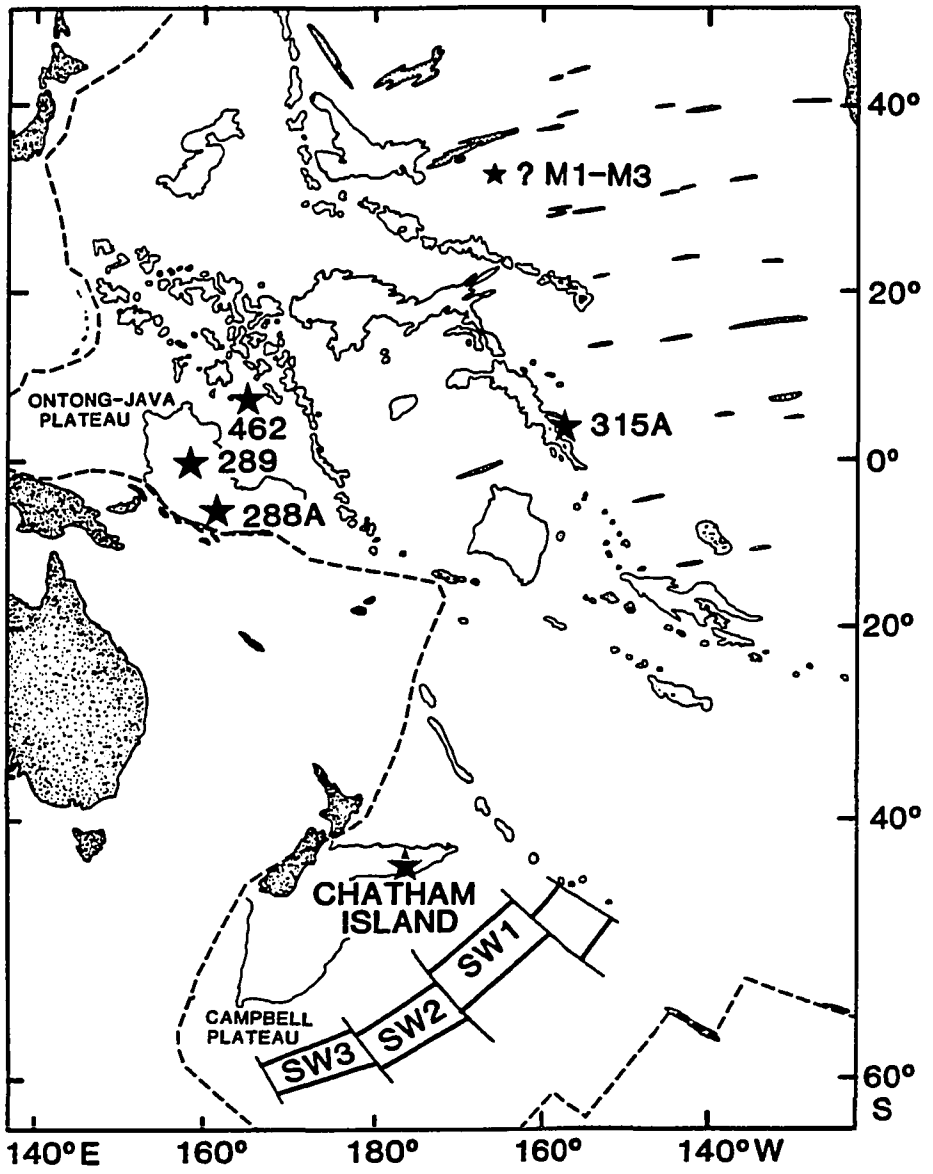

Figure 5.22 Locations of sampling sites of data mentioned in text as recording paleomagnetic poles significantly north of of north Pacific paleomagnetic poles. These data are plotted in Figure 5.21.

5.2 PALEOMAGNETIC IMPLICATIONS FOR INDIVIDUAL SEAMOUNT CHAINS

5.2.1 PALEOMAGNETISM OF LINE ISLANDS SEAMOUNTS

The Line Islands chain is perhaps the longest straight linear feature on the Pacific plate. It extends over 4200 km. from Horizon Guyot at its northwest end to its apparent termination at the northwest end of the Tuamotu Islands. Composed of a series of seamounts, guyots, submarine ridges, and atolls, this chain has fueled much speculation as to its significance to Pacific tectonics, but its origin remains obscure. In 1979, three research cruises were undertaken by the Hawaii Institute of Geophysics to gather geologic and geophysical data in the Line Islands in an effort to better understand its enigmatic features. During these cruises eleven seamounts were surveyed for paleomagnetic analysis. These paleomagnetic results and their implications for the origin and evolution of the Line Islands chain are the subject of this section.

Part of the reason that the Line Islands are so enigmatic is the fact that the chain occurs on Cretaceous Quiet Zone sea floor (Winterer, 1976). The youngest magnetic lineation in the Phoenix and Hawaiian anomaly groups to the west and northwest of the Line Islands are M1 and M0 respectively, with ages of 108 and 113 Ma. (Larson and Hilde, 1975). Anomaly 32, 70-71 Ma. in age (Lowrie and Alvarez, 1981), is located to the east of the Musician seamounts (Moberly et al., 1983). However, this anomaly has not been identified directly to the

east of the Line Islands presumably because of the low paleolatitude of the seafloor at the time of its formation coupled with a scarcity of ship tracks of suitable azimuth crossing the region. Winterer (1976) estimated the age of the seafloor underlying the Line Islands to be about 100 Ma. However, the Line Island chain is not exactly parallel to the probable azimuth of the mid to Late Cretaceous Pacific-Farallon ridge, so the age of the seafloor beneath the Line Islands is more probably variable, ranging from about 110-80 Ma. (Epp, in preparation).

Several investigators have concluded that the Line Islands represent a former boundary of the Pacific plate. Winterer (1976) suggested that many of the Line Islands edifices were formed by volcanism resulting from an abandoned spreading center left behind by an eastward jump of the Pacific-Farallon ridge. A study of the free air gravity field over the Line Islands (Watts et al., 1980) gives some creedence to this hypothesis as it found that many Line Islands seamounts were formed close to the ridge; although, this study did not distinguish between seamounts formed by volcanism related to the spreading center or volcanism from some other source, such as a hotspot located near the spreading center. Orwig and Kroenke (1980) as well as Farrar and Dixon (1981) hypothesized that the Line Islands chain was the site of a long fracture zone. Orwig and Kroenke proposed that the offset along the Line Islands was sinistral whereas Farrar and Dixon preferred dextral shear. In Orwig and Kroenke's model the Line Islands were formed coincidentally with volcanism in the Mid-Pacific Mountains to the northwest at 85 Ma. In Farrar and Dixon's model, the dextral

shear along the chain began in the Maastrichtian and ended during the Eocene.

Morgan (1972) and Epp (1978) considered the Line Islands to be the result of hotspot volcanism. Morgan believed the Line Islands to be contemporaneous to the Emperor chain, but this view appears to be incorrect (Epp, 1978; Haggerty et al., 1982). In contrast, Epp (1978) proposed that the Line Islands volcanism was generated by a hotspot at an earlier time, during the Late Cretaceous. He further attempted to explain some of its features by the interaction of hotspot volcanism with older structural features (Epp, 1978).

Jackson and Schlanger (1976) noted evidence favoring simultaneous volcanism along the north and central Line Islands in the results of Legs 17 and 33 of the DSDP. They suggested that a post-edifice building pulse of volcanism occurred all along the chain uplifting it into the photic zone. This pulse of volcanism appears to have occurred during the Late Cretaceous and is related to widespread volcanism of the same age throughout the western Pacific (Schlanger et al., 1981). Haggerty et al. (1982) found evidence that this volcanism estended to the southern Line Islands, and that there was a subsequent volcanic event in the Eocene.

Unfortunately, the age data from the Line Islands does not clearly favor any one genetic theory. By far the oldest rock of any from the Line Islands was dredged from a seamount in the northern end of the chain near Horizon Guyot and dated at 127 Ma. (Saito and Ozima, 1977); although, some scientists believe that this age is erroneous (D. Clague, personal communication, 1983). Most of the other dated rocks

from the chain appear to be much younger, but the scatter in ages is large. The majority can be divided into two groups of Late Cretaceous (100-70 Ma.) or Eocene (55-40 Ma.) age (Schlanger et al., 1982).

5.2.1.1 LINE ISLANDS SEAMOUNT PALEOMAGNETIC MODELS

Of the eleven Line Islands seamounts surveyed for paleomagnetic analysis, seven gave reliable paleomagnetic results. Several seamounts in the chain had been surveyed previously, but only one, L3, gave reliable results (Harrison et al., 1975). The locations of these seamounts are shown in Figure 5.23.

The magnetic models of seamounts L4-L8 are discussed at length in Sections 4.5.6 to 4.5.9 and those of seamounts L1-L3 can be found in the literature (Harrison et al., 1975; Keating and Sager, 1980; Sager et al., 1982). For each model modifications of the seamount's shape improved the match between the observed and calculated magnetic anomalies. The most common modifications were the extension of the lower layers of the seamount below the sea floor and a removal of some of the summit. As discussed in Chapter 4, these modifications have the following geologic interpretations. The bottom extension may in many circumstances represent the flanks of a seamount buried by sediments deposited after its formation (Harrison, 1971). Some bottom extentions or some part of every bottom extension may be the result of a magnetic root of material remagnetized by the magma rising through the crust to form the seamount. The removal of layers from the top of a seamount

model is usually attributed to a low magnetization value for the seamount's summit. Hyaloclastite material, which is nearly non-magnetic, is often found at the summits and on the flanks of seamounts (see Section 2.5) and its presence is commonly cited as the reason for the non-magnetic properties of many seamount summits (Harrison, 1971). In the Line Islands seamount models the bottom extensions ranged from 750 m. to 1750 m. whereas the portions removed from the summits varied from 0 m. to 1375 m. The deep bottom extensions are probably a result of the bottoms of most Line Islands seamounts being buried by the thick turbidite fans, shed by the Line Islands ridge, that blanket much of the sea floor in the region (Orwig, 1981). Also, the fact that most of the models had some of the summit removed is in accord with the observation that hyaloclastite is commonly dredged from Line Islands seamounts (Natland, 1976; Keating and Sager, 1980).

The models of seamounts L2, L4-L7 required further modifications. L2 was hypothesized to have a reversely magnetized summit resting on a normally polarized base (Sager et al., 1982). L6 was modeled as having two small reversely polarized areas within the bulk of a normally polarized body as well as a base with an intensity of magnetization twice that of its summit. L4, L5, and L7 all had significant portions of each edifice considered to be non-magnetic. These models reflect the complex magnetization structure of most Line Islands seamounts. As seen in Figure 5.23, only 8 of 16 seamounts surveyed in and near the Line Islands gave reliable paleomagnetic results. In the case of the four analyzed in the course of this study that gave poor results, all were so grossly inhomegeneous in their magnetic structure as to display

little correlation between the shape of each volcano and its magnetic anomaly.

Probably the timing of volcanism in the Line Islands lead to the inhomogeneous magnetization structures observed in most of these volcanoes. It will be shown below that half of the modeled seamounts appear to have formed during the Eocene indicating widespread volcanism in the chain at that time. The Eocene, like the entire Tertiary, was characterized by frequent reversals of the geomagnetic field. The seamounts with grossly inhomogeneous magnetic structures probably formed over periods of time encompassing several reversals, whereas those that could be modeled may have formed over a shorter period of time or their volcanism may have fortuitously coincided with a period of a single magnetic polarity. In accord with this hypothesis is the observation that most of the seamounts giving poor results are large valcanoes, likely to have taken a longer period of time to form, whereas most of the seamounts that gave good results were small in size. Additionally, the seamounts modeled in the Line Islands that seem to be the most homogeneous are those that appear to have formed during the Late Cretaceous, a time characterized by few magnetic reversals.

5.2.1.2 LINE ISLANDS SEAMOUNTS VGPs

Four of the modeled seamounts (L4-L7) have VGPs well to the north of most Cretaceous seamount VGPs (Figure 4.2, Figure 5.24). One of these seamounts, L4, has been ^{40}Ar-^{39}Ar dated at 41.9±1.1 Ma. (R. A. Duncan, personal communication, 1982). Seamount L5 is directly adjacent to L4 and their VGPs are close together, so they are likely the same age. These two VGPs agree with a paleocolatitude and a paleoequator of Eocene age as well as three other seamount VGPs from seamounts in the eastern Pacific and Hawaiian chain that are probably Eocene or Early Oligocene age (Figure 5.4; Sager, 1983a). The discovery of Eocene volcanic material on a seamount at 9° S in the southern Line Islands (Haggerty et al., 1982) along with the apparent ubiquity of Eocene K-Ar ages from the Line Islands edifices (Schlanger et al., 1982) indicates that the Eocene volcanic episode occurred along a considerable length of the chain. Thus the most likely age of seamounts L6 and L7, which also have high latitude VGPs near the other Eocene poles (Figure 5.4), is also Eocene.

The other four seamounts giving reliable paleomagnetic results have VGPs consistent with Late Cretaceous ages (Figure 5.24). Three of the four have been dated. L2 has K-Ar ages ranging from 81-89 Ma. (Sager et al., 1982) and a ^{40}Ar-^{39}Ar age of 85 Ma. (Schlanger et al., 1982). The ^{40}Ar-^{39}Ar age of nearby L3 is virtually identical at 84-85 Ma. (Saito and Ozima, 1977). L8, located at 7.5° S, appears to be somewhat younger. Fossils dredged from the edifice are of Late

Campanian-Maastrichtian age (J. A. Haggerty, personal communication, 1982).

Because seamount L8 has a reversed polarity, it is possible to refine its age further. The Campanian and Maastrichtian contain only a few reversed epochs. One of these, corresponding to the Gubbio A- interval (Alvarez et al., 1977), occurs between anomalies 33-34. Its age appears to be in the range 78-86 Ma. depending on the geomagnetic time scale being used. The other reversals all occur between about 68-72 Ma. during intervals Gubbio C- and E- (Alvarez et al., 1977) between anomalies 30-33. Because the identified fossil fragments favor the Maastrichtian or Late Campanian, the younger reversed epochs are indicated. In accord with its inferred age of 68-72 Ma., the VGP of L8 falls nearly in the middle of the area where most Pacific paleomagnetic data of Maastrichtian age predicts the pole for that period to lie (Figure 5.5). Another Line Islands seamount, L1, an undated edifice in the northern end of the chain, gives a VGP that is located near the Maastrichtian Paleomagnetic pole, implying that this seamount is most likely Maastrichtian in age.

L2 and L3 have virtually identical $^{40}Ar-^{39}Ar$ ages of 84-85 Ma., yet their VGPs are separated by 22^{o}. This descrepancy was puzzling until the behavior of the Pacific's APWP became apparent (Section 5.1.9). Between 91-81 Ma. the motion of the Pacific paleopole was very rapid, so a difference of only a few million years in the ages of two volcanoes can result in a large difference in the positions of their VGPs. Although L2 has a radiometric age of 85 Ma., its rocks apear to record the Gubbio A- reversal (Sager et al., 1982). The absolute age

of this epoch is not known precisely. According to some geomagnetic time scales (e.g. Ness et al., 1980), it could include the 85 Ma. radiometric age of L2, but other time scales indicate that this reversal can be as young as 78 Ma. (e.g., Van Hinte, 1978). In this study, an intermediate value is assumed for the age of this reveral, so an age of 83 Ma. was assigned to L2 for the Campanian paleomagnetic pole calculation in Section 5.1.4. The VGP of L3, on the other hand, falls in with the VGPs of seamounts in the range 86-89 Ma. Although L3's 84 Ma. age was retained in the calculation of the Santonian paleomagnetic pole (Section 5.1.5), this seamount may be slightly older.

5.1.2.3 TECTONIC IMPLICATIONS FOR THE LINE ISLANDS

Seamount paleomagnetic results from the Line Islands augument the radiometric and fossil age determinations from other seamounts in the chain that were not studied paleomagnetically. Apparently volcanism has been recurrent in the chain with episodes occuring during the Late Cretaceous and Eocene. Because reliable paleomagnetic results are available for only eight Line Islands seamounts, it is impossible to place very rigid constraints on the spatial distribution of the different volcanic episodes. All of the seamounts giving reliable paleomagnetic results in the central part of the chain record Eocene VGPs, implying that the Eocene volcanic pulse may have been heavy there. Together with the identification of Eocene volcanism in the

southern Line Islands, the paleomagnetic data shows that the Tertiary volcanism occurred at least from 8^{o} N to 9^{o} S.

All of the volcanoes having Cretaceous VGPs are located in the north and south ends of the chain. This observation could be misconstrued to imply the lack of Cretaceous volcanoes in the central Line Islands; however, such a hypothesis would be at odds with studies of DSDP cores from this part of the chain (Jackson and Schlanger, 1976) that indicate that Late Cretaceous volcanism also occurred in the central Line Islands.

The southern Line Islands seamount from which Eocene volcanic material was obtained (KD-45 in Figure 5.23) also yielded Late Cretaceous fossils (Haggerty, 1982; Haggerty et al., 1982). These findings imply that the seamount existed during the Cretaceous and reawakened with volcanism during the Tertiary. Of course, from the small amount of material recovered from the seamount it is impossible to determine whether the volcanism occurred only during the Late Cretaceous and Eocene, or whether it occurred continuously or intermittently in the interim. However, the key point is that the Eocene volcanism seems to have occurred on a pre-existing edifice in this instance. Thus it is not clear whether the Eocene seamounts studied paleomagnetically were formed entirely during the Tertiary or whether they represent resurgent volcanism in older volcanoes.

If the Tertiary volcanic event commonly occurred in pre-existing volcanoes, then there exists the possibility that some of the paleomagnetic field directions derived from the magnetic modelling might be misleading. The north Pacific APWP shows that seamounts

formed during the Late Cretaceous probably formed 20-30° south of their present positions. Likewise, Eocene seamounts have undergone about 13° of northward drift since their formation. Thus the maximum difference in the inclination of the two periods at any point in the chain is about 24°. If the Eocene volcanic rocks make up the majority of a given volcano, then it probably will give an Eocene VGP when modeled. Rice et al. (1980) suggest that only 40% of a volcano need be comprised of the younger material to effectively remagnetize the entire edifice. On the other hand, if the amount of Eocene volcanism is small, its magnetic properties should not greatly affect the Cretaceous magnetic signature. Between the two extremes will be seamounts combining both Cretaceous and Eocene magnetic directions. If the distribution of the volcanic material from both periods is relatively uniform throughout a seamount then the paleomagnetic direction calculated from its magnetic anomaly should be the vector sum of the magnetizations of the two periods. If the Eocene volcanism occurred on a seamount during a reversed epoch or if the newer material only remagnetized part of the edifice, the resultant magnetic anomaly may be complex. This might explain why many Line Islands seamounts seem to have complicated anomalies. The only seamounts having apparently reliable models that might be adversely affected by remagnetization would be those of the four Cretaceous edifices (L1-L3,L8). Although L1 is of uncertain age and might be affected, L2, L3, and L8 all have VGPs consonant with other paleomagnetic data of similar age. Hence, remagnetization does not appear to have occurred in these seamounts.

The paleomagnetic data gives interesting insights to the evolution of the Line Islands, but not their origin. It appears that the Line Islands were a long chain of seamounts and islands during the Cretaceous (Jackson and Schlanger, 1976; Haggerty et al., 1982) extending through most of the present day length of the chain. The data presented here favors no one of the proposed genetic mechanisms. However, the results presented here clearly demonstrate that the volcanic history of the Line Islands has been complex and that a very detailed study of the chain will be necessary to sort out the various phases of its evolution.

The paleomagnetic data can be used to infer something of the timing of the Eocene volcanism. All of the Eocene seamount VGPs group together very closely as seen in Figures 5.4 and 5.24. This behavior suggests that the Eocene volcanism was short-lived. Although the "far-sided-effect" that causes Miocene and perhaps Oligocene Pacific paleomagnetic poles to be located in the same region seems to invalidate this conclusion, a detailed study of the timing of this effect (Epp et al., 1983) indicates that this bias was small prior to about 24 Ma. Hence, if the Eocene volcanic pulse were of long duration, say 5-10 Ma. before or after the mean age of these poles, a greater smearing of the pole positions along the APWP would be expected.

The age inferred for the Eocene paleomagnetic data, approximately 41-42 Ma., seems to be significant. These seamounts were probably formed at about the same time that the Hawaiian-Emperor bend records a large change in the direction of the Pacific plate's motion with

respect to the mantle. As shown in Figure 5.23, the motion of the Line Islands chain over the mantle prior to the time of the Hawaiian-Emperor bend was almost along its length. However, after about 43 Ma. the motion of the chain over the mantle is more oblique to its trend. A reasonable hypothesis for the widespread Eocene volcanism in the Line Islands is thus as follows. The Cretaceous Line Islands represented a zone of weakness in the lithosphere. This zone of weakness might have resulted from an abandoned spreading ridge, a fault zone, or even lithosphere thinned by the thermal effects of a hotspot. Volcanism in the Line Islands resumed during the Eocene because of a large change in the intra-plate stress field. During the Cretaceous and early Tertiary the Pacific's motion suggests that the stress was more or less along the long axis of the chain; however, in the Eocene the stress orientation changed so that it was more oblique to the chain, tending to pull apart previously healed cracks and fractures in the crust and lithosphere. A similar mechanism has been proposed for resurgent volcanism in the Mathematicians Seamounts (Vanko and Batiza, 1982; Watkins et al., 1982). If this hypothesis is true, then contemporaneous volcanism should be found in many other Pacific seamount chains. Perhaps the Eocene volcanic material underlying the limestone cap of Enewetak Atoll in the Marshall Islands (Ladd et al., 1953; Kulp, 1963) is evidence of this event.

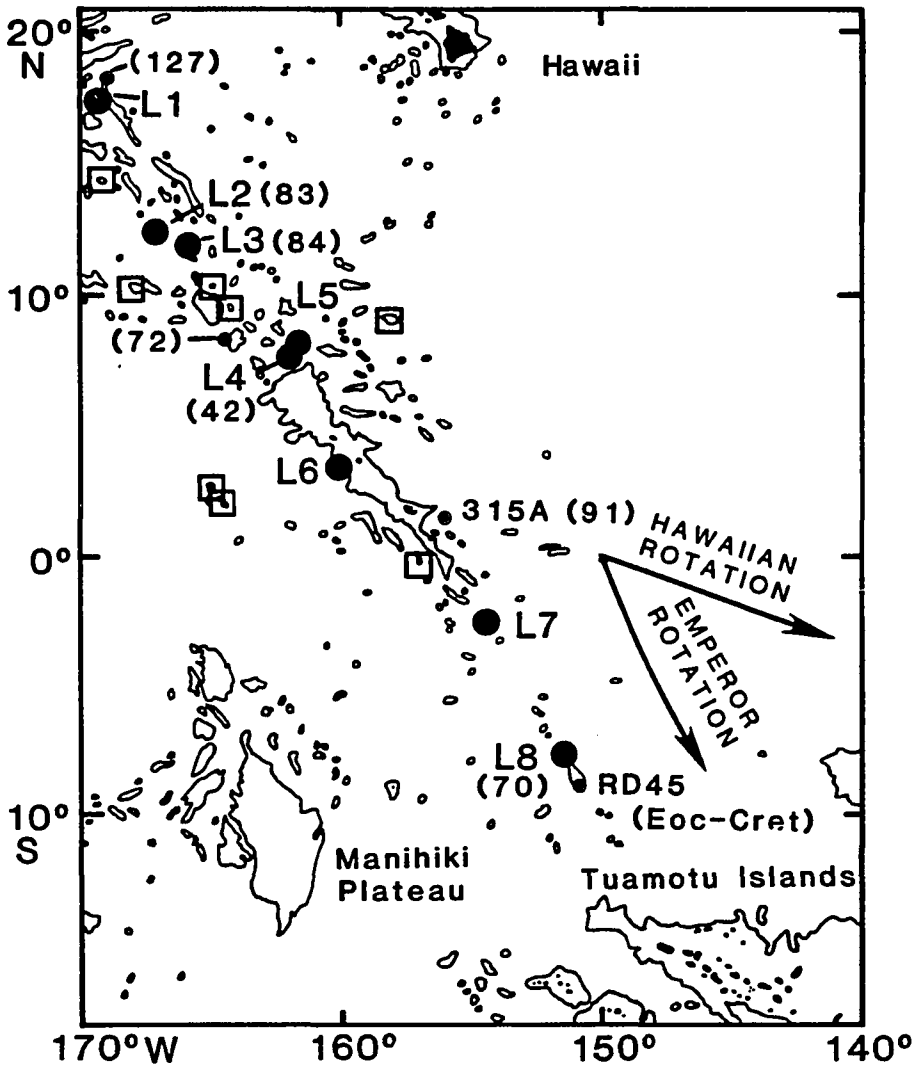

Figure 5.23 Locations of Line Islands seamounts used for paleomagnetic analysis. Large filled circles show locations of seamounts that gave apparently reliable results. Boxes show seamounts that have given apparently unreliable results. Small dots show dated edifices; ages given in parenthesis. Location of RD-45 mentioned in text is also shown. Arrows show the direction of the motion of the mantle with respect to the lithosphere just before and after 43 Ma.

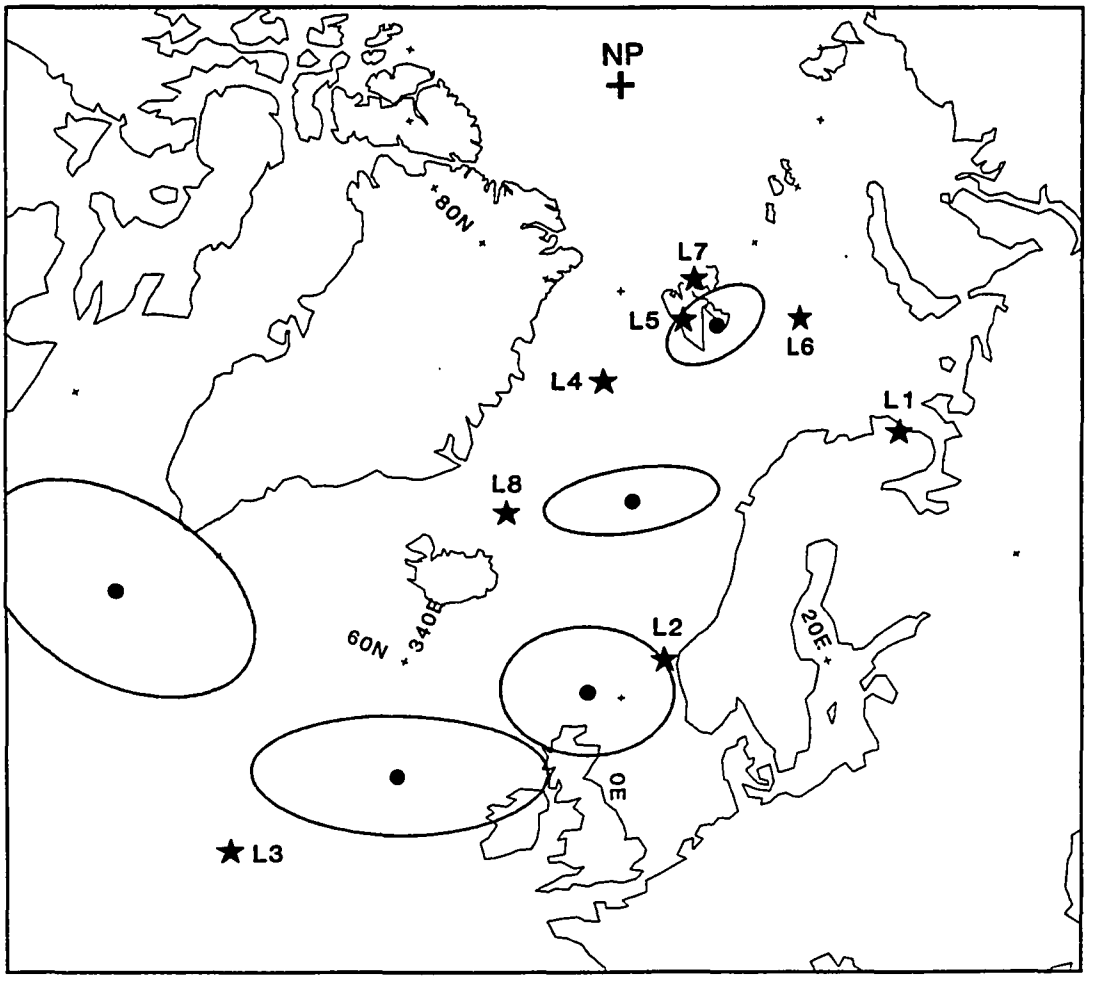

Figure 5.24 Comparison of Line Islands VGPs with paleomagnetic poles. VGPs are shown as stars; paleomagnetic poles, as in Figure 5.2. Map projection is polar equal area.

5.2.2 PALEOMAGNETISM OF MUSICIANS SEAMOUNTS

To the northwest of the Hawaiian Islands is a province of seamount and submarine ridges known as the Musicians Seamounts (Figure 5.25). These volcanoes were apparently formed by Cretaceous volcanism, but their origin remains obscure. Much of our present knowledge of this province comes from a large number of north-south magnetic and bathymetric tracklines run through the region by the National Oceanic and Atmospheric Administration during the mid-1960's (Rea, 1969). During the summer of 1980 two Hawaii Institute of Geophysics cruises sailed to the Musicians Seamounts for the purpose of collecting geologic samples and geophysical data. Six seamounts were surveyed especially for paleomagnetic study to complement the four that had previously yielded paleomagnetic results (Harrison et al., 1975). Paleomagnetic studies were also made of seven additional Musicians Seamounts combining the HIG and NOAA data.

Because the southern boundary of the Musicians province is not well defined, it is appropriate to include discussion of the paleomagnetic results from seamounts around the Hawaiian Islands in this section. Many seamounts in this region have previously been studied paleomagnetically (Richards et al., 1967; Francheteau et al., 1970). Five new reliable paleopoles are presented in this study for seamounts in the vicinity of the Hawaiian Islands; four of these are pertinent to the following discussion. These new paleopoles along with the ten new reliable paleopoles from the Musicians province brings the total number of seamounts giving reliable results in this region to 24,

making it the most intensely studied region in the world using seamount paleomagnetism.

Several prominent bathymetric trends are seen in the Musicians Seamounts (Figure 5.25). The most characteristic feature of the province is a series of east-west ridges in the eastern Musicians. The best developed and most regular of these ridges occur in the southeast part of the province, south of the Murray Fracture Zone. Those to the north of the fracture zone are less regular, associated with many large seamounts, and are located on a broad uplift called the "Musicians Horst" by Rea and Naugler (1971). Two chains of seamounts are evident in the Musicians. One begins at about 34^{o} N, 167^{o} W and trends to the southeast until it meets the Murray Fracture Zone. Its continuation to the south of the fracture zone is uncertain. The other seamount chain runs almost due north-south along 162^{o} W. It begins in the area of the Musicians Horst and apparently continues past the Murray Fracture Zone south to the vicinity of the Hawaiian Islands. Interestingly, these two seamount chains intersect near the Murray Fracture Zone at Katchaturian Seamount.

The southeast trending seamount chain occurs along a line where most of the north Pacific fracture zones appear to bend (Rea, 1970). Rea and Naugler (1971) suggested that the Musicians formed by volcanism along zones of weakness in this "bending line." They explained the origin of the east-west ridges by volcanism along short-lived transform faults that were operative during their proposed "bending" and realignment of spreading directions. Four additional hypotheses have been suggested for the mechanism that might have formed the Musicians

Seamounts. They are a pulse of coeval volcanism throughout the entire province, volcanism along short ridge segments as the direction of spreading along the Pacific-Farallon ridge shifted from southwest-northeast to east-west (Moberly et al., 1983), volcanism associated with a single hotspot and its interactions with the ridge crest, and volcanism associated with two hotspots and the interaction of the first with the ridge (Epp, 1978; Moberly et al., 1983).

Moberly et al. (1983) favor the latter of these models. Their scenario for the formation of the seamounts in the province proceeds as follows (Figure 5.26). They hypothesize that the age of the sea floor beneath the northern Musicians is 90-100 Ma. whereas that beneath the southern Musicians is 80-85 Ma. old. The first volcanism in the province erupted in the northwest edifices of the southeast trending chain. These seamounts began to form when a hotspot, previously located beneath the Farallon plate, passed under the spreading center and beneath the Pacific plate at about 100 Ma. From 100-88 Ma. the southeast trending chain formed as the Pacific passed northwest over the hotspot. The northern east-west ridges formed along transform segments between the ridge crest and the hotspot as the direction of spreading reoriented slightly. At approximately 88 Ma., the hotspot passed beneath the Murray Fracture Zone back to the Farallon plate thereby terminating the southeast trending chain. However, soon thereafter the hotspot either returned to the Pacific plate or the spreading ridge jumped to the hotspot and the southern east-west ridges were formed along transform faults between about 85-80 Ma.

At approximately 75 Ma. another hotspot began to move through the region. Its initial eruptions were in the northern Musicians where it paralleled the older hotspot chain. At 70 Ma. it lay beneath the Musicians Horst and contributed to the volcanic pile already there. From 70-60 Ma. the Pacific plate moved north over this hotspot to create the south trending chain of seamounts. The beginning and end of this hotspot chain are obscure as there appears to be no significant trail of volcanoes to the north of the Musicians or to the south of the Hawaiian chain to record where this hotspot came from or where it went.

5.2.2.1 MUSICIANS SEAMOUNT PALEOMAGNETIC MODELS

Paleomagnetic models for ten seamounts in the Musicians province are discussed in Sections 4.5.10 to 4.5.19. The four models of seamounts in the vicinity of the Hawaiian Islands are presented in Sections 4.5.2, 4.5.3, and 4.5.5. The only reversely polarized edifices in the entire region are the eastern tip of the Rameau Ridge, the southernmost large east-west ridge, and Paumakua Seamount (H12), located just to the south of the Rameau Ridge. With few exceptions, the Musicians Seamounts analyzed paleomagnetically have very simple and smooth magnetic anomalies apparently resulting from homogeneous internal magnetization distributions. Because of the simplicity of most of their magnetic anomalies, the GFRs of the Musicians Seamounts are generally high; the mean GFR for the 14 Musicians in Table 4.1 is 4.6.

Unlike the Line Islands seamount models discussed in Section 5.2.1, the Musicians models rarely required large sub-sediment extensions. All but three had 250 m. or less added below the ocean bottom. Of these three, two had 500 m. extensions, and the third had a 950 m. extension of uncertain significance because of the limited areal sampling of the mountain's magnetic anomaly (Section 4.5.11). The lack of large bottom extensions on these seamount models is in accord with seismic reflection and refraction studies indicating that the sedimentary cover in the region is thin (Wallin, 1982).

The amount of summit removed from Musicians Seamount models varied considerably. Four seamounts (M4,M8,M11,M12) had unmodified tops. The rest have from 250 m. to 750 m. of summit removed. No obvious regional trend exists for the summit modifications. They apparently reflect individual variations in the character of the volcanism of each seamount.

Like the Musicians Seamounts, H5, H6, and H12 all have simple anomalies. None of the models of these three seamounts required an extension of the bottom, but each had 500 m. to 750 m. removed from its summit. In contrast, seamount H1, located near the islands of Oahu and Kauai, required a deep (1000 m.) bottom extension to match its magnetic anomaly. Seismic reflection data taken just to the south of this seamount show deep accumulations of sediment derived from the Hawaiian Islands (Wallin, 1982) that help explain the need for this bathymetric modification. The best model of H1 also required the removal of 800 m.

of its summit and gave a magnetization direction close to the present-day geomagnetic field direction. An interpretation of this paleomagnetic direction is given in Section 5.2.3.

5.2.2.2 MUSICIANS SEAMOUNTS VGPS

VGPs from the Musicians Seamounts and those from the seamounts around the Hawaiian Islands are shown in Figure 5.27. In both groups the VGPs are seen to lie generally near the APWP (except the VGP from H1) from Turonian-Santonian age to Maastrichtian age. One remarkable aspect of the VGP distribution of the Musicians Seamounts is the tendency for the VGPs of neighboring seamounts to fall close together. Notice that M4, M6, and M11, from the western central Musicians, have VGPs located between the Turonian and Santonian paleomagnetic poles. The M1-M3 VGPs are located between the Campanian and Santonian paleomagnetic poles. The VGPs for M7-M10, from the northern Musicians, are all located between the Maastrichtian and Campanian poles. Also, the VGPs for M11, M12, and H12, located in the southern east-west ridges or slightly further south, fall in a small group near the Maastrichtian paleomagnetic pole. These observations suggest that this paleomagnetic data is quite accurate and that for the most part the differences between Musicians VGPs are the result of age differences or tectonic motion rather than scatter resulting from imperfect determination of the paleomagnetic directions.

This apparent accuracy is indeed fortunate, for few seamounts in the region have been dated and the paleomagnetic information can be used to infer the temporal distribution of volcanism in the province. The dated seamounts in the area are shown in Figure 5.28. Seamount H3 and Cross seamounts, just south of the Hawaiian chain, have K-Ar ages of 87.7-91.3 Ma. and 81.0-87.7 Ma., respectively (Dymond and Windom, 1968). Paumakua (H12) and Kauluakalana (H1) seamounts have K-Ar ages of 65 Ma. and 80 Ma. (M. Pringle, personal communication, 1982); whereas, the only dated Musicians edifices are Rachmaninov (M4) and Katchaturian (M6) with K-Ar ages of 88.8 Ma. and 66.9 Ma. (Clague and Dalrymple, 1975).

In Figure 5.28 an age has been assigned each of the seamounts in the Musicians-Hawaii region depending on the position of its VGP along the north Pacific APWP. These inferred ages are called magnetic ages to distinguish them from more reliable age dates (e.g., K-Ar, ^{40}Ar-^{39}Ar). In an attempt to quantify the accuracy of these VGPs, the distance of each from the APWP was measured. Along the APWP, tectonic motion of the paleopole is impossible to separate from modeling errors; however, the VGP scatter perpendicular to the APWP should be nearly independent of the tectonic motion. Therefore, the distances of the VGPs from the APWP provide a one dimensional estimate of the VGP scatter. The mean error for the Musicians VGPs is 2.5° and for the Hawaiian area VGPs (excluding H1) it is 4.2°. Using Fisher statistics, the 95% confidence interval of the Musicians VGPs is $\pm 1.7^{\circ}$ and that of the Hawaiian area VGPs is $\pm 3.7^{\circ}$. Combined, the two groups yield a 95%

confidence interval of $\pm 1.8^{o}$. As the slowest rate of APW that occurred between the Turonian and Maastrichtian is 0.75^{o}/Ma., these estimates suggest that the magnetic age of a Musicians seamount should have a resolution of about 2-3 Ma. and for a seamount in the area near Hawaii, the resolution should be about 5 Ma. However, the danger of making this sort of inference is that a seamount of 80 Ma. age, for example, might have a VGP that falls closer to the Maastrichtian paleomagnetic pole, where it should be found, because of inaccuracies inherent in the process of determining a paleomagnetic direction from a seamount. In such an instance the magnetic age may be misleading, so it is advisable to look for patterns in the magnetic ages of seamounts rather than placing too much emphasis on individual magnetic ages for making tectonic interpretations.

The magnetic ages of the seamounts in this region can be divided into four age categories: between Turonian-Santonian (M4,M6,M11,H3,possibly M2), Campanian (M1,M3,M10,H2,H9,possibly M2,H8), between Campanian-Maastrichtian (M7,M8,M9,M14,H7), and Maastrichtian (M12,M13,H5,H6,H10,H12,possibly M5,H4). The magnetic ages for M4, H3, and H12 are in accord with their K-Ar ages, as expected because these seamounts were used in the calculation of the APWP. Additionally, the Maastrichtian paleocolatitude from GPC3, located to the east of the Musicians, agrees with the VGP from Maastrichtian aged H12, implying that the agreement of the seamount's K-Ar and magnetic ages are not fortuitous. In contrast, M6 has an magnetic age of Turonian-Santonian, but its K-Ar age is Maastrichtian. However, this particular K-Ar age is not considered to be accurate on technical grounds (Moberly et al.,

1983). Also, a large difference exists between the apparent and K-Ar ages of seamount H1. This seamount has a magnetization vector close to the present direction of the geomagnetic field and thus its magnetic age is zero. In this case, the K-Ar age of 80 Ma. is probably the better estimate of the seamount's true age because the paleomagnetic direction may be the result of a large induced component of magnetization.

5.2.2.3 TECTONIC IMPLICATIONS FOR MUSICIANS-HAWAIIAN SEAMOUNTS

Even a cursory examination of the magnetic ages of the Musicians is enough to dispel any notion that these seamounts formed by any simple mechanism. Volcanism seems to have occurred in the province over a span of about 25 Ma. from the Turonian to the Maastrichtian. There is a general trend for volcanoes to have younger magnetic ages from west to east. Thus the hypotheses that these seamounts formed by coeval volcanism or from a single hotspot appear untenable.

The two hotspot model of Moberly et al. (1983) fares poorly as well. Although their prediction that some of the seamounts in the Musicians Horst region should be borderline between Maastrichtian and Campanian in age appears to be substantiated, almost all of their other predictions do not fit the magnetic ages. First of all, both the southeast and south trending seamount chains in the northern Musicians appear to have age progressions in the opposite direction to that predicted by the two hotspot model. The oldest seamounts in these two

chains are near the Murray Fracture Zone whereas the apparently younger ones are further north. If this age progression is correct, then these chains could not have been formed by hotspot volcanism as they would imply (against all other evidence) that the Pacific plate was moving southward with respect to the mantle during the Late Cretaceous. Another discrepancy between the magnetic ages and the two hotspot model is the apparent Maastrichtian ages of the seamounts in the southeast Musicians predicted to have an age of 80-85 Ma. by Moberly et al. (1983).

Rea and Naugler's (1971) bending line hypothesis appears to be untenable as well. A zone of weakness may underlie the Musicians, and this zone of weakness may relate to the mechanism that makes the fracture zones in the northern Pacific seem to bend, but a source of volcanism that could give rise to the observed pattern of magnetic ages is difficult to imagine. The reorienting ridge hypothesis does not seem to work either. According to the magnetic age map (Figure 5.28), many of the seamounts were formed either during or just prior to the Maastrichtian. By that time, the spreading ridge, as shown by anomalies 30-32 on magnetic anomaly maps, was far to the east (Moberly et al., 1983). Consequently, in order to make this hypothesis workable, one must postulate a large eastward jump of the Pacific-Farallon ridge at the close of the Cretaceous.

The magnetic age map also implies that the volcanism that formed the eastern Musicians Seamounts also occurred further south. To the south of the Hawaiian Islands, seamounts H4-H6 have VGPs interpreted as Maastrichtian. Seamount H10, to the east of Hawaii, also has a

Maastrichtian apparent age. These Maastrichtian volcanoes appear to be superimposed upon older volcanoes as these seamounts are surrounded by edifices with apparent and K-Ar ages ranging from Campanian to Turonian.

Rather than giving a clear picture of the tectonic processes that formed the Musicians Seamounts, the seamount paleomagnetic results have confounded the issue. None of the proposed models for the evolution of the province seem to easily explain the paleomagnetic results. The paleomagnetic data appears to be very consistent, but the overall picture it gives makes it difficult to derive a tectonic model. This problem may result from several phases of superimposed volcanism in the area or there may have been relative tectonic displacements or rotations of small crustal blocks that make the magnetic ages misleading. For example, the difference between the predicted and apparent ages for M1-M3 was cited in Section 5.1.10 as possible evidence of a block that may have been decoupled from the rest of the Pacific. Although there is no evidence for a plate boundary to set off these seamounts from the rest of the Pacific, it must nonetheless be conceeded that the Musicians are a complex group of seamounts and that it will be very difficult to decipher the course of events that occurred in the region without better age control. Until such data is available, the conclusions based on the magnetic ages must be considered tentative.

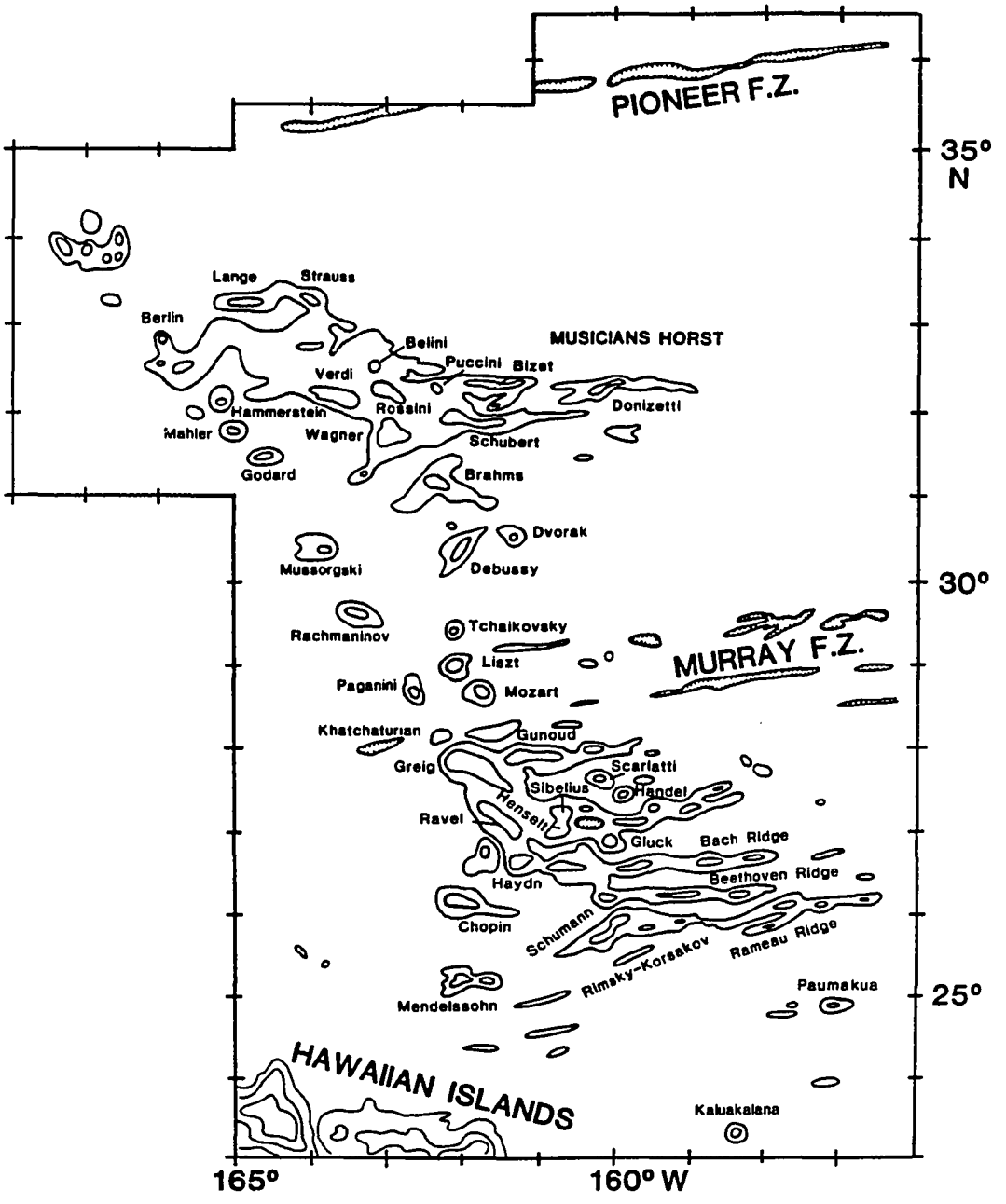

Figure 5.25 Sketch map of Musicians Seamounts showing major edifices and trends. (redrawn from Rea and Naugler, 1971).

Figure 5.26 Two hotspot model for the formation of the Musicians Seamounts. Details given in text. (from Moberly et al. 1983)

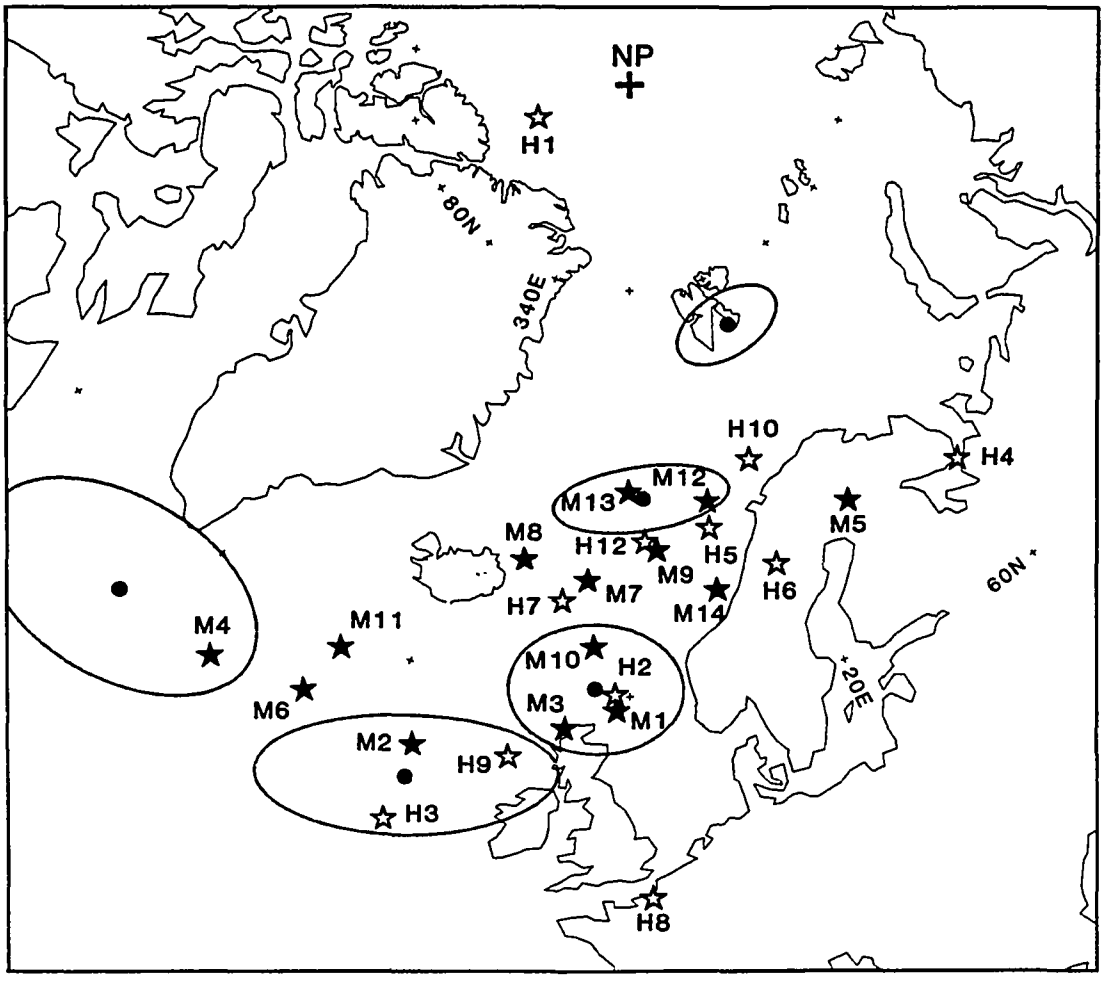

Figure 5.27 Comparison of Musicians and Hawaiian area seamount VGPs with the north Pacific paleomagnetic poles. Musicians VGPs are shown by solid stars; Hawaiian area VGPs are shown by open stars. Map projection is polar equal area.

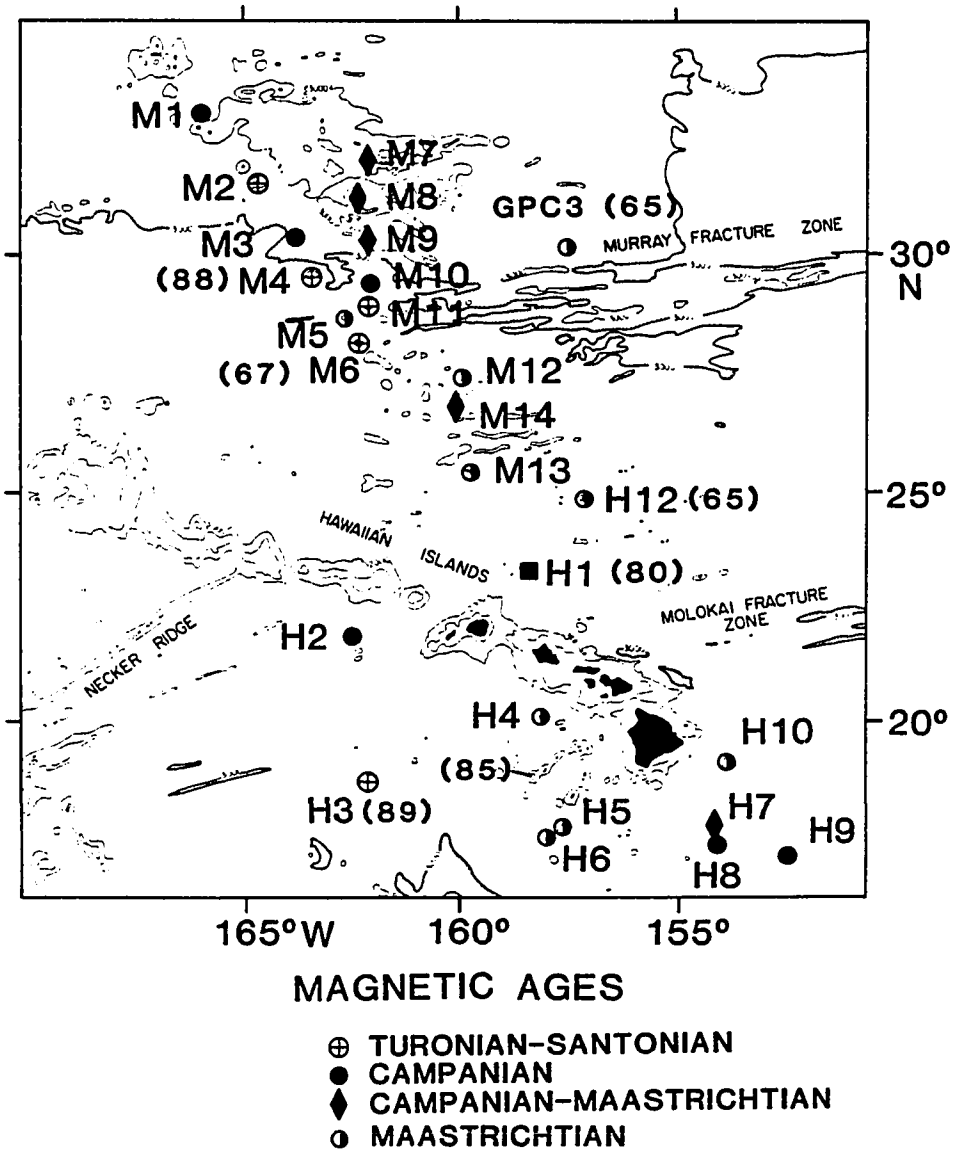

Figure 5.28 Magnetic ages for Musicians and Hawaiian area seamounts. Radiometric ages and fossil age (GPC3) are given in parenthesis. See text for definition of magnetic age.

5.2.3 PALEOMAGNETISM OF OTHER SEAMOUNT GROUPS

Comparing Figure 4.2 with Figure 5.2, it can be seen that the trend of the seamount VGPs follows the trend of the APWP in a general way. As many of the VGPs fall near the APWP, it seems that the technique of assigning magnetic ages to undated seamounts, as done in the analysis of the Musicians Seamounts, may be used to advantage elsewhere. However, magnetic ages are difficult to define for most of the western Pacific seamount groups because of the age ambiguity where the APWP doubles back on itself. Seamounts with VGPs in the area of the Atlantic west of England and south of Greenland may have either Early Cretaceous or Late Cretaceous ages. In the interpretation of the Musicians and Line Islands seamounts it was possible to make a distinction because these seamount chains are on sea floor that is most likely Late Cretaceous in age. Also, most of the VGPs from these two groups are located along the APWP from Santonian to Eocene where there is no age ambiguity. Be that as it may, some useful observations can still be made about several groups of western Pacific seamounts.

Seamounts C1-C5 are an interesting group because, judging from their VGPs, they appear to be much younger than the sea floor upon which they rest. All of these seamounts are located in the central Pacific basin between the equator and the Mid-Pacific Mountains. C3-C5 are on sea floor containing the Phoenix group of magnetic lineations (Larson, 1976). C1 and C2 are on apparently older seafloor further to the north. It is impossible to give a magnetic age for C5 because its VGP is located on the ambiguous section of the APWP (Figure 5.29a) and

the sea floor beneath it appears to be Early Cretaceous or older.

On the other hand, C1-C4 all have VGPs that are located somewhat to the east of the Maastrichtian pole. Their Fisher pole is at 66.9° N, 17.0° E and has an A_{95} of 8.2°. This circle of confidence overlaps most of the Maastrichtian pole's error ellipse and thus a magnetic age of Maastrichtian can be assigned to these seamounts. Because none of these seamounts are dated, it is impossible to ascertain whether they really are on the order of 50 Ma. younger than the underlying crust, or whether some tectonic displacement (such as that discussed in Section 5.1.10) has caused a misleading paleomagnetic direction.

The five seamounts in the Mid-Pacific Mountains also give interesting results. Only one of these, P5, has been dated. This volcano, Darwin Guyot, has a minimum age of 106-109 Ma. from coral fragments dredged from its flanks (Harrison et al., 1975). It is not actually located on the uplift that underlies most of the other Mid-Pacific Mountains to the south of it (Nemoto, in preparation) and its VGP is by far the farthest south of any of those of the Mid-Pacific Mountains studied (Figure 5.29b).

All of the other Mid-Pacific Mountains have magnetization directions implying less than 20° of northward drift. However, their declinations vary greatly. The VGP for P1 is at the extreme western end of the Pacific VGP distribution, perhaps because of its low reliability (Section 4.5.20). In contrast, the VGP of P2, with a GFR of 2.7, falls among the Maastrichtian poles. The VGPs of P3 and P4 lie

in Greenland where Jurassic age VGPs might be expected according to Figure 5.2. Nemoto (in preparation) suggests that the plateau upon which P1-P4 rest is Jurassic in age. Perhaps P3 and P4 are the same age as the underlying uplift.

The large scatter of the Mid-Pacific Mountains VGPs indicates that magnetic ages assigned to these edifices may be unreliable. The scatter may be caused by actual age differences among the edifices, or it may be a result of the magnetic interference of the underlying plateau in the modeling process.

Three other seamounts have VGPs that fall near the geomagnetic north pole (Figure 5.29c). Each seamount (H1,W10,W12) has a high GFR, so the magnetization vector derived from each seamount should be reliable. In Section 2.7 it was demonstrated that a seamount whose magnetization is predominantly induced should have its VGP located near the geomagnetic pole. That certainly seems to be the case for these three seamounts; however, in all of the analyses of the other seamount VGPs, none of those used for the pole calculations was obviously biased by an induced component. If some seamounts are as greatly affected as H1, W10, and W12 appear to be, then it seems probable that some others ought to be affected to a lesser extent, but at least measureably so. Perhaps as more seamount paleomagnetic results become available, such seamounts will become more obvious.

It is possible, however, to give alternative explanations for the positions of the three VGPs. Although it has a K-Ar age of 80 Ma., H1 may record the present geomagnetic field direction because of remagnetization of the volcano by recent volcanism. It is located on

the Hawaiian arch in an area where volcanism less than a few million years old has been postulated to have occurred because of the flexing of the lithosphere by the weight of the Hawaiian Islands (Normark and Shor, 1968; Wallin, 1982). W10 and W12 may also have recorded recent episodes of volcanism, although they are in a section of the Pacific where recent volcanism is unexpected. Alternatively, as these two seamounts are on sea floor that appears to be Jurassic in age (Hilde et al., 1977), they may record a Jurassic paleofield direction that is even further north than the polar circle predicted by the Site 307 paleocolatitude in Figure 5.2.

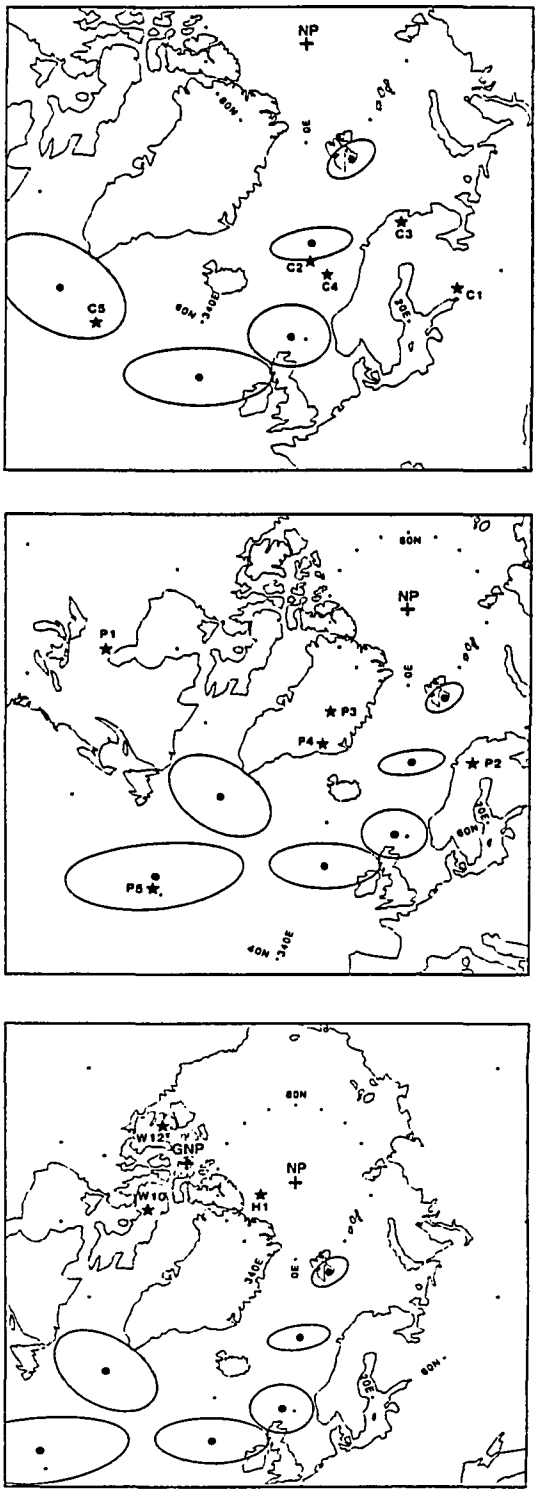

Figure 5.29 Comparison of other seamount VGPs with paleomagnetic poles. (a) central Pacific basin seamounts; (b) Mid-Pacific Mountains seamounts; (c) seamounts showing possible induced magnetizations.

TABLE 5.1 CRETACEOUS AND EARLY TERTIARY PALEOMAGNETIC POLES

Age (Ma.)	Location		95% Confidence Ellipse		
	Lat(N)	Lon(E)	Semi-Axis Length Major	Minor	Azimuth of Major Axis
41 ± 5	77.5	21.2	2.9	1.5	77
68 ± 3	69.8	1.6	4.1	1.6	83
81 ± 3	60.3	357.0	3.9	3.2	89
87 ± 3	54.4	342.6	6.8	3.0	71
91 ± 4	55.4	315.7	6.7	4.5	76
104 ± 6	41.4	317.5	11.3	4.1	35
119 ± 12	57.9	339.2	10.8	3.5	66

TABLE 5.3 PACIFIC PLATE/HOTSPOT ROTATION POLES AND RATES

Age Range (Ma.)	Position Lat(N)	Position Lon(E)	Backtracked Position Lat(N)	Backtracked Position Lon(E)	Rate (°/Ma.)
0- 1	36	284	36.0	284.0	0.9
1- 16	69	280	68.9	278.6	0.9
16- 20	78	237	74.1	234.9	0.9
20- 43	59	306	62.6	313.6	0.7
43- 67	15	255	9.3	283.2	0.75
67-140	36	284	41.2	294.1	0.75

Reference: Epp and Tuthill (in preparation)

5.4 CONCLUSIONS

This study has examined many aspects of seamount paleomagnetism: the method itself. the tectonic implications from seamount paleomagnetic data for the Pacific plate as a whole, and the inferences of this data for the spatial and temporal distribution of volcanism in several seamount chains and groups. Accordingly, the conclusions that follow are divided into three sections addressing each of these topics.

5.4.1 SEAMOUNT PALEOMAGNETIC MODELING

A detailed examination of the assumptions made in modeling seamounts for paleomagnetic study pointed out several problems that can result in misleading results. The greatest source of error seems to arise from assuming an inhomogeneously magnetized seamount to be homogeneously magnetized. Often, such inhomogeneity appears to be caused by a seamount's eruptions spanning a geomagnetic polarity change. However, the remagnetization of a volcano by resurgent, post edifice building volcanism may also be a factor. An additional source of inhomogeneity is a laterally asymmetric distribution of non-magnetic material within a seamount. Many seamounts have non-magnetic summits, but this inhomogeneity is rarely a problem. It usually does not significantly bias the magnetization vector derived from the seamount and it can be easily modeled by removing the top layers of the

bathymetric model of the seamount. However, if the non-magnetic material is concentrated more on one flank of the volcano, misleading paleomagnetic results may be obtained if the edifice is assumed to be homogeneously magnetized. Although this problem does not appear to affect most submarine basaltic volcanoes, it may be a major source of error for the modeling of more explosive, ash-producing island arc volcanoes.

Useful paleomagnetic models can be constructed for some inhomogeneously magnetized seamounts by explicitly including sections of the seamount that are either non-magnetic or of opposing polarity. This technique often works if the volume of the inhomogenieties within the volcano are small. In any case, paleomagnetic results from inhomogeneously magnetized seamounts must be treated with care and compared for reliability to the results of other seamounts of similar age from the same plate. Because goodness of fit parameters do not always indicate poor results, this sort of test is a wise procedure for all seamount paleomagnetic results.

Another source of error in the determination of seamount paleomagnetic vectors arises from interfering crustal magnetic anomalies. The GFRs of seamounts located on seafloor containing large amplitude magnetic lineations are usually low and their VGPs are often more scattered than those of seamounts located on magnetically homogeneous seafloor. An example of this effect are the Tripod Seamounts from the eastern Pacific. Low GFRs and scattered VGPs are also characteristic of the Mid-Pacific Mountains modelled here. The reason appears to be that these seamounts are located on a plateau that

produces a magnetic field that interferes with the modeling of the seamounts resting on it. In contrast, homogeneously magnetized seamounts located on magnetically quiet seafloor often have high GFRs and display very small amounts of VGP scatter. The Musicians Seamounts are a good example of this phenomenon.

The seamount paleopoles were also examined for possible bias caused by either induced magnetization or the demagnetization effect. Demagnetization factors were calculated for several groups of seamount VGPs of approximately the same age using a least-squares procedure. In no case was the demagnetization factor significantly different from unity, indicating that the bias caused by the demagnetization effect is small. The bias caused by induced magnetization also appears to be small. In every case in which well-dated, reliable seamount paleomagnetic data was combined with other paleomagnetic data of the same age to calculate a mean paleomagnetic pole, the seamount data was in excellent agreement with the other data. However, three seamounts have VGPs that fall near the geomagnetic north pole and it was explained that these VGP positions might result from induced magnetism. If this conclusion is true, then the magnetization of each of these seamounts must be almost entirely induced. The fact that no other seamounts give results suggesting any significant induced component is puzzling and may indicate that some other factor may be responsible for the unusual VGP positions.

An additional source of error in the determination of seamount paleomagnetic vectors is the assumption that the seamount magnetic anomaly contains a planar regional field. In some instances the use of

a planar regional may be justified, but most authors have routinely included it in every model. All of the seamounts studied here have magnetization parameters calculated both with and without a planar regional. The scatter in VGPs is clearly greater for the models including the planar regionals, implying that their use should be less universal.

5.4.2 PACIFIC PLATE TECTONICS

VGPs from 26 seamounts having apparently reliable radiometric, fossil, or inferred ages were combined with available DSDP paleomagnetic data, magnetic lineation skewness inclinations, and DSDP equator transits to calculate seven mean paleomagnetic poles defining the APWP of the north Pacific. These paleopoles represent the Eocene, Maastrichtian, Campanian, Santonian, Turonian, Albian, and Barremian.

For the Tertiary and Late Cretaceous (81 Ma. to present), the APWP is a refinement of previously published studies. Along this section of the polar path a relatively continuous northward drift of the Pacific plate is indicated. The apparent polar wander along this segment of the APWP is modified by non-dipole geomagnetic field components and true polar wander. The results of this study agree with published accounts suggesting that there was a significant "far-sided effect" caused by persistant non-dipole magnetic field components in the late Tertiary and that true polar wander displaced the paleomagnetic data of Cretaceous-Tertiary boundary age towards the Pacific by about 12^{o}.

The oldest part of the APWP begins along the polar circle of the paleocolatitude from basalts cored at DSDP Site 307, of Late Jurassic age. A southward drift of the Pacific plate is indicated from the Jurassic until some time in the Early Cretaceous. During the Albian (about 104 Ma.) the APWP turns sharply from a southwest trend to a northerly trend. Another abrupt bend occured during the Turonian (approximately 91 Ma.) at which time the APWP turns towards the east. Between the Turonian and Campanian the apparent polar wander was very rapid (about 2-5 five times the rates of apparent polar wander recorded since) and almost along a line of latitude. This east-west phase of apparent polar wander crosses the Early Cretaceous segment of the APWP between the Albian and Barremian poles to form a mid-Cretacous loop. At about 81 Ma., the APWP takes another sharp turn, this time to the north, into the familiar Late Cretaceous-Tertiary segment.

The onset of the phase of rapid apparent polar wander is not well constrained in age because of the scarcity of Early Cretaceous paleomagnetic data; however, it appears to have begun about the same time as the Cretaceous Quiet Time. Likewise, the rapid polar wander appears to have stopped at the end of the Cretaceous Quiet Time. This latter finding is better constrained by the paleomagnetic data placing the end of the rapid polar wander within a few million years of 81 Ma. These results amplify the hypotheses of other authors who have noted that the Cretaceous Quiet Time was a tectonically disturbed period for the Pacific with fast spreading, large ridge jumps, and widespread volcanism. Furthermore. these results suggest that disturbances within the mantle and core have a direct effect upon plate motion.

True polar wander and long term non-dipole geomagnetic field components were noted to affect the paleomagnetic data of Late Cretaceous and Tertiary age. Likewise, their effects probably bias the APWP for earlier times so that the observed apparent polar wander cannot be entirely attributed to plate motion. Large discrepancies have been found between the observed and plate/hotspot motion model predicted positions of the paleomagnetic poles for the Early and Late Cretaceous. Such differences have been attributed to true polar wander or non-dipole magnetic field errors; however, no evidence has been found in published true polar wander studies or continental APWPs for the mangnitude of true polar wander or non-dipole components implied by the large discrepancies found here between the observed and hotspot-predicted paleomagnetic pole postions. Hence, it is assumed here that currently accepted models of plate/hotspot relative motion for the Early and Late Cretaceous are inadequate and that the APWP mostly reflects the tectonic movements of the Pacific plate.

A speculative explanation is proposed to explain the pre-Campanian APWP. Southward drift of the Pacific plate caused the Late Jurassic-Barremian paleomagnetic data to be closer to the pole than the later data. During the Albian, the Pacific's southward motion changed to north northwest with respect to the mantle around a pole at 36^{o} N, 284^{o} E. This pole is currently used by several authors to explain Pacific plate/hotspot motion for the entire mid to Late Cretaceous because many Cretaceous hotspot chains are parallel to its small circles. At about 91 Ma. the plate motion shifted abruptly to a rapid rotation (about 3 times the present plate/hotspot rotation velocity) around a pole

estimated to be at about 65° N, 190° E. For most of the Pacific this rotation caused an east-west drift over the mantle. Because the shift in plate/hotspot motion appears to have been nearly 90° and the implied plate/hotspot velocity was high, many of the northwest trending seamount chains that formed during the Albian-Turonian motion end abruptly and do not appear to be connected to any younger chains.

It is proposed here that the Marcus-Wake seamount chain, stretching from the northern end of the Marshall-Gilbert-Ellice Island chain to the Bonin Trench, is a previously unrecognized hotspot chain recording this east-west motion. Additionally, it is proposed that the sharp bend in the APWP at about 81 Ma. records a large change in plate motion that manifests itself in the bend between the Marcus-Wake seamounts and the Marshall-Gilbert-Ellice seamounts. Furthermore, the bend in the northern Emperor Seamount chain is hypothesized to be the result of the same change in plate motion and the segment of the Emperor chain northwest of this bend is shown to be approximately parallel to small circles of the 65° N, 190° E pole. This hypothessis, of course, implies that the present age assigned to the north Emperor bend is about 10 Ma. too young and that the currently accepted value of the plate/hotspot rotation rate around the Emperor pole is too fast.

The validity of the single Pacific plate concept is addressed in this study and it is noted that the agreement among the paleomagnetic data from most of the north Pacific is remarkably good, implying that no plate boundaries have intervened to cause relative motion among any of the data sampling locations. However, it was also noted that

several DSDP sediment paleomagnetic studies (from sites 288A, 289, 315A, 462) consistently record the position of the paleopole to be closer to the geographic pole than the rest of the paleomagnetic data. Some authors have dismissed this discrepancy as an inclination error, but it is consistent between sites and only occurs at several equatorial drilling sites. These data also agree with paleomagnetic data from the south Pacific. Consequently, it is suggested here that the discrepancy may in fact have a tectonic origin with relative motion having occurred between the north and south Pacific. The equatorial and south Pacific paleomagnetic data is too sparse to identify a possible plate boundary or to pin down the beginning and end of the relative motion, but the boundary must allow sites 288A, 289, 315A, and 462 to be connected to the south Pacific be active as recently as 40 Ma.

5.4.3 LINE ISLANDS, MUSICIANS SEAMOUNTS AND OTHER SEAMOUNT GROUPS

Seven new seamount VGPs were calculated for Line Islands seamounts bringing to eight the total number of seamounts in this chain giving reliable results. The paleomagnetic data is consistent with radiometric age dating and other geologic information that indicate that volcanism occurred during the Late Cretaceous and the Eocene. Half of the seamounts giving reliable paleomagnetic results have Eocene VGPs indicating that the Eocene volcanic pulse was pervasive. From the paleomagnetic data alone it is impossible to determine what tectonic

mechanism first formed the Line Islands, but they appear to have been a long, linear chain during the Late Cretaceous. However, the Eocene volcanism appears to have occurred at the same time as the Hawaiian-Emperor bend (about 42-43 Ma.). This volcanic pulse was probably the result of the large change in the intra-plate stress field at that time causing zones of weakness, originally caused by the formation of the Line Islands, to open up allowing magma to ascend from the mantle.

Volcanism in the Musicians Seamounts also appears to have been complex. The Musicians VGPs show very little scatter because of the homogeniety of their magnetizations. Consequently, these VGPs hug the APWP and a magnetic age was assigned to each seamount depending on the location on the APWP of its VGP. The magnetic ages were then used to complement the few radiometric ages from the province. The magnetic ages indicate that volcanism in the Musicians spanned about 25 Ma. from the Turonian to the Maastrichtian. However, the magnetic ages do not agree with any proposed hypothesis for the origin of these seamounts. There is a general trend for the older seamounts to be on the west side of the province and the younger seamounts to be on the east side, but there are no obvious linear magnetic age progressions that would suggest that any of the seamounts were formed by one or more hotspots. The oldest Musicians Seamounts are found near the Murray Fracture Zone. These appear to be Turonian-Santonian in age. The seamounts in the area of the Musicians Horst generally appear to be of Campanian-Maastichtian boundary age, whereas those in the southeast part of the province, near the east-west ridges, appear to be Maastrichtian in age. Several seamounts just to the south of the present day Hawaiian Islands

also have Maastrichtian magnetic ages suggesting that the volcanism that formed the seamounts in the southeastern part of the Musicians province may have been active in this region as well.

Several other groups of seamounts give interesting paleomagnetic results. Four undated seamounts, found on Aptian age or older crust in the central Pacific basin, have VGPs that cluster near the Maastrichtian paleomagnetic pole. Thus it appears that these seamounts may be approximately 50 Ma. younger than the crust upon which they rest. However, with no supporting age information from these volcanoes, the possibility that their young magnetic ages may be caused by tectonic displacement cannot be ruled out.

Five seamounts from the western Mid-Pacific Mountains have been analyzed paleomagnetically. Four of these seamounts are located on a plateau that underlies many of the Mid-Pacific Mountains. The other one is found to the north of this plateau and is the only one of these seamounts that has been dated. It has a fossil age of 106-109 Ma. and was used for the calculation of the Albian paleomagnetic pole. The other seamounts have scattered VGPs. One falls near the Maastrichtian pole, two near the Late Jurassic polar circle from DSDP Site 307, and the fourth is well to the west of most of the Cretaceous seamount VGPs. The scatter appears to be due to declination differences between these seamounts perhaps caused by the interference of the magnetic anomaly of the underlying plateau in the modeling process. All of these seamounts have nearly identical inclinations that indicate an average of only about 20^{o} of northward drift, about $5\text{-}10^{o}$ less than might be expected of mid-Cretaceous seamounts. From the APWP it is seen that seamounts

with this amount of northward drift must either be rather young (Maastrichtian) or old (Early Cretaceous-Jurassic).

APPENDIX A: LINEAR LEAST-SQUARES SOLUTIONS FOR MAGNETIZATION PARAMETERS

In Chapter 2 expressions for the magnetic anomaly of a body in terms of its magnetization parameters were given. It was stated that these expressions could be used to determine the magnetization parameters of a seamount from observations of its bathymetry and magnetic field using a linear least-squares technique. Details of these least-squares calculations are given in here.

Equation (12) from Chapter 2 corresponds to the magnetic anomaly calculated with a constant offset. As this regional field was used for most of the paleomagnetic calculations done in this study, it will be treated first and in greatest detail. The text follows Plouff (1975). Equation (12) is expressed

$$T' = J_l B_1 + J_m B_2 + J_n B_3 + C_o. \qquad (12)$$

Here T' is the total field anomaly at some point in space; J_l, J_m, J_n, the components of the magnetization vector; B_1, B_2, B_3, volume integrals determined from the shape of the magnetic body; and C_o, the constant offset between the observed and calculated magnetic anomalies. In this equation it has been assumed that the susceptibility of the seamount's rocks is zero, i.e., that the magnetization is entirely remanent.

In the linear least squares method, one wishes to minimize the sume of the squares of the residuals, $\sum(T_o - T')^2$, or

$$S = \sum_i (T_o - J_1B_1 - J_mB_2 - J_nB_3 - C_o)^2$$

where T_o is the observed total field anomaly and the summation is over the N field observations of T_o. Therefore, partial derivatives are taken of S in terms of each of the parameters to be determined, i.e., $\delta S/\delta J_1$, etc., and set equal to zero. This procedure yields the following system of equations:

$$\begin{aligned}
C_oN + J_1\sum B_1 + J_m\sum B_2 + J_n\sum B_3 &= \sum T_o \\
C_o\sum B_1 + J_1\sum B_1^2 + J_m\sum B_1B_2 + J_n\sum B_1B_3 &= \sum T_oB_1 \\
C_o\sum B_2 + J_1\sum B_2B_1 + J_m\sum B_2^2 + J_n\sum B_2B_3 &= \sum T_oB_2 \\
C_o\sum B_3 + J_1\sum B_3B_1 + J_m\sum B_3B_2 + J_n\sum B_3^2 &= \sum T_oB_3
\end{aligned} \qquad \text{(A1)}$$

This is an over-determined system of equations linear in J_1, J_m, J_n, and C_o and may be solved by standard matrix inversion techniques. However, in the form of (A1) some of the sums are very large numbers of which significant figures will be lost when stored in a computer. This problem is solved in the following manner (Carnahan et al., 1969; Plouff, 1975). The first of the equations (A1) is solved for C_o,

$$C_o = \sum T_o/N - J_1 \sum B_1/N - J_m \sum B_2/N - J_n \sum B_3/N, \qquad (A2)$$

and (A2) is substituted into the remaining three equations. Defining $B_4 = T_o$; J_1, J_m, $J_n = J_k$ $(k = 1...3)$; and

$$P_{jk} = [\sum B_j B_k - (\sum B_j)(\sum B_k)/N]/N,$$

equations (A1) can be expressed in the matrix form

$$P_{jk} * J_k = P_{4j} \quad (j,k = 1..3) \qquad (A3)$$

and solved for the J_k by standard matrix inversion techniques. C_o is then calculated by substituting the magnetization parameters calculated in (A3) back into (A2). This formulation has an advantage over (A1) because the P_{jk}, called product moments, are generally numbers of the order of unity and thus no significant figures are lost by computer truncation. Additionally, the matrix inversion is made simpler by reducing the size of the matrix from 4x4 to 3x3 and the product moments can be used to calculate statistical parameters as follows.

The variance of the calculation is estimated by

$$S^2 = (P_{44} - J_1 P_{41} - J_m P_{42} - J_n P_{43})/(N-4). \qquad (A4)$$

It is, of course, an indication of the accuracy of the inversion and smaller values of (A4) suggest higher accuracy. Another parameter that is useful for assessing the accuracy of the calculation is the multiple correlation coefficient

$$MCC = [(J_1P_{41} + J_mP_{42} + J_nP_{43})/P_{44}]^{1/2} . \qquad (A5)$$

The value of (A5) ranges from 0 to 1 with a value of unity indicating a perfect fit between the observed and calculated anomalies.

If it is desired to calculate a planar regional field along with the magnetization parameters, equation (13),

$$T' = J_1B_1 + J_mB_2 + J_nB_3 + C_1x + C_2y + C_o , \qquad (13)$$

must be put into the form of (A3) by adding two more parameters to the matrix. (A3) becomes

$$P_{jk} * J_k = P_{6j} \quad (j,k = 1...5) \qquad (A6)$$

with $J_4 = C_1$ and $J_5 = C_2$. With the added parameters, the variance and multiple correlation coefficient become

$$S^2 = (P_{66} - J_1P_{61} - J_mP_{62} - J_nP_{63} - C_1P_{64} - C_2P_{65})/(N-6)$$

and

$$MCC = [(J_1P_{61} + J_mP_{62} + J_nP_{63} + C_1P_{64} + C_2P_{65})/P_{66}]^{1/2}.$$

The reader can easily see how the equations above can be modified to calulate the magnetization parameters of additional magnetic bodies. Each new body adds three more magnetization parameters to be calculated and hence three more rows and columns to (A6).

A least-squares calculation for the susceptibility alone was not done in the analyses of the seamounts in this study because the remanent magnetization is usually much stronger than the induced magnetization. However, the technique for solving for the best least-squares susceptibility is given here for reference. Once again the text follows the derivation by Plouff (1975). Starting with the equation from Chapter 2 for the magnetic anomaly in terms of the susceptibility, k,

$$T' = J_{ind}B + C_o,$$

where $J_{ind} = kH$ and $B = lB_1 + mB_2 + nB_3$, the standard normal equations for a least-squares solution are obtained,

$$C_oN + J_{ind}\sum B = \sum T_o \qquad \text{(A7)}$$

$$C_o \quad B + J_{ind} \sum B^2 = \sum T_o B.$$

As before, the summation is over the N field observation points. Making these definitions:

$$P_{xx} = \sum B^2 - (\sum B)^2/N$$

$$P_{xy} = \sum T_o B - (\sum T_o)(\sum B)/N$$

$$P_{yy} = \sum T_o^2 - (\sum T_o)^2/N ,$$

(A7) can be solved for C_o and J_{ind},

$$C_o = \sum T_o - J_{ind} \sum B/N$$

$$J_{ind} = P_{xy}/P_{xx} .$$

Because it has been assumed that the remanent magnetization, J_r, is zero, equations (5) from Chapter 2 reduce to

$$J_x = J_{ind} l$$

$$J_y = J_{ind}^m$$

$$J_z = J_{ind}^n$$

and these three components of the magnetization are used to calculate the susceptibility. For this calculation, the coefficient of correlation and variance are

$$R = P_{xy}/(P_{xx}P_{yy})^{1/2}$$

and

$$S^2 = P_{yy}(1-R^2)/P_{xx}(N-2).$$

The susceptibility and remanent magnetization can also be calculatied concurrently. With the possible exception of Grossling (1970) who does not make it clear whether the susceptibilities used in his calculations are assumed or calculated, no one has tried such a simultaneous inversion for both a remanent vector and susceptibility. In order to do so, the magnetic anomaly is written with both remanent and induced components

$$T' = J_r(LB_1 + MB_2 + NB_3) + J_{ind}B_4 + C_o$$

or

$$T' = J_1B_1 + J_mB_2 + J_nB_3 + J_{ind}B_4 + C_o.$$

In a manner analogous to that used to derive (A3) and (A6), the following matrix equation is obtained:

$$P_{jk} * J_k = P_{5j} \quad (j,k = 1...4)$$

where the remanent magnetization components are defined as before and $J_4 = J_{ind}$. The P_{jk} are determined as before and C_o is

$$C_o = (\sum T_o - J_1 \sum B_1 - J_m \sum B_2 - J_n \sum B_3 - J_{ind} \sum B_4)/N.$$

The correlation coefficient and variance can also be derived in the same manner as before.

Thus one can theoretically determine both the remanent magnetization and the volume susceptibility of the rock of a seamount with a single least-squares inversion. Practically, it may not be so easily accomplished. If the directions of the induced and remanent magnetizations are not very different, then it may be nearly impossible to distinguish between the two and the values of the magnetizations determined in such an inversion may not be valid. A better approach would be to design the inversion routine so that a range of susceptibilities could be specified in the program. The routine would then test each to see which gives the best fit.

APPENDIX B: SEAMOUNT SURVEYS

There is no simple answer to the question "what is the best seamount survey?" because seamounts vary greatly in size, shape, and the complexity of their magnetic anomalies. A few tracklines may be sufficient to describe a conical seamount with a simple magnetic anomaly, yet several days of ship time may be needed to make a good survey of a large seamount with a complex anomaly. Often it is not possible to have a preconcieved idea of a seamount survey pattern because many seamounts are mis-positioned or poorly represented on bathymetric charts.

Seamount paleomagnetism is not particularly demanding of the accuracy of survey data. Most of the seamount models described in Chapter 4 are based on 250 m. bathymetric contours and 50 or 100 nT. magnetic contours. A reasonably good description of the overall shape of the seamount and its anomaly is all that is needed. This is indeed fortunate considering the viscissitudes of navigation in the open ocean and the sizable magnetic field variations that must be removed from the survey data.

Although Loran C radio-navigation may be used in coastal areas and in a few other places where transmitter geometries are favorable, for most of the Pacific Ocean, this method does not give sufficiently accurate positional information for seamount surveying. Likewise, Omega radio-navigation, even though available world-wide, is also rarely accurate enough for seamount surveys. Most open ocean

navigation is accomplished using Doppler satellites. Navigation by Doppler satellite usually consists of a series of position "fixes" linked by dead reckoning calculations. A position fix is derived from calculations using orbital parameters transmitted by the satellite and range determinations gleaned from the Doppler shift of the satellite's signal (Guier, 1966). The reliability of a fix depends on many factors, but most fixes that fit conventional acceptance standards are within 0.9 km. of the true position (Talwani et al., 1966). Though the frequency of fixes varies with the region of the world where the ship is located, a fix can usually be expected every few hours on the average, even in the remotest parts of the Pacific.

Between fixes, an educated guess (called "dead reckoning") of the ship's position is made. These calculations take into account the ships's speed and heading, currents, and wind drag (Rose, 1974); however, if too many hours elapse between satellite fixes, the calculated dead reckoning postion may be in error by many kilometers. Situations particularly vulnerable to such errors are those of heavy seas when the speed log is especially inaccurate, long periods between fixes (particularly those with many turns), and during and after dredge stations when the ship's speed is low and heading variable. All of these problems make the job of contouring the bathymetric and magnetic data that much more difficult. It is a rare seamount survey that does not contain at least one poorly navigated track that must be substantially repostioned. In general, one must use both the bathymetry and magnetic anomaly to adjust such errant tracks so that they fit into the survey with a minimum of track crossing error.

It may be very difficult in some sparse surveys to find a unique corrected position for some tracklines. In such a case, there is usually nothing to be done other than to make a best-guess correction and keep the problem in mind when interpreting the magnetic anomaly. However, navigational problems such as these rarely have a deletereous effect on a seamount's bathymetric model because small changes in the seamount's shape have little effect on the magnetic anomaly at the sea surface. On the other hand, such errors make it difficult to properly contour the magnetic anomaly, particularly if large diurnal corrections must be made or data collected at another time must be fitted into the suevey. In these tasks the differences between magnetic values at track crossings are important pieces of information, but large navigational errors give them misleading values.

Three example survey patterns are shown over a hypothetical seamount in Figure B.1. Of course, there are many adequate ways to survey a seamount, but this figure aims to point out a few salient features that are important in undertaking a survey. Looking back to Figure 2.6, the reader will see that magnetic anomaly morphology varies greatly even for a homogeneously magnetized seamount. Sometimes a minimum of the anomaly is located over the seamount summit, but at other times the maximum gradient of the anomaly is located there. Usually a survey that includes all of the seamount out to the lowest closed contour will include enough of the anomaly to completely characterize it, but occasionally the survey will be better if extended somewhat farther from the summit. Consequently, the scientist in charge of the survey must actively monitor the survey while it is in

progress to make sure that both the shape of the seamount and its magnetic anomaly are adequately defined.

However, several generalizations can be made about proper surveys. A good survey should have at least on north-south line. A trackline oriented in this manner should sample close to the maximum and minimum values of the anomaly as well as the maximum gradient of the anomaly between the maximum and minimum centers. These features must be adequately described to constrain the inclination and intensity of the magnetization vector. The north-south line alone is obviously insufficient for an entire survey because information of the lateral extent of the anomaly minimum and maximum are needed to constrain the declination of the magnetization. East-west tracklines are to be avoided whenever possible because they can sometimes be unfortunately positioned to give little information on the shape of the anomaly. Figure 2.6 shows that nearly every anomaly has at least one region, usually in the important high gradient area, in which an east-west track would be nearly parallel to the contours and thus sample a virtually constant magnetic field.

Each of the surveys shown in Figure B.1 has merits and disadvantages. The "clover leaf" pattern has been used most often in this study. Among its advantages are the facts that it has no directional bias and it covers eight points of the compass in short amount of time. It also has very good coverage near the summit, which is desirable because the material nearest to the surface has the greatest effect on the magnetic anomaly measured at the sea surface. Notice in Figure B.1 that the tracklines near the summit do not all

cross precisely at the summit. By purposely orienting some of the tracks to bracket the peak, a better picture of the summit area can be had. This pattern also has several disadvantages. It presupposes some knowledge of the location and shape of the seamount. If the first crossing does not go near the summit, then the pattern is difficult to complete. Also, the multidirectional nature of this survey is guaranteed to put the ship parallel to the waves at some point and thus it may be dangerous to use in rough weather.

The "zig-zag" pattern in Figure B.1 can be useful for finding a mis-postioned seamount. Also, it can be a good foul weather survey as the zig-zags can be oriented into and with the prevailing seas--usually the best tacks to take in rough seas. However, the pattern can present some problems. Unless a tie line is run back across the survey, as illustrated in the figure, the ship tracks will nowhere cross each other leaving no crossing errors to be used for navigational or magnetic corrections. Additionally, an unlucky surveyor may miss all or most of the maximum or minimum of the magnetic anomaly. Figure B.1 also shows a "rectangular" pattern that as shown is very similar to the zig-zag pattern. It is the most consumptive of ship time of the three, but it can be a particularly good survey if two sets of perpendicular lines are run across the seamount.

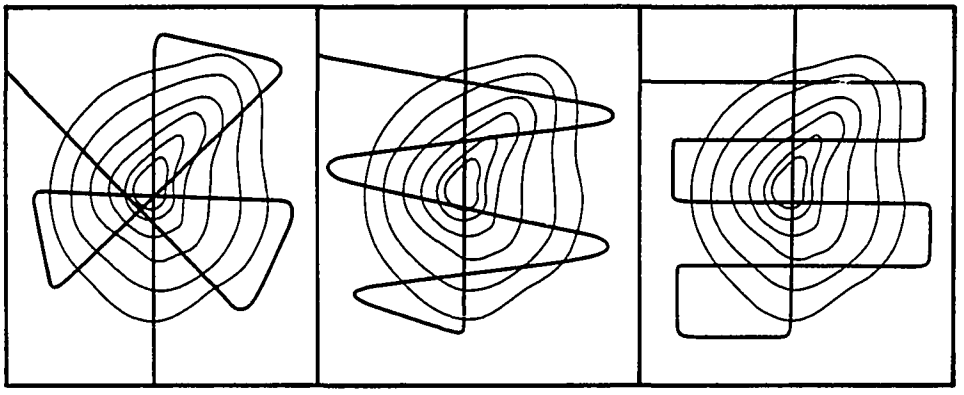

Figure B.1 Three example seamount survey patterns. (Left) "clover leaf"; (middle) "zig-zag"; (right) "rectangular".

APPENDIX C: SEAMOUNT MODELING - STEP BY STEP

This appendix is written as a guide for the novice seamount modeler. it is hoped that the instructions below will save such a reader precious time in the beginning stages of a magnetic modeling project. A few of the instructions are specific to the magnetic inversion program used in this study, one written by Donald Plouff of the U. S. Geological Survey office at Menlo Park. However, most of the instructions will be of use even to those readers wishing to use a different modeling program.

STEP 1: Gather all bathymetric, magnetic, and seismic reflection data. Every bit of data helps and often previous cruises have crossed the seamount of interest. Check the archives of the National Geophysical and Solar-Terrestrial Data Center in Boulder, Colorado. Plot ship tracks, bathymetry, and magnetics at a large scale for contouring. In this study the most useful map scale was found to be about 36 inches/degree. Time marks should be plotted on the ship tracks at 10-15 min. intervals to aid in making magnetic diurnal corrections.

STEP 2: Contour the bathymetric and magnetic data. Check the crossing errors in both the bathymetry and magnetics to look for navigational errors. Most tracks will have to be shifted slightly, on the order of 0.5-1.0 kilometers, and sometimes there is one poorly navigated track in a survey that is off by several kilometers. Remember when fitting such tracks into the survey that some of the

magnetic crossing errors are the result of magnetic field variations and not navigational error. Contour the bathymetry using echo-sounding and seismic reflection records (when available) as a guide. A contour interval of 250 m. is sufficient for seamount modeling. Make diurnal corrections to the magnetic data as discussed in Section 3.2 and contour the magnetic anomaly. For large anomalies a contour interval of 100 nT. is sufficient and for smaller anomalies 50 nT. will do.

STEP 3: Prepare the bathymetric model. On a large sheet of tracing paper laid over the bathymetric map, draw polygons that approximate the shapes of the contours. For each observation point, the computer program must make one calculation for each polygon side, so it is desirable to use the minimum number of observation points and polygon vertices possible to adequately sample the magnetic anomaly and represent the shape of the seamount. The best approximation of the seamount shape is obtained by placing the top and bottom of the vertical prism that each polygon represents halfway between the contours (e.g., for a 250 m. contour interval, the top of the 2000 m. prism would be at 1875 m. and the bottom at 2125 m.). The deeper layers need fewer polygons and vertices because short wavelength magnetic fields are attenuated rapidly with distance from the plane of observation. In this study the usual practice was to use 250 m. prisms for the upper 1.5 km. of a seamount and 500 m. prisms below.

Often an extension of the seamount below the ocean bottom will improve the model. Add about 1 km. of extension onto the bottom of the seamount model. If seismic reflection records are available to help constrain the shape of these layers, so much the better. However, the

seismic penetration is often insufficient to be of much help. The method of extension that usually works best is one which keeps the same overall shape and slope of the visible part of the seamount; although, occasionally an extension with vertical sides works better. The usefulness of this extension will be tested in later steps.

STEP 4: Pick an origin for the model in the southwest corner of the survey area; x values will be northward and y values, eastward (in Plouff's program). Digitize the vertices of the polygon model and put them into proper format for input to the magnetic modeling program.

Digitize the magnetic anomaly. In Plouff's program the magnetic anomaly values may be input either as a rectangular grid, random points, or a single transect. Some authors prefer to use magnetic values digitized only along the ship tracks. This technique requires the random point method. Alternatively, a grid may be constructed, referenced to the origin, and the magnetic anomaly digitized at its intersections. The former method is probably the more objective of the two, but the latter is easier to use in modelling and graphical display. That is the reason rectangular gridding has been used almost exclusively in this study. A grid size of 1 nautical mile has been found a useful compromise between being fine enough to adequately sample all of the variations of the magnetic anomaly and yet not being too cumbersome computationally. The grid sizes in this study range from about 100 points to 625 points.

Pick an area of the magnetic anomaly to be inverted. This area should include only parts of the anomaly that are well constrained with data. If there is not very much data, then digitizing the anomaly

along the ship tracks should be used so that the contouring does not add a bias.

STEP 6: Determine the direction and intensity of the geomagnetic field at the survey site. In this study the 1975 IGRF was used to calculate the inclination, declination, and intensity of the geomagnetic field given the latitude, longitude, and date of the survey.

STEP 7: Begin modeling. Run the program with the whole seamount including the bottom extension and not the GFR value. Take away the bottom extension layer by layer noting the GFR each time. The maximum GFR indicates the amount of extension that produces the best model. Now repeat this procedure taking away the top layers one by one. The best top of the model will be indicated by the highest GFR value as before. Most seamounts require some bottom extension or summit reduction, but not all (see the seamount model descriptions in Chapter 4). This is the basic model. Further improvements may be accomplished by making subtle changes in the seamount's shape or magnetization structure; however, these more complex models should be treated with suspicion unless they produce results in agreement with other paleomagnetic data.

REFERENCES

Abdel-Monem, A., N. D. Watkins, and P. W. Gast, 1971, Potassium-argon ages, volcanic stratigraphy, and geomagnetic polarity history of the Canary Islands: Lanzarote, Fuerteventura, Gran Canaria, and La Gomera, Am. J. Sci., 271, 490-521.

Abdel-Monem, A., N. D. Watkins, and P. W. Gast, 1972, Potassium-argon ages, volcanic stratigraphy, and geomagnetic polarity history of the Canary Islands: Tenerife, La Palma, and Hierro, Am. J. Sci., 272, 805-825.

Ade-Hall. J. M., H. P. Johnson, and P. C. Ryall, 1976, Rock magnetism of basalts, Leg 34, Init. Rept. DSDP, 34, 459-468.

Akasofu, S. I. and S. Chapman, 1967, Geomagnetic storms and auroras, in Physics of Geomagnetic Phenomena, v. 2, S. Matsushita and W. H. Campbell, eds., Academic Press, New York, 1113-1152.

Alvarez, W., M. A. Arthur, A. G. Fischer, W. Lowrie, G. Napoleone, I. Premoli-Silva, and W. M. Roggenthen, 1977, Upper Cretaceous-Paleocene geomagnetic reversal time scale, Geol. Soc. Am. Bull., 88, 383-389.

Arora, B. R. and N. S. Sastri, 1977, Some features of the variability associated with solar and lunar daily variations, Geophys. J. Roy. Astr. Soc., 50, 235-241.

Arrhenius, G. O., Pelagic Sediments, 1963, in The Sea, v. 3, M. N. Hill. ed., Interscience, New York, 655-727.

Atwater, T., 1970, Implications of plate tectonics for the Cenozoic evolution of western North America, Geol. Soc. Am. Bull., 81, 3513-3536.

Atwater, T. and H. W. Menard, 1970, Magnetic lineations in the northeast Pacific, Earth Planet. Sci. Lett., 7, 445-450.

Bargar, K. E. and E. D. Jackson, 1974, Calculated volumes of individual shield volcanoes along the Hawaiian-Emperor chain, J. Res. U. S. Geol. Survey, 2, 545-550.

Baraclough, D. R. and E. B. Fabiano, 1977, Grid values and charts for the IGRF 1975.0, IAGA Bull, no. 38, IUGG Publications office, Paris.

Barr, S. M., 1974, Seamount chains formed near the crest of the Juan de Fuca Ridge, northeast Pacific Ocean, Mar. Geol., 17, 1-19.

Basaltic Volcanism Study Project, 1981, Distribution and morphology of basalt deposits on planets, in Basaltic Volcanism on the Terrestrial Planets, Pergamon Press, New York, 702-802.

Batiza, R., 1977, Age, volume, compositional and spatial relations of small isolated oceanic central volcanoes, Mar. Geol., 24, 169-183.

Batiza, R., 1982, Abundances, distribution and sizes of volcanoes in the Pacific Ocean and implications for the origin of non-hotspot volcanoes, Earth Planet. Sci. Lett., 60, 195-206.

Bennett, D. J. and F. E. M. Lilley, 1973, an array study of daily magnetic variations in southeast Australia, J. Geomag. Geoelectr., 25, 39-62.

Bhargava, B. N. and A. Yacob, 1969, Solar cycle response in the horizontal force of the earth's magnetic field, J. Geomag. Geoelectr. 21, 385-396.

Bhattacharji, S., 1979, Convective plumes, magma chamber development, penetrative magmatism and intraplate rifting, (abstract), Hawaii Symposium on Intraplate Volcanism and Submarine Volcanism, Abstract Volume, Hilo, Hawaii, July 16-22, 1979, 35.

Bingham, C., 1964, Distribution on the sphere and on the projective plane, Ph. D. dissertation, Yale University.

Blakely, R. J. and R. L. Christiansen, 1978, The magnetization of Mount Shasta and implications for virtual geomagnetic poles determined from seamounts, J. Geophys. Res., 83, 5971-5978.

Blakely, R. J. and A. Cox, 1972, Identification of short polarity events by transforming marine magnetic anomalies to the pole, J. Geophys. Res., 77, 4339-4349.

Bonatti, E., 1967, Mechanisms of deep-sea volcanism in the south Pacific, in Researches in Geochemistry, v. 2, P. Abelson, ed., J. W. Wiley and Sons, New York, 453-491.

Briden, J. C., A. M. Hurley, and A. G. Smith, 1981, Paleomagnetism and Mesozoic-Cenozoic paleocontinental maps, J. Geophys. Res., 86, 11,631-11,656.

Briden, J. C. and M. A. Ward, 1966, Analysis of magnetic inclination in bore cores, Pure Appl. Geophys., 63, 133-152.

Cain, J. C. and R. E. Sweeney, 1973, The POGO data, J. Atm. Terr. Phys., 35, 1231-1247.

Campbell, W. H., 1967, Geomagnetic pulsations, in Physics of Geomagnetic Phenomena, v. 2., S. Matsushita and W. H. Campbell, eds., Academic Press, New York, 822-909.

Cande, S. C., 1976, A paleomagnetic pole from Late Cretaceous Marine magnetic anomalies in the Pacific, Geophys. J. Roy. Astr. Soc., 44, 547-566.

Carnahan, B., H. A. Luther, and J. O. Wilkes, 1969, Applied Numerical Methods, J. W. Wiley and Sons, New York, 604 pp.

Chapman, S. and J. Bartels, 1940, Geomagnetism, v. 1 and v. 2, Oxford Univ. Press, London, 1018 pp.

Chapman, S. and K. S. Raja Rao, 1965, The H and Z variations along and near the equatorial electrojet in India, Africa, and the Pacific, J. Atm. Terr. Phys., 27, 559-581.

Clague, D. A. and G. B. Dalrymple, 1975, Cretaceous K/Ar ages of volcanic rocks from the Musicians Seamounts and the Hawaiian Ridge, Geophys. Res. Lett., 2, 305-308.

Clague, D. A. and R. D. Jarrard, 1973, Tertiary Pacific plate motion deduced from the Hawaiian-Emperor chain, Geol. Soc. Am. Bull., 84, 1135-1154.

Cockerham, R. S. and J. M. Hall, 1976, Magnetic properties and paleomagnetism of some DSDP Leg 33 basalts and sediment and their tectonic implications, J. Geophys. Res., 81, 4207-4222.

Cockerham, R. S. and R. D. Jarrard, 1976, Paleomagnetism of some Leg 33 sediments and basalts, Init. Rept. DSDP, 33, 631-647.

Coupland, D. H. and R. Van der Voo, 1980, Long-term nondipole components in the geomagnetic field during the last 130 m.y., J. Geophys. Res., 85, 3529-3548.

Cox, A., 1975, The frequency of geomagnetic reversals and the symmetry ot the nondipole field, Rev. Geophys. Space Phys., 13, 31-51.

Cox, A. and R. R. Doell, 1962, Magnetic properties of the basalt in Hole EM7, Mohole project, J. Geophys. Res., 67, 3997-4004.

Cox, A. and R. G. Gordon, 1983, Paleolatitudes determined from paleomagnetic data from vertical cores, submitted to Rev. Geophys. Space Phys.

Creer, K. M., D. T. Georgi, and W. Lowrie, 1973, On the representation of the Quaternary and late Tertiary geomagnetic fields in terms of dipoles and quadrupoles, Geophys. J. Roy. Astr. Soc., 33, 323-345.

Crough, S. T. and D. M. Jurdy, 1980, Subducted lithosphere, hotspots, and the geoid, Earth Planet. Sci. Lett., 48, 15-22.

Currie, R. G., 1966, The geomagnetic spectrum from 40 days to 5.5 years, J. Geophys. Res., 71, 4579-4598.

Currie, R. G., 1976, Search for an annual line in geomagnetic activity at middle latitudes, J. Geophys. Res., 81, 2935-2937.

Dalrymple, G. B., M. A. Lanphere, and D. A. Clague, 1980, Conventional and $^{40}Ar-^{39}Ar$ K-Ar ages of volcanic rocks from Ojin (Site 430), Nintoku (Site 432), and Suiko (Site 433) seamounts and the chronology of volcanic propagation along the Hawaiian-Emperor chain, Init. Rept. DSDP, 55, 659-676.

Darwin, C., 1842, The structure and distribution of coral reefs, in The Geology of the Voyage of the Beagle, v. 3, Smith, Elder, and Co., London, 214 pp.

Diller, D. E., 1982, Contributions to the geology of west Maui volcano, Hawaii, M. Sc. thesis, University of Hawaii, Honolulu, 237 pp.

Duncan, R. A., 1981, Hotspots in the southern oceans--an absolute frame of reference for motion of the Gondwana Continents, Tectonophys., 74, 29-42.

Duncan, R. A. and I. McDougall, 1976, Linear volcanism in French Polynesia, J. Volc. Geotherm. Res., 1, 197-227.

Dunlop, D. J. and C. J. Hale, 1977, Simulation of long-term changes in the magnetic signal of the oceanic crust, Can. J. Earth Sci., 14, 716-744.

Dymond, J. and H. L. Windom, 1968, Cretaceous K/Ar ages from Pacific ocean seamounts, Earth Planet. Sci. Lett., 4, 47-52.

Dzurisin, D., L. A. Anderson, G. P. Eaton, R. Y. Koyanagi, P. W. Lipman, J. P. Lockwood, R. T. Okamura, G. S. Punawai, M. K. Sako, and R. M. Yamashita, 1980, Geophysical observations of Kilauea volcano, Hawaii 2. Constraints on the magma supply during November 1975-September 1977, J. Volc. Geotherm. Res., 7, 241-269.

Emilia, D. A. and R. L. Massey, 1974, Magnetization estimation for nonuniformly magnetized seamounts, Geophysics, 39, 223-231.

Epp, D., 1978, Age and tectonic relationships among volcanic chains on the Pacific plate, Ph. D. dissertation, University of Hawaii, Honolulu, 199 pp.

Epp., D., 1982, Hotspots and hotlines in the Pacific, (abstract), The Origin and Evolution of seamounts conference, Lamont-Doherty Geological observatory, November 17-19, 1982, Palisades, New York.

Epp., D., W. Sager, F. Theyer, and S. R. Hammond, 1983, Hotspot/spin axis motion or far-sided effect?, Nature, 303, 318-320.

Elsasser, W. M., 1955, Hydromagnetism I: a review, Am. J. Phys., 23, 590-609.

Fabiano, E. B., N. W. Peddie, D. R. Barraclough, and A. K. Zunde, 1982, International Geomagnetic Reference Field 1980-Charts and Grid Values, IAGA Bulletin No. 47, U.S. Geological Survey Circular 873. U.S. Government Printing office, Washington, D.C., 142 pp.

Farrar, E. and J. M. Dixon, 1981, Early Tertiary rupture of the Pacific Plate: 1700 Km of dextral offset along the Emperor Trough-Line Islands lineament, Earth Planet. Sci. Lett., 53, 307-322.

Fisher, R. A., 1953, Dispersion on a sphere, Proc. Roy. Soc. Lond., A217, 295-305.

Fiske, R. S. and E. D. Jackson, 1972, Orientation and growth of Hawaiian volcanic rifts: the effect of regional structure and gravitational stresses, Proc. Roy. Soc. Lond., A329, 299-326.

Fox, P. J. and N. D. Opdyke, 1973, Geology of the oceanic crust: magnetic properties of oceanic rocks, J. Geophys. Res., 78, 5139-5154.

Francheteau, J., J. G. Sclater, and H. Craig, 1969, Magnetization of a recently discovered seamount in the central Pacific, Geophysics, 34, 645-651.

Francheteau, J., C. G. A. Harrison, J. G. Sclater, and M. L. Richards, 1970, Magnetization of Pacific seamounts: a preliminary polar curve for the northeastern Pacific, J. Geophys. Res., 75, 2035-2061.

Furumoto, A. S., 1978, Nature of the magma conduit under the east rift zone ot Kilanea Volcano, Hawaii, Bull. Volcanol., 41, 435-453.

Gordon, R. G., 1982, The late Maastrichtian paleomagnetic pole of the Pacific plate, Geophys. J. Roy. Astr. Soc., 70, 129-140.

Gordon, R. G., 1983, Late Cretaceous apparent polar wander path of the Pacific plate: evidence for a rapid shift of the Pacific hotspots with respect to the paleomagnetic axis, Geophys. Res. Lett., in press.

Gordon, R. G. and C. D. Cape, 1981, Cenozoic latitudinal shift of the Hawaiian hotspot and its implications for true polar wander, Earth Planet. Sci. Lett., 55, 37-47.

Gordon, R. G. and A. Cox, 1980a, Paleomagnetic test of the early Tertiary plate circuit between the Pacific basin plates and the Indian plate, J. Geophys. Res., 85, 6534-6546.

Gordon, R. G. and A. Cox, 1980b, Calculating palaeomagnetic poles for oceanic plates, Geophys J. Roy. Astr. Soc., 63, 619-640.

Gordon, R. G., A. Cox, and C. E. Harter, 1978, Absolute motion of an individual plate estimated from it ridge and trench boundaries, Nature, 274, 752-755.

Grant, F. S. and G. F. West, 1965, Interpretation Theory in Applied Geophysics, McGraw-Hill, New York, 583 pp.

Grindley, G. W., C. J. D. Adams, J. T. Lumb, and W. A. Watters, 1977, Paleomagnetism, K-Ar dating and tectonic interpretation of Upper Cretaceous and Cenozoic rocks of the Chatham Islands, New Zealand, N. Z. J. Geol. Geophys., 20, 425-467.

Gromme, S. and F. J. Vine, 1972, Paleomagnetism of Midway Atoll lavas and northward movement of the Pacific plate, Earth Planet. Sci. Lett., 17, 159-168.

Grossling, B. F., 1970, Seamount magnetism, in The Sea, v. 4, A. E. Maxwell. ed., Interscience, New York, 129-156.

Guier, W. H., 1966. Satellite navigation using integral Doppler data--the AN/SRN-9 equipment, J. Geophys. Res., 71, 5903-5910.

Haggerty, J. A., 1982, The geologic history of the southern Line Islands, Ph. D. dissertation, University of Hawaii, Honolulu. 202 pp.

Haggerty, J. A., S. O. Schlanger, and I. Premoli-Silva, 1982, Late Cretaceous and Eocene Volcanism in the southern Line Islands and implications for hotspot theory, Geology, 10, 433-437.

Hall. J. M., 1977. Does TRM occur in oceanic layer 2 basalts?, J. Geomag. Geoelectr., 29, 411-419.

Hamilton, E. L., 1956, Sunken Islands of the Mid-Pacific Mountains, Mem. Geol. Soc. Am., 64, Waverly Press, Baltimore, 97pp.

Hammond. S. R., D. Epp., and F. Theyer, 1979, Neogene relative motion between the Pacific plate, the mantle, and the earth's spin axis, Nature, 278, 309-310.

Hammond. S. R., L. W. Kroenke, F. Theyer, 1975, Northward motion of the Ontong-Java Plateau between -110 and -30 M.Y.: a paleomagnetic investigation of DSDP Site 289, Init. Rept. DSDP, 30, 415-418.

Hammond. S. R., F. Theyer. and E. Herrero-Bervera, 1980, 0-11 M.Y. paleomagnetic polar wander results from central Pacific oriented sediment cores (abstract). Trans. Am. Geophys. Union, EOS, 61, 218.

Handschumacher, D. W., 1976. Post-Eocene plate tectonics of the eastern Pacific, in The Geophysics of the Pacific Ocean Basin and its Margin, Geophys. Mon. Ser. 19, G. H. Sutton, M. H. Manghnani, and R. Moberly, eds., AGU, Washington, D.C., 177-202.

Harrison, C. G. A., 1970, Magnetization of Atlantic Seamounts, Bull. Mar. Sci., 20. 560-574.

Harrison, C. G. A., 1971, A seamount with a nonmagnetic top, Geophysics, 36, 349-357.

Harrison, C. G. A. and M. M. Ball, 1975, Geophysical observations on an exposed seamount in the Afar depression, Bull. Volc., 38, 26-43.

Harrison, C. G. A., R. D. Jarrard, V. Vacquier, and R. L. Larson, 1975, Palaemagnetism of Cretaceous Pacific seamounts, Geophys. J. Roy. Astr. Soc., 42, 859-882.

Harrison, C. G. A. and T. Lindh, 1982a, A polar wandering curve for North America during the Mesozoic and Cenozoic, J. Geophys. Res., 87, 1903-1920.

Harrison, C. G. A. and T. Lindh, 1982b, Comparison between the hot spot and geomagnetic field reference frames, Nature, 300, 251-252.

Heezen, B. C., I. D. MacGregor, H. P. Foreman, G. Forristall, H. Hekel, R. Hesse, R. H. Hoskins, E. J. W. Jones, A. Kaneps, V. A. Krasheninnikov, H. Okada, and M. H. Ruef, 1973, The Post-Jurassic sedimentary sequence on the Pacific plate; a kinematic interpretation of diachronous deposits, Init. Rept. DSDP, 20, 725-738.

Heezen, B. C., J. L. Matthews, R. Catalano, J. Natland, A. Coogan, M. Tharp, and M. Rawson, 1973, Western Pacific Guyots, Init. Rept. DSDP, 20, 653-723.

Henderson, L. J. and R. G. Gordon, 1981, Oceanic plateaus and the motion of the Pacific plate with respect to the hotspots, (abstract), Trans. Am. Geophys. Union, EOS, 62, 1028.

Herron, E. M., 1972, Sea-floor spreading and the Cenozoic history of the east-central Pacific, Geol. Soc. Am. Bull., 83, 1671-1692.

Hilde, T. W. C., N. Isezaki, and J. M. Wageman, 1976, Mesozoic sea floor spreading in the north Pacific, in The Geophysics of the Pacific Ocean Basin and its Margin, Geophys. Mon. Ser. 19, G. H. Sutton, M. H. Manghnani, and R. Moberty, eds., AGU, Washington, D.C., 205-226.

Hilde, T. W. C., S. Uyeda, and L. Kroenke, 1977, Evolution of the western Pacific and its margin, Tectonophys., 38, 145-165.

Hobbs, B. A. and G. J. K. Dawes, 1979, Calculation of the effect of the oceans on geomagnetic variation with an application to the Sq field during the IGY. J. Geophys., 46, 273-289.

Hollister, C. D., M. F. Glenn, and P. F. Lonsdale, 1978, Morphology of seamounts in the western Pacific and Philippine Basin from multi-beam sonar data, Earth Planet Sci. Lett., 41, 405-418.

Hutton, R., 1967, Sq currents in the American equatorial zone during the IGY-I, seasonal effects, J. Atm. Terr. Phys., 29, 1411-1427.

Irving, E., 1977, Drift of the major continental blocks since the Devonian, Nature, 270, 304-309.

Irving, E., W. A. Robertson, and F. Aumento, 1970, The Mid-Atlantic Ridge near 45°N. VI. remanent intensity, susceptibility, and iron content of dredged samples, Can. J. Earth Sci., 7, 226-241.

Jackson, E. D., 1976. Lineear volcanic chains on the Pacific plate, in Geophysics of the Pacific Ocean Basin and its Margin, Geophys. Mon. Ser. 19, G. H. Sutton, M. H. Manghnani, and R. Moberly, eds., AGU, Washington, D.C., 319-335.

Jackson, E. D., I. Koisumi, G. B. Dalrymple, D. H. Clague, R. J. Kirpatrick, and H. G. Greene, 1980, Introduction and summary of results from DSDP Leg 55, the Hawaiian-Emperor hot-spot experiment, Init. Rept. DSDP, 55, 5-31.

Jackson, E. D., and S. O. Schlanger, 1976, Regional synthesis, Line Islands, Tuamotu chain, and Manihiki Plateau, central Pacific basin, Init. Rept. DSDP, 33, 915-1027.

Jackson, E. D. and T. L. Wright, 1970, Xenoliths in the Honolulu volcanic series, Hawaii, J. Petrol., 11, 405-430.

Jarrard, R. D., 1973. Paleomagnetism of Leg 17 Sediment Cores, Init. Rept. DSDP, 17, 365-375.

Jarrard, R. D. and D. A. Clague, 1977, Implications of Pacific island and seamount ages for the origin of volcanic chains, Rev. Geophys. Space Phys., 15, 57-76.

Jarrard, R. D. and S. Sasajima, 1980, Paleomagnetic synthesis for Southeast Asia: constraints on plate motions, in the The Tectonic and Geologic Evolution of Southeast Asian Seas and Islands, Geophys. Mon. Ser. 23, D. E. Hayes, ed., AGU, Washington, D.C., 293-317.

Jones, F. W., 1974, The perturbation of slowly varying electromagnetic fields by three dimensional conducting bodies, Can. J. Phys., 52. 1195-1202.

Jones, J. G., 1966, Intraglacial volcanoes of southwest Iceland and their significance in the interpretation of the form of the marine basaltic volcanoes, Nature, 212, 586-588.

Jurdy, D. M., 1981, True polar wander, Tectonophys., 74, 1-16.

Jurdy, D. M., 1983, Early Tertiary subduction zones and hotspots, J. Geophys. Res., in press.

Jurdy, D. M. and R. Van der Voo, 1975, A method for the separation of true polar wander and continental drift, including results for the last 55 m.y., J. Geophys. Res., 79, 2945-2952.

Keating, B. and W. Sager, 1980, Watkins Seamount: preliminary paleomagnetic results, J. Geophys. Res, 85, 3567-3571.

Kodama, K., S. Uyeda, and N. Isezaki, 1978, Paleomagnetism of Suiko seamount, Emperor seamount chain, Geophys. Res. Lett., 5, 165-168.

Kodama, K. and S. Uyeda, 1979, Magnetization of Izu Islands with special reference to Oshima Volcano, J. Volc. Geotherm. Res., 6, 353-373.

Kono, M., 1980a, Magnetic properties of DSDP Leg 55 basalts, Init. Rept. DSDP, 55, 723-736.

Kono, M., 1980b, Paleomagnetism of DSDP Leg 55 basalts and implications for the tectonics of the Pacific plate, Init. Rept. DSDP, 55, 737-752.

Koyanagi, R. Y., E. T. Endo, and P. L. Ward, 1976, Seismic activity on the island of Hawaii, 1970 to 1973, in Geophys of the Pacific Ocean Basin and Its Margins, Geophys. Mon. Ser. 19, G. H. Sutton, M. H. Manghnani, and R. Moberly, eds., AGU, Washington, D.C., 169-172.

Kroenke, L. W., 1974, Origin of continents through development and coalescence of oceanic flood basalt plateaus, (abstract). Trans. Am. Geophys. Union, EOS, 55, 443.

Kroenke, L. W., 1981, Cruise report; KK810626-05, 27 October-22 November, 1981, Unpublished manuscript.

Kulp, J. L., 1963. Potassium-Argon dating of volcanic rocks, Bull. Volc., 26, 247-258.

Ladd, H. S., E. Ingerson, R. C. Townsend, M. Russell, and H. K. Stephenson, 1953, Drilling on Eniwetok Atoll, Marshall Islands, Am. Assoc. Pet. Geol. Bull., 37, 2257-2280.

Lancelot, Y. and R. L. Larson, 1975, Sedimentary and tectonic evolution of the northwestern Pacific, Init. Rept. DSDP, 32, 925-939.

Larson, R. L., 1976. Late Jurassic and Early Cretaceous evolution of the western central Pacific Ocean, J. Geomag. Geoelectr. 28, 219-236.

Larson, R. L. and C. G. Chase, 1972, Late Mesozoic evolution of the western Pacific ocean, Bull. Geol. Soc. Am., 83, 3627-3644.

Larson, R. L. and T. W. C. Hilde, 1975, A revised time scale of magnetic reversals for the Early Cretaceous and Late Jurassic, J. Geophys. Res., 80, 2586-2594.

Larson, R. L. and W. Lowrie, 1975, Paleomagnetic evidence for motion of the Pacific plate from Leg 32 basalts and magnetic anomalies, Init. Rept. DSDP, 32, 571-577.

Larson, R. L. and S. O. Schlanger, 1981, Geological evolution of the Nauru Basin and regional implications, Init. Rept. DSDP., 61, 841-862.

Le Pichon, X. and M. Talwani, 1964, Gravity survey of a seamount near 35°N 46°W in the North Atlantic, Mar. Geol., 2, 262-277.

Lines, L. R. and F. W. Jones, 1973, The perturbation of alternating geomagnetic fields by three-dimensional island structures, Geophys. J. Roy. Astr. Soc., 32, 133-154.

Lonsdale, P. and R. Batiza, 1980, Hyaloclastite and lava flows on young seamounts examined with a submersible, Geol. Soc. Am. Bull., p. I., 91, 545-554.

Lowrie, W., 1973. Viscous remanent magnetization in oceanic basalts, Nature, 243, 27-30.

Lowrie, W., 1974, Oceanic basalt magnetic properties and the Vine and Matthews hypothesis, J. Geophys., 40, 513-536.

Lowrie, W. and W. Alvarez, 1981, One hundred million years of geomagnetic polarity history, Geology, 9, 392-297.

Lowrie, W. and D. E. Hayes, 1975, Magnetic properties of oceanic basalt samples, Init. Rept. DSDP, 28, 869-878.

Lowrie, W., R. Lovlie, and N. D. Opdyke, 1973, Magnetic properties of Deep-Sea Drilling Project basalt from the north Pacific Ocean, J. Geophys. Res., 78, 7647-7660.

Lumb, J. T., M. P. Hochstein, and D. J. Woodward, 1973, Interpretation of magnetic measurements in the Cook Islands, South-west Pacific Ocean, in The Western Pacific Island Arcs, Marginal Seas, Geochemistry, P. J. Coleman, ed., Crane, Russak, and Co., Inc., New York, 79-101.

Macdonald, G. A., 1972, Volcanoes, Prentice-Hall, Inc., Englewood Cliffs, N. J., 510 pp.

Macdonald, G. A. and A. T. Abbott, 1972, Volcanoes in the Sea, The University Press of Hawaii, Honolulu, 441 pp.

Machado, F., 1970, Oceanic fissure eruptions, subvolcanic intrusions and volcanic manga chambers, Bull. Volcanol., 33, 1229-1235.

Malahoff, A., G. M. McMurtry, J. C. Wiltshire, and H. W. Yeh, 1982, Geology and chemistry of hydrothermal deposits from active submarine volcano Loihi, Hawaii, Nature, 298, 234-239.

Marshall, M., 1978, The magnetic properties of some DSDP basalts from the north Pacific and inferences for plate tectonics, J. Geophys. Res., 83, 289-308.

Marshall, M. and A. Cox, 1971, Effect of oxydation on the natural remanent magnetization of titanomagnetite in suboceanic basalt, Nature, 230, 28-31.

Marshall, M. and A. Cox, 1972, Magnetic changes in pillow basalt due to sea floor weathering, J. Geophys. Res., 77, 6459-6469.

Mason, R. G., 1963. The equatorial electrojet in the central Pacific, Scripps Inst. Oceanog. Rept. 63-13, 29 pp.

Matsushita, S., 1967a, Solar quiet and lunar daily variation fields, in Physics of Geomagnetic Phenomena, v. 1, S. Matsushita and W. H. Campbell, eds., Academic Press, New York, 302-424.

Matsushita, S., 1967b, Geomagnetic distrubances and storms, in Physics of Geomagnetic Phenomena, v. 2., S. Matsushita and W. H. Campbell. eds., Academic Press, New York, 793-819.

Matthews, D. J., 1939, Tables of the velocity of sound in pure water and sea water for use on echo-sounding and sound ranging, 2nd ed., H. D. 282, Admiralty Hydrogr. Dep., London, 52 pp.

Matthews, J. L., B. C. Heezen, R. Catalano, A. Coogan, M. Tharp, J. Natland, and M. Rawson, 1974, Cretaceous drowning of reefs on Mid-Pacific and Japanese guyots, Science, 184, 462-464.

Mayaud, P. N., 1977, The equatorial counter-electrojet--a review of its geomagnetic aspects, J. Atm. Terr. Phys., 39, 1055-1070.

Mayaud, P. N., 1978, Morphology of the transient irregular variations of the terrestrial magnetic field and their statistical laws, Ann. Geophys., 34, 243-276.

McBirney, A. R., 1963. Factors governing the nature of submarine volcanism, Bull. Volcanol., 26, 455-469.

McBirney, A. R., 1971, Oceanic volcanism: a review, Rev. Geophys. Space Phys., 9, 523-556.

McElhinny, M. W., 1973. Paleomagnetism and Plate Tectonics, Cambridge University Press, Cambridge, 358 p.p.

McNutt, M. and R. Batiza, 1981, Paleomagnetism of northern Cocos seamounts: constraints on absolute plate motion, Geology, 9, 148-154.

Menard, H. W., 1964, Marine Geology of the Pacific, McGraw-Hill, New York, 271 pp.

Merrill, R. T. and R. E. Burns, 1972, A detailed magnetic study of Cobb Seamount, Earth Planet Sci. Lett., 14, 413-418.

Merrill, R. T. and M. W. McElhinny, 1977, Anomalies in the time-averaged paleomagnetic field and their implications for the lower mantle, Rev. Geophys. Space Phys., 15, 309-323.

Miles, P. R. and D. G. Roberts, 1981, The magnetisation of Rosemary Bank Seamount, Rockall trough, northeast Atlantic, Earth Planet Sci. Lett., 54, 442-448.

Minster, J. B., T. H. Jordan, P. Molnar, and E. Haines, 1974, Numerical modelling of instantaneous plate tectonics, Geophys. J. Roy. Astr. Soc., 36, 541-576.

Moberly, R., J. F. Campbell, and J. M. Sinton, 1983, Musicians Seamounts: control of hospot volcanism by spreading center, transform faults, and earlier intraplate volcanism, Geol. Soc. Am. Bull., in press.

Molnar, P., T. Atwater, J. Mammerickx, and S. M. Smith, 1975, Magnetic Anomalies, bathymetry and the tectonic evolution of the South Pacific since the Late Cretaceous, Geophys. J. Roy. Astr. Soc., 40, 383-420.

Morgan, W. J., 1968, Rises, trenches, great faults and crustal blocks, J. Geophys. Res., 73, 1959-1982.

Morgan, W. J., 1972, Deep mantle convection plumes and plate motions, Am. Assoc. Pet. Geol. Bull., 56, 203-213.

Morgan, W. J., 1981, Hotspot tracks and the opening of the Atlantic and Indian oceans, in The Sea, v. 7, C. Emiliani, ed., J. Wiley and Sons, New York, 443-487.

Nagata, T. and M. Ozima, 1967, Paleomagnetism, in Physics of Geomagnetic Phenomena, v. 1., S. Matsushita and W. H. Campbell, eds., Academic Press, New York, 103-180.

Nakamura, K., 1977, Volcanoes as possible indicators of tectonic stress orientation--principle and proposal, J. Volc. Geotherm. Res., 2, 1-16.

Natland, J. H., 1976a, Petrology of volcanic rocks dredged from seamounts in the Line Islands, Init. Rept. DSDP, 33, 749-777.

Natland, J. H., 1976b, Possible volcanologic explanations for the origin of flat-topped seamounts and ridges in the Line Islands and Mid-Pacific mountians, Init. Rept. DSDP, 33, 779-787.

Nayudu, R., 1962, A new hypothesis for origin of guyots and seamount terraces, in Crust of the Pacific Basin, Geophys. Mon. Ser. 6, G. A. Macdonald and H. Kuno, eds., AGU, Washington, D.C., 171-180.

Ness, G., S. Levi. and R. Couch, 1980, Marine magnetic anomaly timescales for the Cenozoic and Late Cretaceous: a precis, critique, and systhesis, Rev. Geophys. Space Phys., 18, 753-770.

Nordlie, B. E., 1973. Morphology and structure of the western Galapagos volcanoes and a model for their origin, Geol. Soc. Am. Bull., 84, 2931-2956.

Normark, W. R. and G. C. Shor, 1968, Seismic reflection study of the shallow structure of the Hawaiian arch, J. Geophys. Res., 73, 6991-6998.

Onwumechilli, A., 1967. Geomagnetic variations in the equatorial zone, in Physics of Geomagnetic Phenomena, v. 1., S. Matsushita and W. H. Campbell, eds., Academic Press, New York, 426-507

Orwig, T. L., 1981, Channeled turbidites in the eastern central Pacific Ocean, Mar. Geol., 39, 33-57.

Orwig, T. L. and L. W. Kroenke, 1980, Tectonics of the eastern central Pacific basin, Mar. Geol., 34, 29-43.

Osbourne, D. G., 1966. Correlations beetween quiet-day magnetic ranges J. Atm. Terr. Phys., 28, 45-51.

Ozima, M., M. Honda, and K. Saito, 1977, ^{40}Ar-^{39}Ar ages of guyots in the western Pacific and discussion of their evolution, Geophys. J. Roy. Astr. Soc., 51, 475-485.

Ozima, M., I. Kaneoka, and S. Aramaki, 1970, K-Ar ages of submarine basalts dredged from seamounts in the western Pacific area and discussion of oceanic crust, Earth Planet. Sci. Lett., 8, 237-249.

Ozima, M., M. Ozima, and I. Kaneoka, 1968, Potassium-Argon ages and magnetic properties of some dredged submarine basalts and their geophysical implications, J. Geophys. Res., 73, 711-723.

Parker, R. L., 1972, The determination of seamount magnetism, Geophys. J. Roy. Astr. Soc., 24, 321-324.

Peddie, N. W. and E. B. Fabiano, 1982, A proposed International Geomagnetic Reference Field for 1965-1985, J. Geomag. Geoelectr.. 34, 357-364.

Peirce, J. W., 1976. Assessing the reliability of DSDP paleolatitudes, J. Geophys. Res., 81, 4173-4187.

Peirce, J. W., C. R. Denham, and B. P. Luyendyk, 1974, Paleomagnetic results of basalt samples from DSDP Leg 26, Init. Rept. DSDP, 26, 517-527.

Petersen, N., 1978, Rock and paleomagnetism of basalts from Site 396B, Leg 46, Init. Rept. DSDP, 46, 357-362.

Petersen, N., U. Bleil, and P. Eisenach, 1978, Rock and paleomagnetism of Leg 42A, Hole 373A basalts, Init. Rept. DSDP, 42, 881-886.

Petersen, N., U. Bleil, and P. Eisenach, 1979, Rock and paleomagnetism of Leg 43 basalts, Init. Rept. DSDP, 43, 773-780.

Piddington, J. H., 1967. A hydromagnetic model of geomagnetic storms and auroras, in Physics of Geomagnetic Phenomena, v. 2, S. Matsushita and W. H. Campbell, eds., Academic Press, New York, 1203-1241.

Pitman, W. C., III and D. E. Hayes, 1968, Sea-floor spreading in the Gulf of Alaska, J. Geophys. Res., 73, 6571-6580.

Plouff, D., 1975, Derivation of formulas and FORTRAN programs to compute magnetic anomalies of prisms, Nat. Tech. Inf. Service No. PB-243-525, U. S. Dept. of Commerce, Springfield, Va., 90 pp.

Plouff, D., 1976, Gravity and magnetic fields of polygonal prisms and application to magnetic terrain corrections, Geophysics, 41, 727-741.

Price, A. T., 1967, Electromagnetic induction within the Earth, in Physics of Geomagnetic Phenomena, v. 1, S. Matsushita and W. H. Campbell, eds., Academic Press, New York, 235-298.

Prince, R. A., G. R. Heath, and M. Kominz, 1980, Paleomagnetic studies of central north Pacific sediment cores: stratigraphy, sedimentation rates, and the origin of magnetic stability, Geol. Soc. Am. Bull., part II, 91, 1789-1835.

Rastogi, R. G. and K. N. Iyer, 1976, Quiet day variation of geomagnetic H-field at low latitudes, J. Geomag. Geolelectr., 28, 461-479.

Rastogi, R. G., N. B. Trivedi, and N. D. Kaushika, 1966, Night-time sudden commencements in H within the equatorial electrojet region, J. Atm. Terr. Phys., 28, 131-136.

Rea, D. K., 1969, Bathymetry and magnetics of a region (POL-21-3) 29° to 35°N, 155° to 165°W, ESSA Tech. Rept. ERL 146-POL4, Washington, U. S. Government Printing Office, 23 pp.

Rea, D. K., 1970, Changes in structure and trend of fracture zones north of the Hawaiian Ridge and relation to seafloor spreading, J. Geophys. Res., 75, 1421-1430.

Rea, D. K. and F. P. Naugler, 1971, Musicians Seamounts province and related crustal structures north of the Hawaiian Ridge, Mar. Geol. 10, 89-111.

Rice, P. D., J. M. Hall, and N. D. Opdyke, 1980, Deep drill 1972: a paleomagnetic study of the Bermuda Seamount, Can. J. Earth, Sci., 17, 232-243.

Richards, M. L., V. Vacquier, and G. D. Van Voorhis, 1967, Calculation of the magnetization of uplifts from combining topographic and magnetic surveys, Geophysics, 32, 678-707.

Riddihough, R. P., 1971, Diurnal corrections to magnetic surveys--an assessment of errors, Geophys. Prosp., 19, 551-567.

Roden, R. B., 1964, The effect of an ocean on magnetic diurnal variations, Geophys. J. Roy. Astr. Soc., 8, 375-388.

Roden, R. B. and C. S. Mason, 1964, The correction of shipboard magnetic observations, Geophys. J. Roy. Astr. Soc., 9, 9-13.

Rose, J. C., 1974, Open ocean navigation accuracy considerations for marine gravity requirements, in Proceedings of the International Symposium on Applications of Marine Geodesy, Marine Tech. Soc., Washington, D. C., 113-122.

Ryan, M. P., R. Y. Koyanagi, and R. S. Fiske, 1981, Modeling the three-dimensional stucture of macroscopic magma transport systems: application to Kilauea volcano, Hawaii, J. Geophys. Res., 86, 7111-7129.

Sager, W. W., 1983a, A Late Eocene paleomagnetic pole for the Pacific plate, Earth Planet. Sci. Lett., 63, 408-422.

Sager. W. W., 1983b, Paleomagnetism of Abbott Seamount and implications for the latitudinal drift of the Hawaiian hotspot., J. Gephys. Res., in press.

Sager. W. W., G. T. Davis, B. H. Keating, and J. A. Philpotts, 1982, A geophysical and geologic study of Nagata Seamount, northern Line Islands, J. Geomag. Geoelectr., 34, 283-305.

Sager. W. W. and B. H. Keating, 1982, Implications of western Pacific seamount magnetism for the motion of the Pacific plate, (abstract), Tran. Am. Geophys. Union, EOS, 63, 916.

Saito, K. and M. Ozima, 1976, ^{40}Ar-^{39}Ar ages of submarine rocks from the Line Islands: implications on the origin of the Line Islands, in The Geophysics of the Pacific Ocean Basin and its Margin, Geophys. Mon. Ser. 19, G. H. Sutton, M. H. Manghnani, and R. Moberly, eds., AGU, Washington, D. C., 369-374.

Saito, K. and M. Ozima, 1977, ^{40}Ar-^{39}Ar geochronological studies on submarine rocks from the western Pacific area, Earth Planet. Sci. Lett., 33, 353-369.

Sayre. W. O., 1981, Preliminary report on the paleomagnetism of Aptian and Albian limestones and trachytes from the Mid-Pacific mountains and Hess Rise, Deep Sea Drilling Project, Leg 62, Init. Rept. DSDP, 62, 983-994.

Schimke, G. R. and C. G. Bufe, 1968, Geophyisical description of a Pacific Ocean seamount, J. Geophys. Res., 73, 559-569.

Schlanger, S. O., M. O. Garcia, J. Haggerty, B. H. Keating, J. J. Naughton, J. A. Philpotts, W. Sager, and R. A. Duncan, 1982, Geologic evolution of the Line Islands, (abstract), The Origin and Evolution of Seamount Conference, Lamont-Doherty Geological Observatory, Palisades, N. Y., Nov. 17-19, 1982.

Schlanger, S. O., H. C. Jenkyns, and I. Premoli-Silva, 1981, Volcanism and vertical tectonics in the Pacific basin related to global Cretaceous transgressions, Earth Planet. Sci. Lett., 52, 435-449.

Schlanger, S. O. and R. L. Larson, 1981, Underway geophysical data from Deep Sea Drilling Project Leg 61: navigation, bathymetry, magnetics, and seismic profiles, Init. Rept, DSDP, 61, 771-813.

Schlanger, S. O. and I. Premoli-Silva, 1981, Tectonic, volcanic, and paleogeographic implications of redeposited reef faunas of Late Cretaceous and Tertiary age from the Nauru Basin and Line Islands, Init. Rept. DSDP, 61, 817-827.

Schlapp, D. M., 1968, World-wide morphology of day-to-day variability of Sq, J. Atm. Terr. Phys., 30, 1761-1776.

Schlapp, D. M., 1973, Hour-to-hour variability of Sq, J. Atm. Terr. Phys., 35, 827-831.

Schouten, H., 1971, A fundamental analysis of magnetic anomalies over ocean ridges, Mar. Geophys. Res., 1, 111-144.

Schouten, H. and S. C. Cande, 1976, Paleomagnetic poles from marine magnetic anomalies, Geophys. J. Roy. Astr. Soc., 44, 567-575.

Sclater, J. G. and R. D. Jarrard, 1971, Preliminary paleomagnetic results, Leg 7, Init. Rept. DSDP, 7, 1227-1234.

Sharma, P. V., 1978, Geophysical Methods in Geology, Elsevier, New York, 428 pp.

Shaw, H. R. and E. D. Jackson, 1973, Linear island chains in the Pacific: result of thermal plumes or gravitational anchors?, J. Gephys. Res., 78, 8634-8652.

Simkin, T., 1972, Origin of some flat topped volcanoes and guyots, in Studies in Earth and Space Sciences, Geol. Soc. Am. Mem. 132, R. Schagam and R. B. Hargraves, eds., GSA, Boulder, Colorado, 183-193.

Stearns, H. T. and G. A. Macdonald, 1942, Geology and groundwater resources of the island of Maui, Hawaii, Hawaii Div. Hydr. Bull. No. 7, 344 pp.

Steiner, M. B., 1981a, Paleomagnetism of the Cretaceous section, Site 462, Init. Rept. DSDP, 61, 711-716.

Steiner, M. B., 1981b, Paleomagnetism of the igneous complex, Site 462, Init. Rept. DSDP, 61, 717-729.

Steiner, M. B., 1982, An investigation of ulvospinel compostion and cation migration during maghemitization in Deep Sea Drilling Project Leg 61 titanomagnetites, J. Geophys. Res., 87, 5361-5374.

Suarez, G. and P. Molnar, 1980, Paleomagnetic data and pelagic sediment facies and the motion of the Pacific plate since the Late Cretaceous, J. Gephys. Res., 85, 5257-5280.

Suyenaga, W., 1979, Isostasy and flexure of the lithosphere under the Hawaiian Islands, J. Geophys. Res., 84, 5599-5604.

Swanson, D. A., 1971, Magma supply rate at Kilauea volcano, 1952-1971, Science, 175, 169-170.

Talwani, M., 1965, Computation with the help of a digital computer of magnetic anomalies caused by bodies of arbitrary shape, Geophysics, 30, 797-817.

Talwani, M., L. Dorman, J. Worzel, and G. M. Bryan, 1966, Navigation at sea by satellite, J. Geophys. Res., 71, 5891-5902.

Tamaki, K., M. Joshima, and R. L. Larson, 1979, Remanent Early Cretaceous spreading center in the central Pacific basin, J. Geophys. Res., 84, 4501-4510.

Telford, W. M., L. P. Geldart, R. E. Sheriff, and D. A. Keys, Applied Geophysics, Cambridge University Press, 860 pp.

Thiede, J., W. E. Dean, D. K. Rea, T. L. Vallier, and C. G. Adelseck, 1981, The geologic history of the Mid-Pacific Mountains in the central north Pacific Ocean--a systhesis of Deep-Sea Drilling Studies, Init. Rept. DSDP, 62, 1073-1120.

Tomoda, Y., H. Fujimoto, A. Uchiyama, and I. Nakano, 1982, Determination of the geomagnetic daily variation in total force on board a ship, J. Geomag. Geoelectr., 34, 241-244.

Turner, D. L., R. D. Jarrard, and R. B. Forbes, 1980, Geochronology and origin of the Pratt-Welker seamount chain, Gulf of Alaska: a new pole of rotation for the Pacific plate, J. Geophys. Res., 85, 6547-6556.

Turner, D. L. and R. D. Jarrard, 1982, K-Ar dating of the Cook-Austral Island chain: a test of the hot-spot hypothesis, J. Volc. Geotherm. Res., 12, 187-220.

Uyeda, S., 1978, The New View of the Earth, W. H. Freeman and Co., San Francisco, 217 pp.

Uyeda, S., M. D. Fuller, J. C. Belshe, and R. W. Girdler, 1963, Anisotropy of magnetic susciptibility of rocks and minerals, J. Geophys. Res., 68, 279-291.

Uyeda, S. and M. L. Richards, 1966, Magnetization of four Pacific seamounts near the Japanese Islands, Earthquake Res. Inst. Bull., 44, 179-213.

Vacquier, V., 1962, A machine method for computing the magnitude and direction of magnetization of a uniformly magnetized body from its shape and a magnetic survey, Proceedings Benedum Earth Magnetism Symposium, 123-137.

Vacquier, V., 1972, Geomagnetism in Marine Geology, Elsevier, New York 185 pp.

Vacquier, V. and S. Uyeda, 1967, Paleomagnetism of nine seamounts in the western Pacific and of three volcanoes in Japan, Earthquake Res. Inst. Bull., 45, 815-848.

van Andel, T. H., 1974, Cenozoic migration of the Pacific plate, northward shift of the axis of deposition, and paleobathymetry of the central equatorial Pacific, Geology, 2, 507-510.

van Andel, T. H., G. R. Heath, and T. C. Moore, 1975, Cenozoic History and Paleoceanography of the Central Equatorial Pacific, Geol. Soc. Am. Mem. 143, GSA, Boulder, Colorado, 134 pp.

Van Hinte, J. E., 1978, A Cretaceous time scale, in Contributions to the Geologic Time Scale, AAPG studies in Geology, No. 6, AAPG, Tulsa, Oklahoma, 269-287.

Van Voorhis, G. and J. Walczak, 1963, Summary of magnetization computations for Kelvin Seamount, unpublished manuscript M-8-63, Marine Sciences Dept., U. S. Naval Oceanographic Office, Washington, D. C., 19 pp.

Vanko, D. A. and R. Batiza, 1982, Gabbroic rocks from the Mathematician Ridge failed rift, Nature, 300, 742-744.

Vestine, E. H., 1967. Main geomagnetic field, in Physics of Geomagnetic Phenomena, v. 1, S. Matsushita and W. H. Campbell, eds., Academic Press, New York, 181-233.

Vogt, P. R., 1969, Can demagnetization explain seamount drift?, Nature, 224, 574-576.

Vuagnat, M., 1975, Pillow lava flows: isolated sacks or connected tubes?, Bull. Volc., 39, 581-589.

Wallin, B. H., 1982, The northern Hawaiian deep and arch: interpretation of geologic history from reflection profiling and echo character mapping, M. Sc. thesis, University of Hawaii, Honolulu, 133 pp.

Watkins, E., R. Batiza, and D. Vanko, 1982, Petrology and significance of alkalic volcanic rocks erupted at the Mathematician Ridge and Clarion Fracture Zone, eastern Pacific, (abstract). Trans. Am. Geophys. Union, EOS, 63, 473.

Watts, A. B., J. H. Bodine, and N. M. Ribe, 1980, Observations of flexure and the geological evolution of the Pacific Ocean basin, Nature, 283, 532-537.

Weissel, J. K., D. E. Hayes, and E. M. Herron, 1977, Plate tectonics synthesis: the displacements between Australia, New Zealand, and Antarctica since the Late Cretaceous, Mar. Geol., 25, 231-277.

Wentworth, C. K. and A. E. Jones, 1940, Intrusive rocks of the leeward slope of the Koolau range, Oahu, J. Geol., 48, 975-1006.

Wilson, R. L. and M. W. McElhinny, 1974, Investigation of the large scale palaeomagnetic field over the past 25 million years. Eastward shift of the Icelandic spreading ridge, Geophys. J. Roy. Astr. Soc., 39, 570-586.

Winterer, E. L., 1973, Sedimentary facies and plate tectonics of equatorial Pacific, Am. Assoc. Pet. Geol. Bull., 57, 265-282.

Winterer, E. L., 1976. Anomalies in the tectonic evolution of the Pacific, in The Geophysics of the Pacific Ocean Basin and its Margin, Geophys. Mon. Ser. 19, G. H. Sutton, M. H. Manghnani, and R. Moberly, eds., AGU, Washington, D. C., 269-278.

Winterer, E. L., P. F. Lonsdale, J. L. Matthews, and B. R. Rosendahl, 1974, Structure and acoustic stratigraphy of the Manihiki Plateau, Deep Sea Res., 21, 793-814.

Wolejszo, J., R. Schlich, and J. Segoufin, 1974, Paleomagnetic studies of basalt samples, Deep Sea Drilling Project, Leg 25, Init. Rept. DSDP, 25, 555-572.

Woods, M. T. and G. F. Davies, 1982, Late Cretaceous genesis of the Kula plate, Earth Planet. Sci. Lett., 58, 161-166.

Woodward, D. J. and M. P. Hochstein, 1970, Magnetic measurements of the Cook Islands, South-west Pacific Ocean, N. Z. J. Geol. Geophys., 13, 207-224.

Worsley, T. R., 1973. Calcareous nannofossils: Leg 19 of the Deep Sea Drilling Project, Init. Rept. DSDP, 19, 741-750.

Yacob, A. 1966. Seasonal parameters of the equatorial electrojet at different longitudinal zones, J. Atm. Terr. Phys., 28, 581-597.